

UNIVERSIDAD POLITECNICA DE VALENCIA

DEPARTAMENTO DE CIENCIA ANIMAL



UNIVERSITAT  
POLITÈCNICA  
DE VALÈNCIA

**“Study of requirements and design of sensors for monitoring water quality and feeding process in fish farms and other environments”**

*TESIS DOCTORAL*

Autora:

**PARRA BORONAT, Lorena**

Directores

**LLORET MAURI, Jaime**

**RODILLA ALAMÁ, Miguel**

Tutor:

**JOVER CERDÁ, Miguel**

*Valencia, Junio del 2018*



# Abstract

There are many efforts done in the aquaculture to reach its sustainability, although in reality, it is far from being sustainable. Its negative impacts on the environment can be prevented and corrected by the use of sensors, developing precision aquaculture. The water quality affects to the fish performance. The temperature and salinity are some factors that affect to the fish growth. Nevertheless, other factors such as turbidity, photoperiod and dissolved oxygen among other can affect to the fish feeding needs. To adjust the amount of feed needed is crucial to ensure the sustainability of the aquaculture and to increase the economic profit of the facilities. Monitoring the water quality allows estimating the feed needs. However, it is not enough. To monitor the fish behavior, especially during the feeding period can help to adapt the provided feed. Then, if it is so clear that the monitoring can help to the aquaculture production, why we do not see this monitoring systems in the aquaculture facilities? Why in most of the facilities the feed is given manually without considering the fish feeding behavior?

Nevertheless, the current price of the sensors for monitoring the fish farms is extremely high. The employed sensors are in most of the cases, the same that are used for oceanography. The proposed systems in the literature only cover some water quality parameters and usually do not consider fish feeding behavior. It is need low-cost sensors suitable for aquaculture monitoring. Those sensors must also be low-energy consumption, easy to use and with the option to include them in a network in order to send the data. Thus, we can use these sensors and sensors network to monitor the activity, to send alarms if it is necessary and to automatize processes. Moreover, including Internet, the data can be seen remotely. The use of those sensors can help to the aquaculture production.

In this thesis, we show the study of requirements and design of sensors for monitoring water quality and feeding process in fish farms and other environments. First, we study in detail the requirements of sensors in aquaculture. Then, we show the state of the art of the current sensors for water quality monitoring and for aquaculture monitoring.

Following, we present the design and development of some low-cost sensors and their applications in fish farm facilities with open system and recirculating system. Moreover we show a complete system which monitors up to 10 parameters including water quality (temperature, salinity, turbidity and presence of hydrocarbon/oil layer), tank environment (water level, illumination, presence of workers), and fish feeding behavior (shoal swimming depth, estimation of changes on shoal swimming velocity and feed falling). Moreover, it accomplishes the features of low-cost and low energy consumption. The estimated price for proposed system is less than 100€ per tank. In addition, we show the use of some of the aforementioned sensors for automatic adjustment of fish feeding process.

Finally, some of the developed sensors are plied in other natural aquatic areas such as mangroves, and estuaries. Moreover, an intelligent system for pollution monitoring and tracking in water bodies are presented.

# Resumen

Se están realizando muchos esfuerzos en la acuicultura para alcanzar la sostenibilidad, sin embargo aún está lejos de ser sostenible. Sus impactos sobre el medio ambiente pueden prevenirse y corregirse mediante el uso de sensores, desarrollando la conocida como acuicultura de precisión. La calidad del agua afecta el rendimiento de los peces. La temperatura y la salinidad son algunos factores que afectan al crecimiento de los peces. Sin embargo, otros factores como la turbidez, el fotoperíodo y el oxígeno disuelto entre otros pueden afectar a las necesidades nutritivas de los peces. Ajustar la cantidad de alimento necesario es crucial para garantizar la sostenibilidad de la acuicultura y para aumentar el beneficio económico de las instalaciones. Al monitorear la calidad del agua, es posible estimar las necesidades de alimentación. Sin embargo, no es suficiente. El monitoreo del comportamiento de los peces, especialmente durante el período de alimentación, puede ayudar a adaptar el alimento proporcionado. Entonces, si está tan claro que el monitoreo puede ayudar a la producción acuícola, ¿por qué no vemos este sistema de monitoreo en las instalaciones acuícolas? ¿Por qué en la mayoría de las instalaciones la alimentación se da manualmente sin considerar el comportamiento de alimentación de los peces?

El precio de los sensores para monitorizar las piscifactorías es extremadamente alto. Los sensores empleados son, en la mayoría de los casos, los mismos que se utilizan para la oceanografía. Los sistemas propuestos en la literatura cubren pocos parámetros de calidad del agua y generalmente no consideran el comportamiento de alimentación de los peces. Son necesarios sensores de bajo costo adecuados para la monitorización de la acuicultura. Esos sensores deben ser de bajo costo, bajo consumo de energía, fáciles de usar y con la posibilidad de incluirlos en una red para enviar los datos. Por lo tanto, podremos utilizar esta red de sensores y sensores para controlar la actividad, enviar alarmas si es necesario y automatizar los procesos. Además, si incluimos Internet, los datos se pueden ver de forma remota. El uso de esos sensores puede ayudar a la producción acuícola.

En esta tesis mostramos el estudio de los requisitos y el diseño de sensores para monitorizar la calidad del agua y el proceso de alimentación en piscifactorías y otros entornos. Primero estudiamos en detalle los requisitos de los sensores en acuicultura. Luego mostramos el estado del arte de los sensores actuales para el monitoreo de la calidad del agua y para el monitoreo de la acuicultura.

A continuación, presentamos el diseño y desarrollo de nuestros propios sensores de bajo costo y su aplicación en instalaciones de piscifactorías con sistema abierto y sistema de recirculación. Además, mostramos la posibilidad de monitorizar hasta 10 parámetros incluyendo calidad del agua (temperatura, salinidad, turbidez y presencia de hidrocarburo / capa de aceite), ambiente del tanque (nivel de agua, iluminación, presencia de trabajadores) y comportamiento de alimentación de peces (profundidad de natación de bajura, estimación de los cambios en la velocidad de nado de bajíos y la caída de alimento). El sistema propuesto, capaz de monitorear todos estos parámetros, tiene un bajo coste y bajo consumo de energía. El precio estimado es inferior a 100 € por tanque. Además, mostramos el uso de algunos de los sensores antes mencionados para el ajuste automático del proceso de alimentación de peces.

Finalmente, mostramos como algunos de los sensores desarrollados se utilizan en otras áreas acuáticas naturales como manglares y estuarios. Además, se presenta un sistema inteligente para monitorear y rastrear la contaminación en los cuerpos de agua.

# Resum

S'estan realitzant molts esforços en l'aqüicultura per assolir la sostenibilitat, malgrat això, encara està lluny de ser sostenible. Els seus impactes sobre el medi ambient es poden prevenir i corregir mitjançant l'ús de sensors, desenvolupant la coneguda com a aqüicultura de precisió. La qualitat de l'aigua afecta el rendiment dels peixos. La temperatura i la salinitat són alguns factors que afecten el creixement dels peixos. A més a més, altres factors com la terbolesa, el fotoperíode i l'oli dissolt entre uns altres poden afectar a les necessitats nutritives dels peixos. Ajustar la quantitat d'aliment necessari és crucial per garantir la sostenibilitat de l'aqüicultura i per augmentar el benefici econòmic de les instal·lacions. Al monitoritzar la qualitat de l'aigua, és possible estimar les necessitats d'alimentació. No obstant això, no és suficient. Monitoritzar el comportament dels peixos, especialment durant el període d'alimentació, pot ajudar a adaptar el subministrament alimentari. Aleshores, si es tan clar que el monitoratge pot ajudar a la producció aqüícola, per què no veiem aquest sistema de monitoratge en les instal·lacions aquàtiques? Per què a la majoria de les instal·lacions la alimentació es dona manualment sense considerar el comportament alimentari dels peixos?

El preu dels sensors per controlar les piscifactories és extremadament alt. Els sensors empleats són, en la majoria dels casos, els mateixos que es fan servir per a l'oceanografia. Els sistemes proposats en la literatura monitoritzen pocs paràmetres de qualitat de l'aigua i generalment no consideren el comportament dels peixos durant l'alimentació. Són necessaris sensors de baix cost adequats per a la monitorització de l'aqüicultura. Aquests sensors han de ser de baix cost, baix consum d'energia, senzills d'usar i amb la possibilitat d'incloure'ls en una xarxa per enviar-los. Per tant, podrem utilitzar aquesta xarxa de sensors i sensors per controlar l'activitat, enviar alarmes si és necessari i automatitzar els processos. A més, si incloem Internet, les dades es podran veure de forma remota. L'ús d'aquests sensors pot ajudar a la producció aqüícola.

En aquesta tesi es mostra l'estudi dels requisits i el disseny de sensors per a monitoritzar la qualitat de l'aigua i el procés d'alimentació en piscifactories i altres entorns. Primer, estudiem en detall els requisits dels sensors en aqüicultura. A continuació, es mostra el estat de l'art dels sensors actuals per al monitoratge de la qualitat de l'aigua i per al monitoratge de l'aqüicultura.

A continuació, presentem el disseny i desenvolupament dels nostres propis sensors de baix cost i la seva aplicació en instal·lacions d'aqüicultura amb sistema obert i sistema de recirculació. A més, mostrem la possibilitat de monitoritzar fins a 10 paràmetres, incloent-hi la qualitat de l'aigua (temperatura, salinitat, terbolesa i presència d'hidrocarburs / capa d'oli), ambient del tanc (nivell d'aigua, il·luminació, presència de treballadors) i alimentació del consum de peces (profunditat de natació de baix, estimació dels canvis en la velocitat de naixement de baixos i la caiguda d'aliment). El sistema proposat, capaç de controlar tots aquests paràmetres, té un baix cost i baix consum d'energia. El preu estimat és inferior a 100 € per tanc. A més, mostrem l'ús d'alguns dels sensors abans esmentats per a l'ajust automàtic del procés d'alimentació de peces.

Finalment, mostrem com alguns dels sensors desenvolupats es fan servir en altres àrees aquàtiques naturals com manglars i estuaris. A més, es presenta un sistema intel·ligent per monitoritzar i rastrejar la contaminació en els cossos d'aigua.

# Agradecimientos

Querría agradecer en primer lugar a mis directores, Jaime Lloret y Miguel Rodilla y mi tutor Miguel Jover por todo lo mucho que me ha enseñado y apoyado en este proyecto. Y en concreto a Jaime Lloret por la oportunidad que me ha dado de trabajar con él y su grupo de investigación. En segundo lugar le quiero dar las gracias a Sandra Sendra y José Miguel Jimenez por haberme guiado y ayudado en algunos puntos de este trabajo incluso desde la distancia. Por explicarme y ayudarme en cierto tipo de conocimientos que tal vez se alejan un poco de mi ámbito de trabajo. También quiero agradecer a Miran Taha, Laura García y Javier Rocher con quien he colaborado en el laboratorio habitualmente.

Por último a mi familia, a mi pareja Borja Mengual y a mis amigos quienes me habéis dado ánimos para proseguir y que nunca habéis dudado de que alcanzaría todo lo que me propusiera. Sobre todo a ti, Borja, has creído en mí hasta cuando yo no creía, has comprendido las noches y fines de semana de trabajo, las estancias lejos de casa y siempre has conseguido ayudarme. Muchas gracias a todos, esto no hubiese sido posible sin vosotros.

# TABLE OF CONTENTS

<b>LIST OF FIGURES</b> .....	xii
<b>LIST OF TABLES</b> .....	xvii
<b>LIST OF ACRONYMS</b> .....	xix
<b>1. INTRODUCTION</b> .....	1
1.1. Introduction and motivation .....	2
1.1.1. The aquaculture and its sustainability .....	2
1.1.2. Open issues when monitoring the aquaculture.....	3
1.1.3. The information and communication technologies and the WSN.....	5
1.2. Research goals.....	8
1.3. Precedents .....	9
1.4. Contributions.....	10
1.5. Structure .....	12
<b>2. RELATED WORK</b> .....	14
2.1. Introduction.....	15
2.2. Effects of the environmental parameters on fish.....	15
2.2.1. Effects of temperature .....	15
2.2.2. Effects of salinity .....	17
2.2.3. Effects of photoperiod.....	22
2.2.4. Effects of dissolved oxygen .....	25
2.2.5. Effects of other parameters.....	27
2.2.5.1. Effects of light:.....	27
2.2.5.2. Effects of turbidity:.....	28
2.2.5.3. Effects of pH .....	29
2.2.6. Discussion on the effects of environmental parameters on fish .....	29
2.3. Physical sensors for water quality monitoring for precision aquaculture .....	33
2.3.1. Requirements of aquaculture sensors .....	34
2.3.2. Temperature .....	36
2.3.3. Salinity .....	38
2.3.4. Dissolved oxygen .....	40
2.3.5. Turbidity.....	41
2.3.6. Discussion and future challenge on sensors for fish farms monitoring.....	43
2.4. Current systems for aquaculture monitoring .....	46
2.4.1. Data gathering systems.....	47

2.4.2.	Monitoring systems for fish farms .....	47
2.4.3.	Monitoring systems for general aquatic environments .....	50
2.5.	Related work on conductivity meters .....	52
2.6.	Related work on hydrocarbon detection.....	53
2.7.	Conclusion.....	55
<b>3.</b>	<b>DEVELOPED SENSORS .....</b>	<b>57</b>
3.1.	Introduction.....	58
3.2.	Salinity sensor .....	61
3.2.1.	First models .....	61
3.2.1.1.	Material and methods.....	61
3.2.1.1.1.	Based on a hall sensor .....	62
3.2.1.1.2.	Based on an inductive coil.....	62
3.2.1.1.3.	Developed tests .....	63
3.2.1.2.	Results .....	65
3.2.1.2.1.	Comparative of prices of the developed sensors and current commercial sensors	69
3.2.1.2.2.	Discussion .....	70
3.2.2.	The copper coils as conductivity sensors .....	70
3.2.2.1.	Material and methods.....	70
3.2.2.1.1.	Description of coils models.....	71
3.2.2.1.2.	Test bench .....	71
3.2.2.2.	Results .....	72
3.2.2.2.1.	Comparison of models and Discussion .....	75
3.2.3.	Studying the combination of solenoid and toroid.....	76
3.2.3.1.	Material and methods.....	76
3.2.3.2.	Results and Discussion .....	78
3.2.3.2.1.	Minimum cell volume .....	78
3.2.3.2.2.	Linear ranges and sensibility .....	79
3.2.3.2.3.	Verification process.....	81
3.2.4.	Evaluating the combination of two solenoids for conductivity monitoring in fish farms	82
3.2.4.1.	Background theory .....	82
3.2.4.2.	Test bench .....	83
3.2.4.3.	Results .....	84
3.2.4.3.1.	Physical characterization of the sensor.....	85
3.2.4.3.2.	First test: Changes in the number of spires maintaining the spires relationship	86



3.2.4.3.3.	Second and third test: Change the spires relation.....	86
3.2.4.3.4.	Forth test: Change the wire diameter.....	88
3.2.4.3.5.	Fifth test: Change the coil diameter .....	88
3.2.4.3.6.	Summary of tests for physical characterization of the sensor and election of prototype .....	89
3.2.4.3.7.	Determination of minimum cell volume .....	90
3.2.4.3.8.	Calibration.....	92
3.3.	Turbidity sensor.....	94
3.3.1.	Material and methods .....	94
3.3.1.1.	Background.....	94
3.3.1.2.	Design and development of the turbidity sensor .....	94
3.3.1.3.	Turbidity samples .....	95
3.3.2.	Results and Discussion.....	96
3.3.2.1.	Different turbidity sources .....	96
3.3.2.2.	Distinguish between turbidity sources.....	97
3.3.2.3.	Intelligent algorithm.....	101
3.3.2.4.	Verification process.....	102
3.3.2.5.	Comparison with current sensor systems and suitability for fish farms...	103
3.4.	Hydrocarbon sensor.....	104
3.4.1.	Material and methods .....	104
3.4.2.	Results .....	105
3.5.	Conclusion.....	106
<b>4.</b>	<b>IMPLEMENTATION IN FISH FARMS .....</b>	<b>109</b>
4.1.	Introduction.....	110
4.2.	A system to control the salinity and water level in the fish farms facilities.....	111
4.2.1.	System description .....	111
4.2.1.1.	Salinity Sensor .....	111
4.2.1.2.	Wireless module.....	114
4.2.1.3.	Sensor to measure the water level .....	114
4.2.1.4.	Signal generation.....	115
4.2.1.5.	Server implementation collect data.....	117
4.2.2.	Autonomous System to Control Automatically the water Salinity .....	119
4.2.3.	Real Measurements and network test.....	121
4.3.	WSN for monitoring the turbidity in fish farms.....	124
4.3.1.	System description .....	124
4.3.1.1.	Turbidity sensor development .....	125

4.3.1.2.	Employed Node .....	126
4.3.1.3.	WSN deployment .....	126
4.3.1.4.	Architecture.....	127
4.3.2.	WSN Performance.....	129
4.4.	System for monitoring the cage, the water quality, and the fish behavior .....	133
4.4.1.	Materials and Methods .....	133
4.4.1.1.	Architecture.....	133
4.4.1.2.	Sensors .....	135
4.4.1.2.1.	Water parameters.....	135
4.4.1.2.2.	Tank parameters .....	137
4.4.1.2.3.	Feeding parameters .....	138
4.4.1.2.4.	Other sensors .....	138
4.4.1.3.	Node .....	139
4.4.2.	Results and discussion.....	140
4.4.2.1.	Results of the water quality sensors .....	140
4.4.2.2.	Results of the tank sensors .....	142
4.4.2.3.	Results of the fish behavior sensors.....	143
4.4.2.4.	Comparison with other systems and price of the employed components	147
4.5.	Automatic system for the adjustment of the feeder process to the fish demand .....	148
4.5.1.	System description .....	148
4.5.1.1.	Scenario description .....	149
4.5.1.2.	Node and sensors description .....	149
4.5.2.	Results and discussion.....	150
4.5.2.1.	Calibration of the feed detection system.....	150
4.5.2.2.	Calibration of fish presence sensor .....	154
4.5.2.3.	Verification process.....	155
4.5.2.4.	Simulation of feeding process .....	158
4.5.2.5.	Comparison with current systems .....	160
4.6.	Conclusion.....	160
<b>5.</b>	<b>IMPLEMENTATION IN OTHER ENVIRONMENTS .....</b>	<b>163</b>
5.1.	Introduction .....	164
5.2.	Proposed System for estuaries and mangrove forests .....	166
5.2.1.	Proposed system.....	166
5.2.1.1.	Salinity Sensor .....	167
5.2.1.2.	Wireless module.....	168
5.2.2.	Server deployment for data gathering .....	170

5.2.3.	Real Measurements and network test .....	170
5.3.	Application of the WSN for oceanic climate monitoring.....	172
5.3.1.	Proposal Description .....	172
5.3.1.1.	Multisensor buoy .....	172
5.3.1.2.	Design of wireless node .....	173
5.3.2.	Sensors for marine parameters monitoring .....	174
5.3.2.1.	Water temperature sensor .....	175
5.3.2.2.	Water Salinity Sensor .....	176
5.3.2.3.	Water Turbidity Sensor .....	180
5.3.2.4.	Hydrocarbon detector sensor .....	182
5.3.3.	Sensors for Weather parameters monitoring .....	184
5.3.3.1.	Sensor for environmental Temperature .....	184
5.3.3.2.	Relative Humidity .....	185
5.3.3.3.	Wind speed and direction .....	187
5.3.3.4.	Solar Radiation sensor .....	191
5.3.3.5.	Rainfall Sensor .....	193
5.3.4.	Mobile platform and Network Performance.....	195
5.3.4.1.	Data acquisition system based on Android .....	195
5.4.	Smart system for detecting and tracking pollutants in water .....	197
5.4.1.	Proposed System .....	197
5.4.1.1.	Proposed sensor node.....	197
5.4.1.2.	Designed Algorithm.....	200
5.4.2.	Network Performance .....	201
5.5.	Conclusion.....	204
<b>6.</b>	<b>CONCLUSIONS AND FUTURE WORK.....</b>	<b>205</b>
6.1.	Introduction .....	206
6.2.	Conclusions .....	206
6.3.	Future work .....	207
6.4.	Fulfillment of the objectives and difficulties found during the process .....	208
6.5.	Publications derived from the PhD .....	208
	<b>Bibliography.....</b>	<b>211</b>

## LIST OF FIGURES

### Chapter 1:

Figure 1. 1 Factors that affect the fish performance in aquaculture facilities	3
Figure 1. 2 Main benefits of monitoring environmental parameters when feeding	4
Figure 1. 3 Main applications of underwater WSNs.	7

### Chapter 2:

Figure 2. 1 Studied factors for all the effects	30
Figure 2. 2 Stage of development of fish tested in growth studies and its susceptibility to changes	30
Figure 2. 3 Studied factors in growth tests and effects	30
Figure 2. 4 Stage of development of fish tested in survival studies and its susceptibility to changes	31
Figure 2. 5 Studied factors in survival tests and effects	31
Figure 2. 6 Stage of development of fish tested in behavior studies and its susceptibility to changes	33
Figure 2. 7 Studied factors in behavior tests and effects	33
Figure 2. 8 Employed technology on temperature sensors	46
Figure 2. 9 Employed technology on salinity sensors	46
Figure 2. 10 Employed technology on dissolved oxygen sensors	46
Figure 2. 11 Employed technology on turbidity sensors	46

### Chapter 3:

Figure 3. 1 Structure of the laboratory test bench for Hall sensor.	63
Figure 3. 2 Structure of the laboratory test bench for Two Coils.	63
Figure 3. 3 Laboratory set-up with the probe in the air	63
Figure 3. 4 Laboratory set-up with the probe in the water.	63
Figure 3. 5 The first solenoid of the first test, which has an assay tube in the center.	64
Figure 3. 6 The second solenoid for the first test, which is coiled on a plastic tube that serves as a container	64
Figure 3. 7 Representation of the data for 5V for test A and test B	67
Figure 3. 8 Representation of the data for 10 V for test A	67
Figure 3. 9 Representation of the data for 20V for test A	67
Figure 3. 10 Representation of the data of Table 3.10	69
Figure 3. 11 Representation of the data of Table 3.11	69
Figure 3. 12 Output voltage for first model.	73
Figure 3. 13 Output voltage for second model.	73
Figure 3. 14 Output voltage for third model.	73
Figure 3. 15 Output voltage for fourth model.	73
Figure 3. 16 Relation between water conductivity and output voltage for Model 1 at 500kHz.	74
Figure 3. 17 Relation between water conductivity and output voltage for Model 2 at 500kHz.	74
Figure 3. 18 Relation between water conductivity and output voltage for Model 3 at 2000kHz.	75
Figure 3. 19 Relation between water conductivity and voltage registered in the Model 4 at 150kHz.	75
Figure 3. 20 The conductivity sensor Model 4 with the components.	77
Figure 3. 21 Possible scenarios of measurement attending to the size of the container	77
Figure 3. 22 Dependence of the Sensor signal with the volume of water obtained in the test of minimum cell volume	79
Figure 3. 23 Correlation between the water conductivity and the Sensor signal Model 4 at the working frequency.	80
Figure 3. 24 Conductivity of our sensor vs. Conductivity of commercial device.	82
Figure 3. 25 The employed coils and its magnetic field	82
Figure 3. 26 Electric circuit of the sensor	84
Figure 3. 27 Picture of the test bench for one of the measurements	86

Figure 3. 28 Example of possible behaviors of different prototypes	86
Figure 3. 29 Induced voltages for best frequencies of prototypes from 1 to 4 at test 1	89
Figure 3. 30 Induced voltages for best frequencies of prototypes from 5 to 9 at test 2	89
Figure 3. 31 Induced voltages for best frequencies of prototypes from 5' to 9' at test 3	89
Figure 3. 32 Induced voltages for best frequencies of prototypes 3, 11, 12 and 14 at tests 4 and 5	89
Figure 3. 33 Example of containers of water that accomplish the minimum cell volume A) and do not accomplish it B).	91
Figure 3. 34 Results of first test to find out the minimum cell volume	92
Figure 3. 35 Results of second test to find out the minimum cell volume	92
Figure 3. 36 Representation of data of calibration process	93
Figure 3. 37 Representation of the prototype and its electronic scheme	95
Figure 3. 38 Resistance of LDR and photodiode with samples of <i>Isochrysis galbana</i>	97
Figure 3. 39 Resistance of LDR and photodiode with samples of <i>Tetraselmis chuii</i>	97
Figure 3. 40 Resistance of LDR and photodiode with samples of Sediment	97
Figure 3. 41 Regression models with confidence intervals for different turbidity sources with a green light	99
Figure 3. 42 Regression models with confidence intervals for different turbidity sources with yellow light.	100
Figure 3. 43 Regression models with confidence intervals for different turbidity sources with red light.	101
Figure 3. 44 Decision algorithm	102
Figure 3. 45 Data from the verification process.	103
Figure 3. 46 Data gathered in real time.	103
Figure 3. 47 Disposition of the light source, detector and water sample	105
Figure 3. 48 Set up of the experiments to select the best light source.	106
Figure 3. 49 Output voltage registered at the photoreceptor output using different light colors.	106
Figure 3. 50 Output voltage registered at the photoreceptor output using the selected light of test 1 after 10 repetitions, represented the mean with the standard deviation.	106

#### Chapter 4:

Figure 4. 1 Design on PVC coverage.	112
Figure 4. 2 Sensors with and without isolating cover	112
Figure 4. 3 Distance measuring sensor unit	114
Figure 4. 4 Distance sensor position in fish tanks.	115
Figure 4. 5 Distance to water vs. output voltage.	115
Figure 4. 6 Program code for Flyport to create a square signal.	116
Figure 4. 7 Stages of our proposed system	116
Figure 4. 8 Square signal generated by the Flyport.	117
Figure 4. 9 Sine wave obtained at the output of induced coil overlapped with the generated square signal.	117
Figure 4. 10 TPC Socket connection process and packet exchange between server and client.	118
Figure 4. 11 Program code for Flyport configuration as Socket Client.	119
Figure 4. 12 Architecture and sensors distribution.	120
Figure 4. 13 Flow diagram to control the system	121
Figure 4. 14 Scenario used during our test bench.	122
Figure 4. 15 Consumed bandwidth by a node when sending data from 4 level sensors.	122
Figure 4. 16 Consumed bandwidth by a node when sending data from one salinity sensor	123
Figure 4. 17 Consumed bandwidth by a node when sending data from the level sensor.	123
Figure 4. 18 Delay between TCP streams.	124
Figure 4. 19 Histogram of the delay between TCP messages.	124
Figure 4. 20 Calibration of the optical IR sensors	125
Figure 4. 21 Flyport module	126
<b>Figure 4. 22 Network topology</b>	127
Figure 4. 23 Physical topology adapted to the fish farm facility structure	128
Figure 4. 24 System operation	129
Figure 4. 25 Packets per second in different scenarios	130

Figure 4. 26 Packet loss rate in different scenarios	130
Figure 4. 27 Number of retransmitted packets in different scenarios	130
Figure 4. 28 Server appearance showing reception tank information	131
Figure 4. 29 Server appearance showing production tank information	132
Figure 4. 30 Alarm appearance at the smartphone	132
Figure 4. 31 Network topology proposed	134
Figure 4. 32 Architecture of the proposed system	134
Figure 4. 33 Operation algorithm for the water variables and tank variables	135
Figure 4. 34 Operation algorithm for fish behavior algorithm	136
Figure 4. 35 Operation algorithm for feed falling sensor	136
Figure 4. 36 Employed components for sensor to monitor the water quality	137
Figure 4. 37 Employed components for sensor to monitor the tank	138
Figure 4. 38 Detail of the location of feed fallen detector	139
Figure 4. 39 Compatible module with Arduino Mega 2560 connected to WiFi module and MicroSD card reader	140
Figure 4. 40. Data and code of the temperature sensor	141
Figure 4. 41 Data and code of the turbidity sensor	141
Figure 4. 42 Data and code of the oil layer sensor	142
Figure 4. 43 Data and code of the light sensor	142
Figure 4. 44 Data and code of the presence sensor	143
Figure 4. 45 Experiments to demonstrate the operation of fish behavior sensor, preliminary test	144
Figure 4. 46 Average LDR resistance in different point with and without the fish	144
Figure 4. 47 Data gathered by the fish presence sensor	144
Figure 4. 48 Data gathered by the fish presence sensor	145
Figure 4. 49 Fish shoal in tested scenarios	146
Figure 4. 50 Code for presence	146
Figure 4. 51 State of variable fish presence of one sensor in different scenarios	146
Figure 4. 52 Data gathered by the fish presence sensor	146
Figure 4. 53 Data gathered by the feed falling sensor	147
Figure 4. 54 Proposed system for feed supply	149
Figure 4. 55 Control node description	150
Figure 4. 56 Code for obtaining the histograms	151
Figure 4. 57 Red histogram of pictures without feed	152
Figure 4. 58 Red histogram of pictures with feed	152
Figure 4. 59 Green histogram of pictures without feed	152
Figure 4. 60 Green histogram of pictures with feed	152
Figure 4. 61 Blue histogram of pictures without feed	152
Figure 4. 62 Blue histogram of pictures with feed	152
Figure 4. 63 Summation of pixels with brightness values between 0 and 15 in the red histogram	153
Figure 4. 64 Summation of pixels with brightness values between 0 and 15 in the green histogram	153
Figure 4. 65 Summation of pixels with brightness values between 0 and 15 in the blue histogram	153
Figure 4. 66 Gathered Vout values in the calibration test	155
Figure 4. 67 Employed pictures for the verification test	157
Figure 4. 68 Summation of pixels with brightness values between 0 and 15 in the blue histogram in the verification test	157
Figure 4. 69 Box Whiskers graphic of summation of pixels with brightness values between 0 and 15 in calibration and verification test	157
Figure 4. 70 Gathered Vout values in the verification test	158
Figure 4. 71 Box Whiskers graphic of Vout in calibration and verification test	158
Figure 4. 72 Operation algorithm	159
Figure 4. 73 Result of applying the algorithm to the data of a simulated feeding period	160

## Chapter 5:

Figure 5. 1 Evolution of mangrove forests between 1984 and 2010	164
Figure 5. 2 Estuary with a WSN for outflow plume monitoring	167

Figure 5. 3 Network topology for mangrove monitoring.....	167
Figure 5. 4 Conductivity sensor.....	168
Figure 5. 5 Induced voltages at different conductivities.....	169
Figure 5. 6 Calibration results.....	169
Figure 5. 7 Salinity node architecture.....	169
Figure 5. 8 Electronic design of our low-cost salinity sensor.....	169
Figure 5. 9 Socket connection between client and server.....	170
Figure 5. 10 Program code for Flyport configuration as Socket Client.....	171
Figure 5. 11 Flyport IDE during test.....	171
Figure 5. 12 Web interface.....	172
Figure 5. 13 Consumed bandwidth in bits/s.....	172
Figure 5. 14 Multisensor buoy,.....	173
Figure 5. 15 Float of the buoy with the sensors.....	173
Figure 5. 16 FlyPort Module.....	174
Figure 5. 17 Diagram with all connections and the proposed architecture.....	174
Figure 5. 18 NTC for the water temperature sensor.....	175
Figure 5. 19 Electronic circuit of the water temperature sensor.....	175
Figure 5. 20 Programming code to read the analog input from water temperature sensor.....	176
Figure 5. 21 Temperature measured vs. output voltage.....	176
Figure 5. 22 Salinity sensor.....	177
Figure 5. 23 Output voltage of the salinity sensor as a function of the frequency.....	178
Figure 5. 24 Oscilloscope during the tests.....	178
Figure 5. 25 PWM signal and the resulting sine wave.....	178
Figure 5. 26 Electronic design of the low-cost salinity sensor.....	178
Figure 5. 27 Frequency response of our BPF.....	178
Figure 5. 28 Programming code for the PWM signal generation.....	179
Figure 5. 29 Programming code to read the analog input of the salinity sensor.....	179
Figure 5. 30 Water salinity as a function of the output voltage.....	180
Figure 5. 31 Comparison between our measures and the predicted measures.....	180
Figure 5. 32 Schematic of the turbidity sensor.....	181
Figure 5. 33 Calibration results of the turbidity sensor.....	181
Figure 5. 34 Comparison of measures in both equipment.....	182
Figure 5. 35 Sensor for hydrocarbon.....	183
Figure 5. 37 Operation of the sensor.....	183
Figure 5. 38 Test bench with orange light.....	183
Figure 5. 39 Output voltage for the six lights used.....	184
Figure 5. 40 Output voltage as a function of the light.....	184
Figure 5. 41 Sensor to measure the ambient temperature.....	184
Figure 5. 42 Behavior of TC1047 and its equation.....	184
Figure 5. 43 Program code for reading analog input for the ambient temperature sensor.....	185
Figure 5. 44 Test bench of the ambient temperature sensor.....	185
Figure 5. 45 Electrical connections for HIH-4000.....	186
Figure 5. 46 RH in % as a function of the output voltage compensated in temperature.....	186
Figure 5. 47 Relative humidity measured during two months.....	186
Figure 5. 48 Design of our anemometer.....	187
Figure 5. 49 Relationship between the output voltage in DC motor and the rotation speed.....	188
Figure 5. 50 Measures of wind speed in a real environment.....	188
Figure 5. 51 Sensor Hall.....	189
Figure 5. 52 Diagram of operation for the wind direction sensor.....	189
Figure 5. 53 Angle calculation as a function of the sensors Hall values.....	190
Figure 5. 54 Output voltage as a function of the magnetic field.....	190
Figure 5. 55 Output voltage of each sensor as a function the wind direction.....	191
Figure 5. 56 Measures of the wind direction in real environments.....	191
Figure 5. 57 Circuit diagram for the solar radiation sensor.....	192
Figure 5. 58 Circuit used in our test bench.....	192
Figure 5. 59 Program code for the solar radiation sensor.....	192
Figure 5. 60 Output voltage of both LDRs and the average value.....	193

<i>Figure 5. 61 Results of the solar radiation gathered during 2 months in a real environment.....</i>	<i>193</i>
<i>Figure 5. 62 Rainfall sensor and the basic electronic scheme.....</i>	<i>194</i>
<i>Figure 5. 63 Results of Rainfall gathered during 2 months in a real environment. ....</i>	<i>194</i>
<i>Figure 5. 64 Protocol to perform a connection with the buoy, using a VPN.....</i>	<i>196</i>
<i>Figure 5. 65 Screenshot of our Android applications to visualize the data from the sensors. ....</i>	<i>196</i>
<i>Figure 5. 66 Consumed bandwidth.....</i>	<i>197</i>
<i>Figure 5. 67 Designed device .....</i>	<i>198</i>
<i>Figure 5. 68 Top view of the device.....</i>	<i>198</i>
<i>Figure 5. 69 Waspnote and GPS receiver .....</i>	<i>198</i>
<i>Figure 5. 70 Devices initially positioned inside the stain .....</i>	<i>199</i>
<i>Figure 5. 71 Devices positioned to start the displacement.....</i>	<i>199</i>
<i>Figure 5. 72 Devices at the boundary of the pollution.....</i>	<i>199</i>
<i>Figure 5. 73 Algorithm to reach the edge of pollution.....</i>	<i>201</i>
<i>Figure 5. 74 Algorithm for devices placed at the same distance .....</i>	<i>201</i>
<i>Figure 5. 75 Communication protocol to establish the connection between the devices.....</i>	<i>201</i>
<i>Figure 5. 76 Number of Broadcast packets registered for AODV and DSDV protocols.....</i>	<i>203</i>
<i>Figure 5. 77 Number of control packets registered for AODV and DSDV protocols .....</i>	<i>203</i>
<i>Figure 5. 78 Consumed bandwidth for AODV and DSDV protocol.....</i>	<i>203</i>

Chapter 6:

There are not Figures in this chapter



## LIST OF TABLES

### Chapter 1:

There are not Tables in this chapter

### Chapter 2:

<i>Table 2. 1 Summary of the temperature effects on growth. * Represents higher TL. ....</i>	<i>16</i>
<i>Table 2. 2 Summary of the temperature effects on survival. (-) means no available information. ....</i>	<i>18</i>
<i>Table 2. 3 Summary of the salinity on growth. * Not represents highest SGR, it represents FI. ** Represent TL *** Represent BW. N.E. means No Effect. ....</i>	<i>19</i>
<i>Table 2. 4 Summary of the salinity effects on survival on early stages of development (-) means no available information. ....</i>	<i>21</i>
<i>Table 2. 5 Summary of the salinity effects on survival of juvenile fish. N.E. means No Effect.....</i>	<i>22</i>
<i>Table 2. 6 Summary of the photoperiod effects on growth * Not represents higher SGR, represents length. N.E. means No Effect. ....</i>	<i>24</i>
<i>Table 2. 7 Summary of the photoperiod effects on survival. N.E. means No Effect.....</i>	<i>25</i>
<i>Table 2. 8 Summary of the dissolved oxygen effects on growth * Not represents higher SGR, represents TL or **FCR. N.E. means No Effect. ....</i>	<i>26</i>
<i>Table 2. 9 Summary of the oxygen effects on survival. N.E. means No Effect.....</i>	<i>27</i>
<i>Table 2. 10 Commercially available sensors for temperature monitoring.....</i>	<i>38</i>
<i>Table 2. 11 Commercially available sensors for salinity monitoring .....</i>	<i>40</i>
<i>Table 2. 12 Commercially available sensors for oxygen monitoring .....</i>	<i>42</i>
<i>Table 2. 13 Commercially available sensors for turbidity monitoring. ....</i>	<i>43</i>
<i>Table 2. 14 Commercially available sensors for monitoring.....</i>	<i>45</i>

### Chapter 3:

<i>Table 3. 1 Values of voltage and current used to power the solenoid in the first test of DC current and sensor based on Hall sensor .....</i>	<i>64</i>
<i>Table 3. 2 Values of electric conductivity of water samples of the first set of test.....</i>	<i>64</i>
<i>Table 3. 3 Values of frequencies used at 12V .....</i>	<i>64</i>
<i>Table 3. 4 Values of electric conductivity of water samples.....</i>	<i>65</i>
<i>Table 3. 5 Results of the induced current in air .....</i>	<i>65</i>
<i>Table 3. 6 Magnetic field (mT) values at different conductivities and frequencies with 12V (AC) with Solenoid 1 (with the test tube). ....</i>	<i>65</i>
<i>Table 3. 7 Magnetic field (mT) values at different conductivities and frequencies with 12V (AC) using Solenoid 2 (without the test tube.).....</i>	<i>66</i>
<i>Table 3. 8 Magnetic field (mT) values when measuring different conductivities at different DC voltages</i>	<i>66</i>
<i>Table 3. 9 Measures obtained at 20 V of DC .....</i>	<i>67</i>
<i>Table 3. 10 Induced coil voltage at different frequencies when the environment changes .....</i>	<i>68</i>
<i>Table 3. 11 Induced coil voltage at different frequencies when the voltage in the air is fixed at 2.8v.....</i>	<i>68</i>
<i>Table 3. 12 Price of the components for sensor 1 (Hall sensor + solenoid).....</i>	<i>69</i>
<i>Table 3. 13 Price of the components for sensor 2 (two solenoids) .....</i>	<i>69</i>
<i>Table 3. 14 Comparative of prices of different sensors on the market.....</i>	<i>70</i>
<i>Table 3. 15 Models of coils used in tests to compare the different configurations of coils combination (S: Solenoid, T: Toroid).....</i>	<i>72</i>
<i>Table 3. 16 Samples used in tests to compare the different configurations of coils combination.....</i>	<i>72</i>
<i>Table 3. 17 Comparative of best results for four models.....</i>	<i>76</i>
<i>Table 3. 18 Height of water (cm) in the test of minimum cell volume and the output sensor signal (V) ...</i>	<i>78</i>
<i>Table 3. 19 Diameter of the container (cm) in the test of minimum cell volume and the output signal (V) .....</i>	<i>79</i>
<i>Table 3. 20 Characterization of the linear ranges of the sensor Model 4.....</i>	<i>81</i>
<i>Table 3. 21 Output Voltage for unknown samples. ....</i>	<i>81</i>

<i>Table 3. 22 Features of solenoids used in the tests .....</i>	<i>85</i>
<i>Table 3. 23 Summary of frequencies used for each prototype. ....</i>	<i>87</i>
<i>Table 3. 24 Frequency of working for each prototype .....</i>	<i>89</i>
<i>Table 3. 25 Cost comparison of copper in each prototype .....</i>	<i>90</i>
<i>Table 3. 26 Verifying measures and the relative and absolute error.....</i>	<i>93</i>
<i>Table 3. 27 Sensibility of our prototype with the mathematical model (3) at different ranges .....</i>	<i>93</i>
<i>Table 3. 28 Price of the electronic components for the low cost smart turbidimeter.....</i>	<i>95</i>
<i>Table 3. 29 Concentration of gasoline in the samples .....</i>	<i>105</i>

Chapter 4:

<i>Table 4. 1 Comparative between isolated prototypes.....</i>	<i>113</i>
<i>Table 4. 2 Verification of the calibration process .....</i>	<i>126</i>
<i>Table 4. 3. Summary of characteristics of the current system and our proposal .....</i>	<i>147</i>
<i>Table 4. 4 Summary of characteristics of the current system and our proposal .....</i>	<i>148</i>

Chapter 5:

<i>Table 5. 1 Coils Features (I).....</i>	<i>168</i>
<i>Table 5. 2 Coils Features (II).....</i>	<i>177</i>
<i>Table 5. 3 Concentration and Turbidity of the Samples.....</i>	<i>182</i>
<i>Table 5. 4 Results Verifying the Samples .....</i>	<i>182</i>
<i>Table 5. 5 Average value of the output voltage for the best cases .....</i>	<i>183</i>
<i>Table 5. 6 Energy consumption of each node .....</i>	<i>199</i>
<i>Table 5. 7 Simulation Parameters.....</i>	<i>202</i>

Chapter 6:

There are not Tables in this chapter

## **LIST OF ACRONYMS**

Absorption coefficient per unit length  
(A/D) Analog-to-Digital Converter module  
(AC) Alternative current  
(ADV) Acoustic doppler velocimetry  
(ANN) Artificial neural networks  
(AP) Access Point  
(AR) Acoustic recording  
(BN) Box nodes  
(BPF) Band pass filter  
(BSI) Acoustic backscattering intensity  
(BV) Britheness values  
(*Cond.*) Conductivity  
(DARS) Dynamic Ad Hoc Routing Simulator  
(DB) Database  
(DC) Direct current  
(DIDSON) Dual-frequency Identification Sonar  
(DO) Dissolved oxygen  
(EC) Electric conductivity  
(EO) Earth Observation  
(EQS) Environmental Quality Standards  
(FCE) Feed Conversion Efficiency  
(*FE<sub>x</sub>*) Feed falling sensor  
(FF) Flip-Flop  
(FI) Feed Intake  
(*FI<sub>x</sub>*) Fish behavior sensors  
(FL) Fuzzy logic  
(FLI) Fish Learning Index  
(GPS) Global Position System  
(GSM) Global System for Mobile communications  
(HPF) High-pass filter  
(ICSP) In-Circuit Serial Programming  
(ICT) Information and Communication Technologies  
(IMV) Indicator of MV  
(INDC) Induced coil  
(*I<sub>o</sub>*) Light intensity of a source  
(IoT) Internet of Things  
(IR) Infrared  
(*I<sub>t</sub>*) Transmitted light  
(*l*) Length of the light pass  
(L:D) Hours of light : Hours of dark  
(LDO) Luminescent Dissolved Oxygen  
(LDR) Light Dependent Resistor  
(LED) Light-emitting diode  
(LOD) Limits of detection  
(LPF) Low pass filters  
(MUX) Multiplexer  
(MV) Shoal mean velocity  
(*n*) Refractive index

(NI) No information  
(NTC) Negative temperature coefficient  
(NTU) Nephelometric Turbidity Unit  
(ORP) Oxidation Reduction Potential  
(POWC) Powered coil  
(PRT) Platinum resistance thermometers  
(PSU) Practical units of salinity  
(PTC) Positive temperature coefficient  
(*r*) Particle size  
(RF) Radio Frequency  
(RH) Relative humidity  
(RI) Region of interest  
(*Rir*) Resistance of the IR photodiode  
(RMP) Recognized Maritime Picture  
(ROV) Operated underwater vehicle  
(RTD) Resistance temperature device  
(S) Solenoid  
(SEV) Satellite-Extended- Vessel Traffic Service  
(SL) Salinity sensors  
(SpCond) Specific conductance  
(SS) Suspended sediments  
(SVM) Support Vector Machine  
(T) Torodid  
(*t*) Turbidity  
(TDS) Total dissolved solids  
(*TH<sub>x</sub>*) Thresholds for each variable  
(TIG) Turbidity of *Isochrysis galbana*  
(TL) Level sensors  
(TL) Total Length  
(TS) Turbidity of sediment  
(TTC) Turbidity of *Tetraselmis chuii*  
(*T<sub>v</sub>*) Reference value for each tank variables  
(TWi) Tanks rows  
(UV) Ultraviolet light  
(UWSN) Underwater wireless sensor networks  
(Vout) Voltage Output  
(VPN) Virtual private network  
(Vpp) Peak to peak voltage  
(WFD) Water Framework Directive  
(WLAN) Wireless Local Area Network  
(WSN) Wireless sensor networks  
(*W<sub>v</sub>*) Reference value for each water variables  
( $\theta$ ) Scatter angle  
( $\lambda$ ) Wavelength



# **1. INTRODUCTION**

## **1.1. Introduction and motivation**

### **1.1.1. The aquaculture and its sustainability**

Due to the increase in human population all around the world, there is a higher demand to increase food production. Data provided by United Nations point out that the population will increase up to 9.7 billion by 2050 and about 11.2 billion by 2100 (UN, 2015). It is important to plan how to provide food quality in safe and sustainable conditions. According to FAO (2014) statistics, the aquaculture production is growing while fish captures are stabilized. It demonstrates that aquaculture is the only future option to provide fish for consumption to the world population.

Furthermore, while in all around the world the aquaculture is growing, in European Union and especially in Spain, the aquaculture production has been stabilized. In the last decade, the aquaculture growth around 6.4% annually and only 1.2% in the European Union. This evidences the existence of several limitations for the development of the aquaculture in the European Union (APROMAR, 2017)

Aquaculture is a promising option to offer sustainable fish meet, and it will allow to considerably increase the fish consumption by 2050 (Merino et al., 2012). It can be implemented under different conditions. Some facilities are deployed in the sea, while other facilities are placed inland. In inland facilities, fish are kept in tanks that can vary in size and materials. In facilities that perform intensive aquaculture, many efforts are taken in order to maximize the performance of the fish. The fish performance depends on different factors: environmental factors (Rubio et al., 2005), production factors (Adewolu et al., 2008), and biotic factors (Kestemont et al., 2003). In the facilities, it is possible to control some of those factors. Halogen lights are used over each tank to provide illumination to the tanks. With light, it is possible to change the photoperiod and modify the behavior of the fish in order to enhance their performance (Biswas et al., 2008). Moreover, filters can be used at the water entrance to eliminate the turbidity. Thus, the negative effects of turbidity are reduced improving the fish performance (Ardjosoediro & Ramnarine, 2002). Other factors as water temperature or water conductivity are not usually modified, although it is possible to modify them. Water temperature and conductivity can change the feeding needs of fish kept in the tanks (Rubio et al., 2005). Moreover, if fish are stressed their feeding consumption falls and the performance decrease. Many factors can cause stress on fish.

Countries with the highest marine fish aquaculture production are Norway, China, Chile, and Indonesia. Despite the possibilities of aquaculture, its fast and uncontrolled growth is producing some negative environmental impacts (Buschmann et al., 2009). Once the aquaculture has demonstrated that can cover the fish meet demand, its next step is to reach the sustainability. So that, it needs to integrate and minimize the environmental costs of its production. In order to have a sustainable aquaculture, its impacts must be reduced. These impacts include habitat destruction, water pollution due to aquaculture wastes, the need of fish meal and fish oil for feed production, among others (Primavera, 2006). The use of new technologies can help to minimize these impacts. The accumulation of organic matter in the sea floor is one of the big deals to reach the sustainability. This organic matter comes from the uneaten food and the fish dregs (Borja, 2011). Moreover, the mineralization of organic matter will produce other changes in the environment. The changes can include variation in water coloration and an increase of organic matter, derived from phytoplankton, deposition (Yoshikawa et al., 2012). There are several options to solve the aforementioned problems such as perform cleaning actions in the sediments. Nevertheless, the solutions are expensive solutions. Considering that the environmental problems rarely affect the fish production, the companies do not take care of the cleaning tasks. The adjustment of the feed supplied to the fish cages may be other solution that benefits to the environment and to the companies. Thus, no feed will sediment to the seafloor. Moreover, for the companies will suppose an economic saving because all the supplied feed is used for the growth of fish (Garcia et al. 2011). Different

manners to feed the fish in the fish farms are available, each one presents the different percentage of uneaten feed. However, some of them are only used for experimentation. In fish farms, the fish are fed to satiety this is the most employed feeding strategy. Although certain parameters are considered, the workers feed the fish until they perceive that the fish are not eating. The considered parameters are the feeding rate depending on the fish weight and the water temperature. However, this feeding strategy has a loss of feed of 8% (Garcia et al. 2011). These feed falls to the sea floor causing the problems described in the previous paragraphs.

### 1.1.2. Open issues when monitoring the aquaculture

Other activities, such as agriculture or mammal and bird farming, have reduced their impacts using technology to monitoring their activity. These techniques are englobed on the concept of precision agriculture or precision farming. There are several examples of those applications on agriculture (Primicerio et al., 2012), (Garcia-Sanchez et al., 2011) and (Lloret et al., 2011a) and on farming (Martinelli et al., 2009), (Nadimi et al., 2008). (Sendra et al., 2013a). Those techniques have also been planned for aquaculture (Lloret et al., 2011b), (Kai et al., 2012) and (Costa et al., 2009). However, it is not yet clear which parameters must be monitored. Although some proposals for precision aquaculture have been published, few real implementations can be found

Besides reducing the potential impacts, monitoring fish and water parameters have other positive impacts. In aquaculture, fish are maintained in cages or tanks and fed. Huge efforts had been made to obtain better feeds and to minimize their dependence on fish products for feed (Amaya et al., 2007), (Robinson K. et al., 2008) and (Hernández et al., 2007). Nevertheless, other factors affect to fish growth and survival, see Figure. 1.1. The monitoring of abiotic parameters and the adaptation of production techniques are crucial for aquaculture sustainability. However, there is no consensus on what parameters should be monitored. Factors such as temperature, salinity or photoperiod are critical for fish and many authors have studied their effects. But other parameters such as light intensity, dissolved oxygen, turbidity, and others can alter the well-being of the fish. When those environmental parameters do not have the optimal value, several effects appear, such as changes in growth, survival, natatorium behavior, immunity response or reproductive success ratio among others.

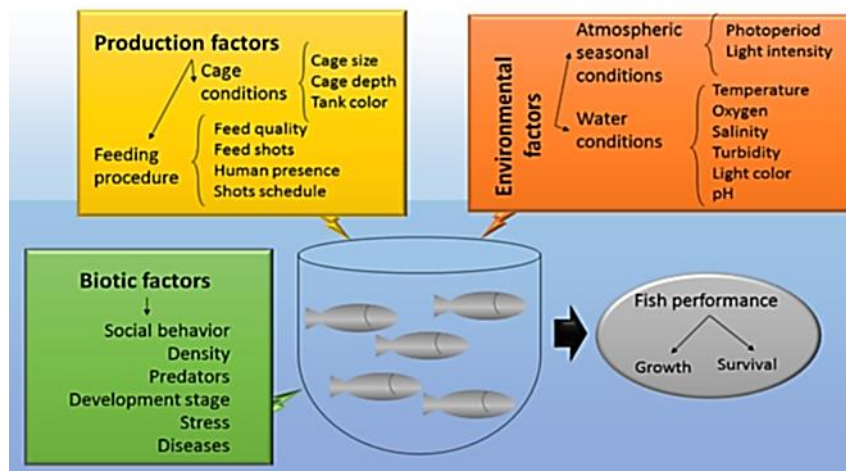


**Figure 1. 1** Factors that affect the fish performance in aquaculture facilities

There are two main different types of aquaculture facilities for fish production according to their emplacement, the marine, and the inland. The marine facilities are exposed to natural water changes. In those facilities, there are juvenile fish with high survival rate and their growth is affected by the changes in the environmental parameters. Some parameters change according to



annual cycles such as the temperature of photoperiod. While other parameters change randomly, due to current changes or sporadic pollutants, which cause changes in pH, turbidity and light intensity or color. In marine facilities, it is not possible to control the water parameters, but it is possible to adapt their actions to the environmental parameters in real time (for example changing the amount of dispensed feed or changing the feeding time).

On the other hand, in the inland facilities, the water is taken from the sea or from the river, depending on the fish species, and the water is led by pipes to the tanks. The inland facilities may operate in open or closed systems according to the use of water recirculation. The ones with open systems have no control of water conditions; however, they can isolate the fish during a short period of time by closing input/output water pipes. This can prevent possible damages when there is a pollutant in the river or sea. Nevertheless, keeping fish in those conditions can cause other problems related to dissolved oxygen or nitrogenous compounds. The inland facilities with closed systems have higher control of water conditions. They can have a heater or cooler devices to change the water temperature, filters to reduce turbidity and oxygen injectors to increase oxygen concentration among others systems. Those facilities can have high benefits when they use sensors to monitor the water parameters. They can monitor the water parameters to modify them or to adapt their actions accordingly. In inland facilities, the most sensitive fish stages are cultivated reproducers, eggs, and larvae are maintained carefully. In the larval stage, the critical factor is the survival.

The water monitoring thus can have two different objectives, adapt the actions to the conditions in real time or modify them. Some examples of adaption actions are the following: (I) reduce/increase the amount of feed, (II) close/open the water input pipe. Moreover, the facilities with closed circuit may use the water parameters monitoring with the purpose of changing those parameters to the optimal values. These are some examples: (I) increase/reduce the water temperature with heat exchangers, (II) increase/reduce the salinity with other water supplies, (III) modify the watercolour by using different algae concentration, (IV) modify the turbidity by the activation of filters or (V) close/open the air injectors.

When the feed needs are adapted to the water conditions, many benefits can be obtained. They are exposed in Figure 1.2. These benefits are linked to the environment, which let the industry obtain a more sustainable activity and reduces operating costs. It also impacts on the wellbeing of the fish.

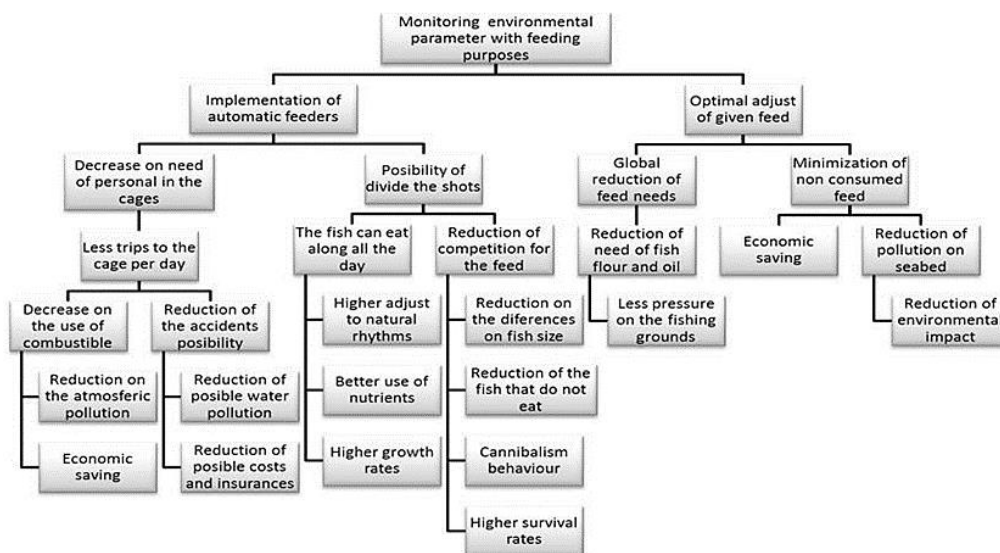


Figure 1. 2 Main benefits of monitoring environmental parameters when feeding

### 1.1.3. The information and communication technologies and the WSN

In recent years, the development of different Information and Communication Technologies (ICT) in conjunction with the creation of low-cost small sensors have made possible to monitor many processes. Wireless sensor networks (WSN) are a clear example as they are often used for farming purposes. WSNs are composed of small devices (nodes) that are able to sense data from the environment. The nodes have the capability to communicate between them. To collect data from the natural environments, these nodes should be sensors able to detect changes in physical and chemical magnitudes generated by events in the medium.

WSNs research works have increased hugely in recent years due to the many types of applications (Bri et al.2009), (Bri et al., 2010). WSNs are composed of sensors, that sense data from the environment; nodes, that receive the sensed data and process them. Due to their low memory and limited battery (Mohsin et al., 2012), nodes cannot store a lot of data, so they must send it. As WSNs can be composed by hundreds of nodes they need to self-organize based on different network architectures and use protocols to communicate. These protocols should have into consideration several aspects such as the energy constrains (Wang et a., 2014), security in data transmission and have to be tolerant to network failures (Xing et al., 2014) in order to maintain a correct network performance.

Sensor nodes are mainly composed of 4 different modules (Fereydooni et al., 2015). First, the sensing module, which performs the data acquisition, can be composed of one or more sensors that sense one or more environmental parameters and the sensing processing module. The central processing unit performs the processing and storage operations with the received data. The wireless transceiver module is in charge of the wireless communications and can use different wireless technology as radio frequency, Wi-Fi, ZigBee. Finally, the power supply module, which should provide a continuous and stable power to the rest of modules, is composed of batteries and a power management system. It is recommendable to have some energy harvesting system and implement some energy saving strategies (Anastasi et al., 2009).

Nowadays there are many researches focused on WSNs. A WSN consists of a set of devices wirelessly connected which are able to obtain information from the environment. Most of these devices usually present low processing capacity and reduced memory. Developers always try to design devices with very low power consumption. In order to gather information from the environment, these devices need sensors capable of detecting chemical or physical magnitudes from the environment and transform them into electric variables (Garcia et al., 2010). The most common physical variables that are often measured are relative humidity, temperature, conductivity, vibration, among others. From the point of view of the WSNs, it is common to include power saving techniques in order to improve the energy consumption efficiency (Compte et al., 2011).

The use of WSNs offers lots of advantages. With them, it is easier taking data with specific data gathering systems (Meghanathan & Mumford, 2013) from extreme environments like volcanoes or deep oceans. They can bring real-time data from a remote place which is being monitored and inform the users on possible problems and events through different technologies. WSNs are able to give data in intervals defined by the users as a function of the type of the monitored environment and device accuracy. In addition, WSNs facilitates the process of taking measures because the data can be obtained without the need of taking in-situ samples and send them to a laboratory. Finally, one of the main problems of the sensors is the continuous need for calibration. The WSN and UWSN are composed by (I) the sensing module, (II) the central processing unit, (III) the transceiver module and (IV) the battery unit (Fereydooni et al., 2015). To use UWSN for underwater monitoring, a special transceiver module is necessary (Sendra et al, 2015a). The fact of having multiple devices distributed along an area, communicating each other and sending information about the physicochemical parameters is very attractive for several environments. However, we should consider the drawbacks these mediums present, especially in underwater environments where the dispersive character of water worsen the data transmission (Das & Thampi, 2017). Using those WSN, there is no need of going continuously to the place understudy to take samples in order to analyze them at the laboratory. Comparing

with traditional sampling and analysis procedure in the chemical laboratory, WSNs offer several advantages. Besides the aforementioned displacements, the consumption of chemical reagents (which can be expensive and pollutant) and the destruction of the sample (precluding a repetition of the analysis) are some advantages. Other advantages are related to the real-time monitoring and the possibility of taking intelligent decisions (Mamoune et al., 2015). Using WSN there is no need to wait till the sample is carried to the laboratory in order to perform the analysis. For these reasons, the use of WSN is dramatically increasing. Moreover, sensing modules adapted to the underwater environment and requiring low maintenance are needed (Sendra et al., 2015b). For these reasons, the best option for sensing modules is physical sensors which, compared with chemical or biochemical sensors, require low maintenance. In particular, they do not need continuous calibration or partial replacement over time (as in the case of membranes or electrolytes). Therefore, physical sensors are most suitable for UWSN. Water quality has to be monitored continuously in aquaculture to ensure good management of the daily activity. The data gathered from the water quality facilitates to take different actions in order to prevent damages or to adapt the feeding process. However, the technology needed for it is still in development or is expensive.

WSNs have been used for monitoring the three vigor (Kameoka et al., 2017), greenhouses (Wang et al., 2016) and citrus crops (Sawant et al., 2007). Moreover, WSNs are employed to monitor the state of farm animals such as goats (Nadimi et al., 2011) or cows (Handcock et al., 2009). Even some systems have been proposed for monitoring fish farms, they will be analyzed individually in the related work section. The majority of them are based on monitoring water quality including just a couple of water parameters to be monitored. Moreover, they usually employ commercial probes. The commercial probes for underwater monitoring have a high cost. Thus, if a WSN were to be utilized to monitor several parameters using commercial probes in all the production tanks, the cost of the system would be unaffordable for the fish farms. Moreover, other authors propose systems for monitoring fish behavior, in the related work section, we will analyze each proposal. Therefore, if we aspire to measure different parameters in fish farms facilities with WSN, it is crucial to reduce the cost of the sensors and include a wider variety of parameters in the same system.

The main issue in applying these technologies to precision aquaculture is the different environment where the underwater wireless sensor networks (UWSN) and the remotely operated underwater vehicle (ROV) would have to be deployed. On the one hand, wireless communication between underwater devices is complicated, especially in the case of high bandwidth and long distances (Sendra et al., 2015a). On the other hand, the need for a waterproof isolation for the sensors to ensure long-term monitoring hinders the manufacturing of underwater sensors.

The majority of applications are implemented on land. But these nodes could be deployed in a changing medium and in that case we would need to locate the sensors (Chowdhury et al., 2016), (Elkin et al. 2017). Even that the majority of WSNs are developed for terrestrial applications, the marine applications are becoming an important area. The  $\frac{3}{4}$  of our planet is covered by water. The human impact in oceans is becoming more and more evident. The need for continuous monitoring of underwater environments can be covered by using WSNs. Terrestrial and underwater WSNs have some differences. The environment in underwater WSNs is more aggressive than in terrestrial WSNs, so the deployed devices will require major protection: water isolation to avoid corrosion and biofouling. Because of the waves from tidal and ships can produce movements in the WSNs, the system must be prepared to assume these movements and changes of locations from its initial deployment. Generally, underwater WSNs are used to cover higher areas than terrestrial WSNs (Nguyen et al., 2012), the energy consumption will be higher and the signals are attenuated in the underwater environments. So, it is important to implement energy-efficient techniques in data processing (Liu et al., 2015), (Jain et al., 2015) and energy harvesting solutions (Zhou et al., 2014) to prolong the network lifetime (Legakis et al., 2015) and network stability. The price of devices used in underwater WSNs is

usually higher than in terrestrial WSNs. In addition, sensor nodes in underwater WSNs are placed in a specific place along the water column, so flotation and mooring devices are needed (Albaladejo et al., 2010). Finally, the wireless communication technology in terrestrial WSNs use different radio frequencies, however in underwater WSNs the water produces an important attenuation on radio frequencies, so there are many deployments using other technologies such as sound or light (Dong, 2009).

Underwater sensors can be placed at the bottom, at the surface or at different points along the water column. The sensed parameters can change depending on the point where the sensors are placed and the objective of the WSN. For example, in environments without light, there is no need to measure Chlorophyll and in environments far from human impact, there is no need to measure the presence of hydrocarbons. Table I shows the main parameters that can be sensed as a function of the place where sensor nodes are placed in the water column. Although there is a large list of parameters, the most common ones are Temperature, pH, turbidity and Dissolved Oxygen (Albaladejo et al., 2010).

According to (Xu et al., 2014), underwater WSNs are mainly applied to general ocean sensing and monitoring, water quality monitoring, fish farms monitoring, coral reef monitoring and marine shellfish monitoring (See Figure 1.3.). However, the theoretical applications are wider (Gkikopouli et al., 2012), (Akyildiz et al., 2005). We can highlight the ocean sampling networks, environmental monitoring, disaster prevention, assisted navigation, mine reconnaissance, military purposes or undersea explorations, but there are very few works published showing real deployments. The nodes and sensors for underwater WSN must be waterproof, robust and have low energy recruitments or energy harvesting techniques. Those specifications usually increase the cost of the sensors and sensor nodes, thus increasing the investment of the fish farms.

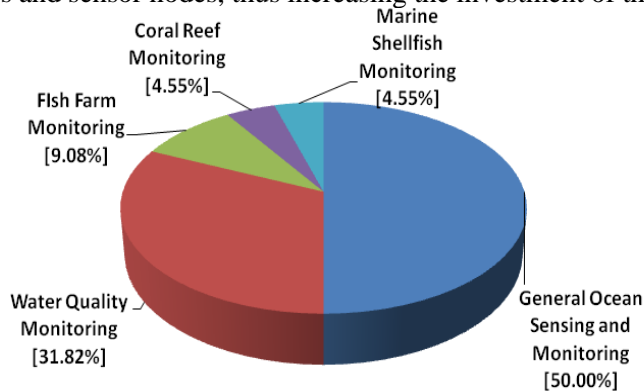


**Figure 1. 3** Main applications of underwater WSNs.

According to (Albaladejo et al., 2010), underwater WSNs are mainly developed in Europe (26 references), North America (19 references), China (21 references) and Australia (12 references). The main topologies used for this purpose are star topology and topologies partially connected (Albaladejo et al., 2010). There are a huge variety of protocols specifics for underwater environments such as VBF, HH-VBF, and FBR. Each one of them has benefits and drawbacks. It has no sense to select one of them as a function of our scenarios (Ayaz et al., 2011).

The main challenges for underwater WSNs are (Dong et al., 2009) (FAIMMS, 2014):

- Sensors protection to avoid corrosion, biofouling and ensure the isolation of the water.
- Advanced buoy design with low cost, waterproof and strong stability. It should also have an energy harvesting system and a mooring system.
- Energy harvesting system design. There are several renewable power sources that can be used in the ocean like seawater generator, tidal power or wind energy.
- System stability and reliability.
- Distributed localization and time synchronization. Continuous changes in sensors can affect the precision of location and the time of data is crucial for good analysis.

At this moment, with the current economic situation of the fish farms companies is not feasible to implement WSN for aquaculture monitoring if we do not offer low-cost solutions.

Lloret et al. (2015) described one example of WSN for this purpose. The number of needed sensors estimated was between 68 and 200 for a group of 6 cages. Thus, the first step to achieve a truly precision aquaculture is the creation of a low-cost WSN. Once we have low-cost sensors available we need to show its operation in laboratory conditions and in production tanks. Then, the fish farm companies can see the benefits of implementing WSN. The companies need to be sure of the cost-effectiveness of this inversion. Thus, we need to show up the recovery of the capital invested in terms of feed saving, considering the price of uneaten feed and the price of the WSN.

## 1.2. Research goals

In this subsection, we present the objectives and the work plan to reach our goal, to design, develop and deploy a WSN able to monitor the water quality and fish behavior in fish farms and other natural environments. First, the objectives are described as simple goals that have been accomplished.

- Selecting the environmental parameters that may affect the fish performance including fish growth, survival, and natatorium behavior.
  - Studying and reviewing the main literature about the effects of environmental variable on fish growth, survival and natatorium behavior
  - Choosing the parameters that should be monitored in our developed system
  - Differentiating between water parameters and environmental parameters
- Designing and developing physical sensors with low-cost capable to measure the selected parameters in an underwater environment.
  - Studying and reviewing the current technologies for monitoring each one of the selected underwater parameters.
  - Choosing the best available technology for sensing each underwater parameter.
  - Describing the current challenges and future trends in the field of the underwater physical sensors
- Creating the physical part of the required sensors for monitoring the water parameters and environmental parameters.
  - Calibrate the developed sensors
  - Performing the laboratory assays to calibrate each sensor considering the working range needed in the aquaculture facilities.
  - Obtain the mathematical equations that model the performance of each sensor.
  - Employing these equations for programming the node.
  - Verify the calibration performed with new data in aquaculture tanks and or aquariums
- Selecting the best location for each calibrated sensor in order to gather the data optimally.
  - Evaluating the changes in each environmental parameter along fish farm facilities.
  - Defining the location of each sensor in the tank
- Creating smart algorithms to automate processes in the fish farms to enhance the fish well-being and the environmental sustainability.
  - Considering the use of emergency turn off systems for the nodes located underwater
  - Considering the possible turning on/off actuators in the fish farm facilities
  - Considering the need for alarm messages and its receivers.
- Gather data from the physicochemical parameters and from the fish behavior.

- Deploying the sensors in aquariums to gather data from water quality producing changes in the water and environment parameters.
- Deploy the sensors in aquaculture tanks to gather data from fish swimming behavior and feeding behavior

Besides of these objectives, there are other secondary goals related to the environmental sustainability and fish wellbeing in the fish farms. The first one is the reduction of cost in fish farms due to the adjustment of feeding process thanks to the use of sensors. Moreover, the use of sensors and alarms will allow the appearance of precision aquaculture that considers the involved parameters. In addition, we pretend to use the lessons learned and the developed sensors for monitoring water quality in other natural environments.

### 1.3. Precedents

The idea to create a WSN for aquaculture monitoring is not entirely a new issue. We can find several examples in the literature, which will be analyzed in the related work section. Nevertheless, the conjunction of low-cost sensors, the possibility of monitoring water quality and fish behavior and the application of smart algorithms is not found in the literature. The conjunction of these three factors in the same proposal is very interesting and novelty.

The starting point of this PhD Thesis was my Master's Tesis where we propose the use of low-cost sensors for conductivity monitoring and the published papers of one of my PhD directors (Mauri & Mauri, 2007), (Lloret et al., 2011) and (Garcia et al., 2011). In these publications, the research group proposes a monitoring and control sensor system for fish feeding in marine fish farms. However, they were not able to deploy the system due to several issues. The main one was the high cost of each sensor for water quality and feed falling monitoring. Thus, the need for a low-cost system was detected. Without low-cost sensors, it was not possible to design in detail a WSN for aquaculture monitoring. Furthermore, a thesis from a college has shown the impacts of the aquaculture facilities on the sea floor and its recovery after the cessation of activity (Higón, 2014).

The idea of creating our own low-cost sensors was born from the thesis of one college in the research group (Compte, 2013). In her thesis, she had to develop some low-cost sensors based on simple electronic components. Basing on this idea and the recent need for low-cost underwater sensors this thesis was started.

The designed sensors in this thesis are used to control and monitor processes in fish farms in order to achieve the sustainability in the feeding procedure and ensure the fish wellbeing. Moreover, the possibility to have low-cost sensors opens new research lines where the sensors can be applied for other purposes as monitor water quality in groundwater, estuaries or open sea.

This thesis was partially supported by the following projects and grants:

- Project “Desarrollo de sensores subacuáticos para la monitorización del comportamiento de los peces con el objetivo de mejorar la productividad y sostenibilidad en una granja marina”. “UPV. Vicerrectorado de Investigación Desarrollo e Innovación”. 16/12/2012 – 15/12/2013. IP: Jaime Lloret Mauri (UPV).
- Project “Red Cognitiva Basada en Grupos de Sensores Colaborativos para el Sensado y Monitorización del Entorno Acuático”, “Ministerio de Ciencia y Tecnología”. TEC2011-27516. 01/01/2012 – 31/12/2014. IP: Jaime Lloret Mauri (UPV).
- Grant “Ayuda para la contratación de personal investigador en formación de carácter predoctoral” by the “Conselleria de Educación, Investigación, Cultura y Deporte”, Reference ACIF/2014/245.
- Grant “Ayudas para contratos predoctorales de Formación del Profesorado Universitario FPU (Convocatoria 2014)” by the “Ministerio de Educación, Cultura y Deporte”, Reference FPU14/02953.

Once we start to develop low-cost sensors for fish farms we discovered the opportunities of applying these systems in other environments such as groundwater, estuaries or marine protected areas.

Finally, to make the proposed system useful in fish farms we considered the energy issues. Thus, we developed several algorithms that allows deciding if the node has to send or save the gathered data in order to save energy to increase the network lifetime.

There are several works related to this thesis, but all of them have been used to research new concepts about water quality and fish behavior monitoring. For this reason, these works will be referenced in their corresponding chapters in order to introduce ideas or solution in each chapter.

## **1.4. Contributions**

In this section, we are going to show a summary of every contribution performed on behalf this dissertation. The contributions of this thesis are linked to the aforementioned goals. They are the following ones:

1. Collect all the knowledge about the effects (growth, survival or changes on behavior) caused by the environmental parameters, published in the last years. We select those effects because growth is the most important factor in the juvenile fish, while survival is critical for larvae stages. The natatorium behavior in relation to water parameters is important for further research, mainly when researchers relate the fish behavior with fish needs (feeding among other). The parameters included in our work are temperature, salinity, photoperiod, dissolved oxygen, turbidity, light (intensity and color) and pH. Those are the main environmental parameters that appear in research papers related to the studied effects.
2. Summarise the different available physical sensors for water quality monitoring to promote precision aquaculture. Physical sensors proposed in papers, patents and also commercial products are included. In addition, we discuss the challenges of using physical sensors and UWSN, which encompass the improvement of underwater wireless communication, the inclusion of energy harvesting and the adoption of energy-efficient protocols. In terms of the sensors, we focus on the challenges related to the reduction of costs and long-term operations.
3. Show up the opportunities of conductivity monitoring employing inductive sensors based on generated and induced magnetic fields. For this purpose, different combinations are evaluated. First, the opportunity of using a sensor hall for detecting the magnetic fields are studied. Then, the combination of powered and induced copper coils are widely studied. Several combinations of toroids and solenoids with different structures are tested in order to select the best combination. Our main goal is to check what combination of coils offers the best results and sensitive. We will also extract the best working frequency and the relation between conductivity and the output signal of our models. The best combination, two solenoids, are evaluated changing its characteristics such as the number of spires of the powered coil, number of spires of the induced coil, the diameter of coils and diameter of the copper wire. For this purpose, we prepare some laboratory samples with different values of conductivity. As well we obtain the minimum volume of water needed to cover all the generated magnetic field.
4. Present the design and development of a low-cost hydrocarbon/oil sensor. The sensor is based on the photoluminescence effect linked to the hydrocarbons. We use light-emitting diodes (LEDs) with different wavelength as a light source and a photoreceptor as a light detector. The sensor will be able to detect the presence of a fine layer of hydrocarbon/oil on the water. With our sensor it is not possible to determine the amount of hydrocarbon/oil.

5. Design and develop a low-cost smart turbidimeter. The smart turbidity sensor will be able to distinguish phytoplanktonic turbidity from sedimentary turbidity. This new turbidimeter is based on optical methods. Different LEDs with different wavelength (i) infrared (IR), (ii) green, (iii) yellow, and (iv) red are used to emit a light source. Two light detectors are used, a light dependent resistance (LDR) to detect visible light (180°) and photodiodes for detecting infrared light. These LEDs are powered by a voltage of 4.5V. The proposed sensor offers two improvements compared to existing commercial sensors: (i) the low-cost of the sensor and (ii) its capability to differentiate sedimentary turbidity from phytoplanktonic turbidity. This sensor will help us to control sensitive areas and monitor fish farms. Moreover, it can be used in other activities or environments where a bloom of algae can be produced or the turbidity has to be controlled.
6. The aim of this dissertation is to design and deploy a low-cost WSN to monitor fish feeding process and water quality in aquaculture tanks. The system is composed by sensors that measure different parameters of the water quality (such as temperature, turbidity or conductivity, among others), of the tank conditions (such as illumination and water level), and of the fish feeding behavior (such as swimming depth and velocity and fallen pellets). Moreover, the system has other sensors, such as the humidity sensor, that actuates as an emergency turn-off system to prevent damages caused by water in the node and other electronic circuits. In addition, presence sensors are placed in each tank to control the possible effects in the fish behavior of the passage of the workers near the tanks. A total of three nodes control the different parameters in each tank. The nodes are wirelessly connected to an Access Point (AP) that sends the data to a server. The data is available on the local area network and on the internet. Besides, the system is able to send alarm messages to different workers if abnormal situations are detected.
7. Design and deployment of a smart system for data gathering in estuaries using WSNs. The system is based on a WSN that monitors the outflow plume of a river and send data gathered to a server. Each node has a conductivity sensor, which are deployed to monitor the advance direction of the outflow plume. The server saves the data in a database (DB). All developed parts, both wireless communication and a conductivity sensor, are tested with real samples in real scenarios.
8. Present a specific conductivity sensor for groundwater monitoring. The sensor is based on solenoid coils and covers all the requirements for groundwater environments. It can be easily isolated from the environment with different materials. It does not need periodic calibration and has low energy consumption, so it can be left in groundwater for long-term monitoring. The operational range of the sensor fits perfectly with groundwater monitoring requirements. The sensor is robust and easy to clean (if necessary).
9. Propose a smart system based on a mobile WSN, where sensor nodes detect, track and locate pollution stains. Nodes are small ships provided with a solar panel to power the system, which is placed inside the polluted area and move till the boundary of the polluted area by using intelligent algorithms. After some time all sensor nodes will be delimiting the pollution stain.
10. Design of an oceanographic multisensor buoy for ocean monitoring in the Mediterranean Sea. The system is based on 2 set of low-cost sensors that are able to collect data from the water, such as salinity, temperature or turbidity and from the weather, such as temperature, relative humidity or rainfall among others. The system is held in a buoy which maintains the system isolated from the water to avoid possible problems of oxidation. The data gathered by all sensors are processed using a microcontroller. Finally, the buoy is connected with the base station through a wireless



connection using a FlyPort module. The whole system and the individual sensors have been tested in a controlled environment. This proposal could be used for monitoring other areas with special ecological interest and for monitoring and supervise several aquaculture activities.

## **1.5. Structure**

Considering the need for monitoring the aquaculture activity to reach the sustainability and to ensure the fish wellbeing, the rest of the dissertation is structured as follows:

Chapter 2 presents the state of the art of the topics included in this dissertation. First, the knowledge about the effects of environmental parameters in fish growth, survival and natatorium behavior is shown. We need to review the literature to define the parameters that must be monitored by our WSN. Moreover, we present a survey on the current technologies for water quality monitoring, focused on the selected parameters. In order to perform an exhaustive review of the current technologies, papers, patents and commercial devices have been studied. Finally, the available solutions for aquaculture monitoring presented in papers are shown and the gap in the current solutions is identified.

Chapter 3 shows the designed and developed sensors based on simple electronic components. According to the conclusions of Chapter 2 we develop the following low-cost sensors. First, we show the design of the conductivity sensor. Our low-cost conductivity sensor is based on the inductive method in which two coils are used to measure the conductivity of a liquid. The designed device is completely new and different compared with the current devices. We show the different combinations of coils tested in order to select the best conductivity sensor. Next, the design of a turbidity sensor is presented. As a novelty, our sensor is capable to differentiate between turbidity sources (phytoplankton or turbidity). The calibration in the laboratory and its verification are presented. Finally, Chapter 3 describes a sensor capable to detect the presence of hydrocarbon or oil layer over the water surface.

Following, Chapter 4 presents the partials deployment of the presented sensors in Chapter 3. All the deployments are proposed for inland fish farms because in this case, we can combine the sensors and actuators. In sea fish farms we only can deploy the sensors. For this reason, our proposed deployments are in inland fish farms where fish are kept in tanks. Here we showed the implementations in different scenarios. The first scenario shows the chance of having two water sources for the same fish farms. Thus we can adjust the water quality in the fish farms according to the water quality of each source. The parameter monitored, in this case, is the conductivity of the water and the water level in the tanks. The second shown scenario is based on control the water temperature and water turbidity. It has a control system capable to isolate some tanks if the value of turbidity in the reception tank reaches a preset value. Moreover, in this scenario humidity sensors were included in the nodes in order to have an emergency shutdown system to prevent further damages if water enters into the box. In addition, we evaluate the efficiency of the deployed system in terms of network performance. Thus, we can decide how many nodes we can use with a single AP. When we are planning the WSN we need to plan where to establish the AP and the number of AP needed. In the third, we show the new deployment in fish farms with the learned lessons from Chapter 4. The main detected problem is the need to reduce the data exchange between the nodes and AP. If we pretend to add more sensors and more nodes in each cage it is not feasible to need 1 AP every 5 nodes. In the deployment shown in Chapter 5, we propose to have 3 nodes in each tank and up to 10 sensors per tank. In this Chapter, we show the development of the fish behavior and feed falling sensors. Moreover, we include in this deployment temperature sensor, presence sensor and light sensor among others. The objective is to monitor the water quality, the cage environment, and the fish behavior. Thus, we can improve the feeding process and detect fish stress, changes in fish swimming velocity or depth, in order to relate this event to the water quality. Moreover, we present a smart algorithm to minimize the amount of data exchanged between the node and the AP with the purpose of reducing the number of needed APs. In addition, this smart algorithm

will reduce the energy waste increasing the network lifetime. The last case shows an automatic adjustment of feed supply velocity. We propose to increase the efficiency of the feeding system using two different sensors. The first one is a sensor which is able to monitor the mean fish depth velocity. The second employed sensor is able to detect the feed falling. Combining these data it is possible to adjust the feed supply velocity.

Chapter 6 presents the application of those systems in other natural protected environments where we detect that the use of sensors to control water quality may be useful. The first example is the use of conductivity sensors to monitor the estuaries. In the estuaries, there is an equilibrium between the freshwater from the river and the salty water from the sea. Many species as mangroves need a certain value of conductivity in the water to germinate. Because of the reduction of river flow the salty water enters in the estuaries. Thus, the monitoring of the water conductivity can help to manage the minimum river flow to ensure the conservation of mangroves. The second example is the application of several sensors for water quality and meteorological conditions to monitor of sensible habitats like the phanerogams meadows in the Mediterranean Sea. The last example is the use of an intelligent system to detect the presence of pollution, hydrocarbon in this case, and track this pollution in a water body.

In Chapter 7, although each chapter has its own conclusions, we are going to provide the conclusions as a whole. Moreover, in this chapter, we describe some future works related to use of sensors to achieve the precision aquaculture. It also includes the list of publications derived from the PhD.

## **2. RELATED WORK**

## 2.1. Introduction

As the one of the objectives of this PhD Thesis is to select the environmental parameters that may affect to the fish performance including fish growth, survival and natatorium behavior, it is necessary to perform an exhaustive review. Moreover, we pretend to develop new technologies to measure those parameters. Thus, the state of art of the current available sensors for water quality monitoring must be set.

In addition, it will be necessary to know the current proposals for fish farms monitoring proposed in the literature. In order to find the shortcomings in the current systems, we will present the proposals and will analyze their suitability. The requirements to ensure that our proposal can promote the spread of the precision aquaculture are the following ones:

- Low cost of the entire system, including sensors, nodes, software (if needed) and low-energy consumption.
- Access the data from anywhere and at anytime
- Monitoring the fish activity during the feeding behavior as a fish position in the tanks and feed falling detection
- Monitoring the water quality including several parameters such as temperature, salinity, and turbidity among others.
- Monitoring the environment of the tank including several parameters such as water level, illumination, and presence of workers among others.

In this chapter, the state of the art in different areas is shown. Section 2 presents a description of the effects of temperature, salinity, photoperiod, dissolved oxygen, turbidity, light and pH on growth, survival and natatorium behavior. Following, Section 3 defines the current technologies for monitoring those parameters. The state of the art of the current systems for aquaculture monitoring is shown in Section 4. Section 5 presents some specific related work on conductivity measurement using coils. Section 6 shows the state of the art of the methods for hydrocarbon detection. Finally, Section 6 presents the conclusion of this chapter.

## 2.2. Effects of the environmental parameters on fish

In this section, we show a review on the effects of environmental parameters on fish performance. We collect the current knowledge of each parameter and analyze its effects on growth, survival and natatorium behavior. The evaluated parameters are the following ones: temperature, salinity, photoperiod, dissolved oxygen, light, turbidity, and pH.

### 2.2.1. Effects of temperature

In this section the effects of the water temperature on fish are shown. The temperature is one of the environmental parameters with more changes. It changes along the world and along the year. It even changes with the depth. Its variation along the year is necessary to ensure the reproduction of the fish. The global warming and local spills can produce abnormal variations on temperature.

Several authors studied the effects of different temperatures on fish growth on larvae. Baras *et al.* (2001) studied the effect of the temperature on the first stages of life of *Oreochromis niloticus*. The highest Total Length (TL) was reached at 30°C. The effect of the temperature on the first stages of life of *Paralichthys olivaceus* was studied by Dou *et al.* (2005). The highest TL was reached at 18°C and at 21.5°C. Trotter *et al.* (2003) studied the effect of the temperature on *Latris lineata* larvae. It was between 14°C and 19°C. The effect of the temperature on *Hippoglossus hippoglossus* larvae was studied by Lein *et al.* (1997a). Larvae reared at 8°C presented higher TL and weight. Azaza *et al.* (2008) studied the effect of the temperature on fry of *Oreochromis niloticus*. The Specific Growth Rate (SGR) at 30°C was 8% higher than at 26°C and Feed Conversion Efficiency (FCE) was lowest at 30°C and 26°C.

The majority of studies are performed with juvenile fish, as can be seen below. Wang *et al.* (2009) studied the effect of temperature on small juvenile of *Sander lucioperca*, SGR at 28°C was 67% higher than at 20°C and the FCE was 33% higher. The effect of the temperature on

juvenile of *Rachycentron canadum* was studied by Sun *et al.* (2006), the SGR at 27°C was 67% higher than at 23°C and the FCE was 26% higher at 27°C than at 23°C. Person-Le Ruyet *et al.* (2004) studied the effect of the temperature on juvenile of *Dicentrarchus labrax*. It presented the highest SGR at 26°C, but authors did not find differences in FCE and Feed Intake (FI) at different temperatures. The effect of the temperature on post-smolts *Salmo salar* was studied by Handeland *et al.* (2008). They observed that fish had the highest SGR and the lowest FCE at different temperatures for different fish sizes. The same effect was detected by Imsland *et al.* (2006) with *Anarhichas minor*. Person-Le Ruyet *et al.* (2006) also studied the effect of the temperature on juvenile of *Pollachius pollachius*, the SGR at 15°C was 32% higher than at 18°C and the FCE was 20% lower. The effect of the temperature on juvenile of *Scophthalmus maximus* was studied by Van Ham *et al.* (2003), authors found that the SGR at 16 °C and 22 °C did not present differences. However, the FCE was 13% lower at 22°C than at 16°C. Luo *et al.* (2013) studied the effect of the temperature on juveniles of *Anguilla marmorata* and *Anguilla bicolor pacifica*, both species presented the highest SGR at 28°C. The effect of the temperature on juvenile of *Anarhichas minor* was studied by Hansen and Falk-Petersen (2002), the fish presented the highest weight at 12°C. The details of the experiments are shown in Table 2.1.

**Table 2. 1** Summary of the temperature effects on growth. \* Represents higher TL.

Authors	Specie	Stage	Period (days)	Range of Temp.	Temp. with highest SGR
Baras <i>et al.</i> (2001)	<i>Oreochromis niloticus</i>	larvae	28	27.2 - 39	27.9 *
Dou <i>et al.</i> (2005)	<i>Paralichthys olivaceus</i>	larvae	16	14.6 - 21.5	18 - 21.5 *
Trotter <i>et al.</i> (2003)	<i>Latris lineata</i>	larvae	17	12 - 18	16 *
Trotter <i>et al.</i> (2003)	<i>Latris lineata</i>	larvae	14	15 - 21	17 *
Lein <i>et al.</i> (1997a)	<i>Hippoglossus hippoglossus</i>	larvae	-	4 - 12	8 *
Azaza <i>et al.</i> (2008)	<i>Oreochromis niloticus</i>	fry	28	22 - 34	26
Wang <i>et al.</i> (2009)	<i>Sander lucioperca</i>	juvenile	56	20 - 28	28
Sun <i>et al.</i> (2006)	<i>Rachycentron canadum</i>	juvenile	21	23 - 35	27
Person-Le Ruyet <i>et al.</i> (2004)	<i>Dicentrarchus labrax</i>	juvenile	84	13 - 29	26
Handeland <i>et al.</i> (2008)	<i>Salmo salar</i>	post-smolts	84	6 - 18	11 - 14
Person-Le Ruyet <i>et al.</i> (2006)	<i>Pollachius pollachius</i>	juvenile	84	9 - 21	15
Imsland <i>et al.</i> (2006)	<i>Anarhichas minor</i>	juvenile	204	4 - 12	6 - 8
Van Ham <i>et al.</i> (2003)	<i>Scophthalmus maximus</i>	juvenile	53	16 - 22	22
Hansen and Falk-Petersen (2002)	<i>Anarhichas minor</i>	juvenile	63	8 - 12	12
Luo <i>et al.</i> (2013)	<i>Anguilla marmorata</i>	juvenile	45	8 - 33	28
Luo <i>et al.</i> (2013)	<i>Anguilla bicolor pacifica</i>	juvenile	45	8 - 33	28

The effects of temperature on survival were also studied by several authors in different freshwater and saltwater species. The studies were focused on the first stages of development, eggs or larvae reared under different temperatures.

Nevertheless, some authors studied the effect on eggs when the reproducers were kept under

selected temperatures. The effects of temperature on mature females of *Salmo salar* in the pre-spawning period on the egg quality were studied by King *et al.* (2003). Egg fertility and survival were highest at the lowest temperature (14°C). The same effect on *Oncorhynchus mykiss* was studied by Pankhurst *et al.* (1996), the highest egg survival rate was reached at 12°C. Davies and Bromage (2002) also studied the effect on *Oncorhynchus mykiss*. When they lowered the temperature below the environmental values, the eggs showed a decrease performance. Suquet *et al.* (2005) studied the effect of the temperature on mature males and females of *Pollachius pollachius*. The highest egg number, fertilization and hatching rates were reached at 8°C.

Following, we present the experiments performed on eggs and larvae. Okamura *et al.* (2007) studied the effect of the temperature on the first stages of *Anguilla japonica*. The highest survival rate was reached at 25°C. Watanabe *et al.* (1995) studied the effect of the temperature on eggs and larvae of *Epinephelus striatus*. The eggs reared at 26°C had the highest larvae survival. Kurokawa *et al.* (2008) studied the effect of the temperature on the first stages of *Anguilla japonica*. The best hatching rate and larval survival results were reached between 22°C and 26°C. The effect of the temperature on eggs incubation and larvae of *Abramis brama* was studied by Kucharczyk *et al.* (1997). The highest survival rate, 94.3%, was reached at 21.1°C while at 18.5°C and 22.9°C the survivals fall to 87.6% and 27.4%. Moreover, larvae present highest survival at 27.9°C.

Baras *et al.* (2001) studied the effect of the temperature on *Oreochromis niloticus*. The minimum mortality was related to temperatures from 24°C to 33°C. Dou *et al.* (2005) studied the effect of the temperature in the first stages of life of *Paralichthys olivaceus*. The highest survival rate was reached at 15°C. The effect of the temperature on larvae of *Latris lineata* was studied by Trotter *et al.* (2003). Fish have maximum survival at 16°C. The effect of the temperature on survival of larvae of *Hippoglossus hippoglossus* was studied by Lein *et al.* (1997a). Larvae reared at 4°C presented a higher chance of survival and lower level of deformities than at other temperatures. Azaza *et al.* (2008) studied the effect of the temperature on fry of *Oreochromis niloticus*. The highest survival, 98%, was reached at 32°C, while at 34°C the survival rate was 74%. The effect of the temperature on juvenile of *Anarhichas minor* was studied by Hansen and Falk-Petersen (2002). Fish presented the highest chances of survival at 8°C. Luo *et al.* (2013) studied the effect of the temperature on juveniles of *Anguilla marmorata* and *Anguilla bicolor pacifica*. *Anguilla marmorata* presented the highest survival rate between 18°C and 33°C and *Anguilla bicolor pacifica* presented the highest chances of survival between 28°C and 33°C. More details can be seen in Table 2.2.

The thermoregulatory swim of *Salmo salar* in cages with stratified water was studied by Johansson *et al.* (2009). The results show that fish swimming preferences are a combination of different factors such as temperature conditions, social factors and motivations.

### 2.2.2. Effects of salinity

Following, we show the effects of the salinity on fish. The salinity changes geographically along the world. However, it does not change along the year as the temperature does. Some regions, like the Mediterranean Sea and Red Sea, have higher salinity values. The salinity is a limiting parameter for several fish species. Even that there are some fishes that can live under changing saline conditions, others need specific values to survive or to reproduce.

The effects of salinity on the growth of different fish species have been the object of study for several authors. A summary of the results of those experiments can be seen in Table 2.3. The effect of low salinities was studied by Imsland *et al.* (2008) on juveniles of *Hippoglossus hippoglossus*. The highest SGR and FCE (27% higher than other values at 32‰) values were related with salinities of 15‰ and 25‰. Foss *et al.* (2001) studied the same effect on *Anarhichas minor* and they did not find any effect on the final weight, SGR, FCE or FI. Rubio *et al.* (2005) also presented the effects of reduced salinities on food consumption of *Dicentrarchus labrax*.

**Table 2. 2** Summary of the temperature effects on survival. (-) means no available information.

Authors	Specie	Stage of development	Period (days)	Range of Temp.	Temp. with higher survival
King <i>et al.</i> (2003)	<i>Salmo salar</i>	mature - egg	91	14 - 22	14
Pankhurst <i>et al.</i> (1996)	<i>Oncorhynchus mykiss</i>	mature - egg	>60	9 - 21	12
Davies and Bromage (2002)	<i>Oncorhynchus mykiss</i> <i>Pollachius</i>	mature - egg	730	-	-
Suquet <i>et al.</i> (2005)	<i>pollachius</i>	mature - egg	-	8 - 12	8
Okamura <i>et al.</i> (2007)	<i>Anguilla japonica</i> .	egg	20	19 - 31	25
Kucharczyk <i>et al.</i> (1997)	<i>Abramis brama</i>	egg	-	13.2 - 26.8	- 21.1
Kucharczyk <i>et al.</i> (1997)	<i>Abramis brama</i>	larvae	21	13.2 - 34	27.9
Watanabe <i>et al.</i> (1995)	<i>Epinephelus striatus</i>	egg - larvae	-	26 - 30	26
Kurokawa <i>et al.</i> (2008)	<i>Anguilla japonica</i> <i>Oreochromis</i>	egg - larvae	-	18 - 30	22 - 26
Baras <i>et al.</i> (2001)	<i>niloticus</i> <i>Paralichthys</i>	larvae	28	27.2 - 39 14.6	24 - 33 -
Dou <i>et al.</i> (2005)	<i>olivaceus</i>	larvae	16	21.5	15
Trotter <i>et al.</i> (2003)	<i>Latris lineata</i>	larvae	17	12 - 18	14 - 18
Trotter <i>et al.</i> (2003)	<i>Latris lineata</i> <i>Hippoglossus</i>	larvae	14	15 - 21	15 - 19
Lein <i>et al.</i> (1997a)	<i>hippoglossus</i> <i>Oreochromis</i>	larvae	-	4 - 12	4
Azaza <i>et al.</i> (2008)	<i>niloticus</i>	Fry	28	19 - 36.5	32
Hansen and Falk-Petersen (2002)	<i>Anarhichas minor</i> <i>Anguilla</i>	juvenile	63	8 - 12.	8
Luo <i>et al.</i> (2013)	<i>marmorata</i> <i>Anguilla</i> <i>bicolor</i>	juvenile	45	8 - 33	18 - 33
Luo <i>et al.</i> (2013)	<i>pacifica</i>	juvenile	45	8 - 33	23 - 33

Maximum FI appear at 25‰. Juveniles of *Umbrina cirrosa* were exposed to low salinity by Mylonas *et al.* (2009). The maximum length, weight and SGR were reached between 10‰ and 40‰ (93% higher than at 4‰), but it gave the lowest FCE (almost 50% lower than at 4‰). The effects on juvenile of *Sparus aurata* were studied by Laiz-Carrión *et al.* (2005). Fish had the highest SGR at 12‰ (4% higher than at 38‰). The exposure of juveniles of *Centropomus parallelus* to low salinity conditions was made by da Silva Rocha *et al.* (2005). They did not detect effects at 15 days, but at 30 days of exposure, the highest SGR was reached at 5‰. Sampaio and Bianchini (2002) evaluated the growth of *Paralichthys orbignyanus*. At 30‰ fish presented 25% higher SGR than at 0‰. Juveniles of *Solea senegalensis* were exposed to low salinity water by Arjona *et al.* (2009). The maximum SGR was reached at 25‰ and 38‰. The value was three times higher than at 15‰. The effect of different saline conditions on juveniles of *Argyrosomus japonicus* was tested by Fielder and Bardsley (1999). FCR was minimum at 5‰. The value was 69% lower than at 10‰, and 40% lower than at 20‰.

**Table 2. 3** Summary of the salinity on growth. \* Not represents highest SGR, it represents FI. \*\*

Represent TL \*\*\* Represent BW. N.E. means No Effect.

Authors	Specie	Stage of development	Period (days)	Range of Salinity	Salinity with higher SGR
Imsland <i>et al.</i> (2008)	<i>Hippoglossus hippoglossus</i>	juvenile	129	15 - 32	12 - 25
Foss <i>et al.</i> (2001)	<i>Anarhichas minor</i>	juvenile	84	12 - 34	N.E.
Rubio <i>et al.</i> (2005)	<i>Dicentrarchus labrax</i>	juvenile	35	0 - 25	25*
Mylonas <i>et al.</i> (2008)	<i>Umbrina cirrosa</i>	juvenile	84	4 - 40	10 - 40
Laiz-Carrión <i>et al.</i> (2005)	<i>Sparus aurata</i>	juvenile	100	6 - 38	12
da Silva Rocha <i>et al.</i> (2005)	<i>Centropomus parallelus</i>	juvenile	15	5 - 30	N.E.
da Silva Rocha <i>et al.</i> (2005)	<i>Centropomus parallelus</i>	juvenile	30	5 - 30	5
Sampaio and Bianchini (2002)	<i>Paralichthys orbignyanus</i>	juvenile	90	0 - 30	30
Arjona <i>et al.</i> (2009)	<i>Solea senegalensis</i>	juvenile	90	15 - 38	25 - 38
Fielder and Bardsley (1999)	<i>Argyrosomus japonicus</i>	juvenile	20	5 - 35	5
Sampaio <i>et al.</i> (2007)	<i>Paralichthys orbignyanus</i>	juvenile	18	5 - 30	20 - 30**
Zhang <i>et al.</i> (2010)	<i>Takifugu flavidus</i>	larvae	20	0 - 45	15 - 25**
Yan <i>et al.</i> (2004)	<i>Fugu obscurus</i>	juvenile	36	0 - 35	8
Denson <i>et al.</i> (2003)	<i>Rachycentron canadum</i>	juvenile	70	5 - 30	30
Resley <i>et al.</i> (2006)	<i>Rachycentron canadum</i>	juvenile	56	5 - 30	5
Okamura <i>et al.</i> (2009)	<i>Anguilla japonica</i>	larvae	55	17.5 - 35	17.5**
Sampaio and Bianchini (2002)	<i>Paralichthys orbignyanus</i>	juvenile	90	0 - 30	30
Tsuzuki <i>et al.</i> (2007)	<i>Centropomus parallelus</i>	juvenile	50	5 - 35	15- 35 **
Partridge and Jenkins (2002)	<i>Acanthopagrus butcheri</i>	juvenile	183	0 - 60	12 - 48
Partridge and Jenkins (2002)	<i>Acanthopagrus butcheri</i>	juvenile	122	0 - 12	N.E.
Luz <i>et al.</i> (2008)	<i>Carassius auratus</i>	juvenile	21	0 - 10	0 - 6
Wang <i>et al.</i> (1997)	<i>Cyprinus carpio</i>	juvenile	920	0.5 - 10.5	0.5
Saoud <i>et al.</i> (2007)	<i>Siganus rivulatus</i>	juvenile	42	10 - 40	N.E.
Garcia <i>et al.</i> (1999)	<i>Aristichthys nobilis</i>	fry	28	0 - 6	0 - 2***
Tandler <i>et al.</i> (1995)	<i>Sparus aurata</i>	larvae	32	25 - 40	25 ***
Martínez-Palacios <i>et al.</i> (2004)	<i>Chirostoma estor estor</i>	larvae	2	0 - 15	10 - 15

Sampaio *et al.* (2007) studied the effect of lower salinities on different stages of *Paralichthys orbignyanus* the highest TL appeared between 20‰ and 30‰. Zhang *et al.* (2010)



studied the effect of low salinities on larvae of *Takifugu flavidus*. The highest SGR was obtained with 15‰ to 25‰. The effect of different saline conditions on juveniles of *Fugu obscurus* was studied by Yan *et al.* (2004). The maximum SGR was reached at 8‰. It was 180% higher than at 0‰ and 228% higher than at 35‰. Denson *et al.* (2003) studied the effect of low salinities on juveniles of *Rachycentron canadum*. SGR was maximum at 30‰. It was 24% higher than at 15‰. Resley *et al.* (2006) also studied the effect on juveniles of *Rachycentron canadum*. The highest SGR value was reached at 5‰. Okamura *et al.* (2009) studied the effect of low salinities on larvae of *Anguilla japonica*. The maximum TL was reached at 17.5‰. The effect of different saline conditions was tested on *Paralichthys orbignyanus* by Sampaio and Bianchini (2002). The highest SGR was reached at 30‰. It was 25% higher than at 0‰. Tsuzuki *et al.* (2007) evaluated the effect of salinity on juveniles of *Centropomus parallelus*. The maximum TL was found between 15‰ and 35‰. Partridge and Jenkins (2002) studied the effect of different salinities on juveniles of *Acanthopagrus butcheri*. The highest SGR were obtained from 12‰ to 48‰.

Moreover, the effect of high salinities was also studied by several authors like Luz *et al.* (2008) with *Carassius auratus*. The maximum body weight and SGR and minimum FCE was obtained for salinities from 0‰ to 6‰. A similar experiment was developed on *Cyprinus carpio* by Wang *et al.* (1997). Fish presented highest SGR at 0.5‰. It was 6% higher than at 2.5‰. However, the optimal FCE was reached at 2.5‰. Saoud *et al.* (2007) studied the effect of high and low salinities on juveniles of *Siganus rivulatus*. Authors did not find effects on growth. The effects on *Aristichthys nobilis* were evaluated by Garcia *et al.* (1999). Fry exposed to different salinities had higher Body Weight (BW) between 0‰ and 2‰. The effect of high and low saline conditions on larvae of *Sparus aurata* was studied by Tandler *et al.* (1995). BW was 16% higher at 25‰ than at 32.5‰. Martínez-Palacios *et al.* (2004) studied the effect of different salinities on larvae of *Chirostoma estor estor*. Fish presented the maximum SGR from 10‰ to 15‰.

The effects of salinity on survival were studied mainly in the early stages of development: eggs, larvae, fry and fingerling. Fashina-Bombata and Busari (2000) studied the effect of high salinities on the early stage of *Heterobranchus longifilis*. The maximum hatch rate was reached under 0 to 4.5‰ conditions. Larvae expressed maximum survival at 0‰ and fingerlings between 0 and 7‰. The effect of different saline conditions were tested on eggs of *Acanthopagrus butcheri* by Haddy and Pankhurst (2003). The maximum survival and hatch rate was obtained at salinities from 30 to 35‰. The effect of different saline conditions were tested on eggs of *Anguilla japonica* by Okamoto *et al.* (2009). The maximum hatching and survival rates appeared from 30 to 33‰. Smith *et al.* (1999) studied the effect of different salinities on eggs and larvae of *Paralichthys lethostigma*. The highest hatch rate was obtained from 10 to 35‰ and the maximum larvae survival rate from 5 to 30‰. Sampaio *et al.* (2007) studied the effect of low salinities on different stages of *Paralichthys orbignyanus*. Hatching only occurred at 35‰ and larvae survival its maximum at 30‰. Zhang *et al.* (2010) studied the effect of low salinities on eggs and larvae of *Takifugu flavidus*. The highest survival on eggs appeared between 10 and 20‰ while the larvae survival was higher from 15 to 35‰. Martínez-Palacios *et al.* (2004) studied the effect of different salinities on larvae of *Chirostoma estor estor*. The maximum survival rates were reached from 5 to 15‰. The effect of different saline conditions was tested on larvae of *Hippoglossus hippoglossus* by Lein *et al.* (1997b). Maximum survival was obtained at salinities between 26.5 and 31.5‰. Okamura *et al.* (2009) studied the effect of low salinities on larvae of *Anguilla japonica*. The highest survival rates were reached at 17.5‰. The effects of different saline conditions on larvae of *Sparus aurata* was studied by Tandler *et al.* (1995). The survival was 3.5 times higher at 25‰ than at 40‰. The effects on *Aristichthys nobilis* was evaluated by Garcia *et al.* (1999). The fry exposed to different salinities had higher survival at salinities from 0 to 6‰. More information can be seen in Table 2.4.

**Table 2. 4** Summary of the salinity effects on survival on early stages of development (-) means no available information.

Authors	Specie	Stage of development	Period (days)	Range of Salinity	Salinity with higher SGR
Fashina-Bombata and Busari (2000)	<i>Heterobranchus longifilis</i>	egg	-	0 - 15	0 - 4.5
Fashina-Bombata and Busari (2000)	<i>Heterobranchus longifilis</i>	fry	4	0 - 15	0
Fashina-Bombata and Busari (2000)	<i>Heterobranchus longifilis</i>	fingerling	4	0 - 15	0 - 7
Haddy and Pankhurst (2003)	<i>Acanthopagrus butcheri</i>	egg	-	0 - 35	30 - 35
Okamoto <i>et al.</i> (2009)	<i>Anguilla japonica</i>	egg	-	24 - 42	30 - 33
Smith <i>et al.</i> (1999)	<i>Paralichthys lethostigma</i>	egg	-	0 - 35	10 - 35
Smith <i>et al.</i> (1999)	<i>Paralichthys lethostigma</i>	larvae	3	0 - 30	5 - 30
Sampaio <i>et al.</i> (2007)	<i>Paralichthys orbignyanus</i>	egg	-	10 - 35	35
Sampaio <i>et al.</i> (2007)	<i>Paralichthys orbignyanus</i>	larvae	4	0 - 30	30
Zhang <i>et al.</i> (2010)	<i>Takifugu flavidus</i>	egg	-	0 - 45	10 - 20
Zhang <i>et al.</i> (2010)	<i>Takifugu flavidus</i>	larvae	20	0 - 45	15 - 35
Tandler <i>et al.</i> (1995)	<i>Sparus aurata</i>	larvae	32	25 - 40	25
Garcia <i>et al.</i> (1999)	<i>Aristichthys nobilis</i>	fry	4	0 - 16	0 - 6
Martínez-Palacios <i>et al.</i> (2004)	<i>Chirostoma estor estor</i>	larvae	2	0 - 15	5 - 15
Lein <i>et al.</i> (1997b)	<i>Hippoglossus hippoglossus</i>	larvae	49	20.3 - 42.2	- 26.5 - 31.5
Lein <i>et al.</i> (1997b)	<i>Hippoglossus hippoglossus</i>	larvae	19	24 - 39	27.5 - 31.5
Okamura <i>et al.</i> (2009)	<i>Anguilla japonica</i>	larvae	55	17.5 - 35	17.5

However, some authors studied the effects of salinity on juvenile fish, their results can be seen in Table 2.5. The effects of different saline conditions on juveniles of *Fugu obscurus* was studied by Yan *et al.* (2004). At salinity levels of 8 and 18‰ the survival rate was 100%. It was 25% higher than at 0‰ and 37% higher than at 35‰. Denson *et al.* (2003) studied the effect of low salinities on juveniles of *Rachycentron canadum*. The chances of survival were the same for saline conditions of 15‰ and 30‰. In addition, Resley *et al.* (2006) studied the effect on juveniles of *Rachycentron canadum*. The highest survival rate was reached at 15‰. The effect of different saline conditions was tested on *Paralichthys orbignyanus* by Sampaio and Bianchini (2002). No effects were detected on the survival rates. Saoud *et al.* (2007) studied the effect of different salinities on juveniles of *Siganus rivulatus*. The fish had the same chances of survival, 100%, for all the conditions. Juveniles of *Centropomus parallelus* were exposed to different salinities by Tsuzuki *et al.* (2007). No effects have been found on survival rates. Partridge and Jenkins (2002) studied the effect of different salinities on juveniles of *Acanthopagrus butcheri*. Maximum survival rate was obtained from 12‰ to 60‰. Moreover, the effect of low saline

conditions was tested on juveniles of *Anarhichas lupus* by Le François *et al.* (2004). No mortality occurred in the test. Finally, the effect on larvae and juveniles of *Argyrosomus japonicus* in different saline conditions was tested by Fielder and Bardsley (1999). The fish had the same survival, around 80%, from 5 to 35‰. At 0.6‰ all the fish died.

**Table 2. 5** Summary of the salinity effects on survival of juvenile fish. N.E. means No Effect

Authors	Specie	Period (days)	Range of Salinity	Salinity with higher SGR
Yan <i>et al.</i> (2004)	<i>Fugu obscurus</i>	54	0 - 35	8 - 18
Denson <i>et al.</i> (2003)	<i>Rachycentron canadum</i>	70	5 - 30	15 - 30
Resley <i>et al.</i> (2006)	<i>Rachycentron canadum</i>	56	5 - 30	15
Sampaio and Bianchini (2002)	<i>Paralichthys orbignyanus</i>	90	0 - 30	N.E.
Saoud <i>et al.</i> (2007)	<i>Siganus rivulatus</i>	42	10 - 42	N.E.
Tsuzuki <i>et al.</i> (2007)	<i>Centropomus parallelus</i>	50	5 - 35	N.E.
Partridge and Jenkins (2002)	<i>Acanthopagrus butcheri</i>	183	0 - 60	12 - 60
Partridge and Jenkins (2002)	<i>Acanthopagrus butcheri</i>	122	0 - 12	0 - 12
Le François <i>et al.</i> (2004)	<i>Anarhichas lupus</i>	133	7 - 28	N.E.
Fielder and Bardsley (1999)	<i>Argyrosomus japonicus</i>	28	5-35	

### 2.2.3. Effects of photoperiod

Next, the effects of alterations on natural photoperiod are shown. Photoperiod is also an environmental parameter that changes along the year and it is different depending on the latitude. In the equatorial zone, the photoperiod has minimum changes along the year, while in the polar zones the changes are bigger. The changes in the photoperiod are necessary for a correct maturation of fishes.

The effect of changing photoperiods or simulated photoperiods at different moments of the year on fish growth were studied by several authors. Endal *et al.* (2000) established that receiving 24 hours of light (L):0 hours of dark (D) from January to July produce that smolts of *Salmo salar* maximize their growth. Taylor *et al.* (2006) found that the best growth and FCR were found after exposing fry of *Oncorhynchus mykiss* to longer photoperiods from autumn to spring. Kissil *et al.* (2001) studied the effect of long photoperiod on juveniles of *Sparus aurata* during 11 months. Three different photoperiods were used: natural photoperiod, long-day photoperiod, and skeleton. The fish under long-day photoperiod presented the highest growth and lower FCR. Handeland and Stefansson (2001) studied the effect of photoperiod on post-smolt *Salmo salar* during 111 days. The used photoperiods were: (I) 24L:0D during the whole period, (II) 9 weeks 12L:12D followed by 7 weeks 24L:0D, (III) 12 weeks 12L:12D followed by 4 weeks 24L:0D and (IV) natural photoperiod. The best results were obtained with the first and second treatments.

By the other side, the effects on larvae of *Amphiprion melanopus* of different continuous photoperiods on fish growth were studied by Arvedlund *et al.* (2000). The maxim LT were obtained at a photoperiod of 16L:8D. Fielder *et al.* (2002) studied the effect of different photoperiods on larvae of *Pagrus auratus*. Fish larvae had higher TL from 18L:6D to 24L:0D than at shorter photoperiods. Barlow *et al.* (1995) studied the effect of the photoperiod on larvae and juvenile of *Lates calcarifer*. The TL at 16L:8D and 24L:0D was 18% higher than at 8L:16D. The effect of different photoperiods on larvae of *Solea senegalensis* was studied by Cañavate *et al.* (2006). No differences were found on growth with different photoperiods. Stuart

and Drawbridge (2012) studied the effect of the photoperiod on larvae of *Seriola lalandi* and *Atractoscion nobilis*. Solely *Atractoscion nobilis* attained higher length under longer photoperiods. The effect of long-day photoperiod on fry of *Oreochromis niloticus* was studied by Rad *et al.* (2006). Under 24L:0D the fish SGR was 8% higher and the FCE 25% lower than under the natural photoperiod. The effect of different photoperiods on fry *Oreochromis niloticus* was studied by El-Sayed and Kawanna (2004). The fry presented higher SGR between 18L:6D and 24L:0D. The SGR at 18L:6D and 24L:0D was 7% higher than at 12L:12D. Adewolu *et al.* (2008) studied the effect of the photoperiod on fingerlings of *Clarias gariepinus*. The SGR at 0L:24D was 59% higher than at other photoperiods. The effect of the photoperiod on juveniles of *Pagrus major* was studied by Biswas *et al.* (2006). The achieved SGR at 24L:0D was 17% higher than at 6L:6D. The effect of long photoperiods on juvenile of *Scophthalmus maximus* was studied by Imsland *et al.* (1997). The maximum SGR was obtained at 24L:0D. The effect of different photoperiods on juvenile of *Huso huso* was studied by Bani *et al.* (2009). No differences were found in SGR or FCE. The effect of different photoperiods on larvae and juvenile of *Miichthys miiuy* was studied by Shan *et al.* (2008). Authors did not find any differences in SGR. Schütz and Nuñez (2007) studied the effect of photoperiod on post-larvae of *Salminus brasiliensis*. No correlation was found between growth and photoperiod. The effect of photoperiod on juvenile of *Pleuronectes ferrugineus* was studied by Purchase *et al.* (2000). No effects were found. Aride *et al.* (2006) studied the effect of different photoperiods on juvenile of *Colossoma macropomu*. Fish under 0L:24D had higher SGR, almost 3 times higher than under 24L:2D. The effect of long photoperiods on juvenile of *Cyprinus carpio* was studied by Danisman-Yagci and Yigit (2009). Again, no differences were found on growth parameters under different photoperiods. See Table 2.6 for more information.

Sigholt *et al.* (1995) studied the effect of short photoperiods on smolts of *Salmo salar* during 7 months. The first 3 groups had a simulated winter, the fourth had a short simulated winter starting from different months, the fifth had a long photoperiod during the entire test and the last one had a natural photoperiod. The mortality rates were higher in groups with simulated winter in the first months. The rest of the groups had a mortality of 15% or less.

Other authors studied the effects of continuous photoperiod on different fish. Arvedlund *et al.* (2000) studied the effect of different photoperiods on larvae of *Amphiprion melanopus*. No effects were found on chances of survival. Fielder *et al.* (2002) studied the effect of different photoperiods on larvae of *Pagrus auratus*. Fish larvae had higher survival rates between 12L:12D and 24L:0D than under shorter photoperiods. The effect of different photoperiods on larvae of *Miichthys miiuy* was studied by Shan *et al.* (2008). The larvae with no light died after 7 days, because they were not able to feed. The rest of photoperiods did not cause any effects on mortality. Barlow *et al.* (1995) studied the effect of photoperiod on larvae and juvenile of *Lates calcarifer*. No differences were found on the survival rate. The effect of different photoperiods on larvae of *Solea senegalensis* was studied by Cañavate *et al.* (2006). The larvae presented the same chances of survival under different photoperiods. Stuart and Drawbridge (2012) studied the effect of photoperiod on larvae of *Seriola lalandi* and *Atractoscion nobilis*. *Seriola lalandi* reached a higher survival rate at 24L:0D and no effects were detected on *Atractoscion nobilis*. Schütz and Nuñez (2007) studied the effect of photoperiod on post-larvae of *Salminus brasiliensis*. No effects were found. El-Sayed and Kawanna (2004) studied the effect of different photoperiods on fry and fingerlings of *Oreochromis niloticus*. The fry had 17% more chances of survival under 24:0 than under 12:12. The same survival rates was found in different conditions in fingerlings. Adewolu *et al.* (2008) studied the effect of the photoperiod on fingerlings of *Clarias gariepinus*. The fish had higher survival rates under 0L:24D, 14% higher than with other photoperiods. This is because under dark conditions the fish spend the most of the time resting. The effect of different photoperiods on juvenile of *Huso huso* was studied by Bani *et al.* (2009). The survival rate was 25% higher from 12L:12D to 24L:0D. The effect of the photoperiod on juvenile of *Pleuronectes ferrugineus* was studied by Purchase *et al.* (2000). No survival differences were found.

**Table 2. 6** Summary of the photoperiod effects on growth \* Not represents higher SGR, represents length. N.E. means No Effect.

Authors	Specie	Stage of development	Period (days)	Range of Phot. (L:D)	Phot. with higher SGR
Arvedlund <i>et al.</i> (2000)	<i>Amphiprion melanopus</i>	larvae	25	12:12 - 24:0	16:8*
Fielder <i>et al.</i> (2002)	<i>Pagrus auratus</i>	larvae	12	0:24 - 24:0	18:6 - 24:0*
Fielder <i>et al.</i> (2002)	<i>Pagrus auratus</i>	larvae	21	12:12 - 24:0	18:6 - 24:0*
Barlow <i>et al.</i> (1995)	<i>Lates calcarifer</i>	larvae	9	8:16 - 24:0	16:8 - 24:0*
Barlow <i>et al.</i> (1995)	<i>Lates calcarifer</i>	larvae	19	12:12 - 24:0	N.E.
Cañavate <i>et al.</i> (2006)	<i>Solea senegalensis</i>	larvae	14	14:0 - 24:0	N.E.
Stuart and Drawbridge (2012)	<i>Seriola lalandi</i>	larvae	8	12:12 - 24:0	N.E.
Stuart and Drawbridge (2012)	<i>Atractoscion nobilis</i>	larvae	8	12:12 - 24:0	24:0*
Rad <i>et al.</i> (2006)	<i>Oreochromis niloticus</i>	fry	168	18:6 - 24:0	24:0
El-Sayed and Kawanna (2004).	<i>Oreochromis niloticus</i>	fry	60	6:18 - 24:0	18:6 - 24:0
El-Sayed and Kawanna (2004).	<i>Oreochromis niloticus</i>	fingerlings	90	6:18 - 24:0	N.E.
Adewolu <i>et al.</i> (2008)	<i>Clarias gariepinus</i>	fingerlings	70	0:24 - 24:0	0:24
Biswas <i>et al.</i> (2006)	<i>Pagrus major</i>	juvenile	56	6:6 - 24:0	24:00:00
Imsland <i>et al.</i> (1997)	<i>Scophthalmus maximus</i>	juvenile	545	18:6 - 24:0	24:0
Bani <i>et al.</i> (2009)	<i>Huso huso</i>	juvenile	56	0:24 - 24:0	N.E.
Shan <i>et al.</i> (2008)	<i>Miichthys miiuy</i>	juvenile	52	0:24 - 24:0	12:12 - 24:0
Purchase <i>et al.</i> (2000)	<i>Pleuronectes ferrugineus</i>	juvenile	70	12:12 - 24:0	N.E.
Purchase <i>et al.</i> (2000)	<i>Pleuronectes ferrugineus</i>	juvenile	112	12:12 - 24:0	N.E.
Biswas <i>et al.</i> (2008)	<i>Oplegnathus fasciatus</i>	juvenile		6:6 - 24:0	N.E.
Arde <i>et al.</i> (2006)	<i>Colossoma macropomum</i>	juvenile	50	0:24 - 24:0	0:24
Danisman-Yagci and Yigit (2009)	<i>Cyprinus carpio</i>	juvenile	90	12:12 - 24:0	N.E.

Tucker *et al.* (2006) studied the effect of a short photoperiod on *Pagrus auratus*. No significant differences were found on survival. Biswas *et al.* (2008) studied the effect of the photoperiod on *Oplegnathus fasciatus*. All the fish survived the test. The effect of long photoperiods on juvenile of *Cyprinus carpio* was studied by Danisman-Yagci and Yigit (2009). Again, no differences were found in the survival rates under different photoperiods. Biswas *et al.* (2005) studied the effect of photoperiod on *Pagrus major*. No differences were observed on survival rate. The effect of different photoperiods on juvenile of *Colossoma macropomum* was studied by Arde *et al.* (2006). No mortality occurred during the experiment. More information can be seen in Table 2.7.

**Table 2. 7** Summary of the photoperiod effects on survival. N.E. means No Effect.

Authors	Specie	Stage of development	Period (days)	Range of Phot. (L:D)	Phot. with higher survival
Arvedlund <i>et al.</i> (2000)	<i>Amphiprion melanopus</i>	larvae	25	12:12 - 24:0	16:8
Fielder <i>et al.</i> (2002)	<i>Pagrus auratus</i>	larvae	12	0:24 - 24:0	12:12 - 24:0
Fielder <i>et al.</i> (2002)	<i>Pagrus auratus</i>	larvae	21	12:12 - 24:0	N.E.
Shan <i>et al.</i> (2008)	<i>Miichthys miiuy</i>	larvae	52	0:24 - 24:0	12:12 - 24:0
Barlow <i>et al.</i> (1995)	<i>Lates calcarifer</i>	larvae	9	8:16 - 24:0	N.E.
Barlow <i>et al.</i> (1995)	<i>Lates calcarifer</i>	larvae	19	12:12 - 24:0	N.E.
Cañavate <i>et al.</i> (2006)	<i>Solea senegalensis</i>	larvae	14	14:0 - 24:0	N.E.
Stuart and Drawbridge (2012)	<i>Seriola lalandi</i>	larvae	8	12:12 - 24:0	24:0
Stuart and Drawbridge (2012)	<i>Atractoscion nobilis</i>	larvae	8	12:12 - 24:0	N.E.
Schütz and Nuñer (2007)	<i>Salminus brasiliensis</i>	post-larvae	-	0:24 - 24:0	N.E.
El-Sayed and Kawanna (2004).	<i>Oreochromis niloticus</i>	fry	60	6:18 - 24:0	18:6 - 24:0
El-Sayed and Kawanna (2004).	<i>Oreochromis niloticus</i>	fingerlings	90	6:18 - 24:0	N.E.
Adewolu <i>et al.</i> (2008)	<i>Clarias gariepinus</i>	fingerlings	70	0:24 - 24:0	0:24
Bani <i>et al.</i> (2009)	<i>Huso huso</i>	juvenile	56	0:24 - 24:0	12:12 - 24:0
Purchase <i>et al.</i> (2000)	<i>Pleuronectes ferrugineus</i>	juvenile	70	12:12 - 24:0	N.E.
Purchase <i>et al.</i> (2000)	<i>Pleuronectes ferrugineus</i>	juvenile	112	12:12 - 24:0	N.E.
Tucker <i>et al.</i> (2006)	<i>Pagrus auratus</i>	larvae	32	12:12 - 18:6	N.E.
Biswas <i>et al.</i> (2008)	<i>Oplegnathus fasciatus</i>	juvenile	-	6:6 - 24:0	N.E.
Danisman-Yagci and Yigit (2009)	<i>Cyprinus carpio</i>	juvenile	90	12:12 - 24:0	N.E.
Biswas <i>et al.</i> (2006)	<i>Pagrus major</i>	juvenile	56	6:6 - 24:0	N.E.
Arde <i>et al.</i> (2006)	<i>Colossoma macropomum</i>	juvenile	50	0:24 - 24:0	N.E.

#### 2.2.4. Effects of dissolved oxygen

In this subsection, the effects of changes in dissolved oxygen are shown. Dissolved oxygen (DO) is a limiting factor for several species. Generally, the level of oxygen in the water is the result of the equilibrium between water and atmosphere. However in aquaculture is possible to increase the level of oxygen using aerators. An increment on the organic matter in the water and the presence of certain microorganism can cause a reduction of oxygen concentration.

Thetmeyer *et al.* (1999) studied the effect of 40% (hypoxia), 86% (control) and fluctuating saturation from 40% to 86% each 770 minutes on *Dicentrarchus labrax* during 1 month. The SGR was higher for the control treatment and did not present any difference between hypoxia and the oscillating treatment. No differences on FCE were found.

The effects of hypoxia and hyperoxia have been studied by different authors; more information about the following references can be seen in Table 2.8. The effect of dissolved

oxygen on larvae of *Oncorhynchus mykiss* was studied by C. S. Ciuhandu *et al.* (2005). The weight by which the fish increased was lower under hypoxia conditions. The effect of the dissolved oxygen on juvenile *Oreochromis niloticus* was studied by Tran-Duy *et al.* (2008). The fish presented 3 times higher FI and the fastest growth at higher oxygen concentrations. Pichavant *et al.* (2001) studied the effect of low oxygen concentrations on juveniles of *Dicentrarchus labrax* and *Scophthalmus maximus*. In hypoxia conditions fish gain less weight and the FI was lower. No changes on FCE were detected. The effect was more pronounced in *Scophthalmus maximus*. Filho *et al.* (2005) studied the effect of low oxygen concentrations on *Leporinus elongatus*. The FCR was higher at oxygen concentrations of 3.91 mg/L and FI was the same from 3.91 to 6.94. The effect of hypoxia on the growth on *Scophthalmus maximus* was studied by Pichavant *et al.* (2000). The highest weight and FI were obtained at 7.2mg/L of oxygen. The effect of the dissolved oxygen on the growth of *Oreochromis aureus* was studied by Papoutsoglou and Tziha (1996). The weight of the fish was three times higher at 6.51 mg/L than at 2.63 mg/L.. Person-Le Ruyet *et al.* (2002) studied the effect of oxygen supersaturation on juveniles of *Scophthalmus maximus*. No differences on SGR, FCE and FI were found. Foss and Imsland (2002) demonstrated with *Anarhichas minor* the effects on SGR after a period of hypoxia. During the hypoxia, fish exposed to lower oxygen concentration, have a reduction on the SGR. After the hypoxia, fish exhibit a compensatory growth under normal conditions. Foss *et al.* (2002) studied the effect of low oxygen concentration on *Anarhichas minor*. The FCE did not present differences and feeding rate was 31% higher from 9.6 to 14mg/L. No changes on FCE on *Anarhichas minor* under normoxia and hyperoxia were detected by Foss *et al.* (2003). Braun *et al.* (2006) studied the effect of low dissolved oxygen on *Rhamdia quelen*. The maximum SGR was reached from 4.1 to 6.16mg/L.

**Table 2. 8** Summary of the dissolved oxygen effects on growth \* Not represents higher SGR, represents TL or \*\*FCR. N.E. means No Effect.

Authors	Specie	Stage of development	Period (days)	Range of oxygen (mg/L)	Level with higher SGR
C. S. Ciuhandu <i>et al.</i> (2005)	<i>Oncorhynchus mykiss</i>	larvae	36	5 - 15	10 - 15
Tran-Duy <i>et al.</i> (2008)	<i>Oreochromis niloticus</i>	juvenile	25	3 - 5.6	5.6
Pichavant <i>et al.</i> (2001)	<i>Scophthalmus maximus</i>	juvenile	42	3.2 - 7.4	7.4*
Pichavant <i>et al.</i> (2001)	<i>Dicentrarchus labrax</i>	juvenile	42	3.2 - 7.4	7.4*
Filho <i>et al.</i> (2005)	<i>Leporinus elongatus</i>	juvenile	7	1.92 - 6.94	3.9 - 6.94
Pichavant <i>et al.</i> (2000)	<i>Scophthalmus maximus</i>	juvenile	45	3.5 - 7.2	7.2*
Papoutsoglou and Tziha (1996)	<i>Oreochromis aureus</i>	juvenile	200	2.63 - 6.51	6.51
Person-Le Ruyet <i>et al.</i> (2002)	<i>Scophthalmus maximus</i>	juvenile	30	6.9 - 26.6	N.E.
Foss and Imsland (2002)	<i>Anarhichas minor</i>	juvenile	75	4 - 14.5	9.6 - 14.5
Foss <i>et al.</i> (2002)	<i>Anarhichas minor</i>	juvenile	76	5 - 14.5	9.6 - 14.5*
Foss <i>et al.</i> (2003)	<i>Anarhichas minor</i>	juvenile	56	9.6 - 14.5	N.E.**
Braun <i>et al.</i> (2006)	<i>Rhamdia quelen</i>	juvenile	30	1.96 - 6.16	4.1 - 6.16

The effects of dissolved oxygen on survival rates were studied to a lesser extent. The effect of the hyperoxia on larvae of *Oncorhynchus mykiss* was studied by C. S. Ciuhandu *et al.* (2005). No effects have been detected. The effect of the low oxygen concentrations on juvenile *Oreochromis niloticus* was studied by Tran-Duy *et al.* (2008). Again, no effects were found on survival. Braun *et al.* (2006) studied the effect of low dissolved oxygen on *Rhamdia quelen*. The fish under 0.4mg/L to 1.04mg/L have high mortality. This information is summarized in Table 2.9.

**Table 2.9** Summary of the oxygen effects on survival. N.E. means No Effect.

Authors	Specie	Age	Period (days)	Range of oxygen (mg/L)	Level with higher survival
Tran-Duy <i>et al.</i> (2008)	<i>Oreochromis niloticus</i>	juvenile	25	3 - 5.6	N.E.
C. S. Ciuhandu <i>et al.</i> (2005)	<i>Oncorhynchus mykiss</i>	larvae	36	5 - 15	N.E.
Braun <i>et al.</i> (2006)	<i>Rhamdia quelen</i>	juvenile	4	0.4 - 1.68	1.68

Finally, the effects on behavior are presented. The effect of 1.5, 0.8 and 0.3 mg/L during 180 minutes on the behavior of *Oreochromis niloticus* was studied by Xu *et al.* (2006). At 0.8 mg/L fish showed more active behavior than at 0.3mg/L. At 1.5mg/L fish stayed a longer time at the water surface, for aquatic surface respiration. Israeli & Kimmel (1996) studied the effect of 1 and 8 mg/L of dissolved oxygen during two trials of 50 minutes on behavior of *Carassius auratus*. In hypoxia conditions fish presented an ascendant displacement and a reduction in the swimming speed.

### 2.2.5. Effects of other parameters

In this subsection, the effects of other parameters such as turbidity, light color and intensity or pH are shown. Those parameters are less studied than the previous ones.

#### 2.2.5.1. Effects of light:

First, the effects of light, its intensity, and color are shown. Similarly, some papers about the coloration of the tanks are included. Generally, the light intensity depends on the meteorological conditions and the turbidity of the water. While the coloration of the water depends on the phytoplankton communities that can proliferate or the presence of some pollutants.

The effects of light on growth have been studied by several authors. It is possible make a division between light colour experiments, light intensity experiments, and the effects of tank or water colour. The effect of white, red and blue with 100 or 300 lux light during 158 days on *Cyprinus carpio* was studied by Karakatsouli *et al.* (2010). Under blue light they presented the lowest final weight, the light intensity had no effect. The effect of the light intensity and water coloration on larvae of *Gadus morhua* was studied by van der Meeren *et al.* (2007). Two different light intensities were used in combination with different water colours, green or clear during 33 days. No differences were found on SGR at different treatments. Monk *et al.* (2006) studied the effect of different light regimes on larvae of *Gadus morhua*. Fish were exposed to three different light regimes. The first regime consisted of 2200 lux during the whole period, the second on 2200 lux until day 24 and 600 lux until day 55. Tthe last regimen consisted on 2200 lux until day 36 and 600 lux until the end. The larvae that reached highest weight and length were the fish from the second treatment. Collett *et al.* (2008) studied the effect of 23-34, 163-204 and 270-315 lux on juveniles of *Argyrosomus japonicus* during 56 days. No differences were found on weight, FCR or FI under the different light intensities tested. The effect of tank colour on larvae of *Gadus morhua* was studied by Monk *et al.* (2008). Tanks of different



colourations, light walls and dark bottoms or dark walls and light bottoms were used. No growth differences were observed. Duray *et al.* (1996) studied the effect of two different colours (tan or black) on larvae of *Epinephelus suillus*. After 14 days the TL was significantly higher in the tan tanks.

Next, the effects of light on fish survival are shown. Monk *et al.* (2006) studied the effect of fluctuating light with intensities of 2200 lux and 600 lux on larvae of *Gadus morhua* exposed. No differences were found on the survival rates. The effect of the light intensity and the water coloration on larvae of *Gadus morhua* was studied by van der Meeren *et al.* (2007) during 33 days. The survival was higher in green water, no differences were observed on light intensities. The effect of tank colour (light/dark walls and dark/light bottoms) on larvae of *Gadus morhua* was studied by Monk *et al.* (2008). No differences on survival were observed. Duray *et al.* (1996) studied the effect of two different tank colour (tan or black) on the larvae stage of *Epinephelus suillus*. After 14 days no effects were found on survival rates. The effect of different light intensities, 0, 500, 1000 and 3000 lux on larvae of *Plectropomus leopardus* during 5 days was studied by Yoseda *et al.* (2008). No differences were found on survival rates. Cerqueira and Brügger (2001) studied the effect of 0 lux to 2500 lux on larvae of *Centropomus parallelus*. Higher survivals were related to light intensities from 200 to 1500 lux. Collett *et al.* (2008) studied the effect of 23-34, 163-204 and 270-315 lux on juveniles of *Argyrosomus japonicus* during 56 days. No differences were found on survival rates.

Finally, the tests based on the effects of light on fish behavior are shown. The effect of different light colours and intensities during 24 hours on larvae of *Melanogrammus aeglefinus* was studied by Downing and Litvak (2001). Under white light, the maximum feeding rate (3 preys per larvae approximately) was reached between 20 and 1500 lux. Under blue light, similar feeding rates were reached at only 80 lux. Under green light, the feeding rate was much lower. Juell and Fosseidengen (2004) pointed out that the swimming depth of *Salmo salar* was highly correlated to natural or artificial light intensity.

#### 2.2.5.2. Effects of turbidity:

Following the effects of turbidity are presented. The turbidity of the water depends on the presence of sediments or the planktonic communities. The concentration of sediments in the water can be related to the meteorological conditions and the increase of rains.

The effects of turbidity on growth are studied by a few authors. Sweka and Hartman (2001) studied the effect of maintaining juvenile of *Salvelinus fontinalis*. Fish were maintained at 10 different turbidity conditions from 0.85 to 44.75 NTU during 5 days. The higher the turbidity the higher SGR. The effect of 0 to 500 mg of sediment/L during 21 days on growth of *Erimonax monachus* and *Cyprinella galactura* was studied by Sutherland and Meyer (2007). *Erimonax monachus* had the highest SGR at 0mg/L while *Cyprinella galactura* had the highest SGR from 0 to 50mg/L. The effect of turbidity on larvae of *Stizostedion vitreum*, from hatching to 17 days, was studied by Rieger and Summerfelt (1997). The growth was faster in turbid water. Ardjosoediro and Ramnarine (2002) studied the effect of turbidity levels of 0 to 200 mg of clay/L on fry of red tilapia, [(*Oreochromis aureus* x *O. niloticus*)x(*O. mossambicus* x *O. hornorum*)]. After 56 days, the lower the turbidity the higher final weight. No effects were found on SGR or FCE.

Furthermore, the effects of turbidity on survival are presented next. Effects of turbidity on larvae of *Stizostedion vitreum* was studied by Rieger and Summerfelt (1997). The tests started at the moment of hatching and had a duration of 17 days. There were no differences in survival rates. Ardjosoediro and Ramnarine (2002) studied the effect of turbidity levels of 0 to 200 mg of clay/L on fry of red tilapia. After 56 days, the maximum survival rates were found at 0 and 50mg/L.

The effect of turbidity (0, 5, 20, 50 and 300mg of kaolin/l) on schooling behavior of *Plecoglossus altivelis*, *Engraulis japonicas* and *Seriola quinqueradiata* was studied by Ohata *et*

al. (2013). High levels of turbidity negatively affected the schooling formation of *Seriola quinqueradiata*, moderate turbidities had a positive effect on the schooling behavior of two other species.

### 2.2.5.3. Effects of pH

Lopes et al. (2001) studied the effect of pH from 5.5 to 8.5 on survival and growth of larvae of *Rhamdia quelen* during 21 days. The growth and survival was higher at pH of 8 and 8.5 than at other conditions. Heydarnejad (2012) studied the effect of pH on survival and growth on juveniles of *Cyprinus carpio* during 21 days. From pH 6 to 8.5 the survival rate was 100%. The highest mean weight was reached at pH of 8. The FCE was equally good at pH from 7.5 to 8.5. The effect of pH from 3 to 10.5 on survival of fry of *Rhamdia quelen* was studied by Zaions and Baldisserotto (2000) during 96h. The groups maintained at level of pH between 4 and 8.5 presented a survival of 100%.

## 2.2.6. Discussion on the effects of environmental parameters on fish

In this section, we are going to present some statistics about the most studied parameters and the most used species in the experiments. First, the data about the environmental parameters is shown in Figure 2.1. The most studied parameter, according to the number of papers collected, is the salinity with 27%, followed by photoperiod with 22% and temperature with 21%. The less studied one is the pH with only 3 papers. The most studied specie is *Salmo salar*, followed by *Anarhichas minor* and *Oreochromis niloticus*. From the 25 species that appear in more than one paper, 10 of them are aquaculture species with different levels of production. Alternatively, 7 species had aquaculture production at specific moment but they are not aquaculture species. Finally, the remaining 8 species, never had aquaculture production. It is possible to see that most of this research is performed with aquaculture species, because of the high commercial interest. Regarding to species habitat, 16 of those species belong to saltwater habitat and 9 species belong to freshwater. This reflects that the majority of the efforts are made with species from marine environment, linked to production in sea cages. If we look at only to the top 10 most used species, only one is not related to aquaculture, the *Anarhichas minor*.

From this point, the statistics are related to the number of experiments provided instead to the number of published papers, because one paper can include data from growth and survival or various stages of development. More information can be obtained if we pay attention to the development stage of fish used in the test and the observed effects. For growth studies, we can analyse the development stage of fish used in the test, see Figure 2.2. Different colours represent different stages of development and solid or striped sections mean authors have found an effect or have not found an effect. For growth studies, the most used fish were juvenile, followed by larvae. In studies where fry, smolt or post-smolt fish were used, in 100% of cases authors found a correlation between the studied parameter and growth. In experiments with juvenile fish, in 55% of the experiments, in the majority of cases there exists a relation between environmental parameters and fish growth (47% in total). Only in 8% of the cases authors did not find a correlation. While for larvae fish, 32% of the growth experiments, authors found out a correlation in 27% of total growth studies. Only in 5% of the cases authors did not. Regarding to the studied parameters in relation with fish growing and their effects, see Figure 2.3, temperature, salinity and photoperiod are the most studied ones. Experiments that focused on temperature, turbidity or pH found a correlation in the 100% of cases. The experiments with different salinities represent the 28% of total growth studies. In 24% of those experiments, authors found a correlation and in 4% they did not. The studies where authors did not find a correlation were made with *Anarhichas minor* maintained at low salinities (Foss *et al.*, 2001). The other experiments with N.E. are performed with *Centropomus parallelus* during low period at low salinities. The same authors demonstrated that for longer periods growth is affected by salinity (Person-Le Ruyet *et al.*, 2006). Concerning the photoperiod experiments, 27% of total growth studies, in 18% of these authors found an effect and 9% did not. In the case of dissolved

oxygen, studied in 14% of the growth test, in 12% of those tests authors found effects on fish growth. However, in the remaining 2% of the test, authors did not find a correlation. The test where authors did not find any relation was the test with juveniles of *Scophthalmus maximus* (Person-Le Ruyet *et al.*, 2002) in supersaturation conditions. However, in a similar experiment performed with smaller *Scophthalmus maximus* with different oxygen concentrations, show that the changes in dissolved oxygen have an effect on fish growth. (Pichavant *et al.* (2001).

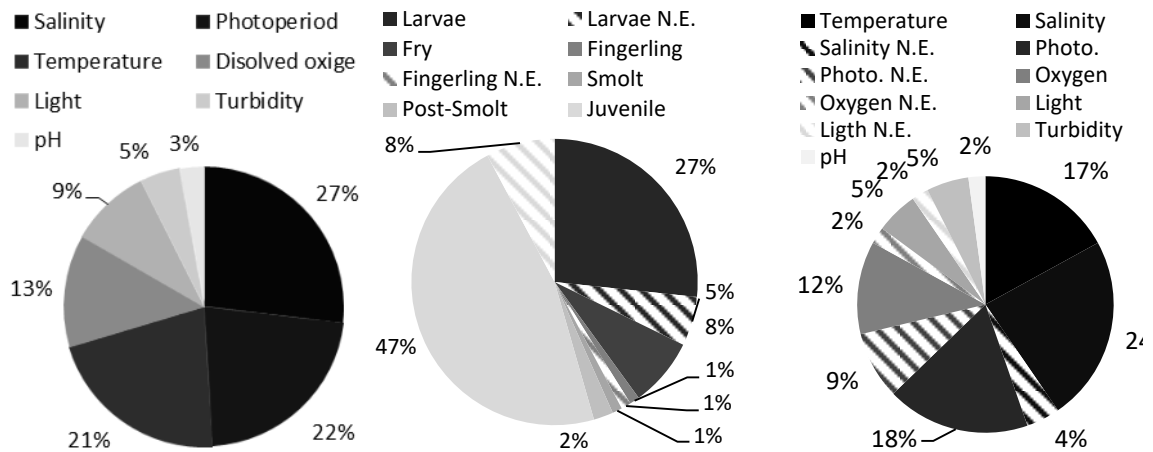


**Figure 2. 1** Studied factors for all the effects **Figure 2. 2** Stage of development of fish tested in growth studies and its susceptibility to changes **Figure 2. 3** Studied factors in growth tests and effects

We are going to focus on the experiments where authors found effects on growth. For photoperiod, authors found out that on species such as *Salmo salar* and *Oncorhynchus mykiss*, natural changes during the year enhance growth (Cerqueira & Brügger, 2001), (Handeland & Stefansson, 2001), (Taylor *et al.*, 2006). However, species such as *Oreochromis niloticus*, *Pagrus major* and *Scophthalmus maximus* reach the maximum growth under permanent light (24L:0D). While *Amphiprion melanopus* reach under long photoperiods (16L:8D) (Watanabe *et al.*, 1995), (Biswas *et al.*, 2006), (Imsland *et al.*, 1997) and (Arvedlund *et al.*, 2000). Regarding to dissolved oxygen, from the 11 studies developed where authors found a relation, 7 of them are made to evaluate the effect of low oxygen concentrations. In those cases, the best growth is always related to higher oxygen concentration. In all the studies fish present the maximum growth between 5.6 and 7.4mg/l, nevertheless those are values of mild hypoxia. It is expected that at higher concentrations fish present higher growth. No big differences are found between optimal values of different fish species. The other experiments were made with fish kept at high and low dissolved oxygen concentration, to analyse the compensatory growth. Authors found that the maximum growth is correlated with 9.6mg/l. Under hypoxia, fish present a compensatory growth but not under hyperoxia (Foss *et al.*, 2012), (Foss *et al.*, 2013) and (Foss and Imsland, 2012). The studies with salinity demonstrate that unlike the oxygen concentration each species presents its own optimal salinity value. As is expected with freshwater species, the less the salinity the higher growth. Nevertheless, some species that are saltwater fish present their maximum growth at lower salinities than was expected. *Hippoglossus hippoglossus* or *Sparus aurata* are a good example, both of them have their optimal growth at 15 and 12 PSU respectively (Imsland *et al.*, 2008) and (Laiz-Carrión *et al.*, 2005). Those values are far away from the salinity values where they are usually maintained in aquaculture. For this reason, it is very important to have the chance to change the salinity in aquaculture facilities. The tests with temperature, point out the same as salinity tests, each species presents its optimal value of

temperature. However, it is possible to group fish in cold water fish of warm water fish. *Pollachius pollachius*, *Anarhichas minor* and *Salmo salar* reach its maximum growth at temperatures lower than 12°C (Person-Le Ruyet *et al.*, 2006): (Imsland *et al.*, 2006) and (Handeland *et al.*, 2008). *Anarhichas minor* presents the lowest optimal temperature at 6°C (Imsland *et al.*, 2006). On the other side, the group with higher optimal temperatures presents the maximum growth at temperatures between 22 and 28°C (Wang *et al.*, 2009), (Sun *et al.*, 2006), (Person-Le Ruyet *et al.*, 2004) and (Van Ham, 2003). The effect of light was studied only in a few tests. With species such as *Cyprinus carpio*, authors demonstrated that with small fish red light enhances the growth. However, with bigger fish (up to 51.88 g) no effects have been found (Karakatsouli, 2010). Turbidity has a clear negative effect on the studied species, *Erimonax monachus*, *Cyprinella galactura* and *Salvelinus fontinalis* (Sutherland *et al.*, 2007) and (Sweka *et al.*, 2001). In all the studies, growth decreases as the turbidity decrease.

For survival studies we can analyse the development stage of fish used in the survival test, see Figure 2.4. As in Figure 2.2, different colours represent different stages of development, while authors found or not an effect is represented in solid or striped sections. Unlike the growth studies, the survival studies are focused on the first stage of development, eggs (15% of total survival studies) and larvae (44% of survival studies). The studied environmental parameters in eggs were only salinity and temperature. Juvenile fish were used in 28% of the studies, only in 14% of the experiments authors found a correlation between the studied parameter and the survival. All the studies performed with larvae exposed to different salinity or temperature conditions show a clear relation between those factors and larval survival. The sole experiment performed with different turbidity values shows no relation between turbidity and larval survival. In juvenile fish, the parameters that affect all the studies were dissolved oxygen and temperature. Regarding to the analysed parameters on survival experiments, see Figure 2.5, the most studied parameter is the salinity (33%). The temperature, used on 22% of survival experiments, it is highly correlated with survival. In all the experiments authors found a correlation. The photoperiod, 26% of the experiments, produce effects only in 9% of the total while in 17% does not produce any effect.

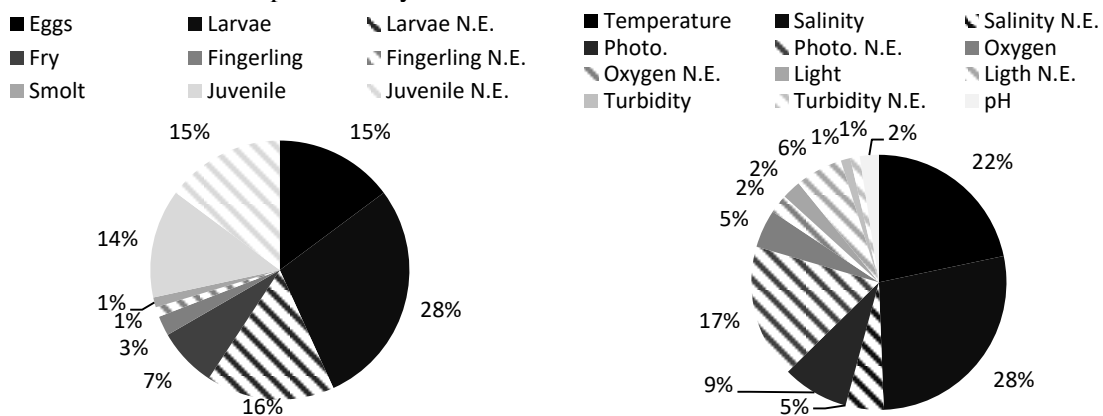


**Figure 2. 4** Stage of development of fish tested in survival studies and its susceptibility to changes **Figure 2. 5** Studied factors in survival tests and effects

In continuation, we are going to focus on the experiments where authors found survival relation with studied environmental parameters. For photoperiod, authors found that species such as *Oreochromis niloticus*, *Seriola lalandi* and *Salminus brasiliensis* reach higher survival rates under continuous light conditions (El-Sayed & Kawanna, 2004), (Stuart & Drawbridge, 2012), (Schütz & Nuñez, 2007). In the case of *Oreochromis niloticus* the study was performed with fish of different sizes and only the smaller fish, 0.02 g, presented this relation between

photoperiod and survival. Similar relation was found with *Miichthys miiuy*, their maximum death rates were related to continuous dark conditions. Nevertheless, no differences were observed in other photoperiods (Shan *et al.*, 2008). On the other hand, *Clarias gariepinus* presented its maximum survival rates under continuous dark conditions (Adewolu *et al.*, 2008). Other fish such as *Huso huso*, had its optimum photoperiod in 12L:12D. In those conditions juveniles reach their maximum survival rates. The changes on photoperiod can also affect the survival rates on *Salmo salar*. In A simulated winter experiment after the fish are moved to the sea, we can see an increase in mortality (Sigholt *et al.*, 1995). Different species present different preferences of photoperiod. The study with different oxygen concentrations with juveniles of *Rhamdia quelen* points out that it can resist the low oxygen concentration without decreasing the survival until 1.68 mg/L (Braun *et al.*, 2006). Alternatively, the experiments with salinity where authors found a correlation are detailed now. In general terms, the typical freshwater species have higher survival rates at lower salinities. The *Fugu obscurus* which is euryhaline fish maintain its high survival rates from 8 to 18 PSU. The majority of saltwater species present their higher survival rates between 25 and 35 PSU. But, there are some species that present the maximum survival between 15 and 0 PSU and are common in oceans (Resley *et al.*, 2006), (Zhang *et al.*, 2010a). There are some studied species such as *Rachycentron canadum*, *Takifugu flavidus* or *Argyrosomus japonicus* that present the best performance at different salinities, according to the stage of development. *Rachycentron canadum* present the highest survival at low salinities after hatching (between 0 and 3 PSU). However, as the fish gain weight survival at higher salinities increases, reaching the same effects on survival from 15 to 30 PSU (Faulk & Holt, 2006), (Resley *et al.*, 2005) and (Denson *et al.*, 2003). The same effect was found in *Argyrosomus japonicus*, that presents a lower tolerance to high salinity in larval stage. The highest survival rate is related to 5PSU. Then, juvenile fish present the highest survival at 12.5PSU (Fielder & Bardsley, 1999). Finally, *Takifugu flavidus*, have the maximum survival rates at 10 PSU during the egg and hatched stage and at 25 PSU during larval stage (Zhang *et al.*, 2010a). There is a pattern in those species, the initial development stages needs water with lower salinity. The opposite tendency is found in the specie *Paralichthys orbignyanus*. The eggs presented the highest survival rates at 35 PSU while the larvae reached highest survival rates at 30 PSU (Smith *et al.*, 1999), (Sampaio *et al.*, 2007).

The optimal temperatures, where fish show maximum survival rates goes from 8°C in the case of juveniles of *Anarhichas minor*, larvae of *Hippoglossus hippoglossus*, and eggs of *Pollachius pollachius* to 36°C in the case of larvae of *Oreochromis niloticus* (Hansen & Falk-Petersen, 2002), (Faulk & Holt, 2006), (Suquet *et al.*, 2004) and (Baras *et al.*, 2001). A described for salinity, one specie can have different survival rates for the same salinity at different stages of development. The eggs of *Abramis brama* present the highest survival rate at 18.5 °C while the larval stage reaches this at 28 °C (Kucharczyk *et al.*, 1997). The survival of *Abramis brama* at high temperatures increases with the age of the fish. The opposite effect can be found out in *Oreochromis niloticus*, the larval stage has the highest survival rates between 26 and 35°C but the fry fish achieve this at 26°C (Baras *et al.*, 2001) and (Azaza *et al.*, 2008). In this case, higher survival rates at high temperatures seem to be reduced such as the fish growth. (as the fish grows)?? The effect of light and other parameters are explained below. Larvae of *Gadus morhua* were affected by light intensity, larvae present higher chance of survival at lower light intensities (van der Meer *et al.*, 2007). Contrastingly,, larvae of *Plectropomus leopardus* present the maximum survival rate at 1000lux (Yoseda *et al.*, 2008). Larvae of *Centropomus parallelus* present 0% of survival under dark conditions, and a relatively good survival rate from 200 to 2500 lux (Cerqueira & Brügger, 2001). The larvae are also sensitive to the tank color. *Epinephelus suillus* has higher survival rates in tan tanks (Duray *et al.*, 1996). All these variations are related to hunting strategies, some fish only use their visual sense to hunt such as *Centropomus parallelism*, and under dark conditions they are unable to feed. While other species such as *Gadus morhua* are able to use other senses. This explanation is the same for the experiments with different turbidity levels. Both, turbidity and light intensity can hinder the

successful hatching of fish. However, the effects of turbidity may depend on the type of particles that causes the turbidity. Turbidity caused by green algae has a positive effect on larvae (van der Meeren *et al.*, 2007). Finally, the effect of pH was studied on *Rhamdia quelen* and *Cyprinus carpio*. The larvae of *Rhamdia quelen* presented highest survival rates at 8 and 8.5pH. However,, the fry of *Rhamdia quelen* have a higher tolerance and present the same survival from 3.8 to 8.5pH (Lopes *et al.*, 2001), (Zaions & Baldisserotto, 2000) and (Heydarnejad, 2012). The effect of pH was only studied on freshwater fish.

For natatorium behavior studies, we can analyze the development stage of fish used in the experiments, see Figure 2.6. Different sections represent different stages of development and the striped or solid section indicates that authors found or did not find an effect. In 50% of the tests larvae fish were used and juvenile fish on other 50%. In all the cases, the behavior was related with the studied parameter. Regarding to the studied parameters and their effects, see Figure 2.7, oxygen, temperature, light and turbidity were analyzed.

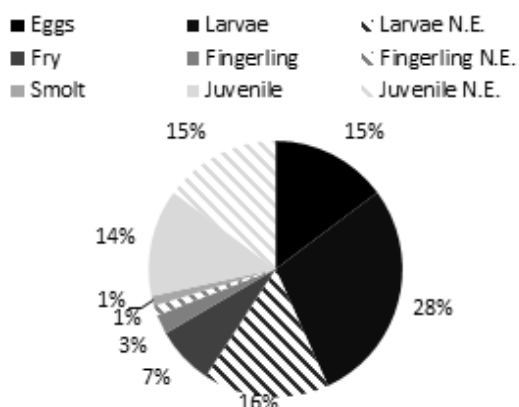


**Figure 2. 6** Stage of development of fish tested in behavior studies and its susceptibility to changes

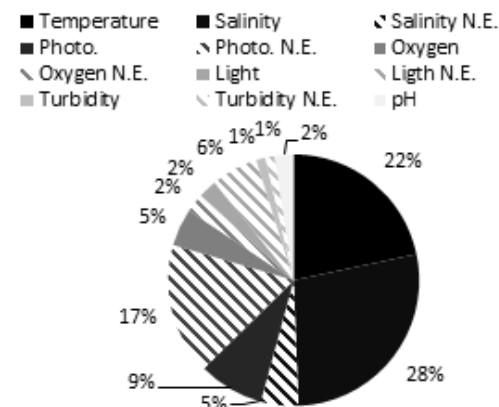


**Figure 2. 7** Studied factors in behavior tests and effects

All the studies using different oxygen concentrations point out that the behavior of fish changes according to the oxygen concentration. The observed behavior is an ascendant movement of schooling under low oxygen concentration (Xu *et al.*, 2006) and (Israeli & Kimmel, 1996). The changes on temperature were evaluated in one experiment. The results show that behavior was related with temperature, but also with social patterns. In the studies with light, authors found out that under different light fish exhibit different natatorium profundities (Juell & Fosseidengen, 2004). Finally, turbidity is related to the schooling formation and its effects may be positive or negative according to the affected species.

### 2.3. Physical sensors for water quality monitoring for precision aquaculture

In this section, we present a review of the existing technologies for water quality monitoring. First, we show the requirements of the sensors that are going to be used for aquaculture monitoring. Following, we expose the current options for monitoring for of the most important parameters: temperature, salinity, dissolved oxygen, and turbidity. Those parameters correspond to the factors analyzed in the previous section. However, as the photoperiod and light are measured above the water they are not included in this survey. The pH is not included because there is not yet a clear relation with the growth or survival of fish.

### 2.3.1. Requirements of aquaculture sensors

In this section, the requirements and challenges for the sensors that will be used for precision aquaculture are shown. Although WSN are widely used in a variety of different areas for terrestrial applications, such as health monitoring (Alrajeh et al., 2014), disaster prevention (Chen et al., 2013) and precision agriculture (Lloret et al., 2011a), their use in the marine environment is still limited. As explained before, this underuse is caused by the special water attributes, the high cost of underwater sensors and failures because of the harsh environment. Battery issues and the difficulties of energy harvesting, telecommunication problems and sparse deployment are some of the challenges for the UWSN (Yick et al., 2008). However, some low-cost underwater sensor proposals have been developed in the last years. To ensure suitability for aquaculture facilities, these sensors have to fulfil certain requirements. Different papers have already described the challenges for UWSN (Heidemann et al., 2012). However, applying UWSN in of the field of aquaculture has some peculiarities which are addressed below.

First, the sensors have to be able to sense data over longer periods without having to be cleaned, maintained or replaced. The sensors in the fish farm will be deployed at different points. If sensors require attention, it would be necessary to allocate divers for maintenance tasks. Some sensors may be placed in hard to reach places. Therefore, a sensor that needs daily calibration or weekly cleaning would not be suitable for long-term monitoring, which renders all chemical sensors, as they require periodical calibration, unsuitable. Sensors with membranes or electrolytes that need replacements should also be avoided.

Second, the sensor nodes have limited battery power and the signal transmission consumes a great percentage of it. It is therefore important that the sensors have low energy demands to ensure long-term monitoring. If different options are available to measure the same parameters, it is important to select the option with low energy consumption. Periodical battery changes should be avoided for the same reason as explained above for cleaning or maintenance. Reducing energy consumption is essential, also in terms of communication, such as using energy-efficient protocols.

Third, seawater is a harsh environment. Salinity can cause corrosion and the currents can move the sensors and cause collisions. It is therefore important that the sensors are robust and have a protective layer. To prevent corrosion, the layer and any sensing part that will be in contact with the water must not contain any metallic materials. Therefore, the use of plastics and methacrylate is recommended (Harnett et al., 2008). Waterproof insulation must be ensured. Depending on the depth, different options can be used, from simple waterproof silicone to special O-rings. In some cases, the use of deflectors or other structures to ensure proper orientation of the sensor with the changing currents of after collisions have to be considered.

Fourth, it should be noted that the sea is full of organisms (phytoplankton, zooplankton, macroinvertebrates, algae and fish) which can alter the sensors. In the open sea, the available surface for living beings is limited. Every object that remains in the water will be subjected to biofouling. Different organisms, from microorganisms to macroinvertebrates, will colonise every submerged surface, resulting in alterations in the buoyancy, the shape and the size of the sensor package. Some microorganisms can alter the sensor surface via biocorrosion and change the transparency and colour. Dead plankton can be deposited on the package; hence, the potential light path must be properly designed. Several sensors are based on optical effects and need a light path on their packages. Those transparent sections should be placed in a proper orientation to avoid deposition and biofouling. Photosynthetic organisms can generate oxygen bubbles that modify the light beam in optic sensors; in this case, sensors based on light effects should be avoided.

Macroinvertebrates will tend to use the nooks and crannies of the devices as hiding places, which might cause obstruction of the water current, therefore causing a reduction of the water exchange. In this case, the data may not represent the value of the surrounding water. If the sensors must be placed in a nook, is recommendable to add a grating to prevent

macroinvertebrates from entering. The material of the grating must withstand biofouling and corrosion to ensure long-term operation.

Fish can hit or bite the packages and therefore, fragile and soft parts should be covered. Fish such as *Sparus aurata* usually present biting behavior in fish farms, related to different stress sources. This is also the case for *Pomatomus saltatrix*, a common predator. Such behavior has been related to net holes (Moe et al, 2007, Sanchez-Jerez et al., 2008). To avoid damage caused by fish bites, the recommendation is to use packages with a spherical shape and with a diameter larger than the mouth of the fish. Thus, if spherical shapes are used there will be no points that stand out or edges in the package where the fish can bite. Another recommendation is to use dissuasive measures as sharp shapes in the sensors placed out of the net.

The fifth consideration is focused on the effects that sensors may cause on the fauna. It is important to ensure that no harmful effects on fish and other living beings are generated. We need to consider that compared to other sensor applications, in fish farm monitoring, this is critical, as the animals cannot move away from potential harmful effects. For this reason, some sensing techniques must be avoided, in particular sensors that use (i) ultraviolet light (UV), (ii) acoustics beams that can be felt by fish and (iii) magnetic fields that disturb their activity. The UV light can reduce growth rates in larvae and diminish its immune function (Häder et al, 2011). The acoustic beams that produce high sound levels cause damages in the sound sensors cells, which can produce hearing loss (Popper et al., 2003). Moreover, there are fish species that are magneto-sensitive (Öhman et al., 2007). It is important to ensure that the sensors do not alter fish swimming and feeding activities. Moreover, we need to ensure that sensors do not attract surrounding fauna, which can modify fish behavior and produce stress. It is therefore crucial to test the potential harmful effects of the proposed sensors under laboratory conditions before using them on site.

Another problem of UWSN is the location of the sensor itself (Han. et al., 2015). In sensors, such as current meters, the ability of the sensor to move and get oriented is needed. In this case, deflectors can be used to orient the sensor with the current. On the other hand, there are sensors that need to be in a fixed position with a specific orientation, avoiding any movement. Therefore, it might be necessary to include an anchor system. Although these systems can be added after the creation of the sensor, it is important to consider whether there is a need to have a fixed location. Devices with moving parts should be avoided, as such parts are susceptible to clogging.

Finally, sensors suitable for aquaculture and, generally, for marine monitoring, are relatively expensive (Partan et al., 2007). The costs of fabrication, deployment and recovery are significantly higher than those for terrestrial applications. In terrestrial applications, generally, the sensors are spread in the horizontal plane, while in marine monitoring; they are spread in the horizontal and the vertical planes, requiring the use of more sensors. It should be expected that a percentage of the total placed sensors are lost as a result of e.g. shock rupture or taken by the flow, which makes replacement from time to time necessary.

In summary, underwater sensors must be low maintenance, low cost, low battery consuming, robust, waterproof, non-metallic, withstand biofouling and have no effects on organisms. If possible, optical sensors should be avoided. It is important to study the threshold values of the hearing ability of fishes and the effects of magnetic fields.

On the other hand, there are some advantages compared with other applications, mainly the fact that high accuracy is not important. While for other applications, high accuracy is needed, in aquaculture, the level of required accuracy is lower. Assuming that the sensors will be used for water monitoring to determine fish needs, a change of 0.01°C or 0.01 PSU will not affect the fish. It is, however, important to study in detail the minimum variation of different parameters that affect fish.

Another advantage is that no minimised systems are needed. In other applications, such as in e-health, small sensors are important to minimise potential discomforts, but this is not the case for aquaculture. The use of large sensors is even recommended, as small ones are easily



lost and can be eaten by fish. Fish such as *Dicentrarchus labrax* do not exhibit biting behavior, but can eat the entire device.

### 2.3.2. Temperature

This section discusses the different temperature sensors. Water temperature is mainly a factor of solar radiation and shows spatial and temporal variation. Annual cyclical changes are necessary for the correct sexual development and reproduction of fish (Pankhurst et al., 1996). The temperature is stratified along the water column and along the earth's surface. For aquaculture, water temperature is the most important water parameter because it is highly correlated to fish performance. The effect of temperature has been studied by several authors. Sander *luciooperca* presents the highest growth at higher temperatures (Wang et al., 2009) while *Oreochromis niloticus* presents its maximum survival rate at 32°C (Azaza et al., 2008). In marine fish farms, the changes in water temperature are related to annual cycles, meteorological conditions, changes in currents and climatic change. In the inland facilities with open water circuits, the temperature changes can be higher than in marine fish farms. Nevertheless, heat exchange can be used to control the temperature.

There are several techniques for temperature sensing, which mainly fall into the two categories electric devices and non-electric devices. Electric devices need to be in contact with the sensed object, and the thermocouples are based on the Seebeck effect. They are composed of two different, connected metal conductors, usually made of copper, nickel, iron, platinum, rhodium and different alloys. Thermocouples are inexpensive, small and highly robust (Childs et al., 2000). Although they present low accuracy. They are used for several applications, even for water temperature monitoring as Dickson (1994) does.

The resistance of conductor materials (such as copper, gold, nickel, platinum or silver, among others) changes with the temperature. The resistance temperature device (RTD) has a higher accuracy than thermocouples, and the sensing range depends on the used material, i.e. from –100 to 100°C for copper (Childs et al., 2000). Two different RTDs are available on the market; RTDs with higher accuracy made of platinum and RTDs commonly known as thermistors. The platinum resistance thermometers (PRT) have a platinum coil wired over a glass made of quartz or mica. The PTR is mainly used to measure the water temperature of air conditioner systems. There is a linear relation between resistance and temperature and it is relatively stable. An increase in temperature produces an increase in resistance.

On the other hand, the thermistors are characterized by less accuracy, with a positive or a negative relation between resistance and temperature, depending on the material. They are known as negative temperature coefficient (NTC) or positive temperature coefficient (PTC). The NTC is commonly used for water temperature sensing (Rayne et al., 2008), water heating systems (Vieira & Mota, 2009). The PTC is used for water temperature monitoring (Nikolic et al., 2013).

Semiconductors, such as transistors or diodes, can also be used for temperature sensing. They are useful for sensing temperatures between -55 and 150°C, with an accuracy higher than 1°C. Their operation is based on the p–n junction and the temperature dependence of the forward voltage drop. Diode thermometers are widely used because the relation between temperature and voltage drop is almost linear. Two of the most used semiconductors are Si and GaAs. While Si diodes are cheaper, GaAs diodes have a higher output. There are different examples of applications of diodes for water temperature sensing as was done by Emery et al. (2012).

Another option for temperature sensing is the use of a capacitance thermometer. Some materials, such as strontium titanate, present different electric permittivity at different temperatures. Capacitance thermometers present the maximum accuracy at temperatures of 100 K or lower and are used for applications with low temperatures or the presence of high magnetic fields, but are not suitable for water temperature sensing. Less common sensing methods are the

noise thermometry or the use of quartz thermometers. Noise thermometry is based on the thermal fluctuation of conductor materials and used for ultra-low temperatures in the millikelvin range (Lusher et al., 2001). Quartz thermometers are based on the vibration frequency of piezoelectric materials, with a sensing range from 4.2 to 500 K (Rubin, 1997); they are mainly used for cryogenic measurements (Pavey et al., 2003).

In contrast, non-electronic devices make use of the thermal expansion of materials with temperature. Based on the thermal expansion, it is possible to distinguish gas, the liquid-in-glass thermometers and the thermal expansion of solids. However, it is difficult to use this principle to create a sensor. In recent years, several chemical compounds have been discovered that present different colorations under different temperatures. Thermochromic liquid crystals can be extended over a surface, forming a thin film. The temperature produces reversible changes in their coloration and they are used when the range of temperature variation is limited and high accuracy is needed, e.g. for medical applications (Chik et al., 2013) or the study of heat transfer in microscopic electronic components (Segura et al., 2015). Thermographic phosphors are characterized by changes in their light emission at different temperatures (Khalid & Kontis, 2008) and enable to measure from cryogenic levels to 2,000°C and offset sensitivities of 0.05°C, with an accuracy of 0.1–5% (Childs et al., 2000). They are used for several applications, including heat transfer in engines (Fuhrmann et al., 2013). Heat-sensitive paints are temperature-sensitive crystalline solids, and the changes of coloration are not reversible. They are used for several applications, such as the detection of boundary layer transition for aerodynamic profile tests (Klein et al., 2013)

These three different groups of chemical compounds are, however, not suitable for aquaculture monitoring. Their principal characteristic is the high precision, a characteristic that is not needed for our purpose. These chemical compounds must be sprayed over a surface and need to be in contact with the sensed objective. One of our requirements is to avoid, if possible, the contact between the sensing element and the water. Moreover, the degradation and the price of these materials render them unsuitable for our purpose.

Sensing techniques that do not require contact with the sensed medium are based on changes in electromagnetic radiations of an object at different temperatures. Different techniques are used for different temperature ranges. Infrared thermography can be used from 50 to 6,000 K. The infrared spectrum is composed of wavelength from 0.75 to 1,000  $\mu\text{m}$ . Different materials can be used to detect IR emissions, and this method is used for different purposes. Nevertheless, it is required that the sensor package has an optical window between the sensed element and the IR detector. As discussed above, optical solutions should be avoided when other options are available. Other methods based on the measurement of the electromagnetic spectrum are available, but they are only suitable for higher temperatures. Acoustic thermography is another option to measure the temperature of liquids and works with frequencies lower than 100 Hz. The speed of sound in water depends on the water temperature (Childs et al., 2000), and sound propagation is higher in warm water than in cooler water. Acoustic thermography can be used for different purposes, even for detecting changes in deep-ocean temperature (Woolfe et al., 2015). Its use has been described for deep oceans where other methods are not suitable. However, the equipment is expensive and requires an acoustic emitter and a receiver. Its use in shallow waters is not extended because of the existence of other options. Compared with the use of electric devices, acoustic thermography and infrared thermography are more expensive and have a higher energy consumption.

The best option for temperature monitoring in water is the use of electric devices, especially the RTD or the thermistor. Those sensors need to be in contact with the sensed medium, the water. Although our requirements include the need to avoid contact between the sensor and the water, they are the best option. There is a possibility to use a heat conductor package for the electric device. Therefore, we isolated the sensor, avoiding many problems. The RTD and

thermistors have a high working range, adequate accuracy, and low price. Table 2.10 shows some of the commercial devices for temperature monitoring in underwater environments. Several companies offer different solutions for temperature monitoring. The RTDs and thermistors seem to be the most common solutions.

**Table 2. 10** Commercially available sensors for temperature monitoring

Type of sensor	Fabricant	Range (°C)	Reference
Thermistor	In-Situ Inc	-5 to 50	(Aqua TROLL 400, 2017)
Thermistor	In-Situ Inc	-5 to 50	(Aqua TROLL 600, 2017)
Thermistor	In-Situ Inc	-5 to 50	(smarTROLL RDO, 2017)
Thermistor	In-Situ Inc	-5 to 50	(smarTROLL, 2017)
Thermistor	In-Situ Inc	0 to 50	(RDO Titan, 2017)
Thermistor	In-Situ Inc	-5 to 50	(TROLL 9500, 2017)
Thermistor	Eureka water probes	-5° to 50	(Eureka Manta2 Temp, 2017)
Thermistor	Aquatec Group	- 2 to 30	(AQUAlogger 520, 2017)
Thermistor	Aquatec Group	- 2 to 30	(AQUAlogger 530, 2017)
Thermistor	Aquatec Group	- 2 to 30	(AQUAlogger 540, 2017)
Thermistor	OTT	- 5 to 50	(OOT Temp, 2017)
No Information	Saiv A/S	- 2 to 40	(TD301/TD303, 2017)
No Information	Saiv A/S	- 2 to 40	(SD204, 2017)
No Information	Saiv A/S	- 2 to 40	(SD208, 2017)
NTC	SEBA	-5 to 50	(MPS-D3 type, 2017)
NTC	SEBA	-5 to 50	(MPS PTEC, 2017)
NTC	SEBA	-5 to 50	(MPS-K16/Qualilog16, 2017)
NTC	SEBA	-5 to 50	(MPS-D8/Qualilog8, 2017)
Thermocouple	Hanna	max 450	(HI766B1, 2017)
Thermistor	Hanna	-50 to 150	(HI762W, 2017)
Thermocouple	Hanna	max 250	(HI766TR1, 2017)
Thermocouple	Hanna	max 900	(HI766E1, 2017)
Thermocouple	Hanna	max 900	(HI766PE1, 2017)
Thermistor	Hanna	-50 to 150	(HI765P, 2017)
Thermistor	Hanna	-50 to 150	(HI762L, 2017)
No Information	Hanna	-5 to 50	(HI9829, 2017)
No Information	YSI	0 to 45	(5200A Multiparameter, 2017)
No Information	YSI	0 to 45	(5500D MultiDO t, 2017)
No Information	YSI	0 to 45	(5400 MultiDO, 2017)
Thermistor	INW TempHion	-5 to 70	(T1/T1R, 2017)
Thermistor	INW TempHion	-5 to 40	(CT2X, 2017)

### 2.3.3. Salinity

Salinity in water is related to the presence of different ions. It is also known as electric conductivity (EC) and usually expressed in Siemens per meter (S/m), practical units of salinity (PSU) or mg/l. The value of the EC is related to the salinity and the total dissolved solids (TDS). For aquaculture, EC is a critical parameter, and changes in salinity result in alterations of fish growth and survival survival (Rubio et al., 2005; Resley et al., 2006). In marine facilities, water stratification, atmospheric changes and water currents can modify the regular values of salinity. Those facilities will need to control the salinity at different points in the horizontal and the vertical planes. Therefore, the sensors must be adapted to different pressures. In inland facilities, it is easier to monitor water EC in input pipes.

Water density, light refraction and electrical conductivity are the three physical parameters related to salinity (Postolache et al., 2012). The measuring of water density using a precise

vibrating flow densimeter was widely used in the 1970s and 1980s in oceanographic studies. However, other techniques, based on light refraction or on EC, have become more practical over time and currently, no salinity sensors based on a precise vibrating flow densimeter can be found. The optical methods are based on the correlation between the refraction angle of an incident beam of light and the water salinity. When a light beam travels from reference water to sample water, the light has a refraction effect. Recording the point where the beam impacts, it is possible to know the salinity of the water sample. Based on this effect, several authors present different sensor proposals (Zhao et al., 2009; Zhao et al., 2002; Esteban et al., 1999; Zhao et al., 2003), distinguishing salinities from 0 to 50 PSU. Their range of measurements meets the requirements of salinity sensors for aquaculture. However, in the underwater environment, this system is not the most appropriate one because of the need to maintain a clean crystal surface. As mentioned before, there are several problems, such as biofouling, sediment precipitation and oxygen bubbles, which will impede the use of optical systems.

There are two options to measure EC, the conductive and the inductive method, of which the conductive method is the most used one and based on the water resistivity. Two or more electrodes are used to calculate the conductivity. The conductance,  $G$ , is the reciprocal of the electrical resistance,  $R$ , as shows (Eq. 2.1). While the conductivity,  $\sigma$ , depends on the resistance and on the cell constant,  $Kc$ , it has to be calculated for each design (Eq. 2.2). The  $Kc$  depends on the length of the electrode,  $l$ , and the area of the electrode,  $A$  (Eq. 2.3.). Based on this theory, different designs appear. The simplest design is based on two electrodes (Russ et al., 2010). However, the design with two electrodes can cause water polarisation. For this reason, other authors have used more electrodes, and the design using four electrodes seems to be most common (Ramos et al., 2005; Ramos et al., 2008). Other designs use six electrodes (Brown et al., 1988). Some authors, based on the electrode design, create a small cell with a microfluidic channel and microelectrodes (Gong et al., 2008; Huang et al., 2011; Kim et al., 2013). However, the main issue with this methodology, in the case of aquaculture monitoring, is the requirement that the electrodes stay in contact with the water, which can cause corrosion, biofouling and sedimentation, thereby altering the  $Kc$ . In aquaculture systems, such electrodes would require continuous cleaning and are therefore not suitable.

$$G = \frac{1}{R} \quad (2.1)$$

$$\sigma = Kc \times G \quad (2.2)$$

$$Kc = \frac{l}{A} \quad (2.3)$$

The inductive method is based on the use of two coils. The first coil is powered by an alternating current and generates a magnetic field. The intensity of the magnetic field is modified by the medium and the generated electric field. In the secondary coil, the magnetic field induces an electric field that can be correlated to the water salinity. As in the conductive method, different designs appear. The simplest one is formed by two one-turn coils (Kleinberg et al., 1989). The use of two toroidal coils was the most studied approach and is presented in different publications (Pham et al., 2008; Wood et al., 2010). Although this methodology is less used it presents some advantages, mainly the possibility to isolate the sensing element, the coils, from the water.

For these reasons, the use of the inductive methodology to measure EC is the best option for salinity monitoring in fish farms. It is a cheap method, highly accurate and its measurement range fits with the requirements of aquaculture facilities. The devices can be isolated from the environment and at the used frequencies, no harmful effects on fish have been detected. Table 2.11 shows some of the currently used commercial sensors, of which the majority are based on electrodes. Nevertheless, an inductive sensor can be obtained from DPF sensors.

### 2.3.4. Dissolved oxygen

Dissolved oxygen is a measure of the concentration of oxygen in the water. For aquaculture, dissolved oxygen measurement is crucial. For adequate fish development, a minimum oxygen concentration is required, depending on the fish species. The negative effects of hypoxia on fish growth have been widely demonstrated by several authors, e.g. Tran-Duy et al. (2008) for *Oreochromis niloticus* or Ciuhandu et al. (2005) for *Oncorhynchus mykiss*. The concentration of oxygen in the water is a result of the equilibrium with the oxygen in the atmosphere, representing oxygen solubility, which depends on the pressure, salinity and temperature (Garcia and Gordon, 1992). The reduction of dissolved oxygen is caused by the presence of organisms (respiration and decomposition of organic matter by bacteria) and by some chemical reactions. On the other hand, the increase of oxygen concentrations is caused by photosynthesis. In marine facilities, a reduction of oxygen concentration under normal conditions is not common. However, some situation, such as an algae bloom, can produce a high oxygen demand during the night. In inland facilities, some adverse situations can cause a reduction of oxygen concentrations in shallow waters. Those situations are generally associated with high temperatures. In addition, some situations in aquaculture require the water to be kept in the tanks during long periods, resulting in low dissolved oxygen levels.

**Table 2. 11** Commercially available sensors for salinity monitoring

Type of sensor	Fabricant	Range	Reference
Four-ring electrode	Hanna	0 to 200 mS/cm	(HI9828, 2017)
No information	Hanna	0 to 200 mS/cm	(HI9829, 2017)
Four-ring electrode	Hanna	0 to 200 mS/cm	(HI769828-3, 2017)
Four-ring electrode	Hanna	0 to 200 mS/cm	(HI763100, 2017)
Four-ring electrode	Hanna	0 to 200 mS/cm	(HI7609829-3, 2017)
Four-ring electrode	Hanna	0 to 200 mS/cm	(HI7698194-3, 2017)
Electrodes	PCE Instruments	0 to 200 mS/cm	(PCE-PHD 1, 2017)
No information	PCE Instruments	0 to 12% of salt	(PCE-SM 11, 2017)
Electrodes	PCE Instruments	0 to 20 mS/cm	(PCE-CM 411, 2017)
Electrodes	Crison	10 to 80 mS/cm	(Conductivity 53 88, 2017)
Electrodes	Crison	0.1 to 10 mS/cm	(Conductivity 53 90, 2017)
Electrodes	Crison	0.5 to 80 mS/cm	(Conductivity 53 92, 2017)
Electrodes	Crison	0.5 to 80 mS/cm	(Conductivity 53 98, 2017)
Electrodes	Crison	500 to 50 mS/cm	(Conductivity 53 99, 2017)
Electrodes	Crison	0.1 to 50 mS/cm	(Conductivity 53 95, 2017)
Electrodes	Crison	1 to 200 mS/cm	(Conductivity 53 96, 2017)
Electrodes	In-Situ Inc	5 to 100 mS/cm	(Aqua TROLL 400, 2017)
Electrodes	In-Situ Inc	0 to 350 mS/cm	(Aqua TROLL 600, 2017)
Electrodes	In-Situ Inc	5 to 100 mS/cm	(SmarTROLL, 2017)
Electrodes	In-Situ Inc	5 to 112 mS/cm	(TROLL 9500, 2017)
Electrodes	Eureka Probes	0 to 100 mS/cm	(Eureka Manta+ Cond, 2017)
Electrodes	OTT	0 to 100 mS/cm	(OOT Cond, 2017)
Inductive cell	Saiv A/S	0 to 70 mS/cm	(SD204, 2017)
Inductive cell	Saiv A/S	0 to 80 mS/cm	(SD208, 2017)
Four electrodes	SEBA	0 to 200 mS/cm	(MPS-D3 type, 2017)
Four electrodes	SEBA	0 to 200 mS/cm	(MPS PTEC, 2017)
Four electrodes	SEBA	0 to 200 mS/cm	(MPS-K16/Qualilog16, 2017)
Four electrodes	SEBA	0 to 200 mS/cm	(MPS-D8/Qualilog8, 2017)
No Information	YSI	0 to 200 mS/cm	(5200A Multiparameter, 2017)
Four-pole electrode	INW TempHion	0 to 300 mS/cm	(CT2X, 2017)

There are different techniques to measure dissolved oxygen. The reference method is the Winkler test, which is based on a titration (Winkler, 1888). It is a complex method that requires the addition of different reagents and cannot be used in a sensor. Nevertheless, it can be used for

the sensor calibration. There are two main groups of developed sensors, namely electrochemical and optical sensors. Electrochemical sensors are similar to the Clark electrode (Clark et al., 1953), which is an amperometric sensor based on the electrochemical cell. It is formed by a cathodic working electrode made of platinum, embedded in a cylindrical insulator and a ring-shaped silver anode. The used electrolyte is KCl. An oxygen-permeable membrane is employed in some of the designs. The designs present different membranes (see Mackereth et al., 1964; Glasspool and Atkinson, 1998; Martínez-Máñez et al., 2004) and use thick film technology. Other designs (Luz et al., 2006), used a modified glassy carbon electrode; the design proposed by Xu et al. (2008) is an example of a low-cost design. The main disadvantages of the sensors that present a permeable membrane are the dependence of the oxygen diffusivity on the pressure. Moreover, they need to be cleaned periodically (Sosna et al., 2007). There are, however, other designs without membranes (Sosna et al., 2007), which serve as prototypes for laboratory use, but are not suitable for in situ measurements. A needle-type dissolved oxygen microelectrode array sensor (Lee et al., 2007) or a microelectrode sensor designed by Sosna et al. (2008) are other examples. Nevertheless, those designs need continuous maintenance. The electrodes have to be in contact with the water and sedimentation, biofouling or air bubbles can disturb the measurement.

Optical sensors are based on collisional quenching by molecular oxygen of a certain chemical compound embedded in a support matrix (Chu and Lo, 2010). Two main groups of chemical complexes are used, based on platinum (II) (Trettnak et al., 1996; Yeh et al., 2006) or ruthenium (II) (Trettnak et al., 1998; McDonagh et al., 2001; Sin et al., 2004; Jorge et al., 2004; Evans et al., 2006).

The optical oxygen sensors are the best option for in-situ monitoring and are used for long-term monitoring. Nevertheless, the chemical compounds employed in these sensors usually degrade over time and need replacement. Moreover, they are relatively expensive, which impedes their use in aquaculture facilities. Furthermore, biofouling and sedimentation can obstruct the contact between water and the sensing element. For this reason, it will be necessary to search for a region of the light spectrum in the UV light that allows measuring the absorbance of light and correlates it with the dissolved oxygen. Table 2.12 shows the currently used sensors to measure dissolved oxygen. Most of them are optical sensors, while only three are based on the Clark cell. Different companies offer solutions for different ranges

### 2.3.5. Turbidity

Turbidity is a measure of the transparency of water, and reduced turbidity is related to the presence of suspended sediments (SS). For aquaculture, turbidity increase can cause several problems as the effect of turbidity on fish is complex. In some species, such as *Erimonax monachus*, increased turbidity causes a reduction in growth (Sutherland and Meyer, 2007). In other species, such as *Stizostedion vitreum*, maximum growth is reached at highest turbidity (Rieger and Summerfelt, 1997). Turbidity can be caused by inert particles such as sedimentary turbidity, related to river discharge. Moreover, it can be caused by living particles, such as plankton. In marine facilities, abrupt changes in turbidity are not usual and generally related to high phytoplankton blooms or some adverse methodological conditions. However, inland facilities can be affected by sedimentary or planktonic turbidity. In this case, the use of filters can reduce its effects. Nevertheless, it is important to monitor turbidity in order to take the necessary steps. Turbidity can be measured using different techniques. Some of these techniques, such as the use of a Secchi disk, gravimetric methodology or the Imhoff cone, are not suitable for automatic and remote techniques. Techniques based on light effects are related to the Beer-Lambert law (Eq. 2.4), which quantifies the transmitted light,  $I_t$ , as a function of the light intensity of a source,  $I_0$ , the absorption coefficient per unit length,  $a$ , the turbidity,  $t$  and the length of the light pass,  $l$ , (Postolache, et al., 2002a).

$$I_t = I_0 \times e^{-(a \times t)l} \quad (2.4)$$

Based on the previous equation, there are three different methodologies to measure water turbidity. Nephelometers are based on the measurement of the scattered light. The light sensing component is usually positioned at 90°, or a lower angle, from the light source. This method is usually employed to measure samples with low turbidity values (Lambrou et al., 2009). There are few proposals based on this methodology (e.g. Tokhtuev et al., 2005), where a diode is used as a light emitter and a photodiode as a light detector. Another example can be found in Lambrou et al. (2009), with a sensing range from 0 to 120 NTU.

**Table 2. 12** Commercially available sensors for oxygen monitoring

Type of sensor	Fabricant	Range	Reference
Optic	Hach	0 to 20 mg/L	(LDO® Model 2, 2017, 2017)
Clark cell	Hach	No information	(5500 Clark DO Sensors, 2017)
Optic	Hach	0 to 40 ppm	(5740 sc DO Sensors, 2017)
Optic	Hach	0 to 2 ppm	(9582 sc DO Sensors, 2017)
Optic	Hach	0 to 80 ppm	(Orbisphere 311xx, 2017)
Optic	Hach	0 to 80 ppm	(Orbisphere A1100, 2017)
Optic	Hach	0 to 40 ppm	(Orbisphere K1100/K1200, 2017)
Optic	Hach	0 to 40 ppm	(Orbisphere M1100, 2017)
No information	Hanna	0 to 50 mg/L	(HI9829, 2017)
Optic	In-Situ Inc	0 to 50 mg/L	(RDO PRO-X, 2017)
Optic	In-Situ Inc	0 to 50 mg/L	(RDO Titan, 2017)
Optic	In-Situ Inc	0 to 50 mg/L	(Aqua TROLL 400, 2017)
Optic	In-Situ Inc	0 to 50 mg/L	(Aqua TROLL 600, 2017)
Optic	In-Situ Inc	0 to 50 mg/L	(SmarTROLL RDO, 2017)
Optic	In-Situ Inc	0 to 50 mg/L	(SmarTROLL, 2017)
Optic	In-Situ Inc	0 to 50 mg/L	(TROLL 9500, 2017)
Clark cell	In-Situ Inc	0 to 20 mg/L	(TROLL 9500, 2017)
Optic	Eureka Water Probes	0 to 20 mg/L	(Eureka Manta2 DO, 2017)
Optic	Zebra-Tech	No information	(D-Opto Sensor, 2017)
Optic	INW TempHion	0 to 25 ppm	(DO/GDL, 2017)
Optic	INW TempHion	0 to 25ppm	(DO2, 2017)
No information	SEBA	0 to 25 mg/L	(MPS-K16/Qualilog16, 2017)
Optic	SEBA	0 to 40 mg/L	(MPS-D8/Qualilog8, 2017)
Clark cell	SEBA	0 to 40 mg/L	(MPS-D8/Qualilog8, 2017)
Optic	YSI	0 to 60mg/L	(5200A Multiparameter, 2017)
Optic	YSI	0 to 50 mg/L	(5500D MultiDO t, 2017)
Optic	YSI	0 to 60mg/L	(5400 MultiDO, 2017)
Optic	YSI	0 to 50 mg/L	(ProODO, 2017)

The second methodology, using turbidimeters, is focused on the absorption of the light. The undissolved particles cause light scattering and light absorption. This methodology is proposed for samples with high turbidity values (Lambrou et al., 2009). Some examples of prototypes based on this methodology can be found in the literature. One turbidimeter uses a diode with the peak wavelength at 950 nm and an IR photodiode with a sensing range from 0 to 1,000 NTU (Sendra et al., 2013b). Other authors presented a similar prototype as (Giuffre et al., 1999) or improved the existing prototype as Biard (1996). In this case, the author added a second photodiode next to the light emitted to evaluate the light intensity before passing through the sample. Similarly, Bartz (1994) and Shenoy et al. (2012) placed the detector at 360° from the emitter and used a lent to reflect the light.

In the ratio turbidimeter, two light detectors are used, placed at 180° and 90°. This methodology is recommended for water with high turbidity levels and coloured samples. Sensing ranges are from 0 to 18 NTU (Mylvaganaru and Jakobsen, 1998) or from 0 to 120 NTU (Lambrou et al., 2009). An improvement was presented by Postolache et al, (2002a, 2002b), who proposed to use an extra photodetector, resulting in a system with one emitter and three

detectors at 90°, 180° and 270°. With this enhancement, the authors increased the sensing range to 1,000 NTU.

There is, however, another physical principle to measure turbidity. The presence of suspended sediments produces alterations in an acoustic beam. The use of high-frequency acoustic beams to measure turbidity presents better results because it is independent of the particle size. Clifford et al. (1995) demonstrated that the particle size affects the turbidity readings. For this reason, the use of acoustic doppler velocimetry (ADV) seems a better option for monitoring water turbidity. There are different options to relate the SS with the sound alterations. The first one is to use a probe for measuring the acoustic backscattering intensity (BSI). Several authors have studied the relation between BSI and turbidity (Kawanisi and Yokosi 1997; Voulgaris and Meyers 2004; Trevethan et al., 2007; Chanson et al., 2008). Besides, the acoustic beam amplitude can be used to estimate turbidity (Vousdoukas et al., 2011). Chanson et al. (2011) presented both methodologies with good correlations. Finally, the sound noise ratio signal indicates that the scattered sound pulses are correlated to turbidity (Marttila et al., 2010).

After analysing all current options for turbidity measurement, two main groups could be distinguished. First, sensors based on an optical beam, where absorption, refraction or both are measured. Another option is the use of an acoustic beam. In this case, both options present their own problems. Optical methods should be avoided. However, acoustic methods employ higher energy than optical methods. Moreover, acoustic sensors are usually more expensive than optical sensors. For these reasons, we suggest the use of optical methods for turbidity monitoring. The use of scattering or backscattering methods depends on the expected turbidity values. Table 2.13 shows the currently used commercial sensors based on light effects. No company offers solutions based on acoustic effects. The majority present a range between 0 and 4,000 NTU.

**Table 2. 13** Commercially available sensors for turbidity monitoring.

Type of sensor	Fabricant	Range	Reference
Optic	In Situ Inc	0 to 2,000 NTU,	(TROLL 9500, 2017)
Optic	In-Situ Inc	0 to 4,000 NTU	(Aqua TROLL 600, 2017)
Optic	Eureka Water Probes	0 to 3,000 NTU	(Eureka Manta2 Turb, 2017)
Optic	Aquatec Group	0 to 2,000 NTU	(AQUAlogger 210TY, 2017)
Optic	OOT	0 to 3,000 NTU	(OOT Turb, 2017)
Optic	SEBA	0 to 1,000 NTU	(MPS-K16/Qualilog16, 2017)
Optic	SEBA	0 to 1,000 NTU	(MPS-D8/Qualilog8, 2017)
No information	INW TempHion	0 to 3,000 NTU	(Turbo, 2017)
Optic	Hach	0 to 4,000 NTU	(Solitax series, 2017)
Optic	Hach	0 to 9,999 NTU	(TSS series, 2017)
Optic	Hach	0 to 4,000 NTU	(Highline sc, 2017)
Optic	Hanna	0 to 1,000 NTU	(HI9829, 2017)

### 2.3.6. Discussion and future challenge on sensors for fish farms monitoring

This subsection presents a review of the current options for water quality monitoring. The challenges for water quality monitoring in the fish farm environment are shown and the required characteristics of the employed sensors for long-term monitoring are detailed. Although the use of sensors is common for terrestrial applications, such as monitoring agricultural and livestock processes, its use in underwater environments is reissued. The main reasons are the differences between air and water environments. The characteristics of the underwater and, especially, saline environments can cause alterations in the sensor. Because of this, many measures must be taken to protect the sensors from the harsh environment. Waterproof packages or of the avoidance of materials that corrode are possible solutions. Furthermore, there are certain restrictions to access the sensors. Therefore, in long-term monitoring, it is important to minimise replacement. The need for battery replacement and cleaning must be considerably reduced.



Hence, it is extremely important to reduce the energy consumption of the sensor, which stresses the need for sensing methods with low energy requirements. Moreover, those sensors must have low maintenance needs. In general terms, optic sensors must be avoided because they need to be cleaned frequently. However, if no other option is feasible, a proper orientation can be chosen to avoid sedimentation and to reduce maintenance. The effect of change the orientations must be studied in order to find the best option to reduce the accumulation of sediment. In general it is preferred vertical orientations than horizontal ones. To avoid damage by fish, special shapes and sizes can be selected. The use of spherical shapes in the sensors inside the cage will ensure that the sensors will not cause any damage to the fish if they collide with or bite the sensor. Sensors need to be available at low costs if we pretend to impulse the use of sensors for precision aquaculture.

For the review of different methodologies for temperature, salinity, dissolved oxygen and turbidity measures, papers and patents were analysed in order to prepare a selection of the most suitable options for water quality monitoring. According to the challenges and needs described above, the best options to sense each parameter were selected. For temperature monitoring, the best option is to use electronic devices such as RTD or thermistors. They are cheap, easy to isolate and sufficiently adequate. Usually, they consume low amounts of energy and can be easily powered with a normal sensor node such as Flyport, Waspote or Arduino. The best option for salinity monitoring is the measurement of EC by the use of inductive methods. The coils used for these methods can be isolated from the water. Depending on the coil, the sensors consume low amounts of energy. Furthermore, they are cheap and can be powered with a regular node. For turbidity measurement, optical sensors are most suitable, either scattering or backscattering methods. They are cheaper than the use of acoustic beams and require less amounts of energy. The use of a light source and detector can be easily implemented in a node of a WSN. Although the use of a light beam should be avoided, this is the best option in this case. For dissolved oxygen monitoring, there are two groups of sensors, ones based on collisional quenching and ones based on the Clark electrode. Unfortunately, both of them need regular maintenance and replacement. However, there are no other options at this moment. The most appropriate option for long-term monitoring is the use of optical sensors. The main advantage of this sensor is its robustness. Nevertheless, it is important to remark that optical sensors for dissolved oxygen monitoring are usually more expensive.

Next, data about the real implementations based on the commercial available devices. First, the different technologies employed in the available probes are shown. The following factories including In-Situ Inc, SEBA, Hanna, YSI, Eureka water probes, Aquatec Group, OTT, Saiv A/S, INW TempHion, Crison, PCE Instruments, Zebra-Tech, and Hach were studied to elaborate Figures 2.8 to 2.11. Up to 100 sensors for 13 factories were analyzed to elaborate Figures 2.8 to 2.11. In Figures 2.8 to 2.11, it is possible to see the number of sensors in each category and the percentage of each category. The companies offer the following solutions for temperature monitoring, see Figure 2.8. The RTDs and thermistors seem to be the most common solutions. Our analyses considering the options described in Section 2.3.1 conclude that the best option was to use RTD or the thermistors for water quality monitoring. The commercial devices use the same option pointed out previously. Figure 2.9 shows the currently used commercial sensors, of which the majority are based on electrodes. Nevertheless, an inductive sensor can be obtained from Saiv A/S. In section 2.3.3 we conclude that the best option was to use the inductive sensors. Most of the commercial devices are not yet including this technology. We can expect that the inductive technology will be used in the future for water quality monitoring. Figure 2.10 shows the currently used sensors to measure dissolved oxygen. Most of them are optical sensors, while only three are based on the Clark cell. In Section 2.3.4 we conclude that the best option was the optic sensors and the commercial devices are mainly using the optic methods. However, it is necessary to point that the optic methods require maintenance due to the membranes. Figure 2.11 shows the currently used commercial sensors based on light effects. No company offers solutions based on acoustic effects. Our

recommendation in Section 2.3.5 was to use the optical sensors. All the available options in the market goes in this direction. Finally, the information about few devices capable to monitor the listed parameters in this section is shown in Table 2.14. It is possible to see that the enterprises mentioned in Table 2.14 are producing probes that can be employed in aquaculture facilities. As Table 2.14 includes only the probes founded that are able to measure all the parameters selected in this subsection, many probes from different factories are not included. The main disadvantage of the current available sensors is its price. From some sensors there is no information (NI) about the used technology. Water temperatures in marine waters range from 0 to 29.5°C (Locarnini et al., 2010), and all the presented sensors are suitable for temperature monitoring according to their operational range. Generally, marine water salinity ranges from 29 to 38 mg/L (Antonov et al., 2010), all the sensors are able to cover this range of salinities. The average oxygen concentration in the water surface ranges from 4.6 in the tropics and 9.0 mg/L in the Arctic (Garcia and Gordon, 1992, without any significant changes throughout the year. In aquaculture facilities, the oxygen concentration can diminish. All the included sensors in Table 2.14 present an operational range suitable for the range of dissolved oxygen at the sea surface. The range that present the turbidity sensors above are adequate for the expected levels in the fish farms.

**Table 2. 14** Commercially available sensors for monitoring

Factory	Temperature		Salinity		Dissolved oxygen		Turbidity		Ref.
	Type	Range (°C)	Type	Range (mS/cm)	Type	Range (mg/l)	Type	Range (NTU)	
In-Situ Inc	Thermistor	-5 to 50	Electr.	0 to 350	Optic	0 to 50	Optic	0 to 4,000	Aqua TROLL 600
In-Situ Inc	Thermistor	-5 to 50	Electr.	5 to 112	Optic & Clark cell	0 to 50 & 0 to 20	Optic	0 to 2,000	TROLL 9500
SEBA	NTC	-5 to 50	4 Electr.	0 to 200	N.I.	0 to 25	Optic	0 to 1,000	MPS-K16/Qualilog16
SEBA	NTC	-5 to 50	4 Electr.	0 to 200	Optic	0 to 40	Optic	0 to 1,000	MPS-D8/Qualilog8
Hanna	N.I.	-5 to 50	N.I.	0 to 200	N.I.	0 to 50	Optic	0 to 1,000	HI9829

In the future, the challenges in underwater sensing for aquaculture monitoring will be based on long-term monitoring. To address this goal, it will be necessary to encourage researchers to develop new physical methods for turbidity and dissolved oxygen monitoring. The reduction of biofouling is one of the major challenges in terms of reducing maintenance needs. The investigation of materials that withstand corrosion and biofouling processes is crucial. Moreover, the inclusion of energy harvesting techniques in underwater environments will facilitate long-term monitoring, without the need of battery replacement. The most important challenge is that the developed sensors have no negative effects on fish, which requires studies with live organisms. Further, the sensors should not cause any effects after short or chronic exposure, in fish swimming and feeding behavior and feeding or changes in the immunological system.

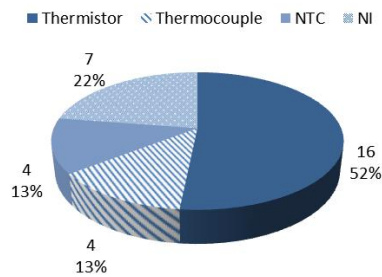


**Figure 2. 8** Employed technology for temperature

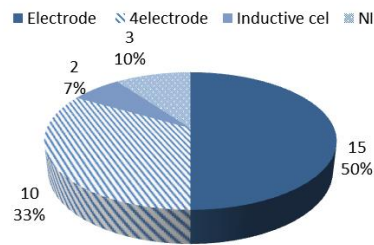


**Figure 2. 9** Employed technology for salinity

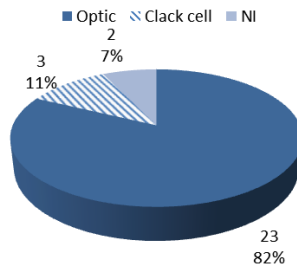


**Figure 2. 10** Employed technology for dissolved oxygen

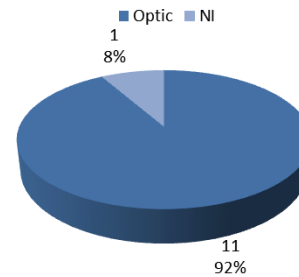


**Figure 2. 11** Employed technology for turbidity

In the future, the challenges in underwater sensing for aquaculture monitoring will be based on long-term monitoring. To address this goal, it will be necessary to encourage researchers to develop new physical methods for turbidity and dissolved oxygen monitoring. The reduction of biofouling is another challenge in terms of reducing maintenance needs. The investigation of materials that withstand corrosion and biofouling processes is crucial, and the new methods will have to require lower amounts of energy. Moreover, the inclusion of energy harvesting techniques in underwater environments will facilitate long-term monitoring, without the need of battery replacement. The most important challenge is that the developed sensors have no negative effects on fish, which requires studies with live organisms. Further, the sensors should not cause any effects after short and chronic exposure, mainly in terms of altered fish swimming behavior and feeding activities or changes in their immunological system.

For some parameters, such as salinity and temperature, the commercially available sensors meet all the requirements for water quality monitoring in aquaculture facilities, as compared to other sensors. Research in new sensing technologies is an emerging and important field. Recently, the WSN has demonstrated several benefits for process monitoring. Data gathered in conjunction with artificial intelligence and remote actuators can facilitate the automatization of many activities, improving efficiencies from an economical and environmental point of view. Our future work will be focused on using the selected sensors to create a WSN for water quality monitoring in aquaculture facilities. We will also propose to include data about feed consumption and implement artificial intelligence techniques to build an intelligent system for fish farm monitoring, with the overall aim to improve aquaculture efficiency.

## 2.4. Current systems for aquaculture monitoring

In this section, we present a review of the existing systems for data gathering and for fish farm monitoring. We will divide the possible systems for fish farm monitoring between those systems that allows measuring the water quality and the systems that allows measuring the fish behavior.

### **2.4.1. Data gathering systems**

In this subsection different data gathering systems are presented. There are several authors who are currently working on technologies aimed to reduce the energy waste. We can see a classification of these techniques presented by O. Diallo et al. (2015). When an alternative data gathering system is proposed, it is necessary to evaluate its effectiveness and to do it, many tests are required. The evaluation of a WSN consumes high amount of resources and time, even higher than the time spend for developing the systems itself. The performance of laboratory test bench and simulations can help us to avoid the real deployments. In this sense, J. Wang et al. developed an adaptive data gathering scheme based on the introduction of an autoregressive model which used their recent work on the emerged compressive sensing theory (Wang et al., 2012). This proposal was able to perform a correlation between the value of the sensed data collected by a node and the data gathered by its neighbors. In this proposed system, the number of measures carried out depended on the variation of the sensed parameter and the degree of required accuracy. In addition their model was capable of detecting any reading out of bounds. Their experimental results performed with real data made evident the high effectiveness and efficiency of this proposal. Nevertheless, the packets loss of sensed data make very difficult the data reconstruction by using of the autoregressive model. This implies the system performance degradation.

The first design for large-scale WSNs that applied the compressive sampling theory to data gathering process was presented by C. Luo et al. (2009). The test bench was performed in a scenario with several nodes. As authors commented, the obtained sensed data showed a clear spatial correlation. The results proved the high efficiency and robustness of the proposed system. These results were due to reduction of global scale communication cost without the needed of having intensive computation systems or complex transmission control systems.

The software and hardware design of MPWNodeZ was presented by R. Morais et al. (2008). Authors implemented three different energy harvesting techniques in their proposal in order to recharge the batteries. This proposal was designed to sense data from large areas and sends them through a wireless acquisition device based on ZigBee technology. The presented proposal was designed to develop precision viticulture in vineyards placed in the Demarcated Region of Douro. Two different tests were carried out. The first one was carried out in the laboratory while the second test was performed in a real field of vineyards. The results show the good performance of their proposal. It could be adapted to precision viticulture.

Our proposal presents some advantages over the current ones. First, our devices work under the IEEE 802.11g standard which reduces the implementation costs. Moreover it offers larger coverage area, thus the number of devices needed to cover an area will be low. The selected device presents a small size which is perfect for environmental and rural monitoring. Although the use of the IEEE 802.11 wireless technology supposes higher energy consumption, the selected device has one of the smallest energy requirements of the commercial devices.

### **2.4.2. Monitoring systems for fish farms**

In this subsection, the state of art of the systems for fish farm monitoring is shown. Several authors propose different systems for water quality monitoring. Water quality monitoring and fish behavior monitoring are crucial to improve the efficiency of aquaculture.

Wireless Sensor Networks (WSN) have become a solution for performing water quality monitoring. Espinosa-Faller and Rendón-Rodríguez (2012) presented a WSN-based water monitoring system. The system employed ZigBee to transmit the information gathered by the sensors from the recirculating system. Then, the information was stored in a MySQL database. Temperature, pressure, and dissolved oxygen was measured throughout the day. When a problem was detected, an SMS or an E-mail was forwarded to alert the person responsible for the facility. Another WSN-based water monitoring system was presented by Zhang et al. (2010). The system was able to measure pH, water temperature, water level and dissolved oxygen. The

data was forwarded to a database that provided the information to the software to be monitored in real-time. The software was developed employing Visual studio 2005 and separates logic, display and data layers to improve scalability and reusability. Lastly, warnings were forwarded via SMS or graphical device twinkle to the users. WSN is employed as well for the recirculating monitoring system proposed by Lin et al. (2011). The system was composed of a three-layer architecture comprised of the remote layer, the server layer and the client layer that obtained, transported, and displayed the information gathered on water temperature, conductivity, salinity, and pH. Moreover, a software solution was developed as well to monitor the obtained information by accessing a Postgre SQL server employing a Wireless Local Area Network (WLAN). Huang et al. (2013) presented a WSN-based water quality monitoring system that gathered data on pH, water temperature and dissolved oxygen. A real-time interface allowed the display of the data numerically and graphically. Several testing results were provided displaying fluctuations during the day. These results show a 1.40% of relative error for pH, 0.27% for temperature and 1.69% for dissolved oxygen. The water quality monitoring system presented by Simbeye and Yang (2014) measured pH, water level, water temperature, and dissolved oxygen and employed ZigBee to forward the data. They used the LabView software to display the obtained information. Furthermore, several experiments regarding communication performance, battery performance and sensor readings were performed over a period of six months. Results showed the fluctuations of these parameters throughout the day. Zhu et al. (2010) designed a water quality monitoring system for fish farms. It employed artificial neural networks (ANN) to forecast water quality to prevent losses. The data acquisition node measured water and room temperature, percentage of dissolved oxygen saturation, dissolved oxygen concentration, pH, electrical conductivity, and salinity employing a variety of sensors. The data was then forwarded to a server to be remotely accessed. Encinas et al. (2017) proposed an IoT-based water monitoring system for aquaculture. They employed an Atlas Ph Probe digital sensor, an analog temperature sensor and an Atlas Dissolved Oxygen Probe as well as an Arduino node that employed a ZigBee module to forward the information to a MySQL database. Moreover, the system utilized 200 mA/h rechargeable batteries and was able to perform for 8 h. The information was able to be visualized through a desktop or a mobile application. Han et al. (2007) designed an environment monitoring system specific to aquaculture farms. They measured water quality, fish food and the medication provided to the fish. For water monitoring, they employed sensors to achieve data on conductivity, temperature, dissolved oxygen, and air saturation. The user interface allowed monitoring of the parameters from a graph and a log. Furthermore, the system was able to alarm users when the fish disease was propagated to provide treatment. Cario et al (2017) a water quality monitoring system for fish farms. The system was composed of SUNSET (Software Defined Communication Stack) for networking purposes and Hydrolab Series 5 probes for data acquisition. The measured parameters were temperature, pH, luminescent Dissolved Oxygen (LDO), salinity, Oxidation Reduction Potential (ORP) and specific conductance (SpCond). Moreover, energy consumption was reduced employing new sleep and wake-up mechanisms. Another water monitoring system was presented by by Hongpin et al. (2015). Their system employed ZigBee and GPRS modules with a STM32F103 chip. They also employed a Pt1000 temperature sensor and a YCS-2000 dissolved oxygen sensor as well as other sensors to measure pH and ammonia. The obtained information could be monitored with a computer program developed with Labview. This program allowed monitoring of each parameter in a separate graph as well as numerically. Results showed a packet loss rate of 0.43%. Shifenf et al. (2007) propose an aquiculture environment monitoring system that employed Radio Frequency (RF) and Global System for Mobile communications (GSM) to measure temperature and dissolved oxygen. Two algorithms were designed to determine the performance of the monitoring center and the different substations. Substations performed a 24-h uninterrupted data acquisition and forwarded the information in real-time.

The techniques employed to monitor fish behavior usually utilize optic and acoustic techniques. Papadakis et al. (2012) implemented a fish behavior monitoring system that was able to monitor 9 fish tanks at the same time employing computer-vision. They evaluated stock density as a stress factor. Their system was able to be controlled remotely and provided real-time images of the fish. The obtained results showed a significant statistical difference in treatment comparison only for the experiment performed with the undamaged mesh. A survey of other existing vision-based systems for fish behavior monitoring was presented by Saberioon et al. (2016). They defined the two major areas of applications for optical sensors as pre-harvesting and during cultivation, and post-harvesting situations. They also performed a discussion on fish monitoring technologies such as machine vision, hyperspectral imaging, thermal imaging, and x-rays. They summarized the applications of optical sensors for fish monitoring into five types being fish sorting, fish quality, physical attributes, chemical attributes, and food security. A monitoring behavior system based on a flat passive integrated transponder antenna array was presented by Armstrong et al. (1996). They employed their system to record the movements of salmon shoals. Several experiments were performed employing different quantities of salmon for each test. The obtained results showed a success rate higher than 99%. Moreover, fish presented no unusual behavior to the antenna array. Conti et al. (2006) employed acoustics for monitoring fish behavior, growth, and density. Their experiments were performed over sardines, rockfish and sea bass deployed in tanks. They employed the scattering cross section to determine the behavior of the fish and to trig an alarm when anomalies were detected. They were able to monitor the growth-rate of the fish as well employing a first-order polynomial equation and a second-order polynomial equation. An imaging sonar referred as Dual-frequency Identification Sonar (DIDSON) was utilized by Zhang et al. (2004) to monitor swimming pattern and the length of Chinese sturgeons. Experiments were performed with over 2500 targets. Authors were able to find a relation between swimming pattern and body length from the obtained data. The lengths detected by DIDSON were 35.6% shorter than the ones obtained from manual measurements. Moreover, results showed that fish mostly swam in a circular motion and close to the net. Ruff et al. (2002) performed stereo Image analysis to monitor fish. They were able to measure shape, size position and spatial orientation of a fish. Three different experiments were performed in fish tanks with a depth of 3 m and 1 m of cross-section. All experiments had four stages being calibration, image acquisition, identification of the measurement points and 3D position calculation. Results showed an error between 3% and 5% for determining the length of the fish. A GPS tracking device was employed by Sims et al. (2009) to monitor sunfish *Mola mola*. The system was able to monitor the position with an approximate accuracy of 70 m. Experiments were performed on three different fish with sizes varying from 0.6 m to 1 m. The route performed by the fish was able to be visualized in a map. Moreover, Data on the speed of the fish was acquired and displayed on graph locating each measure on the map by adding a dot on the route. Karimanzira et al. (2014) presented a guidance system for a fish behavior and water quality monitoring system that employed an autonomous underwater vehicle. The vehicle was provided with a conductivity and oxygen optode sensor, as well as a spectrometer. LED cameras were also attached to the vehicle to observe fish behavior. The vehicle was able to navigate through the cages without colliding with them. As a result, the vehicle was able to obtain information without any collision.

Feeding is another important factor to owners of fish farms as excess feed increases the production cost and contaminates the water. For that reason, the number of researches on fish feeding solutions is constantly increasing. A fish feeding system that considered the behavior of fish in order to determine the best time to provide the food was presented by AlZubi et al. (2016). The hardware design included an automatic dispenser, a webcam and an interface circuit. The camera detected the number of fish that went to the feeding area, when the Fish Learning Index (FLI) was higher than the threshold, the system provided food. Results showed

the variation of the number of times food is provided for eight days. Atoum et al. (2015) introduced a feeding system for aquaculture tanks that employs visual signal processing. The system included a decision-making process to determine whether fish are eating or not, and detection of excess feed. Excess feed was detected employing two different methods, being a Support Vector Machine (SVM) based refinement classifier and a correlation filter. Bórquez-Lopez et al. (2017) performed a comparison between mathematical functions and fuzzy logic (FL) feeding techniques for shrimp farming. Authors determined that dissolved oxygen influences feeding rate the most, a 74%, and temperature influences it in a 26%. Moreover, they concluded that FL is the better strategy saving up to a 35% of feed without affecting growth or survival. Papandroulakis et al. (2002) presented an automated feeding system for intensive fish farms. The system considered the necessary amount of plankton that had to be distributed to each tank. Experiments were performed applying the proposed method to four groups of sea bream and comparing it with the results obtained from two groups fed with the standard method. A reduction between 30% and 40% in labor was achieved and the use of *Artemia nauplii* decreased by 40%. M. Garcia et al., (2011) presented a fish feeding system that employed sensors that determine when fish need feed. Sensors were deployed both inside and outside the cage. These were temperature, oxygen, displacement speed, biomass distribution placement and pellet detection sensors for the internal part of the cage and presence and water current sensors for the outside. Covès et al. (2006) performed in a set of experiments were an on-demand feeding system was employed to provide feed to 50 sea bass. The two experiments were conducted during 55 and 69 days respectively. Moreover, a PIT tag was utilized to determine whether fish activated the trigger or not. Results showed a 67% and 74% of the fish in experiments 1 and 2 activated the trigger at least once. Furthermore, two fish in experiment 1 were responsible for 82% of the triggers and one fish in experiment 2 was responsible of 77% of the triggers.

#### **2.4.3. Monitoring systems for general aquatic environments**

In this subsection, we present a selection of papers where different sensors are used for monitoring aquatic environments. Many of them propose the water monitoring to obtain real-time information about parameters such as quality, component analysis, etc. Among these, we find the following ones:

O'Flynn et al. (2007) described the operation of "SmartCoast", a Multi Sensor System for water quality monitoring. The system is aimed at providing a platform capable of meeting the monitoring requirements of the Water Framework Directive (WFD). The key parameters under investigation include temperature, phosphate, dissolved oxygen, conductivity, pH, turbidity and water level. Authors also presented a WSN platform developed at Tyndall, with "Plug and Play" capabilities, which allows the sensor integration as well as the custom sensors under development within the project. Their results indicated that a low power wireless multi sensor network implementation is viable.

Kröger et al. (2002) stated that biosensors have great potential in the marine environment. The development of biosensors for taking measurements in-situ is a difficult challenge and that work is underway to address some of the issues raised. While the ability to make such observations is the ultimate goal of most developments, the ability to make decentralized measurements in the field rather than having to process collected samples in specialized laboratories is a significant advance which should not be overlooked. This is an area where biosensors are likely to find their initial significant applications: the low-cost, user-friendly test that can be carried out to pre-screen samples, possibly helping to focus the sample collection effort for further detailed chemical analysis.

Thiemann and Kaufmann (2002) present algorithms for the quantification of the trophic parameters, the Secchi disk transparency and a method to measure the chlorophyll concentration based on the hyperspectral airborne data. The algorithms were developed using in-situ reflectance data. These methods were validated by independent in-situ measurements resulting in

mean standard errors of 1.0–1.5 m for Secchi disk transparency and of 10–11 mg/l for chlorophyll regarding the case of HyMap sensors. The multitemporal applicability of the algorithms was demonstrated based on a 3-year database. With the complementary accuracy of Secchi disk transparency and chlorophyll concentration, and the additional spatial and synchronous overview of numerous contiguous lakes, this remote sensing approach gives a good overview of changes that can then be recorded more precisely by more extensive in-situ measurements.

The water quality monitoring at a river basin level to meet the requirements of the Water Framework Directive (WFD) poses a significant financial burden using conventional sampling and laboratory tests based on techniques presented by O'Flynn et al. (2010). They presented the development of the DEPLOY project. The key advantages of using WSNs are the following ones:

- Higher temporal resolution of data than the ones provided by traditional methods.
- Data streams from multiple sensor types in a multi-station network.
- Data fusion from different stations could help to achieve a better understanding of the catchment as well as the value of real time data for event monitoring and catchment behavior analysis.

Data from monitoring stations can be analyzed and transmitted to a remote office/laboratory using wireless technology in order to be statistically processed and interpreted by an expert in these kind of systems. Rising trends for any constituent of interest or breaches of Environmental Quality Standards (EQS) will alert relevant personnel who can intercept serious pollution incidents by evaluating changes in water quality parameters. To detect these changes it is necessary to perform measurements several times per day. The capabilities of DEPLOY system for continuously taking samples and communicating them allow reducing monitoring costs while providing better coverage of long-term trends and detecting fluctuations in parameters of interest.

Güttler et al. (2013) present new results for the characterization of the Danube Delta waters and explore multi-sensor turbidity algorithms that can be easily adapted to this purpose. In order to study the turbidity patterns of Danube Delta waters, optical remote sensing techniques were used to capture satellite images of more than 80 medium with high spatial resolution.

Albaladejo et al. (2012) explain and illustrate the design and implementation of a new multisensor monitoring buoy system. The sensor buoy system offers a real opportunity to monitor coastal shallow-water environments. The system design is based on a set of fundamental requirements. The main ones are the low cost of implementation, the opportunity of applying it in coastal shallow-water marine environments, suitable dimensions to be deployed with very low impact over the medium, the stability of the sensor system in a shifting environment like the sea bed, and the total autonomy of power supply and data recording. Authors have shown that the design cost and its implementation is low. This implies that it can be integrated in a WSN and, due to the properties of these systems, they will remain stables in aggressive and dynamic environments like the sea. Authors have identified the basic requirements of the development process of the electronic and mechanical components necessary to assembly a sensor.

Jianxin et al. (2011) proposed a new method to measure marine parameters of marine power systems. The system performs a synchronous sampling and distributed data fusion, which is based on the optimal state estimation. The single-sensor measuring data is accurately estimated by the Kalman filter, and the multi-sensor data behavior is globally estimated as a combination these data. The simulation test shows that the measured parameters obtained with the method based on multi-sensor data fusion present more accuracy and stability than the results obtained by the direct measurement method with single-sensor.

Vespe et al. (2008) presented an overview of the Satellite-Extended- Vessel Traffic Service (SEV) system for in-situ and Earth Observation (EO) data association. The description of the cognitive data correlation concept shows the benefits brought to the resulting Recognized Maritime Picture (RMP) in supporting decision making and situation awareness applications. They show the results of multi-technology integration and its benefits brought in terms of suspect vessel detection and propagation tracking. The navigational and geographical knowledge is exploited for the final data association implementation. The vessel motion features and the scenario influence are used to estimate the degree of correlation confidence. The tactical scenario



depiction has also shown the improvement in maritime traffic for coastal and open waters surveillance.

Sousa-Lima et al. (2013) presented an inventory list of fixed autonomous acoustic recording (AR) devices, including acronyms, developers, sources of information and a summary of the main capabilities and specifications of each AR system. The devices greatly vary in capabilities and costs. There are small and hand-deployable units for detecting dolphin and porpoise clicks in shallow water and larger units that can be deployed in deep water to record at high-frequency bandwidths for over a year, but they must be deployed from a large vessel. The capabilities and limitations of the systems reviewed are discussed in terms of their effectiveness in monitoring and studying marine mammals.

Some more interesting research works can be found in (Lloret, 2013), but no one has the same features and purpose than this dissertation.

## **2.5. Related work on conductivity meters**

There are some works in the related literature where the authors develop conductivity meters. This section presents a review of those works.

In first place, an example of some work where the authors create a conductivity meter based on the traditional methodology, the pass of an electric current through the water sample.

Medrano et al. (2007) developed their own conductivity meter for liquids with low electrical conductivity (measuring directly the conductivity of the water). The minimum value that they were able to measure was  $200\text{pSm}^{-1}$ , with an error of 10%. They measure with different distances between both electrodes (0.5 to 2.5 mm) and different voltages (-10 to 10V). Wei et al. (2010) proposed a new seawater conductivity sensor (also based on the capacity of water to transmit the electricity), which uses a bipolar pulse to avoid the effect of electrode polarization. They also propose a temperature composition with different formulas for 3 ranges of temperature 1 °C to 10 °C, 10 °C to 20 °C and 20 °C to 30 °C. The sensor is able to self-compensate and self-tuning. H. Ramos et al. (2006) created a low cost in-situ four electrode conductivity cells. It is suitable to take measurements from estuarine waters.

As far as we know, the use of the interaction in the electromagnetic field has not been used to measure the water conductivity yet (at least in the published works). Moreover, there are few papers describing the process that occurs when an electromagnetic field passes through water with different electrical conductivities and how to use it as an electrical conductivity sensor. However, there are some commercial sensors, that use two coils to measure the induction, but they present higher prices.

There are several application fields where it is possible to measure some environmental parameters as a function of magnetic field interaction. We can find works related to astrophysics where magnetic fields are used to characterize stars (Johns-Krull, 2007) or in agriculture to measure the soil electric conductivity (Martínez et al., 2010). The use of the alteration on the magnetic field used to measure the conductivity is used also in the study of saline soils (López-Bruna and Herrero, 1996) (Olivier Job et al., 1998). In those works two coils are used, the energy passes through one of them and a charge to the other coil which is induced. The charge on the second coil depends on the salinity of the soil.

In order to be able to perform all needed measurements, it is important to characterize the coils and their interaction with the medium. We can find several papers where authors try to measure the water salinity and conductivity using different kinds of coils. However, it is complicated determining which coil configuration presents better efficiency and results.

Ribeiro et al. (2006) presented an inductive conductivity cell to measure the electrical conductivity of the salty water. The sensor is constructed as a double transformer to be utilized to measure the water salinity in the sea and estuaries. Authors used two toroidal cores provided with one single winding which have equal number of turns. The coils were stacked within a plastic container. The electromotive forces developed in the water give rise to electrical currents

which act as the secondary currents of one transformer and the primary currents of the other. The intensity of these currents is related to the electric conductivity of the medium. Authors used the electric current in the water to provide the magneto-motive force necessary to magnetize a second ferromagnetic core, inducing a voltage in the secondary winding which is correlated to the conductivity of the water.

Ramos, et al. (2005) presented a four electrode cell without metallic grids on the tops for water quality monitoring in estuaries and oceans. It is formed by a plastic tube, with two ring-shaped electrodes inside, and two metallic tips to measure the output voltage. Authors were also carried out the experimental characterization of the cell versus frequency, temperature and salt concentration. As results show, the temperature is not an influent factor in the conductivity measurements and the geometry of conductivity cell was found as an independent factor for conductivity measurements.

Natarajan et al. (2007) measured the fluid conductivity using the radio frequency (RF) phase detection. The sensor is formed from two 1.5 mm thick toroidal coils of area 1 sq. inch and a separation between them of 3mm. The feed coil and the sense coil are connected to the sensor electronics using phase stable RF cables. One of the coils is fed with an input RF signal of known frequency while the second coil acts as a sensing coil and receives the coupled signal. Authors calculated the conductivity by converting a phase change between two signals to an output voltage. The results show that it is possible to define four lineal ranges which as a function of the conductivity fluid.

Finally, Cui and Sun (2007) presented an inductive level sensor based on a cylinder vessel wound by electric coils outside with magnetic fluid. In this case, authors used this sensor for detecting level and small inclination angles against horizontal plane. The composition of this sensor allows magnetic fluid used as a variable inductance core to detect level and small tilt of a body against horizontal plane. Authors analyzed the operation of their sensor depending on different pumping frequency. They concluded that the sensitivity of this level sensor is proportional with magnetic susceptibility of magnetic fluid, with the peak current as well as with the pumping frequency through the driving coil. They added that the sensitivity of this level sensor is independent with the value of tilting angle against horizontal plane. As far we know, there is no works which analyze different coil configurations to measure the water conductivity. For this reason, we cannot define the best configuration for our conductivity sensor.

## **2.6. Related work on hydrocarbon detection**

In this section, we are going to show a summary of the related work in the area of hydrocarbon sensors. Different sensors present different operational principles. In this section, we also discuss the feasibility of the real application of each proposed sensor in a sensor network for water quality monitoring.

Péron et al. (2009) presented a sensor able to detect the presence of polycyclic aromatic hydrocarbons in artificial sea water. They used the technique of surface-enhanced Raman scattering. A gold colloidal monolayer was used as an active substrate. As polycyclic aromatic hydrocarbons authors used naphthalene and pyrene. They used different concentration, from 0.01ppm to 10 ppm of naphthalene and from 0.01 ppm to 0.1 ppm of pyrene. This sensor is suitable for detecting low concentrations of hydrocarbons when they are mixed with the water.

An optical sensor was presented by MacLean et al. (2003). The sensor was able to detect the presence of hydrocarbons related to spills. The technique employed by the sensor is the standard optical time domain reflectometry. The sensor consisted on a wire which is in contact with the water. The signal intensity changes when is in contact with the spills. Field test were performed, in the first one a wire of 375m was deployed in the sea. At specific length, 1m of the wire was saturated with petrol. The signal of the sensor reveals the presence of hydrocarbons at the correct length. The maximum time that the wire was placed in the sea was 2 weeks, it

confirms that the wire can resist at least this time in harsh conditions. The sensor seems that has good applications to monitoring lineal areas, like the places where tubes for hydrocarbons transport are placed. However the applications for monitoring natural environments are no good. If is necessary to monitoring a squared area using that sensor, the amount of wire needed increase, because of the linearity of the sensor.

McCue et al. (2006) presented their sensor for hydrocarbon detection in water. They used a mid-infrared wavelength as a source. As a detector, authors used a silver halide fibre optic cable coated with a polymer. In the laboratory test authors used benzene as hydrocarbon at four different concentrations, from 500ppm to 2000ppm. They test optic fibre coated with the polymer and uncoated. The one that has better response was the coated. The sensor was able to work in dynamic pattern. However the sensor was not tested in the environment. The design of the sensor is optimum for laboratory conditions but its applications for monitoring real environments is not clear.

Other sensor based on infrared light was presented by Albuquerque et al., (2005). Authors created a probe to measure the presence of hydrocarbon in seawater. The light source employed in their test was a tungsten lamp. InGaAs detector was used as a detector, with a range of detection from 850nm to 1800nm. Authors used different compounds as hydrocarbons. They used benzene, toluene, ethylbenzene and m-Xylene. Different concentrations of each compound were used. For toluene the minimum concentration was 27mg/L and the maximum 237mg/l. Benzene presented the higher concentration with up to 375mg/l. This sensor was presented as a laboratory sensor for analyse processed samples, however its application for analyse real samples is not clear.

The most spread way to detect the presence of spills in the water is the use of remote sensing. However if we want to detect the spill with low delay, the use of sensors in the water is the most indicated technology. The current sensors have some deficiencies, or they are specific for laboratory conditions, or they have to be in contact with the water. The contact with such harsh environment can cause drifts in the sensor calibration, corrosion, deposition of sediments and other problems that are going to reduce the time that the sensor can be in the environment before the need of clean or replacement. The sensor that we present has the advantage that it doesn't need to be in contact with the water.

Chen et al., (2014) present a WSN mechanism for monitoring and tracking the movement of pollution in water named AquaView. They focus their work on the organization and communication of the nodes. Those nodes do not have de capability to move and they are deployed randomly over the spillage area with an aerial vehicle. The first task of the nodes is to self-organize into clusters. Once the clusters are established, they self-locate in different quadrants (I to IV) obtaining their coordinates. Then each node communicates with its neighbors to check if they are in the boundary of the spill or not. Finally, the information is sent as a report with the coordinates of the boundary sensors. In the simulations they found that their mechanism reduces the communication overhead during the monitoring of the pollution. Their results point that AquaView is a good mechanism for monitoring and tracking of pollution in water environments.

Alkandari (2011) present a proposal of a WSN for water quality monitoring [9]. Their proposal is focused for shallow water environments, developed with low cost constrictions and using a hierarchical communication structure. The nodes use ZigBee technology for communication due its low power consumption. The sensors sense different water parameters as temperature, pH and dissolved oxygen. All the nodes structure themselves into cluster groups. Authors develop some real test of their system in a pool first with stable temperature and latter with variable temperature. Their results show that the system is able to sense and sent the information in real time and detect correctly the changes in sensed parameters. Authors conclude that the developed system has low cost, low energy consumption and also in time consumption.

Rasin and Abdullah (2009) present other WSN for water quality monitoring with low budged. Authors develop both the hardware and the software necessary for its proposal. The sensors used

sense pH, turbidity and temperature of water. The signal of sensor is processed in the sensor node, they use a ZigBee ZMN2405HP module due to its low consumption and high power transmission. The node is powered with a 9V battery. Authors perform some real test to measure the power consumption, coverage and the Link Quality Indicator. Their results show that the nodes can run during 12 hours using a rechargeable battery of 170 mA.H. But more test are need to determine the optimum coverage and Link Quality Indicator.

Wang et al., (2009) propose a system for remote water quality monitoring based on WSN. The developed system has low cost sensor nodes with low power consumption. Comparing the developed system with traditional ones some advantages is archive. Common batteries can be used to power the system. The proposed system has a simple architecture. The nodes are organized in clusters that use ZigBee technology to communicate. And the coordinators send the data to the monitoring central computer with GPRS technology. It shows the data of the water quality in real time or view the historical data. Authors point that the results of their test ensure that the system is able to run stably, however the authors do not bring any information about what test were performed or if those test were real test or simulations.

Yue and Ying, (2011) present other WSN for water quality monitoring. Their proposal has a novel architecture, aimed to monitoring different specific sites instead a general area, and sends the data in real time. The whole system, sensor and nodes are powered with an energy harvesting system, a solar panel. The energy obtained is stored in a battery of 12V. The communication between nodes and base station are based on IEEE 802.15.4. The sensors used for water monitoring sense parameters as pH, Redox potential and turbidity. The main advantages of proposed system are its low energy consumption, low carbon emissions and its high flexibility for deployment.

Finally, Harchi et al., (2008) describe the implementation of a node specific for oil spill monitoring. Authors propose to use ZigBee technology for communications inside the clusters. Of the whole WSN system authors focus their investigation on the partitioned network. Authors perform several simulations in order to evaluate the importance of cluster parameters and they use Opnet Modeler as a simulation tool. The cluster algorithm has two stages; the first one is neighbor discovery and cluster head selection while the second one is the cluster building and maintenance and in these stages they use four broadcast messages. Several clustering protocols have been described in the literature with little variations and authors propose their own protocol and in their simulations taking into account that nodes can move and different values of  $\alpha$ . They performed 900 simulations. And their results point that their protocol is optimum for water pollution monitoring.

## **2.7. Conclusion**

Finally, we show our conclusions after setting the state of the art in the fields of fish biology, available technologies for water quality monitoring in fish farms and current systems for fish farms monitoring.

In this chapter we have shown how the different environmental parameters affect to fish performances. This section pretends to be a guide for promoting the precision aquaculture. Keeping the values of the environmental parameters under the optimal conditions allows maximizing the growth and reducing the mortality. This subsection shows a summary of the current state of the art on the effects of the environmental parameters on fish. Our future work is focused on reviewing all sensors and technologies for water quality monitoring in aquaculture surroundings in order to propose an optimum system for precision aquaculture.

Following, we analyze the existing options for water parameters monitoring focusing on temperature, salinity, dissolved oxygen and turbidity. We discovered that for some parameters such as temperature, conductivity and turbidity, it will be easy to adapt the existing sensors for our purposes. Nevertheless, for the dissolved oxygen nowadays there is no possibility to create a physical sensor.

The aforementioned systems in Section 2.4, 2.5 and 2.6 measure the water quality considering only a couple of parameters (between 2 and 4 parameters) obviating other important factors to monitor such as the turbidity of the water. Moreover, many of the papers do not

specify the used sensors, or they employ expensive sensors, resulting in a high-cost system that is difficult to implement in fish farms with few resources. From the observed papers in Section 2.4, no one of them develops their own sensors. In addition, the authors do not consider the location of the sensors in the tank. Furthermore, fish behavior monitoring is not usually incorporated in the same system increasing the investment owners have to do in order to improve the efficiency of their fish farm.

On the other hand, there are some systems to monitor fish behavior and feed falling systems. Most feeding management systems rely on fish behavior in order to determine whether fish are eating or not. They do not consider in conjunction the feed falling and the fish behavior.

We can summarize that no one of the proposed systems covers our premises. Thus, it is necessary to develop our own proposal in order to have a system which can boost the creation of commercial solutions for precision fish farming.

The ideal system must monitor at least the following parameters: temperature, salinity, photoperiod, dissolved oxygen, light, turbidity, and fish movement. Nevertheless, as the sensors for dissolved oxygen are expensive and it will be hard to develop a new system for its monitoring, we are not going to include these type of sensors in our proposal.

Finally, work presented in this chapter have been published in the following references (Parra et al., 2018a).

### **3. DEVELOPED SENSORS**

### 3.1. Introduction

In this chapter, we are going to show the developed physical sensors. These sensors will be able to measure physical and chemical parameters of water quality. In this chapter, the sensors are designed, developed and calibrated employing simple electronic components without using any node to gather the data. Thus, the results will be shown as a relation between a physicochemical parameter and resistance or conductivity of the physical sensor.

First, the conductivity sensors will be shown. The conductivity is defined as the capability of a matter or medium to permit the pass of electricity through it. It is measured in Siemens/meter or microhoms/cm (Light et al., 2005). Electric conductivity is also defined as the natural property of each body which represents how ease the electrons can pass through it. The electrical conductivity of liquids is related to the presence of salts, which generates positive and negative ions, because they are able to carry electric energy through the solution. Those ions are called electrolytes or electrolytic conductors. The electrical conductivity depends on the temperature of the solution. Because the temperature changes, it can also change the values of the ions, solubility, and solution viscosity among other issues (Zhiyao et al., 2005)

The conductivity measurement is a very important factor in several areas such as oceanography, agriculture, aquaculture or industry. The spatial and temporal monitoring of this parameter can be an important factor to prevent possible damages to fauna and flora or material damages. In some cases, it is necessary a great number of sensors to perform a correct monitoring. When the high spatial resolution is required, the number of sensors should be calculated according to the needs of the installation and their purpose. The increase in the number of sensors entails major installation cost. If we want to extend the use of these devices in wireless sensor networks for monitoring, for example, industrial processes, we need to develop more economic sensors maintaining the required quality and accuracy.

There are different ways to measure the electrical conductivity of the water. The traditional one is to measure the conductivity or resistance offered by the water. It can also be measured by using diamagnetic and paramagnetic proprieties of the water with a different concentration of salty ions. The paramagnetic substances increase the value of the magnetic field. Moreover, the diamagnetic substances drive down the magnetic field. Generally, each material has both kinds of behaviors but predominates one of them.

The magnetic fields are composed of electrical charges, which react with the environment. Those charges can attract or repel themselves and their behavior depends on the chemical or physical forces of the environment. Electric and magnetic charges represent different aspects of the same event. When there is no electric or magnetic charge, the electron's loads are not agitated. When an attractive force is applied, the electron's loads are agitated and begin to move in the direction of the applied force. In the case of water, its chemical composition determines the effects in the magnetic field. The interaction occurred between the electrical charges and the water molecules can cause that some atoms lose their electrons, those atoms are ionized or charged. As a result, these atoms attempt to recover the missing electrons. The combination of the ionized atoms and the magnetic fields causes the formation of an electric current in the water.

When an electromagnetic field passes through a material or medium, the measurement of the changes of the electromagnetic field can bring information about some of its proprieties. In the water medium, the measurement of electric conductivity can bring information about water quality and the concentration of dissolved salts. This is important in many areas such as water management, agriculture, aquaculture or groundwater supplies. In the case of agriculture, it is very important to know the salinity of the water used in the irrigation process; because when the soil is irrigated with water that contains a high concentration of salts can produce salinization of the irrigated soils in the long term. It is estimated that 50% of cultivated fields are suffering this kind of salinization (Reddy et al., 2006). In the case of aquaculture in fresh or sea waters, changes in salinity can cause the death of the cultured species, causing huge economic losses. Moreover, the saline intrusion is causing great damages in the groundwater supplies, which

would lead to obtaining not drinkable waters at the time. Unpolluted fresh water is becoming a limiting resource in some regions, so the saline intrusion in the aquifers of those regions must be controlled to ensure the availability of the water quality.

All these problems can be prevented and corrected using the proper control. Sensor networks, where sensor nodes are sensitive to conductivity changes, can bring an early warning signal, which allows applying the necessary measures to prevent harmful effects. In order to develop this sensor network, the first step is to develop a physical sensor able to measure the conductivity, which must be as cheap as possible, because, for example, to measure the environment of an aquaculture installation many sensors are needed. Low maintenance is also required for the sensors, so the contact between the water and the sensor should be minimized.

As the previous section concludes, the current conductivity sensors are based on the conductivity methods. Therefore, the sensors based on inductive methods are better for long-term monitoring. Nevertheless, there is not much information about the operation of those sensors in the literature. Thus, several tests were done in order to achieve an inductive conductivity sensor able to monitor the changes in conductivity in fish farms.

Following, the developed turbidity sensor is described. We design new turbidity sensors based on light absorption. For these turbidity sensors, we employ light with different wavelength in order to distinguish different substances in the water such as sediment of phytoplankton.

The increase in human population and the changes of land use increase the turbidity levels in water (Fabricius et al., 2016). The monitoring of turbidity, for different purposes, has become an important issue. Turbidity is caused by suspended particles in water; these substances may be organic or inorganic. The inorganic ones are mainly composed of sediments, while the organic ones are mainly algae, microorganism, etc... (MPCA, 2017 and APHA, AWWA, WEF, 2012). Turbidity measurements are necessary for water quality monitoring. It is measured in natural resources, because of the negative effects on ecosystems (Smith & Davis-Colley, 2001). Moreover, it is measured in drinking water (Beaudeau et al., 2014), or in irrigation water (PNUMA, 2017). The principal effects of turbidity in the ecosystems are (I) reduction of visibility, (II) reduction of light penetration and photosynthesis process or (III) clogging of gills and other adverse physical effects on fish and eggs (Bruton, 1985 and Wilber & Clarke 2001) among others. However, in some cases, the quantitative value of turbidity is not enough, because different types of turbidity may cause different effects. One example is in the fish farms, where the turbidity generated by sediments and the one generated by phytoplankton can require different actions to prevent further damages. For this reason, the characterization of turbidity is needed in the fish farms and in many other cases.

In fish farming, the increase of turbidity causes a reduction of fish performance. The effects of turbidity on fish growth and survival have been studied by different authors. Sutherland & Meyer (2007) maintained two fish species from 0 to 500 mg/l of sediment during 21 days. Their results showed that *Erimonax monachus* presented the highest SGR at 0 mg/l while *Cyprinella galactura* presented it from 0 to 50mg/l. Ardjosoediro & Ramnarine (2002) maintained red tilapia during 56 days at different turbidity values, from 0 to 500 mg/l of clay. Fish presented higher weight at the end of the experiments when the level of turbidity was lower. The maximum survival rates were reached from 0 to 50mg/l.

The opportunity of monitoring the values of turbidity at the water input in the aquaculture facilities is useful in order to take different actions to prevent further damages in fish production. It can be especially valuable for inland facilities with open water circuit. In the facilities where larval and reproducers are kept those sensors are crucial to ensure the water quality in the production tanks. However, different types of turbidity cause different effects on fish. Suspended sediment may cause gill damage. *Cyprinella galactura* shows no gill damage from 0 to 50 mg/l of sediment, moderate damage at 100 mg/l and severe at 500 mg/l (Sutherland & Meyer, 2007). Au et al., (2004) founded a correlation on *Epinephelus coioides* between gill damage and suspended sediments. Hess et al., (2015) studied the changes in gills morphology



on clownfish larvae exposed to suspended sediments. They conclude that fish exposed to 45 mg/l of sediments or more, had excessive mucous discharge and growth of protective cell layers. Moreover, in facilities with larvae culture, the technique of greenwater is widely used to increase the growth and survival of larvae (Faulk & Holt, 2005 and Palmer et al., 2007). This technique consists of adding algae in the water of the larvae tanks. However, this technique requires aeration to ensure the appropriate oxygen levels and to avoid the phytoplankton sedimentation. Recently, the use of clay has been studied as a substitute for phytoplankton in *Anoplopoma fimbria* (Lee, 2015a and Lee et al., 2017). However, the use of the greenwater technique requires the use of aeration to ensure that the oxygen concentrations do not decrease during dark periods. Different turbidity can cause different effects on fish and some specific actions must be taken. For this reason, it is necessary to have an automatic method to monitor the turbidity and to characterize it. Then, we can differentiate between two types of turbidity in fish farms, sedimentary turbidity, and phytoplanktonic turbidity. The worse possible conditions are related to the appearance of phytoplankton turbidity during dark periods (night or dark photoperiod in the tanks). In those conditions, the phytoplankton starts to consume the oxygen in the water and may require the activation of the aeration in order to prevent hypoxia conditions in the tanks. Moreover, some algae species may produce toxic products.

There are other areas where characterize the turbidity may be useful. The possibility to detect and track phytoplankton blooms is interesting in some ecosystems, Parra et al. (2015) proposed a similar system with hydrocarbons. The algae bloom formed by some species are considered as an abnormal situation in ecosystems that can cause eutrophication. Moreover, in some cases, those algae blooms can produce water pollution because of the production of some toxic compounds by the algae. Besides, in dark conditions, the algae blooms may consume high quantities of dissolved oxygen.

The most common method for measuring turbidity is the optical sensors. Optical sensor works by emitting a beam of light and detecting the amount of light that reaches the detector. Three techniques exist for optical sensing, according to the measuring angles. If the angle is  $90^\circ$  it is called nephelometric, if the angle is  $180^\circ$  it is called absorptimeters and if the angle is found between  $90^\circ$  to  $180^\circ$  it is called backscattering (Bin Omar & Bin MatJafri, 2009). Different techniques are applied to measure different turbidity levels (Lambrou et al., 2009). Takaaki et al., (2012) used 5 stations with optical sensors to monitor sediment transported in rivers. Schoellhamer & Wrightl (2003) used optical turbidity sensors for continuous measurement of suspended solids discharged in rivers. Stubblefield et al., (2007) used nephelometric turbidometry for determining suspended solids in a lake. The Secchi disk, a traditional method, consists of the introduction of a disk into the water, the distance in which we stop observing the disk is inversely proportional to the turbidity (Lee, 2015b). However, this methodology is not suitable for continuous monitoring. There are other methods such as acoustic sensors or the use of satellite images. Chanson et al., (2008) and Ward et al., (2013) used acoustic methods to measure the turbidity in rivers. Güttler et al., (2013) and Zheng et al., (2016) used remote sensing in rivers and lakes. The commercial turbidimeters that are currently in the market have two problems. The first one is the high price of the sensor, which may become prohibitive for many applications. The second one is that commercial sensors do not differentiate the type of turbidity (sedimentary or phytoplanktonic). Those are the current gaps in the commercial devices that are avoiding the use of turbidity sensors for monitoring in many applications.

Finally, the hydrocarbon and oil sensor is presented. This sensor is based on the differences in the light reflexion by the water surface and the hydrocarbon or oil layer. The sensor is composed of a LED and an IR photodetector. Several LEDs with different wavelength are tested in order to find the best wavelength to detect the presence of oil or hydrocarbon layer over the water surface. We present the design and development of a low-cost hydrocarbon sensor. The sensor is based on the photoluminescence effect linked to the hydrocarbons. We use as a source different light wavelength from LEDs and a photoreceptor as a detector. The sensor will be able

to detect the presence of a fine layer of hydrocarbon on the water (including the presence of fuel or oils). With our sensor is not possible to determine the concentration of hydrocarbons. The developed sensor will be a feasible option to be included in a sensor network for water quality monitoring. The use of this sensor networks can be applied in some exposed areas as ports, where the presence of hydrocarbons is quite common or in sensitive areas as fish farms or protected areas. In the presence of hydrocarbons, the fish can die by asphyxia because of their skin and gills are covered by the hydrocarbon (Lari et al., 2016).

Even that is not common to have big oil spills in the surrounding of the fish farms, small spills can cause damages. One of the causes of hydrocarbon pollution in oceans are the ship accidents. They generally become an international affair. Hydrocarbon pollution affects several organisms from terrestrial to marine ones. The plants and animals, even the human society are affected. According to Dalton and Jin (2010), between 2002 and 2006 there were up to 7500 spills in US waters. The number of spills caused by vessels has been reduced in the last decades. Nevertheless, the number of spills related to pipelines has quadrupled from 1990 to 2010 (Jernelöv, 2010).

The rest of Chapter is structured as follows. Section 3.2 shows the test done with the conductivity sensors. The development of the turbidity sensor is detailed in Section 3.3. Section 3.4 presents the hydrocarbon/oil sensor. Finally, the conclusions are shown in Section 3.5.

## **3.2. Salinity sensor**

### **3.2.1. First models**

In this subsection, we are going to describe the structure of the conductivity sensors developed for the first tests. There are two different kinds of sensors, in both cases, we generated a magnetic field using a copper solenoid powered by direct current or alternate current. There are two different systems to measure the conductivity. The first one is a sensor is based on the measures of the magnetic field directly through the use of Hall sensor. The second one measures this magnetic field through the induced current on an inductive copper coil.

#### *3.2.1.1. Material and methods*

In these first tests, we pretend to evaluate the possibility to measure the conductivity through alteration in the magnetic field. Our purpose is to detect changes in the electromagnetic field and relate it with the conductivity of the water where it is passing through. It will let us create an electrical conductivity detector. In both cases, the used coils have a solenoid form.

In order to measure the electrical conductivity values, we used a commercial sensor: CM 35+. By using two different methods, we developed two different inductive conductivity sensors. The materials used in these tests are:

- Conductivity meter CM 35+ (Conductivity meter CM 35 +, 2018)
- Generator of AC
- Generator of DC
- Oscilloscope
- Hall sensor Axial Payme
- Tesalameter Phaywe
- Coil of copper of 0.8mm with an empty core
- Coil of copper of 0.8mm coiled covert a plastic tube with an empty core
- Copper coils from a current transformer of 0.4mm and a relation of turns of 1:36.66
- 6 assay tubes
- Salt

In these tests, we obtain the preliminary data to decide on which method we will base our sensor and continue the study.

Our purpose is to detect changes in the electromagnetic field and relate it with the conductivity of the water where it is passing through. It will let us create an electrical conductivity detector. In order to measure the electrical conductivity values, we used a commercial sensor: CM 35 +. By using two different methods, we developed two different inductive conductivity sensors.

Now, we are going to describe the structure of the conductivity sensors developed for the first tests. There are two different kinds of sensors, in both cases, we generated a magnetic field using a copper solenoid powered by direct current or alternate current. There are two different systems to measure the conductivity. The first one is a sensor is based on the measures of the magnetic field directly through the use of Hall sensor. The second one measures this magnetic field through the induced current on an inductive copper coil.

#### 3.2.1.1.1. Based on a hall sensor

For the first method, we prepared an assembly with a solenoid without core that generates the electromagnetic field. In the center of the solenoid, we introduced an assay tube, which is used as a container for the water samples. Moreover, in the center of the solenoid (where the magnetic field is higher), inside the assay tube, we inserted a magnetic field sensor. The solenoid was powered by a direct current (DC) generator or connected to an alternative current (AC) through a transformer from 220V to 12V, depending on the desired output measurements (in Direct Current or Alternating Current). See the explained in Figure 3.1.

The whole structure was fixed using a laboratory support to assure that when the solenoid and the assay tube are removed (in order to change the solution), the position of the sensor respect to the solenoid is maintained. This is very important, because when the position of the sensor over the center of the solenoid changes, vary the values of magnetic field. This backing system is useful only for the height and the vertical movement. The horizontal movement has less importance because the width of the assay tube, the center of the solenoid and the sensor are almost the same and that precluded the horizontal movement.

We prepared a second experience with this system (Hall sensor), a second solenoid without the assay tube, in order to avoid the potential interferences caused by the glass of the assay tube. In this solenoid, the wire that generates the magnetic field envelops the exterior of a plastic tube that is used as a container for the water samples used in previous tests. The rest of the structure was the same as Figure 3.1 except the glass tube.

In both cases, the sensor used was the Hall Axial Payme probe, connected to a Tesalometer Phaywe with a range of measurement from 0 to 2000mT.

#### 3.2.1.1.2. Based on an inductive coil

We also developed a second experiment to study the possibility of measure the electrical conductivity using the generated current on an inductive coil. In order to achieve this goal, we use two copper coils, their wire has a 0.4mm diameter. Those coils were overlapped and do not have a core. The turn relation is 1:36.66. They were part of a voltage transformer that was removed previously. Both coils have a solenoid form. In one coil we introduce AC at different voltages and frequencies, always maintaining a sine wave. This is the powered coil. Meanwhile, we measure the induced current in the other coil, the induced coil.

In the previous case, the water samples are introduced in the center of the magnetic field. At this point, the magnetic field is bigger and the changes are maximum. Thus, we should take the measurements of that specific place. In this case, we want to affect all the magnetic field, so the water must surround the whole space occupied by the magnetic field. So, we introduce both coils inside the water samples. In this case, the water envelops the coils, the core (which is empty) and the exterior.

The coils are isolated from the environment with silicone using a silicone gun to ensure that the water does not enter inside the coils. If there is enamel cracks in contact with the

water, there will be a short. Moreover, the coils had some paper protections, and their permeation can cause changes in the coil properties. In this case, we use a generator of alternating current to power the first coil and an oscilloscope to measure the electric conductivity of the powered and the induced coil. The explained structure is shown in Figure 3.2.

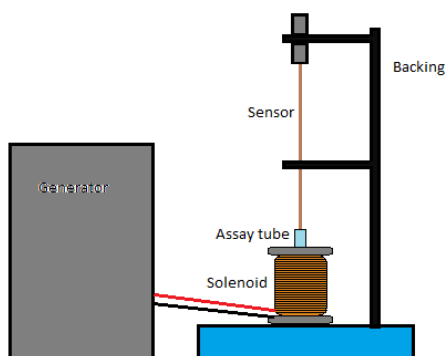


**Figure 3. 1** Structure of the laboratory test bench for Hall sensor.

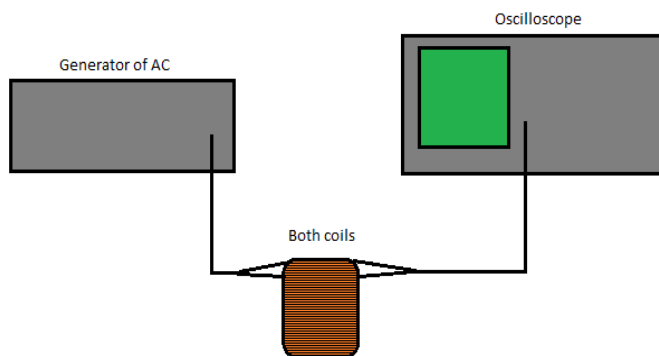


**Figure 3. 2** Structure of the laboratory test bench for Two Coils.

An initial test was performed, first, the coils were in the air, so the magnetic field is completely enveloped of air, and the oscilloscope presents a fixed signal, that signal can be seen in Figure 3.3. When the environment changes and the coils are inside the water, the magnetic field is affected by this water. So the current induced in the inductive coil changes. The new signal can be seen in Figure 3.4. This change can be seen comparing Figures 3.3 and 3.4.

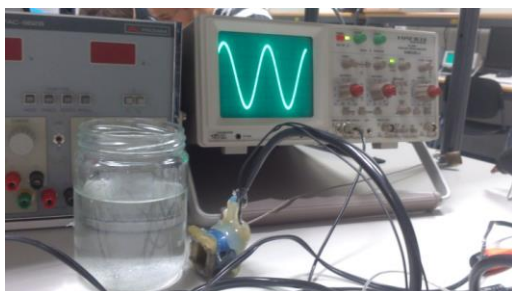


**Figure 3. 3** Laboratory set-up with the probe in the air

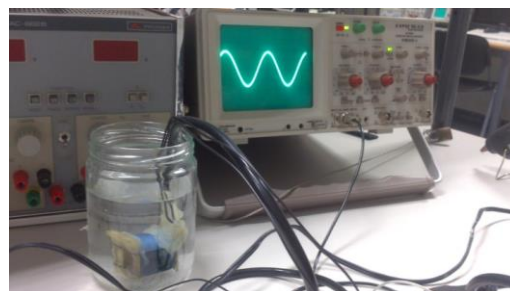


**Figure 3. 4** Laboratory set-up with the probe in the water.

### 3.2.1.1.3. Developed tests

We have done two sets of analysis, one for each methodology. The first one uses the solenoid and the Hall sensor. The purpose of these tests was to demonstrate that differences in the environment can produce alterations in the magnetic field. The second set of analysis was aimed to obtain more sensibility and the reduction of the cost of the sensor. To achieve this goal, we used an inductive coil in which we registered the induced voltage as an output signal instead of a Hall sensor.

Our hypothesis is that we expect to be able to detect changes in the magnetic field when we vary the properties of the environment. In order to know the best point to perform the measures, we performed different tests at different electric conditions.

In the first ones, with DC current, we measured the value of the magnetic field when the generated field by the solenoid passes through different samples with different values of electric conductivity, those values are shown in Table 3.1. We measure the changes of the

magnetic field at different powering conditions; values of used current are shown in Table 3.2. For this experience, we use the structure represented in Figure 3.1, with the solenoid that has a test tube inside.

**Table 3. 1** Values of voltage and current used to power the solenoid in the first test of DC current and sensor based on Hall sensor

<b>Voltage (V)</b>	5	10	15
<b>Current (A)</b>	0.2	0.4	0.6

**Table 3. 2** Values of electric conductivity of water samples of the first set of test

<b>Sample</b>	1	2	3	4	5
<b>Conductivity (mS/cm)</b>	0,002	0,405	191,4	213	285

Later, we measure those samples with AC at 12V, to confirm the different behavior with a different type of current. In this case, the coil is powered using a current transformer from 220V to 12V which was connected to the electrical installation of the laboratory.

With the same purpose as before, to obtain the behavior at different conditions, now we change the frequency of the current. This is aimed to find the best point to perform the rest of measures and obtain the most accurate correlation. The used frequencies to realize the measurements are shown in Table 3.3.

In this case, we use the two solenoids, the first one is the same used in the DC, the solenoid with a test tube inside, see Figure 3.5. The second solenoid is the solenoid coiled on a plastic tube that contains the water, see Figure 3.6. The purpose is to know if an attenuation of the signal due to the glass test tube exists, and if this causes a different changes behavior, that implies less precision.

In order to complete the first test bench, we take measurements at higher DC voltages with the first solenoid, the one that has a test tube. For this test we use different samples, which had different concentration of salts, those conductivities are shown in Table 3.4.

**Table 3. 3** Values of frequencies used at 12V

	<b>AC at 12V</b>			
<b>Frequency (Hz)</b>	15	150	1500	15000

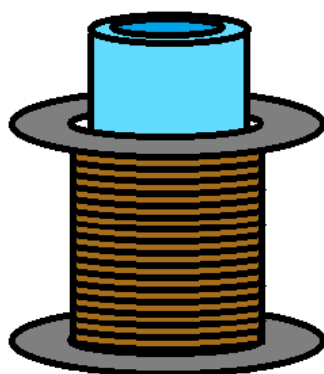


**Figure 3. 5** The first solenoid of the first test, which has an assay tube in the center.



**Figure 3. 6** The second solenoid for the first test, which is coiled on a plastic tube that serves as a container

**Table 3. 4** Values of electric conductivity of water samples

Sample	1	2	3	4	5	6
Conductivity (mS/cm)	0,0028	0,378	1,087	51,2	147,9	194

The second set of laboratory tests is performing using the two overlapped solenoids. The first one is connected to AC at different voltages, using a generator. This coil generates a magnetic field that causes an induction of the second coil. The core of those coils was removed, allowing us to use the air or water as the coil core. Then, we take measurements in both environments, air, and water (in this second case we immersed both coils in a container full of water with high salinity). The measurement of the induced voltage is taken with an oscilloscope by measuring from peak to peak the sine wave. We want to relate the output voltage of the induced coil with the conductivity of the water.

First, we perform several changes of the working frequency. We observe the difference of the induced voltages in the second coil when the environment changes (air or water). This is a preliminary test aimed to find the frequency where the difference between air and water is maximum. Probably at this frequency, the same coil will detect more accurately the changes between different conductivities.

The second test was also performing with different frequencies shown in Table 3.5. But in this case, the voltage of the induced coil is fixed to 2.8V in the air, changing the voltage of the powered coil. Then, we introduce both coils inside a container with salty water and compare it with the obtained voltage after this change. The aim of this test is to find the point where the change of the voltage is higher when we change the environment. This point is important to be found because this will be the point where we will have the maximum precision. This frequency depends on each coil; we made some tests to use it in future tests.

**Table 3. 5** Results of the induced current in air

AC at 2.8V of the induced current in the air										
Frequency (kHz)	0.5	1	2	4	5	6	7	10	20	100

### 3.2.1.2. Results

First, we describe the results obtained in the first set of analysis performed with the solenoid and the commercial sensor. We are going to start showing the results obtained with AC, those results are shown in Table 3.6. We have not appreciated any correlation between the magnetic field and the conductivity of the water at 12V at any frequency. Thus this method is not useful with the employed equipment (maybe with a sensor with higher sensibility we will be able to take this measure).

We repeated the same tests with the second solenoid in order to know if the problems obtained in the previous test are caused by the influence of the glass tube. The results are shown in Table 3.7. In this case, we have not also appreciated any correlation between the magnetic field and the conductivity of the water at 12V, but we have seen a difference in the magnetic field when the environment changes (air or water) only at 15Hz and at 1500Hz.

**Table 3. 6** Magnetic field (mT) values at different conductivities and frequencies with 12V (AC) with

Solenoid 1 (with the test tube).				
Conductivity (mS/cm)	15Hz	150Hz	1500Hz	15000Hz
Without assay tube	269	198	26	3
0,002	269	198	26	3
213	296	198	26	3

**Table 3. 7** Magnetic field (mT) values at different conductivities and frequencies with 12V (AC) using

Solenoid 2 (without the test tube.)				
Conductivity (mS/cm)	15Hz	150Hz	1500Hz	15000Hz
Without water	0.17	0.18	0.16	0.03
0,002	0.16	0.18	0.15	0.03
213	0.16	0.18	0.15	0.03

Now, we present the results obtained with the test when using DC. In this case, we only take measurements with the first solenoid because the other solenoid has fewer turns so the generated electromagnetic field is lower. Also in the previous test, we observed that the influence of the glass tube is not so important.

First, we took measurements with 5 samples with a different concentration of salt and different voltages (shown in Table 3.1 and Table 3.5). The conductivity of the samples has 3 intervals, 1 with the lowest conductivity, 0.002mS, other with low conductivity, 0.405 mS, and 3 samples with high conductivity 192 mS, 213 mS, and 285mS. This distribution allows us to see different issues. First of all, it is possible to distinguish between very different conductivities (low values and high values). Second, it allows us to know the different sensitivities in high conductivities or low conductivities because the sensitivity is different at different ranges for electrical conductivity.

In this case, we did two series of measures at each voltage, to know the repeatability because we have seen that in some cases there is a low repeatability. Those measures are called Test A and Test B, Test A was done before and once in are finished we started again with the measures of Test B.

The results showed us that at high voltages the sensibility increases, but, at the same time, it caused some problems, because a change in the position of the sensor in the magnetic field causes variations in the lecture of the value. At high voltage values, the error committed in a single value is higher than at low voltages. It is so important when taking measurements from different ranges. The results are shown in Table 3.8.

**Table 3. 8** Magnetic field (mT) values when measuring different conductivities at different DC voltages

Environment	Measured at 5V		Measured at 10V		Measured at 15 V	
	Test A (mT)	Test B (mT)	Test A (mT)	Test B (mT)	Test A (mT)	Test B (mT)
Air	2,89	2,90	8,66	8,72	14,89	14,51
Water with conductivity (mS/cm)						
0,002	2,91	2,93	8,68	8,71	14,86	14,56
0,405	2,93	2,96	8,69	8,89	14,82	14,66
191,4	2,93	2,98	8,69	8,89	14,81	14,64
285	2,97	3,01	8,70	8,90	14,82	14,59
213	2,96	3,00	8,73	8,92	14,78	14,62

In Figure 3.7, we can see the representation of the measurements obtained at 5V in test A and test B. In this case, the results show that is possible to distinguish between different conductivities. In all cases, the value of the magnetic field registered in the center of the solenoid increases with the conductivity of the sample. In this case, it is possible to distinguish between samples with low conductivity, but with high conductivities, the sensibility is lower. At low conductivity, a variation in the conductivity of the water of 0.4 mS/Cm causes a variation on the magnetic field of 0.02 mT, but at high concentrations, a variation of 94 mS/cm causes a variation of just 0.04 mT (examples of test A). It shows that at low conductivity values the sensitivity is higher than at high conductivity values. The changes in the magnetic field are almost the same in both tests, test A and test B, with a little increment in test B respect test A. So, at 5 V the repeatability of the measures is good.

In Figure 3.8 the measures obtained at 10 V for test A are shown. The behavior presented when we measure at 10 V in test A is similar to the presented and at 5V, in all cases, the value of the magnetic field registered in the centre of the solenoid, increase with the conductivity of the sample. At low conductivity, a variation in the conductivity of the water of 0.4 mS/Cm causes a variation on the magnetic field of 0.01 mT, but at high concentrations, a variation of 94 mS/cm causes a variation of just 0.04 mT (examples of test A). It demonstrates that at low conductivity values the sensitivity is higher than at high conductivity values, the same that happened in test A and test B at 5 V. The results of test B was not so coherent and did not show a correlation between magnetic field and conductivity. That can be caused because at higher voltages minimum variations in the position of the Hall sensor respect the solenoid causes bigger errors than at lower variations.

We realized also measures at 15 V of two test, but both times yield confusing results, so they are not represented. We think that they may be caused by errors in the position of the sensor respect the magnetic field or because 15 V is not a good input voltage for the sensor.

We also performed measurements at 20V with different samples of water, shown in Table 3.5. The main problem was that at these voltages the coil starts to heat up, and this heat interferes with the measures. So, is very important to realize the measures and turn off the generator that powers the coil. The results are shown in Table 3.9 and represented in Figure 3.9.

**Table 3.9** Measures obtained at 20 V of DC

Conductivity of samples (mS/cm)	0,0028	0,378	1,087	51,2	147,9	194
Magnetic fiel (mT)	50,4	50,2	49,8	48,5	48,2	48

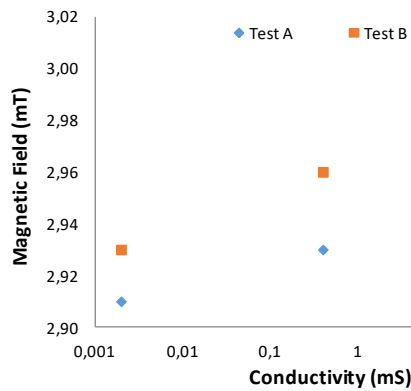


**Figure 3.7** Representation of the data for 5V for test A and test B

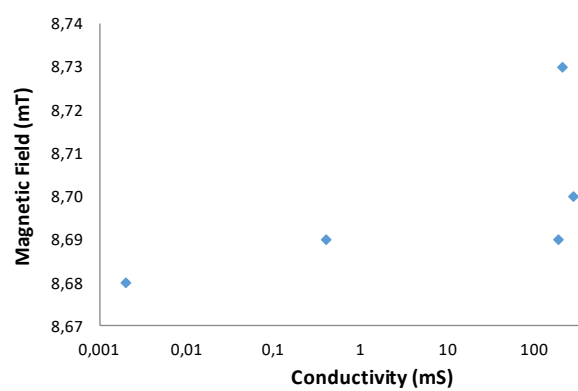


**Figure 3.8** Representation of the data for 10 V for test A

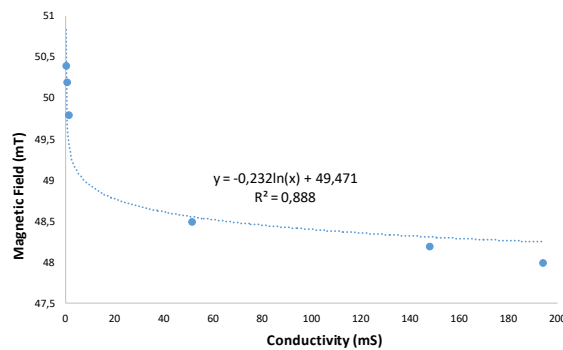


**Figure 3.9** Representation of the data for 20V for test A



This test showed us that there is a good correlation between the changes in the magnetic field and the conductivity of the samples. The magnetic field decreased in all cases when the conductivity increased. This relation can be expressed as a logarithmic function, see Eq. (3.1). In this case, it presents higher sensibility at low values of conductivity.

$$\text{Magnetic Field (mT)} = -0,232 * \ln(\text{Conductivity (mS/cm)}) + 49,471 \quad (3.1)$$

The first set of tests shows us that there is a huge variability in the obtained results, and there is a good correlation in just some cases. Moreover, at high values, where the magnetic field is higher and we expect to have a major sensibility, there are a lot of problems with the heath of the coil. Furthermore, the changes of the position of the Hall sensor respect of the center of solenoid produces errors.

In the first test, we changed the frequency and we observed the voltage in the induced coil in both environments: water and in the air. The results are shown in Table 3.10 and are represented in Figure 3.10. We observed that in the air, voltages increase until 4 kHz. Then, it is maintained until 7 kHz and starts to decrease. Otherwise, in water it increases until 4 kHz, then it starts to decrease. Both environments have the same behavior but different peaks. These behaviors can be interpolated with the following equations: Eq. (3.2) for air and Eq. (3.3) for water. The correlation coefficients are 0.86 for both equations. These results demonstrate us that it is possible to distinguish between salty water and air at any frequency, but some frequencies have higher differences.

$$\text{Voltage of induced coil (V)} = 23 / (-1,071 - 0,01984 * \text{Frequency (kHz)}) \quad (3.2)$$

$$\text{Voltage of induced coil (V)} = 653,4 / \text{Frequency (kHz)} \quad (3.3)$$

We need to know in which frequency the difference between environments is higher, and this is what we did in the second test. We change the frequency, but maintaining the voltage of the induced coil in air at 2.8 V. These results are shown in Table 3.11 and represented in Figure 3.11.

**Table 3. 10** Induced coil voltage at different frequencies when the environment changes

Frequency (KHz)	Voltage (V) in Salty water
0,1	2,4
0,5	2,8
1	2,8
10	1,25
25	1,8
50,8	2
100	3,25
145	2,5
248	2,8
500	3,2
750	3,6

**Table 3. 11** Induced coil voltage at different frequencies when the voltage in the air is fixed at 2.8v

Frequency (KHz)	Voltage (V) measured in	
	Air	Salty water
0,5	15	3
1	18	6,4
2	18	14
4	20	17,5
5	20	13,6
6	20	11,9
7	20	10,4
10	18	8
20	15	5
100	7,6	0,6

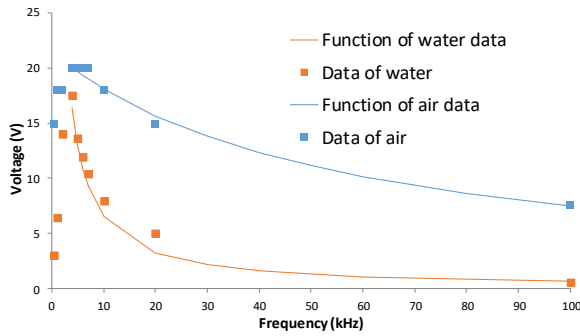


Figure 3. 10 Representation of the data of Table 3.10

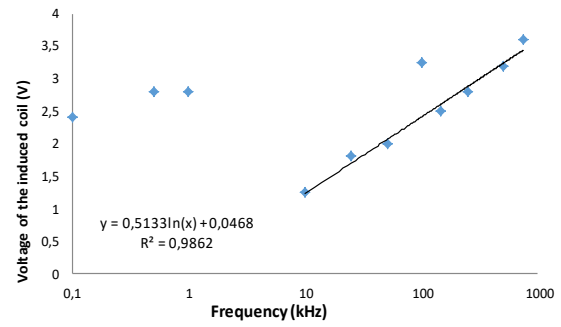


Figure 3. 11 Representation of the data of Table 3.11

In Figure 3.11 we can see that depending on the frequency, the effect of the change of environment can have a different sign (positive sign or negative sign). So the voltage in the water can increase or decrease with respect to the voltages in the air. The value of the voltage in the induced coil was always 2,8V. The point where the sign changes is at 248 kHz. From 10 kHz to 248 kHz the change of environment (air to water) makes to decrease the voltage. This change is higher at 10 kHz and decreases until 248 kHz where is null. From 248 kHz the change of the environment makes to increase the voltage and the difference in voltage increases when the frequency increases. Part of this data (from 10 kHz to 1000 kHz) have a logarithmic behavior and follow the Eq. (3.4):

$$\text{Voltage of induced coil (V)} = 0,5133\ln(\text{Freq. (kHz)}) + 0,0468 \quad (3.4)$$

The best point to take measurements will be the point where the values have higher differences. We can find two different points to take measurements, at high voltages (1000 kHz) and at medium voltages (10 kHz). The maximum differences appear at 10 kHz.

### 3.2.1.2.1. Comparative of prices of the developed sensors and current commercial sensors

In this section, we are going to make a comparison of the prices of the commercial sensors of conductivity and the price of the final assembly of the sensors that we used in these tests. The data of the price of commercial sensors are founded on the different websites of the fabricants, shown in Table 3.12. Meanwhile, the prices of the proposed sensors are calculated according to the necessary materials and the electronic components needed to their assembly, shown in Table 3.12 and Table 3.13. The total price of the first model (Hall sensor + Solenoid) is 42.83€. On the other hand, the total price of the second model (Two Solenoids) is 48.19€.

Table 3. 12 Price of the components for sensor 1

(Hall sensor + solenoid)	
Component	Price (€)
Sensor of Hall Effect	1.64
Voltage regulator +5V (1A output current)	14.50
Voltage regulator -5V (1A output current)	2.73
PIC 16f8775.39	5.39
Digital to Analog converter – 8 bits	8.57
Resistors and capacitors	3
Coil solenoid	7

Table 3. 13 Price of the components for sensor 2

(Two solenoids)	
Component	Price (€)
Voltage regulator +5V (1A output current)	14.50
Voltage regulator -5V (1A output current)	2.73
PIC 16f8775.39	5.39
Digital to Analog converter – 8 bits	8.57
Resistors and capacitors	3
2 x Coil solenoid	14

We can see in Table 3.14 that the price can vary quite a lot from one vendor to another. The cheapest costs around 85.00 €, while the most expensive costs around \$806. The new developed sensors are nearly 50% cheapest than the commercial sensors.

**Table 3. 14 Comparative of prices of different sensors on the market.**

Name	Fabricant	Physical method	Range of values	Price
WQ-COND	Global Water	Conductive	0 to 2000 mS/cm	606€
YSI 5560	YSI	Conductive	-	288€
PCE-CM 41	PCE Holding GmbH	Conductive	0 to 20 mS/cm	85 €
HI 98309	Hanna Instruments	Conductive	0,000 to 1,999 S/cm	122€
HI 720122-1	Hanna Instruments	Inductive	0 to 2000 mS/cm	503€

### 3.2.1.2.2. Discussion

In these tests, we demonstrate that different environments (air, fresh water and, salty water) can produce different alterations in the electromagnetic field, and these alterations can be measured by different methods.

First, by using a solenoid we can measure the values of the electromagnetic field. But the sensibility of this sensor is too low and we need to increase the voltage of the solenoid in order to obtain enough sensibility in the sensor, this produces 2 problems. In the first one, the solenoid heats up and we need to turn off the solenoid between measures because this heat produces interferences (it changes the magnetic field that produces the solenoid). The second one happens because when the magnetic field increases, little changes in the position of the sensor and the solenoid produce erroneous data.

Another way to solve the problem of low sensibility was measuring the electromagnetic field through the induction of a voltage in the second coil. In this case, we are able to distinguish air from salty water at different frequencies. We have observed that the best frequency to measure is at 10 kHz. In some cases, we have been able to distinguish water with low conductivity from high conductivity.

The advantages of these detection methods versus the traditional ones are that we do not need to put in contact the sensors (the two copper coils or the copper coil with the magnetic field sensors) with the environment. So, there is no high degradation of the sensor along the time. This is very important because it means that the sensor can be left at any place with no maintenance. Moreover, because the sensor does not have any perishable part or is not consumed during the measurement, the lifespan of the sensor only depends on the energy source.

The main problem in the first set of tests was that there are important changes in the electromagnetic field when the position of the sensor over the solenoid changes. To prevent this in future tests we propose to create a fixed container for liquids or to make it waterproof and introduce it inside the water. The problem in the second set of tests is that the coils have to be completely isolated. Any hole can make the coils started to drench.

## 3.2.2. The copper coils as conductivity sensors

In this subsection, we are going to describe the structure of the conductivity sensors developed based on two coils. In this test, we will use different coils combination in order to perform an exploratory test to find the best combination. The aim is to find the best combination to use it for conductivity monitoring in fish farms.

### 3.2.2.1. Material and methods

The models of sensors showed in section 2, are based on inductive coils that always use two toroid coils in the same position, one over the other. But in this section, we perform a

comparative study to decide which the best option is. We will use other configurations and compare the results.

For this section the material that we use are the next:

- Conductivity meter CM 35+
- Generator of AC
- Oscilloscope
- Copper coil of 0.4mm, 0.6mm and 0.8mm (See Table 3.15 for more information)
- Nonferus materials to use for coiling surface
- Resistance of 100  $\Omega$
- Capacitor 100nF
- 5 glass containers
- Tap water
- Salt

In order to check what coil configuration present the best performance, we have used different sensor models formed by two coils. In this section, we are going to present 4 models. Each model has been physically characterized taking into account its size, a number of spires, the diameter of enameled copper wire and kind of coil.

#### 3.2.2.1.1. Description of coils models

When a wire conducts an electric current, it is generated a magnetic field wrapped around the wire. Furthermore, when a wire is introduced into a magnetic field, the wire begins to conduct an induced electric current.

We used to types of coils, solenoids, and toroids. We made different configurations using only solenoids, only toroids or toroid, and solenoid. Moreover, we put this coils in different positions of the coils, one over the other and one inside the other.

All models are formed by two coils where the coil with the lowest number of spires is the powered coil (POWC) and it was powered by a sine wave of 8 Volts peak to peak amplitude. This coil induces a current on the induced coil (INDC). The output voltage is proportional to the magnetic field interaction with the fluid of the medium. The magnetic field is affected by the concentration of dissolved salts in the liquid. Table 3.15 shows the models used in our tests and their features.

#### 3.2.2.1.2. Test bench

To perform our test, we have prepared 5 dissolutions with different amount of dissolved salts. In order to prepare our samples, we have used common salt (NaCl) and tap water. Table 3.16 shows the value of TDS and the conductivity of each sample (measured with a calibrated device). The first sample which presents the lowest conductivity corresponds to the tap water. These samples include the conductivity values from freshwater to seawater.

Each model is submerged in the five dissolutions starting with the sample of lowest conductivity. The vessels which contain the dissolutions have a high of 14 cm, but the liquid level is 7.5 cm. The containers have a diameter of 7.9 cm. In all cases, the coils are entirely covered by the dissolution.

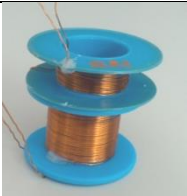



For each model and sample, we are going to perform a frequency scan between 0.1KHz to 800 KHz. because in this range we detect at least a point in the frequency range where we can measure the water conductivity. The third model is measured for a range of 0.1 kHz to 2000 kHz. The water temperature was 23.2°C.

The results of our test will be a voltage value proportional to the current induced in the second coil due to the interaction of the magnetic field with the aqueous medium. From our results, we will be able to determine the best working frequency for each configuration and if it is possible to define a linear working range. The best working frequency will be that which present higher differences in output voltage for each sample. From the results of each model,

we will extract the mathematical expression which will relate the conductivity and the output voltage.

**Table 3.15.**

**Table 3. 15** Models of coils used in tests to compare the different configurations of coils combination (S: Solenoid, T: Toroid)

Model	POW	Features PC	INDC	Features IC
1 	S	Wire Diam.: 0.6 mm Coil Diam.: 29.6 mm Coil High: 13.8 mm - N° of Spires: 21	S	Wire Diam.: 0.6 mm Coil Diam.: 29.6 mm Coil High: 27 mm N° of Spires: 45
2 	T	Wire Diam.: 0.4 mm Inner Coil Diam.: 19.6 mm Outer Coil Diam.: 26.4 mm Coil High: 24.9 mm N° of Spires: 77	T	Wire Diam.: 0.4 mm Inner Coil Diam.: 39.8 mm Outer Coil Diam.: 51.2 mm Coil High: 24.9 mm N° of Spires: 304
3 	S	Wire Diam.: 0.6 mm Coil Diam.: 27.2 mm Coil High: 17.8 m N° of Spires: 31	T	Wire Diam.: 0.8 mm Inner Coil Diam.:30.6 mm Outer Coil Diam.: 44.7 mm Coil High: 22.3 mm N° of Spires: 132
4 	T	Wire Diam.: 0.8 mm Inner Coil Diam.:23.2 mm Outer Coil Diam.: 56.5 mm Coil High: 26.9 mm N° of Spires: 81	S	Wire Diam.: 0.8 mm Inner Coil Diam.:25.3 mm Outer Coil Diam.: 33.6 mm Coil High: 22.6 mm N° of Spires: 324 in 9 layers.

**Table 3. 16** Samples used in tests to compare the different configurations of coils combination

Sample	1	2	3	4	5
Amount of added salt (mg/l)	254	4020	2340	40200	57700
Conductivity (mS/cm)	0.397	6.28	36.6	62.9	90.2

### 3.2.2.2.Results

This section presents the measurement results for our four models. On the one hand, we are going to show the behavior of each model as a function of frequency. After that, we will analyze the relation between water conductivity and output voltage for each model for the frequency of best results

The first model presents similar values of output voltage depending on the frequency. For frequency range of 400 kHz to 600 kHz, this coils combination present different output voltage as a function of water conductivity. The frequency with highest differences between samples is 500 kHz where we have registered 1.5 V for water with the lowest conductivity and 21 V for the sample with the highest concentration of salt. The behavior of first model is shown in Figure 3.12.

Figure 3.13 shows the output voltage for the second model as a function of frequency. In this case, the value of output voltage (in the induced coil) decreases when the water conductivity

increases. In addition, we can see that the output voltage is very similar to water with any salt concentration.

Finally, this model does not present any significant peak in the signal behavior. The optimal frequency for the second model is registered at 500 kHz where we can distinguish between salty water and freshwater.

The third model combines a solenoid and a toroid. This model shows significant results at high frequencies (2000 kHz). In medium and lower frequencies, the registered behavior is very irregular. It starts to be stable for frequencies from 1750 kHz. Figure 3.14 shows the behavior for the third model.

The last model presents two frequencies which can be used for measuring the water conductivity. The first one is registered at 150 kHz with output voltages of 0.65 V for tap water and 4.1 V for water with the highest conductivity. Figure 3.15 shows the measurement results for the fourth model.

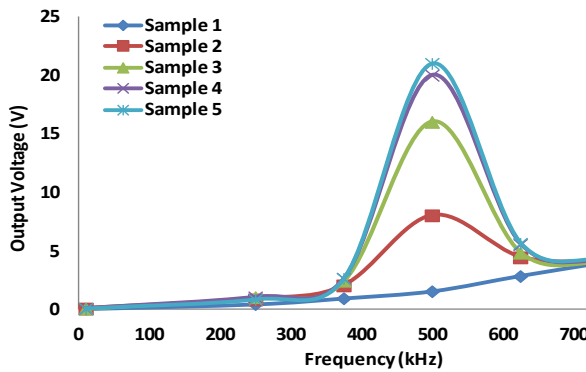


Figure 3.12 Output voltage for first model.

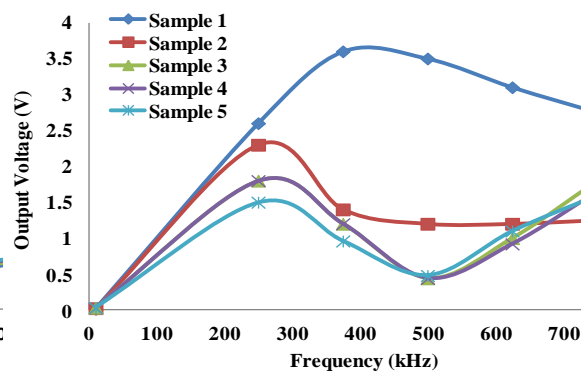


Figure 3.13 Output voltage for second model.

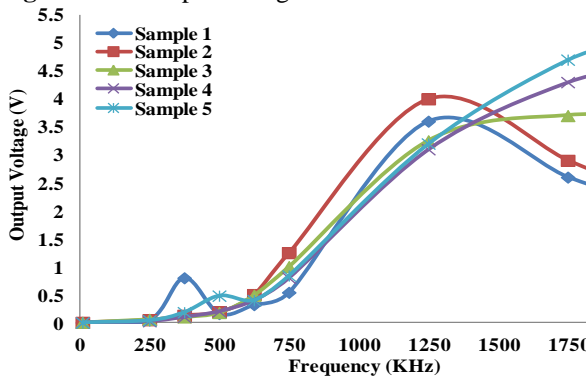


Figure 3.14 Output voltage for third model.

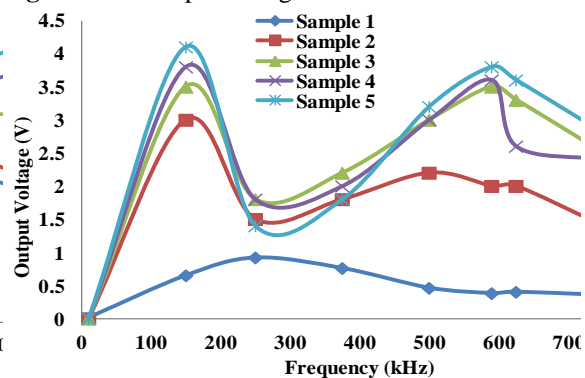


Figure 3.15 Output voltage for fourth model.

Once we have found the best working frequency for each model, we can analyze the operation of each model showing their response in volts as a function of the water conductivity.

In order to analyze the relation of conductivity and output voltage, we are going to take into account two factors:

- Correlation between conductivity and output voltage registered in the induced coil.
- Slope in the linear range.
- If there is a linear working range.

We are only going to consider a linear range when, at least, 4 points are contained in this range and the value of correlation coefficient is higher than 0.95.

For the first model, we have analyzed the relation between output voltage and water conductivity at 500 kHz (See Figure 16). We can use the Eq. (3.5) to model its behavior. Model 1 presents a correlation coefficient of 0.99.

$$V_{out} = 4.653 \cdot \log(0.9833 + C) \quad (3.5)$$

Where  $V_{out}$  is the output voltage induced in the second coil in Volts and C represents the water conductivity in mS/cm.

As we can see in Figure 3.16, the linear range of this model is not clear. The behavior of this combination of coils fits a logarithmic function and we do not have enough points to approximate this behavior to a linear range with enough accuracy.

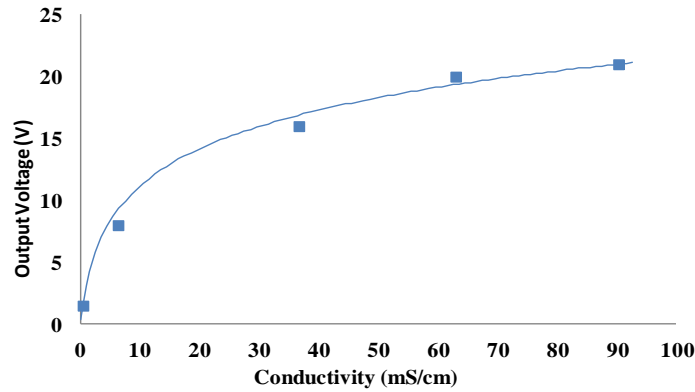


**Figure 3. 16** Relation between water conductivity and output voltage for Model 1 at 500kHz.

Figure 3.17 shows the relation of output voltage as a function of the water conductivity for Model 2. Eq. (3.6) represents the mathematical model for this configuration of coils.

$$V_{out} = 2.446 \cdot C^{-0.3877} \quad (3.6)$$

Where  $V_{out}$  is the output voltage induced in the second coil in Volts and C represents the water conductivity in mS/cm. The correlation coefficient for (2) is 0.9952. In this case there is not a linear clear linear range.

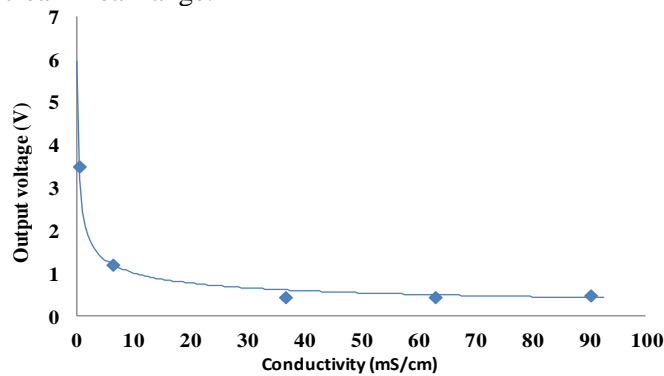


**Figure 3. 17** Relation between water conductivity and output voltage for Model 2 at 500kHz.

The third model shows a linear behavior at 2000 kHz (See Figure 3.18). In this case, the relation between the induced output voltage (V) and conductivity (mS/cm) can be expressed as Eq. (3.7) where the correlation coefficient is 0.98. Finally, Figure 3.19 shows that Model 4 presents a clear linear behavior from 6.28 mS/cm. to 90.2mS/cm. Eq. (3.8) show its

mathematical expression where  $V_{out}$  the output voltage is induced in the second coil in Volts and C represents the water conductivity in mS/cm. The correlation coefficient for (8) is 0.99

$$V_{out} = 0.0324 \cdot C + 2.2675 \quad (3.7)$$

$$V_{out} = 0.013 \cdot C + 2.9637 \quad (3.8)$$

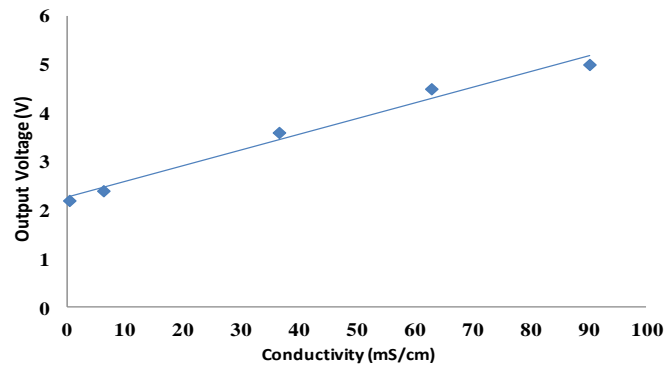


**Figure 3.18** Relation between water conductivity and output voltage for Model 3 at 2000kHz.

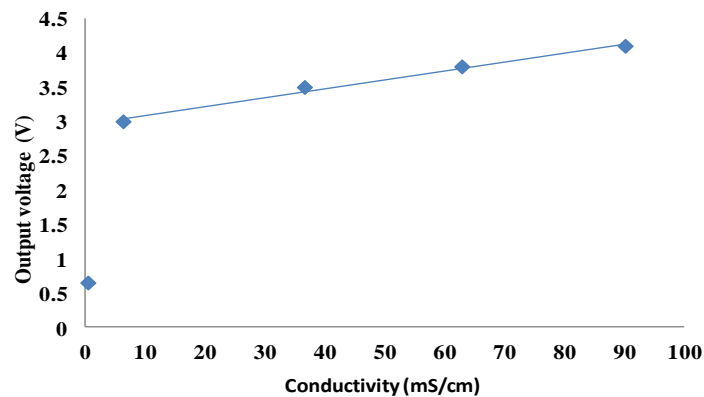


**Figure 3.19** Relation between water conductivity and voltage registered in the Model 4 at 150kHz.

### 3.2.2.2.1. Comparison of models and Discussion

As previous sections show, it is possible to use several combinations of coils to measure the water conductivity. However, Section 3.2.4.1 has shown that some combinations of coils present better performance to measure this parameter. In this section, we are going to compare the results of four models that we have tested. We will also discuss the possible applications of each model.

Table 3.17 shows a summary of best results shown by each model. As we can see, each coil presents different behavior. On the one hand, Model 3 and Model 4 have a linear working range. A low value of slope means that a high variation in the conductivity value generates high variations in the output voltage in the induced coil. The linear range of Model 3 presents higher slope than the one offered by Model 4. However, the optimal frequency for Model 3 is 2000 kHz meanwhile the fourth model places its optimal frequency in 150 kHz. This would be the best option because the cost (economical and energetic) of a prototype with a lower frequency is lower. Model 1 does not have any linear working range but we can approximate its operation as 3 linear working ranges as a function of conductivity. Finally, Model 2 can also be approximated by 3 linear working ranges. The specific applications for this model must be focused on freshwaters areas because at higher values of conductivity, we cannot define a correct value of voltage.



In this section, 3.2.4, we have analyzed 4 configurations of coils to measure the water conductivity. These models combine toroids and solenoids with nonferrous cores. As our measures show, models which present best results are Model 1, Model 3 and Model 4. Previous works have shown other coils combinations. All of them are coils located one after another. But, we have also checked configurations of coils which contains other coils. Finally, we have not used ferrous cores although these avoid the expansion of the magnetic field. Nonferrous cores are more susceptible to magnetic interferences but allow greater frequency range and higher sensitivity.

**Table 3. 17** Comparative of best results for four models.

	Lineal range (mS/cm)	Slope	Optimal frequency (kHz)	Possible camps of applications			
				Estuarine environments	Saline wedges	Irrigation water	Saline environments
Model 1	-	-	500	✓	✓	-	-
Model 2	-	-	500	-	-	✓	-
Model 3	0,397 - 90,2	0,0324	2000	✓	✓	✓	✓
Model 4	6,28 - 90,2	0,013	150	✓	✓	-	-

### 3.2.3. Studying the combination of solenoid and toroid

In this section, we study in detail the possibility of use the combination of two solenoids as a conductivity sensor. We describe the magnetic field of the solenoids with water core and its calibration.

#### 3.2.3.1. Material and methods

In the previous section, we analyzed the results of the measures of different configurations of coil combinations. We concluded that Model 4 is the one that gave best results. It had the wider range to take measurements, from freshwater to seawater. Then, we realized further research with this prototype. In this test, we are going to characterize that sensor and find some important data such as the minimum cell volume, linear range, and sensibility.

- The material used in this section is the following one:
- Conductivity meter CM 35+
- Generator of AC
- Oscilloscope
- Model 4, see Figure 20
- Resistance of 100  $\Omega$
- Capacitor 100nF
- 5 glass containers
- Different containers
- Tap water
- Salt

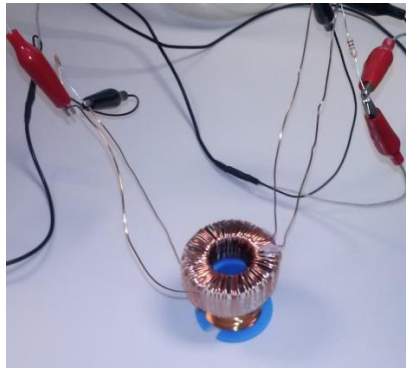


**Figure 3. 20** The conductivity sensor Model 4 with the components.

There are some characteristics that we need to know about our sensor before using it in the real environment. In this section, we are going to establish the laboratory procedures to obtain this data. Moreover, we will explain why is so important to ascertain this characteristic.

When our system is used in an open environment, the volume of the water that envelops the coils is infinite. But in the laboratory test, it's not possible to measure infinite containers. Therefore, the first measure should define the minimum cell volume. The other important factor to bear in mind is the measurement limitation of our sensor and its mathematical model.

One of the parameters to take into account is the dependence of the results with the cell volume.

When we are performing laboratory tests, it is usually used small containers. Due to the container size, the measurements can be modified due to interferences, changes of the medium and reflections in the container walls. Measurements in natural environments are not affected by these effects. We use small containers in order to avoid the waste of water because bigger containers imply bigger volumes of water and salt.

As Figure 3.21 shows, when we have a container too small, the lines of the magnetic field would spread out of the container. In addition, our measurements could be affected by external interferences. However, when our container has a size which can contain the lines of the magnetic field generated by the feed coil, the measurement will be independent of the container volume.

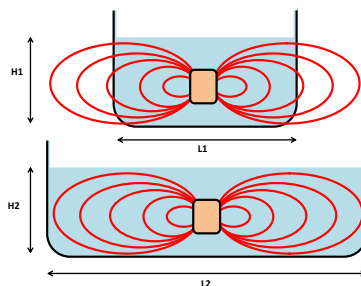


**Figure 3. 21** Possible scenarios of measurement attending to the size of the container

Figure 3.21 shows the two possible scenarios where we can take the measurements. Magnetic lines are represented in red and  $H_1$ ,  $H_2$ ,  $L_1$ , and  $L_2$  are the dimensions of each container.

This test will be composed of two measurements. The first one will be about the measures dependence with the water depth. With this, we will check if covering the sensor is enough to take the correct measurements or if we need to add more water to have accurate measurements. The second test will check if the surface of the water around the sensor affects

significantly the results. For a sample with a fixed conductivity, we will increase the size of the container, keeping the water level. Simultaneously, we will take measures of the output voltage in the induced coil. The minimum cell volume will be the one, which registers a stable value of output voltage in spite of increasing the size of the container.

Before using our sensor, it is important to define its working ranges. This implies to determine the minimum and maximum values of water conductivity where our sensor is able to show a correct correlation between water conductivity and the output signal. In our previous tests, we saw that at higher salt levels the conductivity values of all devices, the commercial ones and our proposal, present unstable values. For this reason, we need to define our working range.

In our experiments, we use tap water to prepare our samples. The sample with the lowest conductivity is tap water and the highest value of conductivity will be the one registered before this effect appears.

On other the hand, the entire working could be approximated by a mathematical expression or by multiple linear ranges. In some occasions, when the device behavior is approximated by some linear ranges, we can obtain better correlation. In order to measure it, we have prepared 35 samples with conductivity values between 0.397 mS/cm and 88.3 mS/cm. Each conductivity value provides us a voltage value. With these values, we will be able to model the behavior of our sensor. Measurements have been performed at 22 °C.

### 3.2.3.2. Results and Discussion

This section shows the results of our test bench. First of all, we are going to analyze the dependence of the measurements with the volume of the container.

After that, we are going to see the relation between the water conductivity and the output voltage of our sensor. Finally, in order to determine the accuracy of our device, a verification process with unknown samples will be performed. The samples are prepared with tap water and common salt (NaCl). The conductivity of each sample is measured with a commercial Conductivity meter CM 35 by Crison Instruments.

Finally, the toroid is powered by a signal generator. It is used a sine wave of 8 V peak to peak amplitude. The induced signal in the second coil (solenoid) is measured by an oscilloscope where both signals can be visualized easily.

#### 3.2.3.2.1. Minimum cell volume

In order to check the minimum value of the cell volume, we have taken the container of 4cm of diameter and, progressively, we have added water to increase the height of water. The first value, 7.1cm, is the minimum height because it is the level of water that covers entirely the sensor. Table 3.18 shows the output voltage for each level.

**Table 3. 18** Height of water (cm) in the test of minimum cell volume and the output sensor signal (V)

Height (cm)	Output sensor signal (V)
7.1	0.7
7.5	0.7
8.1	0.7
8.7	0.7
9.5	0.7

As we can see, the value remains constant in all tests. Then, we can conclude that measurements will be independent of the water level.

The second step shows us the dependence of measures with the surface of the container. In order to achieve this goal, we have prepared 4 containers with the same dissolution and the

same water level. For each container, we have measured the output voltage value. Table 3.19 shows the results of this test.

**Table 3. 19** Diameter of the container (cm) in the test of minimum cell volume and the output signal (V)

Diam. or sides (cm)	Kind of container	Area (cm <sup>2</sup> )	Cell Volume (l)	Output sensor signal (V)
8,6	Round	48.8	0.35	0.7
14,5	Round	165.1	1.17	0.54
18*27	Square	486.0	3.45	0.46
25,5*25,5	Square	650.3	4.62	0.43

As we can see, the changes in the container surface affect the value of the output sensor signal. This test confirms our hypothesis about the dependence of the cell volume and the conductivity measurements. As Figure 3.22 shows, the increase of the area produces an increase of the output sensor signal.

We can model this effect by Eq. (3.9) in order to apply the appropriate correction of the measurements in smaller containers. The correlation coefficient of this expression is 0.98. Where  $V_{out}$  are the signal of the sensors and  $Vol$  is the Volume of the container full of water.

$$V_{out} = 0.4332 + \frac{0.09254}{Vol} \quad (3.9)$$

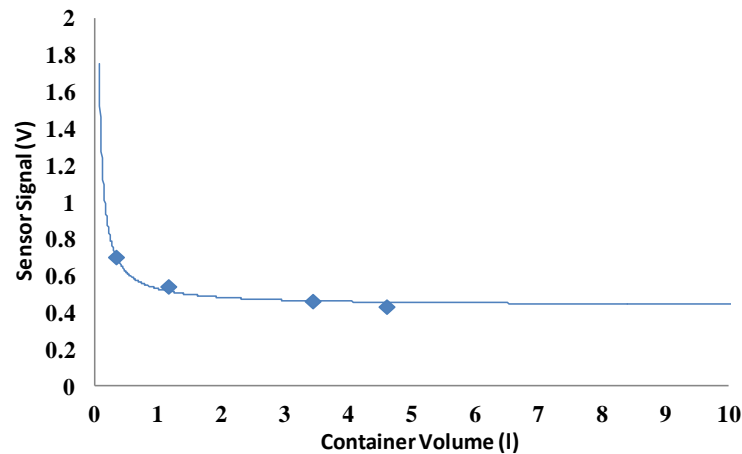


**Figure 3. 22** Dependence of the Sensor signal with the volume of water obtained in the test of minimum cell volume

As Figure 3.22 shows, for 7.845 liters the value of the output sensor signal is stable in 0.43 V. Then, we can conclude that our measures will be independent of the container for volumes higher than 7.845 liters. If we assume a height of 7.1cm, the minimum size of a square container will have a side of 33.24cm. If our container is circular, its radius will be 18.75 cm.

As this sizes are too big to use them in the laboratory we are going to use a container of smaller size (0.35L), and use the equation 9 to convert the sensor output signal if we need to use the sensor in the field.

#### 3.2.3.2.2. Linear ranges and sensibility

This section shows the relation between the water conductivity and the output voltage of our sensor. We are going to present the linear ranges and the sensibility of each one.

The methodology that we use is starting with tap water we add salt, shake it until stabilizing the value of conductivity, measure the conductivity with the commercial conductivity meter and introduce the sensor inside the water container.

As in the previous tests, we saw that the slope of the calibration line had a change, see Figure 3.19, we want to be sure that we have enough points to represent the behavior of the two linear ranges (or more). In addition, we know that at low values of conductivity the slope is bigger so that, at low values of conductivity we are going to perform a lot of points. And when we see that slope changes we will reduce the number of points. Figure 3.23 shows the behavior of our sensor. It relates the output voltage with the water conductivity.

Once we represent the results we can see that there are three linear ranges, the first from 0.397 to 6.56 mS/cm, the second from 6.56 to 22.6 mS/cm, and the last one from 22.6 to 76 mS/cm. The values of voltage registered for this test varied from 0.02 to 7.6V. The slope of each linear range is different. The most sloped is the range that corresponds to the lower conductivity values.

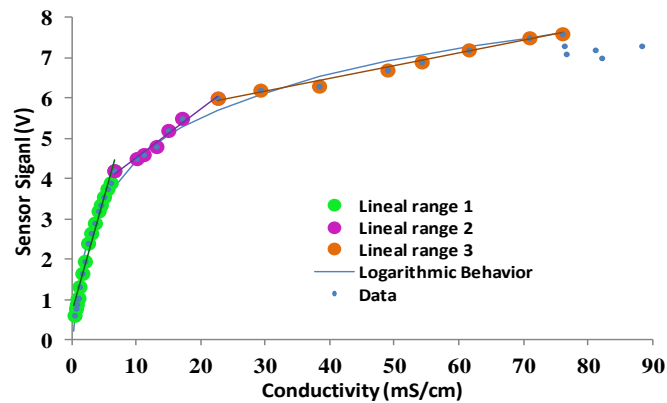


**Figure 3. 23** Correlation between the water conductivity and the Sensor signal Model 4 at the working frequency.

In the linear range 1, Eq. (3.10) can be applied to conductivity values from 0.397 mS/cm to 6.56 mS/cm. These values correspond to output sensor values from 0.2 to 4.2 V. Eq. (3.10) represents the expression of first linear working range with a correlation coefficient of 0.9751. Where  $V_{out}$  is the output voltage of sensor in V and  $C$  represents the conductivity in mS/cm. The second lineal working range is expressed by Eq. (3.11) with a correlation coefficient of 0.9813. Eq. (11) should be applied for values of conductivity from 6.56 mS/cm to 22.6 mS/cm. These values correspond to output sensor values from 4.2 to 6 V. The third lineal working range is applied from from 22.6 mS/cm to 76 mS/cm. The output voltages which correspond to these values are ranged between 6 V to 7.6 V. Eq. (3.12) represents the expression for the third lineal working range. Its correlation coefficient is 0.9872 and  $V_{out}$  is the output voltage of the sensor in V and  $C$  represents the conductivity in mS/cm.

Until now we use linear ranges, with linear equations but we also can adjust the behavior of all our interval of measures to a logarithmic equation by an expression followed by Eq. (3.13). To obtain this equation we use a mathematics software (Eureqa Software, 2015).

$$V_{out} = 0.5894 \cdot C + 0.6037 \quad (3.10)$$

$$V_{out} = 0.1193 \cdot C + 3.3457 \quad (3.11)$$

$$V_{out} = 0.0313 \cdot C + 5.23 \quad (3.12)$$

$$V_{out} = 0.6714 + 0.7999 \cdot \ln(C + C^2) \quad (3.13)$$

Computationally, it is much easier the process of a linear function than a logarithmic function. For this reason, we can consider the option of modeling the behavior of our sensor as a set of linear equations.

For conductivities higher than 76 mS/cm, the sensor presents unstable values of voltage. For this reason, we have limited the use of our sensor for conductivity values up to 76 mS/cm.

The sensibility of our sensor will depend on the linear working range. Its sensibility will also depend on the electronic circuit used to amplify the output signal. In our case, it is easy to get sensibilities of mV. Thus, according to both factors, the sensibility should be 0.002mS/cm for the first linear range, 0.008mS/cm for the second linear range and 0.03mS/cm to the third linear range.

Finally, in Table 3.20, we show a resume of the characteristics of the linear ranges

**Table 3. 20** Characterization of the linear ranges of the sensor Model 4

Linear range	Formula	R2	Slope	Interval range (mS/cm)	Interval range (V)	Sensibility (mS/cm)
1	$V_{out} = 0.5894 \cdot C + 0.6037$	0.98	0.5894	0.397 - 6.56	0.2 - 4.2	0.002
2	$V_{out} = 0.1193 \cdot C + 3.3457$	0.98	0.1193	6.56 - 22.6	4.2 - 6	0.008
3	$V_{out} = 0.0313 \cdot C + 5.23$	0.99	0.0313	22.6 - 76	6 - 7.6	0.03

### 3.2.3.2.3. Verification process

Once we have obtained the correlation equation we should verify it. In order to achieve this goal, we have taken some samples of water from the natural environments. Two of these samples are from two different irrigation channels. The third sample is from the sea (seashore) and another one is from tap water. These samples have an unknown conductivity value.

Samples do not suffer any treatment. We put them in 1.5 liters plastic bottles and we kept them in the refrigerator during the time that they were stored (less than 8 hours). Before performing the measurements, we have homogenized the samples by shaking the bottles.

The first step is to verify the correct behavior of our sensor; we have measured the output voltage of each sample (See Table 3.21).

**Table 3. 21** Output Voltage for unknown samples.

	1	2	3	4
<b>Output Votlage (V)</b>	0.86 V	1.14 V	2.40 V	6.50 V

Estimating the conductivity values by using Eq. 3.10, Eq. 3.11, and Eq. 3.12, we have calculated the results of the water conductivity. In order to compare the estimated conductivity values with the measured values, and the error for the four samples, we provide Figure 24.

Figure 3.24 compares our conductivity measurements and the values of conductivity obtained by a commercial conductivity meter. From Figure 3.24, we can extract the value of correction of our measures. Eq. (3.14) shows the expression which relates the actual conductivity measure and the value of conductivity measured with our sensor. Where  $C_{correct}$  is the conductivity in mS/cm gave by the commercial sensor, and  $C_{measured}$  in the value of conductivity gave by or sensor using Equations 10, 11 or 12 to transform the signal of voltage on value of conductivity.

We discover that we have some kind of error that produce that the signal of our sensor is lower than the signal of the commercial sensor. But using (14) we are able to convert the value of our sensor into real value.

$$C_{correct} = 0.7157 \cdot C_{measured} + 0.0224 \quad (3.14)$$

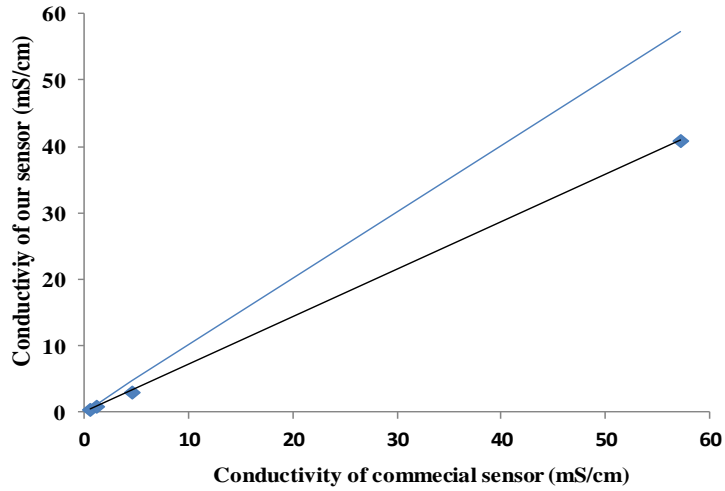


Figure 3. 24 Conductivity of our sensor vs. Conductivity of commercial device.

### 3.2.4. Evaluating the combination of two solenoids for conductivity monitoring in fish farms

In this section, we present the test done with the combination of two solenoids. First we will show some background theory and then we present the multiple prototypes employed and its results.

#### 3.2.4.1. Background theory

To understand the operation of our sensor, we need to understand the concept of mutual inductance. We are going to explain how it works by using the scenario shown in Figure 3.25. We have two coils with a length  $h$ , where  $N_1$  and  $N_2$  are the number of turns of each coil, respectively. Instead of having a ferromagnetic core with a section  $S$  and a relative permeability  $\mu_r$ . We have a space occupied by salt water where the section of the coils is  $N_1$  and the relative permeability  $\mu_{r\_water}$ .

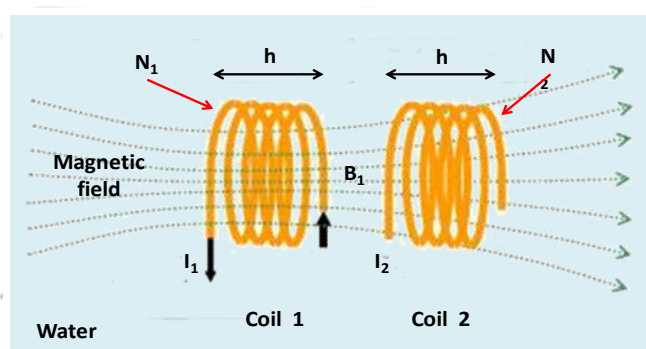


Figure 3. 25 The employed coils and its magnetic field

Throughout the coil 1 a constant current  $I_1$  flows, while the coil 2 is open. To simplify the equations system, let us assume that all lines of the magnetic field created by the coil 1 flow

through the coil 2. Coil 1 creates a magnetic field  $\vec{B}_1$ . This magnetic field is confined to the center of the coil 1, as if it were a core. In this way, the lines of the magnetic field  $\vec{B}_1$  go through the coil 2 and create a magnetic flux  $\Phi_{2,1}$ . The mutual inductance is shown in Eq. 3.15.

$$L_{1,2} = M = \frac{\Phi_{2,1}}{I_1} \quad (3.15)$$

On the other hand, the magnetic field in coil 1 is given by Eq. 3.16:

$$\vec{B}_1 = \mu_{r\_water} \cdot \mu_0 \frac{N_1}{h} \cdot I_1 \cdot \vec{n} \quad (3.16)$$

Where  $\vec{n}$  is unitary vector, parallel to the axis coils and it is directed to the right side. The flow produced on the coil 2,  $\Phi_{2,1}$ , is shown in Eq. 3.17:

$$\Phi_{2,1} = N_2 \cdot \vec{B}_1 \cdot \vec{S} = \frac{\mu_{r\_water} \cdot \mu_0 \cdot N_2 \cdot B_1 \cdot S}{h} \cdot I_1 \quad (3.17)$$

Eq. 3.18 shows the coefficient of mutual inductance:

$$L_{1,2} = M = \frac{\mu_{r\_water} \cdot \mu_0 \cdot N_2 \cdot N_1 \cdot S}{h} \quad (3.18)$$

On the other hand, the electromotive force in coil 2 (**emf**<sub>2</sub>) can be calculated from the magnetic flow produced on the coil 2 which is given by Eq. 3.19.

$$\Phi_{2,1} = M \cdot I_1 \quad (3.19)$$

If  $I_1$  depends on the time, this flow also changes as a function of the time and generates a **emf**<sub>2</sub> which is given by Eq. 3.20.

$$\mathbf{emf}_2 = -\frac{d\Phi_{2,1}}{dt} = -M \cdot \frac{dI_1}{dt} = \frac{M}{\tau} \cdot I_0 \cdot e^{-t/\tau} = \frac{\mu_{r\_water} \cdot \mu_0 \cdot N_2 \cdot B_1 \cdot S}{h \cdot \tau} \cdot I_1 \cdot e^{-t/\tau} \quad (3.20)$$

Where  $\tau$  is related to the working frequency of the induced **emf**<sub>2</sub>.

Finally, we can conclude that the **emf**<sub>2</sub> is related to the medium through the variable  $\mu_{r\_water}$  which is related with the amount of dissolved salts in the water.

#### 3.2.4.2. Test bench

In this section, we explain the components used in the developed tests. We also present the methodology carried out to analyze the dependence between the coil's characteristics and its capability as a salinity sensor.

As it is explained before, there is not any study that accurately evaluates the capability of coils to measure the salinity level of the water. To study the different capability of each prototype, we have performed different tests. In each test, the prototypes are used to measure different saline solutions. We decided to study the effects of different parameters such as the number of spires (test benches 1 to 3), the diameter of the coils (test bench 4) and the effects of different copper wire diameter (test bench 5). Finally, we also studied the performance of each sensor working at different frequencies.

Once the best configuration is selected, an exhaustive calibration is performed. It is also evaluated the effect of water volume in order to determine the minimum cell volume (Parra et al., 2013c).

The methodology used to measure the salinity is based on two solenoids electric coils, one of them is powered by a sinusoidal signal and the second one is connected to an oscilloscope



in order to measure the induced magnetic field. This election is based on our previous works where we studied the best combination of coils (Parra et al., 2013a), (Parra et al., 2013b) and (Parra et al., 2013c). Our results showed that the combination of two coils presented the lowest working frequency where a wide range of salinities could be differentiated. Electric coils are submerged in the water sample. The electric circuit is shown in Figure 3.26. The oscilloscope used is an HM303 and the function generator is an HP 33120A. The signal used to power the coils is a sinusoidal signal with a peak to peak voltage ( $V_{pp}$ ) of 8 V and the used frequencies range from 100 kHz to 4000 kHz.

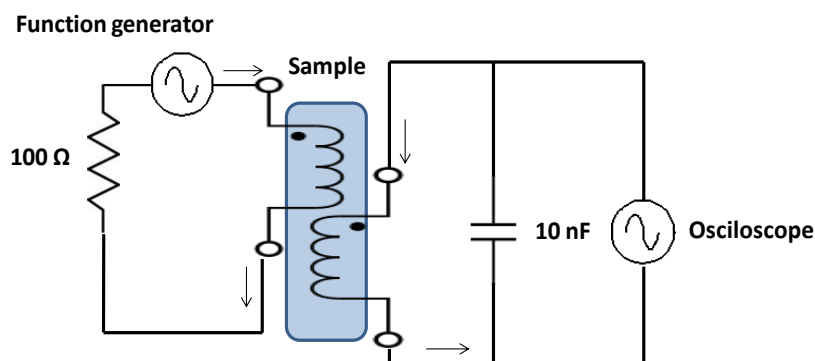


**Figure 3. 26** Electric circuit of the sensor

The solenoids were coiled over a PVC pipe of different diameters (depending on the test). Pipes have diameters of 15 mm, 25 mm and 35 mm. The wire used to form the coils is enamel copper wire. Different diameters of wire are used in different tests. The diameters used are 0.4 mm, 0.6 mm and 0.8 mm. The prepared solenoids had a different number of spires where the smallest one has 5 spires and the biggest one has 120 spires. The characteristics of all solenoids are shown in Table 3.22. Prototypes 5 to 9 were used in two tests using different setups and changing the powered and induced coils so appear twice, one in test 2 and other in test 3. When these prototypes are used in test 2, they are called as 5 to 9 and when these prototypes are used in test 3, prototypes are called as 5' to 9' in order to avoid confusions.

In order to perform our tests, we need to prepare several samples. In our case, 4 different samples have been used. These samples have been prepared using tap water and adding a different amount of salt. The conductivity of each solution is measured using a commercial device (Conductivity Meter CM 35 +). The salty solutions have different salinity levels, i.e., the lowest one has 6.8 mS/cm and the highest one has 90.2 mS/cm. The typical seawater salinity is 52 mS/cm. One of our samples presents salinity close to seawater salinity. The solutions were prepared at 7 °C.

On the other side, we have prepared 30 samples (with salinities between 0.585 mS/cm to 109.5 mS/cm) in order to perform the sensor calibration. The typical salinities registered in the groundwater with low and high levels of saline intrusion were included in this range of values.

All samples are prepared in round glass containers of 72 mm in diameter and 150 mm of high. All the containers had the same amount of water to be able to compare the measures. Containers used in the test to evaluate the minimum cell volume, are also round glass containers. Their diameters are (in cm): 6.3, 7, 8 and 11.7. The biggest container is the one used for determining the minimum cell volume.

### 3.2.4.3. Results

In this section, the test bench results are shown. This section is divided into three subsections in order to better show the obtained results. The first subsection corresponds to the test bench carried out for the salinity sensor characterization, where different configurations

are tested. The second subsection shows the test bench results performed to know the minimum cell volume. Finally, subsection three presents the calibration of our sensor.

**Table 3. 22** Features of solenoids used in the tests

Test	Prototype	Diameter of wire (mm)	Diameter of coils (mm)	Nº of spires of powered coil	Nº of spires induced coil	Spires relation
1	1	0.4	25	5	10	1:2
	2	0.4	25	10	20	1:2
	3	0.4	25	20	40	1:2
	4	0.4	25	40	80	1:2
	5	0.4	25	30	15	1:0.5
2	6	0.4	25	30	30	1:1
	7	0.4	25	30	60	1:2
	8	0.4	25	30	90	1:3
	9	0.4	25	30	120	1:4
3	5'	0.4	25	15	30	1:2
	6'	0.4	25	30	30	1:1
	7'	0.4	25	60	30	1:0.5
	8'	0.4	25	90	30	1:0.3
	9'	0.4	25	120	30	1:0.25
4	3	0.4	25	20	40	1:2
	10	0.6	25	20	40	1:2
	11	0.8	25	20	40	1:2
5	12	0.4	15	40	20	1:2
	3	0.4	25	20	40	1:2
	13	0.4	35	40	20	1:2

#### 3.2.4.3.1. Physical characterization of the sensor

In this subsection, we are going to present the results of the 5 tests performed to study the accuracy of the measurements when the parameters of coils are changed. Figure 3.27 shows the measurement process.

- Firstly, we study the effect of changing the number of spires but maintaining the relation of spires between the induced and the powered coil. For this test bench, we used prototypes from 1 to 4.
- The second test studies the change produced in the sensor performance when the relation of spires changes but maintaining the number of spires in the powered coil. For this test, we used prototypes from 5 to 9.
- The third test changes the number of spires of the powered coil maintaining the number of spires of the induced coil. For this test, we used again prototypes from 5 to 9 but changing the powered coil by the induced coil from the second test.
- Fourth test bench evaluates the effect of changing the diameter of copper wire using 3 different diameters of copper wire while keeping equal the rest of parameters (number of spires of coils and diameter of coil). Prototypes 3, 10 and 11 were used in this test.
- Finally, fifth test bench is performed to check the effect of changing the diameter of coil but maintaining the rest of parameter (wire diameter and number of spires). Prototypes used in this test were prototype 3, 12 and 13.

Moreover, coils are powered at different frequencies. Table 3.22 shows a summary of frequencies used in all tests. It also shows which coil is powered and with which frequency. We have tagged the frequency where the peak is registered with the symbol ✓. The lowest frequency value used to power the coils is 100 kHz. Due to the great variety of coils, the frequencies used to power them are different for each coil. However, we try to maintain some values for all the coils, 100 kHz, 1000 kHz and 1500 kHz. The highest frequency used to power the prototype 1 is 4000 kHz. The prototype that was powered with the lowest frequency is prototype 11, whose maximum frequency was 1500 kHz. Frequencies used to power the

coils are selected according to the points where coils present the mayor differences as a function of the salinity levels.

The frequency where each prototype can be used as a salinity sensor is the frequency where the saline solution produces different alteration of magnetic field and generates changes in the induced voltage. Generally, this frequency is the same that the peak frequency where the induced coil presents its highest voltage. In some cases, prototypes present just one peak frequency, but in other, prototypes present more than one peak frequency (frequencies where the induced voltage is higher than the induced voltages at lower and higher frequencies). Figure 3.28 shows these two possibilities representing the output voltages of the induced coil as a function of working frequency. When we have two or more peak frequencies, the highest one will be called maximum peak frequency.

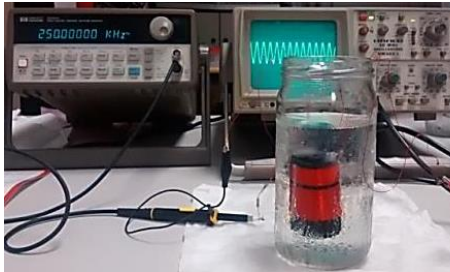


**Figure 3. 27** Picture of the test bench for one of the measurements



**Figure 3. 28** Example of possible behaviors of different prototypes

#### 3.2.4.3.2. First test: Changes in the number of spires maintaining the spires relationship

In this test, we measured the induced magnetic field of the prototypes from 1 to 4 for four different water salinities. For prototype 1, the frequency peak is registered at 3,753 kHz. For prototype 2, the frequency peak is registered at 1,840 kHz. For Prototype 3 the frequency peak is registered at 800 kHz and, finally, for Prototype 4 the frequency peak is registered at 425 kHz. For these four prototypes, it is possible to distinguish the four different samples. Figure 3.29 shows the induced voltage of each prototype for each salinity sample. In all cases, there exists a positive correlation between the induced voltage and the salinity level. This correlation points that these prototypes can be used as salinity sensors. For all cases, when the salinity level increases, the induced voltage also increases.

#### 3.2.4.3.3. Second and third test: Change the spires relation

In these two tests, we measured the induced magnetic field of prototypes from 5 to 9 at four different water salinities. Those prototypes are characteristics because one of the coils has 30 spires and the other one has variable spires (15, 30, 60, 90 and 120). During the second test we measured the induced field in the coils with 30 spires and powered the coils of different spires. Prototype 5 presents two frequency peaks, one at 900 kHz and other at 2,000 kHz. In prototype 6 the frequency peak is registered at 1,200 kHz. In prototype 7 the frequency peak is registered at 900 kHz. Prototype 8 also presents two peaks, one at 800 kHz and other at 1,750 kHz. Finally, prototype 9 presents two peaks, one at 600 kHz and the second one at 1,300 kHz. In this case, not all peak frequencies are useful to detect salinity variations. Only the prototypes 6, 8 and 9 at their peak frequencies offer results that correlate different voltage inductions at different salinities and this is shown in Figure 3.30. All tested prototypes used in test two offer very poor results. There is no clear linearity between data and induced voltage.

On the other hand, as in the first test, in all cases the induced voltage increases as a function of the salinity level. Four of the five prototypes (5, 6, 8 and 9) present two different peaks in the working frequency.

**Table 3. 23** Summary of frequencies used for each prototype.

Freq. (kHz)	Test 1				Test 2					Test 3					Test 4		Test 5	
	P1	P2	P3	P4	P5	P6	P7	P8	P9	P5	P6	P7	P8	P9	P 10	P11	P 12	P13
100	x	x	x	x	x	x	x	x	x	x	x	x	x	x	x	x	x	x
150														x				
200														x		x		
250			x	x		x					x	x	x	x	x			
280														x				
300				x									x	x			x	x
330													x					
350													x	x				
380				x														
400								x				x	x	x		x		
425				✓														
450												x	x			x		
480												✓						
500	x	x	x	x	x	x	x			x	x	x	x		x	x	x	x
550												x				x		
600			x	x					✓					x	x	✓	x	
620																x		
650												x				x		
700			x	x		x			x			x				x	x	
750					x		x	x				x	x		x			
800			✓	x		x		✓				x		x		x	✓	x
850												✓						
900				x	✓	x	✓	x				x	x	x		x	x	✓
950													x					
1000	x	x	x	x	x	x	x	x	x	✓		x	x	x	x	x	x	x
1100					x	x	x	x				x	x	x	x			x
1200						✓						✓	x	✓				
1250		x	x		x		x						x	x	x			
1300						x			x			x	x		x			x
1400						x						x						
1500	x	x	x	x	x	x	x	x	x	x		x	x	x	✓	x	x	x
1600						x							✓					
1700						x						x		x				
1720															x			
1750			x					x										
1800						x						x		x				
1840		✓																
1900						x						x		x				
2000	x	x	x		✓	x	x	x	x	x		x	x	x	x		x	x
2250		x									x				x			
2500	x	x			x	x	x	x	x		x	x	x	x	x			
2600											x							
2700											x							
2750	x	x														x		
2800											x				x			
3000	x	x			x	x	x	x	x	x		x	x	x	x			
3500	x																	
3753	✓																	
4000	x																	

During the third test, we used the prototypes 5' to 9' powering the coils with 30 spires and measuring the induced field in the coils of different spires. The frequency peaks for each prototype are the following; prototype 5' presents two peaks, one at 1,000 kHz and other at 2,700 kHz; Prototype 6' registers the peak at 1,200 kHz; Prototype 7' also presents two peaks, the first one is registered at 480 kHz and the second one appears at 850 kHz. Prototype 8' presents four peaks at 330 kHz, 760 kHz, 1,100 kHz and 1,600 kHz. Finally, Prototype 9' presents three peaks. The first one appears at 280 kHz, the second peak is at 1,200 kHz and the last one is registered 2,800 kHz. The induced voltages at the frequency where prototypes are able to detect changes in conductivity are represented in Figure 3.31. In this case, not all the frequency peaks are useful to detect salinity variations. Thus, prototype 7 is not useful. Four of the five prototypes (5, 7, 8 and 9) present more than one induction peak. Moreover, in all cases at the frequency peak, the induced voltage increases with the salinity of samples.

#### 3.2.4.3.4. Forth test: Change the wire diameter

In these tests, we measured the induced magnetic field of prototypes 3, 10 and 11 using the same four different water samples. All prototypes used in this test have the same number of spires in both coils (20 spires in the powered coil and 40 spires in the induced coil). However, the diameter of copper wire used is different for each one. Prototype 3 is coiled with a copper wire of 0.4 mm. The diameter of copper wire for prototype 10 has 0.6 mm, and prototype 11 uses a copper wire of 0.8 mm. The frequency peak for each prototype is the following: for prototype 3 it is registered at 1,840 kHz, for prototype 10 the frequency peak appears at 1,500 kHz and Prototype 11 presents the frequency peak at 600 kHz. Prototype 10 is not suitable to detect changes in salinity levels working at their frequency peak, but nevertheless prototype 11 can be used for this goal. In Figure 3.32, it is possible to see the relation between the salinity level and the induced voltage of prototype 11 at 600 kHz. In all cases, the induced voltage increases as a function of the salinity working at the frequency peak. The maximum voltages are higher than values in the fourth test. Prototype 11 raises an induced voltage of 8.4 V for the highest salinity sample. Moreover, all the prototypes present just one frequency peak.

#### 3.2.4.3.5. Fifth test: Change the coil diameter

In these tests we measured the induced magnetic field of prototypes 3, 12 and 13 at four different water salinities. Prototypes used in this test have the same number of spires in both coils (20 spires in the powered coil and 40 spires in the induced coil). However, the diameter of coils is different for each one. Prototype 3 has a diameter of 25 mm, while the diameter of coils for prototype 12 is 15 mm and prototype 13 has 35 mm. The frequency peaks for each prototype are the following ones. For Prototype 3 the frequency peak is registered at 800 kHz, for prototype 12 the frequency peak is registered at 800 kHz, and finally, prototype 13 registers the frequency peak at 900 kHz. In this case, all prototypes are able to distinguish between different salinities working at their frequency peaks. Results are shown in Figure 3.32. As we can see, in all cases the induced voltage increases depending on the salinity. Moreover, all these prototypes present only one frequency peak.

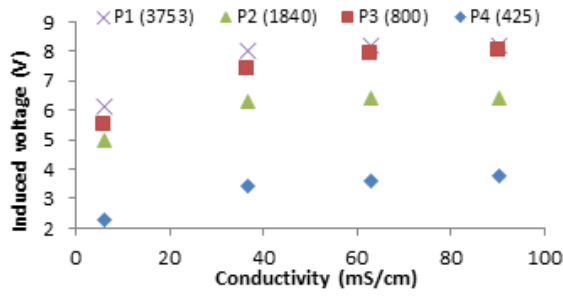


Figure 3.29 Induced voltages for best frequencies of prototypes from 1 to 4 at test 1

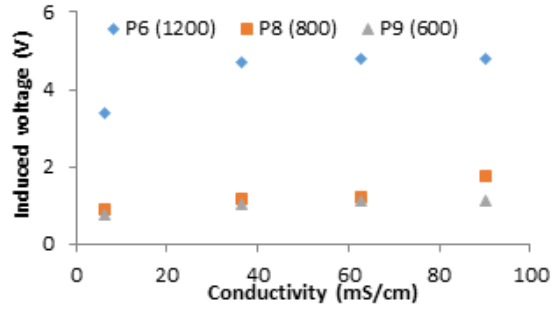


Figure 3.30 Induced voltages for best frequencies of prototypes from 5 to 9 at test 2

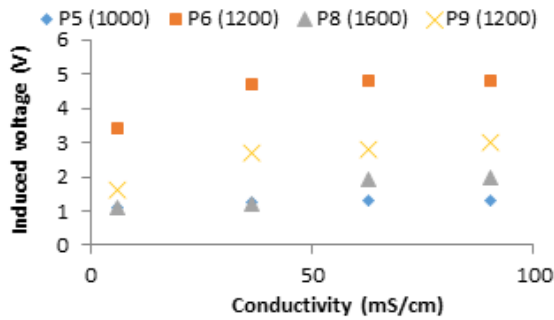


Figure 3.31 Induced voltages for best frequencies of prototypes from 5' to 9' at test 3

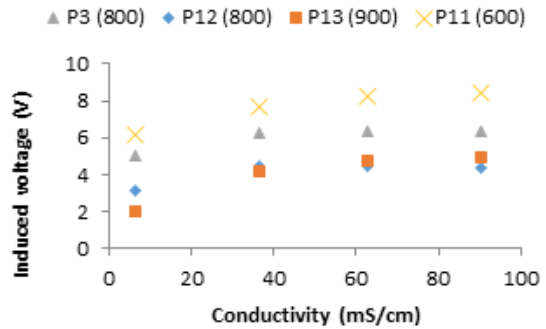


Figure 3.32 Induced voltages for best frequencies of prototypes 3, 11, 12 and 14 at tests 4 and 5

### 3.2.4.3.6. Summary of tests for physical characterization of the sensor and election of prototype

As a summary of the performed tests, we can highlight next facts:

- A total of 13 different prototypes were tested, 4 of them with two different configuration of powered/induced coils.
- Those 17 combinations of coils were powered at frequencies from 100 kHz to 4000 kHz.
- Each combination has one or more peaks of induction at different frequencies
- Generally, peaks of induction represent the frequency where the prototypes are able to detect conductivity changes.
- From 17 different configurations, 14 of them are able to detect conductivity changes.
- The frequency at which the prototypes are able to determine the conductivity is shown in Table 3.33.

Table 3.24 Frequency of working for each prototype

Prototype	Frequency (kHz)	Prototype	Frequency (kHz)	Prototype	Frequency (kHz)	Prototype	Frequency (kHz)
1	3753	6	1200	6'	1200	12	800
2	1840	8	800	8'	1600	13	900
3	800	9	600	9'	1200		
4	425	5'	1000	11	600		

To choose the prototype that will be used as a conductivity sensor, several factors must be considered. These factors are: frequency peak, voltage variation between saline solutions, and size of prototype. It is desirable that the selected prototype presents its frequency peak at low frequencies, since the electric components for the final circuit are cheaper for low frequencies. Higher voltage variation between the saline solutions indicates higher sensibility for the sensor, which makes better the monitoring process. Finally, the coils size (number of spires and diameter) influences on the magnitude of the generated magnetic field and it is desirable not to have big magnetic fields, to avoid the effect of boundaries. Besides, smaller coils have smaller economic cost. From the 14 combinations that are able to determine the variation of conductivity, we have to select one of them. As it is said above, the frequency is very important, so the prototypes with their frequency peaks above 1000 kHz are dismissed as a feasible option. The prototypes that accomplish the premise of low frequency peak are prototype 3, 4, 8, 9, 5', 11, 12 and 13.

Another important factor is the voltage difference between saline solutions, so the prototypes that have less than 2V of difference between saline solution 1 and saline solution 4 are also dismissed as a possible option. The sensors that accomplish all the requirements are prototype 4, 11 and 13. The last factor to take into account is its size. For this reason, Prototype 13 is also dismissed because of its high diameter and it does not present improvement enough over the prototypes with fewer diameters. Finally, prototype 4 and prototype 11 are compared in Table 3.34 from an economic point of view. Attending to the data presented in Table 3.25, the selected device is prototype 4. It costs half than prototype 11. Although this difference is less than a Euro, the number of devices we could need in a medium or large wireless sensor network could be very high, so at the end, the cost difference can be considerable.

**Table 3. 25** Cost comparison of copper in each prototype

<b>Parameter</b>	<b>Prototype 4</b>	<b>Prototype 11</b>
Coil diameter (mm)	25	25
Copper wire diameter (mm)	0.4	0.8
Spires in powered coil	40	20
Spires in induced coil	80	40
Volume of copper wire used (mm <sup>3</sup> )	1184	2369
Price of copper for Prototype (€)	0.42	0.85

#### 3.2.4.3.7. Determination of minimum cell volume

In this subsection, we are going to present the results of the tests performed to determine the minimum cell volume. First of all, we describe the concept of minimum cell volume, defined for the first time in our previous work (Parra et al., 2013c). Finally, the data of the performed tests are presented and analyzed.

As it is described before, there are two main methodologies to measure the conductivity, the inductive and the conductive. In the conductive method, the volume of water is not related with the output voltage. It is only related with the amount of ions, area of copper electrodes and distance between copper electrodes. In inductive methodology the water volume is very important. This is important because of the electromagnetic field produced by the powered coil extends beyond the space occupied by the coils. It is necessary to know the volume that has this electromagnetic field. The minimum cell volume is the minimum water volume necessary to cover all the extension of the magnetic field.

This volume must be covered by water during the calibration and during the sensor operation. Otherwise, the induced voltage will be different generating wrong values of water conductivity. Figure 3.33 explains this situation with two examples. In A) the volume of water

is big enough to cover all the magnetic field represented in yellow lines. However in B) the used container is too small and part of the magnetic field is outside the water. To find out that volume, the easiest way is using a simulator. Nevertheless, there is not any simulator that takes into account the attenuation effect of the electromagnetic waves into water with different conductivities using a coreless coil. Thus the only way is to perform the test described below.

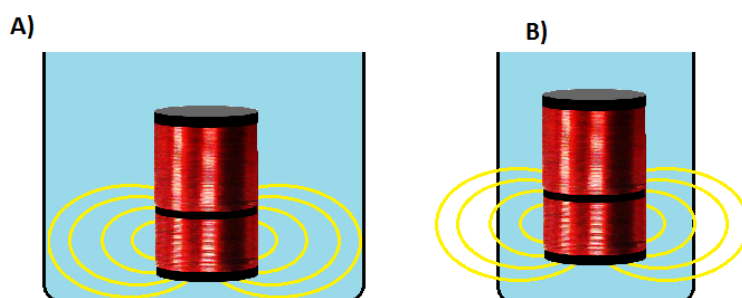


**Figure 3. 33** Example of containers of water that accomplish the minimum cell volume A) and do not accomplish it B).

First test is aimed to find the width of the electromagnetic field generated by the coil. Fixing the height of water and using different glass containers with different diameters, they are filled with the same water sample. The prototype is introduced inside the containers and the value of the induced voltage is recorded. These results can be seen in Figure 3.34, where the obtained data and the analytical model that models the data behavior are represented, see Eq. (3.21).

$$V_{out} (V) = \frac{78.85 - 12.94 \times D(cm)}{150.38 - 25.20 \times D(cm)} \quad (3.21)$$

Where  $V_{out}$  is the induced voltage (in volts) and  $D$  is the diameter of crystal container (in cm). The data corresponds to the output voltage of the induced coil when it is introduced inside the containers with different diameter (from 6.3 cm to 11.7 cm). From Equation 3.21, it is possible to know that the minimum diameter is 25 cm. From this size, when we increase the diameter, the output voltage does not change (at level of second decimal).

The second test performed is aimed to find the height of the electromagnetic field generated by the coil. For this test, the container of 11.7 cm of diameter is used and the height of water was increased after each measure. We started with a height of water that only covers the coils; we call it as 0 cm. Then the level of water is increased with intervals of 1 cm after each measure. The output voltage at each height of water is related with this water level and it is shown in Figure 3.35. The obtained data and the mathematical model (Eq. (3.22)) are shown in Figure 3.35.

$$V_{out} (V) = \frac{0.52 + 0.52 \times H(cm)}{1.40 + H(cm)} \quad (3.22)$$

Where  $V_{out}$  is the induced voltage (in Volts) and  $H$  is the height of water that covers the coil (in cm). From the analytical model, it is possible to extract the height above the coils for the minimum cell volume of 20 cm. At 20 cm above and below the coil, if the height of water increases, the output voltage does not change (at level of second decimal). Considering the height of the coils (8 cm), the height above and below the coils is 20 cm, and the height of the magnetic field extension is 48 cm, then the minimum cell volume is 23.5 L.



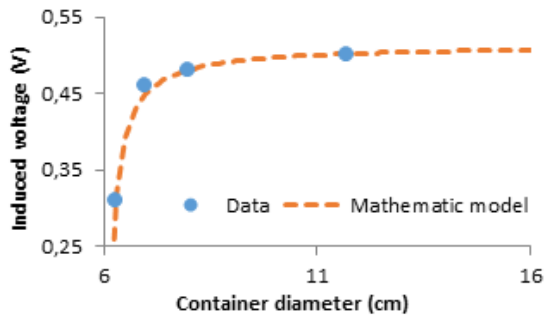


**Figure 3. 34** Results of first test to find out the minimum cell volume

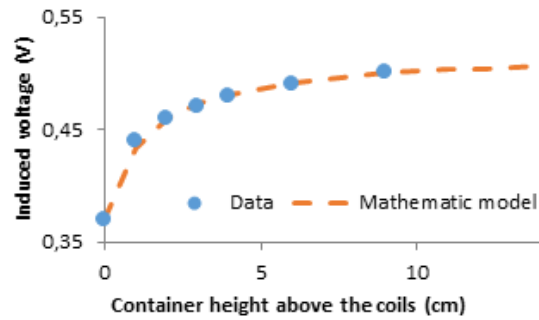


**Figure 3. 35** Results of second test to find out the minimum cell volume

#### 3.2.4.3.8. Calibration

Once the minimum cell volume is known, the calibration can be performed. Nevertheless the volume necessary to accomplish the requirements of minimum cell volume are too high to easily operate under laboratory conditions. Instead of using a container with 48 cm height and 25 cm diameter, a container with 28 cm height and 11.7 cm diameter is used. Thanks to our analytical models, it is possible to calculate the compensated output voltage due to the containers volume used, which is lower than the minimum cell volume. The compensation rate is 3.2%. By using this value is possible to correct the output voltages obtained in this test.

The calibration process is done with more than 30 samples. Starting with lowest conductivity value (0.585 mS/cm) and adding NaCl in small quantities after each measure to increase the salinity level. The value of conductivity is measured after adding NaCl with a conductivity meter CM 35+. The highest value of conductivity tested is 109.5 mS/cm. At each conductivity level, the output voltage of the salinity sensor is recorded. The values of output voltage obtained with the induced coil are corrected by applying a correction factor. When values are corrected, we can see that at 73.8 mS/cm the output voltage is 2.94 V. When the conductivity value increases up to 86.7 mS/cm, the output voltage does not change. After 86.7 mS/cm the output voltage starts to increase again but irregularly. So, 73.8 mS/cm is defined as the last point of our measurable range. Then, the measurable range of our sensor ranges from 0.585 mS/cm to 73.8 mS/cm. However, it is expected that the sensor will be able also to work at lower values. In Figure 3.36 the obtained data are presented. It is divided into two groups; the group Data represents the values that are in the working range; Data out of range presents those values that are out of the working range of the sensor, and Mathematic model is the analytical model that predicts the behavior of our sensor in the working range. The analytical model shown in Equ. 10 is obtained using mathematical software (Eureqa Software, 2015). The analytical model has a correlation coefficient R2 of 0.99 and a mean absolute error of 0.84. In Eq. 3.23 we can see the conductivity (*Cond.*) and its relationship with the induced voltage (IV). The equipment used to measure the output voltage has an acceptable accuracy (0.01 V) compared to the gathered values.

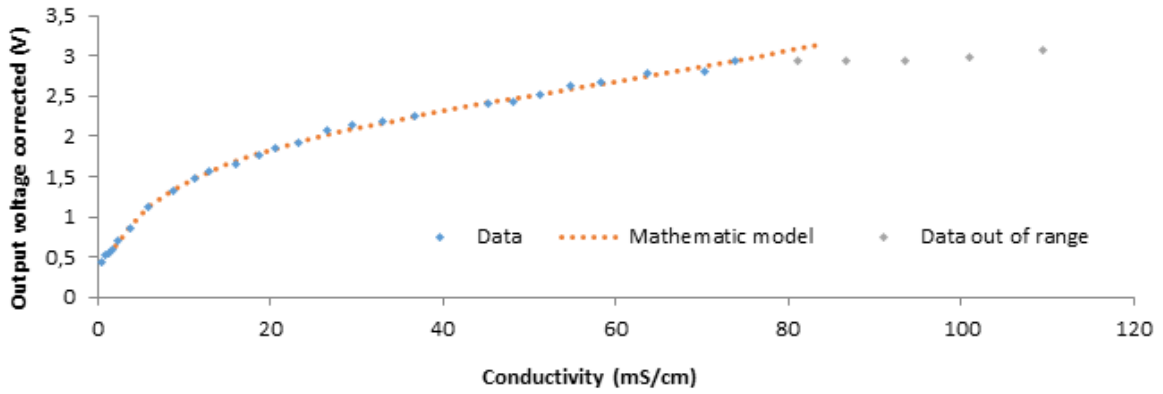


**Figure 3. 36** Representation of data of calibration process

$$Cond. \left( \frac{mS}{cm} \right) = -0.83 \times IV^5(V) + 3.96 \times IV^4(V) - 9.41 \times IV^2(V) + 16 \times IV(V) - 4.93 \quad (3.23)$$

Once the mathematical model is obtained, it is time to verify our model. In order to do it, we used 5 different saline solutions of unknown conductivity. Even that we do not know the conductivity value of the solution, those values are inside the range of the mathematical model. Those solutions are measured with our prototype and the obtained induced voltages are converted into conductivity values in mS/cm using Eq. 3.23. Then, the solutions are measured with the commercial conductivity sensor (CM35+) and we compared the lecture of the commercial device (real value) with our predicted value (equation value). The results are shown in Table 3.26. The absolute error and the relative error of those measures are calculated in order to have some information about the accuracy of our prototype and the mathematical model developed by us. The mean relative error is 2% and the maximum 8%, the mean absolute error is 0.88 mS/cm and the maximum 2.03mS/cm. Those values indicate that our prototype has good accuracy for monitoring the changes of conductivity. The sensibility of our prototype, that is, the minimum variation of conductivity that the prototype is able to detect, is determined by the minimum variation of voltage that we are able to detect. This variation is 0.01V. It is possible to determine the sensibility for different ranges as can be seen in Table 3.27.

**Table 3. 26** Verifying measures and the relative and absolute error

Real Value (mS/cm)	IV (V)	Equation Value (mS/cm)	Relative error (%)	Absolute error (mS/cm)
1.72	0.59856	1.72	0%	0.00
11.38	1.48608	11.37	0%	-0.01
26.7	2.064	28.73	-8%	2.03
45.3	2.3994	44.37	2%	-0.93
58.3	2.6832	59.74	-2%	1.44

**Table 3. 27** Sensibility of our prototype with the mathematical model (3) at different ranges

Sensibility (mS/cm)	From (mS/cm)	To (mS/cm)
0.1	0.6	5.5
0.2	5.5	11.5
0.3	11.5	18
0.4	18.1	28
0.5	28.1	41
0.6	41.1	86.7

### 3.3. Turbidity sensor

#### 3.3.1. Material and methods

In this section, the material and methods are presented. First, the background about the light absorption and the turbidity is detailed. Then, the design and development and price of the turbidity sensor and the origin of turbidity samples are described.

##### 3.3.1.1. Background

In this section, the background of optical sensors is shown. Turbidity is defined as the loss of clarity in water, light may be absorbed, reflected or dispersed (Bin Omar & Bin MatJafri, 2009). Moreover, this parameter is related to the Beer-Lambert law Eq. (3.24) (Postolache et al., 2002). The Beer-Lambert law quantifies the transmitted light ( $I_t$ ), as a function of the light intensity of a source ( $I_o$ ), the absorption coefficient per unit length ( $a$ ), the turbidity ( $t$ ), and the length of the light pass ( $l$ ). From one side, absorption coefficient, and turbidity are related to the turbidity of the water. By the other side, the intensity of a source and length of the light pass are related to the measurement instrument. The value of ( $I_t$ ), can be expressed as a function of the scatter angle ( $\theta$ ), the particle size ( $r$ ), the wavelength( $\lambda$ ), and the optical properties of the particle and the medium such as the refractive index ( $n$ ) Eq. (3.25), (Postolache et al., 2002a).

$$I_t = I_o \times e^{-(a*t)l} \quad (3.24)$$

$$I_t = I_o(\theta, \lambda, r, n) \quad (3.25)$$

##### 3.3.1.2. Design and development of the turbidity sensor

In this subsection the design and the development of our turbidity sensors are detailed. For its design, several conditions must be met. These include low cost, low battery consumption, low maintenance and easiness to clean. As we concluded in the previous section, the most suitable option is the use of light beam for turbidity detection. In the majority of papers, authors use IR light source and IR light detectors. Nevertheless, as the developed turbidity sensor must be able to distinguish between different turbidity sources, more than one light source will be included. One IR and three colour light sources, green, yellow and red. The 5mm IR LED employed is the TSHG6200 (Vishay, 2017a). It has a peak wavelength of 850nm. The 5mm colour LEDs sources have a peak wavelength of 612-625nm (the red one), 581-594nm ( the yellow one) and 562-575nm (the green one). They are the TLLR4400 (Vishay, 2017b). The light receptors used in the sensor are the IR photodiode and the Light Dependent Resistor (LDR) is sensible to a visible light range, the used one is the NSL 19M51 (LDR, 2017). The LDR changes its resistivity depending on the amount of light that impacts on the sensitive part. The higher light intensity, the lower LDR resistance. The employed IR photodiode presents high speed and high radiant sensitivity. Its sensitivity range goes from 790 nm to 1050 nm and the peak appears at 950 nm. The photodiode is manufactured by Vishay, which code is BPW83 (Vishay, 2017c). The photodiode operation is the opposite of the LDR operation. The resistance of the photodiode increases with the light intensity. The price of those materials is detailed in Table 3.28. This price only includes the materials needed for the physical creation of the sensor, the sensing part: LEDs, light detectors, and resistors. The price of the Flyport or other nodes as Arduino or Waspnote that can be used for the same purpose (Parra et al., 2017 and Sendra et al., 2013b) are not included. However, the price of simple compatible Arduino ONE module can be bought by 3.15 €. Besides, the possible resistors needed for the conditioning circuit, to regulate the input signal to the node, must be added. Two voltage divisors must be used for this purpose. For the voltage divisor a resistance should be used. The estimated values of the resistances needed for the photodiode and for the LDR are 6 M $\Omega$ . The price of those resistances

is 0.08 € each one. In Table 3.28, we must add the price of the node and the price of the resistances for the conditioning circuit, so the total price is 8.30 €.

**Table 3. 28** Price of the electronic components for the low cost smart turbidimeter

Component	Code	Producer	Price (€)
IR LED	TSHG6200	Vishay	1.15
Color LED (x3)	TLLR4400	Vishay	0.36 (x3)
IR detector	BPW83	Vishay	0.88
Color detector	NSL 19M51	Advanced Photonix	0.80
Resistor (x4)	PPC470BCT-ND	Vishay	0.27 (x4)
Total			4.99

The prototype can be seen in Figure 3.37 (a). The light detectors are placed at 180° of the light sources. The distance between the light source and light detector are 6.5cm. A pipe made of non-porous crystal with a thickness of 2mm and a diameter of 2.7cm is employed to allow the water pass. The system of light sources and light receptors are placed inside a plastic box in complete darkness. Tubes of PVC are used to conduct the light of the LEDs to the crystal pipe. The same system is used with the receptors. Thus, we ensure that the light received at the light detector is the light of the LED that is not absorbed by the sample. The tubes have a length of 2cm from the light source to the crystal pipe and 1.4cm from the pipe to the receptor. The LEDs are powered using a Flyport module, which offers a constant output voltage of 4.6V. A resistor of 470 Ohms 5% is used between the Flyport and the LEDs to avoid possible damages. The value of resistor of the LDR and the photodiode are measured with a digital multimeter. The LEDs are powered sequentially: IR, red, yellow and green. The scheme of the electronic circuit that includes all the elements cited in Table 3.28 and the conditioning circuit can be seen in Figure 3.37 (b). The Voltage Output (Vout) represents the signal received by the node.

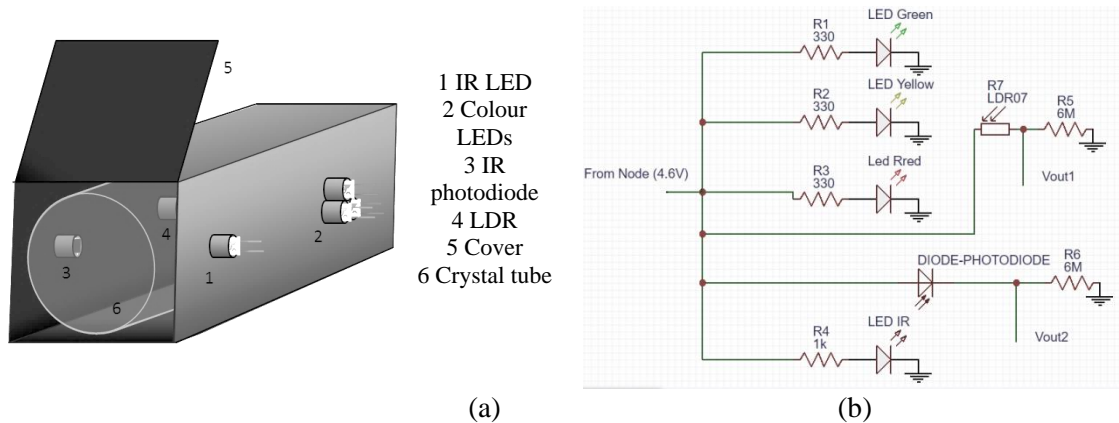


**Figure 3. 37** Representation of the prototype and its electronic scheme

### 3.3.1.3. Turbidity samples

In this subsection, the different samples used in the process of sensor calibration are described. Three different types of samples are employed in the tests; the samples are composed of water and a turbidity source. The water is composed of distilled water and NaCl is added to reach a salinity of 36mg/l. It is necessary to work with that salinity because our objective is to use the sensor for marine water. The turbidity sources employed are *Isochrysis galbana* as brown algae, *Tetraselmis chuii* as green algae and brown silt as sediment. The original samples composed of algae have a concentration of 13.327.658cell/ml *Isochrysis galbana* and 1.818.056cell/ml *Tetraselmis chuii*. The algae used for calibration were obtained from pure cultures of *Isochrysis galbana* and *Tetraselmis chuii*. Both species were grown in filtered and sterilized seawater,

enriched with F/2 medium adapted from Keller et al., (1987). These cultures were maintained at  $25\pm 1^\circ\text{C}$  and continuous aeration, under a 12:12h light:dark photoperiod. Different dilutions of those samples are prepared to calibrate the sensor. The used sediment was obtained from a riverbed. It is composed mainly of silt (67.3%), clay (28.4%), and a small percentage of sand (4.3%). The soil was dried up using an oven at  $40^\circ\text{C}$  during 24h. The coarse materials were removed after the sample was dried up. On the other side, the samples composed of sediment are prepared, each one separately by weighing different amounts of silt and adding 70ml of distilled water.

The salty water was only used for the samples with phytoplankton, to avoid the lysis of the cells. However, to ensure that the different salinities do not affect to our device a prelaminar test was carried out with distilled water and salty water with no turbidity sources. The results show that the diluted salts do not affect to the light absorption.

### 3.3.2. Results and Discussion

In this section, the results are shown and the discussion is done. First, the results of light absorption of different turbidity sources are presented. Following, the mathematical model to distinguish different turbidity samples are shown. Then, the intelligent algorithm is explained and the verification process is carried out. Finally, a comparison between our developed system and the current options is done.

#### 3.3.2.1. Different turbidity sources

In this section, we are going to analyze the results obtained from each one of the turbidity sources. First, the results of the samples that contain *Isochrysis galbana* as a turbidity source are shown. The resistance of the LDR and the IR photodiode are presented in Figure 3.38. The resistance of the IR photodiode increases as the concentration of the turbidity source decreases in a constant and linear pattern. By the other side, the relation between the resistance of the LDR and the turbidity is positive and exponential. It is possible to detect that each light presents different threshold values, from which is not possible to detect changes in turbidity. By the other side, there is a point where resistances maintain constant when the turbidity decreases. These threshold values are reached with the green light at 30% of dilution (3,998,297 cell/mL) with a constant resistance of  $46.76\text{M}\Omega$  and by the yellow light are 20% (2,665,532 cells/mL) of dilution with a constant resistance of  $1.81\text{M}\Omega$ . Those are the limits of detection (LOD) for the brown seaweed. The red light and IR light do not present LOD with the employed samples.

Following, the results with the samples with *Tetraselmis chuii* as a turbidity source are detailed. The results can be seen in Figure 3.39. The resistance of IR photodiode and the LDR are similar to the test with the *Isochrysis galbana*. The LOD is reached with the green light at 5% of dilution (90,903 cells/ml), with a resistance value of  $46.7\text{M}\Omega$ . Moreover, the yellow light presents the LOD at 5% of dilution with a resistance value of  $1.81\text{M}\Omega$ . The maximum resistance is  $92.63\text{M}\Omega$  in green,  $24.27\text{M}\Omega$  in red,  $7.77\text{M}\Omega$  in yellow and  $8.66\text{M}\Omega$  in IR.

Finally, the results with the sediment as a turbidity source are shown in Figure 3.40. As in the other cases, the relation between turbidity and resistance of LDR is exponential. However, in this case, the relation between turbidity and IR photodiode is a negative exponential relation. The LOD was not detected for any light source. Nevertheless, for the green light, an upper limit value has been found. With more than 373 mg/l of sediment and a value of resistance of  $200\text{M}\Omega$ , it is not possible to detect changes in green light absorption. The value of  $200\text{M}\Omega$  corresponds to the highest value or the LDR (resistance in darkness). The sample with the highest concentration gives as a result  $200\text{M}\Omega$  with all the lights.

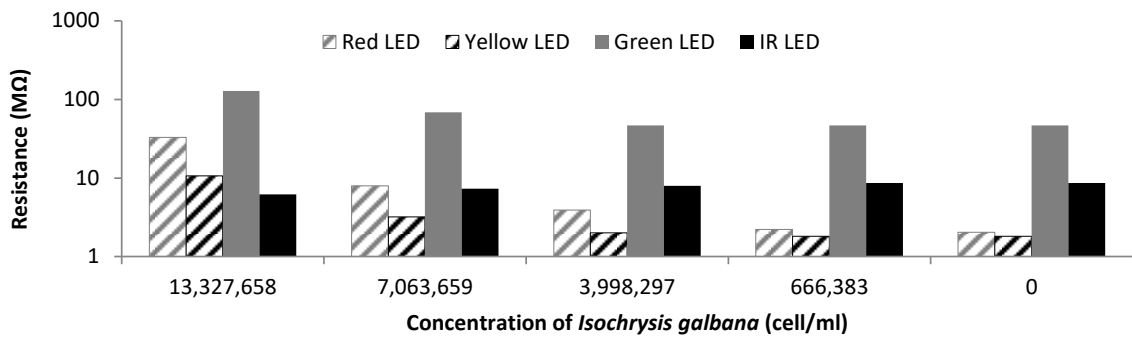


**Figure 3.38** Resistance of LDR and photodiode with samples of *Isochrysis galbana*

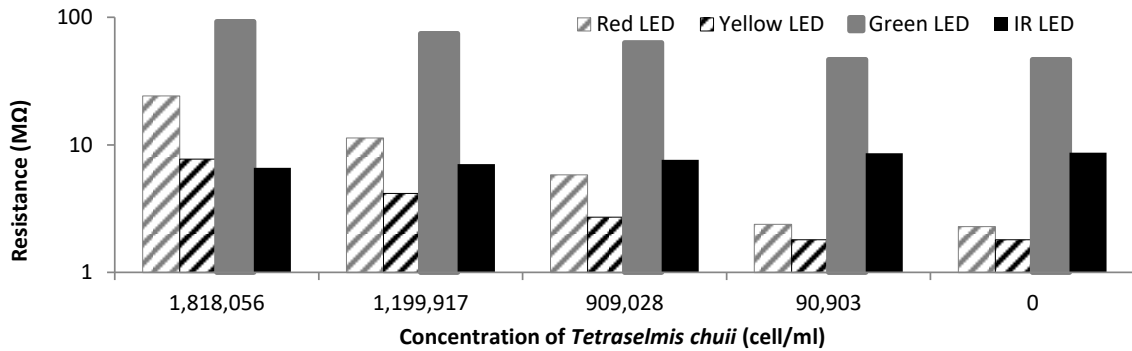


**Figure 3.39** Resistance of LDR and photodiode with samples of *Tetraselmis chuii*

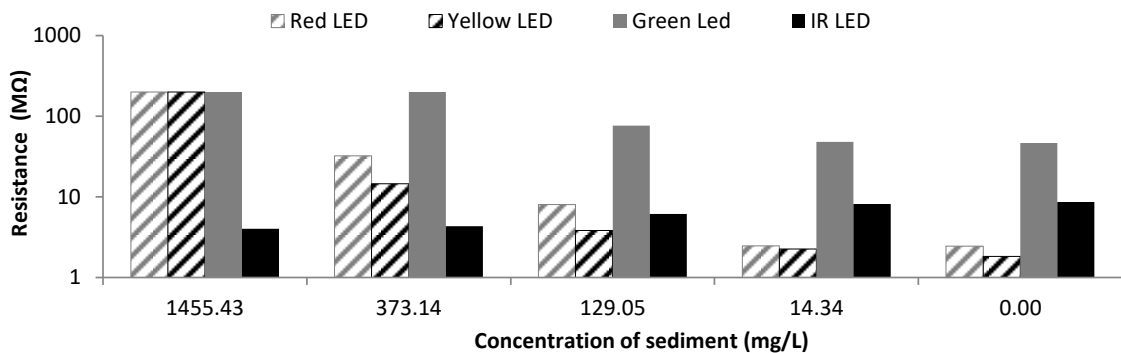


**Figure 3.40** Resistance of LDR and photodiode with samples of Sediment

Our turbidity sensor is capable to distinguish between different concentrations of sediment, from 0 mg/l to 378mg/l. It is possible to distinguish higher values up to 1455 mg/l but only with IR light. For the turbidity generated with seaweed, we can distinguish between different concentrations form 0cells/mL to 13.327.658 cells/mL in *Isochrysis galbana* and from 0cells/mL to 1.818.056 cells/mL in *Tetraselmis chuii*. It is possible to distinguish higher concentration, but they are not tested. With the employed samples no LOD has been found. It is necessary to develop more analysis to found the LOD of the IR light absorption in our system.

### 3.3.2.2. Distinguish between turbidity sources

In this subsection the possibility to distinguish between different turbidity sources is shown. To compare between turbidity sources (sediments, green and brown algae) it is necessary to use turbidity units as Nephelometric Turbidity Unit (NTU). First of all, it is necessary to have a relation between the concentration in mg/l or in cells/mL and the NTU. For this purpose, the Eq. (3.26) shown in Sendra et al., (2013a), is used to relate the mg/l of sediment with NTU.

Moreover, the same design of the IR part of the turbidity sensors was employed and compared with a commercial Turbidimeter, the Hach 2100N. Using this equation it is possible to relate the values of resistance of the IR photodiode ( $R_{ir}$ ) with the turbidity values Eq. (3.27). To obtain the Eq. (3.27) we relate the values of the IR photodiode obtained during the experiment with the values of turbidity in NTU obtained from applying the Eq. (3.26) to the samples of sediment. To relate those values the mathematical software (Eureqa Software, 2015) is used. The Eq. (3.28) and Eq. (3.29) are obtained by relating the values of turbidity in NTU calculated with Eq. (3.27) and the values of concentration for each one of the phytoplankton species.

$$Sediment (NTU) = 1.873 + 0.518 \times Sediment (mg/L) \quad (3.26)$$

$$Turbidity (NTU) = \frac{5209}{1.23 + R_{ir}(M\Omega)^2} - 66.72 \quad (3.27)$$

$$Isochrysis galbana (NTU) = 0.000005 \times Isochrysis galbana \left(\frac{cell}{ml}\right) - 2.6871 \quad (3.28)$$

$$Tetraselmis chuii (NTU) = 0.00005 \times Tetraselmis chuii \left(\frac{cell}{ml}\right) - 1.3232 \quad (3.29)$$

Now, it is possible to compare the resistance values of LDR with different lights for different turbidity sources. Thus, we can find a mechanism to differentiate different turbidity sources. For this purpose the software Statgraphic Centurion (STATGRAPHIC, 2017) is employed. Simple regression is used to obtain an equation that relates the resistance of LDR and the NTU for differences in the turbidity sources. The type of regression model used is an exponential model with a constant and it is based on the minimum squares adjustment. The confidence interval of each model is represented in the following figures. Our objective is, for each one of the lights (green, yellow and red), to present the obtained regression model with their confidence intervals for each turbidity source. Besides, it is necessary to evaluate if it is possible to distinguish different turbidity sources according to the confidence intervals.

First, the results obtained with green light are presented in Figure 3.41. It is possible to see the different regression models with their confidence intervals for each one of the turbidity sources. The different dashes represent different turbidity sources, short dashes for *Tetraselmis chuii*, long dashes for *Isochrysis galbana*, and no dashes for sediment. In squares are presented the gathered data in the previous subsection. The different lines represent the mathematical model in bold and the confidence intervals. The models represented in Figure 3.41 correspond to Eq. (3.30), Eq. (3.31) and Eq. (3.32).  $R_{green}$  ( $M\Omega$ ) represents the value of resistance in  $M\Omega$  of the LDR exposed to green light. The value of  $R_{green}$  ( $M\Omega$ ) for the same turbidity value is different according to the turbidity source. For this reason, we distinguish between  $R_{green}$  if  $IG$  which represents the value of resistance of the LDR with *I. galbana*,  $R_{green}$  if  $TC$  or  $R_{green}$  if  $S$  depending if the turbidity source is *Tetraselmis chuii* or sediment. The turbidity of *Isochrysis galbana* (TIG), *Tetraselmis chuii* (TTC) or sediment (TS) represents the values of turbidity in each test. The correlation coefficients of those mathematical models are 0.985, 0.984 and 0.995 respectively. The means absolute errors are 0.05, 0.03 and 0.04 NTU. According to the confidence intervals, see the Figure 3.41, it is possible to affirm that for values of turbidity higher than 47 NTU, our prototype is able to distinguish between phytoplanktonic turbidity and sedimentary turbidity. However, with green light, our device is not able to distinguish between *Tetraselmis chuii* and *Isochrysis galbana*, according to the confidence intervals.

$$R_{green\ if\ IG}(M\Omega) = e^{(3.75453 + 0.0171214 \times TIG (NTU))} \quad (3.30)$$

$$R_{green\ if\ TC}(M\Omega) = e^{(3.85743 + 0.0134761 \times TTC (NTU))} \quad (3.31)$$

$$R_{\text{green if } S}(\text{M}\Omega) = e^{(3.81816 + 0.00760528 \times TS (\text{NTU}))} \quad (3.32)$$

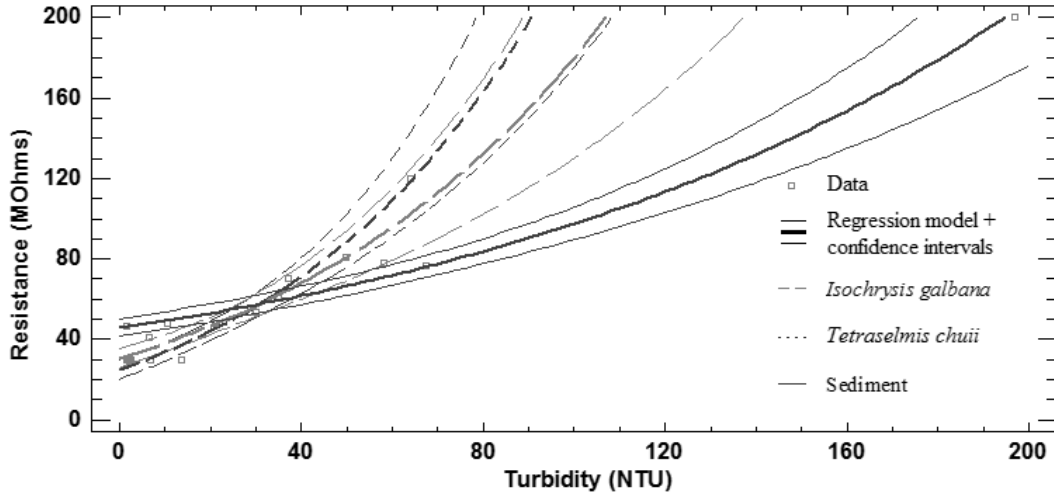


**Figure 3. 41** Regression models with confidence intervals for different turbidity sources with a green light

Now, the results obtained with yellow light are presented. In the Figure 3.42, it is possible to see the three different regression models with their confidence intervals for each one of the turbidity sources. As in Figure 3.41, the different dashes represent different turbidity sources and the different lines represent the mathematical model and the confidence intervals. The Eq. (3.33), Eq. (3.34) and Eq. (3.35) are the models represented in Figure 3.42.  $R_{\text{yellow}}(\text{M}\Omega)$  represents the value of resistance in  $\text{M}\Omega$  of the LDR exposed to yellow light. The value of  $R_{\text{yellow}}(\text{M}\Omega)$  for the same turbidity value is different according to the turbidity source. For this reason, we distinguish between  $R_{\text{yellow if } IG}$  which represents the value of resistance of the LDR with *I. galbana*,  $R_{\text{yellow if } TC}$  or  $R_{\text{yellow if } S}$  depending if the turbidity source is *Tetraselmis chuii* or sediment. Turbidity of *Isochrysis galbana* (TIG), *Tetraselmis chuii* (TTC) or sediment (TS) represents the values of turbidity in each test. The correlation coefficients of the presented mathematical models are 0.989, 0.990, and 0.994 respectively. The means absolute errors are 0.09, 0.06 and 0.06 NTU. According to the confidence intervals, see the Figure 3.42, it is possible to affirm that our prototype is capable to distinguish between phytoplanktonic turbidity and sedimentary turbidity from 21.75 NTU. However, it is not able to distinguish between *Tetraselmis chuii* and *Isochrysis galbana*, according to the confidence intervals with the yellow light.

$$R_{\text{yellow if } IG}(\text{M}\Omega) = e^{(0.432322 + 0.02879 \times TIG (\text{NTU}))} \quad (3.33)$$

$$R_{\text{yellow if } TC}(\text{M}\Omega) = e^{(0.496358 + 0.0291769 \times TTC (\text{NTU}))} \quad (3.34)$$

$$R_{\text{yellow if } TS}(\text{M}\Omega) = e^{(0.606395 + 0.0105505 \times TS (\text{NTU}))} \quad (3.35)$$



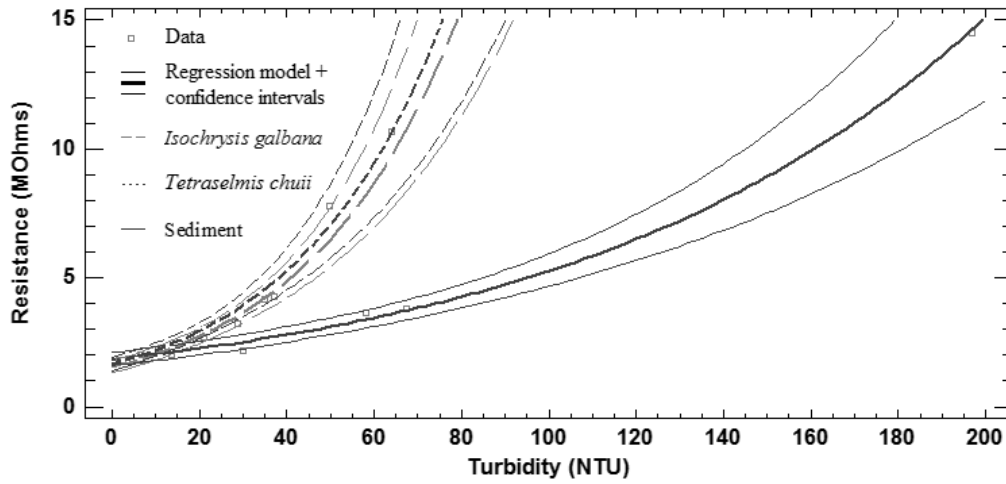


**Figure 3. 42** Regression models with confidence intervals for different turbidity sources with yellow light.

Finally, Figure 3.43 shows the results obtained with red light. It presents the different regression models with their confidence intervals for each one of the turbidity sources. The different dashes represent different turbidity sources. The different lines represent the mathematical model and the confidence intervals such as in Figure 3.41 and 3.42. In Figure 3.43 the regressions models presented correspond to the Eq. (3.36), Eq. (3.37) and Eq. (3.38).  $R_{red}$  ( $M\Omega$ ) is the value of resistance in  $M\Omega$  of the LDR exposed to red light. The value of  $R_{red}$  ( $M\Omega$ ) for the same turbidity value is different according to the turbidity source. For this reason, we distinguish between  $R_{red}$  if  $IG$  which represents the value of resistance of the LDR with *I. galbana*,  $R_{red}$  if  $TC$  or  $R_{red}$  if  $S$  depending if the turbidity source is *Tetraselmis chuii* or sediment. The turbidity of *Isochrysis galbana* ( $TIG$ ), *Tetraselmis chuii* ( $TTC$ ) or sediment ( $TS$ ) represents the values of turbidity in each test. The correlation coefficients of presented regression models are 0.999, 0.999, and 0.990 respectively. The means absolute errors are 0.04, 0.01 and 0.13 NTU for each one.. In this case, it is possible to affirm that our device is able to distinguish between *Tetraselmis chuii* and other turbidity sources from 12 NTU, according to the confidence intervals. Moreover, it is possible to distinguish between *Isochrysis galbana* and sediment from 16 NTU with the red light. Therefore our prototype is capable to differentiate all the tested turbidity sources by using the red light source. For this reason after using the IR light to determine the NTU of the water, the light that will be used to identify the turbidity source is the red light.

$$R_{red} \text{ if } IG (M\Omega) = e^{(0.711176 + 0.0445014 \times TIG (NTU))} \quad (3.36)$$

$$R_{red} \text{ if } TC (M\Omega) = e^{(0.742255 + 0.0488297 \times TTC (NTU))} \quad (3.37)$$

$$R_{red} \text{ if } S (M\Omega) = e^{(0.901301 + 0.0145908 \times TS(NTU))} \quad (3.38)$$

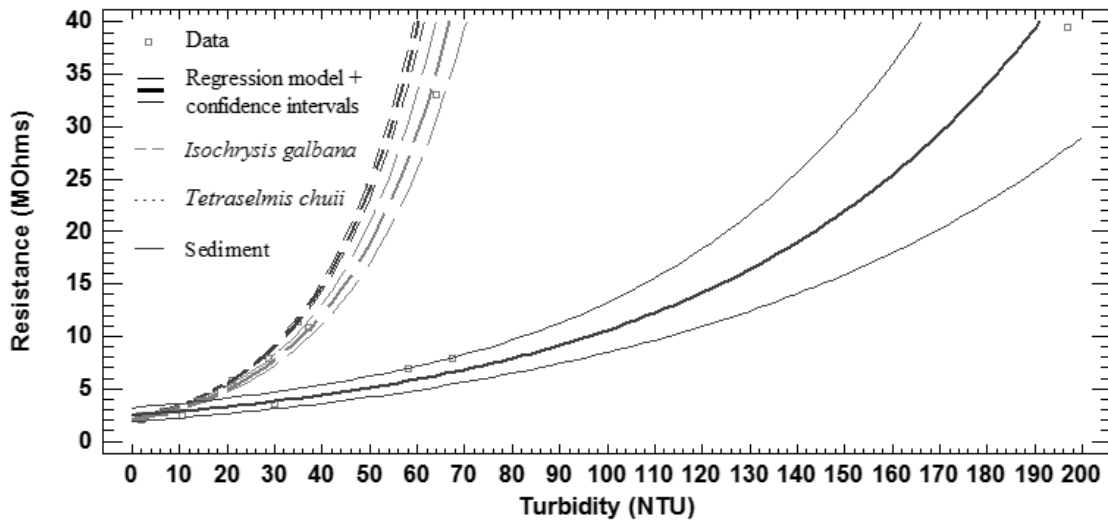


**Figure 3.43** Regression models with confidence intervals for different turbidity sources with red light.

After analyzing all the gathered data and evaluate the confidence intervals of each mathematical model, we can conclude that the best result is obtained with the red light. It is the only light that allows distinguishing between different phytoplankton species. Besides, the red light offers the possibility to distinguish turbidity sources from the level of turbidity of 12 NTU while the other lights only can distinguish at higher turbidities, 16 and 21.75 NTU with yellow and green light. For this reason with the IR and red light, we are able to quantify the turbidity and characterize the turbidity source.

### 3.3.2.3. Intelligent algorithm

In this subsection the algorithm used to evaluate the samples is presented, it can be seen in Figure 3.44. After a measure is done the value of resistance of IR photodiode and the value or resistance of LDR with the red light are analyzed. First, the system turns on the LEDs and gathers the data from the photodiode and the LDR. After gathering the data, the LEDs are turned off. A code in the node is programmed to turn on/off the energy supply of each LED and detector. The LEDs are turned on first. After 3 seconds, the detectors are turned on. Then, after 1 second the photodiode and the IR LED are turned off. Finally, 5 seconds after activating the LDR, it is deactivated. Following, the value of resistance of IR photodiode is used in conjunction with the Eq. (3.27) to obtain the value of turbidity of the sample. Then, the data is tagged with the NTU value. If the NTU value is lower than 12 NTU, the data is tagged as type Undetectable (Und.). However, if the value of NTU is higher than 12 NTU the Eq. (3.36), Eq. (3.37) and Eq. (3.38) are applied. These equations will calculate the value expected *Rred* for a different type of turbidity sources. The model that offers a *Rred* closer to the gathered data assigns the turbidity type. Finally, the sample is tagged with the type of turbidity and with the NTU values and is shown as the result.

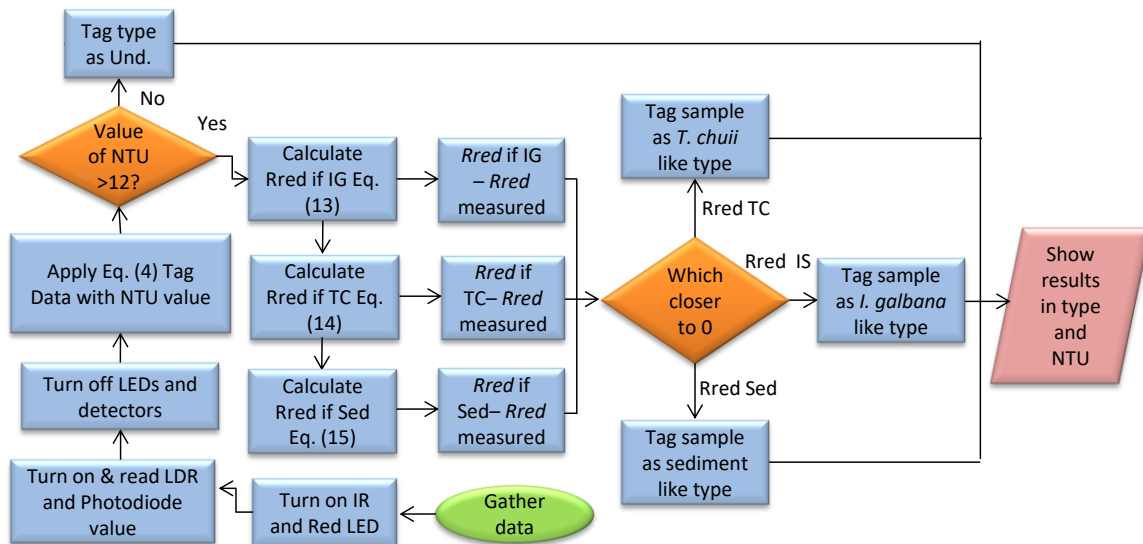


Figure 3. 44 Decision algorithm

### 3.3.2.4. Verification process

In this verification process, we want to confirm that the mathematical model of our system is able to tag correctly the samples and calculate its turbidity. For this test samples were created randomly using the pure samples of algae and sediment. The samples were created by one part of the researchers and they were analyzed by researchers that do not participate in the creation of the samples. The samples were labeled as 1, 2, 3 and 4 and no information about its origin or dilution was added.

The values of resistance with IR and red light, *Rred*, were obtained using the prototype. The values of resistance with yellow and green light were not obtained because we are testing the mathematical model with the red light. First, the values of the resistance with IR light were used to calculate the turbidity of the samples. Two of the samples have turbidity values lower than 10 NTU, so according to our model, it is not possible to assign exactly the type of turbidity. The algorithm can tag the samples anyway, but it will indicate that the veracity of this label cannot be ensured.

For the next step, with the NTU values, the system calculates the expected (*Rred if IG*, *Rred if TC* and *Rred if S* (Eq. 3.36 to 3.38)). Finally, the measured *Rred* is compared with the expected resistance. The source of turbidity is determined by the likeness between the *Rred* and the expected resistance for each type. The results of this process can be seen in Figure 3.45. Figure 3.45 shows the *Rred* and the expected resistances calculated for the turbidity level. The first sample is tag as *I. galbana*, the second sample as sediment, the third as *T. chuii* and the last as sediment. Form the four samples, only one is tagged incorrectly and it was one of the samples with the lowest turbidity. Furthermore, the mean relative and absolute errors in samples used during the verification process are 3.27% and 0.65NTU.

In addition to the verification process, some data about the response time of the photodiode and the LDR when the turbidity changes are shown now. The goal of this test is to show how quick the system can detect changes in the water turbidity. In this test, it is gathered the data from the LDR with red LED and the photodiode during 30 s. The experiment starts with water without any turbidity source, at 9.5 s, and at 17.5 s different amount of sediment was added. The values of resistance of the LDR and the photodiode are shown in Figure 3.46. We can see that the photodiode has a response time of 0.3 s while the LDR needs more time to change the value of the resistance ( $\approx 2$  s).

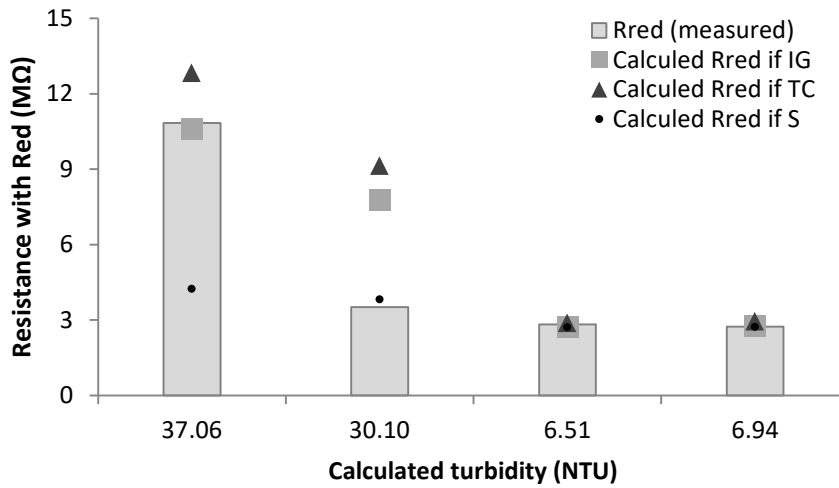


Figure 3.45 Data from the verification process.

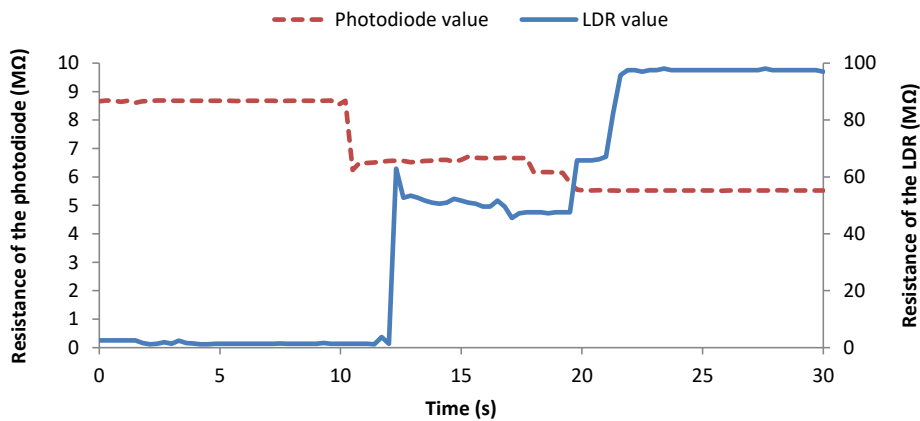


Figure 3.46 Data gathered in real time.

### 3.3.2.5. Comparison with current sensor systems and suitability for fish farms

In this subsection, a comparison between our developed system and the current options are performed. Moreover, we will justify the suitability of this system for fish farms.

The main advantage of the developed device and the algorithm is the capability for characterizing the turbidity. Several authors used different option based on light emission and detection to determine the water turbidity. Sendra et al., (2013a) proposed a low cost turbidity sensor, which is based on an infrared optical sensor placed at 180° of the light source. Their sensor was able to determine the turbidity of water samples, from 0 to 1000 NTU, without differentiating between turbidity sources. Shenoy et al., (2012) developed a turbidity sensor based on optical effects. Two sensors were placed at 360° from the source and a concave mirror was employed at 180° of the light source. The optic fiber was used as a light source and as a sensing element. However, their proposal is not prepared to differentiate between different turbidity sources. J. Rocher et al. (2017) presented the use of a turbidity sensor for fish farms. The sensor was based on an IR emitter and receiver. However, their turbidity sensor was not able to distinguish between different types of sediments. Goddijn-Murphy et al., (2009) analyzed of RGB values obtained with a digital camera. They affirm that there is a significant relationship in the reflectance of red and blue light for yellow substances and blue and green light for chlorophyll. However, they need the use of a digital camera and a posterior image analyzing techniques. Their development is not able to obtain data about the IR region.

Moreover, they do not make a relation between the color and the concentration of the substances.

Different authors proposed the application of remote sensing to quantify the turbidity. Tyler et al., (2006) were able to determine the concentration of suspended solids and chlorophyll in lakes. Sebastia et al., (2012) demonstrated the capability of using remote sensing to determine the concentration of chlorophyll *a* in coastal areas of the Mediterranean Sea. However, the use of remote sensing it is not useful for continuous monitoring due to the low temporal resolution of the images. Moreover, it is not useful for monitoring the changes inside the aquaculture facilities. It can be useful to monitor the changes in the water body from which the water is obtained.

Chanson et al., (2008) proposed to use an Acoustic Doppler Velocimeter (ADV) with backscattering to determine the turbidity in water bodies. Even though this methodology offered good correlation, it is not possible to characterize the origin of the turbidity. Vousdoukas et al., (2011) proposed a similar system. The proposed prototype in this section is able to differentiate different types of turbidity. Moreover, the use of ADV in fish farms facilities is not a suitable option because of the small volume of water and the continuous changes of velocity along the facilities. Our system is not affected by the velocity of the water and the minimum volume of water needed to have a stable value is the volume of the crystal tube. Its diameter is 2.7cm and its length is 7cm. The volume of water that contains the tube is 59.37cm<sup>3</sup>. It is the minimum volume that our system can analyze.

As a summary, the systems based on remote sensing are not suitable for inland fish farms facilities that can be covered or placed inside the building. Besides, the temporal resolution is not enough to ensure a continuous monitoring. The systems based on ADV are able to distinguish turbidity types, but it is not indicated for small water volumes. Then, the most indicated system is the one based on light absorption. The current systems based on light absorption are appropriated for water quality monitoring in fish farms. Nevertheless, they are not able to distinguish between turbidity sources. The developed sensor in this section shows how using two light sources with different wavelength and two detectors it is possible to distinguish different turbidity sources. This system can monitor the turbidity giving, as a result, the water turbidity in NTU and the type of turbidity: sediment, green phytoplankton or brown phytoplankton. For fish farming the capacity to distinguish between types of turbidity is important.

### **3.4. Hydrocarbon sensor**

#### **3.4.1. Material and methods**

In this section, we present the materials employed for the design and calibration of our low cost optic sensor for hydrocarbon detection. We also detail the performed test to evaluate the effectiveness of different light sources to detect the presence of hydrocarbon in the water surface. The principle employed by the sensor to detect the presence of hydrocarbon is the photoluminescence.

According to this principle, if the correct wavelength is used the molecules can absorb a photon and pass to an excited state. To recover their natural state, the molecules emit a photon of other wavelength. This phenomenon allows distinguishing between different molecules, in this case, water of hydrocarbons. We emit light at different wavelength from LEDs to promote the photoluminescence effect. We tested six different light sources. We changed the light wavelength to violet, blue, green, orange, red and white. The emitted light is registered by a photodetector, S186P, able to detect light above 900nm. Both, light source and photodetector are in parallel with an opaque material separating them. That way, the light detected is a result of reflexion and photoluminescence. The light source is placed at 1cm from the sample. The disposition of the source, detector and water is shown in Figure 3.47.

Real sea water is used as water source, and 97 octanes gasoline is employed as hydrocarbon pollutant. The gasoline has been bought in a normal provider. The sea water was filtered and maintained at low temperatures to avoid the proliferation of organisms. Several samples are

prepared at laboratory with different concentration of gasoline. The samples have a total volume of 30ml (seawater and gasoline), and different amounts of gasoline are added at each one. The volume of gasoline added at each sample and the final concentration of each sample can be seen in Table 3.29.

The light intensity recorded by the photodetector is related to the presence or absence of hydrocarbon. The lights with better results are selected for deeper analyses.

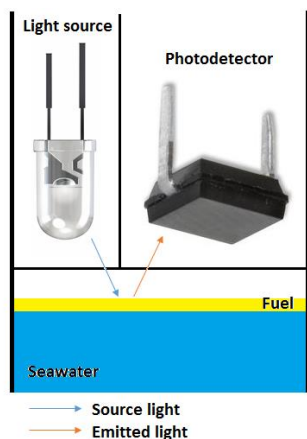


**Table 3. 29** Concentration of gasoline in the samples

Sample n°	Added gasoline 97 octanes (ml)	Gasoline 97 octanes concentration (g/l)
1	0	0
2	2	50
3	4	100
4	6	150
5	8	200
6	10	250

**Figure 3. 47** Disposition of the light source, detector and water sample

### 3.4.2. Results

In this section, we show the results of the performed tests. First, the test with different concentrations of gasoline and different light sources are shown. The test with the lights that offer the best results will be exposed. Finally a statistical analyze of the data of the second test is shown in order to evaluate if the observed differences are statistically significant. Figure 3.48 is a picture taken during the first tests with the sample with white light and a concentration of 0g/l of gasoline.

In the test with different lights and different gasoline concentrations, six lights were employed. Each one has different light color, violet, blue, green, orange, red and white, in order to select the one that offers best results. The results of this test can be seen in the Figure 3.49. We can see that each light offers different results. Blue and green light are not useful at all, they offer the same values when the gasoline is present and when is not. The output voltage registered at 200g/l of gasoline when red light is used is similar to the output value when there is no gasoline, so red light must be rejected. The white, orange and violet light offers good results. The output value in presence of gasoline is different than the output voltage in absence of gasoline. The white and violet are the ones that offer more promising results according to the difference of output voltages in presence or absence of gasoline.

Three light sources are selected to make deeper analysis: violet, orange and white. In this deeper analysis the measures with the samples without gasoline and the sample with lower concentration (50g/l) were repeated 10 times. This way is possible to find the variation in the signal and be sure that the proposed system is able to detect the presence of hydrocarbons in the water.

The results of this test are presented in Figure 3.50. We can see that in all the cases the mean of output voltage is different in absence or presence of gasoline. The white light is the one that presents the highest standard deviation in absence of gasoline, 0.003mV. The orange light is the one that presents lowest standard deviation in both cases, less than 0.0006 mV. The difference

between the means in white light are 0.008 mV for white light, 0.0037 mV for orange light and 0.0072 mV for violet light.

Statistic test were done using Statgraphic Centurion software (STATGRAPHIC, 2017) to validate the observed differences between the means. First of all, the normality of the samples is tested, the values of skewness and kurtosis reveal that the data does not follow a normal distribution. In order to evaluate if the observed difference between the results with and without is statistically significant or not a non-parametric test is used. A Kolmogorov-Smirnov test is used. The value that indicates if the observed difference is statistically significant or not is the p-value. Assuming a confidence level of 95% is possible to assume that the differences observed between lectures in samples with and without gasoline are statistically significant in the three cases. The p-value on all the cases are lower than 0.05.

According that the three light offers good results, different values in absence or presence of gasoline which are statistically significant, is important to select which light will be used in the prototype. To make this decision is important to pay attention to the output values. The light that offers higher output voltages values is the indicated, because of is easier to detect higher voltages. The light with higher voltage is the white light.

The cost of all the electronic components needed to assembly the prototype is only 3€. And its application in real environments lies in the possibility to avoid the direct contact between the sensor and the water. The prototypes were tested at 1cm of the water sample.

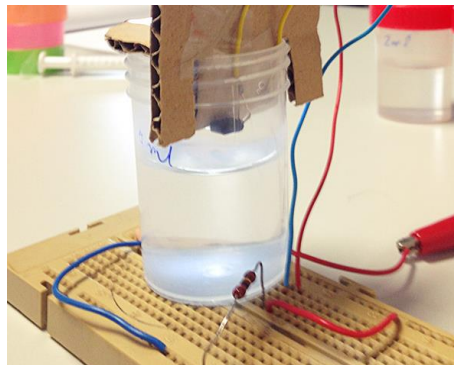


**Figure 3. 48** Set up of the experiments to select the best light source.

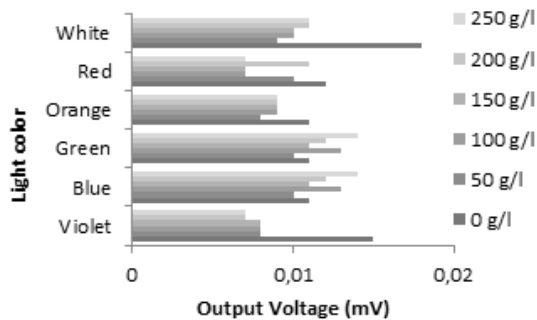


**Figure 3. 49** Output voltage registered at the photoreceptor output using different light colors.

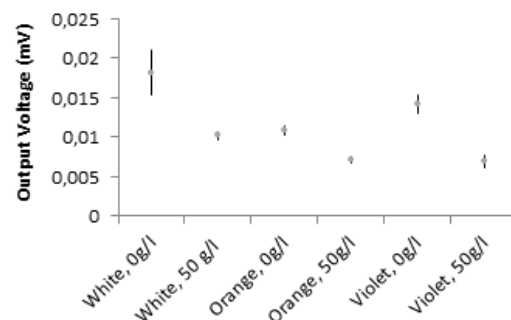


**Figure 3. 50** Output voltage registered at the photoreceptor output using the selected light of test 1 after 10 repetitions, represented the mean with the standard deviation.

### 3.5. Conclusion

In this chapter, we have shown the different sensors developed to test three parameters: conductivity, turbidity, and hydrocarbon.

Regarding to the conductivity sensors, our main objective was to develop a new low-cost, low-maintenance conductivity sensor without contact with the water, reducing the need of continuous calibration and reducing as less as possible the sensibility. It has been achieved successfully.

In the first tests we demonstrated that different environments (air, fresh water and salty water) can produce different alterations in the electromagnetic field, and these alterations can be measured by different methods. But we detect some problems when we are using the Hall sensor. The sensibility of the sensor is too low for our purposes. So, we needed to increase the voltage of the solenoid in order to obtain enough sensibility. This causes a heater of the solenoid that changes the value of the magnetic field when the position of the Hall sensor changes a little.

We choose to measure the alteration of the magnetic field through the changes of the current registered in an inductive coil. We use four different combinations of coils (solenoids and toroids) with different wire diameter and sizes to make a comparison. We saw that each configuration has different optimum frequencies. This frequency can distinguish between different salinities, but not all of them work in the same way. One of them was able to distinguish water samples with low conductivities, however when the conductivity increases the values of sensor signal is the same. So this coil was good to use it in control of irrigation water, but not for our purpose. The others are capable to distinguish freshwater from seawater and different conductivities between them. To decide with one use in the final tests we pay attention at the working frequency, because at lower frequencies, the electronic components needed and the circuit are cheaper. Thus, we chose Model 4 to perform the final test.

In those final tests, we realize some investigations in this sensor. We analyze some factors as the lineal ranges, their sensibility or the minimum cell volume. We saw that there are three lineal intervals with different sensibilities, from 0.002mS/cm to 0.03mS/cm. Moreover, we demonstrate that the volume of the water that surrounds the coils is very important. The high of water needed to use the sensor is just the level of water that covers completely the sensor. However, the surface of water is very important because the magnetic field must be enclosed by water. In the case of our sensor the surface of water needed to realize the measures is 18.75 cm radius.

Finally we perform some measures with samples obtained from the field, with no one treatment, and we identify a drift in our sensor. We have found an analytical relation between the real value and the obtained values by our sensor, and, by using this equation, it is possible to correct the value of conductivity.

One of the main problems when we start the measures is the great variations of behavior that we found at different frequencies. Until we do not finalize the first set of tests we do not know how big the options to continue our test are.

The use of two copper coils submerged under the water was an issue that caused us many problems and made us lose a lot of time. In the first coil that we use, that was part of a current transformer exist thin layers of paper between the layers of copper wire. When this paper gets soaked, the behavior of the coil changes, and we cannot continue the test until the coil dries up. So, we decided to isolate the coil with silicone. But this only retains the water out of the coil for a few period of time. Once the water was inside the coil, we must to remove all the silicone, because with the silicone the coil does not dry up.

Finally, we decided to stop the use of this coil and create our own coils with fewer layers and do not use any other material than the wire of copper. So, the behavior of the coil does not change even if we introduce the coil inside the water for long terms of time.

In further investigations we want to try to avoid that drift, because we think that possibly it is caused by the suspended sediments. Those sediments can interact with the magnetic field but does not interact with the pas of electricity. So, in the next tests we want to measure the turbidity using another developed sensor in other paper (Sendra et al., 2013b). We decide to use it instead of a commercial sensor because this turbidity meter is also a low cost sensor, and one of our objectives is to obtain a low cost sensor.

Moreover, we want to implement this sensor completely with the electronic circuit needed and use this sensor in fishfarms, where changes in the water conductivity can produce huge economic loses.



In addition, we discovered that the current turbidity sensors are not entirely useful for turbidity monitoring in fish farms. There are different turbidity sources, which can cause different effects of fish. For this reason, it was necessary to design, develop and calibrate a turbidity sensor for water. The sensors must be able to determine the turbidity and to differentiate between sedimentary and phytoplanktonic turbidity. The prototype is based on the Beer-Lambert law and the absorption of light by the turbidity. The sensor uses four different light sources with different wavelengths: IR, green, yellow and red. Two different light receptors placed at 180° of light sources were employed, IR photodiode and LDR sensible to the visible spectrum. The calibration was performed with two species of phytoplankton and with sediment. The results show that the prototype is able to distinguish between different algae species and sediment using the value of LDR with the red light as a source. An algorithm was developed to endow our prototype with the ability to differentiate between turbidity sources based on the resistance of the LDR and photodiode. The algorithm is based on the empiric equations obtained in the calibration process. Our findings allow to obtain turbidity measures in fish farms facilities and to characterize this turbidity in order to take the necessary actions to prevent further damages. The proposed sensor can be placed in different parts of the fish farm facilities with the purpose of developing an early alarm system to prevent damages in the production tanks. Therefore, the sensor must be placed at the water entrance, in the reception tank, before the water distribution system.

Our future work is focused on creating a wireless sensor network (WSN) composed by this turbidity sensor and other sensors for water quality monitoring similar to the proposed system by Sendra et al., (2015b). Moreover, we pretend to deploy this WSN in a fish farm facility to control the water parameters along the facility. We will prepare a new set of samples mixing sediment and phytoplankton in order to find out if the sensor can distinguish the percentage of each turbidity source in case of having turbidity caused by two sources. In addition, different types of sediments with different grain-size composition and with the addition of organic matter will be used to improve the calibration of the proposed sensor. Moreover, we want to include our prototype in an alarm system similar to the one developed by J. Rocher-Morant (2017) but including different types of alarms according to the turbidity source. Finally, we show the development of a qualitative sensor which can detect the presence of hydrocarbon over the water layer.

Following, we present a prototype of sensor able to detect the presence of hydrocarbon in the water. The sensor is based on the well known photoluminescence effect linked to the hydrocarbons. In the design of the sensor different light colours are used to excite the molecules of a hydrocarbon, gasoline. The light source is a LED and a photodetector is used as a receptor of the emitted light. We use different concentrations of gasoline in the water to perform the tests. The light that offers best results, white, orange and violet are used for deeply tests. Those tests demonstrate that the light with best results is the white light. It presents higher voltage difference between the measures with and without hydrocarbon. The results of second test were statistically analysed to validate that the observed difference is statistically significant.

The sensor presents good characteristics in order to be applied to detect the presence of spills as a part of a real environment monitoring network. Those characteristics are mainly its low price, less than 3€ the electronic components needed. Also its easy operation and the possibility of avoid the direct contact between sensor and water.

Finally our future work is to use this sensor in real environment as a part of a wireless sensing or network for water quality monitoring in port areas. In the ports is common the presence of hydrocarbons in the upper layer of the water.

Finally, work presented in this chapter have been published in the following references (Parra et al., 2013a), (Parra et al., 2013 b), (Parra et al., 2013c), (Parra et al., 2015c), (Parra et al., 2015d) and (Parra et al., 2018b).

## **4. IMPLEMENTATION IN FISH FARMS**

## 4.1. Introduction

In this chapter, we present the developed systems based on the aforementioned sensors for fish farm monitoring. While in the previous chapter we show some of the developed sensors individually, now we are going to detail the different employed sensors working together. Some new sensors are presented in this chapter as the water level sensor, light sensor, and presence of workers sensor among others. In addition, the system to detect the fish behavior and feed falling is presented.

First, systems that monitor the conductivity and water level in the tanks of fish farms facilities are shown. In this system, we show the possibility of distributing the water with different salinities along the fish farms facilities. This is useful for recirculating systems where different fish are kept. Different fish may have different requirements and may need different conductivity in their water. Moreover, it is known that in recirculating systems the water evaporation produces an increase in the salt concentration in the recirculating water. Thus, it needs a compensation with fresh water. We present a system that monitors the conductivity of the facility and can compensate the salinity with fresh water in order to maintain the thresholds values, set by the fish farm manager, in each tank row. The benefits to adjust the conductivity is to improve the fish performance and fish well-being and therefore increase the economic benefits.

Secondly, we are going to present the design of a network of sensors to monitor the water quality of a fish farm on the mainland. The system is based on two sensors that are placed inside a waterproof box. There is a turbidity sensor and a temperature sensor. This box is crossed by a glass tube where the water passes. A humidity sensor inside the waterproof box is installed to detect the entrance of water inside the box if the humidity sensor detects water in the box it will turn off the sensors, so as to prevent any damage to the electronics. Each group of 3 sensors will be connected to a Flyport that will be connected to an access point via a Wi-Fi connection. The different access points of the plant will be connected to a Switch with an Internet connection via a router. The data collected by Flyport are sent to a server. This data will be accessible both locally and remotely.

Following, the design and deploy a low-cost WSN to monitor fish feeding process and water quality in aquaculture tanks is presented. The system is composed of sensors that measure different parameters of the water quality (such as temperature, turbidity, or conductivity, among others), of the tank conditions (such as illumination and water level), and of the fish feeding behavior (such as swimming depth and velocity and fallen pellets). Moreover, the system has other sensors, such as the humidity sensor, that actuates as an emergency turn-off system to prevent damages caused by water in the node and other electronic circuits. In addition, presence sensors are placed in each tank to control the possible effects in the fish behavior of the passage of the workers near the tanks. A total of three nodes control the different parameters in each tank. The nodes are wirelessly connected to an Access Point (AP) that sends the data to a server. The data is available on the local area network and on the Internet. The system can send alarm messages to different workers if abnormal situations are detected.

Finally, a system for monitoring the feeding process and adjust the feed supply velocity in fish farms. We present a system that automatically adjusts the amount of dispensed feed. In order to do so, the system detects when feed reaches the drainage system. The feed detection is done using CMOS sensors. From the gathered data by the CMOS sensor, we obtain the histograms. After analyzing them we can find a correlation between the number of pixels with certain brightness value and the presence of a feed. Moreover, the height at which fish are swimming is detected by employing Light dependent resistors (LRD) strips deployed from the top to the bottom of the cage. The fish are detected due to the changes in the incident light in the LDR caused by the fish swimming behavior. The fish, covered by scales acts as mirrors, reflecting the light and some of the flashes insides in the LDRs placed in the tanks. We show the calibration and verification process of both sensors. In additions, we present the results of a simulated feeding process with our proposed system and how the feed supply velocity changes.

Our system allows saving feed during feeding time and ensure that all the fish have time to eat, making aquacultural facilities more economically profitable as well as more sustainable.

The rest of the Chapter is structured as follows. Section 4.2 shows the system for distributing water with different conductivity along the fish farms. A WSN for turbidity and temperature in the tanks is shown in Section 4.3. Section 4.4 presents the design and deploy a low-cost WSN to monitor fish feeding process and water quality in aquaculture tanks. The system for monitoring the feeding process and adjust the feed supply velocity is detailed in Section 4.5. Finally, the conclusion and future work are shown in Section 4.6.

## **4.2. A system to control the salinity and water level in the fish farms facilities**

### **4.2.1. System description**

Our goal is to develop and implement a system that should be able to monitor the salinity changes in an area close to the water pipe and in the tanks. It also should be able to prepare a mix of water to feed the aquaculture facilities by selecting water from two sources (the recirculating water and the freshwater) to obtain the desired salinity in each group of tanks. Other sensors will be installed in the aquaculture facility to take information about salinity level. The system will allow the manager of the aquaculture facility to decide the water salinity values required according to the needs. The proposed WSN is composed of nodes connected wirelessly with different technologies. The nodes that monitor the water input pipes are connected to the gateway with WiFi connection. By the other side, the nodes in the facility are connected by Bluetooth, because this technology consumes less energy than WiFi.

The system has two pipes that permit getting water from different places. A common problem in some facilities is the temporal downgrade of the available water quality (related to meteorological alterations, pollution or underwater discharge) and its harmful effects on the fish. However, by having two pipes this problem is reduced. It is possible to select the water from one of the pipes or mix water from both pipes.

The proposed system also includes the water level sensor. This sensor is used to detect the loss of water in one tank. There are different issues that can cause a loss of water in a tank such as the obstruction of the pipes, leakages and even water evaporation. The decrease of the water level has several problems associated. The most important one is the reduction of the available oxygen for the fishes, which can cause the death of the animals. The reduction of spaces is another problem linked to the decrease of the water level. It can cause dangerous behaviors such as fish attacks and stress. Finally, the loss of water due to the evaporation can increase the salinity level of the remaining water.

#### *4.2.1.1. Salinity Sensor*

In this subsection, the salinity sensor of our system is presented. The salinity sensor employed in our system is based on the salinity sensor developed by us in (Parra et al., 2015a) with some improvements. They include the development of a waterproof encapsulation and the consideration that the water volume used for calibration is lower than the volume of the magnetic field. The sensor is isolated from the environment. As we can see in (Wood et al., 2010), all the attempts to isolate the sensor using epoxy material failed. Then, we developed two new alternatives, the first one is to use a silicone based insulating pain. The second is to use two PVC tubes to contain the coils inside as it is shown in Figure 4.1.

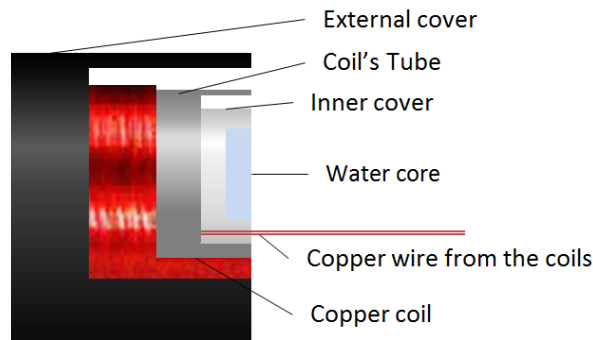


**Figure 4. 1** Design on PVC coverage.

Different coils were used for the isolation test. Due to the experiences are shown in (Wood et al., 2010), we do not use the sensing coil to avoid possible damages, so other prototypes were used. Three different coils were created for this purpose. The coils had 20 spires in powered coil and 40 in the induced coil. The inner diameter of the tube was 1.1 cm and the external diameter was 1.2 cm. The length of the tube with the coils was 4.2cm.

The coil with the waterproof painting was left during 24 hours to dry up before the test. The same period of time was applied to the coil with the PVC protection because some silicon was used. Figure 4.2 shows the different steps to be performed in order to isolate the coils from the water. To make the coil, the first step is to select the support to wind up the copper wire (Figure 4.2 c). After that, we put a new PVC tube that covers both coils. We also cover the top and bottom of the coil in order to avoid any contact with the water. To do so, we use a circular piece of plastic that is glued with thermal silicone (Figure 4.2 -b). Finally, we apply a layer of waterproof paint to seal any pore that may cause water filtration problems (Figure 4.2 -a).

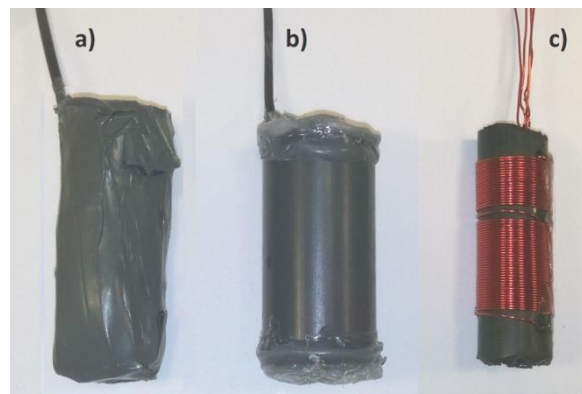


**Figure 4. 2** Sensors with and without isolating cover

In order to evaluate the effects of the waterproof protection on the sensing capacity of the coil, a study is carried out to compare the induced magnetic field. In the case of the coil with waterproof painting the induced magnetic field was almost null. A possible interaction between the varnish and the painting can cause a drastic reduction of the induced magnetic field. The study was done with a saline sample of 43 mS/cm. We took measures from 1000 kHz to 2000 kHz. This data is shown in Table 4.1.

**Table 4. 1** Comparative between isolated prototypes

Freq. (kHz)	Vout (V)	
	PVC Waterproof	No waterproof
2000	2.2	2.4
1800	1.45	1.8
1600	0.78	1.12
1500	0.63	1.01
1400	0.54	0.81
1300	0.43	0.55
1100	0.28	0.39
1000	0.31	0.38

The data are shown in Table 4.1 evidence that the extra PVC tubes for isolating the coil (inner and external cover in Fig. 2) and the air between the covers cause a reduction on the induced magnetic field. This reduction can be expressed as a function of the magnetic field obtained without the PVC tubes. Using the data from Table 4.1 and the Analytical software (Eureqa Software, 2015), we obtain (Eq. 4.1).  $V_{iso}$  represents the output voltage in the isolated coil and  $V_{no\_iso}$  represents the output voltage on the coil without extra PVC tubes. This equation is used to correct the calibration performed in (Parra et al., 2015a) taking into account the attenuation effect of the plastic coverage.

$$V_{iso} (V) = -3.671 - \frac{24.375}{V_{no\_iso}(V) - 6.553} \quad (4.1)$$

Another consideration that must be taken into account is that the generated magnetic field can exceed the volume of the calibration samples. In (Parra et al., 2013b), we calculated the size of the generated magnetic field by the coil. Using the equations of (Parra et al., 2013b) we can correct the obtained output voltage. The loss of the output voltage is 3.2% for that volume of water. This increase must be applied to the calibration in order to use the sensor in the aquaculture environment, where the amount of water is high enough to contain all the magnetic field. The calibration presented in (Parra et al., 2015a) can be corrected considering Eq. 4.1 and the 3.2% of voltage loss, thus it is obtained Eq. 4.2. Eq. 4.2 shows the real correlation between the output voltage, from an isolated coil in Volts, and the water conductivity (mS/cm) in a real scenario.

$$V_{iso}(V) = \frac{\left(-3.671 - \frac{24.375}{0.5084 \times C \left(\frac{mS}{cm}\right)^{0.4004} - 6.553}\right)}{1.032} \quad (4.2)$$

The equation that will be introduced at the server side to calculate the conductivity using the value of output voltage of the sensor is Eq. 4.3:

$$C \left(\frac{mS}{cm}\right) = \sqrt[0.4004]{22.7108 - \frac{24.375}{0.524 \times V_{iso}(V) + 1.867}} \quad (4.3)$$

#### 4.2.1.2. Wireless module

In this subsection, the used wireless module is described. Our smart system for monitoring several parameters in aquaculture tanks is based on a wireless module named FlyPort manufactured by openPICUS. The openPICUS Flyport module can be powered by batteries (between 3.3 and 5V). The module is composed of a Certified WiFi Transceiver 802.11g Microchip MRF24WG0MB module. It also contains a 16 bits low power microcontroller. In this case, our module uses a Microchip PIC24FJ256 Processor, with 256K Flash, 16K Ram and able to execute 16MIPS at 32 Mhz.

In comparison with some other existing wireless modules, the openPICUS FlyPort is characterized by its versatility in programming and wide application range mainly focused on the Internet of Things (IoT). The node consists of two parts, i.e., the WiFi module which contains the transceiver, the processor, the different input/output, buses, etc., and the programmer board named USB Nest.

#### 4.2.1.3. Sensor to measure the water level

The water level sensor proposed for the system is shown in this subsection. GP2Y0A02YK0F (See Figure 4.3) is a distance measuring sensor unit manufactured by SHARP. It is composed of an integrated combination of a position sensitive detector, an infrared emitting diode and a signal processing circuit. According to its features, the reflectivity of the object, the environmental temperature, and the operating duration are not influenced by the distance detection because this device uses the triangulation method. It is able to measure from 20 to 150 cm. It offers an analog output, where the voltage is related to the detected distance.

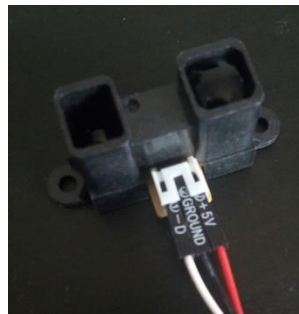


**Figure 4. 3** Distance measuring sensor unit

This sensor is used to detect the water level in fish tanks (See Figure 4.4). It is placed at 20 cm over the water. We have established two thresholds, i.e., the highest level (which corresponds to the regular level) and the lowest level (which corresponds to the critical level). Our fish tanks are continuously monitored in order to ensure that the water maintains the correct water level.

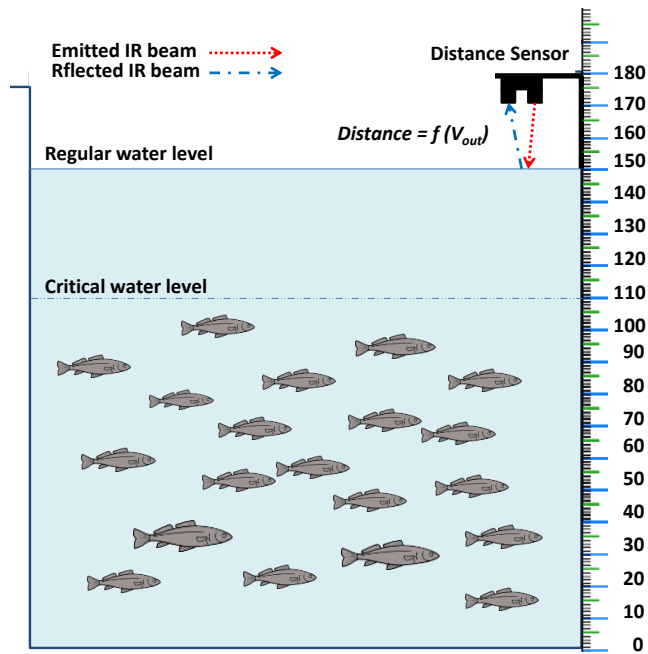


**Figure 4. 4** Distance sensor position in fish tanks.

Finally, to understand and model the behavior of this sensor, we have checked the value of the output voltage as a function of the object distance. Figure 4.5 shows the results, which is very easy to be modeled by an equation. Eq. 4.4 models the behavior given in Fig. 6 with  $R^2 = 0.9528$ .

$$V_{out} (V) = -0.0265 \times \text{Distance}(\text{cm}) + 2.685 \quad (4.4)$$

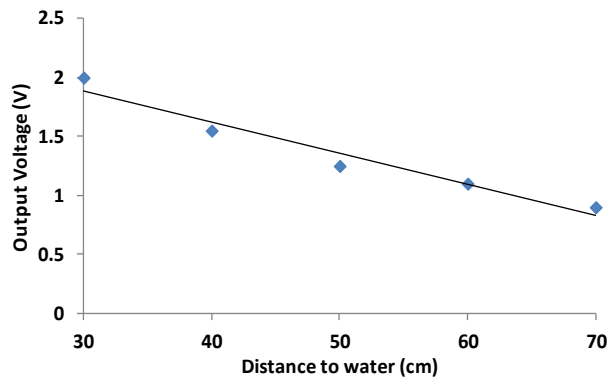


**Figure 4. 5** Distance to water vs. output voltage.

#### 4.2.1.4. Signal generation

The signal generation to feed the salinity sensor is exposed in this subsection. As we explained before, the salinity sensor is composed of two coils; one of them is fed by a signal that records continuous polarity changes. It can be done via square or sine waves. In this case, we have selected square signals, due to their simplicity and less need for electronic components. The other coil is induced by the magnetic field which is affected by the salinity.

In order to generate the square signal, we use the same module. The sensor node generates a



PWM signal. In our case, the duty cycle of the square signal is fixed. In order to implement it, the code shown in Algorithm shown in Figure 4.6 has been used. This code allows to generate the square signal and to gather data from the induced coil. Figure 4.7 shows the different stages of our proposed system. The Flyport generates a square wave to feed the first coil, which is placed in the water medium with the second coil. The second coil receives an induced sine wave, which is received by the Flyport as an input measure (sensed value).

Figure 4.8 shows the square signal generated by the Flyport using the code of Algorithm 1. It is a square signal at 110.30 kHz.

Figure 4.9 shows the sine wave obtained at the output of induced coil overlapped with the generated square signal. We can observe that the received signal has a sinus behavior and the amplitude is slightly smaller than the square signal.

```
#include "taskFlyport.h"

void FlyportTask (){
    const int maxcycle = 65; //here we set max % of brightness
    PWMInit(1,110000,100); //Initialize PWM1 to work at 110 KHz
    PWMOn(p4, 1); //Assign OUT1 as PWM1 and turns it on
    while(1)
    {
        PWMDuty(maxcycle, 1); // Define the duty cycle of square
                               // signal and start signal generator

        myADCValue = ADCVal(1); //Read values from induced coil
        myADCValue = (myADCValue *2.048)/1024; //Convert to
                                               //Voltage value
    }
}
```

**Figure 4. 6** Program code for Flyport to create a square signal.

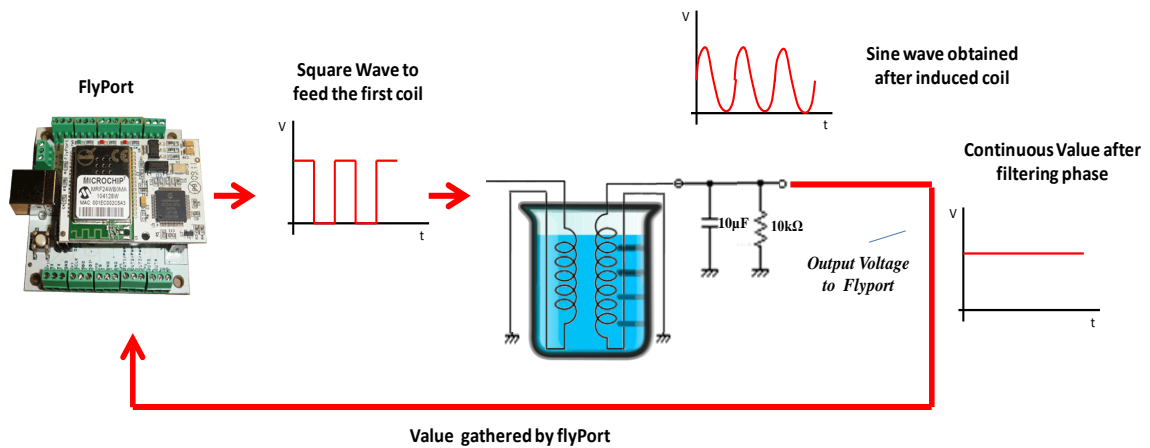


**Figure 4. 7** Stages of our proposed system

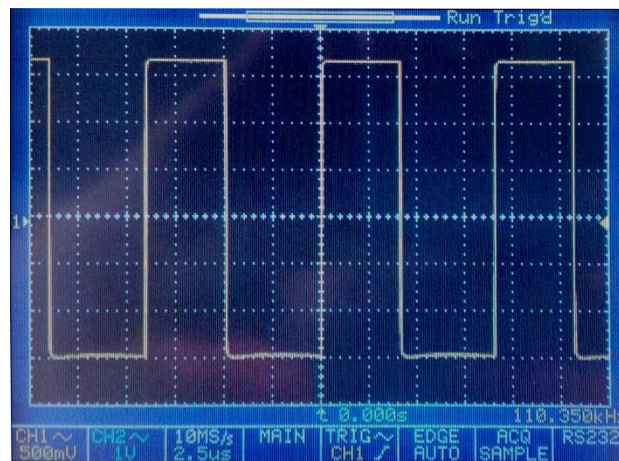


**Figure 4. 8** Square signal generated by the Flyport.

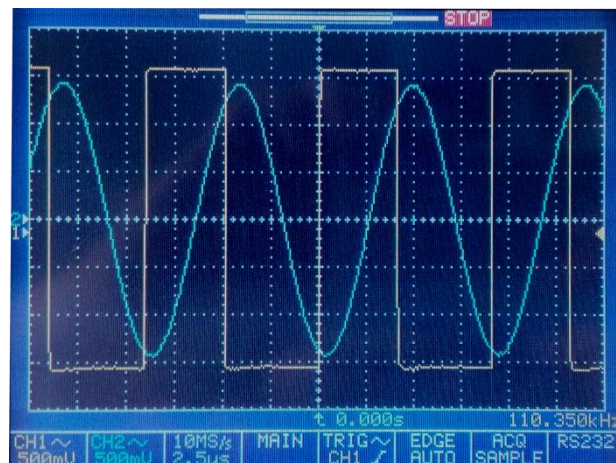


**Figure 4. 9** Sine wave obtained at the output of induced coil overlapped with the generated square signal.

#### *4.2.1.5. Server implementation collect data*

With the goal of gathering and storing data, we have developed a software application that is installed as a service in a server, which requests the node this information and stores it in order to process and make decisions. The application is developed in Java. The information gathered from the sensors is stored in a DB. To implement this, we have selected the connection of devices using sockets. The used of TCP sockets is a widely used and simple method to exchange information. TCP sockets provide a connection-oriented service where data is transferred as a continuous stream. This implies that before transmitting information, a connection must be established between the two devices. In this case, while one of the sockets handles connection requests (server), the other requests the connection (client). After establishing the connection, the server should request data to the client. When the client finishes the data sending, the client sends a Disconnection request packet to the server. After that, the server confirms the disconnection and the server remain in a listening mode while waiting for a new connection. Figure 4.10 shows the packet exchange during a connection.

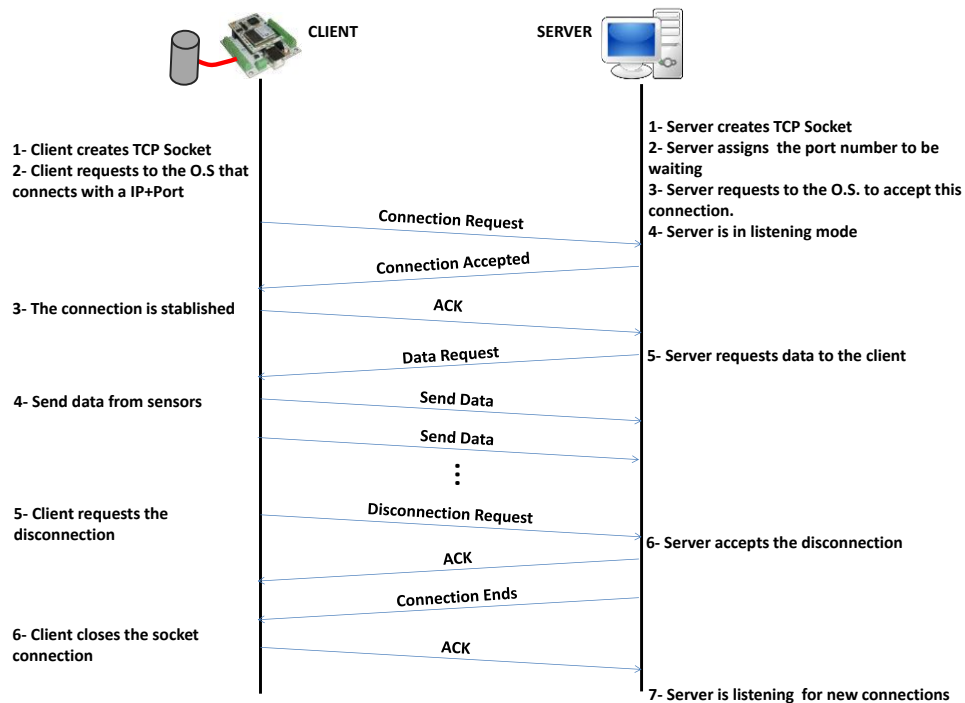


**Figure 4. 10** TPC Socket connection process and packet exchange between server and client.

During the process of server configuration, the user should specify the number of sensors that will provide data and the port number through which the connection establishment and data exchange will be performed. Because the server is implemented using a computer, the application allows to the user choosing the path where the data is going to be saved in a \*.csv file. If an additional module is connected to the server, it automatically generates a new file for storing the data provided by this module. Additionally, we need to supply a specific programming for the Flyport module. The program code used in the Flyport module is shown is Algorithm 2, see Figure 4.11. As we can see, the main aim of this algorithm is generating the needed configurations to create a TCP socket but as the role of client. When a node requests for a new connection to the server, it waits to the server reply. When both devices are connected, the server request the data to the node and then the node send the data through the port 8080.

```

void FlyportTask () {
    TCP_SOCKET sock = INVALID_SOCKET;
    int cnt =0;
    BOOL flagErr = FALSE;
    // Establishment of a wi-fi connection
    WFConnect(WF_DEFAULT);
    while(WFGetStat() != CONNECTED);
    while(!DHCPAssigned);
    vTaskDelay(25);
    UARTWrite(1,"Flyport Wi-fi G connected...hello world!\r\n");
    //Creating the TCP socket connection between clien and server
    sock = TCPClientOpen("192.168.2.3","8080");
    char name[]="Sensor name\r\n"; //Choose a sensor name
    int delay=1000;
    //Selection and configuration or analog inputs

```

```

BOOL analog1 = TRUE;
int adcValue1 = 0;
char uart_msg1 [30];
while(!TCPisConn (sock)) { //Timeout function
if (cnt == 10) {
flagErr = TRUE;
break;
}
vTaskDelay(50);
cnt++;
}
if (flagErr){
UARTWrite (1, "\r\n Error of Timeout\r\n");
}else{
    TCPPutString (sock, name); // sending the sensor name
    while (TCPisConn (sock)) {
if (analog1) {
adcValue1 = ADCVal (1); //write value from ADC 1
sprintf(uart_msg1, "%d\r\n", adcValue1);
TCPPutString (sock, uart_msg1);
UARTWrite (1, uart_msg1); //write value of ADC 1 on the UART port
}
DelayMs(delay); // 1000 msec.= 1 sec
}}}

```

**Figure 4. 11** Program code for Flyport configuration as Socket Client.

#### **4.2.2. Autonomous System to Control Automatically the water Salinity**

One of the biggest problems when working in aquaculture facilities on land (closed-circuits facilities) is the water evaporation from the fish tanks due to the effect of the sun. This would generate the rise in salinity level that could affect the proper development of the fishes. Another major problem is the loss of water due to an accidental leakage. In this section, we explain the architecture developed and the algorithm needed to control the water levels and salinity concentration in the fish tanks.

The control system is shown in Figure 4.12. The water can be taken from both sources. This water is propelled towards the intermediate tanks, where strange elements and other fish that enter through the pipe should be removed. This intermediate step can be used to perform other analyzes. Then, the water is brought to the mixers which are responsible for making mixtures of water in the correct proportions.

After this, the water is driven by each group of tanks that should maintain the same salinity level. In order to propel the water between the mixer and fish tanks, water pumps are used. Water valves are used to control the access of water to the fish tanks. These elements, as well as the salinity and level sensors, are connected and controlled by wireless nodes that receive the control signals required to take the appropriate actions.

This system is adaptable to any type of installation, e.g. open-circuit facilities where water continuously circulates from the sea and other water sources into the tanks of fish and the excess of water are discarded. There are also closed-circuit installations where a fixed volume of water is forced to circulate between the tanks without taking water from external sources.

In order to manage the salinity levels, we have designed an algorithm for the proposed system that allows us to automate the process. Figure 4.13 shows the algorithm used by the

system to have the appropriate salinity level in the tanks. Initially, the system periodically checks the water level in the tanks using the level sensors (TL). If the water level is normal, the system will check the salinity value of each group of tanks using the salinity sensors (SL). If this value is within the established thresholds, the system will send a message to the controller reporting that the situation is correct. This allows us to keep a history of the recorded values. However, if the system detects that the salinity level is not correct (even though the water level is correct), the system will start to drain some water from the affected tank and the controller will receive an alarm message about the status of the installation. Then, the amount of water needed is calculated. The next step will be to measure the salinity values of the sources from which water will be taken. With these values, it is possible to calculate the volume of water that must be taken from each source, so that the water that leaves the mixer is correct to be sent to the fish tanks. This operation will remain active until the tank reaches the correct water level. Finally, the control system will receive a message about the state of the facilities.

After performing this operation, if the salinity value remains outside the thresholds, this task is repeated as many times as needed to achieve the correct salinity values. Such problems often occur in closed-circuit installations where sometimes water evaporation plays an important role in the proper fish production. Finally, if the system detects a loss of water levels, the same process will be repeated, but considering that the registration problem is not related to an increase/decrease of the water salinity.

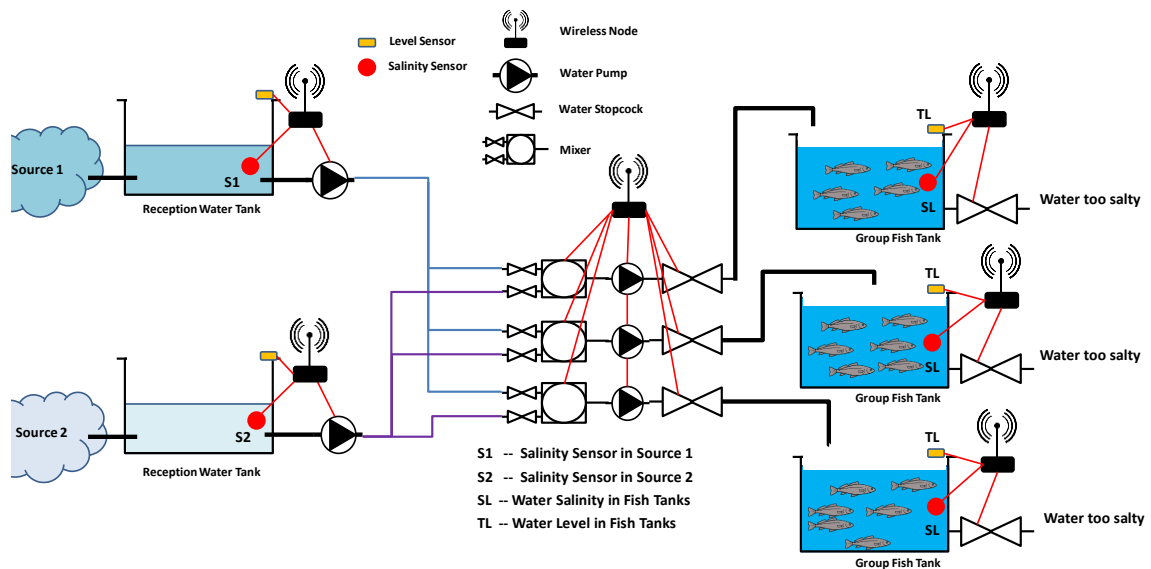


Figure 4. 12 Architecture and sensors distribution.

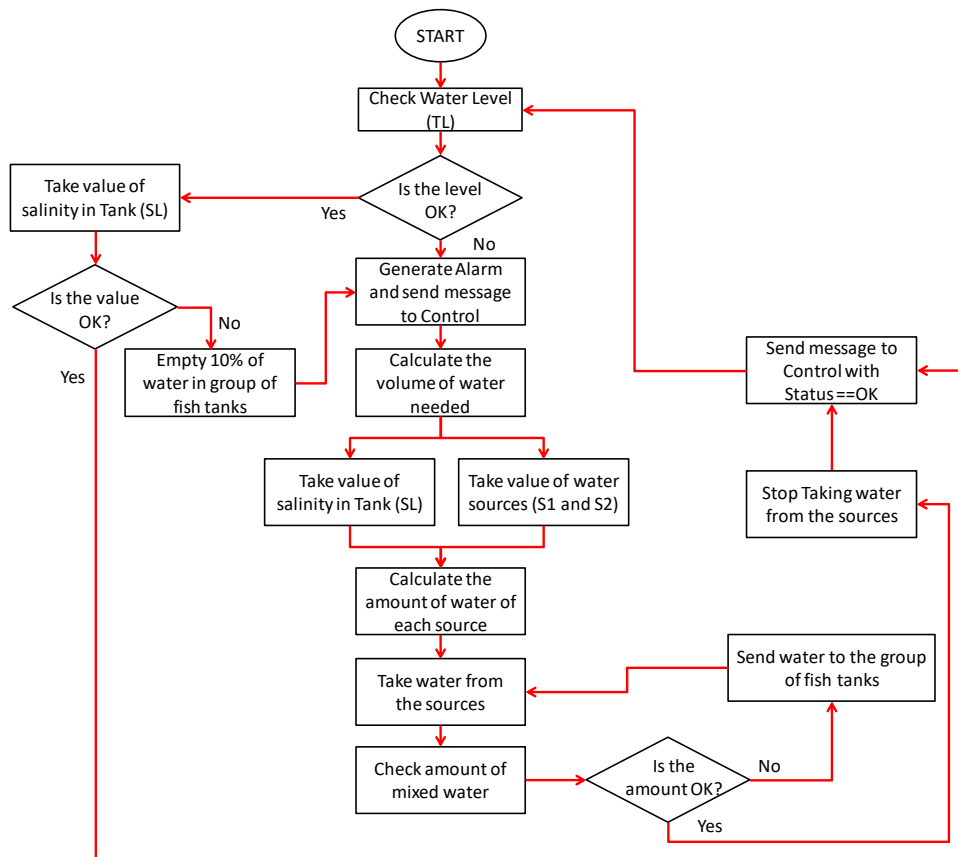
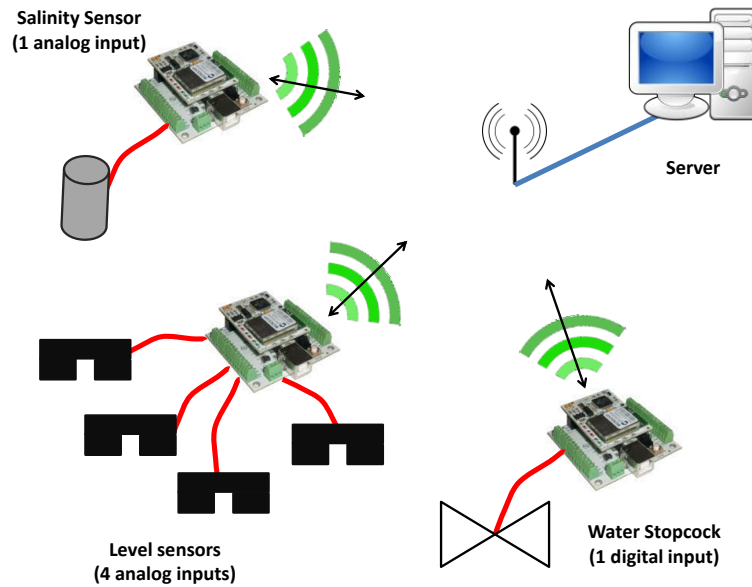


Figure 4. 13 Flow diagram to control the system

### 4.2.3. Real Measurements and network test

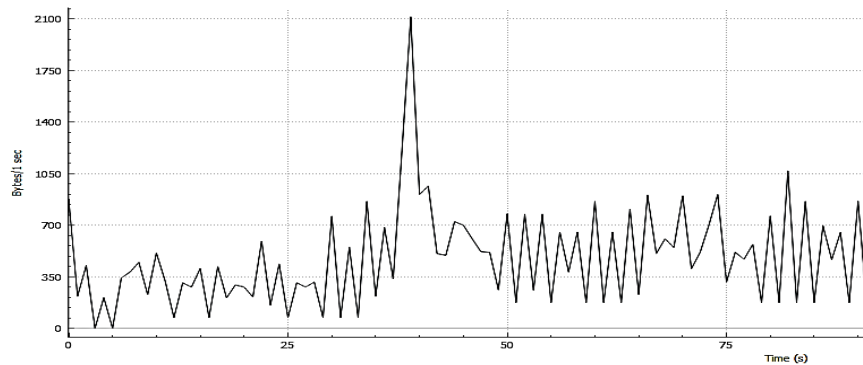
Finally, in order to ensure that our system is able to work properly, we need to check the network performance as well as the response time of the nodes in order to know if the system does not consume too much bandwidth and if it will receive the data with little delay between messages. This section shows the results of the tests about the consumed bandwidth and the delay between received data messages, i.e., the time between TCP packets delivering data from the sensors. It is measured at the server side.

Figure 4.14 shows the scenario used in our tests. In this case, we have tested the consumed bandwidth as a function of the kind of device sending the data and the nature of this input. The test is composed of a server, which is in charge of requesting data and collecting them, and 3 different nodes, i.e., a node that takes measures from a salinity sensor which generates analog data, a node that collect data from 4 level sensors which generates analog data and a node that registers the water stopcock status. In this last case, we only check if the water stopcock is open or not through a digital input.



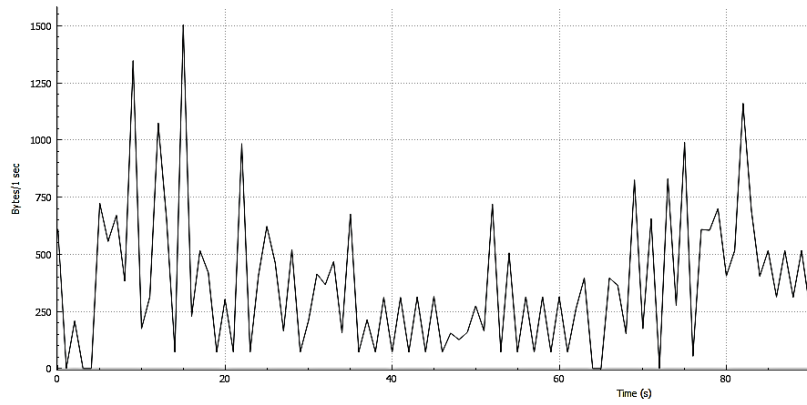
**Figure 4. 14** Scenario used during our test bench.

In order to test each node separately, we only transmitted data with one node each time. Figure 4.15 shows the consumed bandwidth by a node when sending data from 4 level sensors. Data of these sensors are gathered by the analog inputs. As we can see, the average consumed bandwidth is about 400 Bytes/s. There is a peak about 2100 Bytes/s which could correspond to a retransmission of some lost packets. The consumed bandwidth is quite regular.



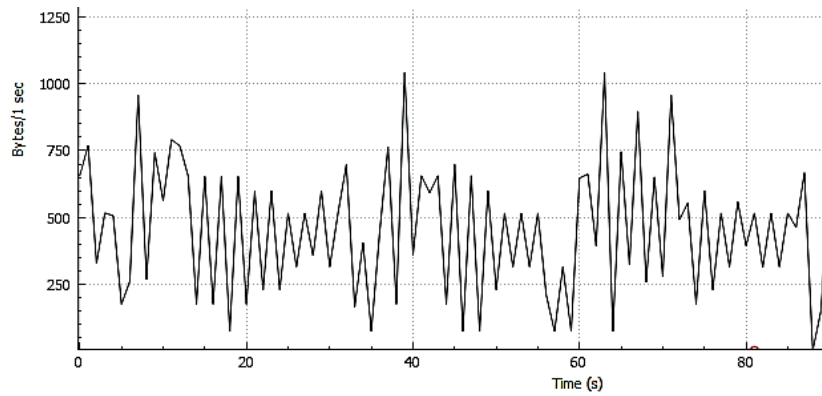
**Figure 4. 15** Consumed bandwidth by a node when sending data from 4 level sensors.

Figure 4.16 shows the consumed bandwidth by a node when sending data from a salinity sensor. Data of this sensor are gathered by the analog input. In this case, the consumed bandwidth is quite variable. We can observe time periods with an average bandwidth of 600 Bytes/s (at the beginning of the test) and other where the average bandwidth is about 210 Bytes/s. We have also observed some peaks higher than 800 Bytes/s.



**Figure 4. 16** Consumed bandwidth by a node when sending data from one salinity sensor

Following, Figure 4.17 shows the consumed bandwidth by a node when taking data from a water stopcock. Data of this sensor is captured through a digital input. In this case, we only take measurements about its status, i.e., if it is open or closed. The behavior, in this case, is quite stable with an average bandwidth of about 400 Bytes/s. There are some few peaks higher than 800 Bytes/s.



**Figure 4. 17** Consumed bandwidth by a node when sending data from the level sensor.

Finally, Figure 4.18 shows the delay between TCP messages delivering data from the sensors with the gathered measurements and their status. During the tests, 92 pairs of TCP streams are sent. We can observe that in all cases, the delay from the previous message to the next one seems to follow a periodical behavior. Additionally, the salinity sensor presents higher peaks with values around 1.2 seconds.



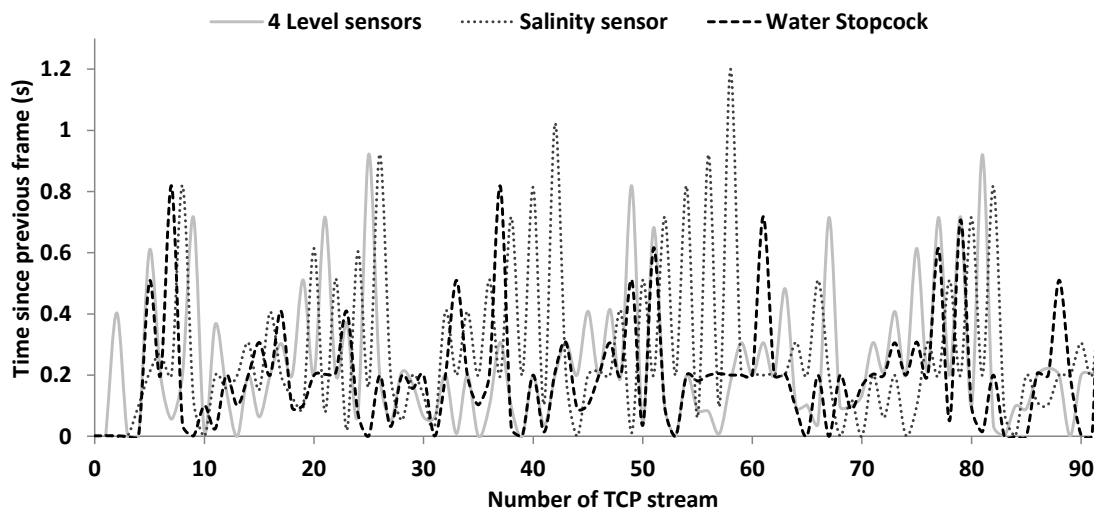


Figure 4. 18 Delay between TCP streams.

Finally, Figure 4.19 shows the histogram to count the number of messages as a function of the delay between TCP streams.

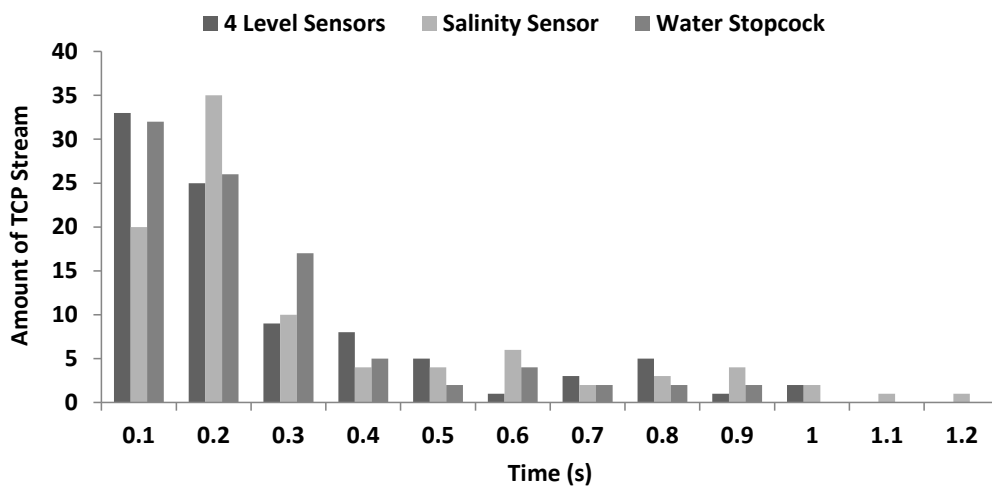


Figure 4. 19 Histogram of the delay between TCP messages.

It is easy to see that the largest number of packets presented a delay between TCP messages smaller than 0.3 seconds. While level sensors and water stopcock concentrate the many packets in times lower than 0.1 ms, salinity sensor have more amount of packets at 0.2 ms.

From these results, we can conclude that our system could be used as a good monitoring system with little delay between the received data.

### 4.3. WSN for monitoring the turbidity in fish farms

#### 4.3.1. System description

In this section, the WSN proposal is presented. First, the development of the employed turbidity sensor is shown. Then, the deployment and some real time measures are detailed. The details of the node used in the WSN are shown. Finally, the architecture is presented.

#### 4.3.1.1. Turbidity sensor development

In this section, the development of the optical sensor employed for turbidity monitoring is presented. To create this sensor, an infrared (IR) light emitter and detector have been used. The sensor is based on the design presented by Sendra et al. (2013b). As a light emitter, an IR LED with peak wavelength of 850nm is selected. As a detector, an IR photodiode with a sensitivity range from 790 to 1050nm is used. The IR LED is placed at 180° from the IR photodiode. The emitter and the receiver are separated by 6.5 cm. From those 6.5cm, 2.7cm are occupied by the water.

In order to calibrate the sensor, different turbidity samples composed of water and sediment are used. The sediment is formed by silt. The reason to use silt is that usually in fish farms the coarse materials and sands are stopped. Only the fine sediments can arrive at the cages. For the calibration of the sensor, 5 different turbidity samples are generated. The sample with less turbidity contains 0mg/L of silt. On the other hand, the sample with the highest turbidity contains 378.55 mg/L. All the samples were homogenized before to perform the measures. The results of the calibration process can be seen in Figure 4.20. The mathematical model that related the response of the photodiode (MΩ) with the turbidity (mg/L) is shown in Eq. (4.5). It presents a correlation coefficient of 0.99918159 and a mean absolute error of 3.8651793. In the equation (1): Turb. represents the turbidity and IR makes reference to the response of the IR photodiode. After the calibration, a verification process is carried out. For this verification process, two new samples were generated and measured. Then, the Eq. (4.5) is applied to evaluate the goodness of the mathematical model. The Eq. (4.6) shows the relation between turbidity and the received signal in volts in the Flyport after using the conditioning circuit. The objective of this conditioning circuit is to ensure that the receiver signal in volts is lower than 2V a voltage divisor is used with a secondary resistance of 2.5 MΩ. The input voltage employed has 4.5V. The resultant output voltage or signal is between 1.24V and 1.65V.

In Table 4.2, the results of the verification process are presented. The maximum absolute error is 4.76 mg/L and the highest relative error is 4.37(%). The verification process shows that the calibration has been performed correctly.

$$Turb. \left( \frac{mg}{L} \right) = 377.36 + \frac{81.14}{IR (M\Omega) - 3.90} - 46.66 * IR (M\Omega) \quad (4.5)$$

$$Turb. \left( \frac{mg}{L} \right) = 2.46 \times e^{3.22 \times Signal (V)} - 136 \quad (4.6)$$

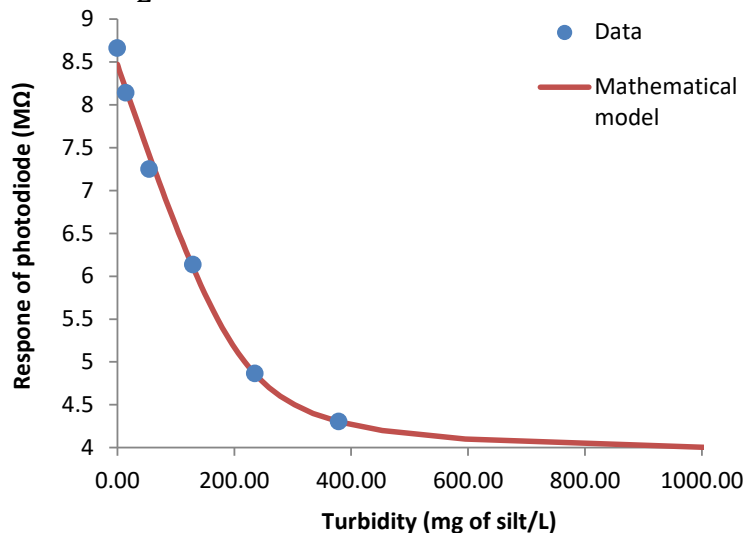


Figure 4. 20 Calibration of the optical IR sensors

**Table 4. 2** Verification of the calibration process

Real Turbidity (mg/L)	Response of IR photodiode (MΩ)	Calculated turbidity (mg/L)	Absolute Error (mg/L)	Relative Error (%)
108.86	6.36	113.618032	4.76	4.37352042
373.14	4.32	369.784656	-3.36	-0.89997734

#### 4.3.1.2. Employed Node

Next, the node employed in our WSN is presented. The chosen node is the Flyport module (Flyport features, 2016) with the USB Nest (see Figure 4.21). It is based on the openPicus platform with open code.

The node includes a 16 Bits processor, the PIC24FJ256, with 256K of flash and 16K de RAM. It supports the wireless connectivity of standards 802.11 b/g/n. The size of this node is 35x48x7 mm and a weight of 11g. It can be powered at 5 or at 3.3V. The node can be seen in Figure 4.21. The main reason to select this module is its flexibility with its several inputs and outputs. The option to use analogic or digital inputs is also suitable for our purposes. Finally, the possibility of programming it for different applications is crucial.



**Figure 4. 21** Flyport module

#### 4.3.1.3. WSN deployment

In this section, the sensor deployment is described. First, the isolation of the sensor and the node are shown. Then, the location of the sensors in the box is detailed. Finally, the distribution of nodes along the fish farm is explained.

Considering that our objective is to monitor the water turbidity will be needed to locate the sensors in the water. Thus, it is necessary to ensure the sealing of the receptacle where the sensors and the Flyport will be placed. The maximum depth where the sensors must be located is lower than 1 m, O-rings will be used to ensure the sealing. A sealed box made of thermoplastic is used for this purpose. The size of the box is 17,5x11,5x7cm. The closure of the box has been modified and tested to ensure the sealing at 1.5m depth in an aquaculture tank. Before to perfume the test, two holes have been done in the box to allow introducing a crystal pipe. The pipe has a diameter of 2.7 cm. It will permit to take the turbidity measures by allowing the water pass along the box. To seal the gasket between the tube and the box a special silicone has been used.

Three sensors have been placed in the sealed box. First, the turbidity sensor is located next to the crystal pipe. The second employed sensor is the temperature sensor. It is based on a Zener diode with 2 terminals. The sensor is already calibrated with an error of 1°C. The temperature sensor is located ensuring the contact with the crystal pipe. This location has been selected because the crystal is better temperature conductor than the plastic. The main reason to use this sensor is due to the temperature is a crucial parameter for fish bioenergetics

performance. The last employed sensor is a humidity sensor. This sensor is located at the bottom of the box. The function of the humidity sensor is an early detection system. The system will detect an increase of humidity in the box in order to prevent water damages caused by water. To power the sensors a 9V battery is employed. To power the Flyport a 5V external battery is used.

The nodes are located in different points of the fish farm, in the production tanks and in the reception tank. In the production tanks, one node is located in the middle of the tank, next to the wall. In the reception tank, two nodes will be located one at the water entrance and the other at the water exit.

#### 4.3.1.4. Architecture

In this section, the topology and operation system of our proposal are shown. The employed topology for our proposal is based on an extended star. The Flyport devices are connected to an access point (AP) by a WiFi connection. The AP is connected to a Switch by Ethernet connection that is connected to a Router to have internet access. The network topology is shown in Figure 4.22. There are two AP where the Flyports are connected and another AP where the other devices are connected. These devices include computers, smartphones, and a server. The server collects all the information gathered by the sensors. The rest of devices can access the server to visualize the data. The information can be accessed in local mode or in remote mode.

The physical topology is conditioned by the fish farm structure. In this section, we use the structure of the majority of the fish farms without recirculation system (See Figure 4.23). Those infrastructures have a big reception tank, which is generally placed on a higher floor than the production tanks. Moreover, there are one or more rooms on both floors designated to offices. The normal conditions in the tanks zone include high humidity and a huge amount of water flowing. In some facilities, they employ saline water. Those conditions favor the corrosion. For this reason, it is important to minimize the network devices included in this zone. Thus, the Switch and the Router are placed in the offices. In the tanks zone, only the AP needed are placed.

At the water entrance and exit of each tank, there are valves that can turn on and turn off the water. Our proposal is to monitor the levels of turbidity in the water of the reception and the production tanks. If an increase of the turbidity is detected in the reception tank is possible to isolate some of the tanks. Not all the tanks have the same fish and not all the fish have the same needs. By the other side, if the humidity sensor gives a lecture higher than 50% will action a system to prevent further damages in this node.

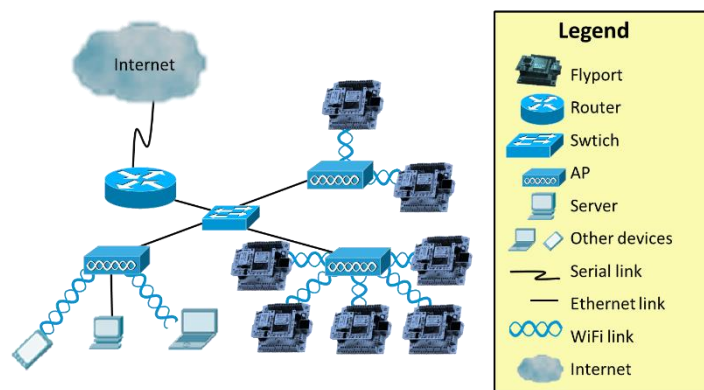
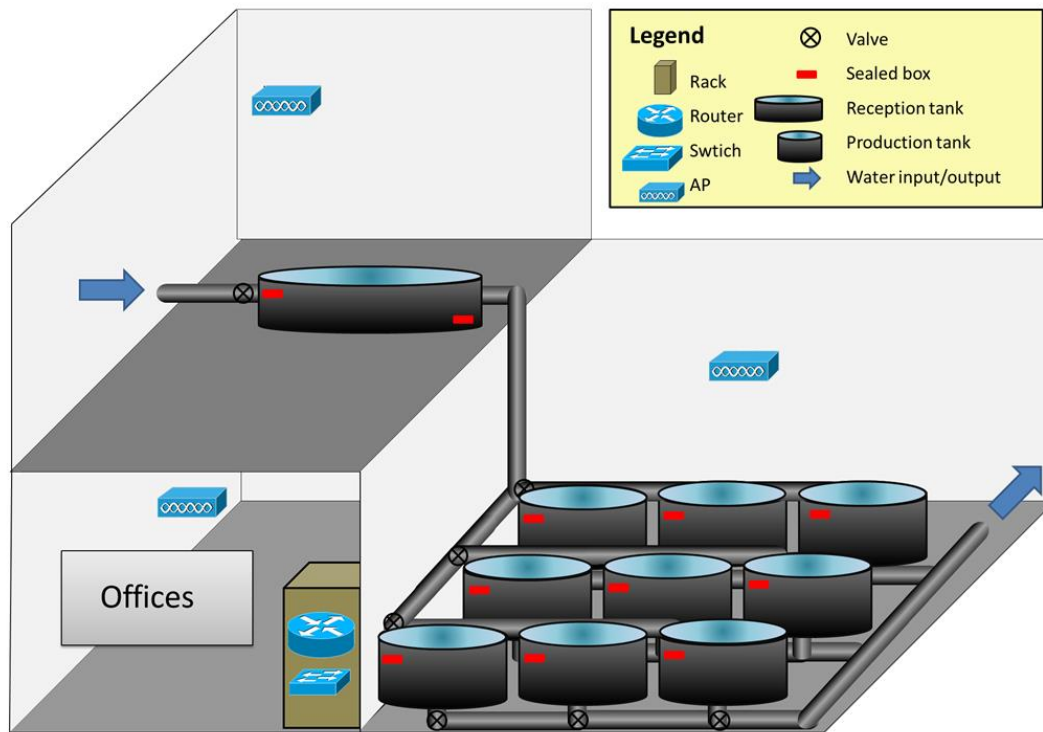


Figure 4. 22 Network topology



**Figure 4.23** Physical topology adapted to the fish farm facility structure

Finally, the algorithm that regulates the operation of the proposed system is detailed (See Figure 4.24). Initially, the tank rows ( $TW_i$ ) are defined as Row 1 ( $TW_1$ ), Row 2 ( $TW_2$ ) and Row 3 ( $TW_3$ ). Each row has each own water quality requirements attending to the fish type that is in each tank row.

Once the Flyport receives the sensor signal identify each signal as Turbidity, Humidity or Temperature according to the analog input. After that, those signals are converted into digital values and transmitted to the server and to the users over HTTP. Only the values of Turbidity and Temperature are transmitted. The data of Humidity is only used as a security mechanism to prevent physical damages in the Flyport.

If this value exceeds an established threshold (50% of relative humidity), a process is triggered. This process will send an alarm to the maintenance workers and will initiate an emergency shutdown in order to avoid electronic damages. In the alarm message, it is indicated the number of the tank where the alarm is generated and a worker will change the sealed box with all the components for a new one. The old sealed box is taken to maintenance to check if there are damages or not and to reboot the system.

By the other side, if the level of Turbidity exceeds the established thresholds of water quality the system will proceed to stop the water flux to some of the tanks. Previously, the person in charge of the production has established the thresholds according to the fish species and stage of development that are being kept in the tanks. Thus, he will establish a threshold to each tank row. At the moment that a row of tanks is isolated from the water flux, a timer will be turned on. This timer will record the time that the tank row has been isolated. This information will be used by the person in charge of the production to restart the water flux even that the water quality remains lower in order to avoid low oxygen concentration in the tanks. Likewise, the alarm that a row has been isolated will be sent also to the workers. The workers must pay special attention to those tanks.

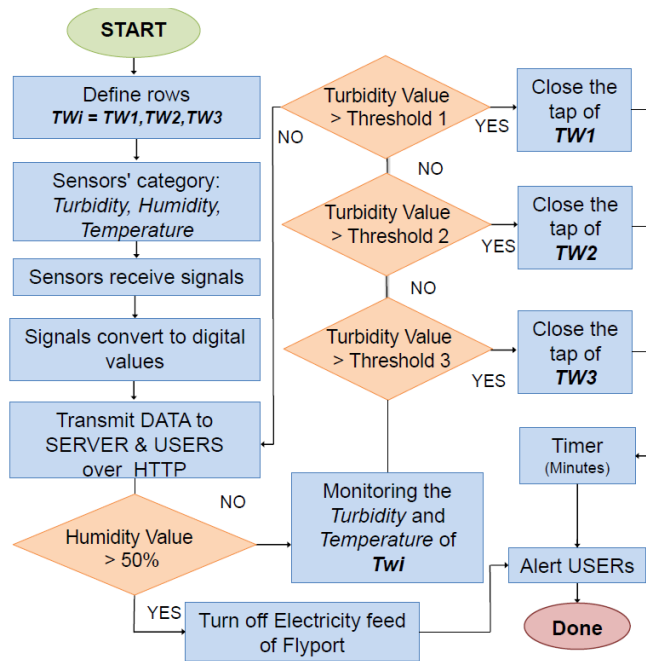


Figure 4. 24 System operation

#### 4.3.2. WSN Performance

In this section, the performance of the WSN is analyzed. Our main objective is to ensure the network performance, obtaining low packet loss rate. However, we also need to minimize the number of AP deployed in the tanks zone. For that, we develop several tests connecting a different number of Flyports to an AP. The network performance will be evaluated next.

The studied network parameters included the transfer packets per second, the rate of packets loss and the retransmitted packets per transmission. Different scenarios have been studied with a different number of wireless nodes connected to an AP. In the scenarios, various wireless nodes will be used which enumerate from 1 Flyport to 10 Flyports connected to the same AP. First, is analyzed the results of the packets per second transmitted in the different scenarios (See Figure 4.25). It is possible to see how as the number of nodes increase the number of packets per second received in the AP increase. The average of packets has been transferred per second throughout the AP with connected 3, 5 and 10 Flyports in a period of the 60s is 70.33, 86.47 and 95.42 pps respectively.

The standard deviation for 3, 5 y 10 wireless nodes is 6.28, 4.55 y 3.43. The results demonstrate that how a number of few connected Flyports use less throughput of packet transmission with high fluctuations.

As shown in Figure 4.25, to have more information about those fluctuations the maximum and minimum amount of packets per second are determined. With 3 Flyports connected the maximum rate is 80 pps and the minimum is 60 pps. For the configurations with 5 and 10 Flyports, the values are 80 and 95 pps for 5 Flyports and 90 and 100 pps for 10 Flyports.

Next, the packet loss rate during 60 sec. is analyzed. In this test, several experiments have been used, from 1 Flyport per AP to 10 Flyports per AP. The results can be seen in Figure 4.26. We can observe that less than two Flyports no packets have been lost in the transmission period. Between 3 to 7 Flyports, less than 1% of the packets are lost. Nevertheless, with more than 8 Flyports per AP the packet loss rate rockets, reaching the 3.5% with 10 Flyports.

As the Flyports supports TCP, it is capable of retransmitting the lost packets. The information related to the retransmitted packets can be seen in Figure 4.27. It is shown the retransmitted packets at intervals of 10 sec. when there are 3, 5 or 10 Flyports connected to the AP. We can see that with 3 Flyport, only in 2 intervals is needed to retransmit packets. In both

cases, 1 packet was retransmitted. For 5 Flyports, in 4 of the intervals packets were retransmitted, the amount of retransmitted packets goes from 1 to 3. In the scenario with 10 Flyports, during 4 intervals retransmitted packets were detected. The maximum number of retransmitted packets was 5. As higher is the number of packets higher retransmission is needed and higher is its variability. In global terms, the scenery with 3 Flyports present 2 retransmitted packets, the number increases to 7 and 14 for 5 Flyports and 10 Flyports respectively.

The best option to minimize the number of AP without losing network performance is to select 5 Flyports per AP.

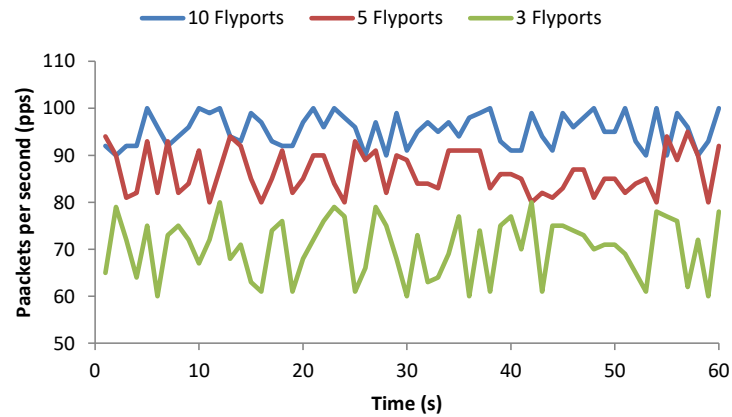


Figure 4. 25 Packets per second in different scenarios

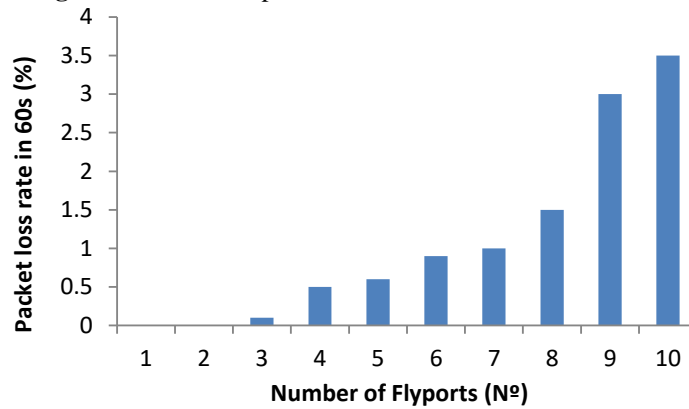


Figure 4. 26 Packet loss rate in different scenarios

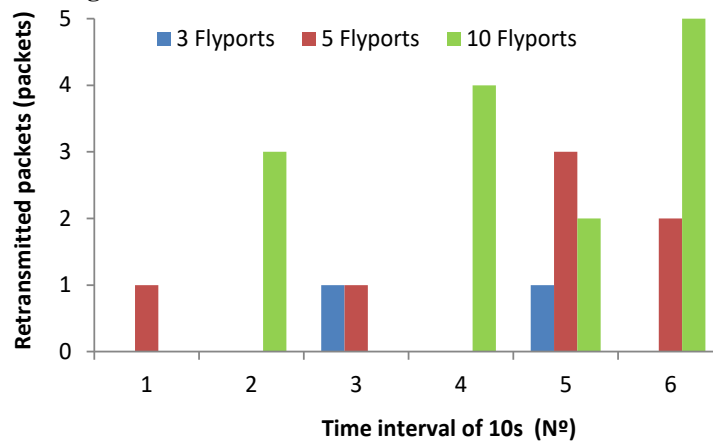


Figure 4. 27 Number of retransmitted packets in different scenarios

Finally, we show the appearance of the different visualization systems. First, in Figure 4.28 we can see the aspect of the data shown in the server after select one node. In the main window of a node that belongs to the reception tank, the server presents the data of the last 60 minutes from turbidity and temperature. In the graphic of turbidity, it is possible to see the currently established thresholds in different colors. In the bottom, we can see if there is an alarm due to turbidity values and the duration of each alarm. From this window, it is possible to select another node to see its data. When the selected node belongs to a production tank the appearance of the window is shown in Figure 4.29. In the upper part, it is possible to see the graphics of temperature and turbidity with the threshold of the selected tank. At the bottom is presented the alarms generated in the last 60 minutes in this tank. Moreover, we can see the timer of the alarms in the last 60 seconds and the timer of the accumulated alarms in this tank in the last 24 hours. The Figure 4.30 presents the information received in a smartphone from two different alarms. On the left is shown the information of one alarm triggered by humidity. The information includes the type of affected tank (production or reception) and the number of the tanks. In the case of a production tank, the alarm will show the number of the tank. In the case of reception tank, the alarm will show if it is the node at the entrance or at the exit of the tank. Moreover, a figure with the exact location of the node is presented. At the right is shown the information of a turbidity alarm. It contains the information of the affected row (Row 1, Row 2 or Row 3). Furthermore, it contains information about the timer or this alarm.

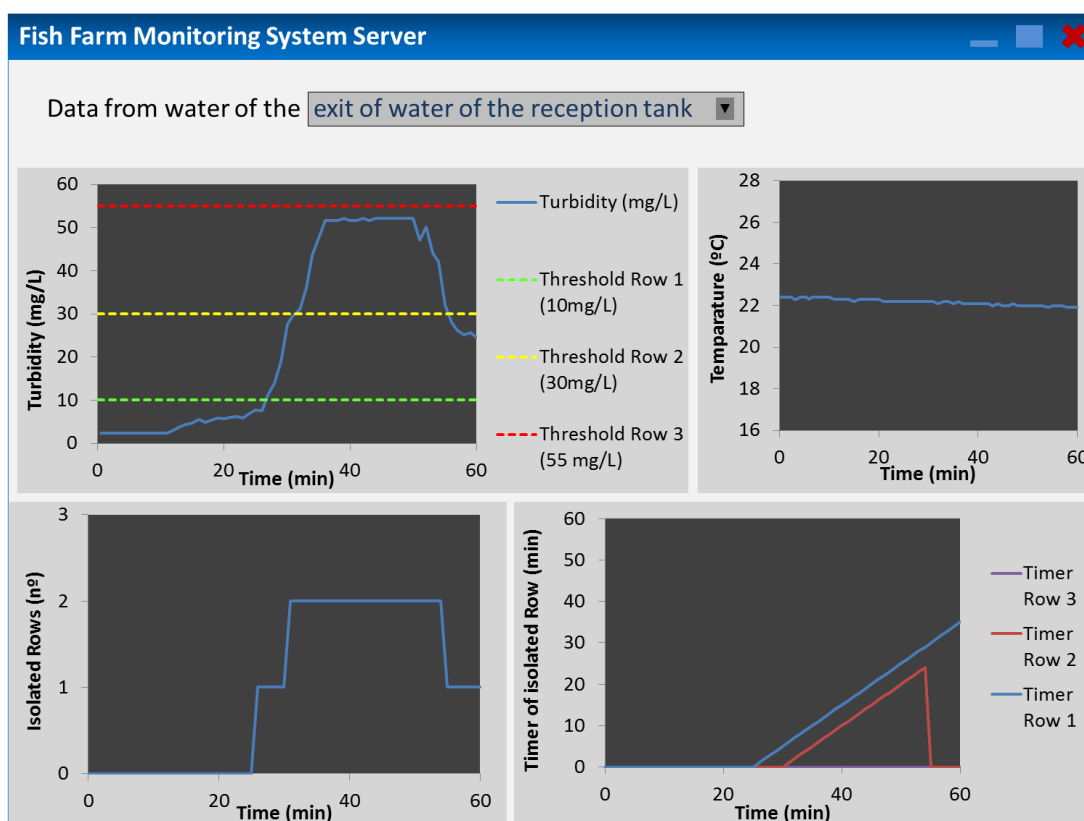


Figure 4. 28 Server appearance showing reception tank information



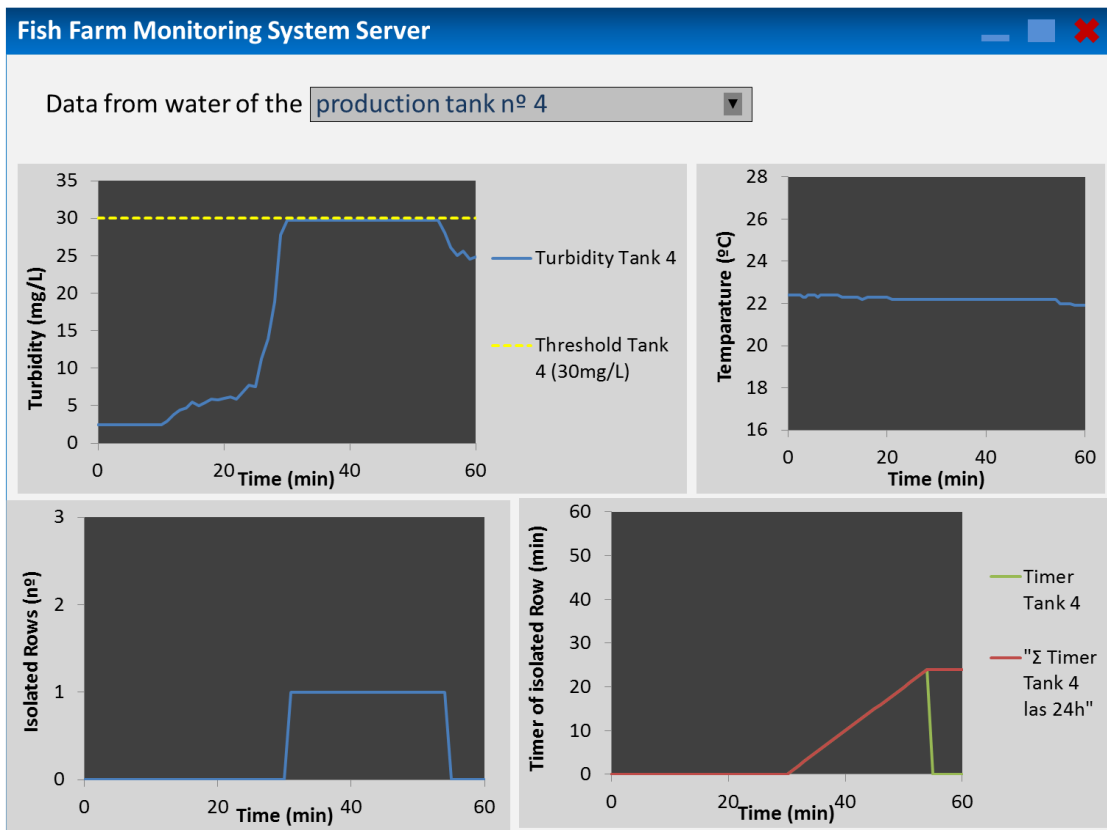


Figure 4. 29 Server appearance showing production tank information

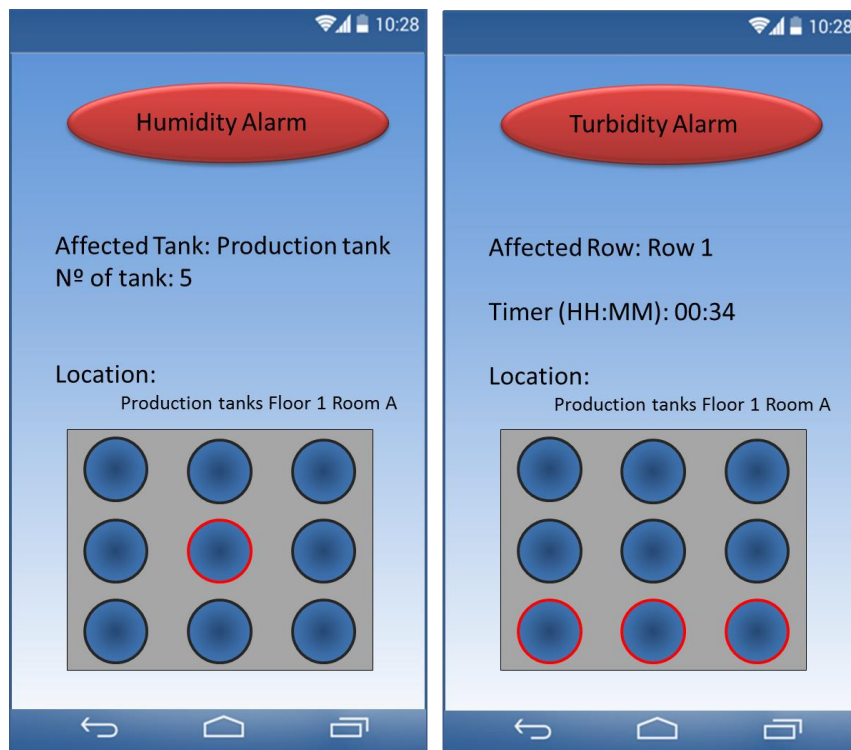


Figure 4. 30 Alarm appearance at the smartphone

## 4.4. System for monitoring the cage, the water quality, and the fish behavior

### 4.4.1. Materials and Methods

In this section, the developed system is detailed. First, the architecture of the proposed system is presented. Second, the employed physical sensors and its conditioning circuits are described. Then, the node and its configuration are presented.

#### 4.4.1.1. Architecture

In this subsection, the architecture of the proposed system is shown. The system is based on sensors for monitoring 10 parameters, including water quality parameters, tank parameters, fish behavior and humidity inside the node boxes. In each production tank, there are three nodes monitoring different parts of the tank. The employed nodes send the data wirelessly to the AP.

First, the physical topology is shown, see Figure 4.31. In the fish farm, a local area network will be deployed. Different box nodes (BN) are placed in several points of the facilities. The nodes are wirelessly connected to the AP using Wi-Fi technology. The APs are connected to the switch with an Ethernet link. Several APs are located at different points of the facilities; some of them are placed in the rooms with the production tanks. However, other APs are placed in the offices and those AP do not send data to the database. Those AP are used to send data to the workers if any alarm messages are generated. Finally, the switch is connected to a router in order to have internet access with a serial connection. The topology is based on an extended star topology.

Figure 4.32 shows the architecture of the entire system, including the database and the smart algorithms applied in the cloud. To save the data and move the computing activity to the cloud, it is possible to opt for a commercial solution such as Amazon Web Services (Amazon Web Services Platform, 2018) or Microsoft Azure (Microsoft Azure Platform, 2018) which implies an additional cost. In our case, we have used an own external web server which can be accessed through the internet. Besides, supervisors who are not located in the fish farm facilities can make an information request to the database from anyplace and anytime. Furthermore, in Figure 4.32 it is possible to see the location of the sensor and BN in the aquaculture tank. The BN 1 contains the following sensors: illumination, water level, oil layer, workers presence and fish behavior sensors. The BN 2 contains the rest of the water quality sensors, which include a temperature sensor, turbidity, and conductivity sensor. Finally, the BN 3 contains the feed fallen detector. In addition, all the BN contains and humidity sensors. In normal condition, the nodes sense and send the data to the database. Once the data arrives at the database, the smart algorithm is applied. If the smart algorithm concludes that the data corresponds to a normal situation no further actions are done. Nevertheless, if the smart algorithm concludes that the data does not fit with the normal situation, an alarm message is sent to the designed worker with the necessary information.

To avoid the energy waste in the sending data, algorithms are can be used in order to send only the relevant data. Thus, we reduce the number of information send reducing, therefore, the energy consumption in the data transmission. The energy consumption is one of the main deals in the WSN (Azizi, 2016) and many protocols have been developed to reduce the energy waste (Shahzad and Cho, 2017), (Wang et al., 2016). First, the thresholds for each variable are set ( $TH_x$ ). Next, the sensor gathers data and save this data as reference value  $X_x$ . A reference value is set for each one of the water variables ( $Wv$ ), including temperature, conductivity, turbidity and oil layer, and for the Tank variables ( $Tv$ ), which include water level, illumination, and workers presence. The next step is to set a clock time = 0. Following, the systems gather new data and it is named as  $Y_x$ . Then, the system checks the data from the humidity sensor. If the data is equal to 1, which indicates that there is humidity in the BN, then the system sends all the

stored data; send an alarm to the workers and turn of this BN. If the humidity sensor gives a value of 0 the operation continues. The  $Y_x$  ta is compared with the  $X_x$ . If the difference is higher than the  $TH_x$ , the stored data is sent to the database. Moreover, the  $Y_x$  is set as  $X_x$ , the clock is set again to 0 and the operation algorithm gathers new data. If the difference between them is not higher than the  $TH_x$  the  $Y_x$  is stored in the SD card of the node and the clock adds one counter more. If the clock value is higher than 3600 (1 hour) all the data is sent to the database. If the clock value is lower than 3600 the  $X_x$  data are maintained and the algorithm follows gathering new data. The entire algorithm can be seen in Figure 4.33.

Another algorithm is used for the fish behavior sensors ( $FI_x$ ), see Figure 4.34. In this case, the node stores de data during 1 minute and then sends all the data to the database. Finally, for the data from the feed falling sensor ( $FE_x$ ), the algorithm shown in Figure 4.35 is applied. Once the data from the sensor is gathered, the data about the interesting band is selected and the data from the other two bands are discarded. Then, the histogram of the selected band is obtained. Finally, the summation of the region of interest (RI) is done. If the summation of the RI is higher to the established  $TH_x$  the data is sent. If not, the algorithm continues gathering new data.

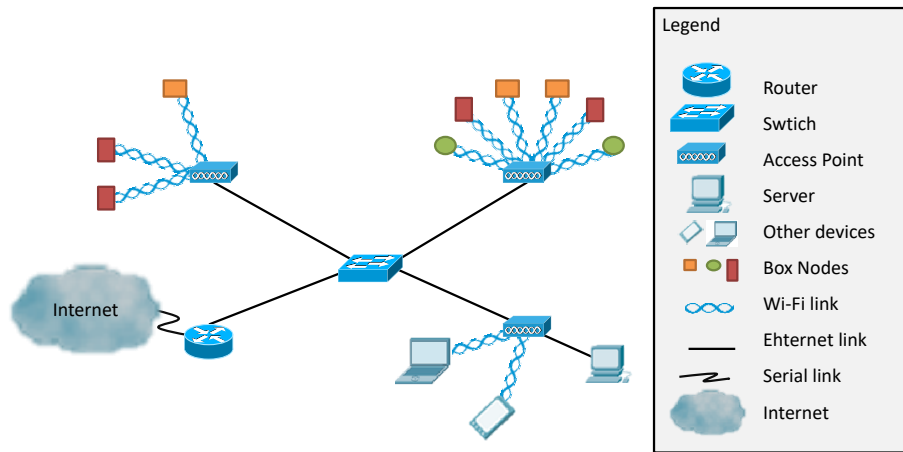


Figure 4. 31 Network topology proposed

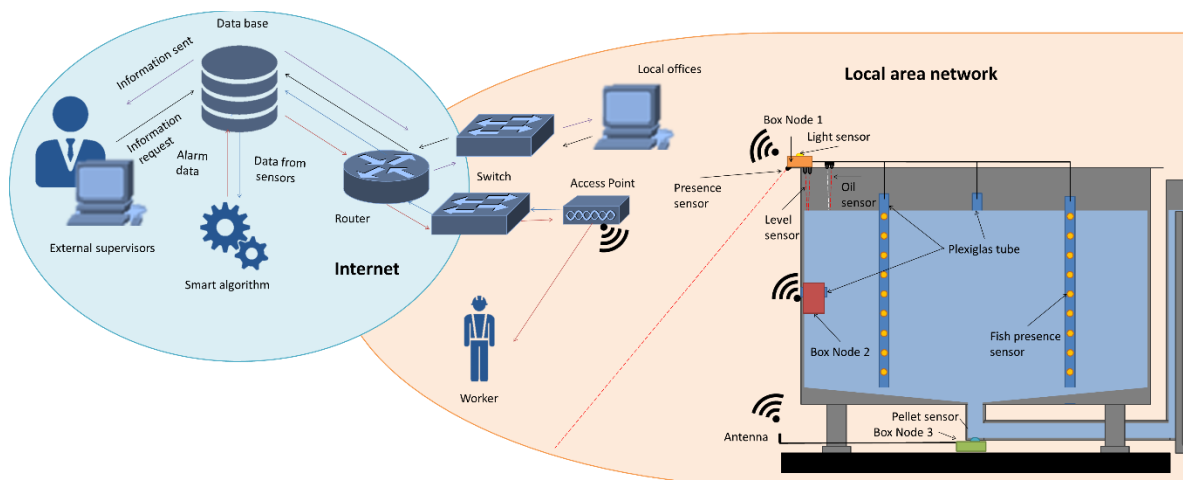


Figure 4. 32 Architecture of the proposed system

#### 4.4.1.2.Sensors

In this subsection, the sensors included in our system are presented. Different types of sensors, including optical sensors, thermal sensors, and magnetic sensors, among others, are used. The sensors are described in three sections. First, the sensors for monitoring water quality are presented. Next, the sensors for cage environment monitoring are shown. Lastly, we describe the sensors for fish feeding behavior.

##### 4.4.1.2.1. Water parameters

For water quality monitoring in fish farms, the physic-chemical parameters monitored by our system are temperature, conductivity, turbidity and the presence of an oil layer in the surface of the water. As it is explained above, to create a low-cost system, the price of the sensors is a limiting factor. For this reason, we create our own sensors based on electronic components with low-cost.

First, we describe the employed sensor for temperature monitoring. There are several options for temperature sensing. The most employed ones for water monitoring are the RTD and the thermistors. The reasons why these are the most used sensors are their high working range, adequate accuracy, and low price. In our case, a thermistor type negative temperature coefficient (NTC) was employed. The NTC presents greater resistance when temperature decreases. The other advantage of the NTC is the linear relationship between resistance and temperature. The employed NTC is the NTCLE413E2103F520L from Vishay (NRC Thermistor Datasheet, 2018). The price of this sensor is 0.96€. The working range of the sensors according to the datasheet is -40°C to 105°C. Our working range will be from 5°C to 35°C. The employed NTC can be seen in Figure 4.36.

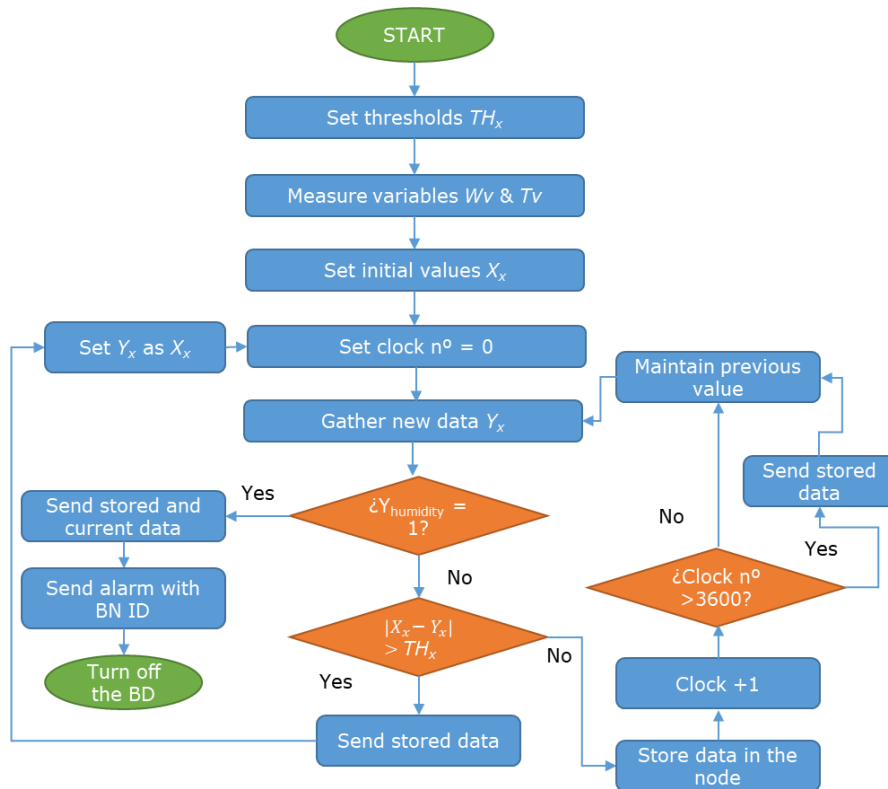


**Figure 4. 33** Operation algorithm for the water variables and tank variables

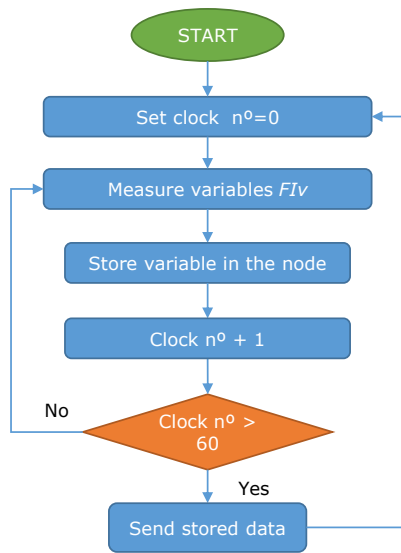


**Figure 4. 34** Operation algorithm for fish behavior algorithm

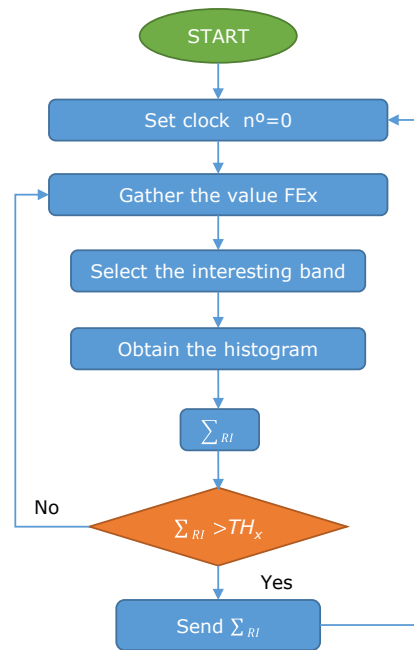


**Figure 4. 35** Operation algorithm for feed falling sensor

Following, the conductivity sensor is presented. As for temperature sensing, different options can be used. In this case, and considering that one of the main requirements is to avoid the contact between the sensing element and the water, we propose the use of the inductive sensor. This sensor is composed of two copper coils. One of the coils is powered by a sine wave. The generated electromagnetic field change depending on the conductivity of the water. The secondary coil, depending on the magnetic field, induces an electric voltage. The employed sensor was described by Parra et al (2015a), Parra et al., (2017). The coils were done with copper wire with 0.4mm of diameter. The coil diameter was 25mm. The powered coil has 40 spires and the induced coil 80 spires. The induced voltage increases when the conductivity of the water increases. In a previous test performed with these coils a PVC tube was used Parra et al (2015a), Parra et al., (2017). Nevertheless, in this case, a crystal cylinder will be used. The working range of the sensor goes from 0 mS/cm to up to 80 mS/cm. In the marine fish farms, the expected salinity goes for 0 mS/cm to 29 and to 38 mg/L (Antonov et al., 2009), that corresponds to a range from 44.9 to 57 mS/cm. The conductivity sensor included in our system can be seen in Figure 4.36.

The turbidity sensor is described below. There are two main methods to measure the turbidity, the acoustic and the optical method. In this case, the optical method is selected. The employed sensor is described in Sendra et al. (2013b). It is composed of an infrared (IR) light emitting diode (LED) and an IR photodetector. The employed IR LED is the TSHG6200 from Vishay (IR LED Datasheet, 2018), the peak wavelength of this LED is 850nm. Moreover, the employed IR photodetector is the BPW83 from Vishay (IR Photodetector Datasheet, 2018). Its range of spectral bandwidth goes from 790 to 1050 nm and its wavelength of peak sensitivity is 950 nm. The IR photodetector offers a fast response, the resistance of the photodetector decreases when the turbidity increases. The relationship between turbidity and resistance is linear in the range from 0 to 250mg/L. If we intend to include higher values, the relationship changes to another type of relation. However, the expected values of turbidity in fish farms are low. Only in adverse conditions, the turbidity values can increase. The turbidity sensor can be seen in Figure 4.36.

The last sensor that monitors the water quality is the oil sensor. This sensor must be able to detect the appearance of an oil layer in the surface of the water. This sensor is based on the

model proposed by Parra et al. (2015d). A white LED is employed to illuminate the water surface and IR photodiode is used to measure the light emission. The employed white LED is the VLHW4100 from Vishay (White LED VLHW4100, 2018), its wavelength emission goes from 400 to 700 nm and the peak wavelength is placed at 450nm. The photodiode is the BPW41N from Vishay (IR Photodiode BPW41N, 2018). The range of spectral bandwidth goes from 870 to 1050 nm with a peak at 950nm. The photodiode is not the same that was used in (Parra et al., 2015d) but their characteristics are the same. Unlike the other sensor, the oil layer sensor is not a quantitative sensor. This sensor is only able to determine the presence of an oil layer but it is not possible to quantify the thickness of the oil layer. The oil sensor can be seen in Figure 4.36.

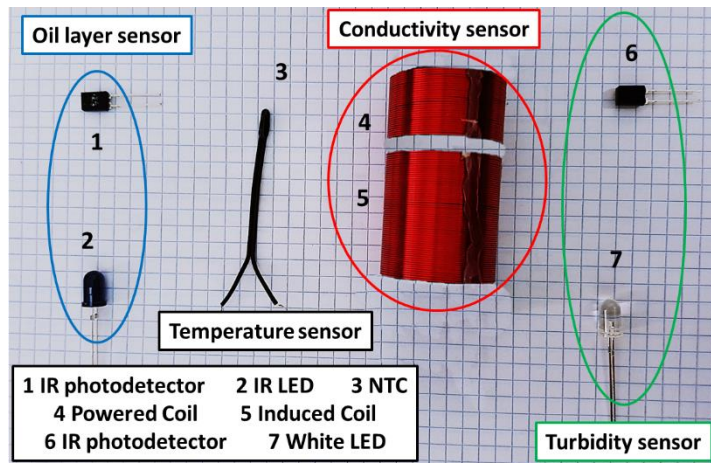


**Figure 4. 36** Employed components for sensor to monitor the water quality

#### 4.4.1.2.2. Tank parameters

Some parameters of the tank and its environments, such as water level, illumination and the presence of workers in the vicinity of the tank, must be monitored. As in water quality sensors, the sensors employed for tank control are simple electronic components sensitive to different light wavelength combined in different ways.

First, the water level sensor is described. There are two main options to measure the level of the water, employing acoustic sensors or optical sensors. To measure the water level, a level sensor based on IR emission and reception was selected (Level Sensor GP2Y0A02YK0F, 2018). This sensor was already tested for fish farms in (Parra et al., 2017). The measurement ranges from 20 to 150 cm. This sensor is already calibrated; the maximum output voltage corresponds to the minimum distance, 20cm. However, the maximum voltage is too high to be connected directly to the node. For this reason, it is necessary to add a conditioning circuit to reduce the maximum voltage. The sensor can be seen in Figure 4.37.

Following, the sensor for monitoring the illumination in the tanks is presented. To measure the luminosity of the halogens that illuminates the tank there are different options. All the options are based on optical sensors. We select to use a light dependent resistance (LDR) for monitoring the illumination, see Figure 4.37. We select the LDR because it has a low price and it provides a fast response. The resistance of the LDR increases with the light intensity. The selected LDR to measure the illumination in the tanks is the NORPS-12 from ADVANCED PHOTONIX (LDR NORPS-12, 2018). It is encapsulated in a humidity resistant coating. Moreover, it is enclosed in a plastic casing. The minimum and maximum resistances are 5.4 k $\Omega$  and 1 M $\Omega$ . Finally, the sensor for detecting the presence of workers in the vicinity of the tanks is shown. This sensor is based on the IR light emission and reception. The system is similar to

the sensor for water level. It has an IR emitter and IR receiver. The sensor can be seen in Figure 4.37.

#### 4.4.1.2.3. Feeding parameters

For monitoring the feeding parameters, the fish behavior and the falling pellets must be measured. Again, low-cost components must be used to ensure the low-cost of the system.

Firstly, the system for monitoring the fish behavior is described. The system is composed of three transparent Plexiglas tubes placed at different points on the inside of the tank. Inside each tube, there are 9 LDR sensors placed at 15 cm from each other. The operation of this sensor is based on the light refraction caused by the fish scales when they are swimming. The majority of the currently available systems are based on the use of acoustic waves or machine vision. However, the systems based on acoustic waves have high energy consumption. On the other hand, the systems based on machine vision require from the high computation. Furthermore, the systems based on machine vision usually do not give information about the swimming depth and swimming velocity of the fish. To control the stress of the fish and their feeding behavior, it is necessary to monitor the swimming depth and swimming velocity. Our system is able to determine the swimming depth and estimate the changes in the swimming velocities. The LDR employed in this system is the NSL 19M51 form Advanced Photonix (LDR NSL 19M51, 2018). The resistance of this LDR varies from  $5k\Omega$  to  $20M\Omega$ . One limitation of our system is that it only can operate when the halogens are turned on.

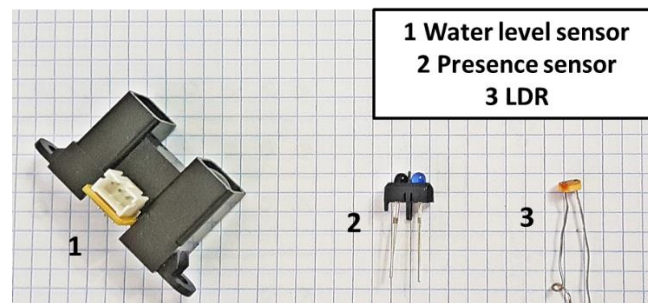


**Figure 4.37** Employed components for sensor to monitor the tank

Nevertheless, as we pretend to monitor the behavior for feeding purposes, the feeding is only provided when the halogens are turned on. During the night, if an abnormal situation occurs and causes stress on the fish, resulting in changes in their swimming depth and/or velocity it will not detect by our system.

The sensor to control the falling pellets is detailed in this paragraph. There are different options for pellet detection. While some authors use acoustic methods others use methods based on cameras. In our proposal, a camera will be used to obtain pictures of the pellets in the effluent pipe. Using the same process shown by Marin et al. (2017) we will obtain the histograms. Then, we can quantify the number of pellets according to the number of pixels with a selected value of brightness. The camera will be placed at the bottom of the water drainage system. It will be necessary to change the elbow pipe by a T shaped one and add a Methacrylate separator as shows Figure 4.38.

#### 4.4.1.2.4. Other sensors

Finally, the humidity level inside the node boxes must be monitored. The humidity node is used to activate an emergency turn off in the BN to prevent further damages caused by the water. It is necessary to consider that the BN2 will be placed inside the water tank and if any damage is caused in the O-Ring of the box the water can enter inside the box. Moreover, in the environment of the production room, the level of relative humidity in the air is very high. Thus,

the NB1 and 3 also must be monitored. The humidity node is the same sensor employed in (Rocher et al., 2017).

#### 4.4.1.3. Node

In this subsection, the employed node and its configuration are detailed. In order to collect the data from all sensors, we have selected a compatible Arduino Mega 2560 module. This microprocessor board has 54 digital input/output pins, 16 analog inputs, 4 UARTs (hardware serial ports), 16MHz crystal oscillator, USB connection, power jack, In-Circuit Serial Programming (ICSP) connector and reset button. In addition, this compatible Arduino Mega module can be supplied from our PC by means of a USB cable or by an external power supply (9 up to 12VDC). However, one of the main drawbacks of this board is that it does not have any type of wireless interface to integrate it in a WSN and the storage capacity of data from the sensors is limited. To solve this problem, we use a Wi-Fi module ESP8266 ESP-01(ESP8266 WiFi Module Features, 2018) and a microSD card reader which will be connected to our microprocessor module as Figure 4.39 shows.

Another important issue to deal when implementing the module is how to collect the signals from the different LDRs in the node of BN1. In this node, the 27 used LDRs must be connected. Moreover, the sensors of humidity, water level, workers presence and illumination are connected too. This issue does not appear in the other nodes. To this end, we select an analog 16x1 multiplexer (MUX). In this case, the Multiplexer (CD74HC4067 16-Channel Analog Multiplexer/Demultiplexer features, 2018) will be chosen. Because we need to collect data from 27 LDRs, it is needed to use two 16x1 MUX. Finally, to join the signals from both, we will use a new 2x1 MUX (74LVC1G3157 Single-Pole Double-Throw Analog Switch, 2018). With this, we will be able to gather data from 30 analog devices.

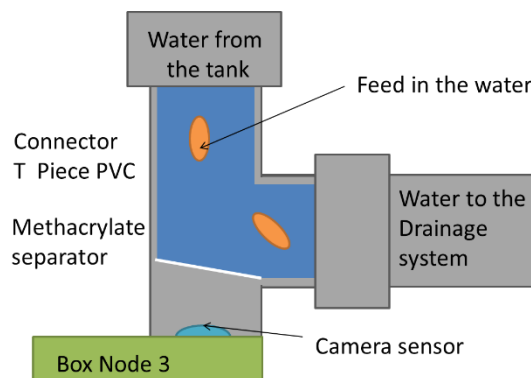


**Figure 4. 38** Detail of the location of feed fallen detector

The resulting operation of this combination of multiplexers works as follow. On the one hand, we have a series of input signals, in our case 32 analog inputs (from AI0 to AI32), which are controlled by the control signals (from C0 to C5). As a function of the control signals, we will select an input signal to drive it to the output. Finally, the STROBE signal enables or disables the multiplexing.



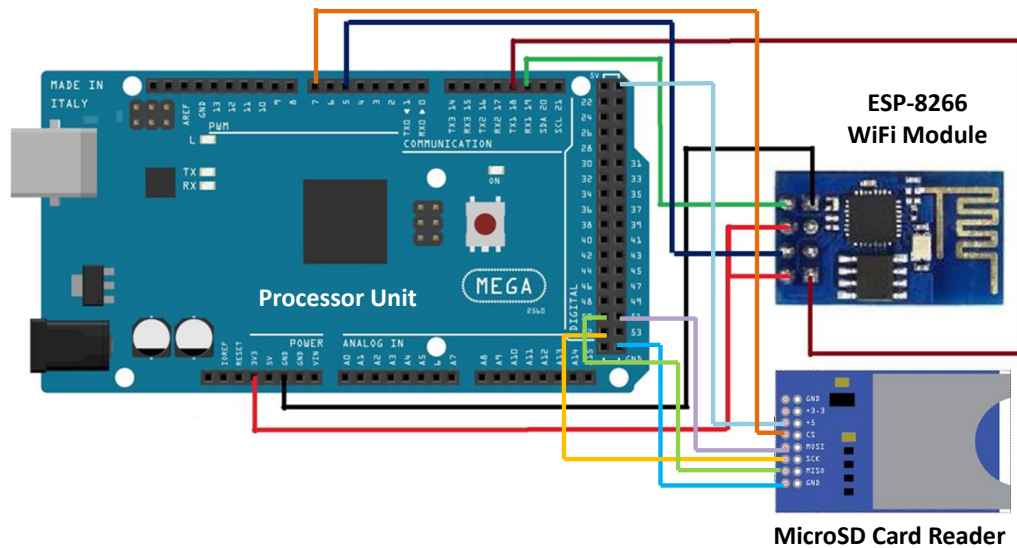


**Figure 4. 39** Compatible module with Arduino Mega 2560 connected to WiFi module and MicroSD card reader

#### 4.4.2. Results and discussion

In this section, the results are shown. First, the results of the calibration of water quality sensors are presented. Following the results of sensors for tank monitoring and fish, behavior monitoring are presented.

##### 4.4.2.1. Results of the water quality sensors

In this subsection, the results of the calibration of the employed sensors for water quality monitoring are shown. In some cases, as turbidity or temperature sensors, calibrations have already been carried out that relate the environmental parameter and the resistance of the electronic component. Nevertheless, for operation in the system, it is necessary to obtain the data as the output voltage ( $V_{out}$ ) that arrives at the node. Moreover, it may be needed to include a voltage divisor to ensure that current in the node is not too high. Thus, it will be necessary to transform the data and to obtain a new calibration equation for the temperature and turbidity sensor. In the case of the conductivity sensor, the same calibration and equations con code that has been used in (Parra et al., 2015a) are employed. Finally, for the oil layer sensor, the calibration shown in (Parra et al., 2015d) is used, the code is presented below.

First, for the temperature sensor, based on the data offered by the manufacturer (NRC Thermistor Datasheet, 2018) it is possible to extract the expected resistances at different temperatures. A voltage divisor must be used in order to maximize the difference of  $V_{out}$  between the minimum and maximum values of resistance of the NTC. An  $R_2$  of  $12K\Omega$  must be used and the NTC is used as  $R_1$ . We can calculate the  $V_{out}$  of the temperature sensor at different temperatures. The data and the mathematical model that follows this data are presented in Figure 4.40 (a). The relation between  $V_{out}$  and Temperature can be seen in equation 1. The correlation coefficient of Eq. 1 is 0.9995. Considering that the resolution of the node is 10 bits and the maximum  $V_{out}$  that can be registered is 3.3V, the minimum difference of  $V_{out}$  that the node is able to detect is 3.2 mV. Thus, the minimum temperature variation that can be detected by our system is 0.1°C. The resolution of the temperature sensor is enough for the aquaculture monitoring. In Figure 4.40 (b) we can see the code used in the node to read the value of the

temperature sensor. The formula that relates the temperature and the voltTemp value is extracted from the Eq. (1).

Following, for the turbidity sensor we use the data shown in (Rocher et al., 2017), where a calibration was already performed. Nonetheless, the data obtained in this calibration must be transformed from the resistance of the IR photodetector to  $V_{out}$ . Once more, a voltage divisor must be used. Using the  $V_{in}$  of 3.3V the IR photodetector as  $R1$  and an  $R2$  of  $6M\Omega$  we maximize the difference between the maximum and minimum  $V_{out}$ . The data after apply the voltage divisor and the mathematical model that adjust to this data are presented in Figure 4.41 (a). The correlation coefficient of the mathematical model, equation 2, is 0.9977. Considering the resolution of the node, the minimum variation of turbidity that can be detected by the turbidity sensor goes from 1.8 NTU in low turbidity conditions to 4 NTU in high turbidity conditions. In Figure 4.41 (b), the code introduced in the node to read the  $V_{out}$  from the turbidity sensor and transform this voltage into turbidity value is shown. The formula that relates the turbidity and the voltTurb value is obtained from relating the data shown in Figure 4.40 (a) being the voltage as the independent variable and the turbidity as the dependent variable. The correlation coefficient of this formula is 0.9993.

The calibration of the oil layer sensor is shown now. The data from the oil sensor can be seen in Figure 4.42 (a). In this case, we only pretend to differentiate the absence to the presence of oil layer. On the one hand, it is possible to see that when there is no oil layer the average  $V_{out}$  is 0.018V, the minimum value is 0.015V. On the other hand, when the oil layer is present the average  $V_{out}$  is 0.010V, with a maximum value of 0.011V. Thus, the threshold value to detect the presence of oil layer is 0.011V. The code for reading the  $V_{out}$  from the oil layer sensor is presented in Figure 4.42 (b).

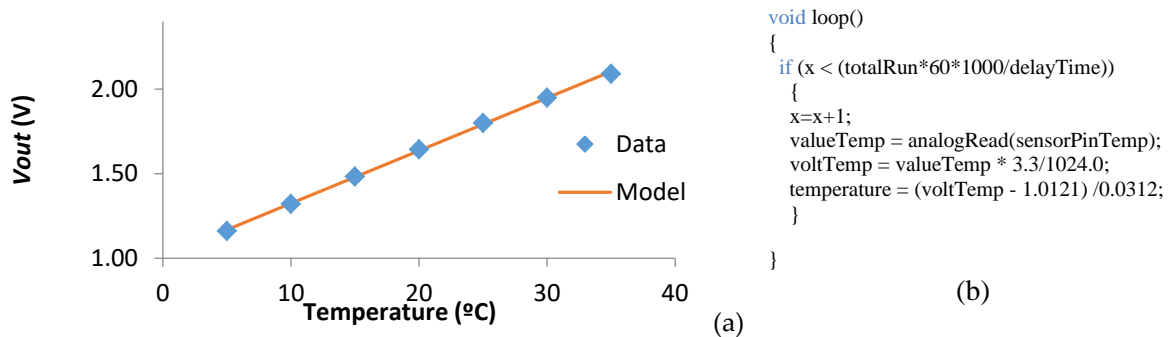


Figure 4.40. Data and code of the temperature sensor

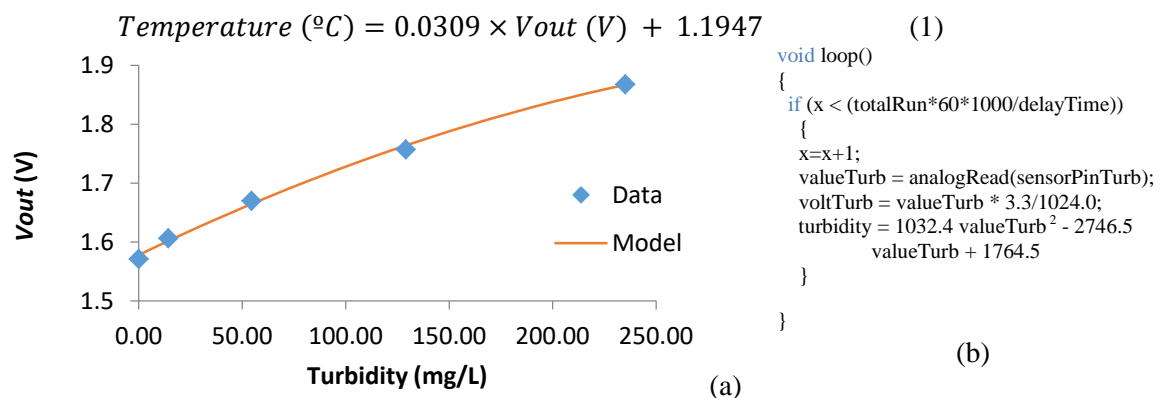


Figure 4.41 Data and code of the turbidity sensor

$$Turbidity (NTU) = 1764.5 + 1032.4 \times V_{out}^2 - 2746.5 \times V_{out} \quad (2)$$

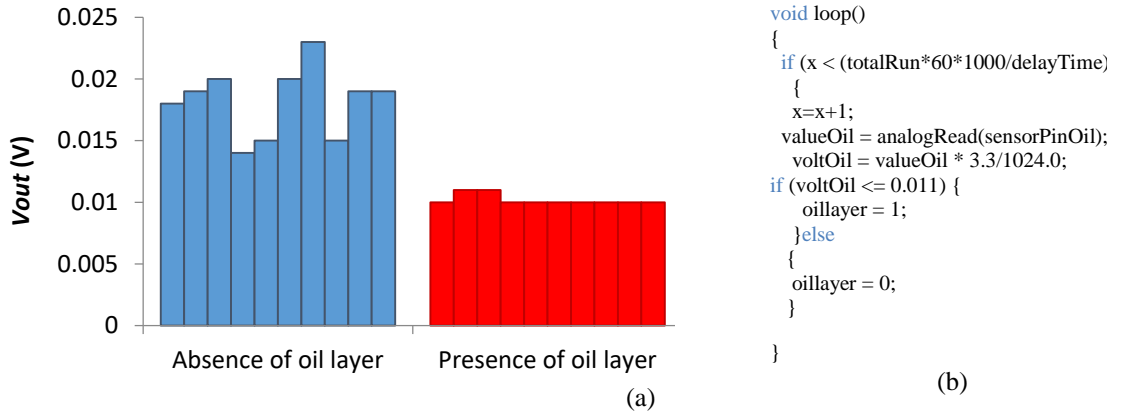


Figure 4.42 Data and code of the oil layer sensor

#### 4.4.2.2. Results of the tank sensors

Following, the results of the calibration from the tank sensors (water level, illumination and presence sensors) are detailed. The data from the water level sensor is obtained from (Parra et al., 2017) because the same level sensor is used in this system. The calibration of the illumination sensor is shown in Figure 4.43 (a). This calibration was done using a  $V_{in}$  of 3.3V the LDR as  $R1$  and an  $R2$  of 2k $\Omega$ . The model presented in Figure 4.43 (a) presents a correlation coefficient of 0.9855 and can be seen in equation (3). Considering the resolution of the node, the minimum variation of light that can be detected by the light sensor goes from 0.1 lux in conditions with low illumination to 42 lux when the illumination exceeds the 1500 lux. In the code introduced in the node to read the  $V_{out}$  from the light sensor and transform this voltage into illumination in lux value is shown in Figure 4.43 (b). The formula that relates the turbidity and the voltLig value is extracted from Eq. (3).

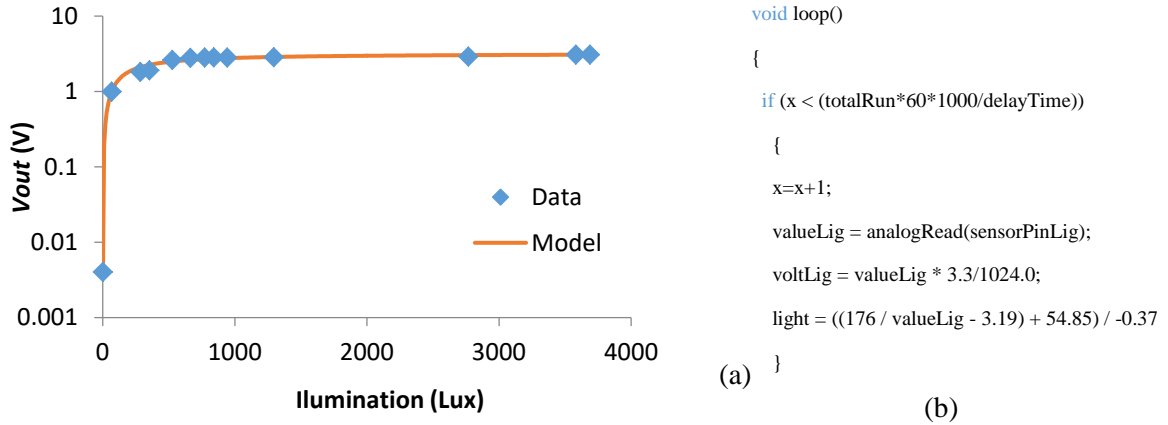
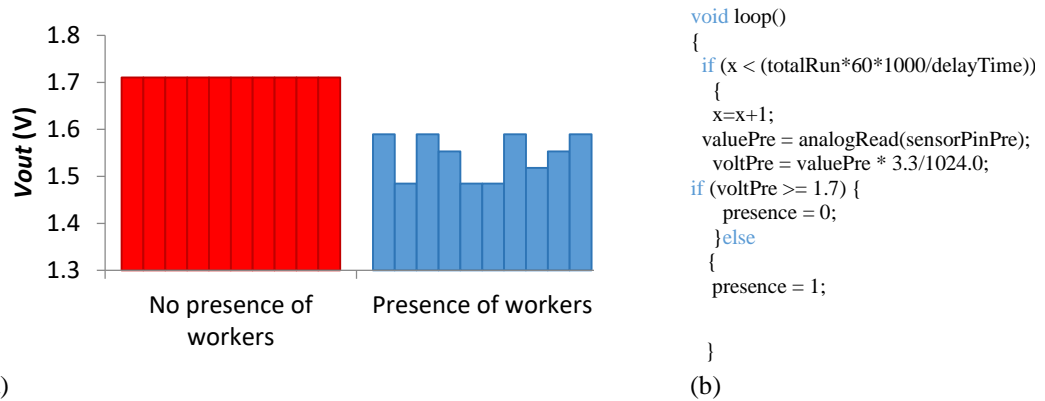


Figure 4.43 Data and code of the light sensor

$$Light (lux) = 3.19 + \frac{176}{-54.85 - 0.37 \times V_{out} (V)} \quad (3)$$

The results of the presence sensor are shown in this paragraph. As for the oil sensor, this sensor is not a quantitative sensor, it is a qualitative sensor. It offers information about if there are or there are not people around the tank. Thus, the calibration of this sensor is done comparing the  $V_{out}$  of the sensor in two scenarios. In the first scenario, there is no presence of any worker. In the second scenario, there is a worker at 50 cm of the tank. The  $V_{in}$  in this test is 3.3 employing an  $R2$  of 2M $\Omega$  and the IR photodiode as  $R1$ . The  $V_{out}$  in both scenarios is

presented in Figure 4.44 (a). The values of  $V_{out}$  without workers are between 1.5 and 1.6 V, while with the presence of workers the  $V_{out}$  increases to 1.7 V. The code of the sensor can be seen in Figure 4.44 (b).



**Figure 4. 44** Data and code of the presence sensor

#### 4.4.2.3. Results of the fish behavior sensors

The results of the fish behavior sensor are shown below. Several tests were done in order to ensure that this system can correctly detect the fish to determine the swimming depth and estimate the swimming velocity. Furthermore, the camera was tested to detect the presence of feed falling.

The first test consists of measuring the resistivity of the employed LDR at different points of an aquarium in the presence (Figure 4.45 (a)) and absence of a fish (Figure 4.45 (b)). For this test, a dead adult of *Sparus aurata* L. has been used. It was necessary to use a dead fish is because it is necessary that the fish remains at the same point during all the experiment. Three repetitions of each measure have been done. In the aquarium, a matrix of 7 per 4 measure points has been set as can be seen in Figure 4.45 (a) as a red dots in the aquarium. The resistance of the LDR has been measured with a multimeter. The average resistance of the LDR in each point of the matrix with and without the fish is presented in Figure 4.46 (a) and (b). It is possible to see that, with the resistance of the LDR we can differentiate when there is or there is not a fish in the aquarium. On the one hand, the lowest resistance when there is a fish is 12.9 k $\Omega$ . On the other hand, the lowest resistance value when the fish is present is 19.7 k $\Omega$ . Thus, the use of LDR for detecting a fish is demonstrated. Once, it has been demonstrated that with the LDR is possible to determine the presence or absence of fish, we need to gather data on living fish. In the first test with a tank, unique LDR was introduced at 60cm depth. The  $V_{out}$  of the presence sensor is shown in Figure 4.47. A  $V_{in}$  of 3.3V and an  $R_2$  of 41K $\Omega$  was used. During the first 10 seconds of measurement, the fish were kept far from the LDR in order to have data without the fish presence. The movement of the fish has been recorded with a camera in order to compare the data of the sensor with the moments that the fish were close to the detector. The time when the fish were close to the LDR are considered as fish presence periods and are colored in red in Figure 4.47. The  $V_{out}$  of the presence sensor is correlated with the presence of fish. When the fish are present the  $V_{out}$  increases to reach values of 1.85 V. The average  $V_{out}$  when the fish are present is 1.63 V. In the periods when the fish are not present, the minimum  $V_{out}$  is 1.37 V and the average 1.39 V

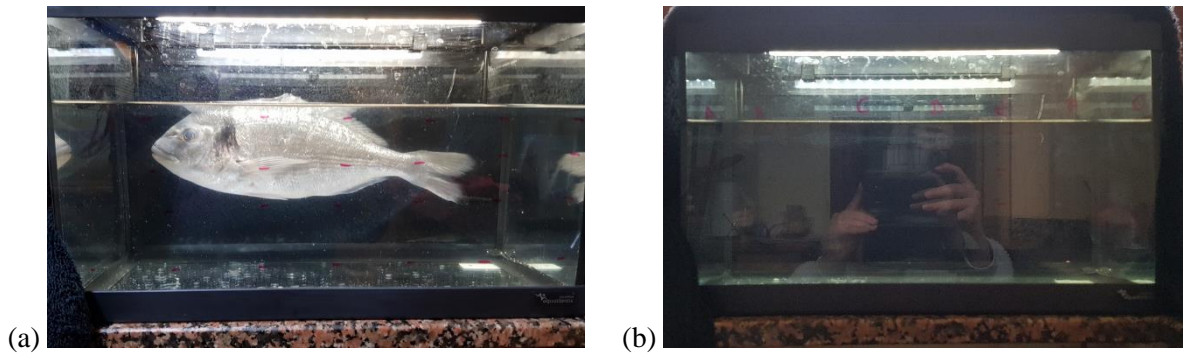


**Figure 4.45** Experiments to demonstrate the operation of fish behavior sensor, preliminary test

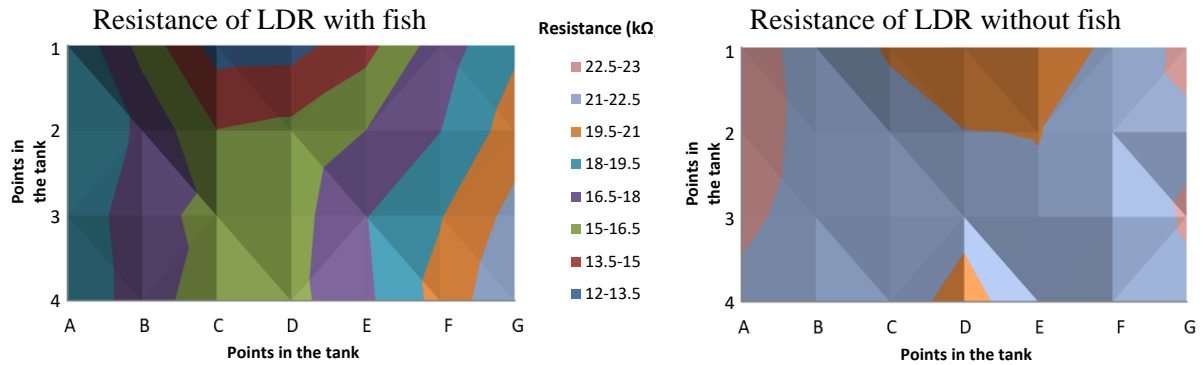


**Figure 4.46** Average LDR resistance in different point with and without the fish

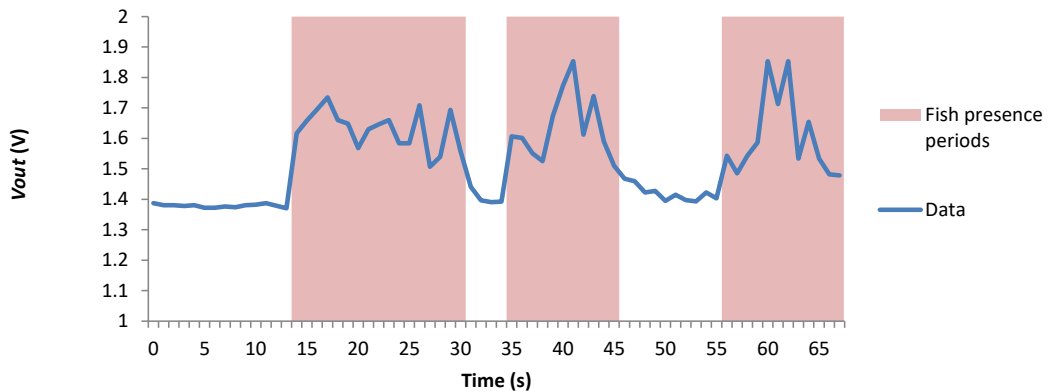


**Figure 4.47** Data gathered by the fish presence sensor

The next two experiments are performed to test the system for fish detection. First, 9 LDR were introduced in the previous tank with the same fish employed in the previous experiment. The *Vout* of each sensor for fish detection is presented in Figure 4.48. The data of 5 different moments or scenarios are presented. In the scenario 1, the fish were not present in the tank. In the rest of scenarios, it is possible to identify the swimming depth by analyzing the *Vout* of the sensor. The maximum value of *Vout* corresponds to the average fish swimming depth. Consequently, it is possible to see that the data of fish detection can be used to determine the fish swimming depth. Unlike with the other sensors where the *Vout* was transformed into the value of the sensed variable before being sent, with this sensor the *Vout* is the sent data. In the database, a smart algorithm will be applied.

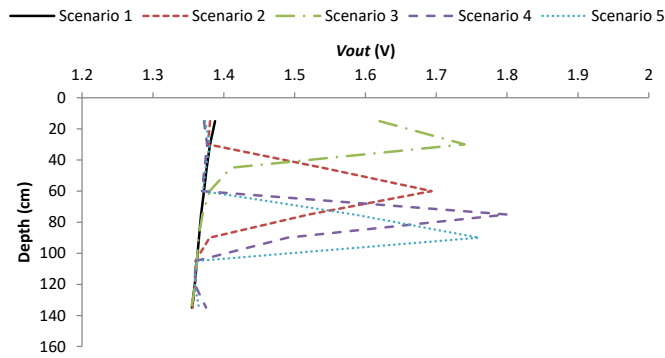


**Figure 4. 48** Data gathered by the fish presence sensor

The last experiment was carried out to estimate the fish swimming velocity. Two scenarios were considered for this test. The first one, when there is low fish density and a small shoal is formed. In this case, the shoal does not form a ring, see Figure 4.49 (a). The second scenario, when there is a higher density and a bigger shoal is formed. In this case, the shoal forms a ring; see Figure 4.49 (b). In this case, instead of representing the  $V_{out}$  of the sensor we process the data with the code (see Figure 4.50) to read this sensor. As this presence sensor gives a qualitative data a threshold value must be set. In the database, it is considered that the fish are present if the  $V_{out}$  is higher to 1.5V, the state of the variable is 1. Consequently, when the value of the  $V_{out}$  received is lower than 1.5V the state of the variable is set to 0. In the first scenario, Figure 4.49 (a), the data after being transformed by the algorithm can be seen in Figure 4.51. In this case, the state of the variable fish presence changes from 0 to 1 periodically, indicating the pass of the fish shoal close to the presence sensor. Thus, it is possible to estimate the shoal mean velocity (MV) by considering that the shoal swims in a circle and estimating that the diameter of this circle is 10% of the tank diameter. The MV will, therefore, be given by the equation 4:

$$MV \left( \frac{m}{s} \right) = \frac{(\phi Tank (m) \times 0.9) \times \pi}{Time\ between\ intervals (s)} \quad (4)$$

Nevertheless, in the scenario 2, it is not possible to measure the fish MV with this methodology. In this case, it is possible to estimate the variations in the velocity using the variations in the  $V_{out}$ . Different fish velocities require different frequencies of propulsion moves. The greater the movement, the faster the changes in illumination received by the LDR. In this case, it will be impossible to establish the MV; but the system can give information about if the MV increase or decrease. Three tests were done in a tank with fish swimming at different velocities. The data from scenario 1 and scenario 2 corresponds to fish swimming at a slower velocity than in scenario 3. The frequency of sensed data in these experiments is the maximum available by the system, 1 data each 0.33 seconds. The  $V_{out}$  data of the three scenarios are presented in Figure 4.52. We can see that in scenario 1 and 2 there is an oscillation similar to a sine pattern between the maximum and minimum  $V_{out}$  values almost constant. However, in scenario 3 this sine pattern is not visible. This is because the flashes produced by the fish scales illuminate the LDR during the very short period of time. The LDR needs little time exposed to the light to reach the maximum value and in the scenario 3, the flashes are shorter than this period of time. Then, the LDR is not able to reach the maximum value reached in the other two scenarios. The best way to differentiate between scenarios is to consider the number of peaks in the  $V_{out}$  that appear in 15 seconds. While in the scenarios 1 and 2 the number of peaks is equal to 5 in the scenario 3 the number of peaks is 11. Therefore, the number of peaks in  $V_{out}$  during 15 seconds is a good indicator of MV (IMV), see equation 5. When the MV increases the number of peaks will increase.

$$IMV = \frac{n^{\circ} \text{ of peaks}}{\text{time (s)}} \quad (5)$$

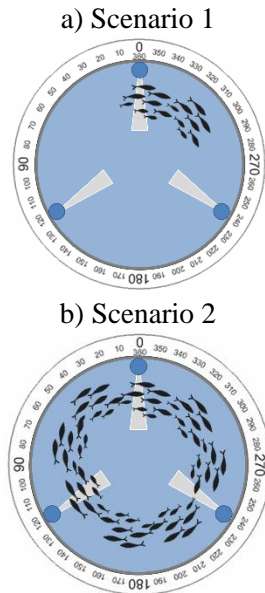


**Figure 4.49** Fish shoal in tested scenarios

```
void loop()
{
  if (x < (totalRun*60*1000/delayTime))
  {
    x=x+1;
    valuePre = analogRead(sensorPinPre);
    voltPre = valuePre* 3.3/1024.0;
    if (voltPre >= 1.5) {
      presence = 1;
    }else
    {
      presence = 0;
    }
  }
}
```

**Figure 4.50** Code for presence sensor

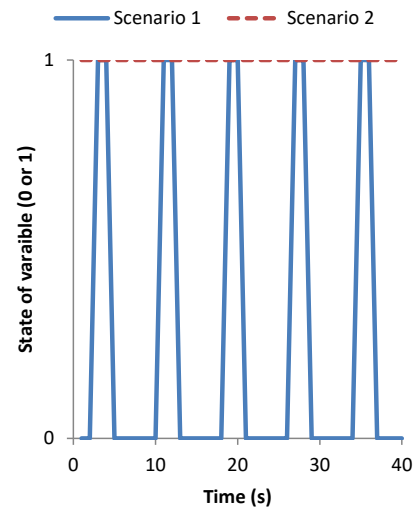


**Figure 4.51** State of variable fish presence of one sensor in different scenarios

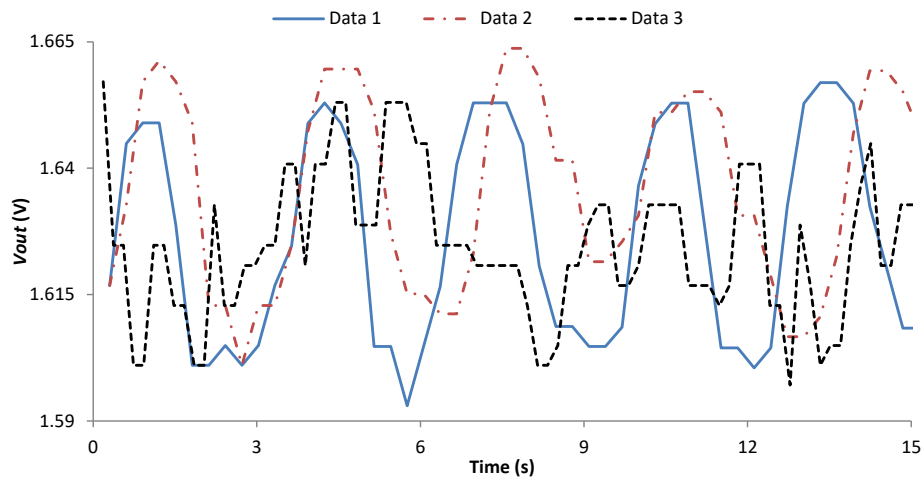


**Figure 4.52** Data gathered by the fish presence sensor

Finally, the results of the sensor employed to detect the feed falling are presented. For the calibration of this sensor, pictures of the drainage tube without pellets and with pellets are analyzed. The histograms of those pictures were obtained using a Matlab library. First, we analyze the red, green and blue histograms to compare the values of the pictures without feed and pictures with feed. The blue histogram is the one that shows the highest differences between both situations. Specifically, in the blue histogram, the region with the highest differences, the RI, is the region of brightness values (BV) between 130 and 150. The  $\sum RI$  of different pictures as the % of pixels in the RI can be seen in Figure 4.53. It is possible to see that in Figure 4.53, the pictures 1 to 4 present values lower than 25% while the pictures 5 to 8 have values higher than 50%. Thus, the threshold for this sensor will be the  $\sum RI$  value of 30%.

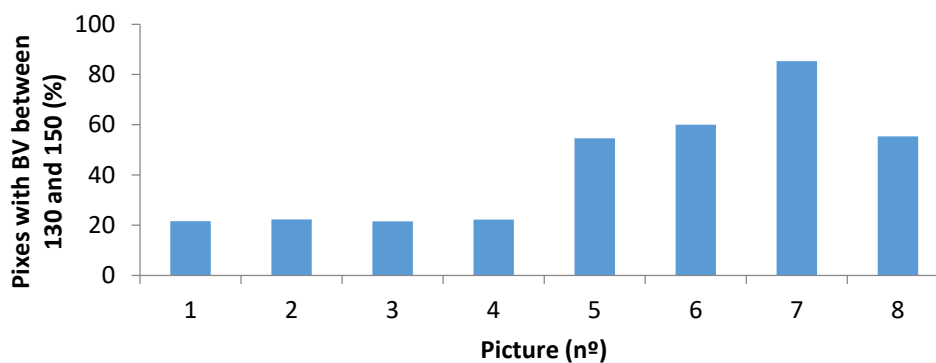


**Figure 4.53** Data gathered by the feed falling sensor

#### 4.4.2.4. Comparison with other systems and price of the employed components

At this point, we are going to perform a comparison between our developed solution and the current systems described in the related work for tanks and ponds, the systems proposed for marine cages are not included. We summarize the characteristics of the current systems and our proposal in Table 4.3. The main differences are that the other systems monitor between 2 and 4 parameters while our systems are capable to monitor 10 parameters. Moreover, the other proposals employ commercial probes and our system is based on our own sensors. Which makes that the price of the system decreases. In our proposal, we also consider the fish movement among the water quality monitoring. Finally, in our solution we showed the location of the sensors in the tank. The majority of the paper do not pay attention to the location of the sensors.

**Table 4.3.** Summary of characteristics of the current system and our proposal

Paper	(Espinosa-Faller, and Redón-Rodríguez, 2012)	(Zhang et al., 2010b)	(Lin et al., 2011)	(Huang et al., 2013)	(Simbeye et al., 2014)	(Zhu et al., 2010)	(Encinas et al., 2017)	(Han et al., 2007)	(Hongpin et al., 2015)	(Shifeng et al., 2007)	Our proposal
Communication technology:	ZigBee	ZigBee	ZigBee	N.I.	ZigBee	ZigBee	LR-WPAN	N.I.	ZigBee	N.I.	WiFi
Applied on::	Tanks	Tank	Tanks	Ponds	Ponds	Tanks	Ponds	N.I.	Tank	Ponds	Tanks
Considers the sensor location?					x						x
Develop their sensors?											x
Store information?	x	x	x	x	x	x	x	x	x	x	x
Send alarm?	x	x		x		x	x	x		x	x
pH		x	x	x	x	x	x		x		x
Water level		x			x						x
Temperature	x	x	x	x	x	x	x	x	x	x	x
Pressure	x										
Dissolved oxygen	x	x		x	x	x	x	x	x	x	
Conductivity			x			x		x			x
Ammonia									x		
Others											x
Fish monitoring											x
Nº monitored parameters	3	4	3	3	4	4	3	3	4	2	10



As a final point, the price of the components to create this WSN for one tank is shown in Table 4.4. The price of employed sensors is 47.44€ and the price of the nodes and their accessories is 40.22€. The most expensive item is the workers presence, this sensor has a cost of 15.23€. All the sensors for water quality have a price of 3.11€. The system for fish detection cost 16.5€ and the camera for feed detection 5.35€. To this price some minor costs as boxes for the nodes or plexiglass tubes must be add. The cost of this system can be assumed by the fish farmers, at least in the tanks with the most sensible and/or expensive fish are kept at the beginning and expand the system in the future. The system presents high scalability and only the need components must be bought.

**Table 4. 4** Summary of characteristics of the current system and our proposal

Purpose	Item	Unitary cost				
		(€)	Units	Cost (€)		
Sensors	Water quality	Temperature	NTCLE413E2103F520L	0.62	1	0.62
		Conductivity	-	0.48	1	0.48
		Turbidity	TSHG6200 IR LED	0.75	1	0.75
	Oli layer		BPW83 IR photodetector	0.38	1	0.38
			VLHW4100 White LED	0.36	1	0.36
	Tank		BPW41N IR photodetector	0.52	1	0.52
		Water level	GP2Y0A02YK0F level sensor	15.23	1	15.23
	Others	Workers presence	TSHG6200 IR LED	0.76	1	0.76
			BPW83 IR photodetector	0.38	1	0.38
		Light	NORPS-12 LDR	1.76	1	1.76
	Node	Fish presence	NSL 19M51 LDR	0.55	30	16.5
		Feed falling	Jtron OV7670 300KP VGA	5.35	1	5.35
	Node	Humidity	HCZ-D5-A Humidity sensor	1.45	3	4.35
Node compatible with Arduino			6.7	3	20.1	
Memory system		Micro SD Card reader	2.19	3	6.57	
		Micro SD Card 4Gb	0.82	3	2.46	
Transmission system		ESP8266 WiFi module	1.58	3	4.74	
		CD74HC4067 16-Channel MUX	0.45	2	0.90	
Multiplexors		74LVC1G3157 Single-Pole Double-Throw Analog				
		Switch	0.45	1	0.45	
Other		Resistances	0.5	10	5	
				Total	87.66	

## 4.5. Automatic system for the adjustment of the feeder process to the fish demand

### 4.5.1. System description

In this section we show the system description. First, we describe the scenario where our system is calibrated and tested. In addition, we detail the hardware part of our system including the employed sensors, node and connections.

#### 4.5.1.1. Scenario description

In this subsection we present the scenario where our system is proposed and the sensors were calibrated. First, we describe the system and its operation. Then we detail the how we test the sensors for the calibration.

The proposed system is able to change the feed supply velocity according to the data gathered by the fish presence sensors and feed falling detector. The system is composed by an automatic feeder tube, which allows to change the feed supply velocity, see Figure 4.54. Four different velocities can be selected, 100%, 50%, 25% and 5% of the usual feed supply velocity. The system always start to feed with the 100% of the velocity. During the feeding process the velocity will decrease according to the sensor signals. The system is controlled by the Arduino which is placed in the exterior of the tank.

The fish presence sensors are placed inside a Plexiglas tube as it was presented in (Parra et al., 2018c). A total of 9 sensors are located along the tank at different depths. The fish presence sensor is composed by LDRs that are able to detect the changes in the received illumination due to the fish moving. The first LDR, LDR 1, is placed at 5cm of the water surface. This is the area where the fish use to be during the feeding process. The second LDR, LDR 2, is located at 30 cm from the water surface. The rest of the LDRs, LDR 2 to LDR 9, are spaced 15cm. The Plexiglas tube with the LDRs is fixed to the tank walls in the same side where the feeder tube dispenses the feed. The Plexiglas tube is sealed in both extremes.

Finally, the feed falling detector is emplaced at the bottom of the tank in the drainage tube. This sensor is composed by a pellet detector sensors an illumination provided by a white LED. The First part of the drainage systems, which usually is composed by an elbow pipe will be changed by a T shaped one and add a Methacrylate separator in one of the shorter sides. Thus, the camera can have full vision of the drainage system without changing the water flow.

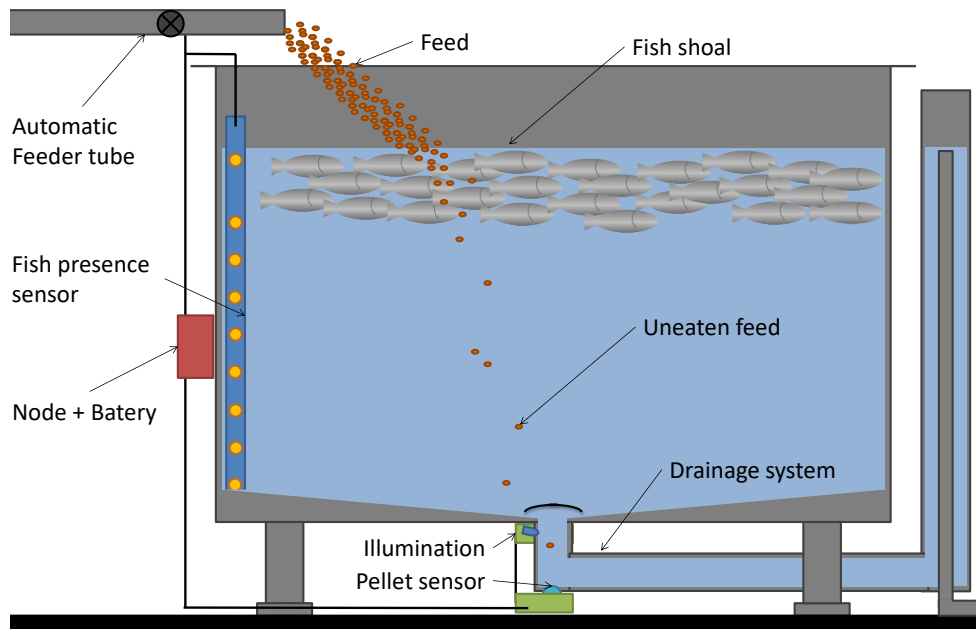


**Figure 4. 54** Proposed system for feed supply

#### 4.5.1.2. Node and sensors description

In this subsection, we present the employed sensors and the selected node are described. .

One of the main elements that forms this system is the control node in charge of monitoring the swimming height of the fish. As Figure 4.55 shows, to develop our control we use an Arduino mega 2560 Rev. 3 board. This board is based on the Atmega2560 microcontroller. It has 54 digital input / output pins (where 14 of them can be used as PWM outputs) and 16

analog inputs, 4 UARTs (hardware ports) and 16 MHz crystal oscillator. In addition, the board contains 256 KB of flash memory, 8 KB of SRAM and 4 KB of EEPROM. The board can be powered by batteries (which is our case) or with an AC-DC adapter.

The node 'operation is as follows. On the one hand, it is not necessary that the set of LDRs is always in operation; it is only required when the process of fish feeding is carried out. Therefore, when the feeder starts pouring food into the water, the node receives a signal to start monitoring. As the fish descends, the node will send different orders to the feeder in order to reduce the speed of food pouring into the water. In this way, the amount of food thrown into the water is adapted to the amount of fish available to eat it. The other important element is the OV7670 camera which controls the instant time the feed start to reach the floor. The OV7670 camera takes pictures with a Resolution of 640×480 VGA and presents a high sensitivity for low-light operation. Due to its low energy requirements, the OV7670 camera module suitable for embedded portable applications. Finally, this implies a lower waste of food which implies important economic improvements in the aquaculture production.

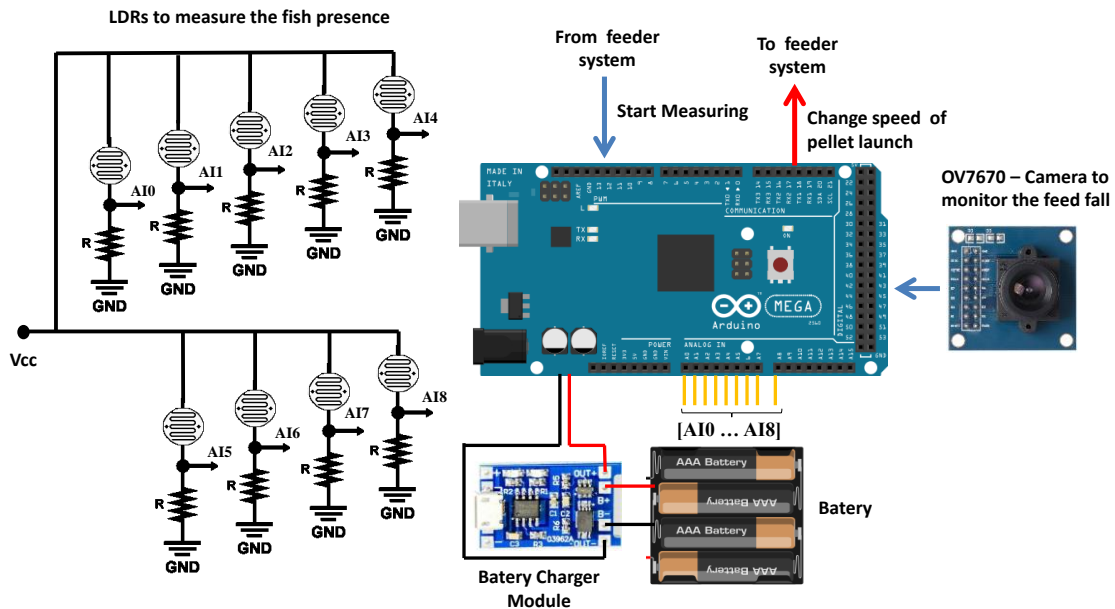


Figure 4.55 Control node description

## 4.5.2. Results and discussion

In this section, we are going to present the results. First, we show the tests done with the camera for feed detection. Then, the calibration of a system for locating the fish in the tank is presented. Following, the verification process of both systems is shown. Finally, we present the operation of the system during a feeding process in aquaculture tanks.

### 4.5.2.1. Calibration of the feed detection system

In this subsection, the calibration of the feed detection system is presented. We gathered 20 pictures without feed in the water and 20 pictures with feed in controlled conditions. The pictures have a size of 640×480 pixels. In order to obtain the histograms, the following code is used, see Figure 4.56.

```

x=imread('picture1.png');
red= x(:,:,1)
green= x(:,:,2)
blue= x(:,:,3)
L=0:1:256
bitcounts1=histc(red,L)
bitcounts2=histc(green,L)
bitcounts3=histc(blue,L)
R=sum(bitcounts1,2)
G=sum(bitcounts2,2)
B=sum(bitcounts3,2)

```

**Figure 4. 56** Code for obtaining the histograms

In order to find in which part of the histogram it is possible to identify the presence of feed in the water, we represent in Figure 4.57 the red histograms of the pictures with feed and, in Figure 4.58, the red histograms of pictures without feed. Figure 4.59 the green histograms of the pictures with feed and in Figure 4.60 the green histograms of pictures without feed. Lastly, Figure 4.61 the blue histograms of the pictures with feed and in Figure 4.62 the blue histograms of pictures without feed. From Figures 4.57 to 4.62 we can highlight the following items. First, the histograms of the pictures without feed are much more similar to each other than the pictures with feed. This is caused because the pictures without feed are almost the same. However, the pictures with feed can be very different. In some cases, as in the pictures 28, 31, 33, 34 or 35, the feed pellet cover almost the 20% of the picture. While in other cases as 21, 24, 26, 29 or 38 the pellet covers less than the 1% of the picture. Thus, there is a high heterogeneity in the pictures with pellets, which will difficult the correct detection of pellets in the pictures. The second idea to highlight is that in general terms, the red, green and blue histograms are quite similar. This is because the main part of the picture (the PVC tube) is dark grey and the water illuminated by the LED system is light grey. In the histograms of the pictures without pellets, we find two main groups of pixels. The first one is formed by pixels with values between 16 and 157. This part of the histograms represents the PVC tube. The second group of pixels has values between 182 and 205, which represents the water illuminated by the flash. Lastly, in Figures 4.57 to 4.62, we can observe that in the pictures with feed there are more pixels in the darkest tones, with low values of brightness (between 0 and 25) than in the pictures without feed. This pattern is found in the three colors. Nevertheless, the difference between the histogram with feed and histogram without feed is greater in the blue histograms.

The next step is to represent the summation of the pixels with lower values of brightness. The summation is done with pixels that present values between 0 and 15. The reason to select those values is due to the pictures without feed which, in general, have a low number of pixels with brightness values lower than 15. The pictures 1 to 20 represent the pictures without pellets that appear in Figure 4.57, Figure 4.59, and Figure 4.61. The pictures 21 to 40 are the pictures with pellets represented in Figure 4.55, Figure 4.60 and Figure 4.62. In Figure 4.63 we present the summation of pixels with low brightness values for red histograms. The summation for green and blue histograms are presented in Figure 4.64 and Figure 4.65. In Figures 4.63 to 4.65, we present the summation of the pictures with and without feed pellets. In Figure 4.63, it is possible to see that the pictures 1 to 20 have a mean value of 937 pixels with brightness values between 0 and 15. The minimum and maximum values in pictures 1 to 20 are 672 (picture 6) and 1219 (picture 4). On the other hand, the mean value in the pictures 21 to 40 is 5038 pixels. Picture 31 present the minimum values, 42 pixels. The maximum value of pixels, 41134 pixels, is found in picture 40.

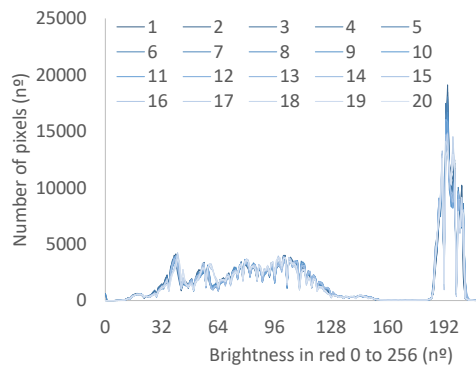


**Figure 4.57** Red histogram of pictures without feed

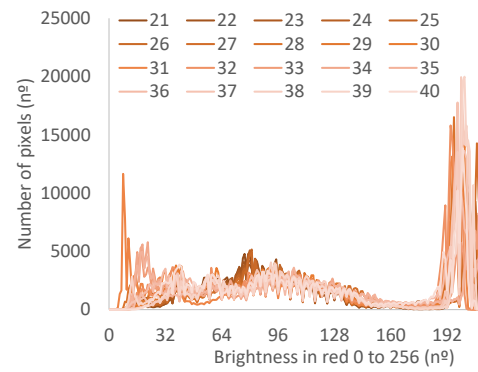


**Figure 4.58** Red histogram of pictures with feed

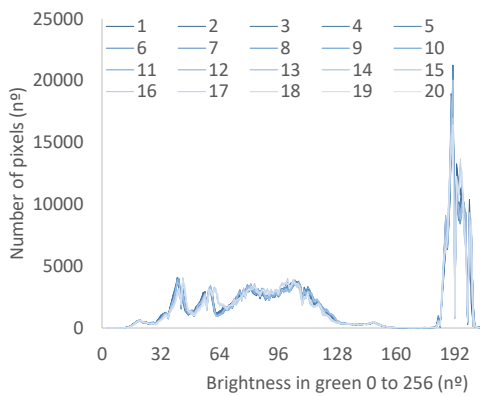


**Figure 4.59** Green histogram of pictures without feed

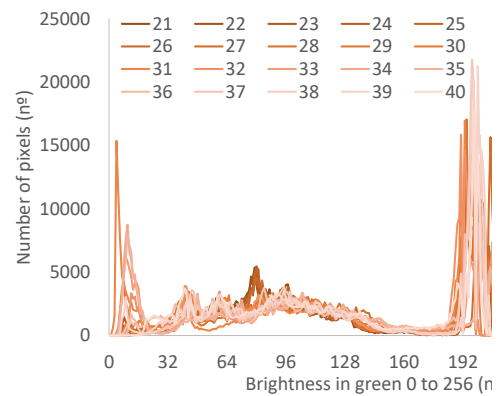


**Figure 4.60** Green histogram of pictures with feed

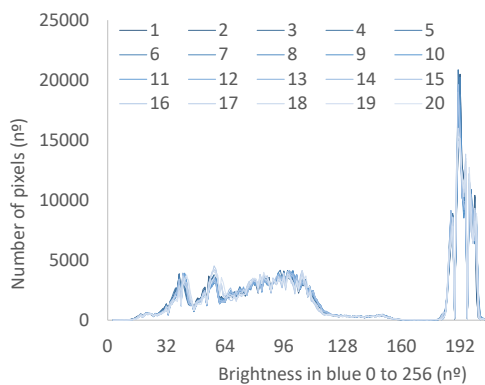


**Figure 4.61** Blue histogram of pictures without feed

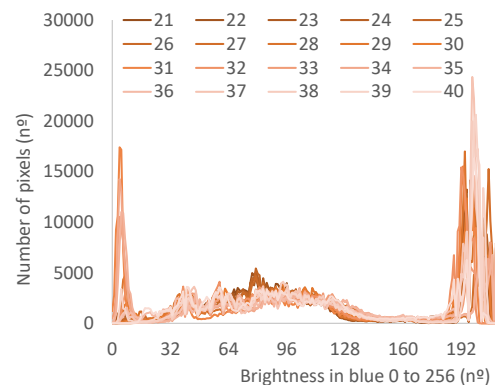


**Figure 4.62** Blue histogram of pictures with feed

Now, we analyze the data from Figure 4.65. In this case, the mean value of pictures 1 to 20 is 285. The mean value of pixels with brightness values between 0 and 15 in pictures without pellets in the green histogram is lower than in the red histogram. The minimum and maximum values in the summation are 154 (picture 20) and 349 (picture 5). Secondly, the pictures 21 to 40 present a mean value of 14645 pixels. The minimum value is found in picture 21 with 236 pixels and the maximum value in picture 31 with 62594 pixels.

Lastly, we present the summation of pixels with brightness values between 0 and 15 from the blue histogram in Figure 4.65. The mean value of pictures 1 to 20 is 279 pixels. The maximum and minimum values in the pictures without pellets are 105 (picture 20) and 473 (picture 2). On the other hand, the mean values of pictures 21 to 40 is 18228 pixels. Picture 40 is the one that presents the lower value, 683 pixels. On the contrary, picture 31 presents the maximum value of pixels with brightness values between 0 and 15, 74005 pixels.

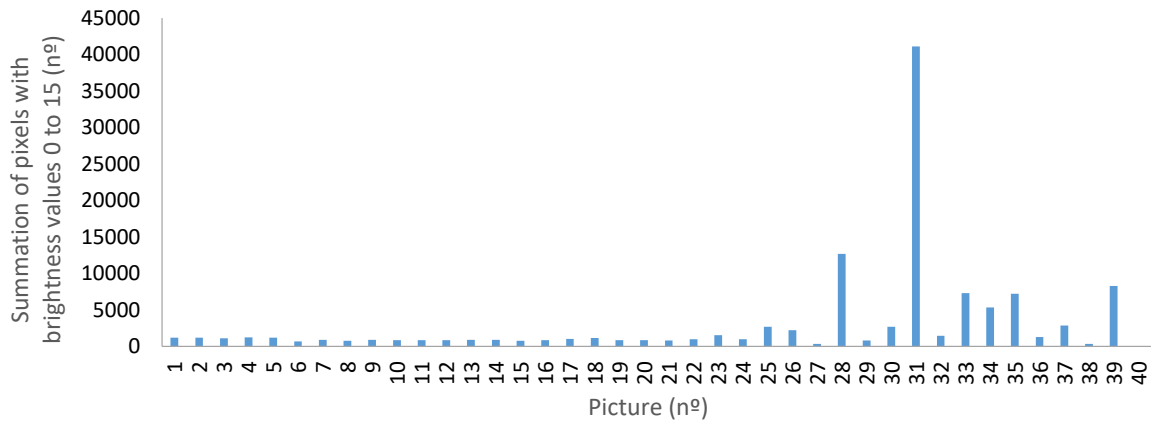


**Figure 4. 63** Summation of pixels with brightness values between 0 and 15 in the red histogram

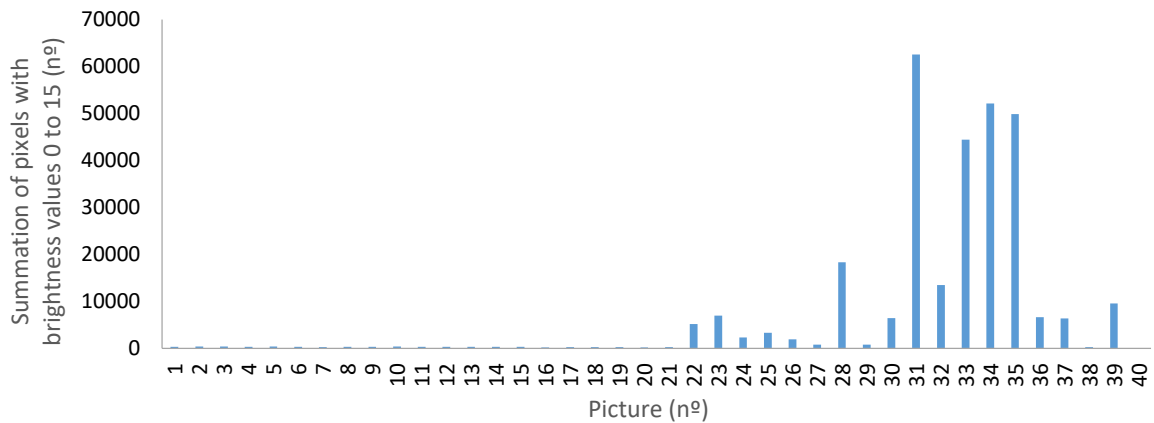


**Figure 4. 64** Summation of pixels with brightness values between 0 and 15 in the green histogram

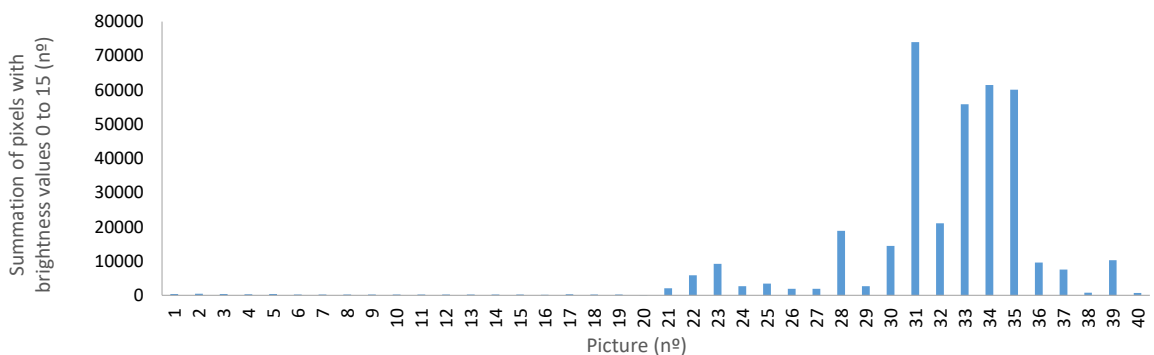


**Figure 4. 65** Summation of pixels with brightness values between 0 and 15 in the blue histogram

As the maximum differences are found in the blue histogram we use this histogram for further analysis with statistical software (STATGRAPHICS, 2017). The first test is a descriptive

analysis to confirm or diminish if the data follows a normal distribution. The data is divided into two variables. The variable A, represents the data from pictures 1 to 20 and the variable B the data from pictures 21 to 40. The descriptive analysis of variable A gives resulting skewness and kurtosis values of 0.876 and 0.417 respectively. Thus, it follows a normal distribution. On the contrary, the results of the test with variable B gives as a result 2.706 and 0.647 as skewness and kurtosis values. Therefore, the variable B does not follow a normal distribution. Consequently, to compare both variables it is necessary to use nonparametric tests. To compare the medians of both variables, the W of Mann-Whitney test is employed. The obtained p-value of this test is 6,77E-8, as it is lower than 0.05, the test concludes that the median of both variables is different. Then, the Kolmogorov-Smirnov is applied to compare the distribution of both variables. The result of the test is a p-value of 0. Thus, it indicates that the distribution of both variables is different. Finally, the Kruskal-Wallis test is done to diminish if the observed differences are due to the randomness of the data or it is because the data in both situations is statistically different. The result of the Kruskal-Wallis test is a p-value of 6,266E-8. As it is lower than 0.05, it indicates that the observed differences are statistically significant. Thus, the proposed system can be used to identify the presence of feed in the water. Based on the obtained values, we will consider as a threshold value, in order to decide whether or not there is feed in the water, a summation of 520 pixels. This value comes from incrementing in a 10% the maximum value of summation in the pictures without feed, picture 2, 473 pixels.

#### 4.5.2.2. Calibration of fish presence sensor

In this subsection, the calibration of the fish presence sensor is shown. This sensor is based on the use of several LDR placed along the tank. For the calibration of the sensor, a small aquaculture tank is employed. A juvenile of *Sparus aurata* is introduced in the tank and the values gathered by the LDR and the fish movement are recorded. After processing the video, we can identify the periods where the fish is in the area of the LDR. The data of the LDR during the test is presented in Figure 4.66. In blue, the voltage of the sensor ( $V_{out}$ ) in each second is represented. The periods when the fish are in the area covered by the LDR are marked in red. We can see in Figure 4.66 that in the periods when the fish is not present,  $V_{out}$  is lower than in the periods when the fish is present. When fish are not present, the values are similar but, when fish are present, the values present high heterogeneity. However, they are always higher than when the fish is not present. The data when fish are not present have a mean value of 1.390 V and a standard deviation of 0.021. The minimum value is 1.371 V and the maximum value is 1.467 V. When the fish are present, the mean  $V_{out}$  is 1.624 V, with a standard deviation of 0.096. The minimum value when fish are present is 1.479 V and the maximum is 1.853 V. As the maximum  $V_{out}$  in the fish presence is lower than the minimum value when the fish is present, it is possible to use this  $V_{out}$  to determine the presence of fish. Now, using the statistical analysis, we are going to evaluate if the values when the fish is present are different from the values when fish are not present. The first step is to assess if the data follows a normal distribution or not. We divide the gathered data into two variables, the first one, variable A, corresponds to the  $V_{out}$  values when the fish is present. On the other hand, the  $V_{out}$  gathered when the fish is not present is considered the data of variable B. Variable A has 46 data in total and, variable B, 55. The descriptive analysis of variable A gives resulting skewness and kurtosis values of 2.008 and 0.316. Thus, it does not follow a normal distribution. The results of the test with variable B for skewness and kurtosis are 6.3094 and 5.696 respectively. In order to evaluate if the observed differences are statistically significant, nonparametric tests must be used. With the W of Mann-Whitney test, we can assess if the medians of both distributions are different. The obtained p-value of the test is 0, as it is lower than 0.05, the test concludes that the median of both variables are different. Then, the Kolmogorov-Smirnov test is performed in order to compare the distribution of variables A and B. The result of the test is a p-value of 0,037. Thus, it indicates that the distribution of both variables are different. Finally, a Kruskal-Wallis test is done to

evaluate the differences in the variance of both variables. The test gives as a result a p-value of 0. Consequently, we can conclude that the differences found in the data when the fish is present and the data when the fish is not present are statistically significant and the sensor can be used to detect the presence of fish. Based on the obtained values, we will consider as a threshold value, in order to decide whether or not fish are present, a  $V_{out}$  of 1.467. In this case, it is not possible to increment in a 10% the maximum  $V_{out}$  in the pictures because the maximum  $V_{out}$  without fish presence is similar to the minimum  $V_{out}$  with fish presence. .

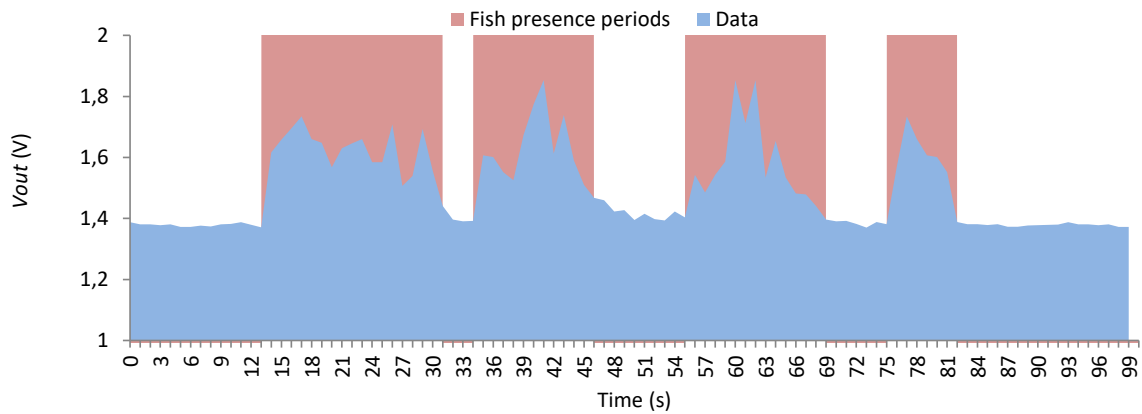


**Figure 4.66** Gathered  $V_{out}$  values in the calibration test

#### 4.5.2.3. Verification process

In this subsection, we detail the verification process for the two sensors developed in the previous subsections. Firstly, we will show the verification process of the feed sensors and then, the verification of the fish presence sensor.

For the verification of the feed sensor, 30 new pictures were used (see Figure 4.67). From these 30 pictures, 15 of them, from pictures 1 to 15, were taken without feed and the other 15, from pictures 16 to 30, were taken with feed. When the selection of the 15 pictures with feed is performed, pictures with a big area covered by the feed as in 21 and 28, and pictures with a small area covered by feed as in 20, 22 and 26, are sought. After applying the same methodology, obtaining the blue histogram and doing the summation of pixels with the brightness value between 0 and 15, the data shown in Figure 4.68 was obtained. In Figure 4.68, the blue bars indicate the summation of pixels with brightness values between 0 and 15 and, the orange line marks the threshold value established in section 4.1., being 520. The first idea that we want to highlight is that all the pictures are correctly classified according to the preset threshold value. The pictures without feed, 1 to 15, present a mean value of 205 pixels. The maximum and minimum values are 292 pixels and 108 pixels. On the other side, the pictures with feed have a mean value of 14427 pixels. Picture 26 presents the minimum value, 3153 pixels, and picture 28 presents the maximum value, 39112 pixels. If we compare the values in the calibration and in the verification test, we can see that, in general terms, the data from the verification test follows the same distribution than the data from the calibration test.

To facilitate the analysis of the distributions of pictures in both the calibration test and verification test, we represent in Figure 4.69 the box whiskers graphics. Firstly, we see the representation of the data from the calibration with and without feed and then, the data from the verification test with and without feed. In this graph, we can see a summary of the data distribution. Primarily, we want to highlight that, once more, the distribution of the data from the pictures without feed in both tests is almost the same due to the low heterogeneity of these



pictures. Moreover, from the distribution of the data of the pictures with feed, we want to foreground that only in the calibration test we found outlier values. The means of both tests are very similar both for the values of pictures with feed, 279 and 205 pixels, and for the pictures without feed, 18228 and 14126 pixels. In addition, the medians are similar, 251 and 218 for pictures without feed, and 8393 and 9658 for pictures with feed. We can note that the medians are much more similar than the means due to the outlier values. Finally, a Median test of Mood is done in order to assess if the medians of the variables from the four samples are identical or not. The result is a p-value of 0. Thus, we can conclude that the medians are different. Therefore, we can conclude that the verification test confirms that the proposed sensor can be used to differentiate the presence or absence of feed and the value of 520 pixels is an optimal threshold value.

Following, we present the verification process of the fish presence sensor. We repeat the same set up than in the calibration process. The data gathered in the verification test can be seen in Figure 4.70. Vout values are represented in blue and the periods when fish are present are indicated in red. The set threshold in section 4.3., 1.467 V, is shown as a black line. In general terms, we can see that the data from the verification test confirms the conclusions of the calibration test. From the 45 gathered values, 10 of them are gathered in the presence of fish. Those 10 values have a mean of 1.615 V. The maximum value is 1.802 V and the minimum 1.490 V. On the other side, the values gathered without the presence of fish have a mean Vout of 1.368 V. The minimum and maximum gathered values of Vout are 1.388 V and 1.354 V. After comparing the values of the calibration and the verification test, it seems that the data follows a similar distribution.

With the purpose of facilitating the comparison of the distributions of the gathered Vout in both the calibration and the verification test, we represent the box whiskers graphic of these data in Figure 4.71. We represent the data from the calibration test with and without fish presence and then, the data from the verification test with and without fish presence. The first idea that we want to highlight is that the distribution of the data from the verification and the calibration test gathered with fish is much more similar to each other than the data without fish. The means of the gathered Vout without fish are 1.390 V and 1.368 V for the calibration and the verification test respectively. On the contrary, the means of Vout with fish presence are 1.624 V for the calibration test and 1.623 V for the verification test. Moreover, the medians are also similar in the verification and calibration test. The medians of Vout with fish presence are 1.381 V and 1.369 V, and the medians without fish are 1.607 V and 1.602 V for the calibration and the verification test respectively. Finally, a Median test of Mood is done in order to assess if the medians of the variables from the four samples are identical or not. The result is a p-value of 0. Thus, we can conclude that the medians are different. Therefore, we can conclude that the verification test confirms that the proposed sensor can be used to differentiate the presence or absence of fish and the value of 1.467 pixels is an optimal threshold value.

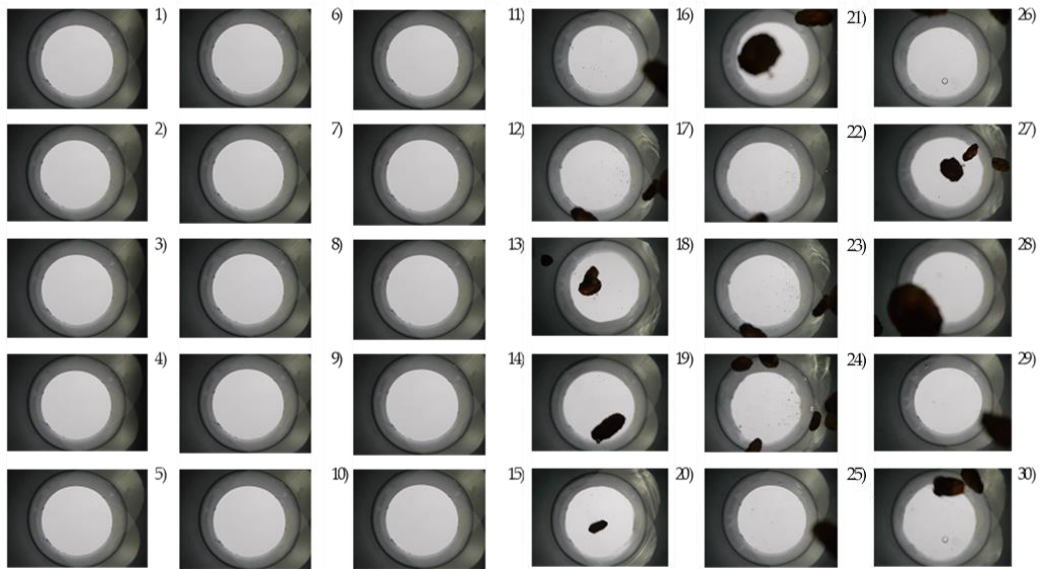


**Figure 4. 67** Employed pictures for the verification test

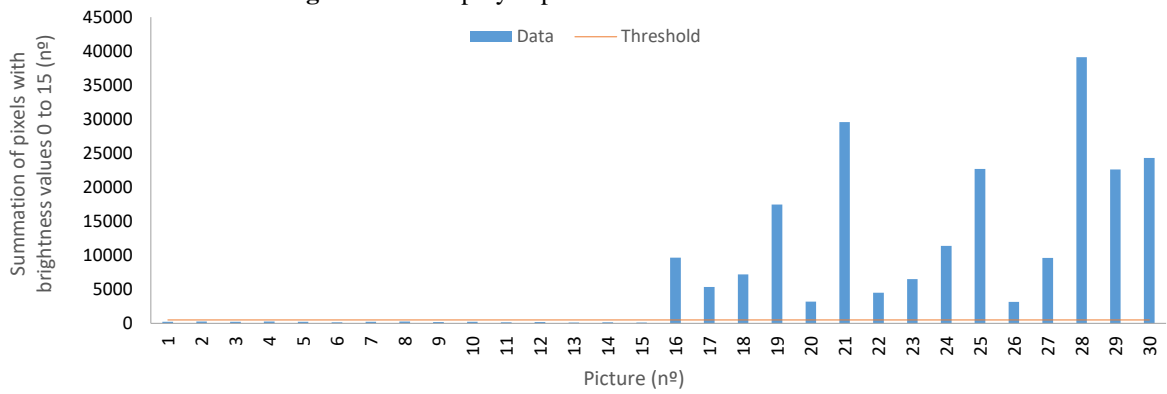


**Figure 4. 68** Summation of pixels with brightness values between 0 and 15 in the blue histogram in the verification test

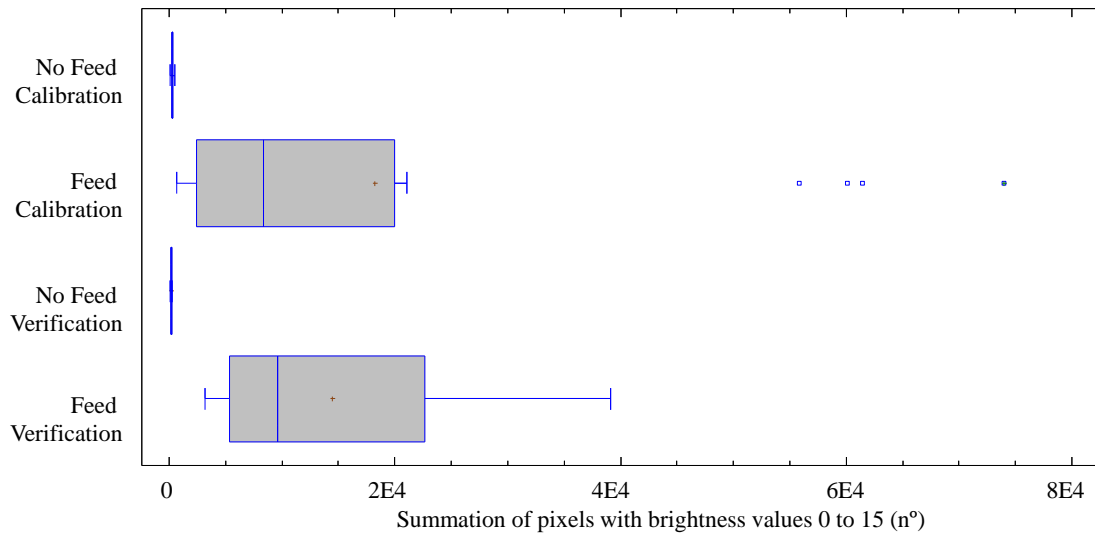


**Figure 4. 69** Box Whiskers graphic of summation of pixels with brightness values between 0 and 15 in calibration and verification test

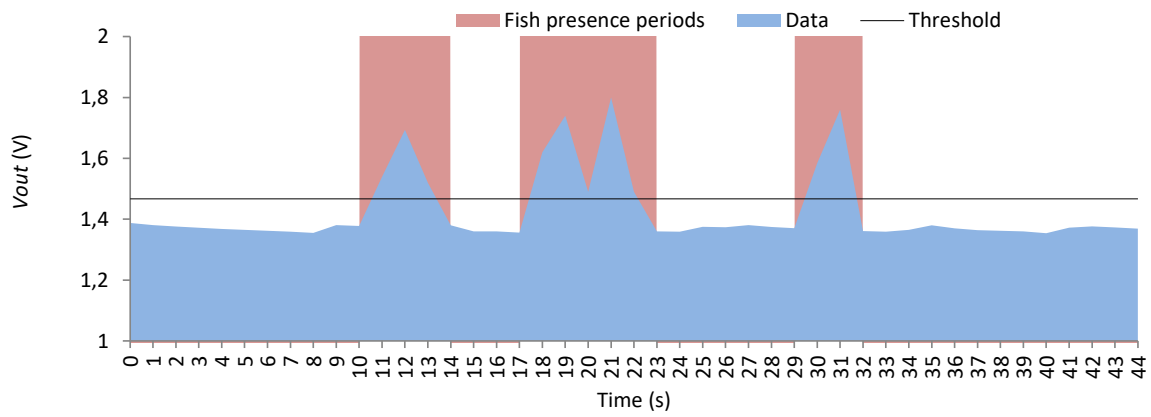


**Figure 4.70** Gathered Vout values in the verification test

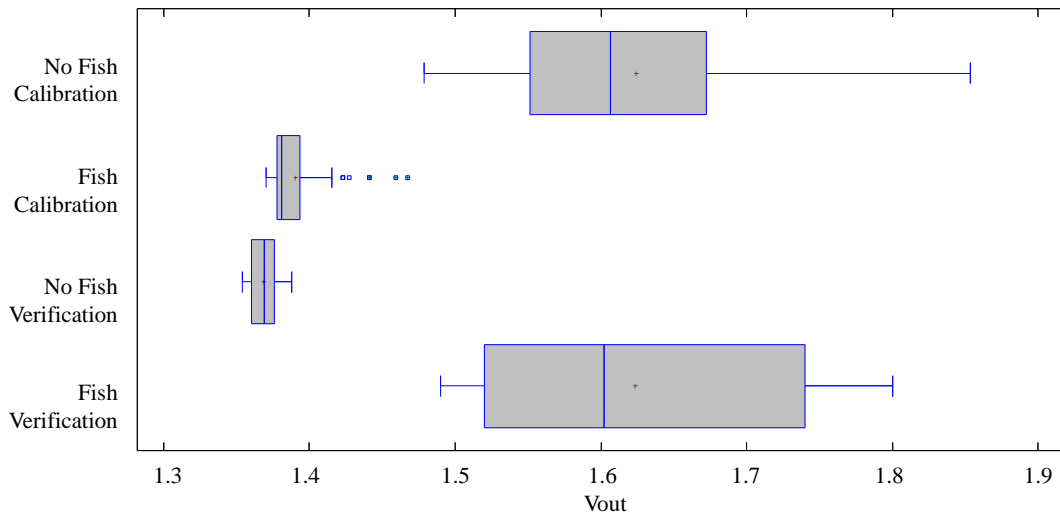


**Figure 4.71** Box Whiskers graphic of Vout in calibration and verification test

#### 4.5.2.4. Simulation of feeding process

In this subsection, we show the gathered data during a simulated feeding process. It is known that during the feeding process the fish shoal rises to the water surface to eat (AlZubi et al., 2016). Thus, when the feed process starts, the fish presence will change, and this change will be detected by the presence sensors. During the first minutes, the fish eats all the supplied feed. However, not all the fish eat at the same time and in the same way. The bigger and more aggressive fish are the first to consume the feed. A few minutes later, when those fish have satiated, the rest of the fish start to eat. At this moment, part of the feed may start to fall. Therefore, it may be necessary to reduce the velocity of feed supplied to avoid feed waste. Nevertheless, usually the feed is supplied with the same velocity all the time. Our system can detect the feed falling in order to reduce the velocity of feed supply.

For our system, the data from the feed presence and the feed falling is used. The purpose of using both data is due to the data of the fish presence indicating if they are eating or not. However, the data from the falling feed indicates the amount of eaten feed. Therefore, for an optimal monitoring, both data are needed. The data from fish presence acts as a trigger for turning off the system while the data from feed falling will trigger the changes in feed supply velocity, see Figure 4.72.

When the feeding monitoring system turns on, the first step is to define the order of the analog inputs 1 to 9, which represent from Vout 1 to Vout 9. The Vout 1 is the Vout of the LDR placed at 5 cm above the water surface. Then, the system starts to gather values from the LDRs. If the Vout 2 to 9 are lower than 1.467 V it means that the whole shoal is in the upper part of the tank and all of them are eating. Thus, the feed velocity must be maintained in 100% and new data must be gathered to continue with the monitoring. Nevertheless, when Vout 2 to 9 are higher than 1.467 V, it means that the whole shoal is not in the upper part of the tank and not all of them are eating. To be sure if all the supplied feed is being consumed, the feed falling system is turned on at 30 s. Then, the pictures are analyzed, is none of the pictures has a summation of pixels greater than 520 pixels it means that the feed is being consumed, no changes are done, and new data is gathered from the LDR. However, if any of the pictures present a summation of pixels higher than 520 pixels, it indicates that not all the feed is being consumed. Therefore, the feed supply velocity must be reduced to 50% of the initial velocity. Again, the data from the LDR is gathered, if the Vout 1 is higher than 1.467 V, it means that none one fish is in the upper part of tanks and we stop the feeding process. However, the expected situation is that some fish may still be eating in the upper part, resulting in the Vout 1 being higher than 1.467 V. After 1 minute, the camera system is turned on again for 30 seconds. If any of the pictures detect feed falling, the velocity of feed supply will change to a 25% of the initial velocity.

The same system described to change from 50% to 25% of the velocity is used to change from 25% to 5% of the initial velocity. The 5% speed is the slower velocity that can be offered by our system. In order to turn off the system, we use the variable of fish presence. At the moment, when the system detects that there are no fish in the upper part of the tank, the feed suppliers stop feeding. Moreover, the system sends all the gathered data and then, the system is turned off until the beginning of the new feeding period.

The system uses fish detection as the trigger because we need to ensure that all of the fish have the chance of eating the feed that they need in order to maximize the fish growth. And it is known that not all the fish eat at the same time. If we do not consider the fish position, our system will stop feeding before all the fish can be satiated. So that, a decrement on the fish growth will be caused causing a reduction in the productivity. On the contrary, if we only use the fish position for the monitoring system, we will not be able to know how to diminish the feed supply velocity and much more feed will not be consumed. Consequently, there will be a percentage of feed waste, which will produce a reduction in the profit of the fish production.

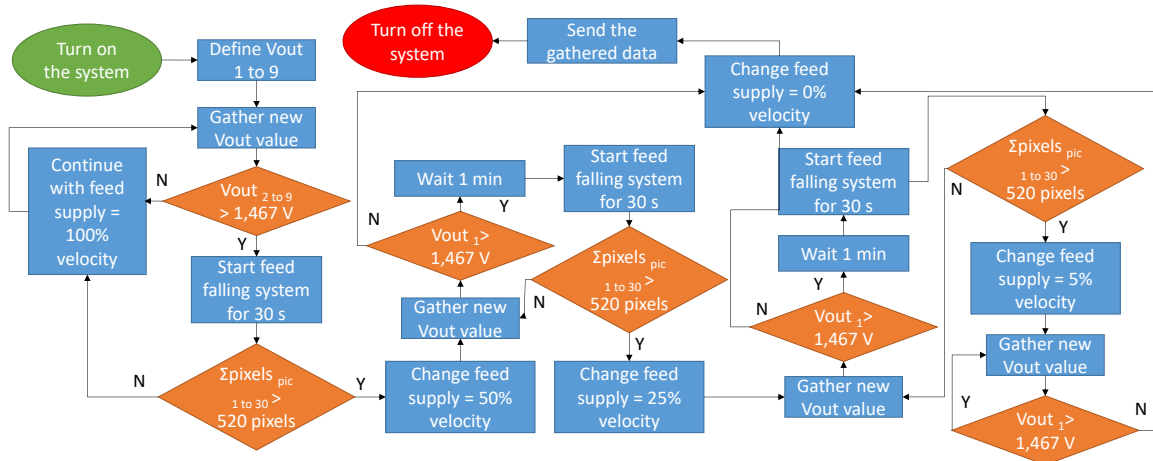


**Figure 4.72** Operation algorithm

Now we show the result of applying the algorithm to the data of a simulated feeding period, see Figure 4.73. We can see the data from the fish presence in Figure 4.73, feed presence (0 or 1)

and feed velocity (100% to 0%). The data from fish presence represents the typical feeding behavior during a normal feeding process. During the first part of the feeding process, all the fish are in the upper part and the Vout of the sensors 2 to 9 give values lower than 1.467. Then, the fish presence in the position 2 to 9 (Fish presence 2 to 9) is equal to 0. And the fish presence in the position 2 (Fish presence 1) is equal to 1 because the Vout of this LDR is higher than 1.467 V. Nevertheless, at second 450, some of the fish moves to the lower part of the tank. Thus, the Fish presence 2 to 9 is equal to 1. At this moment the camera system for feed detection turns on. During the first record, no picture shows a summation of pixels higher than 520, thus the Feed presence is 0. Therefore the feed velocity remains at 100%. After 1 minute, the camera test is repeated. In this case, the pictures reveal that there is feed falling. So that, the feed velocity decrease to 50%. At second 720, the camera detects again feed falling and the velocity is reduced to 25% and, at second 810, the feed velocity decreases to 5%. The feed period ends at second 990 when no fish are detected in the upper part of the tank.

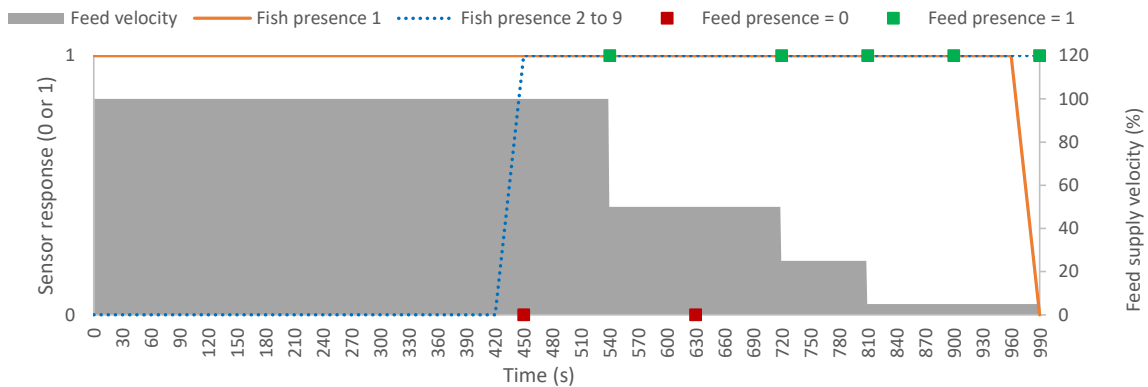


**Figure 4.73** Result of applying the algorithm to the data of a simulated feeding period

#### 4.5.2.5. Comparison with current systems

Currently, the systems to optimize automatically the feed supply in fish farms are very different from each other. First, we found systems with the purpose of determining the best moment to feed as (AlZubi et al., 2016) and (Bórquez-Lopez et al., 2018). Other systems are for on-demand feeding (Covès et al., 2006) or are used for feeding with plankton (Papandroulakis et al., 2002). There is one paper that uses falling feed as the only measure to decrease the feed velocity (Garcia et al., 2011). Finally, there is other proposed system (Atoum et al., 2015) that uses a combination of fish presence and feed falling for adjusting the feed velocity. Nevertheless, they use an overhead camera to determine the position of the fish. Thus, this system is not able to differentiate when the fish are in the upper part of the tank and are eating feed or when they are in the lower part of the tank and they are not eating.

The sensors and algorithm presented in this section suppose an improvement of the current methods for adjusting the feed supply to the fish needs. Moreover, the low cost of the employed components facilitates the possibility to implant this system in aquaculture tanks.

## 4.6. Conclusion

In this chapter, we have shown the different developed systems for fish farm monitoring. Our systems are able to measure water parameters and fish feeding behaviour. Moreover, the system can activate elements as water pumps or reduce the feeding supply velocity and even send alarms to the workers if abnormal situations are detected.

First, we show the design of a smart system for data gathering in aquaculture tanks using a WSN and its deployment have been presented. It has been specially designed for fish farms composed by tanks in land which should take water from two different sources.

It is required to control the water salinity in order to control the fish growth. The system allows the facility manager to increase or reduce the fish growth beyond the temperature changes to cover the market demands

The design and deployment of our system included the salinity sensor and the distance sensor description with their calibrations. We have also shown the wireless module operation, its program code to implement the different functions as well as how to store data in a DB. Finally, we have developed and explained an autonomous algorithm which is able to adapt the system operation to the environment conditions and tank status (water level and salinity value). To carry out the test of our system, real samples and real scenario were used. Regarding to the process of taking measurements, the proposed system presents stable values and during the sending data task the consumed bandwidth is low. This fact makes possible the use of a large number of wireless modules to cover a significant area without registering important delays in transmissions.

Our future work will be focused on using more secure methods for establishing the session between server and clients. In our following implementation, we will use SSL sockets. Moreover, we pretend to extend the use of our application for Wasmote and other well-known wireless modules.

The versatility of this server and the rest of the designed system allow the use of other sensors for monitoring different water parameters. Using some other sensor combination, this system could also be used to monitor fish activity in fish farms (Lloret et al., 2011b) and to automate water supplies for precision agriculture adapting some parts of this system.

Following, the design of a WSN for fish farms monitoring have been presented. All the parts of the network have been tested and shown. First, we have shown the turbidity sensor and the employed node. Then, the operating system is presented and the sealed box is tested. Next, the topology is shown. Finally, the network performance is evaluated and the appearance of the server and the alarms are exposed. The effect of changing the number of Flyports per AP is studied.

As future work, we will introduce authentication system to access to the server and other sensors as (Parra et al., 2015c) will be added to monitor the fish behaviour and other water parameters to automatize some process

In addition, a low-cost WSN for aquaculture monitoring has been shown. The system is able to control the changes in water parameters, tank state and fish behavior during the feeding process. The monitored water parameters are the temperature, conductivity, turbidity, and the presence of oil layer over the water. The tank state parameters monitored by the system are the illumination, the water level and the presence of workers. Finally the fish behavior is monitored with the fish swimming depth sensor and velocity sensor, and the sensor that let us know the amount of feed falling. The topology and architecture have been detailed. The low-cost sensors have been designed, calibrated and deployed. Smart algorithms were designed to diminish the use of energy in the data transference from the node to the database.

The sensors shown in this section can be used to improve the efficiency of the aquaculture and the cost of the entire described system is less than 90€. The sensors are composed by simple electronic components. All the sensors have been calibrated and their suitability for the aquaculture monitoring has been exposed. The greatest efforts have been done with the fish presence sensors and with the feed falling sensor. With the fish presence sensor, several tests were done. First, we performed tests to evaluate the suitability of LDRs to detect the presence of fish were done. Then, different tests were done to determine the presence of fish in different scenarios in order to calculate the fish depth and fish velocity. With the feed falling sensor, test in real scenarios were done in order to gather images of the water drainage system with and without feed. The results shown that with the blue band of the picture it is possible to distinguish the presence of feed with  $\sum RI$ .

As future work, we will estimate the data network requirements such as the number of APs needed in the production rooms. Moreover, we will study the way to send directly the alarm messages to the workers. In terms of sensors, we expect to create a low-cost dissolved oxygen sensor. In addition, with the implantation of this system, it will be possible to apply data mining techniques and artificial intelligence in order to predict the feed needed in each tank. We are

planning to develop the platform to view the data as it was shown in (Khaleeq et al., 2016) with LabVIEW and include the artificial intelligence for diagnosis with the data from the database as it was done in (Chen et al., 2017). We also plan to apply this system to underwater cages as it was done in (Cario et al., 2017)

To close the section, a system to adjust the feed supply velocity was presented. The sensors shown in this section can be used to improve the efficiency of the aquaculture feeding process. The sensors are composed by simple electronic components and can be connected to an Arduino node. The calibration has been shown and the threshold values for detecting fish and feed presence have been found. Moreover, a verification test was done in order to ensure that the threshold values set in the calibration are acceptable. Both verification processes show that the calibrations were done correctly. In addition, we show the operation of the proposed system during a simulated regular feeding process.

As future works, we want to test our fish presence sensor with other fish species. Moreover, we want to test the system for larvae fish, considering no systems are developed to adjust the feed due to the small size of fish and the small size of feed. In addition, we plan to use other light sources as color LEDs to illuminate the drainage system where the pellets are detected in order to evaluate the possibility to differentiated pellets from faeces. The option of use different light sources to differentiated substances in the water have been already used for turbidity (Parra et al., 2018b)

Finally, work presented in this chapter has been published in the following references (Parra et al., 2017), (Rocher et al., 2017), and (Parra et al., 2018c).

## **5. IMPLEMENTATION IN OTHER ENVIRONMENTS**



## 5.1. Introduction

In this chapter, we are going to present the implementation of our developed system in other natural areas. Due to the creation of low-cost sensors and low-cost WSN it was possible to apply this new devices to other environments. During this thesis it was founded a need of monitoring in different endangered or protected aquatic environments. As a results three different proposals appear, the first one for monitoring estuaries, the second one for monitoring the ocean climate and the final one, an intelligent system to track marine pollution.

First, we want to describe the problems in the mangrove forest. Mangroves are the tropical forest systems which are most probably intensively exploited and degraded by human action. As Figure 5.1 shows, in last 25 years, the mangrove lands, located in the "Ciénaga Grande de Santa Marta" (Colombia), have been reduced alarmingly, turning this land into pasture land or soil without any use. Mangroves are the object of many research projects focused on their conservation. This kind of trees is very useful in natural disasters such as tsunamis and they are often used for raising shrimp and fish culture. But nowadays, the population of mangroves is dramatically decreasing because of the increment of salinity in water. The critical salinity level in mangroves depends on each species but generally, salinities higher than 16 ppm (parts per million) make impossible the growth of new individuals (Ye et al., 2005).

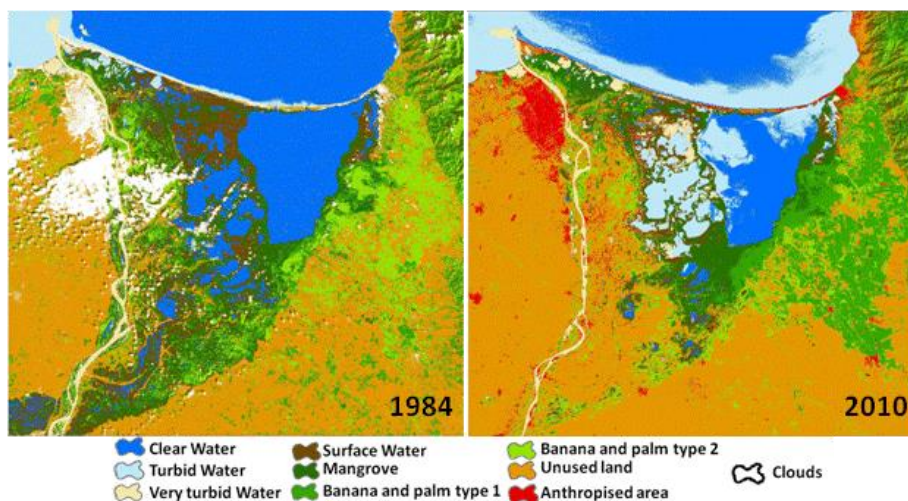


Figure 5. 1 Evolution of mangrove forests between 1984 and 2010.

Thus, in this chapter we present the design and deployment of a smart system for data gathering in estuaries using WSNs. The system is based on a WSN that monitors the outflow plume of a river and send data gathered to a server. Each node has a conductivity sensor which deployment is shown in this section in order to monitor the advance direction of the outflow plume. The server saves the data in a Database (DB). All developed parts, both wireless communication and conductivity sensor, are tested with real samples in real scenarios.

In addition, the monitoring of the climate in the open sea is usually performed with buoys. Those buoys include several sensors with high price. Moreover, the communication is usually done with satellite technologies. With the climatic change it is very important to have cheap options for long term monitoring. It is important to monitor the oceanic climate including the meteorological variables of temperature, wind, rain and solar radiations among others. On the other side, one of the problems related to the climate change is the melting of the ice in the poles (Perovich et al., 2007) and (Markus et al., 2009). For this reason a salinity sensor must be included in this ideal system for climate change monitoring. The changes on water temperature can produce alterations in the ecosystems producing cyanobacteria blooms (Paerl and Huisman, J. (2009) and (O'neil et al., 2012). Thus, turbidity sensors should be added to the buoy.

In this chapter, we are going to present the design of an oceanographic multisensor buoy for ocean monitoring in the Mediterranean Sea. The system is based on 2 set of low-cost sensors that are able to collect data from the water, such as salinity, temperature or turbidity and from the

weather, such as temperature, relative humidity or rainfall among others. The system is held in a buoy which maintains the system isolated from the water to avoid possible problems of oxidation. The data gathered by all sensors are processed using a microcontroller. Finally, the buoy is connected with the base station through a wireless connection using a FlyPort module. The whole system and the individual sensors have been tested in a controlled environment. This proposal could be used for monitoring other areas with special ecological interest and for monitoring and supervise several aquaculture activities. Systems like these ones are used to monitor other underwater environment and threats. In Facility for Automated Intelligent Monitoring of Marine Systems (FAIMMS, 2014.), authors use a system to monitor coral reefs in Australia. In addition, we add a hydrocarbon detection system to the buoy to use this system to control the possible accidental discharges of fuels in the sea.

Moreover, in marine environments, there are different kinds of contaminants that can appear due to ships' accidents, problems in floating structures or products from the land. In spite of the huge capacity of oceans to dilute and disperse the pollution, according to National Geographic (2015), our oceans are at the end of the dilution era.

There is a vast variety of pollutants from inert materials such as plastic or organic pollution (i.e., hydrocarbons or particulate organic matter). The increase of nutrients due to spills can also be considered as pollution. Due to the oceans' high size and the low presence of human beings in open oceans, it is necessary to have a remote way to monitor and detect the presence of pollutants, as well as, to control the water quality. The effect of pollutants depends on the kind of pollutant, the affected area, the removal chance and the time period that this pollutant remains in the affected area. Some of these pollutants affect just a specific group of beings. This is the case of plastic bags for marine turtles that often mistake them for jellyfish and other foods (bags can cause the turtles' death). On the other hand, pollutants like oil spills usually affect to all the beings living in the polluted area.

Fortunately, hydrocarbons can be easily removed from the environment due to its polar properties that make that it does not mix with the water. However, the hydrocarbon spills usually spread quickly and the thickness of the spill is a crucial factor in the decontamination tasks (Denkilkian et al., 2009). Because of this, the rapid detection and tracking of the spill is an important challenge. Traditionally, the detection systems were based on remote sensing. But nowadays, the use of Wireless Sensor Networks (WSN) offers more feasible and useful options (Bri et al., 2009), (Garcia et al., 2010). Different sensors and systems have been developed for hydrocarbon detection as (Denkilkian et al., 2009) and (O'Connell et al., 2011). In recent years, several authors have presented different solution and specific protocols to detect spills and water pollution (Chen et al., 2014), (Harchi et al., 2012). However, current systems do not still have high accuracy and fast location. In contrast to remote sensing systems, the main advantage of WSNs is that they allow knowing the thickness of the spill in addition to the location.

One of the worst problems to remove the hydrocarbon spillages is that hydrocarbons tend to disperse and mix with the water. This dispersion complicates the chance of removing the pollution. As soon begins the decontamination task more efficient will be and more amount of contamination can be removed. While some pollutants affect only one specific animal the hydrocarbon effects can be seen in all the species of the polluted area (Hidalgo et al., 2009):

- Hydrocarbon creates an impermeable layer over the water that avoids the gas exchange between water and atmosphere.
- Oil layers reduce the incident light, affecting the photosynthetic capacity of the phytoplankton
- Birds have several problems such as intestinal problems and skin irritation, among others.
- Fishes death by asphyxia because of their skin and gills are covered by the hydrocarbon.
- Marine mammals are covered by hydrocarbon which causes the loss of their floating capacity.

The use of satellite images is the most common way to detect the spills and determine its dimensions. However, the temporal resolution of some satellite images and the time that takes it to arrive at the interested person are not good enough. To avoid higher damages and increase the

effectivity of decontamination tasks, the detection must be fastest as possible. Because of this, the use of other technology to detect the presence of spillages is needed. The use of sensors has demonstrated to be a feasible option for water quality monitoring.

In addition, we propose a smart system based on a mobile WSN, where sensor nodes detect, track and locate pollution stains. Nodes are small ships provided with a solar panel to power the system, which is placed inside the polluted area and move till the boundary of the polluted area by using intelligent algorithms. After some time all sensor nodes will be delimiting the pollution stain.

Although there are different applications for hydrocarbon detection, the one that we propose in this chapter supposes several improvements. For example in (Chen et al., 2014) the immobile nodes just give an approximated idea of there is the pollution but is impossible to have detailed information about its size or exact position. Moreover, the limited number of nodes and their fixed position can easily lose the pollutions if the ocean currents move the pollutions out of the sensors area. Our system will use ZigBee technology for its communication as (Harchi et al., 2012), (Alkandari et al., 2011), (Rasin et al. 2009), (Yue and. Ying, 2011) due to its low energy consumption and its high coverage. Only in (Yue and. Ying, 2011) authors use energy harvesting techniques for increasing the time that the system can be operating. Our system has also solar panels in order to have a system for long-term monitoring. No one of the related work presented has any smart protocols; the majority of them have cluster architecture while our proposal has different architectures. Finally, of all the related work just two of them (Chen et al., 2014) and (Harchi et al., 2012) are deployed when the pollution is detected the other (Alkandari et al., 2011), (Rasin et al. 2009), (Wang et al., 2009) and (Yue and. Ying, 2011) are left to monitoring a specific area. In our proposal, the nodes are deployed once the pollution is detected. We propose an intelligent system based on a mobile WSN that uses a smart algorithm for detecting, tracking and locating pollution stains.

The rest of section is structured as follows. Section 5.2 shows the different efforts done to apply WSN for estuaries monitoring. Section 5.3 presents a proposed system for climate monitoring in the ocean. An intelligent system for detecting and tracking pollution in the sea is detailed in Section 5.4. Finally, Section 5.5 shows out conclusions.

## **5.2. Proposed System for estuaries and mangrove forests**

### **5.2.1. Proposed system**

To solve the problem of outflow plume monitoring and the changes of salinity in mangroves, we propose the use of a WSN composed of wireless conductivity nodes in the mouth of a river (see Figure 5.2 (a)) at different distances. These nodes are wirelessly connected between them and a node placed on the mainland. In each Flyport we connect several salinity sensors, depending on the height of the water column. We include 1 salinity sensor each 50 cm. In section 3.2.4.3.7 we conclude that the area that one coil can measure have 48 cm heigh.

Moreover, we propose to use this low-cost conductivity sensor formed by two coils to measure the salinity of the land by the interaction of the magnetic field in the water. Wireless nodes are implemented using Flyport modules (Flyport features, 2016) that allow the implementation of wireless sensors networks. Our network consists of a set of wireless sensor nodes scattered in the mangroves (See Figure 5.2 (b)) which send the water information to a server that controls the floodgates (See Figure 5.3). Figure 5.2 (b) shows the deployment of the VLANs along the last kilometers of the Rio Magdalena and the surrounding mangrove forest. In each VLAN we use several Flyports, depending on the terrain, that monitores the water conductivity. Each VLAN has a radius of 2Km. In each Flyport, we connect two salinity sensors that monitores the salinity level in the water surface and another one that measures the saline conditions in the bottom.

This section shows the main characteristic of our proposed system and how to visualize

the monitored data.

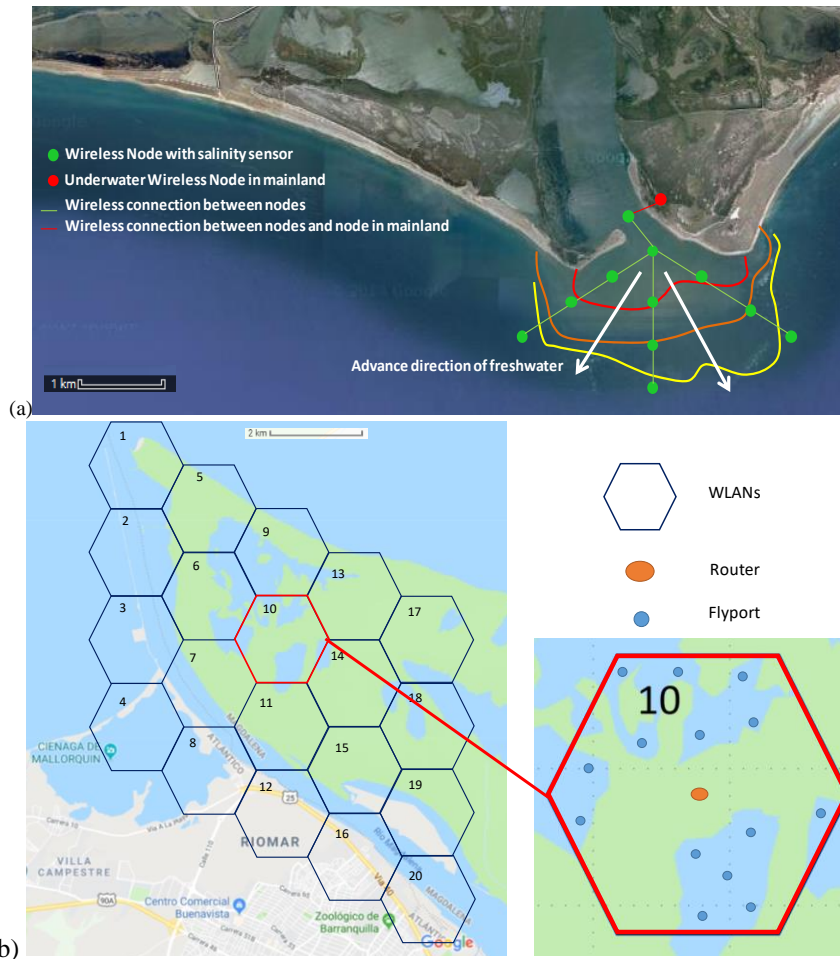


**Figure 5. 2** Estuary and mangrove with a WSN for salinity monitoring

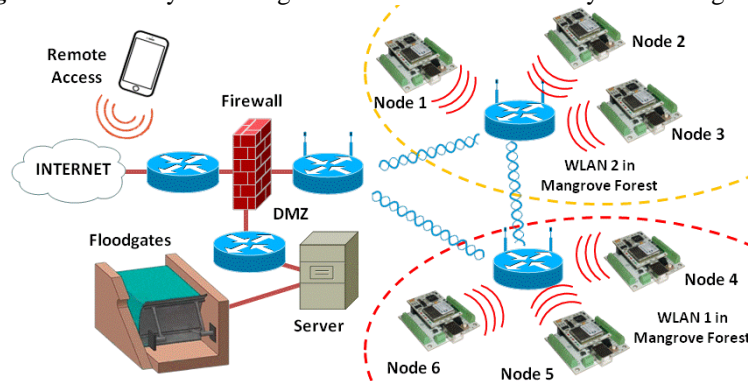


**Figure 5. 3** Network topology for mangrove monitoring

### 5.2.1.1. Salinity Sensor

Most of the conductivity sensors are based on the electrical resistance offered by the water to an electric current. However, we can find conductivity sensors based on an inductive process. The value of induced voltage is related to the water conductivity. In previous papers (Parra et al., 2013a), (Parra et al., 2013 b), (Parra et al., 2013c) we presented several studies in order to develop low-cost conductivity sensors based on induction process. In this case, we have created

a prototype (See Figure 5.4) with the characteristics shown in Table 5.1. Our prototype is based on two coils coiled over a plastic pipe.



**Figure 5. 4** Conductivity sensor

**Table 5. 1** Coils Features (I)

<i>Parameter</i>	<i>Value</i>
Copper wire diameter	0.4 mm
Pipe diameter	25 mm
N° of spires in the powered coil	40
N° of spires in induced coil	80

The most important thing is to know what the working frequency is where the maximum voltage difference as a function of water conductivity is obtained. We measure the induced voltage at 4 different frequencies (from 250 kHz to 1000 kHz). The coil is powered at 8V. The prototype is submerged in three samples with different conductivities, from 32 mS/cm to 58 mS/cm, at a temperature of 7.5 °C. The induced voltage is measured using an oscilloscope. Results are shown in Figure 5.5.

As we can see, the frequency where the sensor is able to differentiate between conductivities is 425 kHz. For the rest of frequencies, the variation of induced voltage with different salinities is almost inappreciable. So, our conductivity sensor will work at 425 kHz.

Once the best working frequency is determined, the sensor should be calibrated. The calibration is performed using several samples of different conductivities and a commercial conductivity device to check the correspondence of our samples. From the obtained values, we can obtain a mathematical equation that relates the induced voltage with water conductivity. These measures were performed using the Flyport module. The FlyPort is configured to send data every 5 seconds. At the end of the testing time, the server is stopped and the values of analog input are stored in our DB. The test was performed during 200 seconds with several repetitions. Figure 5.6 shows the results of the calibration process. In this case, each value represents the average value of these measures gathered for each conductivity value. The lowest conductivity is 0.558 mS/cm which corresponds to 0.43 V. The highest conductivity is 86.7.5 mS/cm which offers an output value of 2.90 V. This calibration has been performed at 28.5 °C. In addition, salinity depends on water temperature, for this reason, we need to add in our mathematical expression a factor to compensate the temperature. The mathematical equation that relates the output voltage and the water conductivity is modeled in Eq. (5.1).

$$V_{out} = (0.5087 * C^{0.4004}) - 5 \quad (5.1)$$

Where  $V_{out}$  is expressed in volts and represents the output voltage induced in the second coil and  $C$  is the water conductivity in S/cm.

#### 5.2.1.2. Wireless module

The proposed system uses a wireless module called FlyPort. It is a programmable compact Wi-Fi module based on the open source platform openPICUS. This module is 5V powered. It is based on the Certified Wi-Fi Transceiver 802.11g Microchip MRF24WG0MB module and 16-bit low power microcontroller Microchip PIC24FJ256 Processor, with 256K Flash, 16K Ram, 16MIPS @ 32Mhz. The advantage of this device against many other wireless nodes is its versatility in programming and wide application range. This module is composed of two parts. The first one has the Wi-Fi module, formed by the transceiver and the processor, as well as different input/output, buses, etc. The second part is the programmer board called

USB Nest.

The main function of this device will be the generation of the sine wave used for feeding our transducer and the acquisition of the resulting signal. As Figure 5.7 shows, the sensor node generates a PWM signal from which we obtain a sinusoidal signal used to power the transducer. The PWM signal needs to be filtered by a band pass filter (BPF) in order to obtain the sinusoidal signal as we know it. Once PWM signal is generated by the microcontroller, it is necessary to filter this signal by a BPF with the center frequency at 150 kHz in order to obtain the desired sine wave. For this design, the BPF was performed by two active Sallen-Key filters of second order configured in cascade, i.e., a low pass filters (LPF) and a high-pass filter (HPF). The cutoff frequencies are 160 kHz and 140 kHz respectively (see Figure 5.8). PWM is generated by the wireless module. The system is initialized to work at 150 KHz. After that, the system generates a width variable pulse which is repeated with a frequency of 150 KHz.

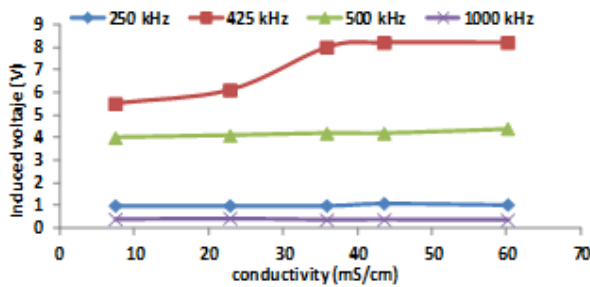


Figure 5. 5 Induced voltages at different conductivities

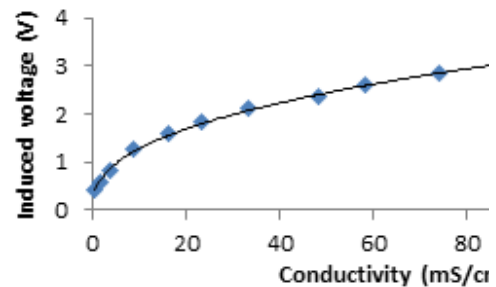


Figure 5. 6 Calibration results

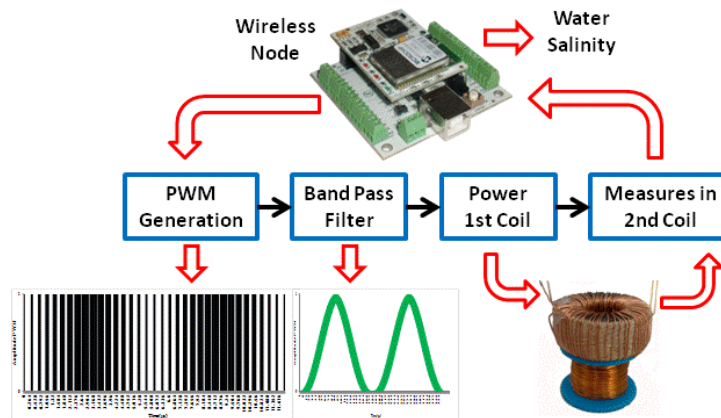


Figure 5. 7 Salinity node architecture

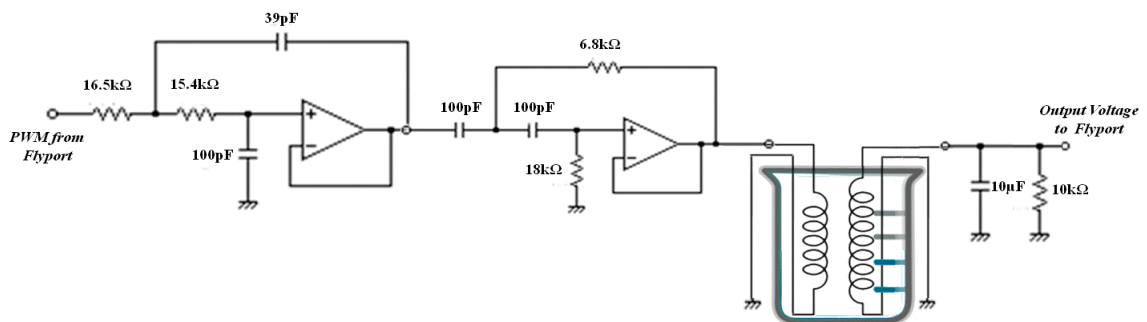


Figure 5. 8 Electronic design of our low-cost salinity sensor

### 5.2.2. Server deployment for data gathering

In order to collect data, we need a server to request to the node this information and store it to process and make decisions for them. For this reason, we have developed a Server application in Java able to store the information from sensors in a database (DB). In this case, we have selected the connection of devices using sockets. The connection of two devices through sockets is a very simple method to exchange information while it is very useful and versatile. After the connection is established, the server request data to the client. When a client has already finished the sending data, the client sends a packet for informing about this status. After that, the connection is closed and the server waits for new connections. (See Figure 5.9).

The server application is developed in Java and its operation is very simple. The server configuration is divided into two steps. Firstly, the user should configure which port the server is going to use for establishing the connection and exchange data (by default, the port number is 8080) and the inputs used. Secondly, the user should choose the path where the data in \*.csv format is going to be saved. When a new module is connected to the server, the server automatically creates a new file for the new module. This new file is stored in the same path that the user previously chose.

Flyport Module also needs a specific programming. Figure 5.10 shows the program code for Flyport module.

In this case, our module is working as a TCP client. The code shows how to configure the analog inputs used in our system and how to create a socket connection as a client. As we can see, when the system requests to the server a connection, it waits for the server reply. After the connection is established, the data is sent to the server through a specific port. In this case, port 8080 is used. Finally, it is possible to configure the number of values that should be stored.

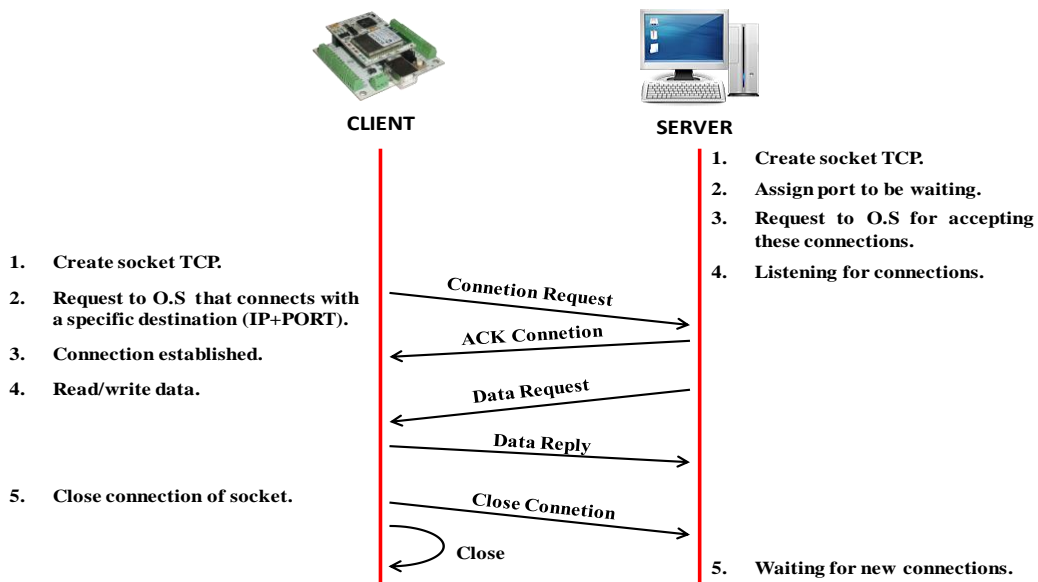


Figure 5. 9 Socket connection between client and server

### 5.2.3. Real Measurements and network test

To ensure the effectiveness of our proposed systems, several tests were performed. They were developed using a FlyPort wireless module. The induced coil is connected to an analog input of the FlyPort who is in charge of gathering data.

Equation 1 is introduced in our application for interpreting the values in a correct way and to implement a salinity control system for water irrigation. During the testing time the values in

real time can be seen through the OpenPicus Flyport IDE software (See Figure 5.11). To make easier the interpretation results, we developed a web interface able to show the current value of sensors as well as the historical data stored in the last 24 hours (See Figure 5.12). The last step was to check the consumed bandwidth by one wireless node when it is transmitting the data gathered to the server. To perform this test, we have captured the network traffic during 200 sec. Figure 5.13 shows the consumed bandwidth in bits/s when a wireless node is working. As we can see, there is a first stage (up to 35 seconds) when the node is establishing the connection with the server. After that, the consumed bandwidth remains stable around 10000 bits/s. Defining the bandwidth consumed by a node, we can know the number of nodes that can be used in our network without high delays.

<pre> void FlyportTask() { TCP_SOCKET sock = INVALID_SOCKET; int cnt =0;     BOOL flagErr = FALSE; // Flyport connects to default network WFConnect(WF_DEFAULT); while(WFGetStat() != CONNECTED); while(!DHCPAssigned);     vTaskDelay(25);     UARTWrite(1,"Flyport Wi-fi G connected...hello world!\r\n"); //Connects the TCP Client to the server sock = TCPClientOpen("192.168.2.3","8080"); char name[]="Sensor name\r\n";//Choose a sensor name int delay=1000; //Enable analog inputs to be used BOOL analog1= TRUE; int adcValue1 = 0; char uart_msg1[30]; </pre>	<pre> while(!TCPisConn(sock)) { //Timeout function if(cnt==10) { flagErr = TRUE; break; } vTaskDelay(50); cnt++; } if(flagErr){ UARTWrite(1,"\r\nTimeout error...\r\n"); }else{ TCPPutString(sock, name); // sending the name while(TCPisConn(sock)) { if(analog1){ adcValue1 = ADCVal(1);//value from ADC channel 1 sprintf(uart_msg1, "%d\r\n", adcValue1); TCPPutString(sock, uart_msg1); UARTWrite(1, uart_msg1); //write on the Uart port } DelayMs(delay); //1000 = 1 sec }} </pre>
---	---

**Figure 5. 10** Program code for Flyport configuration as Socket Client

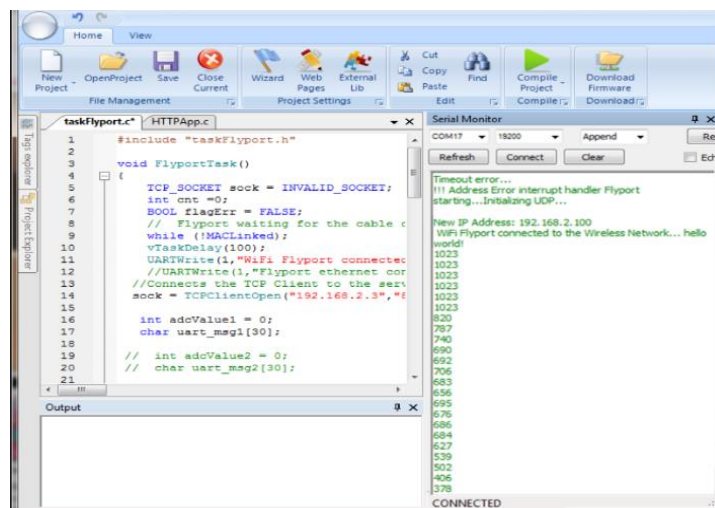


**Figure 5. 11** Flyport IDE during test



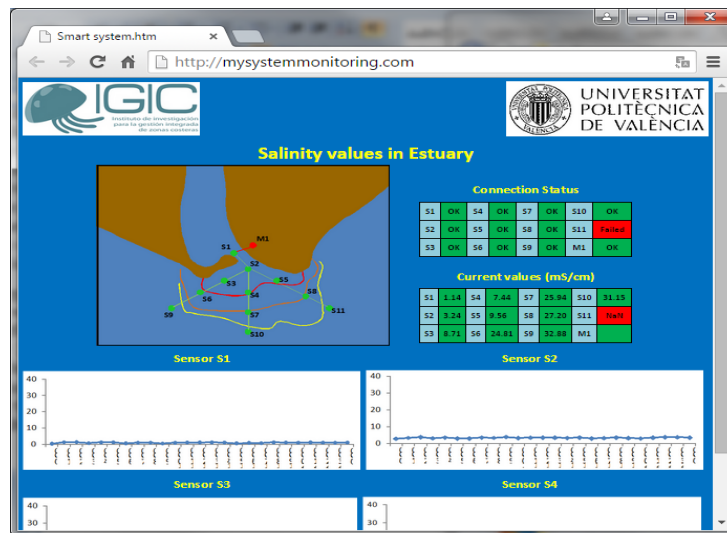


Figure 5. 12 Web interface

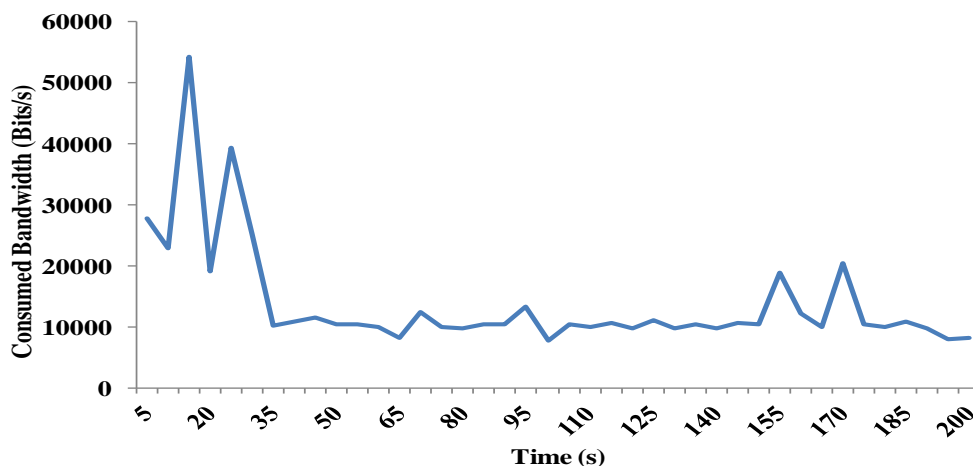


Figure 5. 13 Consumed bandwidth in bits/s

### 5.3. Application of the WSN for oceanic climate monitoring

#### 5.3.1. Proposal Description

The main aim of this section is to develop a multisensor buoy able to collect meteorological and marine parameters and send them to a base station placed in the marine port or mainland. This section explains the main parts of our multisensor buoy as well as the wireless node used to implement our network and where the sensors will be placed in the buoy.

##### 5.3.1.1. Multisensor buoy

The buoy consists of a plastic part or float which provides sufficient buoyancy to the whole system and a fiber structure, which will be in charge of containing all electrical and electronic components, and the battery (See Figure 5.14). The interior of this structure is easily accessible through a small door in its exterior side.

Moreover, the float (See Figure 5.15) has a longitudinal opening that traverses the entire object. Within this opening, the sensors are placed in non-metallic structures. The sensors are always submerged in the water because the buoyancy capacity makes to place the waterline above the sensors. There is an opening to allow the water flow and its exchange without

problems and to avoid the stagnant water. The main reason for locating sensors in this part is to keep them protected against shock and other problems.

Our multisensor system comprises two groups of sensors. The first one is responsible for collecting meteorological parameters such as rainfall, temperature, relative humidity, solar radiation, etc. The second group of sensors is located under the water and they collect data about water conditions. In our case, the system takes measurements of temperature, salinity, turbidity, and presence of fuel.

All sensors are connected to a processor capable of capturing analog signals from our sensors, process them, and wirelessly send these data to the base station located on the mainland.

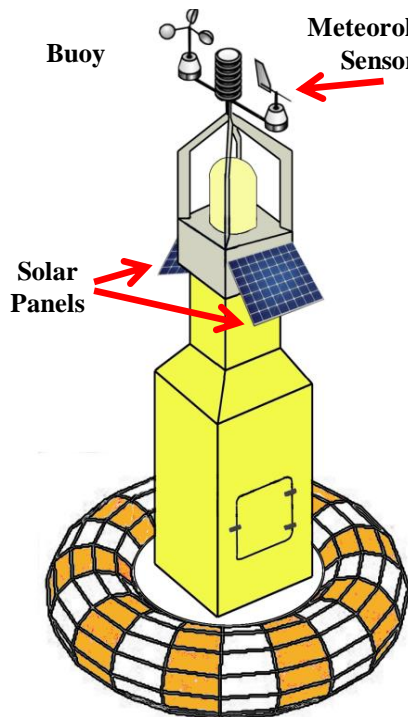


Figure 5.14 Multisensor buoy,

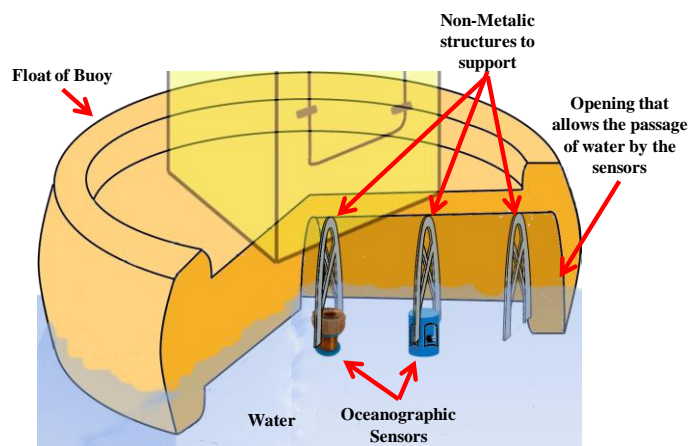


Figure 5.15 Float of the buoy with the sensors.

### 5.3.1.2. Design of wireless node

Our wireless node is based on the wireless module called Openpicus Flyport (Flyport features, 2016). This wireless module is composed of the Certified Transceiver Wi-Fi IEEE 802.11 Microchip MRF24WB0MA and, although it uses the IEEE 802.11 wireless technology, this device presents one of the smallest energy consumption. The main feature of this device is its 16 Bit low power microcontroller Processor Microchip PIC24FJ256, with 256K Flash, 16K Ram, 16Mips@32Mhz. Figure 5.16 shows a view of the top side of this module.

There are several reasons to use this wireless module. The main advantage over existing systems is that it works under the IEEE 802.11 standard which makes fairly inexpensive the purchase of these devices. In addition, it is programmed in C language which permits great versatility in the development of new applications. In addition, it offers an embedded web site that can be used to see the current values gathered by the sensors. Finally, its small size makes this device ideal for several applications such as environmental and rural monitoring (Lloret et al., 2009), agriculture (Lloret et al., 2011b), (Karim et al., 2013), animal monitoring (Sendra et al., 2013a), indoor monitoring (Sendra et al., 2014) or wearable sensors for e-health applications (Jiang et al., 2016), (Lopez-Ruiz et al., 2015) among others.

Finally, because our multisensor buoy is working with 9 different sensors (8 sensors with an analog value as response and a sensor with an ON / OFF response), we need a microcontroller with at least 8 analog inputs. The digital input can be controlled using the Flyport Module. In our case, the device used is 40-Pin Enhanced Flash Microcontrollers with 10-Bit A/D and nanoWatt Technology (PIC18F4520 by Microchip). One of the main characteristics of this device is its 10-bit Analog-to-Digital Converter module (A/D) with up to 13-channels, which is able to perform the auto-acquisition and the data conversion during the sleep mode. Microchip claims that pic18f4520s ADC can go as high as 100K samples per second although our application does not require this sampling rate.

Figure 5.17 shows a diagram with the connection between sensors, the microcontroller and the base station located at the mainland or marine port.

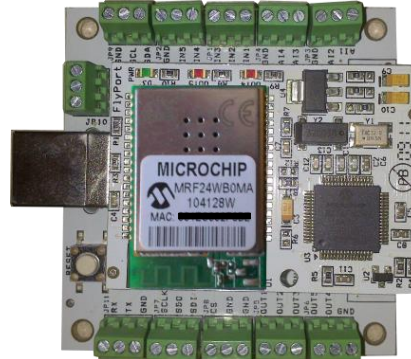


Figure 5. 16 FlyPort Module

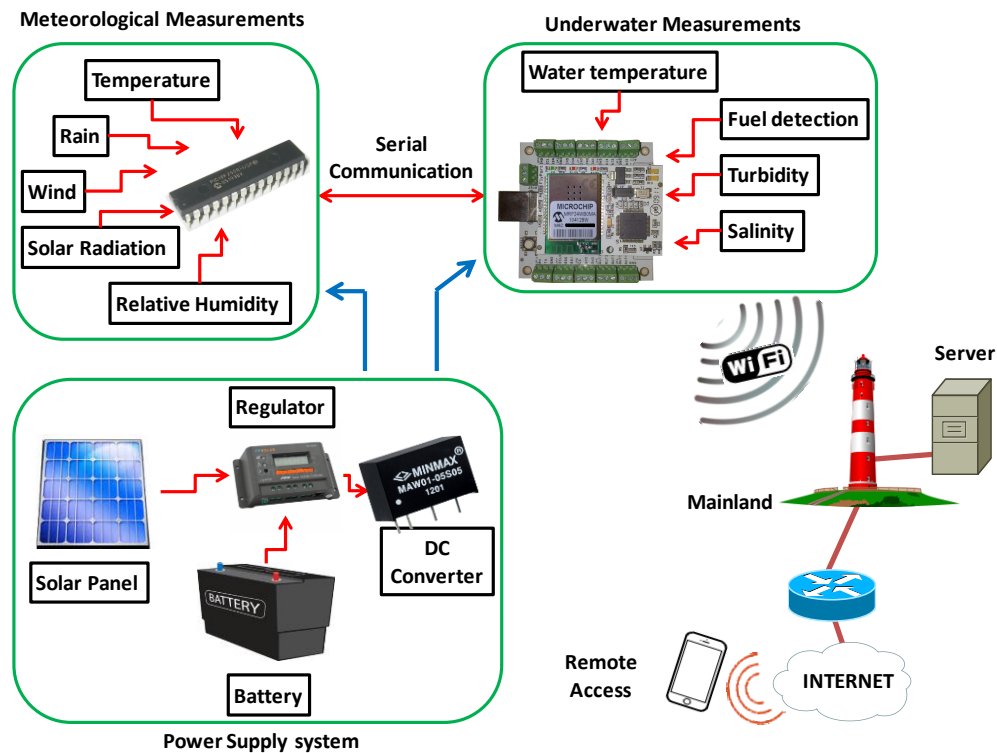


Figure 5. 17 Diagram with all connections and the proposed architecture

### 5.3.2. Sensors for marine parameters monitoring

In this section, we are going to present the design and operation of sensors used to measure marine parameters. For each sensor, we show the electric scheme and mathematical expressions

which relate the environmental parameter magnitudes and electrical values. For our new developments, we will also show the calibration process.

### 5.3.2.1. Water temperature sensor

In order to develop the water temperature sensor, it is used an NTC resistance (Negative Temperature Coefficient) (See Figure 5.18), i.e., as the temperature increases, the carrier concentration and the NTC resistance will decrease its magnitude.

The way to connect this sensor to our circuit is forming a voltage divider and the output of this circuit is connected to an analog input of our wireless node. Our NTC is placed on the lower of the voltage divider. This protects our system. When the current flowing through the NTC is low, we have no problem because heat dissipation is negligible ( $V \cdot I^2$ ). However, if heat dissipation increases, this can affect the resistive value of the sensor. For this reason, the NTC response is not linear but hyperbolic. But the configuration of a voltage divider will make the voltage variation of  $V_{out}$  almost linear.

Regarding the other resistance that forms the voltage divider, it is used a resistance of  $1k\Omega$ . This fact will allow leveraging the sampling range, with a limited power consumption given by the FlyPort. The schematic of the electronic circuit is shown in Figure 5.19.

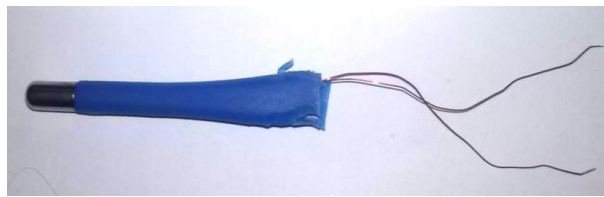


**Figure 5. 18** NTC for the water temperature sensor.

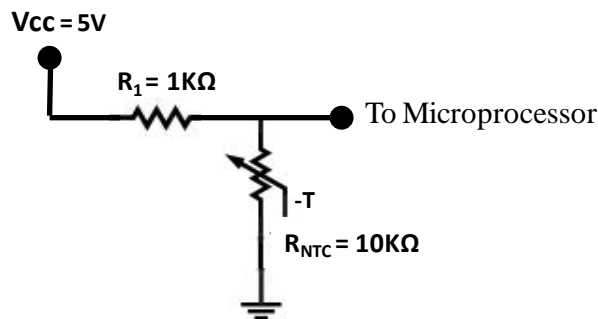


**Figure 5. 19** Electronic circuit of the water temperature sensor.

The output voltage as a function of the temperature (in K) can be modeled by Eq. (5.2):

$$V_{out}(t) = V_{cc} \frac{R_0 \cdot e^{B(\frac{1}{t} - \frac{1}{t_0})}}{R_0 \cdot e^{B(\frac{1}{t} - \frac{1}{t_0})} + R_{sup}} \quad (5.2)$$

Where,  $R_{sup}$  is the superior resistance of the voltage divider formed by this resistance and the NTC.  $R_0$  is the value of the NTC resistance at a temperature  $t_0$  which is 298 K and  $B$  is the characteristic temperature of a material, which is between 2000 K and 5000 K.

We can calculate the temperature in  $^{\circ}\text{C}$  by Eq. (5.3).

$$t(^{\circ}C) = \frac{t_0}{\ln\left(\frac{R_1 \cdot V_{RNTC}}{R_0 \cdot (V_{out} - V_{RNTC})}\right) + 1} - 273 \quad (5.3)$$

Where,  $V_{RNTC}$  is the voltage registered on the NTC resistor,  $R_0$  is the value of NTC resistance at a temperature  $t_0$  which is 298 K and  $B$  is the characteristic temperature of a material.  $V_{out}$  is the output voltage as a function of the registered temperature. Finally,  $t(^{\circ}C)$  is the temperature we need to measure.

To gather the data from the sensor, we need a short program code in charge of obtaining the equivalence between voltage and temperature. Figure 5.20 shows the programming code used.

Finally, the sensor is tested for different temperatures. Figure 5.21 shows the temperature measured as a function of the output voltage.

```
while(1){
  myADCValue = ADCVal(1);
  myADCValue = (myADCValue *2.048)/1024;
  sprintf(buf, "%d", myADCValue);
  vTaskDelay(100);
}
```

**Figure 5. 20** Programming code to read the analog input from water temperature sensor

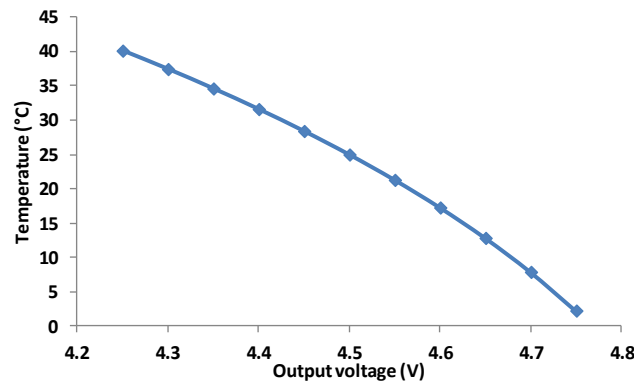


**Figure 5. 21** Temperature measured vs. output voltage

### 5.3.2.2. Water Salinity Sensor

The low-cost salinity sensor is based on a transducer without a ferromagnetic core (Parra et al., 2013a), (Parra et al., 2013b) and (Parra et al., 2013c). The transducer is composed of two coils, one toroid and one solenoid (placed over the toroid). The characteristics of these coils are shown in Table 5.2. Figure 5.22 shows the salinity sensor.

In order to measure water salinity, we need to power one of these coils (the one with fewer spires) with a sinusoidal signal. The amount of solute salts in the water solution affects and modifies the magnetic field generated by the powered coil. The output voltage induced by the magnetic field in the second coil is correlated with the concentration of solute salts. We use this system instead of commercial sensors because our system is cheaper than commercial devices. Another advantage of our system is that it does not require periodic calibrations and it is easy to isolate from the water.

It is important to know the frequency where our system distinguishes different salinity levels with more precision; this frequency is called as working frequency. In order to find this working frequency, we developed several tests using the sinusoidal signal at different frequencies to power the first coil. Tests are performed using 5 samples with different salinity. The samples

were composed of tap water and salt. Their salinities go to tap water up to water highly saturated with salt. The conductivity values typical for seawater and freshwater are included in the samples. To find the working frequency, all samples are measured at different frequencies. Eight different frequencies are tested; the frequencies go from 10 kHz to 750 kHz. The results of these tests are shown in Figure 5.23. It represents the maximum amplitude registered for each sample at different frequencies. The input signal for the powered coil is performed by a function generator (Waycott et al., 2009). To measure the output voltage in the first tests, we use an oscilloscope. Figure 5.24 shows the oscilloscope screen where we can see the input and output sinusoidal waves. We can see that 150 kHz is the frequency where it is possible to clearly distinguish between different samples. At 590 kHz, it is possible to distinguish between all the samples except 17 and 33 ppm. The only frequency that our sensor is able to distinguish between all samples is 150 kHz. This frequency is selected as working frequency.

The main function of the Flyport is the generation of the sine wave used to power our transducer and the acquisition of the resulting signal. The sensor node generates a PWM signal from which we obtain a sinusoidal signal used to power the transducer. The PWM signal needs to be filtered by a band pass filter (BPF) in order to obtain the sinusoidal signal as we know it. Once PWM signal is generated by the microcontroller, it is necessary to filter this signal by a BPF with the center frequency at 150 kHz in order to obtain the desired sine wave. Figure 5.25 shows a PWM signal (as a train of pulses with different widths) and the sine wave obtained after filtering the PWM signal.

The BPF is performed by two active Sallen-Key filters of second order configured in cascade, i.e., a low pass filters (LPF) and a high-pass filter (HPF). The cutoff frequencies are 160 kHz and 140 kHz respectively (see Figure 5.26). PWM is generated by the wireless module. The system is configured to work at 150 KHz. After that, the system generates a variable width pulse which is repeated with a frequency of 150 KHz. Figure 5.27 shows the frequency response of our BPF. Figure 5.28 shows the program code for PWM signal generation.

In order to gather the data from the salinity sensor, we have programmed a small code. The main part of this code is shown in Figure 5.29. As it is shown, the system will take measurements from analog input 1.

Once we know that the working frequency is 150 kHz, we perform a calibration. The calibration is carried out for obtaining the mathematical model that relates the output voltage with the water salinity. The test bench is performed by using more than 30 different samples which salinities go from 0.19 ppm. to 38 ppm. The results of calibration are shown in Figure 5.30.

**Table 5. 2 Coils Features (II)**

		<b>Coils Features</b>	
		<i>Toroid</i>	<i>Solenoid</i>
Wire Diam.		0.8 mm	0.8 mm
Size and core	Inner Coil Diam.:	23.2 mm	Inner Coil Diam.: 25.3 mm
	Outer Coil Diam.:	56.5 mm	Outer Coil Diam.: 33.6 mm
	Coil High:	26.9 mm	Coil High: 22.6 mm
	Core:	Nonferrous	Core: Nonferrous
N° of Spires	81 in one layer	324 layers	9



**Figure 5. 22** Salinity sensor

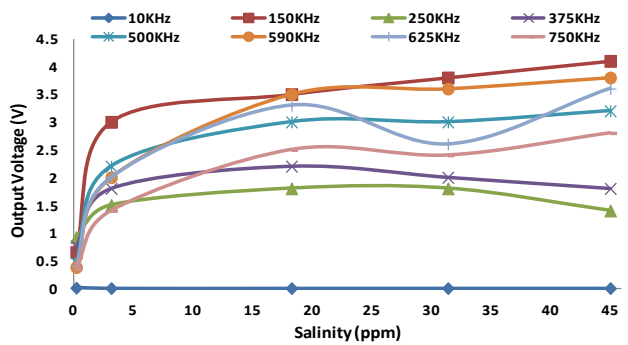


Figure 5. 23 Output voltage of the salinity sensor as a function of the frequency

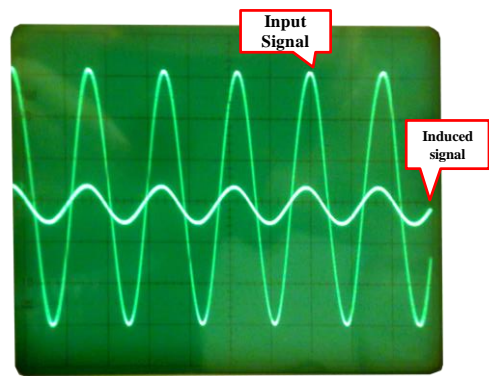


Figure 5. 24 Oscilloscope during the tests

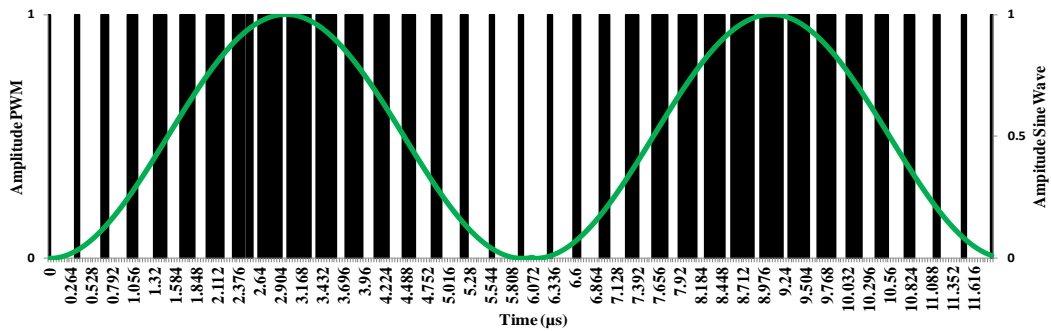


Figure 5. 25 PWM signal and the resulting sine wave

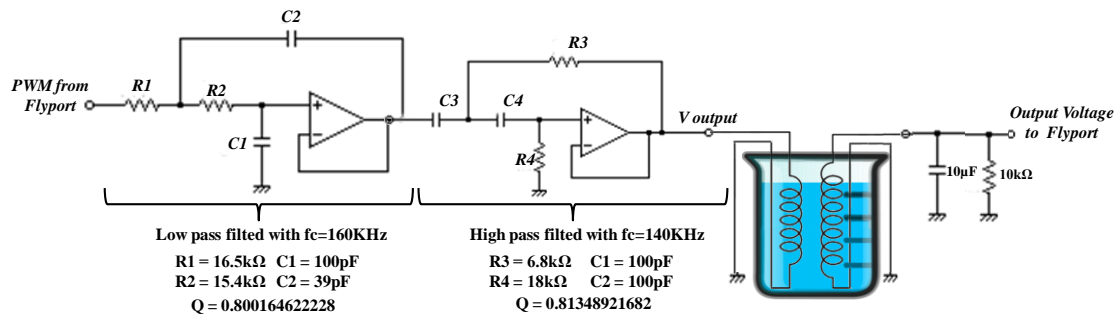


Figure 5. 26 Electronic design of the low-cost salinity sensor

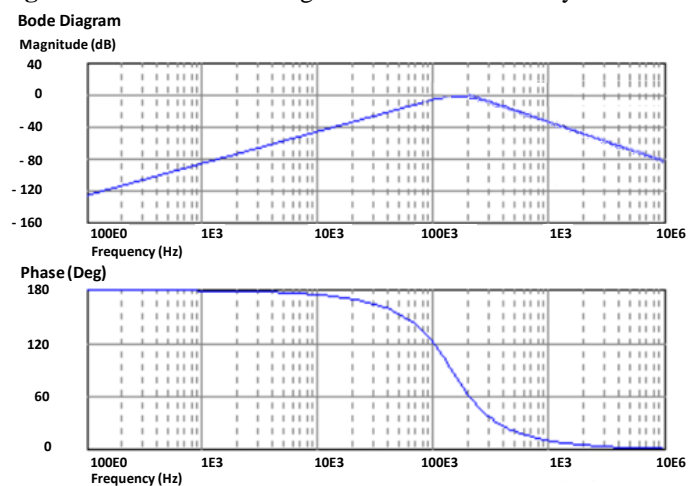


Figure 5. 27 Frequency response of our BPF

We can see that the results can be adjusted by 3 linear ranges with different mathematical equations. Depending on the salinity, the sensor will use one of these equations. The Eq. (5.4) is for salinity values from 0 ppm to 3.28 ppm, Eq. (5.5) is for values from 3.28 ppm. to 11.3 ppm. Finally, Eq. (5.6) is for salinities from 11.3 ppm. to 35ppm. All these equations have a minimum correlation of 0.9751.

Finally, Figure 5.31 compares the measured salinity and the predicted salinity, and we can see that the accuracy of our system is fairly good.

```
#include "taskFlyport.h"
void FlyportTask(){
    const int maxVal = 100;
    const int minVal = 1;
    float Value = (float) maxVal;
    PWMInit(1,1500000,maxVal);
    PWMOn(p9, 1);
    While (1){
        for (Value = maxVal; Value > minVal; Value -
-){
            PWMDuty(Value, 1);
            vTaskDelay(1);
        }
        for (Value = minVal; Value < maxVal; Value +
+){
            PWMDuty(Value, 1);
            vTaskDelay(1);
        }
    }
}
```

**Figure 5. 28** Programming code for the PWM signal generation

```
while(1){
    myADCValue = ADCVal(1);
    myADCValue = (myADCValue
*2.048)/1024;
    sprintf(buf, "%d", myADCValue);
    vTaskDelay(100);
}
```

**Figure 5. 29** Programming code to read the analog input of the salinity sensor

$$V_{out\_1} = 1.1788 \cdot S + 0.6037; R^2 = 0.9751 \quad (5.4)$$

$$V_{out\_2} = 0.2387 \cdot S + 3.3457; R^2 = 0.9813 \quad (5.5)$$

$$V_{out\_3} = 0.0625 \cdot S + 5.23; R^2 = 0.9872 \quad (5.6)$$



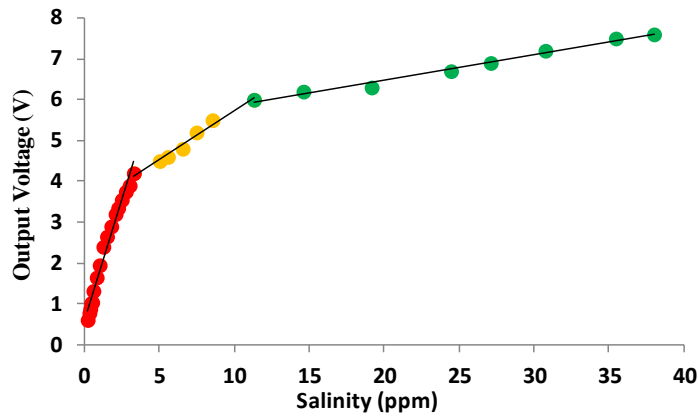


**Figure 5.30** Water salinity as a function of the output voltage.

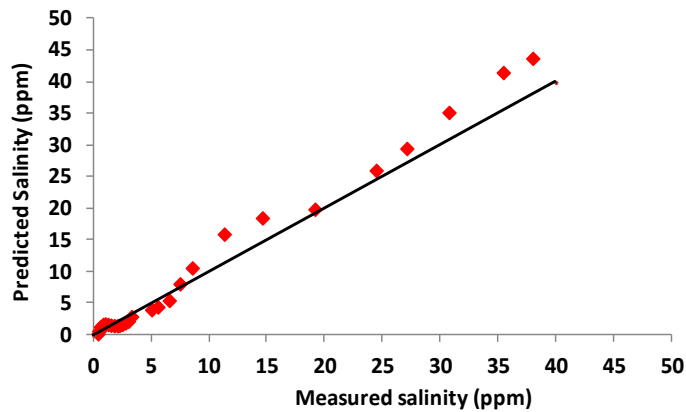


**Figure 5.31** Comparison between our measures and the predicted measures

### 5.3.2.3. Water Turbidity Sensor

The turbidity sensor is based on an infrared LED (TSU5400 manufactured by Tsunamimstar) as a source of light emission and a photodiode as a detector (S186P by Vishay Semiconductors). These elements are disposed at 4 cm with an angle of 180° so that the photodiode can capture the maximum infrared light from the LED (Sendra et al., 2013b).

The infrared LED uses GaAs technology manufactured in a blue-gray tinted plastic package, registering the biggest peak wavelength at 950 nm. The photodiode is an IR filter, spectrally matched to GaAs or GaAs on GaAlAs IR emitters ( $\geq 900$  nm). S186P is covered by a plastic case with IR filter (950 nm) and it is suitable for near-infrared radiation. The transmitter circuit is powered by a voltage of 5 V while the photodiode needs to be fed by a voltage of 15 V. To achieve these values, we use two voltage regulators of LM78XX series which permits a maximum output current of 1 A. The LM7805 is used by the transmitter circuit and the LM7815 is used by the receiver circuit. Figure 5.32 shows the electronic scheme of our turbidity sensor.

In order to calibrate the turbidity sensor, we used 8 samples with different turbidity. All of them were prepared specifically for the experiment at that moment. To know the real turbidity of the samples, we used a commercial turbidimeter, Turbidimeter Hach 2100N, which worked using the same method that our sensor (with the detector placed at 90 degrees). The samples were composed of seawater and sediment (clay and silt), fine material that can be maintained in suspension for the measured time span without precipitate. The water used to prepare the samples were taken from the Mediterranean Sea (Spain). Its salinity was 38.5 PSU. Its pH was 8.07 and its temperature was 21.1°C when we were performing the measures. The 8 samples have different quantities of clay and silt. The turbidity is measured with the commercial turbidimeter. The samples are introduced in specific recipients for their measurement with the turbidimeter. These recipients are glass recipients with a capacity of 30 ml. The concentration of sediments and the

turbidity of each sample are shown in Table 5.3. Once the turbidity of each sample is known, we measured them using our developed system to test it. For each sample, it is obtained an output voltage proportional to each measured turbidity value. Relating to the obtained voltage with the turbidity of each sample, the calibration process is finished and the turbidity sensor is ready to be used. The calibration results are shown in Figure 5.33. It relates the gathered output voltage for each turbidity value. Eq. (5.7) correlates the turbidity with the output voltage. We also present the mathematical equation that correlates the output voltage with the amount of sediment (mg/L) (See Eq. (5.8)). Finally, it is important to say that, based on our experiments, the accuracy of our system is 0.15NTU.

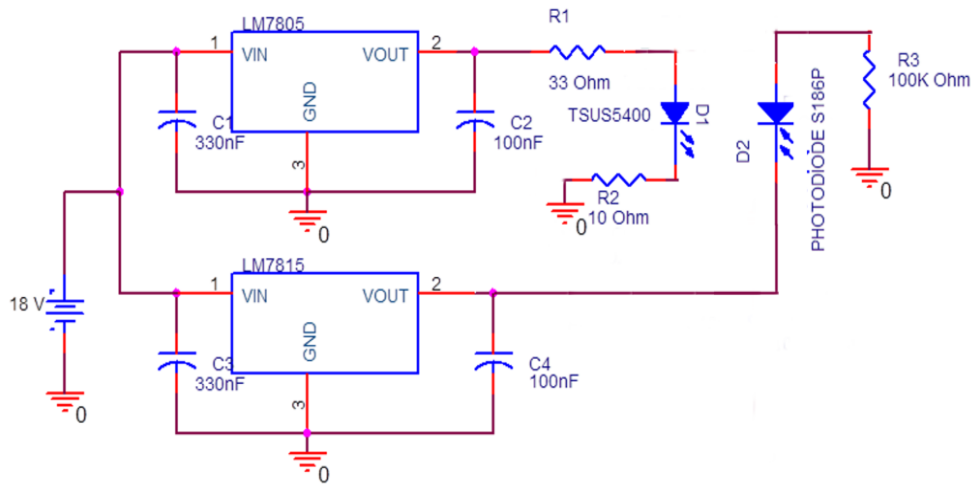


Figure 5. 32 Schematic of the turbidity sensor

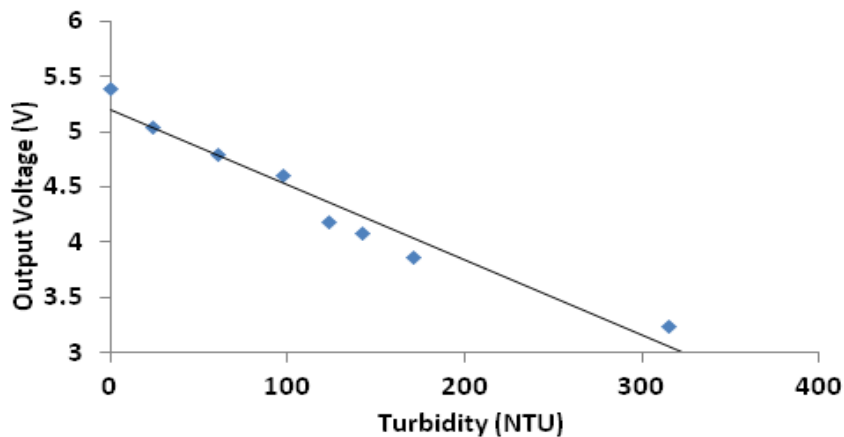


Figure 5. 33 Calibration results of the turbidity sensor

$$\text{Output voltage (V)} = 5.196 - 0.0068 \times \text{Turbidity (NTU)} \quad (5.7)$$

$$\text{Output voltage (V)} = 5.1676 - 116.49 \times \text{Concentration} \left(\frac{\text{mg}}{\text{L}}\right) \quad (5.8)$$

Once the calibration is done, a verification process is carried out. In this process, 4 samples are used. The samples are prepared in the laboratory without knowing neither the concentration of the sediments nor their turbidity.

These samples are measured with the turbidity sensor. The output voltage of each one is correlated to a turbidity measured using Equation 6. The output voltage and the turbidity values are shown in Table 5.4.

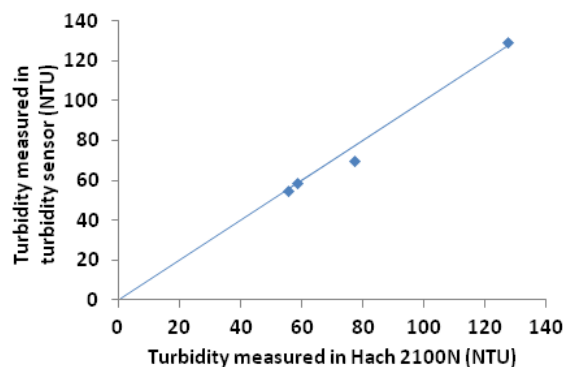
**Table 5. 3** Concentration and Turbidity of the Samples

Sample n°	The concentration of clay and silt (mg/l)	Turbidity (NTU)
1	0	0.072
2	36.33	23.7
3	110.44	60.1
4	175.33	97.2
5	232.10	123
6	260.66	142
7	326.66	171
8	607	385

**Table 5. 4** Results Verifying the Samples

Sample	Output Voltage (V)	Turbidity (NTU)
1	4.67	77.36
2	4.82	55.29
3	4.8	58.24
4	4.33	127.36

After measuring the samples with the turbidity sensor, the samples are measured with the commercial turbidimeter in order to compare them. This comparison is shown in Figure 5.34. We can see the obtained data over a thin line which shows the perfect adjustment (when both measures are the same). It is possible to see that the data are very close, except one case (sample 1). The average relative error of all samples is 3.25% while the maximum relative error is 9.5%. This maximum relative error is too high in comparison to the error of other samples, this makes us think that there was a mistake in the sample manipulation. If we delete this data, the average relative error of our turbidity sensor is 1.17%.

**Figure 5. 34** Comparison of measures in both equipment

#### 5.3.2.4. Hydrocarbon detector sensor

The system used to detect the presence of hydrocarbon is composed by an optical circuit, which is composed by a light source (LED) and a receptor (Photodiode). The Vout signal increases or decreases depending on the presence or absence of fuel in the seawater surface (See Figure 5.35). In order to choose which the best light to implement our sensor is, we used 6 different light colors (white, red, orange, green, blue and violet) as a light source. For all cases, we used the photoreceptor (S186P) as a light receptor. It is cheaper than others photodiodes, but its optimal wavelength is the infrared light. Although the light received by the photodiode is not infrared light, this photodiode is able to sense lights with another wavelength. Both circuits are powered at 5V. A diagram of the principle of operation of the hydrocarbon detector sensor is shown in Figure 5.36.

Finally, the sensor is tested in different conditions. The samples used in these tests are composed of seawater and fuel, which is gasoline of 95 octanes. They are prepared in small plastic containers of 30ml, with different amount of fuel (0, 2, 4, 6, 8 and 10ml), so each sample has a layer of a different thickness of fuel over the seawater. The photodiode and the LED are placed near the water surface, at 1cm, as we can see in Figure 5.37, where orange light is tested.

The output voltages for each sample as a function of the light source are shown in Figure 5.38. Each light has different behaviors and different interactions with the surfaces, and only some of them are able to distinguish between the presence and absence of fuel. The lights, which present bigger difference between the voltage in presence of fuel and without it, are white, orange and violet lights. However, any light is capable of giving us quantitative results. The tests are repeated 10 times for the selected lights in order to check the stability of the measurements and the validity of our sensor. Because our system only brings qualitative results, i.e., between presence and absence of fuel, we only use two samples with different amounts of fuel (0 and 2 ml). The results are shown in Figure 5.39. Table 5.5 summarizes these results.

The results show that these three lights allow detecting the presence of fuel over the water. Nevertheless, the white light is the one which presents the lowest difference in mV between both samples. So the orange or violet lights are the best option to detect the presence of hydrocarbons over seawater.

**Table 5. 5** Average value of the output voltage for the best cases

	Output Voltages (mV)					
	Orange		White		Violet	
	Seawater	With fuel	Seawater	With fuel	Seawater	With fuel
Average value	18.2	10.2	10.9	7.2	14.2	7
Standard Deviation	2.781	0.4216	0.568	0.426	1.229	0.816

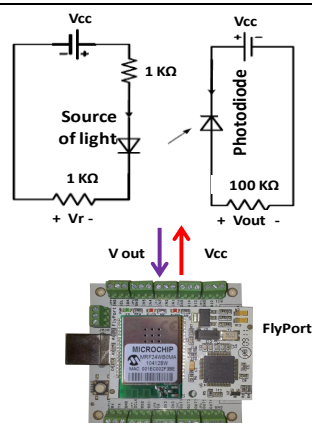


**Figure 5. 35** Sensor for hydrocarbon

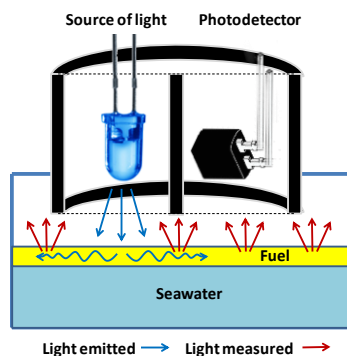


**Figure 5. 36** Operation of the sensor.



**Figure 5. 37** Test bench with orange light

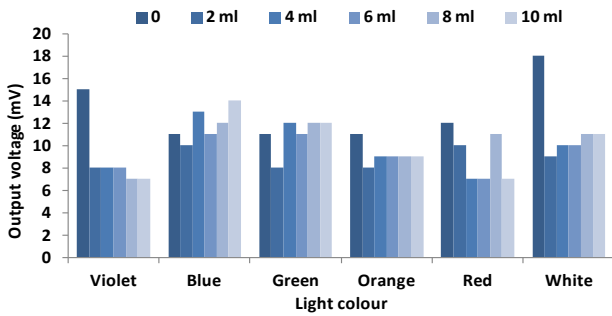


Figure 5.38 Output voltage for the six lights used

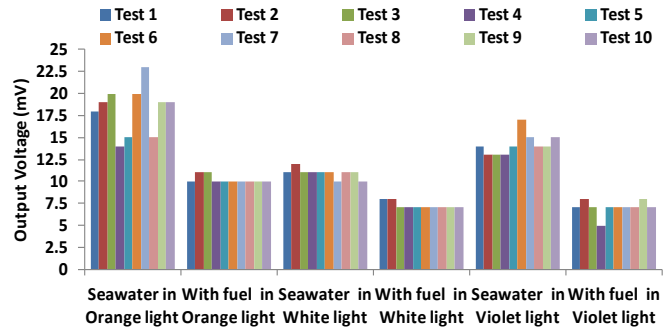


Figure 5.39 Output voltage as a function of the light

### 5.3.3. Sensors for Weather parameters monitoring

This section presents the design and operation of the sensors used to measure the meteorological parameters. For each sensor, we will see the electric scheme and the mathematical expressions relating the environmental parameter magnitudes with the electrical values. We have used commercial circuit integrates that require few additional circuitry.

#### 5.3.3.1. Sensor for environmental Temperature

The TC1047 is a high precision temperature sensor which presents a linear voltage output proportional to the measured temperature. The main reason to select this component is its easy connection and its accuracy. TC1047 can be feed by a supply voltage between 2.7 V and 4.4 V. The output voltage range for these devices is typically 100 mV at -40 °C and 1.75 V at 125 °C.

This sensor does not need any additional design. When the sensor is feed, the output voltage can be directly connected to our microprocessor (see Figure 5.41). Although the operating range of this sensor is between -40 °C and 125 °C, our useful operating range is from -10 °C to 50°C, because this range is even broader than the worst case in the Mediterranean zone. Figure 5.42 shows the relationship between the output voltage and the measured temperature, and the mathematical expression used to model our output signal.

Figure 5.43 shows the program code to read the analog input for the ambient temperature sensor.

Finally, we have tested the behavior of this system. The test bench has been performed for 2 months. Figure 5.44 shows the results obtained about the maximum, minimum and average temperature values of each day.

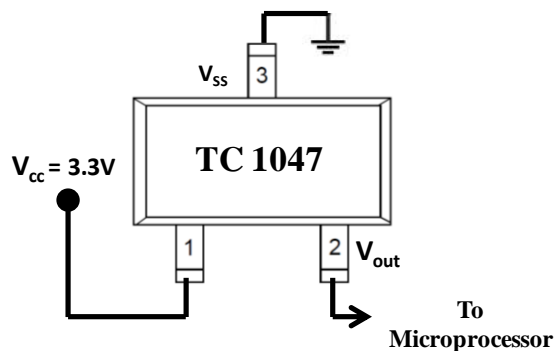


Figure 5.40 Sensor to measure the ambient temperature

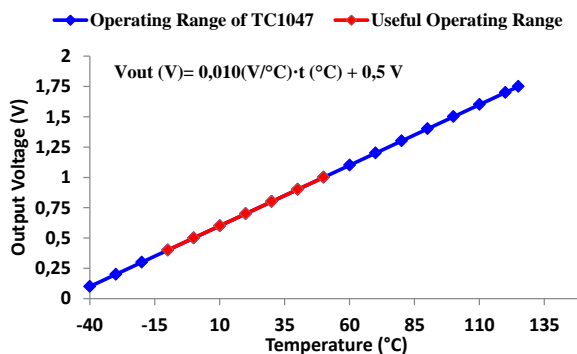


Figure 5.41 Behavior of TC1047 and its equation

```

while(1){
myADCTemp = ADCVal(1);
myADCTemp = (myADCTemp *2.048)/1024;
myADCTemp = myADCTemp *0.010 + 0.5;
sprintf(buf, "%d", myADCValue);
vTaskDelay(100);
}

```

**Figure 5. 42** Program code for reading analog input for the ambient temperature sensor.

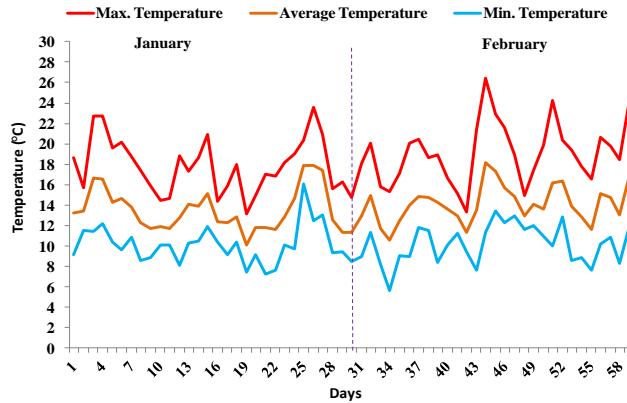


**Figure 5. 43** Test bench of the ambient temperature sensor

### 5.3.3.2. Relative Humidity

HIH-4000 is a high precision humidity sensor which presents a near linear voltage output proportional to the measured relative humidity (RH). This component does not need additional circuits and elements to work. When the sensor is feed, the output voltage can be directly connected to the microprocessor (see Figure 5.45). It is easy to connect and its accuracy is  $\pm 5\%$ , for RH from 0% to 59%, and  $\pm 8\%$ , for RH from 60% to 100%. The HIH-4000 should be feed by a supply voltage of 5V. The operating temperature range of this sensor is from  $-40^{\circ}\text{C}$  to  $85^{\circ}\text{C}$ . Finally, we should keep in mind that the RH is a parameter which depends on the temperature. For this reason, it is needed to perform the temperature compensation as it is shown in Eq. (5.9), (5.10) and (5.11):

$$V_{OUT} = V_{supply} \cdot (0.0062 \cdot RH(\%) + 0.16) \quad (5.9)$$

$$True\ RH(\%) = \frac{RH(\%)}{(1.0546 - 0.00216 \cdot t)} \quad (5.10)$$

$$True\ RH(\%) = \frac{\frac{V_{OUT}}{V_{supply}} - 0.16}{0.0062} \quad (5.11)$$

Where,  $V_{OUT}$  is the output voltage as a function of the RH in %,  $V_{supply}$  is the voltage needed to feed the circuit (in our case it is 5V).  $RH(\%)$  is the value of RH in %,  $True\ RH$  is the RH value, in %, after the temperature compensation and  $t$  is the temperature, expressed in  $^{\circ}\text{C}$ .

Figure 5.46 shows the relationship between the output voltage and the measured RH in %. Finally, we have tested the behavior of this sensor during 2 months. Figure 5.47 shows the relative humidity values gathered in this test bench.

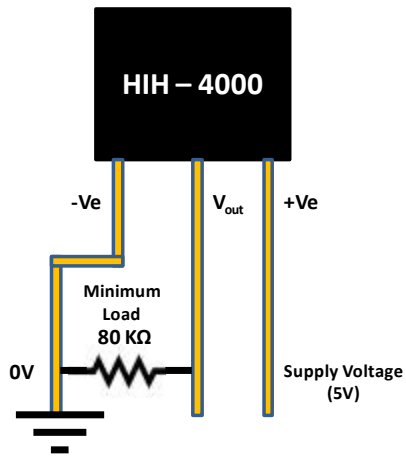


Figure 5. 44 Electrical connections for HIH-4000

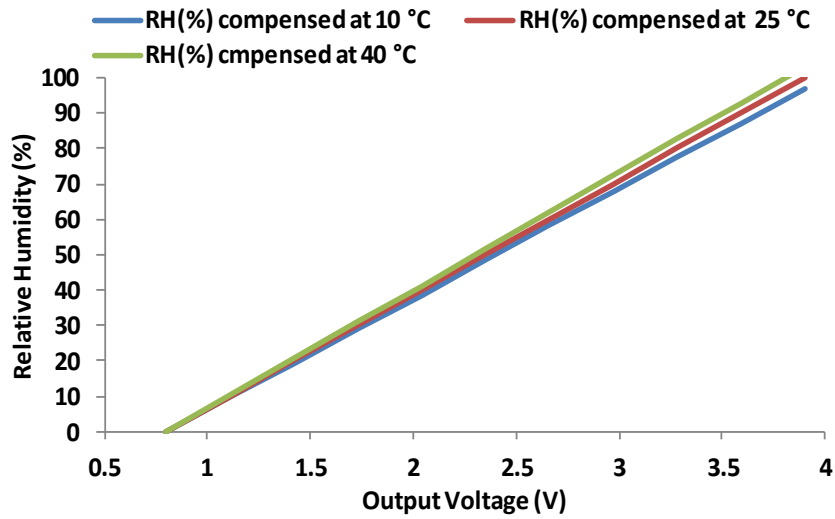


Figure 5. 45 RH in % as a function of the output voltage compensated in temperature

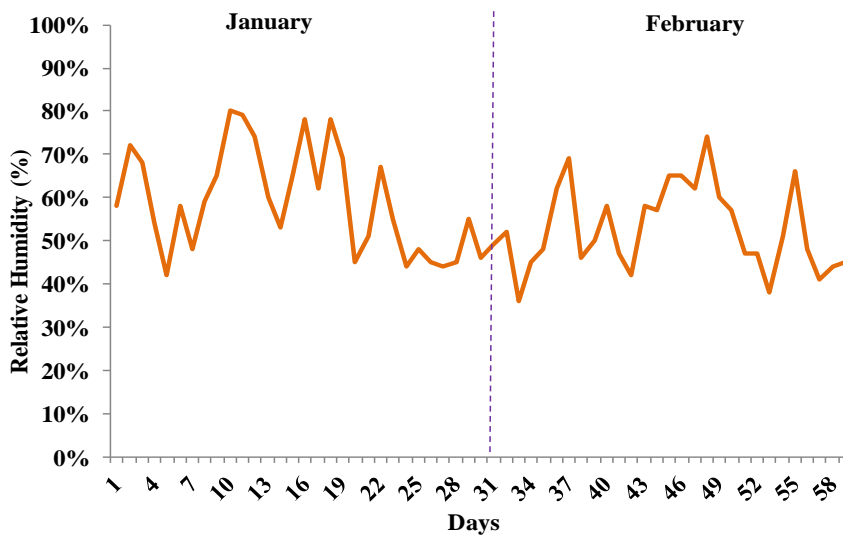


Figure 5. 46 Relative humidity measured during two months

### 5.3.3.3. Wind speed and direction

To measure the wind speed, we use a DC motor as a generator mode, where the rotation speed of the shaft becomes a voltage output which is proportional to that speed. For a proper design, we must consider several details such as the size of the captors wind or the diameter of the circle formed, among others. Figure 5.48 shows the design of our anemometer. We used 3 hemispheres because it is the structure that generates less turbulence. Moreover, we note that a generator does not have a completely linear behavior; the laminated iron core reaches the saturation limit when it reaches a field strength limit. In this situation, the voltage is not proportional to the angular velocity. After reaching the saturation, an increase in the voltage produces very little variation approximating such behavior to a logarithmic behavior.

To implement our system, we use a miniature motor capable of generating up to 3 volts when records a value of 12000 rpm. The engine performance curve is shown in Figure 5.49.

To express the wind speed, we can do different ways. On one hand, the rpm is a measure of angular velocity, while m/s is a linear velocity. To make this conversion of speeds, we should proceed as follows (See Eq. (5.12)):

$$\omega(rpm) = f_{rot} \cdot 60 \rightarrow \omega\left(\frac{rad}{s}\right) = \omega(rpm) \cdot \frac{2\pi}{60} \quad (5.12)$$

Finally, the linear velocity in m/s is expressed as shown in Eq. (5.13).

$$v\left(\frac{m}{s}\right) = \omega\left(\frac{rad}{s}\right) \cdot r \quad (5.13)$$

Where,  $f_{rot}$  is the rotation frequency of anemometer, in Hz,  $r$  is the turning radius of the anemometer,  $\omega\left(\frac{rad}{s}\right)$  is the angular speed in  $\frac{rad}{s}$ , and  $\omega(rpm)$  is the angular speed, in revolutions per minute (rpm).

Given the characteristics of the engine operation and the mathematical expressions, the anemometer was tested during 2 months. The results collected by the sensor are shown in Figure 5.50.

To measure the wind direction, we need a vane. Our vane is formed by two SS94A1 Hall sensors manufactured by Honeywell (see Figure 5.51), which are located perpendicularly. Apart from these two sensors, the vane has a permanent magnet on a shaft that rotates according to the wind direction.

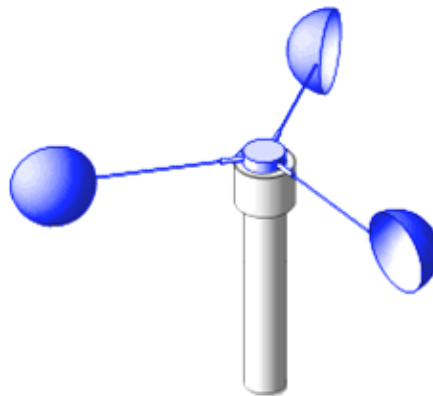


**Figure 5. 47** Design of our anemometer



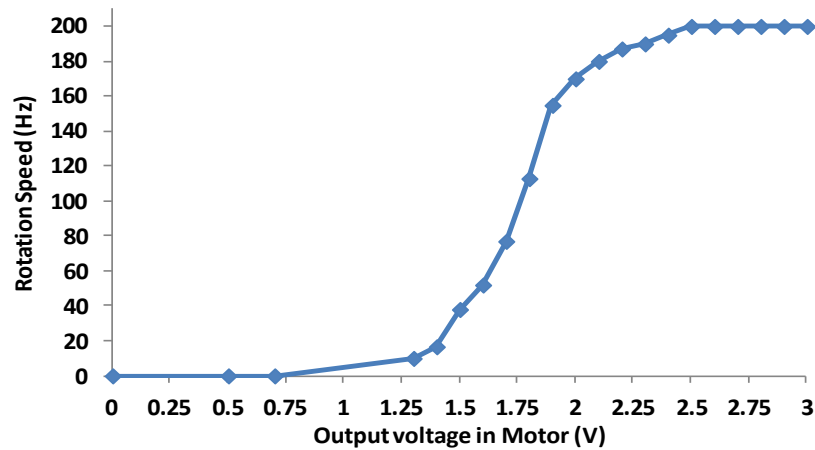


Figure 5.48 Relationship between the output voltage in DC motor and the rotation speed.

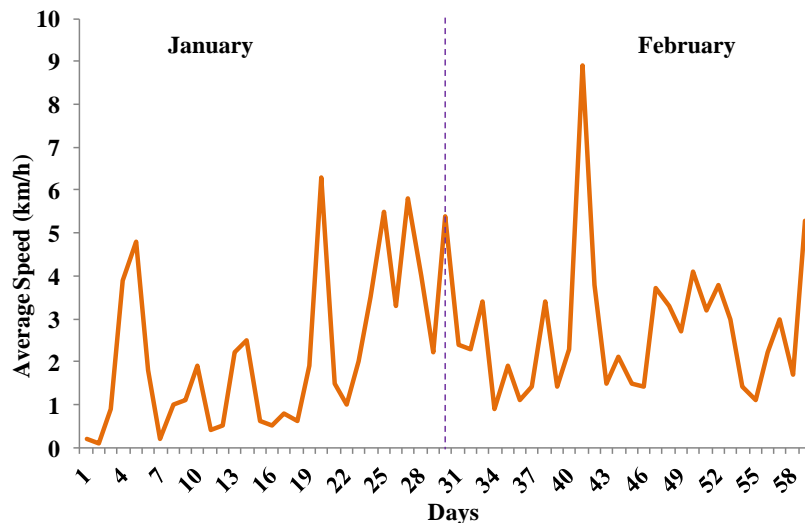


Figure 5.49 Measures of wind speed in a real environment.

Our vane is based on detecting magnetic fields. Each sensor gives a linear output proportional to the number of field lines passing through it, so when there is a linear output with higher value, the detected magnetic field is higher. According to the characteristics of this sensor, it must be fed at least with 6.6 V. If the sensor is fed with 8V, it obtains an output value of 4 Volts per pin, a “0” when it is not applied any magnetic field and a lower voltage of 4 volts when the field is negative. We can distinguish 4 main situations:

- The magnetic field is negative when entering from the South Pole through the detector. This happens when the detector is faced with the South Pole.
- A value greater than 4 volts output will be obtained when the sensed magnetic field is positive (when the positive pole of the magnet is faced with the North pole).
- The detector will give an output of 4 volts when the field is parallel to the detector. In this case, the lines of the magnetic field do not pass through the detector and therefore there is no magnetic field.
- Finally, when intermediate values are obtained, we know that the wind will be somewhere between the four cardinal points.

In our case, we need to define a reference value when the magnetic field is not detected. Therefore, we will subtract 4 to the voltage value that we obtain for each sensor. This will allow us to distinguish where the vane is exactly pointing. These are the possible cases:

- If the + pole of the magnet points to N  $\rightarrow H_2 > 0V$ ;  $H_1 = 0V$ .

- If the + pole of the magnet points to S  $\rightarrow H_2 > 0V$ ;  $H_1 = 0V$ .
- If the + pole of the magnet points to E  $\rightarrow H_1 > 0V$ ;  $H_2 = 0V$ .
- If the + pole of the magnet points to W  $\rightarrow H_1 < 0V$ ;  $H_2 = 0V$ .
- When the + pole of the magnet points to intermediate points  $\rightarrow H_1 \neq 0V$ ;  $H_2 \neq 0V$ .

Figure 5.52 shows the hall sensors diagram, their positions and the principles of operation.

In order to calculate the wind direction, we are going to use the operation for calculating the trigonometric tangent of an angle (see Eq. 5.14).

Where,  $H_2$  is the voltage recorded by the Hall sensor 2,  $H_1$  is the voltage recorded by the Hall sensor 1 and  $\alpha$  represent the wind direction, taken as a reference the cardinal point of East. The values of the hall sensors may be positive or negative and the wind direction will be calculated based on these values. Because for opposite angles the value of the tangent calculation is the same, after calculating the magnitude of that angle, the system must know the wind direction, analyzing whether the value of  $H_1$  and  $H_2$  is positive or negative. It knows it considering the settings shown in Figure 5.53.

After setting the benchmarks and considering the linear behavior of this sensor, we have the following response (see Figure 5.54). Depending on the position of the permanent magnet, the Hall sensors record the voltage values shown in Figure 5.55.

Finally, we gathered measurements with this sensor during 2 months. Figure 5.56 shows the results of the wind direction obtained during this time.

$$\tan \alpha = \frac{H_2}{H_1} \rightarrow \alpha = \tan^{-1} \frac{H_2}{H_1} \quad (5.14)$$



Figure 5. 50 Sensor Hall

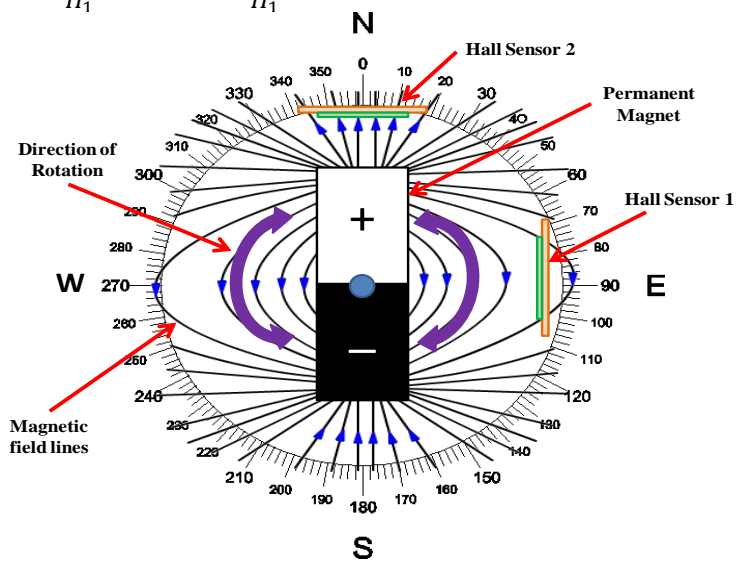


Figure 5. 51 Diagram of operation for the wind direction sensor

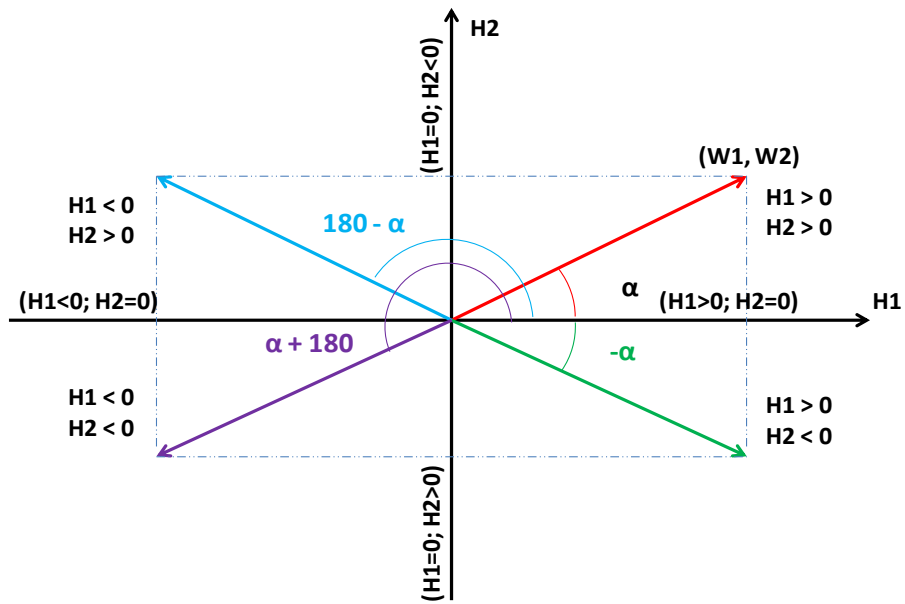


Figure 5.52 Angle calculation as a function of the sensors Hall values

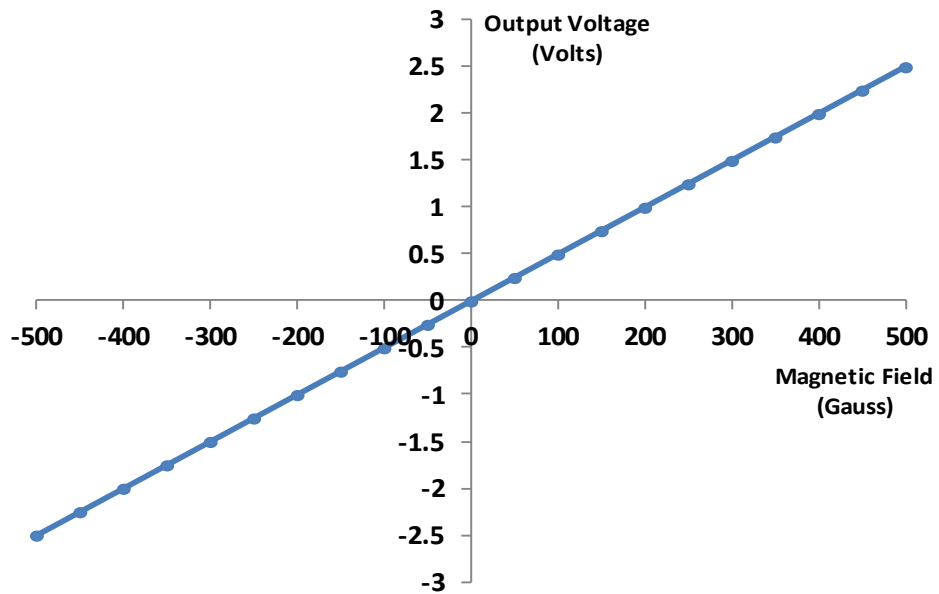


Figure 5.53 Output voltage as a function of the magnetic field

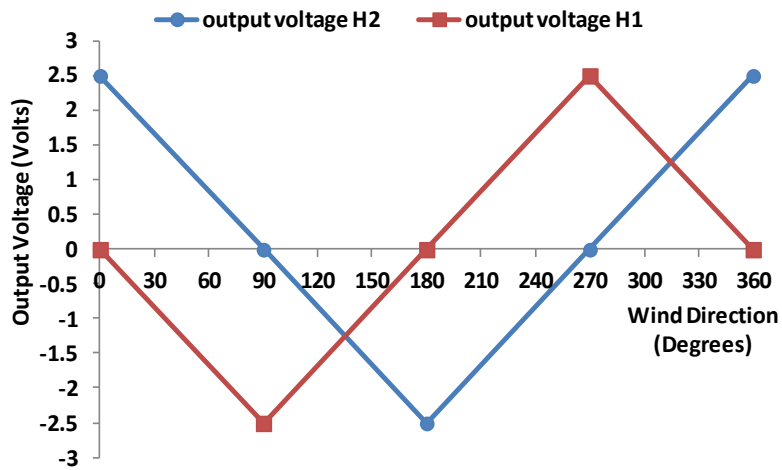


Figure 5. 54 Output voltage of each sensor as a function the wind direction

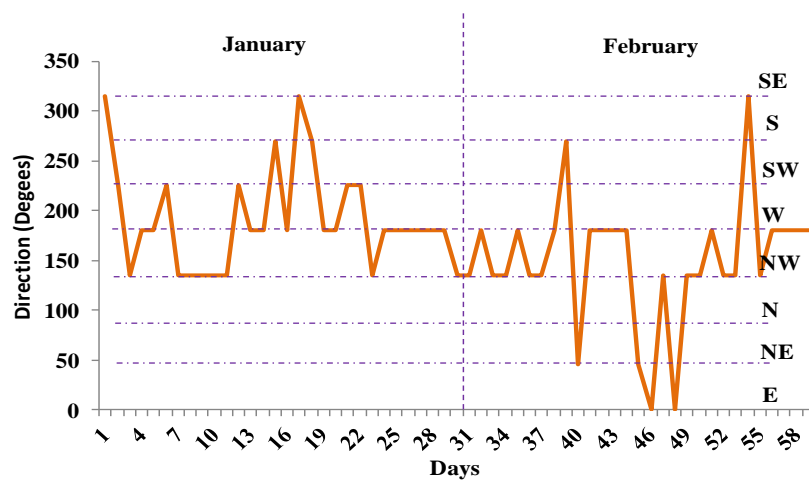


Figure 5. 55 Measures of the wind direction in real environments

#### 5.3.3.4. Solar Radiation sensor

The solar radiation sensor is based on the use of two light-dependent resistors (LDR). The main reason for using two LDRs is because the solar radiation value will be calculated as the average of the values recorded by each sensor. The processor is responsible for conducting this mathematical calculation. Figure 5.57 shows the circuit diagram. The circuit mounted in the laboratory to test its operation is shown in Figure 5.58.

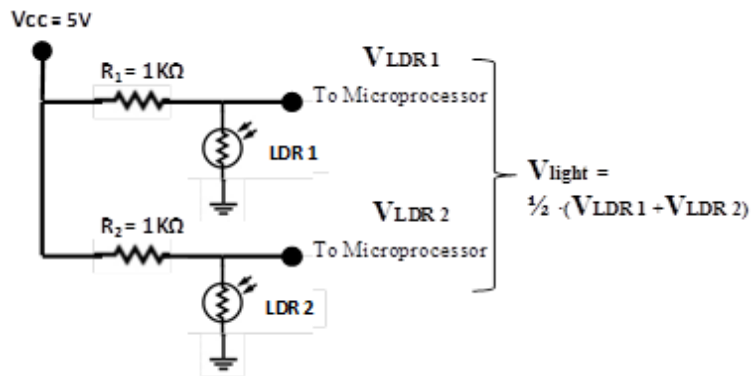
If we use the LDR placed at the bottom of the voltage divider, it will give us the maximum voltage when the LDR is in total darkness, because it is having the maximum resistance to the current flow. In this situation,  $V_{out}$  registers the maximum value. If we use the LDR at the top of the voltage divider, the result is the opposite. We have chosen the first configuration. The value of the solar radiation proportional to the detected voltage is given by the Equation 15:

$$V_{light} = \frac{V_{LDR1} + V_{LDR2}}{2} = \frac{V_{CC}}{2} \cdot \left( \left( \frac{R_{LDR1}}{R_{LDR1} + R_1} \right) + \left( \frac{R_{LDR2}}{R_{LDR2} + R_2} \right) \right) \quad (5.15)$$

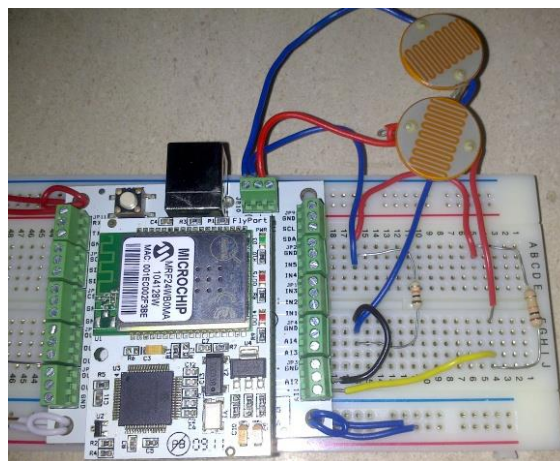
To test the operation of this circuit, we have developed a small code that allows us to collect values from the sensors (see Figure 5.59).

Figure 5.60 shows the voltage values collected during 2 minutes. As we can see, both LDRs offer fairly similar values, however, making their average value, we can decrease the error of the

measurement, due to their tolerances, which in some cases may range from  $\pm 5\%$  and  $\pm 10\%$ . Finally, the sensor is tested for two months in a real environment. Figure 5.61 shows the results obtained in this test.



**Figure 5. 56** Circuit diagram for the solar radiation sensor



**Figure 5. 57** Circuit used in our test bench.

```

while(1){
    ADCVal_LDR1 = ADCVal(1);
    ADCVal_LDR2 = ADCVal(2);
    ADCVal_LDR1 = ADCVal_LDR1 *
        2.048/1024;
    ADCVal_LDR2 = ADCVal_LDR2 *
        2.048/1024;
    Light= (ADCVal_LDR1 + ADCVal_LDR2)/2;
    sprintf(buf, "%d", ADCVal_LDR1);
    sprintf(buf, "%d", ADCVal_LDR2);
    sprintf(buf, "%d", Light);
    vTaskDelay(100);
}

```

**Figure 5. 58** Program code for the solar radiation sensor

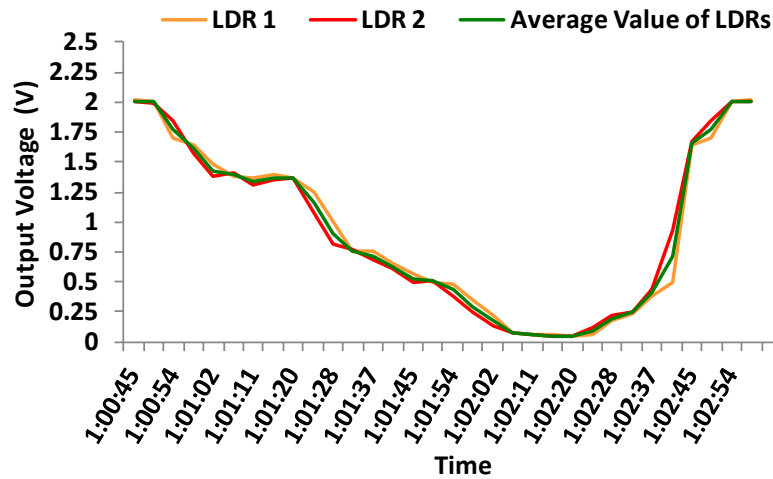


Figure 5. 59 Output voltage of both LDRs and the average value

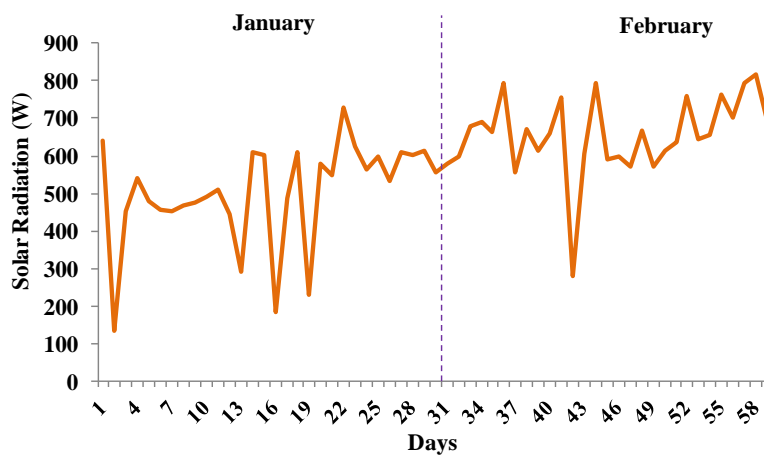


Figure 5. 60 Results of the solar radiation gathered during 2 months in a real environment.

### 5.3.3.5. Rainfall Sensor

LM331 is an integrated converter that can operate using a single source with a quite acceptable accuracy for a frequency range from 1 Hz to 10 KHz. This integrated circuit is designed for both, voltage to frequency conversion and frequency to voltage conversion. Figure 5.62 shows the conversion circuit for the frequency to voltage conversion.

The input is formed by a high pass filter with a cutoff frequency much higher than the maximum input. It makes the pin 6 to only see breaks in the input waveform and thus a set of positive and negative pulses over the  $V_{cc}$  is obtained. Furthermore, the voltage on pin 7 is fixed by the resistive divider and it is approximately  $(0.87 \cdot V_{cc})$ . When a negative pulse causes to decrease the voltage level of pin 6 to the voltage level of pin 7, an internal comparator switches its output to a high state and sets the internal Flip-Flop (FF) to the ON state. In this case, the output current is directed to pin 1.

When the voltage level of pin 6 is higher than the voltage level of pin 7, the reset becomes zero again but the FF maintains its previous state. While the setting of the FF occurs, a transistor enters its cut zone and  $C_t$  begins to charge through  $R_t$ . This condition is maintained (during  $t_c$ ) until the voltage on pin 5 reaches  $2/3$  of  $V_{cc}$ . An instant later, a second internal comparator resets the FF switching it to OFF, then the transistor enters in driving zone and the capacitor is discharged quickly. This causes the comparator to switch back the reset to zero. This state is

maintained until the FF is set with the beginning of a new period of the input frequency and the cycle is repeated.

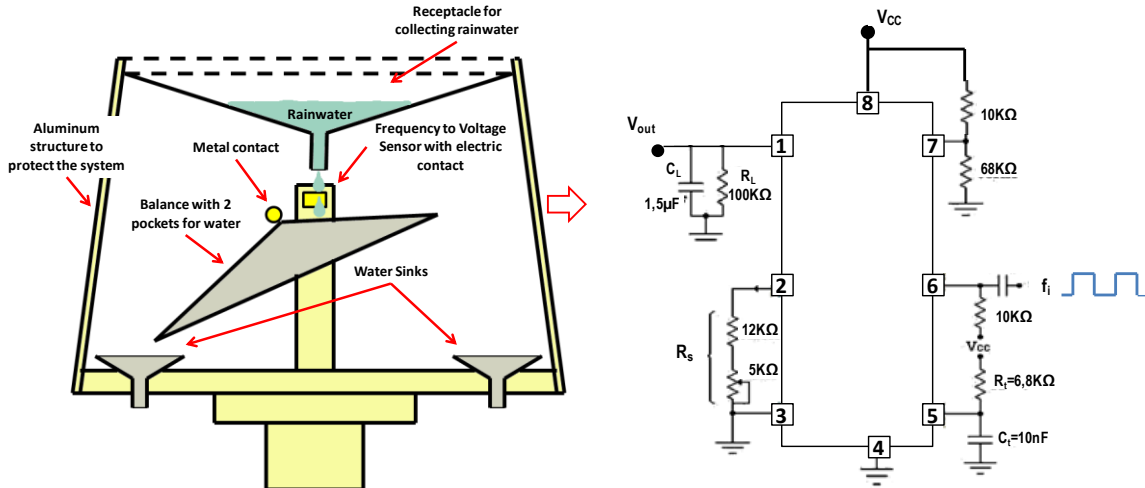


Figure 5.61 Rainfall sensor and the basic electronic scheme

A low pass filter placed at the output pin gives, as a result, a continuous  $V_{out}$  level, which is proportional to the input frequency  $f_{in}$ . As its datasheet shows, the relationship between the input frequency and the output current is shown in Eq. (5.16):

$$I_{average} = I_{pin\ 1} \cdot (1.1 \cdot R_t \cdot C_t) \cdot f_{in} \quad (5.16)$$

To finish the design of our system, we should define the relationship between the  $f_{in}$  and the amount of water. In our case, the volume of each pocket is 10 ml. Thus, the equivalence between both magnitudes is given by:

$$\left\{ \begin{array}{l} 1\text{Hz} \rightarrow 10\text{ml of water} \\ 1\text{l/m}^2 = 1\text{mm} \rightarrow 100\text{Hz} \end{array} \right.$$

Finally, this system can be used for similar systems where the pockets of water can have bigger/lower size and the amount of rainwater and, consequently, the input frequency will depend on it. The rain sensor was tested for two months in a real environment. Figure 5.63 shows the results obtained.

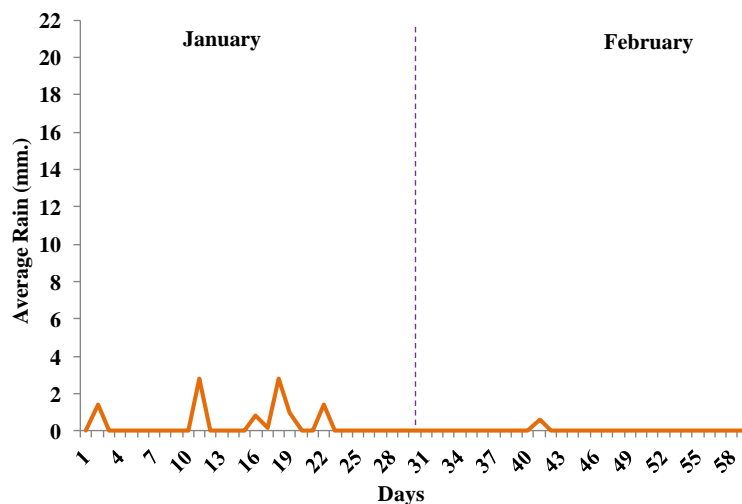


Figure 5.62 Results of Rainfall gathered during 2 months in a real environment.

### 5.3.4. Mobile platform and Network Performance

In order to connect and visualize the data in real-time, we have developed an android application which allows the user to connect to a server and see the data. In order to ensure a secure connection, we have implemented a virtual private network (VPN) protected by authorized credentials (Lin et al., 2014). This section explains the network protocol that allows a user connect with the buoy in order to see the values in real time as well as the test bench performed in terms of network performance, and the android application developed.

#### 5.3.4.1. Data acquisition system based on Android

In order to store the data in a server, we have developed a Java application based on Sockets. The application that shows the activity of the sensors in real-time is developed in Android and it allows the request of data from the mobile devices. The access from computers can be performed through the website embedded in the FlyPort. This section shows the protocol used to carry out this secure connection and the network performance in both cases.

The system consists of a sensor node (Client) located in the buoy, which is connected wirelessly to a data server (this procedure allows connecting more buoys to the system easily). There is also a VPN server which acts as a security system to allow external connections. The data server is responsible for storing the data from the sensors and process them later. The access to the data server is managed by a VPN server that controls the VPN access. The server monitors all remote access and the requests from any device. In order to see the content of the database, the user should connect to the data server following the process is shown in Figure 5.64. The connection from a device is performed by an Android application developed with this goal. Firstly, the user needs to establish a connection through a VPN. The VPN Server will check the validity of user credentials and will perform the authentication and connection establishment. After this, the user can connect to the data server to see the data stored or to the buoy to see its status in real time (both protocols are shown in Figure 5.64, one after the other consecutively). The connection with the buoy is performed using TCP sockets because it also allows us to save and store data from the sensors and process them for scientific studies. The data input/output is performed through *InputStream* and *OutputStream* objects associated to the Sockets. The server creates a *ServerSocket* with a port number as a parameter which can be a number from 1024 to 65534 (the port numbers from 1 to 1023 are reserved for system services such as SSH, SMTP, FTP, mail, www, telnet, etc.) that will be listening for incoming requests. The TCP port used by the server in our system is 8080. We should note that each server must use a different port. When the server is active, it waits for client connections. We use the function *accept()*, which is blocked until a client connects. In that case, the system returns a *Socket*, which is the connection with the client: *Socket AskCliente = AskServer.accept()*.

In the remote device, the application allows configuring the client IP address (Buoy) and the TCP port used to establish the connection (see Figure 5.65-a). Our application displays two buttons to start and stop the socket connection. If the connection was successful, a message will confirm that state. Otherwise, the application will display a message saying that the connection has failed. At that moment, we will be able to choose between data from water or data from the weather (see Figure 5.65-b). These data are shown in different windows, one for meteorological data (see Figure 5.65-c) and water data (see Figure 5.65-d)



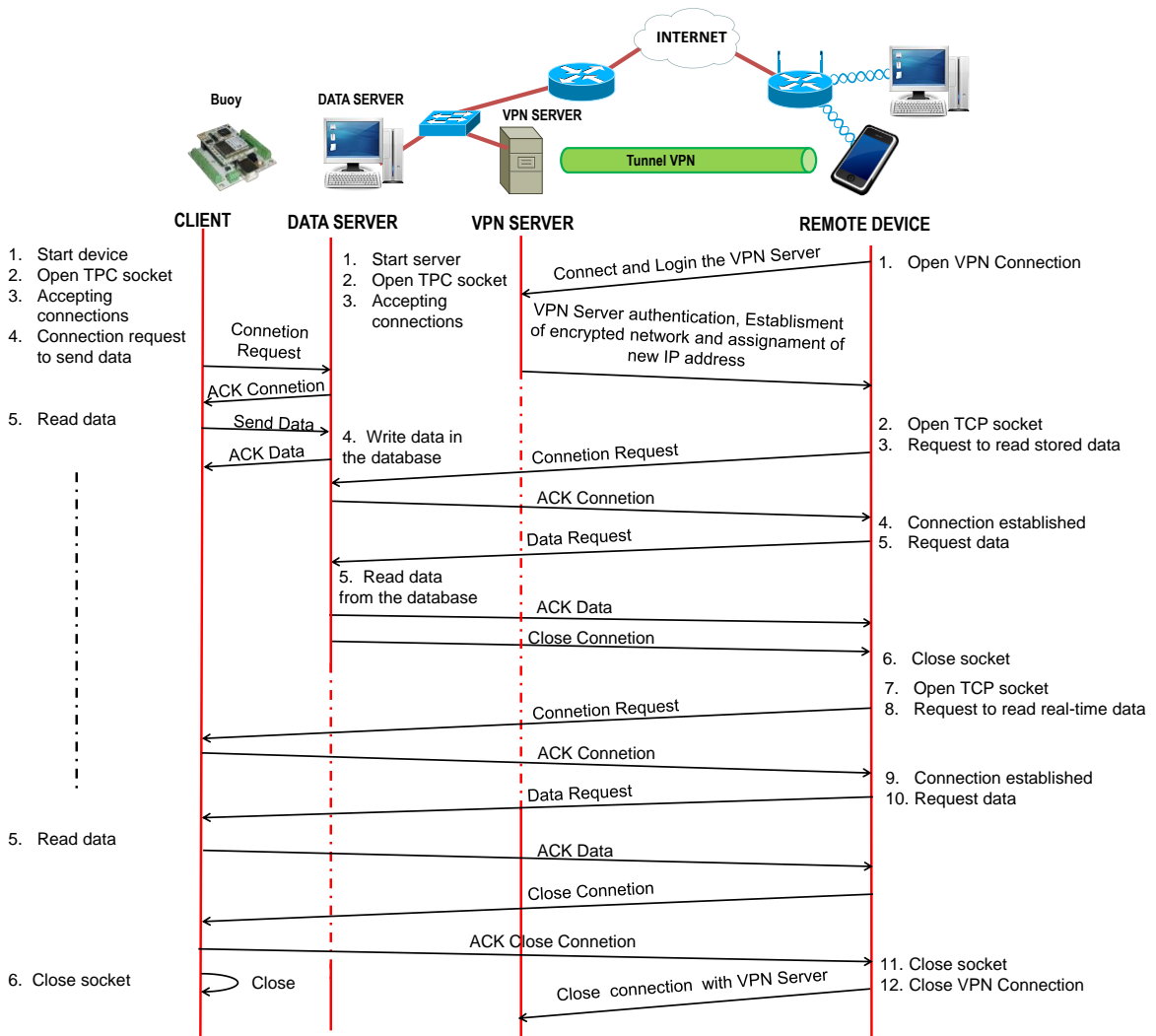


Figure 5. 63 Protocol to perform a connection with the buoy, using a VPN.

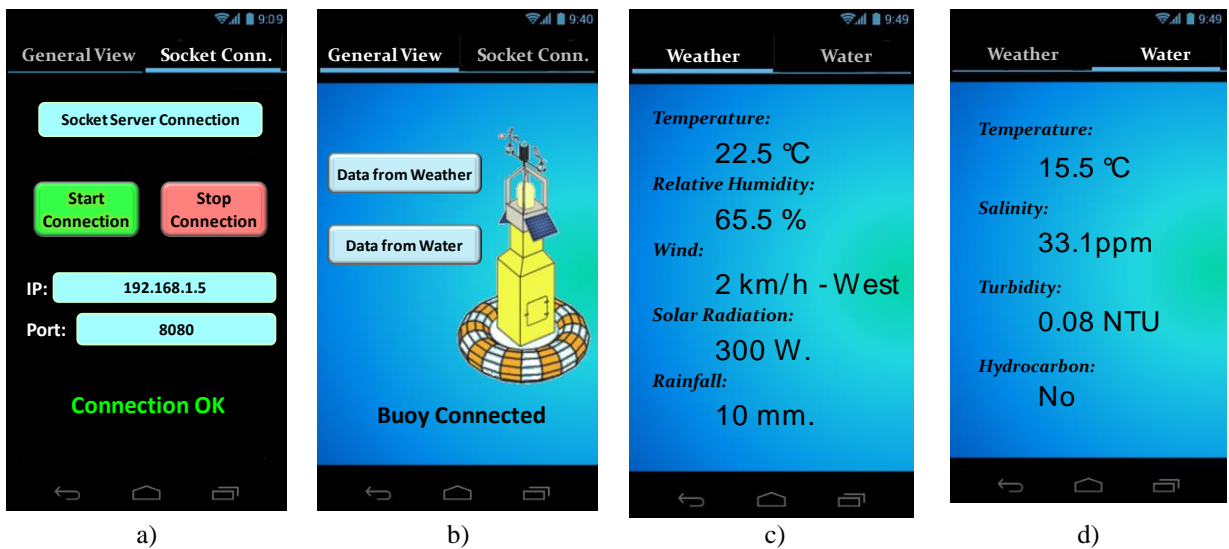


Figure 5. 64 Screenshot of our Android applications to visualize the data from the sensors.

Finally, in order to test the network operation, we carried out a test (see Figure 5.66) during 6 minutes. This test has measured the bandwidth consumed when a user accesses to the client through the website of the node and through the socket connection. As figure 5.66 shows, when the access is performed through the socket connection, the consumed bandwidth has a peak (33kbps) at the beginning of the test. Once the connection is done the consumed bandwidth decreases down to 3kbps.

The consumed bandwidth when the user is connected to the website is 100kbps. In addition, the connection between sockets seems to be faster. As a conclusion, our application presents lower bandwidth consumption than the website hosted in the memory of the node.

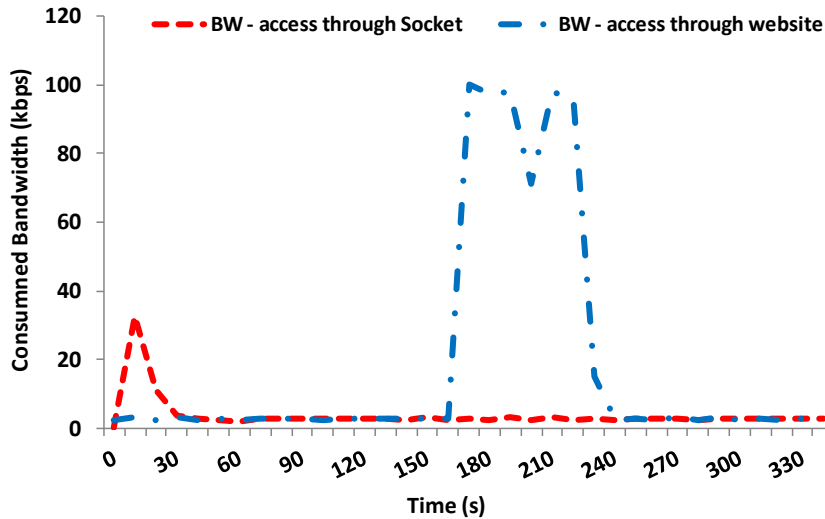


Figure 5. 65 Consumed bandwidth

## 5.4. Smart system for detecting and tracking pollutants in water

### 5.4.1. Proposed System

#### 5.4.1.1. Proposed sensor node

The nodes are small ships provided with a solar panel to power the system. Figure 5.67 shows the designed device. It has two dipoles for its communication using IEEE 802.15.4. They are separated at a distance  $\lambda$  (which is based on the working frequency). They allow connecting to the neighbors, to know which neighbor is closest than the other and which is in the right or the left side (because the signal strength will be higher in one antenna than in the other). It also has a Global Position System (GPS) antenna to know its location, and two sensors to sense the pollution and a small motor and a helix which allow them to move in different directions over the water and oil. Figure 5.68 shows a top view of the device. It is possible to customize the node, but in this case, we propose the use of a commercial module and a GPS antenna (Datasheet of GPS receiver, 2015.) connected to the Waspote through the UART ports (See Figure 5.69). This module is known as Waspote (Features of Libelium Waspote, 2015). Libelium Waspote is a device designed to create WSNs with some quite specific requirements and intended to be deployed in a real scenario. Table 5.6 shows a summary of energy consumption of both devices. It is important to note that our proposal is focused on the wireless needed technologies and the smart algorithm. For the ship movement and stability, Capocci et al. (2017) offers more information. Moreover in adverse conditions, high wind speed or high waves this system may be not useful.

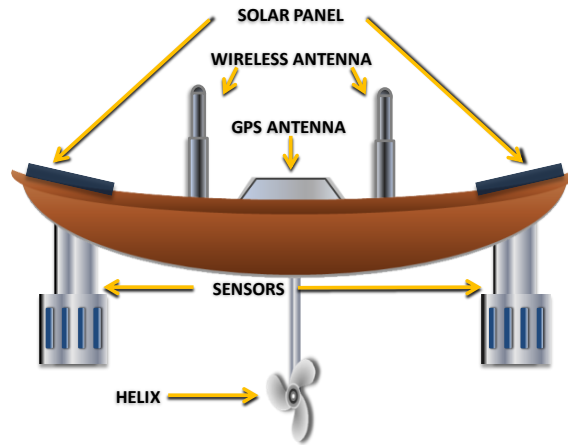


Figure 5. 66 Designed device

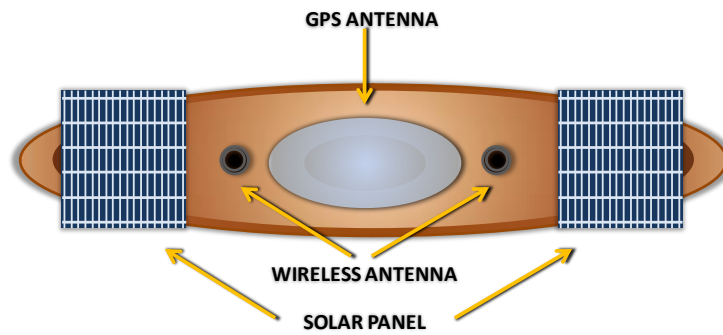


Figure 5. 67 Top view of the device



Figure 5. 68 Wasp mote and GPS receiver

Nodes are placed inside the spill of pollution as it is shown in Figure 6.70. Once nodes are placed in the polluted area, each one starts to move in a random direction to search the boundary of the polluted area. Figure 6.71 shows an example with the direction  $n$  taken by the devices.

When a node arrives at the boundary, but it has just one neighbor (in the right or the left side), it will move to the opposite direction of the neighbor, but keeping at the boundary to find a second neighbor. Then, all devices will move up to be equidistant with its neighbors. When all

nodes are in the boundary and have two neighbors, the polluted area is defined by the coordinates of each node. This information will be sent to the server through. The nodes will move following the movement of the polluted area (due to the wind, water currents or just dispersion) maintaining it equidistant to its neighbors. In Figure 6.72 shows that the devices have reached the edge of pollution and they are placed at the same distance.

The wireless technology used by the nodes to communicate is IEEE 802.15.4 because of its low power consumption.

**Table 5. 6** Energy consumption of each node

Device	Energy consumption			
	<i>Hibernate</i>	<i>Deep Sleep</i>	<i>Mode ON</i>	<i>Sleep</i>
Wasp mote	0.7 $\mu$ A	55 $\mu$ A	15mA	55 $\mu$ A
GPS	25 $\mu$ A	236 $\mu$ A	35 mA	9.2mA

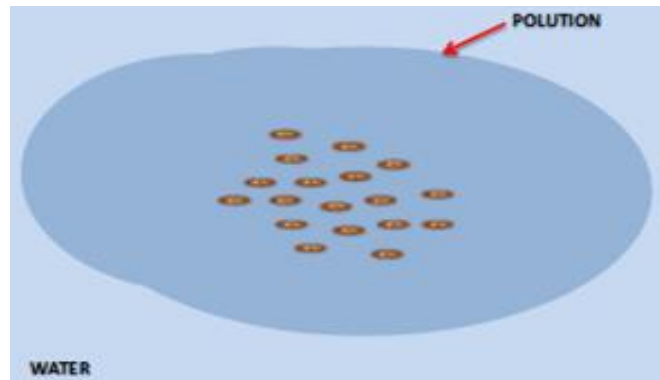


**Figure 5. 69** Devices initially positioned inside the stain

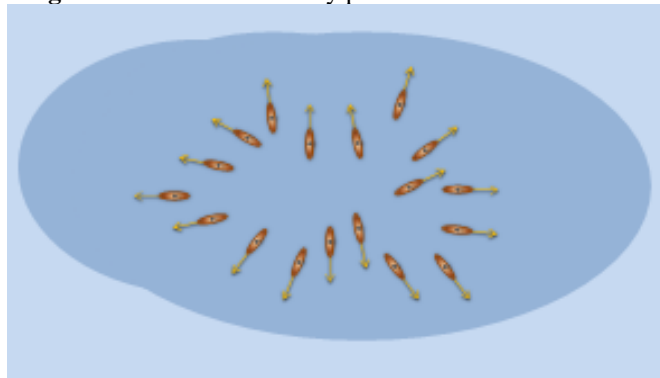


**Figure 5. 70** Devices positioned to start the displacement

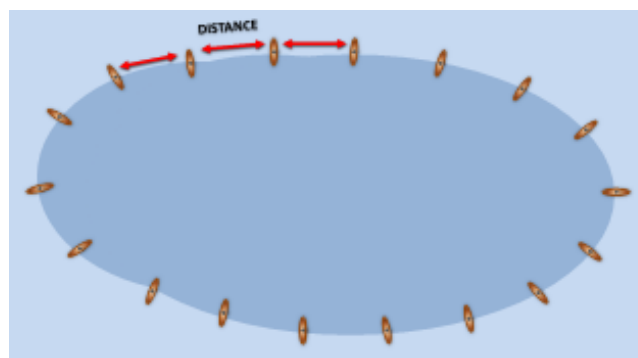


**Figure 5. 71** Devices at the boundary of the pollution

### 5.4.1.2. Designed Algorithm

In this subsection, we explain the designed algorithms.

The first algorithm is used by the nodes to reach the edge of the pollution. Initially, each device begins sensing pollution. If pollution is not detected by the two sensors will not move. If pollution is detected by the two sensors, it obtains a random number between 1 and 360. Then, the device will begin to move in the direction of the grades provided by the random number. Then, it will go straight ahead until one of the sensors senses water instead of pollution. When it happens, the device will stop. Figure 5.73 shows the algorithm to reach the boundary of the pollution.

We also designed an algorithm to keep the devices at the same distance from each other. The devices will begin a neighbor discovery phase. Once it knows all its neighbors, it chooses the closest neighbor on the left side and the closest neighbor on the right side. Then, each device calculates the distance to its neighbor using the value of the received signal strength using Eq. (5.17).

$$RSS = Lo - 20 \cdot \log_{10}(d/1000) - 20 \cdot \log_{10}(f \cdot 1000) \quad (5.17)$$

RSS indicates the received signal strength,  $Lo$  is the output power of the device (jointly with the antenna gain) when it outputs the antenna,  $d$  is the distance in meters and  $f$  is the frequency in GHz. The value of the frequency depends on the channel on which the device is configured.

The objective is to uniformly distribute the devices along the stain of pollution. So each device (except the one that only has one neighbor), will move to be at the same distance of its left and right neighbors while it keeps in the boundary of the stain (one sensor in the pollution and another sensor in the water). Once the devices are distributed a person has just to get close to one device, in order to take the GPS position of all devices (which is routed through the network), and is able to know the dimensions of the stain and its movement along the time. Figure 5.74 shows the algorithm followed by the devices to keep the same distance. The nodes are always trying to achieve the same distance from its neighbors on the right and the left side. Firstly, the node will attempt to locate its discovered neighbor on either side. The node determines the distance to their neighbors and it is positioned equidistant from both neighbors. If it only finds a neighbor, the node will move in the opposite direction to the neighbors' position with the aim of reaching new nodes. Due to the movement of this node, the node closest to him will try to follow it and its adjacent nodes will follow it, forming a cord. The movement of the nodes will cease when all nodes are equidistant.

The communication protocol designed to establish the connection between the devices is shown in Figure 5.75.

The communication protocol is as follows. Initially, each device broadcasts a "Discovery Neighbor" message to all devices under its radio coverage. Each device receiving this message will reply with a "Discovery Ack" message. Then, it will select the closest left and right neighbors by using "Association with the Closest Left Neighbor" and "Association with the Closest Right Neighbor" messages respectively. Neighbors will reply with "Association Ack" message. Then the device will move to keep the same distance to both neighbors. Once devices have been distributed, they will send their GPS position to their neighbors.

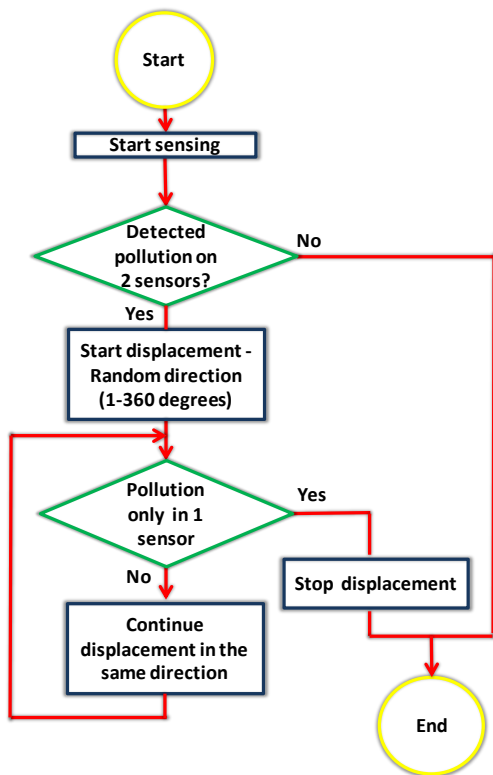


Figure 5. 72 Algorithm to reach the edge of

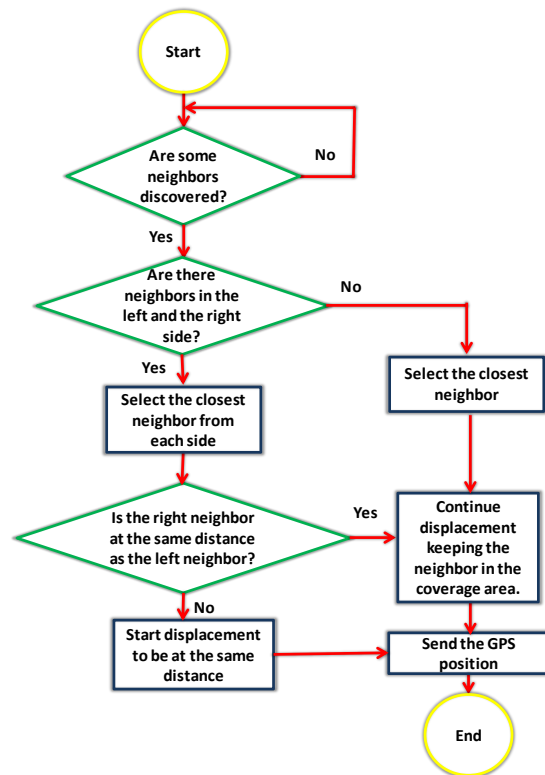


Figure 5. 73 Algorithm for devices placed at the

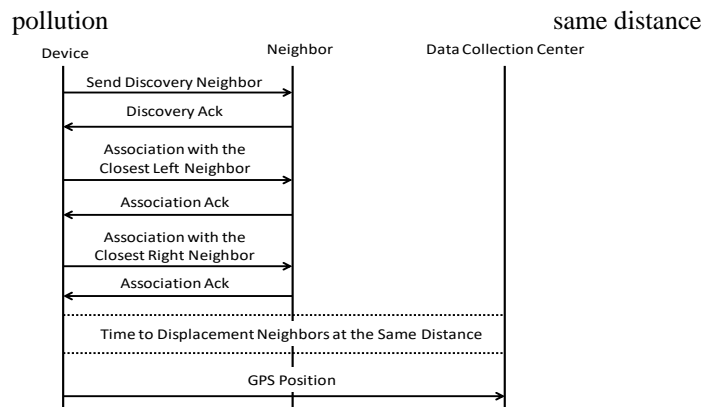


Figure 5. 74 Communication protocol to establish the connection between the devices

### 5.4.2. Network Performance

In order to test the network performance of our smart system, we have simulated the operation of the whole system and its movements using two protocols with different features. On the one hand, we have chosen a reactive protocol where it only tries to find the best routes when it is necessary. In this kind of protocols, it is assumed affordable high latency to the first packet. There is independence between the routes. Finally, although the topology changes, a single route only lives during a limited time. In this case, we have chosen AODV. On the other hand, we have selected DSDV to test a proactive protocol. These protocols are used when the network requires a quick response. In proactive protocols, when a route changes, it can affect any node and the number of useful routes is relatively high compared to all possible.

In this section, we explain the simulation parameters used for both cases and the results obtained in terms of number of broadcast packets, number of control packets and total bandwidth consumed in the network.

To perform these simulations, we have used the Dynamic Ad Hoc Routing Simulator (DARS) (DARS, 2015). It is a freeware tool that allows generating different scenarios and the nodes' movements. The parameters used in our simulations are shown in Table 5.7.

**Table 5.7** Simulation Parameters

Parameter	Simulation Parameters	
	AODV	DSDV
Number of nodes	25	25
Size of Scenario	100m x 700m	100m x 700m
Nodes' speed	0,16 m/s	0,16 m/s
Packet size	512 bytes	512 bytes
Total time of simulation	10 minutes	10 minutes

Initially, all nodes are placed approximately in the middle of the stain. After deciding where they are going to move using the algorithms shown in Figures 5.73 and 5.74, nodes start moving up to reach the boundary of the pollution stain. At this time, all nodes have 2 neighboring nodes (one per side). During the time while the nodes are moving, they are exchanging packets and information. Results are shown in Figure 5.76, Figure 5.77 and Figure 5.78.

Figure 5.76 shows the number of broadcast packets registered for both protocols. On the one hand, we can see that AODV sends periodically some broadcast packets. This happens because, when a node needs to have a useful route, the network is flooded with route request packets. The rest of time nobody needs to transmit information, so the nodes of the network do not send any packet. This is the main reason because the value of broadcast packets remains constant. On the other hand, when nodes are close to each other, the number of broadcast packets is quite high because the network is trying to find the optimal route. As the nodes move away from each other the number of possible routes decreases and consequently, the number of broadcast packets also decreases.

As a consequence of the number of broadcast packets, the nodes generate control packets to reply the network requests. Figure 5.77 shows the number of control packets registered for AODV and DSDV. We can observe similar behavior for both cases where, as nodes are arriving at the edge of the pollution stain (and the number of neighbors decreases), the number of control packets also decrease. However, the number of packets for DSDV is higher than the number of packets for AODV.

Finally, Figure 5.78 shows the consumed bandwidth for the whole network as a function of time. As we can see the biggest difference is detected up to second 225 of simulation, where the nodes are moving and the network topology suffers the most radical changes.

In all three figures (Figure 5.76, Figure 5.77 and Figure 5.78), in the case of DSDV it is observed a zone where the number of packets presents a valley. This happens because of the movement of the nodes. During this period of time, the relative movement between nodes is lower. For AODV, the packets are periodically sent without taking into account the movement of the nodes.

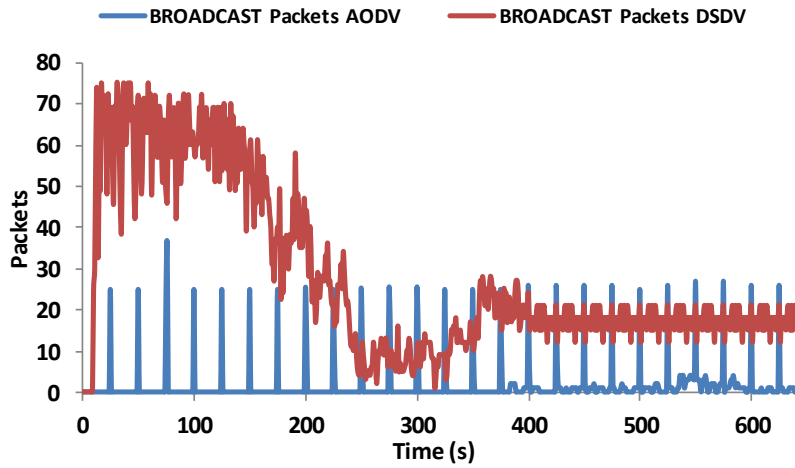


Figure 5. 75 Number of Broadcast packets registered for AODV and DSDV protocols

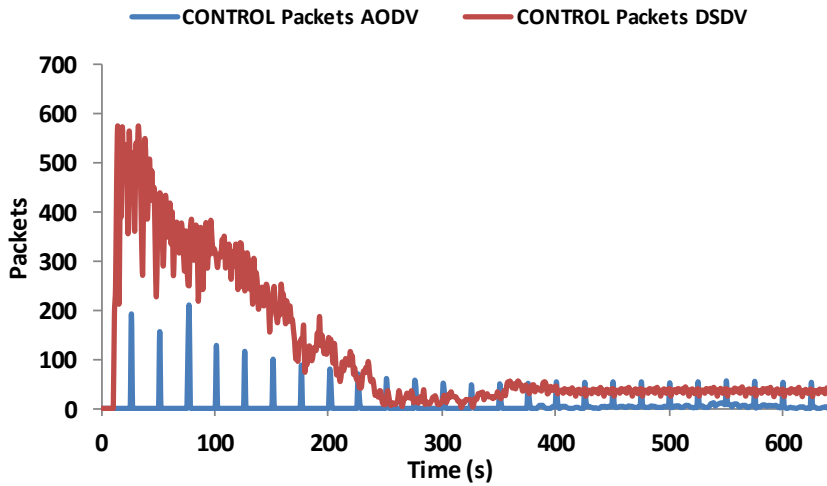


Figure 5. 76 Number of control packets registered for AODV and DSDV protocols

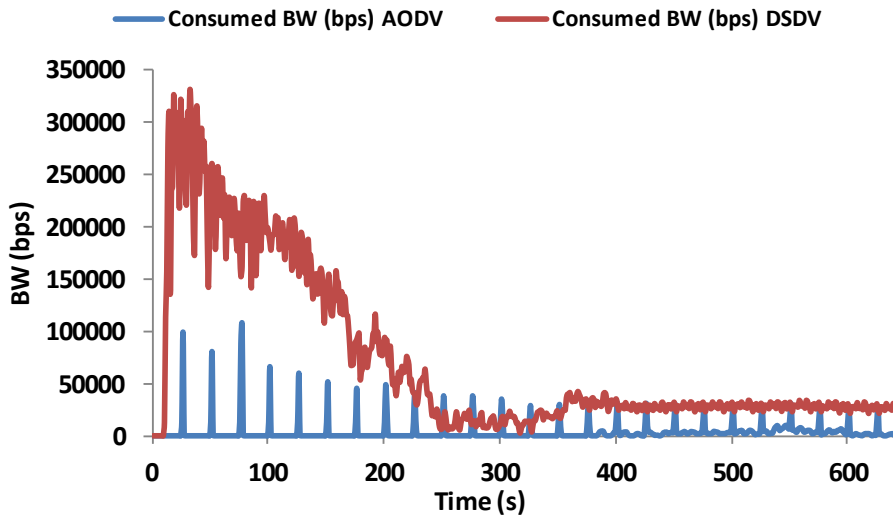


Figure 5. 77 Consumed bandwidth for AODV and DSDV protocol



## 5.5. Conclusion

In this chapter, we have shown the different developed systems for sensible marine environments. Our systems are able to measure different water parameters and meteorological conditions. Moreover, we can send the gathered data by different methods. In addition, we show a system to detect and track pollution in a water body.

First, we have presented a system for monitoring the outflow plume at the river mouth and mangrove forest. We have described the design and deployment of our system in terms of salinity sensor, description of wireless module and server program to store data in a DB. The system has been tested with real samples in real scenarios. The results have been shown on a website that makes easy the observation of salinity evolution. The results show that, regarding salinity measurements, our system presents stable values and the consumed bandwidth is low and we will be able to handle a large number of wireless modules without registering significant delays in communications. As a future work, we would like to use a more secure way of communication using SSLsockets. In addition, we want to extend the use of our application for other well-known wireless modules such as Waspote. Taking advantage of the server configuration, new sensors can be added for monitoring other parameters such as water flow or presence of pollution. The system could also be used to monitor water supplies in precision agriculture.

Following, we have presented an oceanographic multisensor buoy which is able to measure all important parameters that can affect these natural areas. The buoy is based on several low-cost sensors which are able to collect data from water and from the weather. The data collected for all sensors are processed using a microcontroller and stored in a database held in a server. The buoy is wirelessly connected to the base station through a wireless a FlyPort module. Finally, the individual sensors, the network operation, and mobile application to gather data from buoy are tested in a controlled scenario. After analyzing the operation and performance of our sensors, we are sure that the use of this system could be very useful to protect and prevent several damages that can destroy these habitats. The first step of our future work will be the installation of the whole system in a real environment; near to Alicante (Spain). We would also like to adapt this system for monitoring and controlling the fish feeding process in marine fish farms in order to improve their sustainability (Garcia et al., 2011). We will improve the system by creating a bigger network for combining the data of both, the multisensor buoy and marine fish farms, and apply some algorithms to gather the data (Meghanathan & Mumford, 2013). In addition, we would like to apply new techniques for improving the network performance (Rosário et al., 2012), security in transmitted data (Dutta and Annappa, 2014) and its size, by adding an ad hoc network to the buoy (Rosário et al., 2012), as well as some other parameters as decrease the power consumption (Compte et al., 2011).

Moreover, we have proposed an intelligent system based on a mobile wireless sensor network based on IEEE 802.15.4 technology that uses a smart algorithm for detecting, tracking and locating pollution stains. Our nodes are able to move along the polluted area thanks to a small motor. First, nodes calculate their movement direction from a random number. When they reach the stain boundary, nodes run an algorithm that makes them distribute at an equidistant distance to their neighbors. When all nodes are in the boundary and have two neighbors, anyone can take a complete information of the stain just reaching one device. The system has been simulated using AODV and DSDV. Our results show that DSDV routing protocol presents a very high traffic data through the network compared to AODV. This will imply higher energy consumption in the whole network. As future work, we will develop and test our system in a real environment. In addition, we will also test the network operation with another kind of protocols such as hybrid ones. Moreover, we will extend this system to group-based topologies (Lloret et al., 2008a), (Lloret et al., 2008b). Finally, we want to try simulations with a bigger number of nodes in order to analyze the scalability of our structure. We think that in these hypothetical new cases, we will detect an important increase in the number of broadcast packets and a bigger number of packets at the beginning of network operation. However, we are sure that the convergence time will be considerably reduced.

Finally, work presented in this chapter has been published in the following references (Parra et al., 2014), (Parra et al., 2015a), (Sendra et al., 2015b), (Parra et al., 2015b)

## **6. CONCLUSIONS AND FUTURE WORK**

## **6.1. Introduction**

In this chapter, we present the main conclusions of this thesis and the future work related to the different areas.

As at the end of chapters 2 to 5, we have presented the summaries and conclusions about the topics discussed in each of them, in this chapter we are going to present these findings with a global perspective.

We can see at the beginning of this dissertation that there is a lack in the current technological solution for aquaculture monitoring. The aquaculture should take advantage of the opportunities that are offered by the emerging technologies such as sensors, WSN, and IoT among other in order to achieve the sustainability as other activities of the primary sector have been done. Nevertheless, the available options for precision aquaculture are far away from being competitive. Many solutions appear in literature, but they monitor few parameters and are expensive.

In this thesis, we have studied the current options and the needs of aquaculture monitoring systems. Moreover, we have proposed our solution. We designed, developed and deployed our own low-cost sensors for water quality, tank environment, and fish feeding behavior monitoring. In some cases we use the same methods than the current commercial systems, as in the case of turbidity sensors which are based on optical methods. Nevertheless, our turbidity sensors are able to distinguish sediment from phytoplankton and no turbidity sensor in the literature is able to do it. In other cases, as the salinity sensor, our proposal is different to the sensors presented in the literature. Though, the proposed sensors are created bearing in mind the need for low-cost and the use of simple electronic components. All the sensors have been calibrated and verified. Some of the developed sensors are completely new and totally different from the existing options in the literature. This is the case of the fish presence sensor and the feed falling sensor. The proposed sensors are integrated in Chapter 4 in different solutions for many of the problems presented in fish farms. The proposed solutions include (i) a control of the salinity increase in the recirculating systems, (ii) an automatic alarm system to control of turbidity and temperature in open systems, (iii) control of the entire tank status and (iv) automatic adjustment of feed supply velocity.

In addition to the mentioned solutions, because of the opportunity of having low-cost systems for water quality monitoring, different applications have been proposed for other protected aquatic environments. These applications use part of the developed sensors for aquaculture monitoring. Nevertheless, we develop some specific sensors for rain, humidity and wind monitoring.

The rest of the Chapter is structured as follows, Section 6.2 shows the conclusions. The future work is presented in Section 6.3. Section 6.4 shows the fulfillment of the objectives and the difficulties founded during this thesis. Finally, Section 6.5 presents the list of publications derived from the thesis.

## **6.2. Conclusions**

Throughout this dissertation, we have seen the improvement provided by each one of our proposals and deployments. In this subsection, we are going to show a summary of every contribution performed on behalf of this Doctoral Thesis.

In this dissertation, we have presented the main needs of aquaculture monitoring as the effects of different environmental parameters in the fish performance. Moreover, we show the current options for water quality monitoring and the requirements for the sensors employed in aquaculture monitoring. The current systems for aquaculture monitoring are presented and we demonstrated how these systems do not accomplish with the set requirements of the ideal system for precision aquaculture.

The creation of low-cost sensors for water quality monitoring is included in this thesis. The major efforts are done in the creation of the salinity sensor. We conclude that the traditional sensors for salinity monitoring are not the best option for long-term monitoring and that

inductive sensor is needed. However, in the literature, there is no information about the inductive salinity sensors. Thus, many prototypes were created and tested in order to select the prototype with the highest accuracy and lower price. Moreover, a turbidity sensor able to quantify the turbidity and distinguish different turbidity sources was developed. Considering the current sensors for turbidity monitoring and on a prototype created previously by our group (Sendra et al., 2013b) we employ four LEDs with different wavelength to characterize the turbidity. The proposed prototype has a low-cost and a low-energy consumption due to the intelligent algorithm that turns on/off the LEDs and detectors to save energy. Finally, a hydrocarbon sensor was designed and developed. This sensor is based on differences between the refraction and fluorescent effect of water and hydrocarbon. Again, different LED sources were tested. The best results were obtained with the white LED. The obtained sensor was able to detect the presence of hydrocarbon in the water but it was not possible to quantify it.

Following, the integration of those sensors and other ones in applications for aquaculture monitoring has been included in this thesis. The objective was to show how the use of sensors can increase the sustainability and profit of the aquaculture. We proposed different systems to solve some of the problems in the aquaculture inland facilities employing the proposed sensors. The proposed systems can control the water quality including the following parameters temperature, salinity, turbidity (concentration and characteristics), presence of hydrocarbon or oil layer over the water. Moreover, we can monitor other parameters related to the tank environment such as water level, illumination, the presence of workers in the area, and humidity. In addition, the fish feeding behavior can be monitored as the shoal swimming depth and an estimation of changes in velocity and the feed falling. Thus, we can monitor the environment and the fish behavior in order to detect changes and send alarms to correct the possible alterations. Thus, the system will improve the fish well-being and therefore the fish performance. In addition, the adjustment of the feeding process to the fish behavior can increment the economic profit of the facilities. All the employed sensors in our applications are developed in this thesis and present low-cost. Moreover, we have developed different algorithms in order to reduce the energy waste by turning on the systems only when they need, as it was done in the automatic adjustment of the feed supply velocity. Other algorithms were developed to decide if the nodes send the gathered data or not in order to reduce the energy waste and increase the number of nodes per AP. Our price estimation for monitoring each tank with all the developed sensors is lower than 100€, while the current system can cost more than several thousands of euros for each tank. With this low-cost system, we can promote the creation of a truly precision aquaculture.

Finally, we discuss how these sensors can be used in other natural environments were shown. We have developed applications for salinity monitoring in estuaries and mangrove forests, that are endangered and the salinity changes cause a reduction in the germination. In addition, a buoy for monitoring the changes in the oceanic climate was proposed. Lastly, an intelligent system for detecting and tracking pollution in a water body is presented.

### **6.3. Future work**

Following the ideas and proposals presented in this thesis, we can propose different futures projects to continue this investigation.

The first and most obvious future work is to continue with the development of new low-cost sensors that can be useful for aquaculture as the dissolved oxygen sensor. In addition, we pretend to use another turbidity sources to test the proposed turbidity sensor.

Moreover, we pretend to find out other applications for the inductive coils. We plan to use them to detect the feed falling coiling the coils over the drainage system. A recent test has demonstrated that the coils can be used to measure the sediment in the water.

As we developed many sensors we are planning to deploy them in production fish farms and start to collect data in order to apply data mining techniques and find out possible relationships. The systems presented in this thesis have been deployed in research facilities, not

in production facilities.

In addition, we plan to improve the method to measure the fish swimming behavior. Due to the option to use small nodes, we would like to put accelerometers, pressure sensors and a node in the fish farmed fish. This option is only possible for big fishes like salmon or tunas.

Moreover, we would like to adapt our sensors to deploy them in cages in the sea. In order to achieve this, it will be necessary to improve the waterproof isolation.

Finally, with the learned lessons in this thesis, we are going to develop low-cost sensors for optimizing another activity of the primary sector, the irrigation process in the arid regions of North Africa employing nonconventional water sources.

#### **6.4. Fulfillment of the objectives and difficulties found during the process**

In this section, we are going to present the fulfillment of the established objectives in Chapter 1. In addition, we are going to detail the difficulties founded during the thesis.

The set objectives in Chapter 1 were:

- Selecting the environmental parameters that may affect the fish performance including fish growth, survival, and natatorium behavior.
- Designing and developing physical sensors with low-cost capable to measure the selected parameters in an underwater environment.
- Creating the physical part of the required sensors for monitoring the water parameters and environmental parameters.
- Selecting the best location for each calibrated sensor in order to gather the data optimally.
- Creating smart algorithms to automate processes in the fish farms to enhance the fish well-being and the environmental sustainability.
- Gather data from the physicochemical parameters and from the fish behavior.

We can conclude that all the objectives have been fulfilled.

The main difficulties found in this thesis are linked to its multidisciplinary characteristics. I have had to integrate my background knowledge on environmental sciences and on aquaculture with the information related to the ICT. I have to learn about many different areas such as electronics and telecommunications in order to develop my own sensors and to understand how the nodes work. Fortunately, my colleges from different areas helped me to understand many ideas. The opportunity to work in a multidisciplinary team was useful because we had the chance to apply our knowledge and publications in different areas. It helps to have a global vision of each proposal. I consider that the knowledge acquired by my colleges gave me another point of view of the environmental problems and how to propose solutions. However, it was not always easy to integrate my background knowledge with the new ideas from the ICT.

The other difficulty found was related to the fact that our systems cannot be tested in real fish farm production systems. Although at the beginning of my thesis we arranged with an aquaculture producer to allow us to test the proposed system there, the conditions changed and it was no longer possible. Thus, we had to test our systems in laboratory and in aquaculture research facilities.

#### **6.5. Publications derived from the PhD**

Next papers are derived from the research presented in this dissertation or very related to it. The papers that are directly related to the dissertation are the following papers:

Journal papers:

- Parra, L., Sendra, S., Lloret, J., & Bosch, I. (2015). Development of a conductivity sensor for monitoring groundwater resources to optimize water management in smart city environments. *Sensors*, 15(9), 20990-21015.
- Sendra, S., Parra, L., Lloret, J., & Jiménez, J. M. (2015b). Oceanographic multisensor buoy based on low cost sensors for posidonia meadows monitoring in Mediterranean Sea. *Journal of Sensors*, 2015.
- Parra, L., Sendra, S., Lloret, J., & Rodrigues, J. J. (2017). Design and deployment of a smart system for data gathering in aquaculture tanks using wireless sensor networks. *International Journal of Communication Systems*, 30(16).
- Parra, L., Rocher, J., Escrivá, J., & Lloret, J. (2018). Design and development of low cost smart turbidity sensor for water quality monitoring in fish farms. *Aquacultural Engineering*, 81, 10-18.
- Parra, L., Sendra, S., García, L., Lloret, J. (2018). Design and Deployment of Low-Cost WSN Sensors for Monitoring the Water Quality and Fish Behavior in Aquaculture Tanks during the Feeding Process, *Sensors*, 18(3).
- Parra, L., Lloret, G., Lloret, J., Rodilla, M. (2018). Physical sensors for precision aquaculture: A Review, *IEEE Sensor Journal*, 18(10), 3915-3923.
- Parra, L., Sendra, S., García, L., Lloret, J. (2018). The use of sensors for monitoring the feeding process and adjust the feed supply velocity in fish farms, *Journal of Sensors*. (In revision process)

#### Conference papers:

- Parra, L., Karampelas, E., Sendra, S., Lloret, J., & Rodrigues, J. J. (2015). Design and deployment of a smart system for data gathering in estuaries using wireless sensor networks. In *Proceedings of the 2015 International Conference on Computer, Information and Telecommunication Systems*, Gijon, Spain, July 15-17 2015, 1-5.
- Parra, L., Ortuño, V., Sendra, S., Lloret, J. (2013) Low-Cost Conductivity Sensor Based on Two Coils. In *Proceedings of the First International Conference on Computational Science and Engineering (CSE'13)*, Valencia, Spain, 6-8 August 2013, pp. 107-112
- Parra, L., Ortuño, V., Sendra, S., Lloret, J. (2013) Two New Sensors Based on the Changes of the Electromagnetic Field to Measure the Water Conductivity. In *Proceedings of the Seventh International Conference on Sensor Technologies and Applications (SENSORCOMM 2013)*, Barcelona, Spain, 25-31 August 2013; pp. 266-272.
- Parra, L., Ortuño, V., Sendra, S., Lloret, J. (2013) Water Conductivity Measurements Based on Electromagnetic Fields. In *Proceedings of the First International Conference on Computational Science and Engineering (CSE'13)*, Valencia, Spain, 6-8 August 2013; pp. 139-144.
- Parra, L., Sendra, S., Jimenez, J. M., & Lloret, J. (2015). Smart system to detect and track pollution in marine environments. In *Proceedings of the 2015 IEEE International Conference on Communication Workshop*, London, U.K., 8 - 12 Jun 2015 (pp. 1503-1508).
- Parra, L., Sendra, S., Lloret, J., & Rodrigues, J. J. 2014. Low cost wireless sensor network for salinity monitoring in mangrove forests. In *Proceedings of the IEEE SENSORS 2014*, Valencia, Spain, 02 - 05 Nov 2014 (pp. 126-129).
- Parra, L., Sendra, S., Lloret, J., & Bosch, I. (2015). Development of a conductivity sensor for monitoring groundwater resources to optimize water management in smart city environments. *Sensors*, 15(9), 20990-21015.
- Parra, L., Sendra, S., Lloret, J., & Mendoza, J. (2015). Low cost optic sensor for hydrocarbon detection in open oceans. *Instrumentation viewpoint*, (18), 45-45.

Rocher, J., Taha, M., Parra, L., & Lloret, J. (2017). Design and deployment of a WSN for water turbidity monitoring in fish farms. In Proceedings of the 10th IFIP Wireless and Mobile Networking Conference (WMNC), 2017, Valencia, Spain, 25-27 Sept 2017.

## **Bibliography**

- 5200A Multiparameter, <https://www.ysi.com/5200A>. Last access: 19/09/2017
- 5400 MultiDO, <https://www.ysi.com/5400>. Last access: 19/09/2017
- 5500D MultiDO t, <https://www.ysi.com/5500d>. Last access: 19/09/2017
- 74LVC1G3157 Single-Pole Double-Throw Analog Switch, 2018. <https://assets.nexperia.com/>
- Adewolu, M. A., Adeniji, C. A., & Adejobi, A. B. (2008). Feed utilization, growth and survival of *Clarias gariepinus* (Burchell 1822) fingerlings cultured under different photoperiods. *Aquaculture*, 283(1-4), 64-67.
- Akyildiz, I. F., Pompili, D., & Melodia, T. (2005). Underwater acoustic sensor networks: research challenges. *Ad hoc networks*, 3(3), 257-279.
- Albaladejo, C., Sánchez, P., Iborra, A., Soto, F., López, J. A., & Torres, R. (2010). Wireless sensor networks for oceanographic monitoring: A systematic review. *Sensors*, 10(7), 6948-6968.
- Albaladejo, C., Soto, F., Torres, R., Sánchez, P., & López, J. A. (2012). A low-cost sensor buoy system for monitoring shallow marine environments. *Sensors*, 12(7), 9613-9634.
- Albuquerque, J. S., Pimentel, M. F., Silva, V. L., Raimundo, I. M., Rohwedder, J. J., & Pasquini, C. (2005). Silicone sensing phase for detection of aromatic hydrocarbons in water employing near-infrared spectroscopy. *Analytical chemistry*, 77(1), 72-77.
- Alkandari, A. (2011). Wireless sensor network (WSN) for water monitoring system: Case study of Kuwait beaches. *International Journal of Digital Information and Wireless Communications (IJDIWC)*, 1(4), 709-717.
- Alrajeh, N. A., Lloret, J., & Canovas, A. (2014). A framework for obesity control using a wireless body sensor network. *International Journal of Distributed Sensor Networks*, 10(7), 534760.
- AlZubi, H. S., Al-Nuaimy, W., Buckley, J., & Young, I. (2016, March). An intelligent behavior-based fish feeding system. In *Proceedings of the 2016 13th International Multi-Conference on Systems, Signals & Devices (SSD)*, Leipzig, Germany, 21 - 24 Mar 2016, 22-29.
- Amaya, E. A., Davis, D. A., & Rouse, D. B. (2007). Replacement of fish meal in practical diets for the Pacific white shrimp (*Litopenaeus vannamei*) reared under pond conditions. *Aquaculture* 262(2): 393-401.
- Amazon Web Services Platform, 2018. [https://aws.amazon.com/?nc1=h\\_ls](https://aws.amazon.com/?nc1=h_ls) (accessed on 23 February 2018).
- Amazon Web Services Platform, 2018. [https://aws.amazon.com/?nc1=h\\_ls](https://aws.amazon.com/?nc1=h_ls) (accessed on 23 February 2018).
- Anastasi, G., Conti, M., Di Francesco, M., & Passarella, A. (2009). Energy conservation in wireless sensor networks: A survey. *Ad hoc networks*, 7(3), 537-568.
- Antonov, J. I., Seidov D., Boyer T. P., Locarnini R. A., Mishonov A. V., Garcia H. E., Baranova O. K., Zweng M. M., Johnson D. R. (2010). *World Ocean Atlas 2009 Volume 2: Salinity*. S. Levitus Ed. NOAA Atlas NESDIS 69, U.S. Gov. Printing Office, Washington, D.C., 184 pp.
- APHA, AWWA, WEF. *Standard Methods for examination of water and wastewater*. 22nd ed. Washington: American Public Health Association; 2012, 1360 pp. ISBN 978-087553-013-0
- APROMAR (2017). *La Acuicultura en España 2017*. Asociación Empresarial de Productores de Cultivos Marinos en España. Madrid. España.
- Aqua TROLL 400, [https://in-situ.com/wp-content/uploads/2014/11/Aqua\\_TROLL\\_400\\_Manual .pdf](https://in-situ.com/wp-content/uploads/2014/11/Aqua_TROLL_400_Manual.pdf). Last access: 19/09/2017
- Aqua TROLL 600, [https://in-situ.com/wp-content/uploads/2015/09/Aqua\\_TROLL\\_600\\_Spec .pdf](https://in-situ.com/wp-content/uploads/2015/09/Aqua_TROLL_600_Spec.pdf). Last access: 19/09/2017
- AQUAlogger 520, [http://www.aquatecgroup.com/images/products/Technical\\_datasheet\\_AQUA\\_logger520.pdf](http://www.aquatecgroup.com/images/products/Technical_datasheet_AQUA_logger520.pdf). Last access: 19/09/2017
- AQUAlogger 530, [http://www.aquatecgroup.com/images/products/Technical\\_datasheet\\_AQUA\\_logger530.pdf](http://www.aquatecgroup.com/images/products/Technical_datasheet_AQUA_logger530.pdf). Last access: 19/09/2017
- AQUAlogger 540, [http://www.aquatecgroup.com/images/products/Technical\\_datasheet\\_AQUAlogger540.pdf](http://www.aquatecgroup.com/images/products/Technical_datasheet_AQUAlogger540.pdf). Last access: 19/09/2017
- Ardjosoediro, I., & Ramnarine, I. W. (2002). The influence of turbidity on growth, feed conversion and survivorship of the Jamaica red tilapia strain. *Aquaculture*, 212(1-4), 159-165.
- Armstrong, J. D., Braithwaite, V. A., & Rycroft, P. (1996). A flat-bed passive integrated transponder antenna array for monitoring behaviour of Atlantic salmon parr and other fish. *Journal of Fish Biology*, 48(3), 539-541.



- Arvedlund, M., McCormick, M. I., & Ainsworth, T. (2000). Effects of photoperiod on growth of larvae and juveniles of the anemonefish *Amphiprion melanopus*. *Naga, the ICLARM Quarterly* 23(2): 18-23.
- Atoum, Y., Srivastava, S., & Liu, X. (2015). Automatic feeding control for dense aquaculture fish tanks. *IEEE Signal Processing Letters*, 22(8), 1089-1093.
- Au, D. W. T., Pollino, C. A., Wu, R. S. S., Shin, P. K. S., Lau, S. T. F., & Tang, J. Y. M. 2004. Chronic effects of suspended solids on gill structure, osmoregulation, growth, and triiodothyronine in juvenile green grouper *Epinephelus coioides*. *Marine ecology progress series*, 266, 255-264.
- Ayaz, M., Baig, I., Abdullah, A., & Faye, I. (2011). A survey on routing techniques in underwater wireless sensor networks. *Journal of Network and Computer Applications*, 34(6), 1908-1927.
- Azaza, M. S., Dhraief, M. N., & Kraiem, M. M. (2008). Effects of water temperature on growth and sex ratio of juvenile Nile tilapia *Oreochromis niloticus* (Linnaeus) reared in geothermal waters in southern Tunisia. *Journal of thermal Biology* 33(2): 98-105.
- Azizi, R. (2016). Consumption of energy and routing protocols in wireless sensor network. *Network Protocols and Algorithms*, 8(3), 76-87.
- Bani, A., Tabarsa, M., Falahatkar, B., & Banan, A. (2009). Effects of different photoperiods on growth, stress and haematological parameters in juvenile great sturgeon *Huso huso*. *Aquaculture Research* 40(16): 1899-1907.
- Barlow, C. G., Pearce, M. G., Rodgers, L. J., & Clayton, P. (1995). Effects of photoperiod on growth, survival and feeding periodicity of larval and juvenile barramundi *Lates calcarifer* (Bloch). *Aquaculture* 138(1): 159-168.
- Bartz, R. (1994). U.S. Patent No. 5,350,922. Washington, DC: U.S. Patent and Trademark Office.
- Beauveau, P., Schwartz, J., & Levin, R. 2014. Drinking water quality and hospital admissions of elderly people for gastrointestinal illness in Eastern Massachusetts, 1998–2008. *Water research*, 52, 188-198
- Biard, J. R. (1996). U.S. Patent No. 5,589,935. Washington, DC: U.S. Patent and Trademark Office.
- Bin Omar, A. F., & Bin MatJafri, M. Z. 2009. Turbidimeter design and analysis: a review on optical fiber sensors for the measurement of water turbidity. *Sensors*, 9(10), 8311-8335.
- Biswas, A. K., Seoka, M., Inoue, Y., Takii, K., & Kumai, H. (2005). Photoperiod influences the growth performance and stress response of juvenile red sea bream (*Pagrus major*). *Aquaculture* 258(1): 350-356.
- Biswas, A. K., Seoka, M., Ueno, K., Yong, A. S., Biswas, B. K., Kim, Y. S., et al. (2008). Growth performance and physiological responses in striped knifejaw, *Oplegnathus fasciatus*, held under different photoperiods. *Aquaculture* 279(1): 42-46.
- Boeuf, G., & Le Bail, P. Y. (1999). Does light have an influence on fish growth?. *Aquaculture* 177(1): 129-152.
- Boeuf, G., & Payan, P. (2001). How should salinity influence fish growth?. *Comparative Biochemistry and Physiology Part C: Toxicology & Pharmacology* 130(4): 411-423.
- Borja, A. (2011). Los impactos ambientales de la acuicultura y la sostenibilidad de esta actividad. *Boletín. Instituto Español de Oceanografía*, 18(1-4), 41-49.
- Bórquez-Lopez, R. A., Casillas-Hernandez, R., Lopez-Elias, J. A., Barraza-Guardado, R. H., & Martínez-Cordova, L. R. (2018). Improving feeding strategies for shrimp farming using fuzzy logic, based on water quality parameters. *Aquacultural Engineering*.
- Braun, N., De Lima, R. L., Moraes, B., Loro, V. L., & Baldisserotto, B. (2006). Survival, growth and biochemical parameters of silver catfish, *Rhamdia quelen* (Quoy & Gaimard, 1824), juveniles exposed to different dissolved oxygen levels. *Aquaculture Research* 37(15): 1524-1531.
- Bri, D., Coll, H., Garcia, M., & Lloret, J. (2010). A wireless IP multisensor deployment. *International Journal On Advances in Networks and Services*, 3(1).
- Bri, D., Garcia, M., Lloret, J., & Dini, P. (2009, June). Real deployments of wireless sensor networks. In *Proceedings of the Third International Conference on Sensor Technologies and Applications (SENSORCOMM'09)*, Athens (Greece), June 18-23, 009, 415-423.
- Brown, N. L. (1988). New generation CTD system [conductivity-temperature-depth sensor]. *IEEE journal of oceanic engineering*, 13(3), 129-134.
- Bruton, M. N. 1985. The effects of suspensoids on fish. *Hydrobiologia*, 125(1), 221-241.
- Buschmann, A. H., Cabello, F., Young, K., Carvajal, J., Varela, D. A., & Henríquez, L. (2009). Salmon aquaculture and coastal ecosystem health in Chile: analysis of regulations, environmental impacts and bioremediation systems. *Ocean & Coastal Management* 52(5): 243-249.

- Capocci, R., Dooly, G., Omerdić, E., Coleman, J., Newe, T., & Toal, D. (2017). Inspection-class remotely operated vehicles—a review. *Journal of Marine Science and Engineering*, 5(1), 13.
- Cañavate, J. P., Zerolo, R., & Fernández-Díaz, C. (2006). Feeding and development of Senegal sole (*Solea senegalensis*) larvae reared in different photoperiods. *Aquaculture* 258(1): 368-377.
- Cario, G., Casavola, A., Lupia, P. G. M., Petrioli, C., & Spaccini, D. (2017, June). Long lasting underwater wireless sensors network for water quality monitoring in fish farms. In Proceedings of the 60th MTS/IEEE OCEANS Conference in Aberdeen, Scotland, 19–22 June 2017; pp. 1–6.
- CD74HC4067 16-Channel Analog Multiplexer/Demultiplexer features, 2018 <http://www.ti.com/lit/ds/symlink/cd74hc4067.pdf> (accessed on 13 January 2018)
- Cerqueira, V. R., & Brügger, A. M. (2001). Effect of light intensity on initial survival of fat snook (*Centropomus parallelus*, Pisces: Centropomidae) larvae. *Brazilian Archives of Biology and Technology* 44(4): 343-349.
- Chanson, H., Reungoat, D., Simon, B., & Lubin, P. (2011). High-frequency turbulence and suspended sediment concentration measurements in the Garonne River tidal bore. *Estuarine, Coastal and Shelf Science*, 95(2), 298-306.
- Chanson, H., Takeuchi, M., & Trevethan, M. (2008). Using turbidity and acoustic backscatter intensity as surrogate measures of suspended sediment concentration in a small subtropical estuary. *Journal of environmental management*, 88(4), 1406-1416.
- Chen, D., Liu, Z., Wang, L., Dou, M., Chen, J., & Li, H. (2013). Natural disaster monitoring with wireless sensor networks: a case study of data-intensive applications upon low-cost scalable systems. *Mobile Networks and Applications*, 18(5), 651-663.
- Chen, M. C., Chang, W. R., Lin, H. T., & Lee, H. H. (2014). Design and performance evaluation of aquatic-pollution monitoring scheme over a Waterborne Wireless Sensor Network. *Computer Communications*, 40, 51-64.
- Chen, Y., Zhen, Z., Yu, H., & Xu, J. (2017). Application of Fault Tree Analysis and Fuzzy Neural Networks to Fault Diagnosis in the Internet of Things (IoT) for Aquaculture. *Sensors*, 17(1), 153.
- Chik, W. W., Barry, M. A. T., Thavapalachandran, S., Midekin, C., Pouliopoulos, J. I. M., Lim, T. W., ... & Koor, P. (2013). High spatial resolution thermal mapping of radiofrequency ablation lesions using a novel thermochromic liquid crystal myocardial phantom. *Journal of cardiovascular electrophysiology*, 24(11), 1278-1286.
- Childs, P. R. N., Greenwood, J. R., & Long, C. A. (2000). Review of temperature measurement. *Review of scientific instruments*, 71(8), 2959-2978.
- Chowdhury, T. J., Elkin, C., Devabhaktuni, V., Rawat, D. B., & Oluoch, J. (2016). Advances on localization techniques for wireless sensor networks: A survey. *Computer Networks*, 110, 284-305.
- Ciuhandu, C. S., Stevens, E. D., & Wright, P. A. (2005). The effect of oxygen on the growth of *Oncorhynchus mykiss* embryos with and without a chorion. *Journal of fish biology* 67(6): 1544-1551.
- Clark, L. C., Wolf, R., Granger, D., & Taylor, Z. (1953). Continuous recording of blood oxygen tensions by polarography. *Journal of applied physiology*, 6(3), 189-193.
- Clifford, N. J., Richards, K. S., Brown, R. A., & Lane, S. N. (1995). Laboratory and field assessment of an infrared turbidity probe and its response to particle size and variation in suspended sediment concentration. *Hydrological Sciences Journal*, 40(6), 771-791.
- Collett, P. D., Vine, N. G., & Kaiser, H. (2008). The effect of light intensity on growth of juvenile dusky kob *Argyrosomus japonicus* (Temminck & Schlegel 1843). *Aquaculture Research* 39(5): 526-531.
- Compte, S. S. (2013). Deployment of efficient wireless sensor nodes for monitoring in rural, indoor and underwater environments (Doctoral dissertation, Editorial Universitat Politècnica de València).
- Compte, S. S., Lloret, J., Pineda, M. G., & Alarcón, J. F. T. (2011). Power saving and energy optimization techniques for Wireless Sensor Networks. In *Journal of communications* (Vol. 6, No. 6, pp. 439-459). Engineering and Technology Publishing.
- Conductivity meter CM 35 +, [www.crisoninstruments.com/file.php?id=79&lang=es](http://www.crisoninstruments.com/file.php?id=79&lang=es). Last access 21/02/2018
- Conti, S. G., Roux, P., Fauvel, C., Maurer, B. D., & Demer, D. A. (2006). Acoustical monitoring of fish density, behavior, and growth rate in a tank. *Aquaculture*, 251(2-4), 314-323.
- Costa, C., Scardi, M., Vitalini, V., & Cataudella, S. (2009). A dual camera system for counting and sizing Northern Bluefin Tuna (*Thunnus thynnus*; Linnaeus, 1758) stock, during transfer to aquaculture cages, with a semi automatic Artificial Neural Network tool. *Aquaculture* 291(3): 161-167.

- Covès, D., Beauchaud, M., Attia, J., Dutto, G., Bouchut, C., & Begout, M. L. (2006). Long-term monitoring of individual fish triggering activity on a self-feeding system: An example using European sea bass (*Dicentrarchus labrax*). *Aquaculture*, 253(1-4), 385-392.
- CT2X, <http://inwusa.com/wordpress/wp-content/uploads/ct2x.pdf>. Last access: 19/09/2017
- Cui, H., Li, D., & Sun, M. (2009, April). Inductive level measurement sensor with magnetic fluid. In proceedings of 2009 International Conference on Measuring Technology and Mechatronics Automation, April, 11-12, 2009, Zhangjiajie, Hunan, China.
- da Silva Rocha, A. J., Gomes, V., Van Ngan, P., Rocha, M. J. D. A. C., & Furia, R. R. (2005). Metabolic demand and growth of juveniles of *Centropomus parallelus* as function of salinity. *Journal of Experimental Marine Biology and Ecology* 316(2): 157-165.
- Dalton, T., & Jin, D. (2010). Extent and frequency of vessel oil spills in US marine protected areas. *Marine pollution bulletin*, 60(11), 1939-1945.
- Danisman-Yagci, D., & Yigit, M. (2009). Influence of increased photoperiods on growth, feed consumption and survival of juvenile mirror carp (*Cyprinus carpio* Linnaeus, 1758). *Journal of FisheriesSciences.com* 3(2): 146.
- DARS, 2015. <http://dars.sourceforge.net/> [Last access: January 29, 2015].
- Das, A. P., & Thampi, S. M. (2017). Simulation tools for underwater sensor networks: a survey. *Network Protocols and Algorithms*, 8(4), 41-55.
- Datasheet of GPS receiver, 2015. [http://www.mouser.com/ds/2/251/Maestro\\_GPS\\_Receiver\\_A2235\\_H\\_User\\_Manual\\_V12-301680.pdf](http://www.mouser.com/ds/2/251/Maestro_GPS_Receiver_A2235_H_User_Manual_V12-301680.pdf) [Last access: March 19, 2015]
- Davies, B., & Bromage, N. (2002). The effects of fluctuating seasonal and constant water temperatures on the photoperiodic advancement of reproduction in female rainbow trout, *Oncorhynchus mykiss*. *Aquaculture* 205(1): 183-200.
- Denkilkian, H., Koulakezian, A., Ohannessian, R., Chalfoun, M. S., Joujou, M. K. W., Chehab, A., & Elhaji, I. H. (2009). Wireless sensor for continuous real-time oil spill thickness and location measurement. *IEEE Transactions on Instrumentation and Measurement*, 58(12), 4001-4011.
- Denson, M. R., Stuart, K. R., Smith, T. I., Weirlch, C. R., & Segars, A. (2003). Effects of salinity on growth, survival, and selected hematological parameters of juvenile cobia *Rachycentron canadum*. *Journal of the World Aquaculture Society* 34(4): 496-504.
- Diallo, O., Rodrigues, J. J., Sene, M., & Lloret, J. (2015). Distributed database management techniques for wireless sensor networks. *IEEE Transactions on Parallel and Distributed Systems*, 26(2), 604-620.
- Dickson, K. (1994). Tunas as small as 207 mm fork length can elevate muscle temperatures significantly above ambient water temperature. *Journal of Experimental Biology*, 190(1), 79-93. <documents/data-sheet/74LVC1G3157.pdf> (accessed on 13 January 2018).
- Dong, B. (2009, January). A survey of underwater wireless sensor networks. In CAHSI 2009 ANNUAL MEETING, Mountain View, California, USA, January 15–18, 2009 (p. 52).
- Dong, X. Y., Qin, J. G., & Zhang, X. M. (2011). Fish adaptation to oxygen variations in aquaculture from hypoxia to hyperoxia. *Journal of Fisheries and Aquaculture* 2(2): 23.
- Dou, S. Z., Masuda, R., Tanaka, M., & Tsukamoto, K. (2005). Effects of temperature and delayed initial feeding on the survival and growth of Japanese flounder larvae. *Journal of Fish Biology* 66(2): 362-377.
- Downing, G., & Litvak, M. K. (2001). The effect of light intensity and spectrum on the incidence of first feeding by larval haddock. *Journal of Fish Biology* 59(6): 1566-1578.
- Duray, M. N., Estudillo, C. B., & Alpasan, L. G. (1996). The effect of background color and rotifer density on rotifer intake, growth and survival of the grouper (*Epinephelus suillus*) larvae. *Aquaculture* 146(3): 217-224.
- Dutta, R., & Annappa, B. (2014). Protection of data in unsecured public cloud environment with open, vulnerable networks using threshold-based secret sharing. *Network Protocols and Algorithms*, 6(1), 58-75. <electroschematics.com/wp-content/uploads/2015/02/esp8266-datasheet.pdf> (accessed on 13 January 2018).
- Elkin, C., Kumarasiri, R., Rawat, D. B., & Devabhaktuni, V. (2017). Localization in wireless sensor networks: A Dempster-Shafer evidence theoretical approach. *Ad Hoc Networks*, 54, 30-41.

- El-Sayed, A. F. M., & Kawanna, M. (2004). Effects of photoperiod on the performance of farmed Nile tilapia *Oreochromis niloticus*: I. Growth, feed utilization efficiency and survival of fry and fingerlings. *Aquaculture* 231(1): 393-402.
- Emery, N., Caughley, A., Glasson, N., Meier, J., Nation, M., & Tanchon, J. (2012). Co-axial pulse tube development. *Cryocoolers*, 17(1), 135-141.
- Encinas, C., Ruiz, E., Cortez, J., & Espinoza, A. (2017, April). Design and implementation of a distributed IoT system for the monitoring of water quality in aquaculture. In *Proceedings of the Wireless Telecommunications Symposium, Chicago, IL, USA, 26-28 April 2017*, pp. 1-7.
- Endal, H. P., Taranger, G. L., Stefansson, S. O., & Hansen, T. (2000). Effects of continuous additional light on growth and sexual maturity in Atlantic salmon, *Salmo salar*, reared in sea cages. *Aquaculture* 191(4): 337-349.
- ESP8266 WiFi Module Features, 2018. <http://www>.
- Espinosa-Faller, F. J., & Rendón-Rodríguez, G. E. (2012). A ZigBee wireless sensor network for monitoring an aquaculture recirculating system. *Journal of applied research and technology*, 10(3), 380-387.
- Esteban, O., Cruz-Navarrete, M., González-Cano, A., & Bernabeu, E. (1999). Measurement of the degree of salinity of water with a fiberoptic sensor. *Applied optics*, 38(25), 5267-5271.
- Eureka Manta2 Temp, <https://www.waterprobes.com/temperature-water-sondes>. Last access: 19/09/2017
- Eureqa Software. Available online: <http://www.nutonian.com/products/eureqa/> (accessed on 9 August 2015).
- Evans, R. C., Douglas, P., Williams, J. G., & Rochester, D. L. (2006). A novel luminescence-based colorimetric oxygen sensor with a “traffic light” response. *Journal of fluorescence*, 16(2), 201-206.
- Fabricius, K. E., Logan, M., Weeks, S. J., Lewis, S. E., & Brodie, J. 2016. Changes in water clarity in response to river discharges on the Great Barrier Reef continental shelf: 2002–2013. *Estuarine, Coastal and Shelf Science*, 173, A1-A15.
- FAIMMS, 2014. <http://imos.org.au/implementation.html> [Last Access: November 20, 2014]
- FAO (2014) *The State of World Fisheries and Aquaculture 2014*. FAO Fisheries and Aquaculture Department, Rome.
- Fashina-Bombata, H. A., & Busari, A. N. (2003). Influence of salinity on the developmental stages of African catfish *Heterobranchus longifilis* (Valenciennes, 1840). *Aquaculture* 224(1): 213-222.
- Faulk, C. K., & Holt, G. J. 2005. Advances in rearing cobia *Rachycentron canadum* larvae in recirculating aquaculture systems: live prey enrichment and greenwater culture. *Aquaculture*, 249(1), 231-243.
- Features of Libelium Waspote, 2015. <http://www.libelium.com/es/products/waspote/> [Last access: March 19, 2015]
- Fereydooni, M., Sabaei, M., & Eslamlu, G. B. (2015). Energy Efficient Topology Control in Wireless Sensor Networks with Considering Interference and Traffic Load. *Ad Hoc & Sensor Wireless Networks*, 25(3to4), 289to308.
- Fielder, D. S., & Bardsley, W. (1999). A preliminary study on the effects of salinity on growth and survival of mullet *Argyrosomus japonicus* larvae and juveniles. *Journal of the World Aquaculture Society* 30(3): 380-387.
- Fielder, D. S., Bardsley, W. J., Allan, G. L., & Pankhurst, P. M. (2002). Effect of photoperiod on growth and survival of snapper *Pagrus auratus* larvae. *Aquaculture* 211(1): 135-150.
- Flyport features, 2016. <http://store.openpicus.com/openpicus/prodotti.aspx?cprod=OP015351> (Last access: July 27, 2016)
- Foss, A., & Imsland, A. K. (2002). Compensatory growth in the spotted wolffish *Anarhichas minor* (Olafsen) after a period of limited oxygen supply. *Aquaculture Research* 33(13): 1097-1101.
- Foss, A., Evensen, T. H., & Øiestad, V. (2002). Effects of hypoxia and hyperoxia on growth and food conversion efficiency in the spotted wolffish *Anarhichas minor* (Olafsen). *Aquaculture Research* 33(6): 437-444.
- Foss, A., Evensen, T. H., Imsland, A. K., & Øiestad, V. (2001). Effects of reduced salinities on growth, food conversion efficiency and osmoregulatory status in the spotted wolffish. *Journal of Fish Biology* 59(2): 416-426.
- Foss, A., Vollen, T., & Øiestad, V. (2003). Growth and oxygen consumption in normal and O<sub>2</sub> supersaturated water, and interactive effects of O<sub>2</sub> saturation and ammonia on growth in spotted wolffish (*Anarhichas minor* Olafsen). *Aquaculture* 224(1): 105-116.

- Fuhrmann, N., Schneider, M., Ding, C. P., Brübach, J., & Dreizler, A. (2013). Two-dimensional surface temperature diagnostics in a full-metal engine using thermographic phosphors. *Measurement Science and Technology*, 24(9), 095203.
- Garcia, H. E., & Gordon, L. I. (1992). Oxygen solubility in seawater: Better fitting equations. *Limnology and oceanography*, 37(6), 1307-1312.
- Garcia, L. M. B., Garcia, C. M. H., Pineda, A. F. S., Gammad, E. A., Canta, J., Simon, S. P. D., et al. (1999). Survival and growth of bighead carp fry exposed to low salinities. *Aquaculture International* 7(4): 241-250.
- Garcia, M., Bri, D., Sendra, R., & Lloret, J. (2010). Practical deployments of wireless sensor networks: a survey. In *Int. J. Adv. Netw. Serv.*
- Garcia, M., Sendra, S., Lloret, G., & Lloret, J. (2011). Monitoring and control sensor system for fish feeding in marine fish farms. *IET Communications* 5(12): 1682-1690.
- Garcia-Sanchez, A. J., Garcia-Sanchez, F., & Garcia-Haro, J. (2011). Wireless sensor network deployment for integrating video-surveillance and data-monitoring in precision agriculture over distributed crops. *Computers and Electronics in Agriculture* 75(2): 288-303.
- Giuffre, T. R., Figi, B. B., Patel, S. D., & Moyer, T. M. (1999). U.S. Patent No. 5,923,433. Washington, DC: U.S. Patent and Trademark Office.
- Gkikopouli, A., Nikolakopoulos, G., & Manesis, S. (2012, July). A survey on underwater wireless sensor networks and applications. In *Control & Automation (MED)*, In Proceedings of 20th Mediterranean Conference on. *IEEE Control & Automation (MED)*, 2012, Barcelona, España, July 3–6, 2012. p. 1147-1154.
- Glasspool, W., & Atkinson, J. (1998). A screen-printed amperometric dissolved oxygen sensor utilising an immobilised electrolyte gel and membrane. *Sensors and Actuators B: Chemical*, 48(1), 308-317.
- Goddijn-Murphy, L., Dailloux, D., White, M., & Bowers, D. 2009. Fundamentals of in situ digital camera methodology for water quality monitoring of coast and ocean. *Sensors*, 9(7), 5825-5843.
- Gong, W., Mowlem, M., Kraft, M., & Morgan, F. (2008). Oceanographic sensor for in-situ temperature and conductivity monitoring. In Proceedings of the OCEANS 2008 - MTS/IEEE Kobe Techno-Ocean, Kobe, Japan, 8-11 of April, 2008, 1-6.
- Güttler, F. N., Niculescu, S., & Gohin, F. 2013. Turbidity retrieval and monitoring of Danube Delta waters using multi-sensor optical remote sensing data: An integrated view from the delta plain lakes to the western–northwestern Black Sea coastal zone. *Remote Sensing of Environment*, 132, 86-101.
- Haddy, J. A., & Pankhurst, N. W. (2000). The effects of salinity on reproductive development, plasma steroid levels, fertilisation and egg survival in black bream *Acanthopagrus butcheri*. *Aquaculture* 188(1): 115-131.
- Häder, D. P., Helbling, E. W., Williamson, C. E., & Worrest, R. C. (2011). Effects of UV radiation on aquatic ecosystems and interactions with climate change. *Photochemical & Photobiological Sciences*, 10(2), 242-260.
- Han, G., Zhang, C., Shu, L., & Rodrigues, J. J. (2015). Impacts of deployment strategies on localization performance in underwater acoustic sensor networks. *IEEE Transactions on Industrial Electronics*, 62(3), 1725-1733.
- Han, S., Kang, Y., Park, K., & Jang, M. (2007, October). Design of environment monitoring system for aquaculture farms. In Proceedings of the Frontiers in the Convergence of Bioscience and Information Technologies, Jeju City, South Korea, 11-13 October 2007, pp. 889-893.
- Handcock, R. N., Swain, D. L., Bishop-Hurley G. J., Patison, K. P., Wark, T., Valencia, P., Corke, P., O'Neill, C. J. (2009). Monitoring animal behaviour and environmental interactions using wireless sensor networks, GPS collars and satellite remote sensing. *Sensors*, 9(5), 3586-3603
- Handeland, S. O., & Stefansson, S. O. (2001). Photoperiod control and influence of body size on off-season parr–smolt transformation and post-smolt growth. *Aquaculture*, 192(2): 291-307.
- Handeland, S. O., Imsland, A. K., & Stefansson, S. O. (2008). The effect of temperature and fish size on growth, feed intake, food conversion efficiency and stomach evacuation rate of Atlantic salmon post-smolts. *Aquaculture* 283(1): 36-42.
- Hansen, T. K., & Falk-Petersen, I. B. (2002). Growth and survival of first-feeding spotted wolffish (*Anarhichas minor* Olafsen) at various temperature regimes. *Aquaculture Research* 33(14): 1119-1127.
- Harchi, S., Georges, J. P., & Divoux, T. (2012, August). WSN dynamic clustering for oil slicks monitoring. In proceedings of the 3rd International Conference on Wireless Communications in

- Unusual and Confined Areas, ICWCUCA'12, Clermont-Ferrand, France, august 28 – 30, 2012, pp. 1-6.
- Harnett, C. K., Courtney, S. M., & Kimmer, C. J. (2008, May). SALAMANDER: A distributed sensor system for aquatic environmental measurements. In IEEE Instrumentation and Measurement Technology Conference, Victoria, British Columbia, Canada, May 12-15 2008.
- Heidemann, J., Stojanovic, M., & Zorzi, M. (2012). Underwater sensor networks: applications, advances and challenges. *Phil. Trans. R. Soc. A*, 370(1958), 158-175.
- Hernández, M. D., Martínez, F. J., Jover, M., & García, B. G. (2007). Effects of partial replacement of fish meal by soybean meal in sharpsnout seabream (*Diplodus puntazzo*) diet. *Aquaculture* 263(1): 159-167.
- Hernández, M. D., Martínez, F. J., Jover, M., & García, B. G. (2007). Effects of partial replacement of fish meal by soybean meal in sharpsnout seabream (*Diplodus puntazzo*) diet. *Aquaculture* 263(1): 159-167.
- Hess, S., Wenger, A. S., Ainsworth, T. D., & Rummer, J. L. 2015. Exposure of clownfish larvae to suspended sediment levels found on the Great Barrier Reef: Impacts on gill structure and microbiome. *Scientific reports*, 5, 10561.
- Heydarnejad, M. S. (2012). Survival and growth of common carp (*Cyprinus carpio*) exposed to different water pH levels. *Turkish J Veterinary Animal Sci* 36, 245-249.
- HI762L, <http://hannainst.com/products/electrodes-and-probes/temperature/hi762l-air-and-liquid-thermistor-probe-with-handle.html>. Last access: 19/09/2017
- HI762W, <http://hannainst.com/products/electrodes-and-probes/temperature/hi762w-wire-thermistor-probe.html>. Last access: 19/09/2017
- HI765P, <http://hannainst.com/products/electrodes-and-probes/temperature/hi765p-general-purpose-penetration-thermistor-probe-with-colored-handle.html>. Last access: 19/09/2017
- HI766B1, <http://hannainst.com/products/electrodes-and-probes/temperature/hi766b1-90-angle-surface-k-type-thermocouple-probe-with-handle.html>. Last access: 19/09/2017
- HI766E1, <http://hannainst.com/products/electrodes-and-probes/temperature/hi766e1-general-purpose-k-type-thermocouple-probe-with-handle.html>. Last access: 19/09/2017
- HI766PE1, <http://hannainst.com/products/electrodes-and-probes/temperature/hi766pe1-general-purpose-k-type-thermocouple-probe.html>. Last access: 19/09/2017
- HI766TR1, <http://hannainst.com/products/electrodes-and-probes/temperature/hi766tr1-extended-length-penetration-k-type-thermocouple-probe-with-handle-500-mm.html>. Last access: 19/09/2017
- HI9829, <http://hannainst.com/products/portable-meters/hi9829-multiparameter-ph-ise-ec-do-turbidity-waterproof-meter-with-gps-option.html#spec>. Last access: 19/09/2017
- Hidalgo, J. C. (2009). Efectos de los derrames de petróleo sobre los habitats marinos. *Ciencia Ahora*, (24).
- Higón, T. M. (2014). Procesos de intercambio de materiales en la interfase agua-sedimento en piscifactorias marinas en jaulas flotantes (Doctoral dissertation).
- Hongpin, L., Guanglin, L., Weifeng, P., Jie, S., & Qiuwei, B. (2015). Real-time remote monitoring system for aquaculture water quality. *International Journal of Agricultural and Biological Engineering*, 8(6), 136.
- Huang, J., Wang, W., Jiang, S., Sun, D., Ou, G., & Lu, K. (2013). Development and test of aquacultural water quality monitoring system based on wireless sensor network. *Transactions of the Chinese society of agricultural engineering*, 29(4), 183-190.
- Huang, X., Pascal, R. W., Chamberlain, K., Banks, C. J., Mowlem, M., & Morgan, H. (2011). A miniature, high precision conductivity and temperature sensor system for ocean monitoring. *IEEE Sensors Journal*, 11(12), 3246-3252.
- Imsland, A. K., Folkvord, A., Jónsdóttir, Ó. D., & Stefansson, S. O. (1997). Effects of exposure to extended photoperiods during the first winter on long-term growth and age at first maturity in turbot (*Scophthalmus maximus*). *Aquaculture* 159(1): 125-141.
- Imsland, A. K., Foss, A., Sparboe, L. O., & Sigurdsson, S. (2006). The effect of temperature and fish size on growth and feed efficiency ratio of juvenile spotted wolffish *Anarhichas minor*. *Journal of Fish Biology* 68(4): 1107-1122.
- Imsland, A. K., Gústavsson, A., Gunnarsson, S., Foss, A., Árnason, J., Arnarson, I., et al. (2008). Effects of reduced salinities on growth, feed conversion efficiency and blood physiology of juvenile Atlantic halibut (*Hippoglossus hippoglossus* L.). *Aquaculture* 274(2): 254-259.

- IR LED Datasheet, 2018. <https://www.vishay.com/docs/81078/tshg6200.pdf> (accessed on 12 January 2018).
- IR Photodetector Datasheet, 2018. <https://www.vishay.com/docs/81530/bpw83.pdf> (accessed on 12 January 2018).
- IR Photodiode BPW41N, 2018. <http://www.farnell.com/datasheets/2046124.pdf> (accessed on 13 January 2018).
- Israeli, D., & Kimmel, E. (1996). Monitoring the behavior of hypoxia-stressed *Carassius auratus* using computer vision. *Aquacultural engineering* 15(6): 423-440.
- Jain, T. K., Saini, D. S., & Bhooshan, S. V. (2015). Lifetime optimization of a multiple sink wireless sensor network through energy balancing. *Journal of Sensors*, 2015.
- Jernelöv, A. (2010). The threats from oil spills: Now, then, and in the future. *AMBIO: A Journal of the Human Environment*, 39(6), 353-366.
- Jiang, P., Winkley, J., Zhao, C., Munnoch, R., Min, G., & Yang, L. T. (2016). An intelligent information forwarder for healthcare big data systems with distributed wearable sensors. *IEEE systems journal*, 10(3), 1147-1159.
- Jianxin, C., Wei, G., & Hui, H. (2011, December). Parameters measurement of marine power system based on multi-sensors data fusion theory. In *Proceedings of the 2011 8th International Conference on Information, Communications and Signal Processing (ICICS 2011) Singapore, 3 - 11 Dec., 2011*.
- Johansson, D., Ruohonen, K., Juell, J. E., & Oppedal, F. (2009). Swimming depth and thermal history of individual Atlantic salmon (*Salmo salar* L.) in production cages under different ambient temperature conditions. *Aquaculture* 290(3): 296-303.
- Johansson, D., Ruohonen, K., Kiessling, A., Oppedal, F., Stiansen, J. E., Kelly, M., et al. (2006). Effect of environmental factors on swimming depth preferences of Atlantic salmon (*Salmo salar* L.) and temporal and spatial variations in oxygen levels in sea cages at a fjord site. *Aquaculture* 254(1): 594-605.
- Johns-Krull, C. M. (2007). The magnetic fields of classical T Tauri stars. *The Astrophysical Journal*, 664(2), 975.
- Jorge, P. A. S., Caldas, P., Rosa, C. C., Oliva, A. G., & Santos, J. L. (2004). Optical fiber probes for fluorescence based oxygen sensing. *Sensors and Actuators B: Chemical*, 103(1), 290-299.
- Juell, J. E., & Fosseidengen, J. E. (2004). Use of artificial light to control swimming depth and fish density of Atlantic salmon (*Salmo salar*) in production cages. *Aquaculture* 233(1): 269-282.
- Kai, X., Qiuju, Z., Kexiu, L., & Weifeng, S. (2012). Design of monitoring and control system for aquaculture based on ZigBee technology. *Application of Electronic Technique*, 4: 034.
- Kameoka, S., Isoda, S., Hashimoto, A., Ito, R., Miyamoto, S., Wada, G., Watanabe, N., Yamakami, T., Suzuki, K., Kameoka T. A (2017). A Wireless Sensor Network for Growth Environment Measurement and Multi-Band Optical Sensing to Diagnose Tree Vigor. *Sensors*, 17(5), 966
- Karakatsouli, N., Papoutsoglou, E. S., Sotiropoulos, N., Mourtikas, D., Stigen-Martinsen, T., & Papoutsoglou, S. E. (2010). Effects of light spectrum, rearing density and light intensity on growth performance of scaled and mirror common carp *Cyprinus carpio* reared under recirculating system conditions. *Aquacultural engineering* 42(3): 121-127.
- Karim, L., Anpalagan, A., Nasser, N., & Almhana, J. (2013). Sensor-based M2M agriculture monitoring systems for developing countries: state and challenges. *Network Protocols and Algorithms*, 5(3), 68-86.
- Karimanzira, D., Jacobi, M., Pfützenreuter, T., Rauschenbach, T., Eichhorn, M., Taubert, R., & Ament, C. (2014). First testing of an AUV mission planning and guidance system for water quality monitoring and fish behavior observation in net cage fish farming. *Information Processing in Agriculture*, 1(2), 131-140.
- Kawanisi, K., & Yokosi, S. (1997). Characteristics of suspended sediment and turbulence in a tidal boundary layer. *Continental Shelf Research*, 17(8), 859-875.
- Keller, M.D., Selvin, R.C., Claus, W., & Guillard, R.R.L., 1987. Media for the culture of oceanic ultraphytoplankton. *Journal of Phycology*, 23, 633-638.
- Kestemont, P., Jourdan, S., Houbart, M., Mélard, C., Paspatis, M., Fontaine, P., Cuvier, A., Kentouri, M., Barasc, E. (2003). Size heterogeneity, cannibalism and competition in cultured predatory fish larvae: biotic and abiotic influences. *Aquaculture*, 227(1-4), 333-356.
- Khaleeq, H., Abou-ElNour, A., & Tarique, M. (2016). A Reliable Wireless System for Water Quality Monitoring and Level Control. *Network Protocols and Algorithms*, 8(3), 1-14.

- Khalid, A. H., & Kontis, K. (2008). Thermographic phosphors for high temperature measurements: principles, current state of the art and recent applications. *Sensors*, 8(9), 5673-5744.
- Kim, M., Choi, W., Lim, H., & Yang, S. (2013). Integrated microfluidic-based sensor module for real-time measurement of temperature, conductivity, and salinity to monitor reverse osmosis. *Desalination*, 317, 166-174.
- King, H. R., Pankhurst, N. W., Watts, M., & Pankhurst, P. M. (2003). Effect of elevated summer temperatures on gonadal steroid production, vitellogenesis and egg quality in female Atlantic salmon. *Journal of Fish Biology* 63(1): 153-167.
- Kissil, G. W., Lupatsch, I., Elizur, A., & Zohar, Y. (2001). Long photoperiod delayed spawning and increased somatic growth in gilthead seabream (*Sparus aurata*). *Aquaculture* 200(3): 363-379.
- Klein, C., Henne, U., Sachs, W., Beifuss, U., Ondrus, V., Bruse, M., Lesjak, R., Löhr, M. (2014). Application of carbon nanotubes (CNT) and temperature-sensitive paint (TSP) for the detection of boundary layer transition.
- Kleinberg, R. L., Chew, W. C., & Griffin, D. D. (1989). Noncontacting electrical conductivity sensor for remote, hostile environments. *IEEE Transactions on Instrumentation and Measurement*, 38(1), 22-26.
- Kröger, S., Piletsky, S., & Turner, A. P. (2002). Biosensors for marine pollution research, monitoring and control. *Marine pollution bulletin*, 45(1-12), 24-34.
- Kucharczyk, D., Luczynski, M., Kujawa, R., & Czerkies, P. (1997). Effect of temperature on embryonic and larval development of bream (*Abramis brama* L.). *Aquatic Sciences* 59(3): 214-224.
- Kurokawa, T., Okamoto, T., Gen, K., Uji, S., Murashita, K., Unuma, T., et al. (2008). Influence of water temperature on morphological deformities in cultured larvae of Japanese eel, *Anguilla japonica*, at completion of yolk resorption. *Journal of the World Aquaculture Society* 39(6): 726-735.
- Laiz-Carrión, R., Sangiao-Alvarellos, S., Guzmán, J. M., del Río, M. P. M., Soengas, J. L., & Mancera, J. M. (2005). Growth performance of gilthead sea bream *Sparus aurata* in different osmotic conditions: implications for osmoregulation and energy metabolism. *Aquaculture* 250(3): 849-861.
- Lambrou, T. P., Anastasiou, C. C., & Panayiotou, C. G. (2009). A nephelometric turbidity system for monitoring residential drinking water quality. In *Proceedings of the International Conference on Sensor Applications, Experimentation and Logistics*, Athens, Greece, 25 of September, 2009, 43-55.
- Lari, E., Abtahi, B., & Hashtroudi, M. S. (2016). The effect of the water soluble fraction of crude oil on survival, physiology and behaviour of Caspian roach, *Rutilus caspicus* (Yakovlev, 1870). *Aquatic Toxicology*, 170, 330-334.
- LDR NORPS-12, 2018. <http://www.farnell.com/datasheets/409710.pdf> (accessed on 13 January 2018).
- LDR NSL 19M51, 2018. <http://www.farnell.com/datasheets/77395.pdf> (accessed on 13 January 2018).
- LDR, 2017. <http://lunainc.com/wp-content/uploads/2016/06/NSL-19M51.pdf> (Last access: November 22, 2017)
- LDR, 2017. [http://www.farnell.com/datasheets/77395.pdf?\\_ga=2.27766780.1568076438.1510680363-1814763420.1510680363](http://www.farnell.com/datasheets/77395.pdf?_ga=2.27766780.1568076438.1510680363-1814763420.1510680363) (Last access: November 14, 2017)
- Le François, N. R., Lamarre, S. G., & Blier, P. U. (2004). Tolerance, growth and haloplasticity of the Atlantic wolffish (*Anarhichas lupus*) exposed to various salinities. *Aquaculture* 236(1): 659-675.
- Lee, J. H., Lim, T. S., Seo, Y., Bishop, P. L., & Papautsky, I. (2007). Needle-type dissolved oxygen microelectrode array sensors for in situ measurements. *Sensors and Actuators B: Chemical*, 128(1), 179-185.
- Lee, J. S. 2015a. Clay As a Greenwater Alternative for Larval Sablefish *Anoplopoma fimbria*. In *Proceedings of the 145th Annual Meeting of the American Fisheries Society*, Portland, Oregon, 16 – 20 August, 2015.
- Lee, J. S., Cook, M. A., Berejikian, B. A., & Goetz, F. W. 2017. Temporal changes in the suitability of claywater as a greenwater substitute for rearing larval sablefish (*Anoplopoma fimbria*). *Aquaculture*, 470, 11-16.
- Lee, Z., Shang, S., Hu, C., Du, K., Weidemann, A., Hou, W., Lin, J. & Lin, G. 2015b. Secchi disk depth: A new theory and mechanistic model for underwater visibility. *Remote Sensing of Environment*, 169, 139-149.
- Legakis, H., Mehmet-Ali, M., & Hayes, J. F. (2015). Lifetime analysis for wireless sensor networks. *International Journal of Sensor Networks*, 17(1), 1-16.
- Lein, I., Holmefjord, I., & Rye, M. (1997a). Effects of temperature on yolk sac larvae of Atlantic halibut (*Hippoglossus hippoglossus* L.). *Aquaculture* 157(1): 123-135.
- Lein, I., Tveite, S., Gjerde, B., & Holmefjord, I. (1997b). Effects of salinity on yolk sac larvae of Atlantic halibut (*Hippoglossus hippoglossus* L.). *Aquaculture* 156(3): 291-303.



- Level Sensor GP2Y0A02YK0F, 2018. <http://www.farnell.com/datasheets/1386113.pdf> (accessed on 13 January 2018).
- Light, T. S., Licht, S., Bevilacqua, A. C., & Morash, K. R. (2005). The fundamental conductivity and resistivity of water. *Electrochemical and Solid-State Letters*, 8(1), E16-E19.
- Lin, J. L., Hwang, K. S., & Hsiao, Y. S. (2014). A synchronous display of partitioned images broadcasting system via VPN transmission. *IEEE Systems Journal*, 8(4), 1031-1039.
- Liu, Y., Zeng, Q. A., & Wang, Y. H. (2015). Energy-efficient data fusion technique and applications in wireless sensor networks. *Journal of Sensors*, 2015.
- Lloret, J. (2013). Underwater sensor nodes and networks, *Sensors* 13 (9), 11782-11796.
- Lloret, J., Bosch, I., Sendra, S., & Serrano, A. (2011a). A wireless sensor network for vineyard monitoring that uses image processing. *Sensors* 11(6): 6165-6196.
- Lloret, J., Garcia, M., Bri, D., & Sendra, S. (2009). A wireless sensor network deployment for rural and forest fire detection and verification. *sensors*, 9(11), 8722-8747.
- Lloret, J., Garcia, M., Sendra, S., & Lloret, G. (2015). An underwater wireless group-based sensor network for marine fish farms sustainability monitoring. *Telecommunication Systems*, 60(1), 67-84.
- Lloret, J., Garcia, M., Tomás, J., & Boronat, F. (2008b). GBP-WAHSN: a group-based protocol for large wireless ad hoc and sensor networks. *Journal of Computer Science and Technology*, 23(3), 461-480.
- Lloret, J., Palau, C., Boronat, F., & Tomas, J. (2008a). Improving networks using group-based topologies. *Computer Communications*, 31(14), 3438-3450.
- Lloret, J., Sendra, S., Garcia, M., & Lloret, G. (2011b). Group-based underwater wireless sensor network for marine fish farms. In *Proceedings of the 2011IEEE GLOBECOM Workshops (GC Wkshps)*, Houston, USA, Dec. 5 – 9, pp. 115-119
- Locarnini, R. A., Mishonov A. V., Antonov J. I., Boyer T. P., Garcia H. E., Baranova O. K., Zweng M. M., Johnson D. R. (2010). *World Ocean Atlas 2009, Volume 1: Temperature*. S. Levitus, Ed., NOAA Atlas NESDIS 68, U.S. Government Printing Office, Washington, D.C., 184 pp.
- Lopes, J. M., Silva, L. V. F., & Baldisserotto, B. (2001). Survival and growth of silver catfish larvae exposed to different water pH. *Aquaculture International* 9(1): 73-80.
- López-Bruna, D., & Herrero, J. (1996). El comportamiento del sensor electromagnético y su calibración frente a la salinidad edáfica. *Agronomie*, 16(2), 95-105.
- Lopez-Ruiz, N., López-Torres, J., Rodríguez, M. Á. C., de Vargas-Sansalvador, I. P., & Martínez-Olmos, A. (2015). Wearable system for monitoring of oxygen concentration in breath based on optical sensor. *IEEE Sensors Journal*, 15(7), 4039-4045.
- Luo, C., Wu, F., Sun, J., & Chen, C. W. (2009, September). Compressive data gathering for large-scale wireless sensor networks. *Proceedings of the 15th annual International conference on Mobile computing and networking (ACM 2009)*, Beijing, China, September 20–25 2009; 145-156.
- Luo, M., Guan, R., Li, Z., & Jin, H. (2013). The effects of water temperature on the survival, feeding, and growth of the juveniles of *Anguilla marmorata* and *A. bicolor pacifica*. *Aquaculture* 400: 61-64.
- Lusher, C. P., Li, J., Maidanov, V. A., Digby, M. E., Dyball, H., Casey, A., Nyéki, J., Dmitriev, V V., Cowan, B P., Saunders, J. (2001). Current sensing noise thermometry using a low Tc DC SQUID preamplifier. *Measurement Science and Technology*, 12(1), 1.
- Luz, R. D. C. S., Damos, F. S., Tanaka, A. A., & Kubota, L. T. (2006). Dissolved oxygen sensor based on cobalt tetrasulphonatedphthalocyanine immobilized in polytolyllysine film onto glassy carbon electrode. *Sensors and Actuators B: Chemical*, 114(2), 1019-1027.
- Luz, R. K., Martínez-Álvarez, R. M., De Pedro, N., & Delgado, M. J. (2008). Growth, food intake regulation and metabolic adaptations in goldfish (*Carassius auratus*) exposed to different salinities. *Aquaculture* 276(1): 171-178.4.
- Mackereth, F. J. H. (1964). An improved galvanic cell for determination of oxygen concentrations in fluids. *Journal of Scientific Instruments*, 41(1), 38.
- MacLean, A., Moran, C., Johnstone, W., Culshaw, B., Marsh, D., & Parker, P. (2003). Detection of hydrocarbon fuel spills using a distributed fibre optic sensor. *Sensors and Actuators A: Physical*, 109(1-2), 60-67.
- Mamoune, S. E., Ezziyani, M., & Lloret, J. (2015). Towards a new approach for modelling interactive real time systems based on collaborative decisions network. *Network Protocols and Algorithms*, 7(1), 42-63.
- Marín, J.; Rocher, J.; Parra, L.; Sendra, S.; Lloret, J.; Mauri, P.V. (2017). Autonomous WSN for Lawns Monitoring in Smart Cities. In *Proceedings of the 5th International workshop on Big Data and*

- Social Networking Management and Security (BDSN 2017), Hammamet, Tunisia, 30 October 2017–3 November 2017.
- Markus, T., Stroeve, J. C., & Miller, J. (2009). Recent changes in Arctic sea ice melt onset, freezeup, and melt season length. *Journal of Geophysical Research: Oceans*, 114(C12).
- Martinelli, M., Ioriatti, L., Viani, F., Benedetti, M., & Massa, A. (2009, July). A WSN-based solution for precision farm purposes. In *Proceeding of IEEE International Geoscience and Remote Sensing Symposium, IGARSS*, Cape Town, South Africa, 12-17 July of 2009.
- Martínez, A., Rodríguez, R., & Pérez, A. (2010). Influence of the excitement frequency and the distance among coils during sensing of soil electric conductivity by means of a variable magnetic field. *Revista Ciencias Técnicas Agropecuarias*, 19(4), 17-23.
- Martínez-Máñez, R., Soto, J., Lizondo-Sabater, J., García-Breijo, E., Gil, L., Ibáñez, J., ... & Alvarez, S. (2004). New potentiometric dissolved oxygen sensors in thick film technology. *Sensors and Actuators B: Chemical*, 101(3), 295-301.
- Martínez-Palacios, C. A., Morte, J. C., Tello-Ballinas, J. A., Toledo-Cuevas, M., & Ross, L. G. (2004). The effects of saline environments on survival and growth of eggs and larvae of *Chirostoma estor estor* Jordan 1880 (Pisces: Atherinidae). *Aquaculture* 238(1): 509-522.
- Marttila, H., Postila, H., & Kløve, B. (2010). Calibration of turbidity meter and acoustic doppler velocimetry (Triton-ADV) for sediment types present in drained peatland headwaters: Focus on particulate organic peat. *River research and applications*, 26(8), 1019-1035.
- Mauri, G. L., & Mauri, J. L. (2007). Simulator software for marine fish farms sustainability. *WSEAS Transactions on Environment and Development*, 12(3), 214-222.
- McDonagh, C., Kolle, C., McEvoy, A. K., Dowling, D. L., Cafolla, A. A., Cullen, S. J., & MacCraith, B. D. (2001). Phase fluorometric dissolved oxygen sensor. *Sensors and Actuators B: Chemical*, 74(1), 124-130.
- McCue, R. P., Walsh, J. E., Walsh, F., & Regan, F. (2006). Modular fibre optic sensor for the detection of hydrocarbons in water. *Sensors and Actuators B: Chemical*, 114(1), 438-444.
- Medrano, M., Pérez, A. T., & Soria-Hoyo, C. (2007). Design of a conductivity meter for highly insulating liquids. *Journal of Physics D: Applied Physics*, 40(5), 1477.
- Meghanathan, N., & Mumford, P. (2013). Centralized and distributed algorithms for stability-based data gathering in mobile sensor networks. *Network Protocols and Algorithms*, 5(4), 84-116.
- Merino, G., Barange, G., Blanchard, J. L., Harle, J., Holmes, R., Allen, I., Allison, E. H., Badjeck, M. C., Dulvy, N. K., Holt, J., Jennings, S., Mullon, C., Rodwell, L. D. (2012). Can marine fisheries and aquaculture meet fish demand from a growing human population in a changing climate?. *Global Environmental Change*, 22(4), 795-806.
- Microsoft Azure Platform, 2018. <https://azure.microsoft.com/en-us/?v=18.05> (accessed on 23 February 2018).
- Moe, H., Dempster, T., Sunde, L. M., Winther, U., & Fredheim, A. (2007). Technological solutions and operational measures to prevent escapes of Atlantic cod (*Gadus morhua*) from sea cages. *Aquaculture Research*, 38(1), 91-99.
- Mohsin, A. H., Bakar, K. A., & Adekiigbe, A. (2012). A survey of energy-aware routing protocols in mobile ad-hoc networks: trends and challenges. *Network Protocols and Algorithms*, 4(2), 82-107.
- Monk, J., Puvanendran, V., & Brown, J. A. (2006). Do different light regimes affect the foraging behaviour, growth and survival of larval cod (*Gadus morhua* L.)?. *Aquaculture* 257(1): 287-293.
- Monk, J., Puvanendran, V., & Brown, J. A. (2008). Does different tank bottom colour affect the growth, survival and foraging behaviour of Atlantic cod (*Gadus morhua*) larvae?. *Aquaculture* 277(3): 197-202.
- Morais, R., Fernandes, M. A., Matos, S. G., Serôdio, C., Ferreira, P. J. S. G., & Reis, M. J. C. S. (2008). A ZigBee multi-powered wireless acquisition device for remote sensing applications in precision viticulture. *Computers and electronics in agriculture*, 62(2), 94-106.
- MPCA (Minnesota Pollution control Agency), Turbidity: Description, Impact on Water Quality, Sources, Measures Available at : <https://www.pca.state.mn.us/sites/default/files/wq-iw3-21.pdf> (Last access: february 21, 2017).
- MPS PTEC, [https://www.seba-hydrometrie.com/products.html?L=1&tx\\_sebaproducts\\_sebaproducts%5Bproduct%5D=36&tx\\_sebaproducts\\_sebaproducts%5Bprimarycategory%5D=4&tx\\_sebaproducts\\_sebaproducts%5Bsecondarycategory%5D=2&tx\\_sebaproducts\\_sebaproducts%5Baction%5D=show&tx\\_sebaproducts\\_sebaproducts%5Bcontroller%5D=Product&cHash=8c16fc9d5c8bcb6ed76bcb3671dae44d](https://www.seba-hydrometrie.com/products.html?L=1&tx_sebaproducts_sebaproducts%5Bproduct%5D=36&tx_sebaproducts_sebaproducts%5Bprimarycategory%5D=4&tx_sebaproducts_sebaproducts%5Bsecondarycategory%5D=2&tx_sebaproducts_sebaproducts%5Baction%5D=show&tx_sebaproducts_sebaproducts%5Bcontroller%5D=Product&cHash=8c16fc9d5c8bcb6ed76bcb3671dae44d). Last access: 19/09/2017

- MPS-D3 type, [https://www.seba-hydrometrie.com/products.html?L=1&tx\\_sebaproducts\\_sebaproducts%5Bproduct%5D=33&tx\\_sebaproducts\\_sebaproducts%5Bprimarycategory%5D=4&tx\\_sebaproducts\\_sebaproducts%5Bsecondarycategory%5D=2&tx\\_sebaproducts\\_sebaproducts%5Baction%5D=show&tx\\_sebaproducts\\_sebaproducts%5Bcontroller%5D=Product&cHash=6b0d98022a4300b7d2ffe23a7a416fdb](https://www.seba-hydrometrie.com/products.html?L=1&tx_sebaproducts_sebaproducts%5Bproduct%5D=33&tx_sebaproducts_sebaproducts%5Bprimarycategory%5D=4&tx_sebaproducts_sebaproducts%5Bsecondarycategory%5D=2&tx_sebaproducts_sebaproducts%5Baction%5D=show&tx_sebaproducts_sebaproducts%5Bcontroller%5D=Product&cHash=6b0d98022a4300b7d2ffe23a7a416fdb). Last access: 19/09/2017
- MPS-D8/Qualilog8, [https://www.seba-hydrometrie.com/products.html?L=1&tx\\_sebaproducts\\_sebaproducts%5Bproduct%5D=34&tx\\_sebaproducts\\_sebaproducts%5Bprimarycategory%5D=4&tx\\_sebaproducts\\_sebaproducts%5Bsecondarycategory%5D=2&tx\\_sebaproducts\\_sebaproducts%5Baction%5D=show&tx\\_sebaproducts\\_sebaproducts%5Bcontroller%5D=Product&cHash=cbc3e05836f2ef6de80b8f4aaed14fab](https://www.seba-hydrometrie.com/products.html?L=1&tx_sebaproducts_sebaproducts%5Bproduct%5D=34&tx_sebaproducts_sebaproducts%5Bprimarycategory%5D=4&tx_sebaproducts_sebaproducts%5Bsecondarycategory%5D=2&tx_sebaproducts_sebaproducts%5Baction%5D=show&tx_sebaproducts_sebaproducts%5Bcontroller%5D=Product&cHash=cbc3e05836f2ef6de80b8f4aaed14fab). Last access: 19/09/2017
- MPS-K16/Qualilog16, [https://www.seba-hydrometrie.com/products.html?L=1&tx\\_sebaproducts\\_sebaproducts%5Bproduct%5D=35&tx\\_sebaproducts\\_sebaproducts%5Bprimarycategory%5D=4&tx\\_sebaproducts\\_sebaproducts%5Bsecondarycategory%5D=2&tx\\_sebaproducts\\_sebaproducts%5Baction%5D=show&tx\\_sebaproducts\\_sebaproducts%5Bcontroller%5D=Product&cHash=62c28ab8df05470c833395b3a69440f3](https://www.seba-hydrometrie.com/products.html?L=1&tx_sebaproducts_sebaproducts%5Bproduct%5D=35&tx_sebaproducts_sebaproducts%5Bprimarycategory%5D=4&tx_sebaproducts_sebaproducts%5Bsecondarycategory%5D=2&tx_sebaproducts_sebaproducts%5Baction%5D=show&tx_sebaproducts_sebaproducts%5Bcontroller%5D=Product&cHash=62c28ab8df05470c833395b3a69440f3). Last access: 19/09/2017
- Mylonas, C. C., Pavlidis, M., Papandroulakis, N., Zaiss, M. M., Tsafarakis, D., Papadakis, I. E., & Varsamos, S. (2009). Growth performance and osmoregulation in the shi drum (*Umbrina cirrosa*) adapted to different environmental salinities. *Aquaculture*, 287(1): 203-210.
- Mylvaganaru, S., & Jakobsen, T. (1998). Turbidity sensor for underwater applications. In *Proceedings of the IEEE OCEANS'98, Nice, France, 28 of September – 1 of October, 1998*, 158-161.
- Nadimi, E. S., Blanes-Vidal, V., Jørgensen, R. N., & Christensen, S. (2011). Energy generation for an ad hoc wireless sensor network-based monitoring system using animal head movement. *Computers and Electronics in Agriculture*, 75(2), 238-242.
- Nadimi, E. S., Søggaard, H. T., Bak, T., & Oudshoorn, F. W. (2008). ZigBee-based wireless sensor networks for monitoring animal presence and pasture time in a strip of new grass. *Computers and electronics in agriculture* 61(2): 79-87.
- Natarajan, S. P., Weller, T. M., & Fries, D. P. (2007). Sensitivity tunable inductive fluid conductivity sensor based on RF phase detection. *IEEE Sensors Journal*, 7(9), 1300-1301.
- National Geographic, 2015. <http://ocean.nationalgeographic.com/ocean/critical-issues-marine-pollution/> [Last access: January 29, 2015].
- Nguyen, N. D., Zalyubovskiy, V., Ha, M. T., Le, T. D., & Choo, H. (2012). Energy-efficient Models for Coverage Problem in Sensor Networks with Adjustable Ranges. *Adhoc & Sensor Wireless Networks*, 16.
- Nikolic, M. V., Aleksic, O., Radojcic, B. M., Lukovic, M. D., Nikolic, N., & Djuric, Z. (2013). Optimization and application of NTC thick film segmented thermistors. In *Key Engineering Materials* (Vol. 543, pp. 491-494). Trans Tech Publications.
- NRC Thermistor Datasheet, 2018. <https://www.vishay.com/docs/29078/ntcle413.pdf> (accessed on 12 January 2018).
- O'Connell, E., O'Keefe, S., Newe, T., & Lewis, E. (2011, October). Low cost hydrocarbon spillage sensor for the marine environment with interfacing to a mote platform. In *Sensors, 2011 IEEE* (pp. 1558-1561). IEEE.
- O'Flynn, B., Regan, F., Lawlor, A., Wallace, J., Torres, J., & O'Mathuna, C. (2010). Experiences and recommendations in deploying a real-time, water quality monitoring system. *Measurement Science and Technology*, 21(12), 124004.
- O'Flynn, B., Martinez, R., Cleary, J., Slater, C., Regan, F., Diamond, D., & Murphy, H. (2007, October). SmartCoast: a wireless sensor network for water quality monitoring. In *Proceedings of the 32nd IEEE Conference on Local Computer Networks, 2007. LCN 2007. Dublin (Ireland). Oct. 15-18, 2007*
- O'neil, J. M., Davis, T. W., Burford, M. A., & Gobler, C. J. (2012). The rise of harmful cyanobacteria blooms: the potential roles of eutrophication and climate change. *Harmful algae*, 14, 313-334.
- Ohata, R., Masuda, R., Takahashi, K., & Yamashita, Y. (2013). Moderate turbidity enhances schooling behaviour in fish larvae in coastal waters. *ICES Journal of Marine Science* 71: 925–929.
- Öhman, M. C., Sigraý, P., & Westerberg, H. (2007). Offshore windmills and the effects of electromagnetic fields on fish. *AMBIO: A journal of the Human Environment*, 36(8), 630-633.
- Okamoto, T., Kurokawa, T., Gen, K., Murashita, K., Nomura, K., Kim, S. K., et al. (2009). Influence of salinity on morphological deformities in cultured larvae of Japanese eel, *Anguilla japonica*, at completion of yolk resorption. *Aquaculture* 293(1): 113-118.

- Okamura, A., Yamada, Y., Horie, N., Utoh, T., Mikawa, N., Tanaka, S., & Tsukamoto, K. (2007). Effects of water temperature on early development of Japanese eel *Anguilla japonica*. *Fisheries Science* 73(6): 1241-1248.
- Okamura, A., Yamada, Y., Mikawa, N., Horie, N., Utoh, T., Kaneko, T., et al. (2009). Growth and survival of eel leptocephali (*Anguilla japonica*) in low-salinity water. *Aquaculture* 296(3): 367-372.
- Olivier Job, J., Rivera González, M., & González Barrios, J. L. (1998). Algunos usos de la inducción electromagnética en el estudio de los suelos salinos. *Terra Latinoamericana*, 16(4).
- OOT Temp, <http://www.ott.com/es-es/productos/sensores-179/sensor-de-temperatura-355/> Last access: 19/09/2017
- Paerl, H. W., & Tucker, C. S. (1995). Ecology of blue-green algae in aquaculture ponds. *Journal of the World Aquaculture Society*, 26(2), 109-131.
- Palmer, P. J., Burke, M. J., Palmer, C. J., & Burke, J. B. 2007. Developments in controlled green-water larval culture technologies for estuarine fishes in Queensland, Australia and elsewhere. *Aquaculture*, 272(1), 1-21.
- Pankhurst, N. W., Purser, G. J., Van Der Kraak, G., Thomas, P. M., & Forteach, G. N. R. (1996). Effect of holding temperature on ovulation, egg fertility, plasma levels of reproductive hormones and in vitro ovarian steroidogenesis in the rainbow trout *Oncorhynchus mykiss*. *Aquaculture* 146(3): 277-290.
- Papadakis, V. M., Papadakis, I. E., Lampranidou, F., Glaropoulos, A., & Kentouri, M. (2012). A computer-vision system and methodology for the analysis of fish behavior. *Aquacultural engineering*, 46, 53-59.
- Papandroulakis, N., Dimitris, P., & Pascal, D. (2002). An automated feeding system for intensive hatcheries. *Aquacultural Engineering*, 26(1), 13-26.
- Papoutsoglou, S. E., & Tziha, G. (1996). Blue tilapia (*Oreochromis aureus*) growth rate in relation to dissolved oxygen concentration under recirculated water conditions. *Aquacultural Engineering* 15(3): 181-192.
- Parra, L., Karampelas, E., Sendra, S., Lloret, J., & Rodrigues, J. J. (2015a). Design and deployment of a smart system for data gathering in estuaries using wireless sensor networks. In *Proceedings of the 2015 International Conference on Computer, Information and Telecommunication Systems*, Gijón, Spain, July 15-17 2015, 1-5.
- Parra, L., Lloret, G., Lloret, J., Rodilla, M. (2018a). Physical sensors for precision aquaculture: A Review, *IEEE Sensor Journal*, 18(10), 3915-3923.
- Parra, L., Ortuño, V., Sendra, S., Lloret, J. (2013a) Low-Cost Conductivity Sensor Based on Two Coils. In *Proceedings of the First International Conference on Computational Science and Engineering (CSE'13)*, Valencia, Spain, 6–8 August 2013, pp. 107–112
- Parra, L., Ortuño, V., Sendra, S., Lloret, J. (2013b) Two New Sensors Based on the Changes of the Electromagnetic Field to Measure the Water Conductivity. In *Proceedings of the Seventh International Conference on Sensor Technologies and Applications (SENSORCOMM 2013)*, Barcelona, Spain, 25–31 August 2013; pp. 266–272.
- Parra, L., Ortuño, V., Sendra, S., Lloret, J. (2013c) Water Conductivity Measurements Based on Electromagnetic Fields. In *Proceedings of the First International Conference on Computational Science and Engineering (CSE'13)*, Valencia, Spain, 6–8 August 2013; pp. 139–144.
- Parra, L., Rocher, J., Escrivá, J., & Lloret, J. (2018b). Design and development of low cost smart turbidity sensor for water quality monitoring in fish farms. *Aquacultural Engineering*, 81, 10-18.
- Parra, L., Sendra, S., García, L., Lloret, J. (2018c). Design and Deployment of Low-Cost sensors Sensors for Monitoring the Water Quality and Fish Behavior in Aquaculture Tanks during the Feeding Process, *Sensors*, 18(3).
- Parra, L., Sendra, S., Jimenez, J. M., & Lloret, J. (2015b). Smart system to detect and track pollution in marine environments. In *Proceedings of the 2015 IEEE International Conference on Communication Workshop*, London, U.K., 8 – 12 Jun 2015 (pp. 1503-1508).
- Parra, L., Sendra, S., Lloret, J., & Bosch, I. (2015c). Development of a conductivity sensor for monitoring groundwater resources to optimize water management in smart city environments. *Sensors*, 15(9), 20990-21015.
- Parra, L., Sendra, S., Lloret, J., & Mendoza, J. (2015d). Low cost optic sensor for hydrocarbon detection in open oceans. *Instrumentation viewpoint*, (18), 45-45.
- Parra, L., Sendra, S., Lloret, J., & Rodrigues, J. J. (2017). Design and deployment of a smart system for data gathering in aquaculture tanks using wireless sensor networks. *International Journal of Communication Systems*, 30(16).

- Parra, L., Sendra, S., Lloret, J., & Rodrigues, J. J. 2014. Low cost wireless sensor network for salinity monitoring in mangrove forests. In Proceedings of the IEEE SENSORS 2014, Valencia, Spain, 02 - 05 Nov 2014 (pp. 126-129).
- Partan, J., Kurose, J., & Levine, B. N. (2007). A survey of practical issues in underwater networks. *ACM SIGMOBILE Mobile Computing and Communications Review*, 11(4), 23-33.
- Partridge, G. J., & Jenkins, G. I. (2002). The effect of salinity on growth and survival of juvenile black bream (*Acanthopagrus butcheri*). *Aquaculture* 210(1): 219-230.
- Patra, R. K., Nedeveschi, S., Surana, S., Sheth, A., Subramanian, L., & Brewer, E. A. (2007, April). WiLDNet: Design and Implementation of High Performance WiFi Based Long Distance Networks. In 4th USENIX Symposium on Networked Systems Design & Implementation (NSDI '07), Cambridge, MA, USA, April 11–13, 2007, pp 87–100
- Pavey, K. D., Hunter, A. C., & Paul, F. (2003). Real-time evaluation of macromolecular surface modified quartz crystal resonant sensors under cryogenic stress for biological applications. *Biosensors and Bioelectronics*, 18(11), 1349-1354.
- Péron, O., Rinnert, E., Lehaitre, M., Crassous, P., & Compère, C. (2009). Detection of polycyclic aromatic hydrocarbon (PAH) compounds in artificial sea-water using surface-enhanced Raman scattering (SERS). *Talanta*, 79(2), 199-204.
- Perovich, D. K., Richter - Menge, J. A., Jones, K. F., & Light, B. (2008). Sunlight, water, and ice: Extreme Arctic sea ice melt during the summer of 2007. *Geophysical Research Letters*, 35(11).
- Person-Le Ruyet, J., Buchet, V., Vincent, B., Le Delliou, H., & Quemener, L. (2006). Effects of temperature on the growth of pollack (*Pollachius pollachius*) juveniles. *Aquaculture* 251(2): 340-345.
- Person-Le Ruyet, J., Mahe, K., Le Bayon, N., & Le Delliou, H. (2004). Effects of temperature on growth and metabolism in a Mediterranean population of European sea bass, *Dicentrarchus labrax*. *Aquaculture* 237(1): 269-280.
- Pham, T. T., Green, T., Chen, J., Truong, P., Vaidya, A., & Bushnell, L. (2008, September). A salinity sensor system for estuary studies. In Proceedings of the IEEE OCEANS 2008, Quebec City, Canada , 15 – 18 of September, 2008, 1-6.
- Pichavant, K., Person, J., Le Bayon, N., Severe, A., Le Roux, A., & Boeuf, G. (2001). Comparative effects of long-term hypoxia on growth, feeding and oxygen consumption in juvenile turbot and European sea bass. *Journal of Fish Biology* 59(4): 875-883.
- Pichavant, K., Person-Le-Ruyet, J., Le Bayon, N., Severe, A., Le Roux, A., Quemener, L., et al. (2000). Effects of hypoxia on growth and metabolism of juvenile turbot. *Aquaculture* 188(1): 103-114.
- PNUMA, Metodologia para el establecimiento de niveles guía de calidad de agua ambiente para riego Available at : <http://www.pnuma.org/agua-miaac/CODIA%20CALIDAD%20DE%20LAS%20AGUAS/MATERIAL%20ADICIONAL/PONENCIAS/PONENTES/Tema%205%20Niveles%20Guias%20Calidad%20de%20Aguas/NIVELES%20GUIA/2%20-%20Metodologias/3%20-%20Metodologia%20Riego.pdf> (Last access: January 12, 2017).
- Popper, A. N., Fewtrell, J., Smith, M. E., & McCauley, R. D. (2003). Anthropogenic sound: effects on the behavior and physiology of fishes. *Marine Technology Society Journal*, 37(4), 35-40.
- Postolache, O., Girão, P. S., & Pereira, J. M. D. (2012). Water Quality Monitoring and Associated Distributed Measurement Systems: An Overview. *WATER QUALITY MONITORING AND ASSESSMENT*, 25.
- Postolache, O., Girao, P., Pereira, M., & Ramos, H. (2002a). An IR turbidity sensor: design and application [virtual instrument]. Proceedings of the 19th IEEE Instrumentation and Measurement Technology Conference, Alaska, USA, 21-23 of May, 2002, 535-539.
- Postolache, O., Pereira, J. D., & Girao, P. S. (2002b). An intelligent turbidity and temperature sensing unit for water quality assessment. In Proceedings of the Canadian Conference on Electrical and Computer Engineering, Manitoba, Canada, 12-15 of May, 2002, 494-499.
- Primavera, J. (2006). Overcoming the impacts of aquaculture on the coastal zone. *Ocean & Coastal Management* 49(9): 531-545.
- Primicerio, J., Di Gennaro, S. F., Fiorillo, E., Genesio, L., Lugato, E., Matese, A., & Vaccari, F. P. (2012). A flexible unmanned aerial vehicle for precision agriculture. *Precision Agriculture* 13(4): 517-523.

- Purchase, C. F., Boyce, D. L., & Brown, J. A. (2000). Growth and survival of juvenile yellowtail flounder *Pleuronectes ferrugineus* (Storer) under different photoperiods. *Aquaculture Research* 31(6): 547-552.
- Qi, L., Zhang, J., Xu, M., Fu, Z., Chen, W., & Zhang, X. (2011). Developing WSN-based traceability system for recirculation aquaculture. *Mathematical and Computer Modelling*, 53(11-12), 2162-2172.
- Ramos, H., Gurriana, L., Postolache, O., Pereira, M., & Girão, P. (2005). Development and characterization of a conductivity cell for water quality monitoring. In *Proceedings of the Third IEEE International Conference on Systems, Signals & Devices (SSD'2005)*, Sousse, Tunisia, 21-24 of March, 2005, 1-5.
- Ramos, P. M., Pereira, J. D., Ramos, H. M. G., & Ribeiro, A. L. (2008). A four-terminal water-quality-monitoring conductivity sensor. *IEEE Transactions on instrumentation and measurement*, 57(3), 577-583.
- Rad, F., Bozaoğlu, S., Gözükar, S. E., Karahan, A., & Kurt, G. (2006). Effects of different long-day photoperiods on somatic growth and gonadal development in Nile tilapia (*Oreochromis niloticus* L.). *Aquaculture* 255(1): 292-300.
- Rasin, Z., & Abdullah, M. R. (2009). Water quality monitoring system using zigbee based wireless sensor network. *International Journal of Engineering & Technology*, 9(10), 24-28.
- Rayne, S., Henderson, G., Gill, P., & Forest, K. (2008). Riparian forest harvesting effects on maximum water temperatures in wetland-sourced headwater streams from the Nicola River Watershed, British Columbia, Canada. *Water resources management*, 22(5), 565-578.
- RDO Titan, [https://in-situ.com/wp-content/uploads/2014/11/Optical-RDO-Titan-Probe%E2%80%9494Titanium-Probe-for-Process-Monitoring-Control\\_Aqua\\_Specs.pdf](https://in-situ.com/wp-content/uploads/2014/11/Optical-RDO-Titan-Probe%E2%80%9494Titanium-Probe-for-Process-Monitoring-Control_Aqua_Specs.pdf). Last access: 19/09/2017
- Reddy, K. J., Rao, K. V., & Raghavendra, A. S. (2006). *Physiology and Molecular Biology of Stress Tolerance in Plants*. Springer.
- Resley, M. J., Webb, K. A., & Holt, G. J. (2006). Growth and survival of juvenile cobia, *Rachycentron canadum*, at different salinities in a recirculating aquaculture system. *Aquaculture*, 253(1), 398-407.
- Ribeiro, A. L., Ramos, H. M. G., Ramos, P. M., & Pereira, J. D. (2006, September). Inductive conductivity cell for water salinity monitoring. In *Proceedings of XVIII Imeko World Congress, Metrology for a Sustainable Development*, September, 17-22, 2006, Rio de Janeiro, Brazil. (pp. 0018-9464).
- Rieger, P. W., & Summerfelt, R. C. (1997). The influence of turbidity on larval walleye, *Stizostedion vitreum*, behavior and development in tank culture. *Aquaculture* 159(1): 19-32.
- Robinson, E. H., & Li, M. H. (2008). Replacement of soybean meal in channel catfish, *Ictalurus punctatus*, diets with cottonseed meal and distiller's dried grains with solubles. *Journal of the World Aquaculture Society* 39(4): 521-527.
- Rocher, J., Taha, M., Parra, L., & Lloret, J. 2017. Design and deployment of a WSN for water turbidity monitoring in fish farms. In *Proceedings of the 10th IFIP Wireless and Mobile Networking Conference (WMNC), 2017, Valencia, Spain, 25-27 sept 2017*,
- Rosário, D., Costa, R., Paraense, H., Machado, K., Cerqueira, E., Braun, T., & Zhao, Z. (2012). A hierarchical multi-hop multimedia routing protocol for wireless multimedia sensor networks. *Network protocols and algorithms*, 4(4), 44-64.
- Rubin, L. G. (1997). Cryogenic thermometry: a review of progress since 1982. *Cryogenics*, 37(7), 341-356.
- Rubio, V. C., Sánchez-Vázquez, F. J., & Madrid, J. A. (2005). Effects of salinity on food intake and macronutrient selection in European sea bass. *Physiology & behavior* 85(3): 333-339.
- Ruff, B. P., Marchant, J. A., & Frost, A. R. (1995). Fish sizing and monitoring using a stereo image analysis system applied to fish farming. *Aquacultural engineering*, 14(2), 155-173.
- Russ, S. H., Perepa, V., Leavesly, S., & Webb, B. (2010). Novel lowcost salinity sensor for embedded environmental monitoring. In *Proceedings of the IEEE SoutheastCon 2010 (SoutheastCon)*, Concord, USA, 18-21 of March, 2010.
- Saberioon, M., Gholizadeh, A., Cisar, P., Pautsina, A., & Urban, J. (2016). Application of machine vision systems in aquaculture with emphasis on fish: state-of-the-art and key issues. *Reviews in Aquaculture*.
- Sampaio, L. A., & Bianchini, A. (2002). Salinity effects on osmoregulation and growth of the euryhaline flounder *Paralichthys orbignyanus*. *Journal of Experimental Marine Biology and Ecology* 269(2): 187-196.

- Sampaio, L. A., Freitas, L. S., Okamoto, M. H., Louzada, L. R., Rodrigues, R. V., & Robaldo, R. B. (2007). Effects of salinity on Brazilian flounder *Paralichthys orbignyanus* from fertilization to juvenile settlement. *Aquaculture* 262(2): 340-346.
- Sanchez-Jerez, P., Fernandez-Jover, D., Bayle-Sempere, J., Valle, C., Dempster, T., Tuya, F., & Juanes, F. (2008). Interactions between bluefish *Pomatomus saltatrix* (L.) and coastal sea-cage farms in the Mediterranean Sea. *Aquaculture*, 282(1-4), 61-67.
- Saoud, I. P., Kreydiyyeh, S., Chalfoun, A., & Fakhri, M. (2007). Influence of salinity on survival, growth, plasma osmolality and gill Na<sup>+</sup>-K<sup>+</sup>-ATPase activity in the rabbitfish *Siganus rivulatus*. *Journal of Experimental Marine Biology and Ecology* 348(1): 183-190.
- Sawant, S., Durbha, S. S., & Jagarlapudi, A. (2017). Interoperable agro-meteorological observation and analysis platform for precision agriculture: A case study in citrus crop water requirement estimation. *Computers and Electronics in Agriculture*, 138, 175-187.
- Schoellhamer, D. H., & Wright, S. A. 2003. Continuous measurement of suspended-sediment discharge in rivers by use of optical backscatterance sensors. *IAHS PUBLICATION*, 28-36
- Schütz, J. H., & Nuñez, A. P. D. O. (2007). Growth and survival of dorado *Salminus brasiliensis* (Pisces, Characidae) post-larvae cultivated with different types of food and photoperiods. *Brazilian Archives of Biology and Technology* 50(3): 435-444. doi:
- SD204, 2017, <http://www.saivas.no/visartikkel.asp?a rt=2>. Last access: 19/09/2017
- SD208, 2017, <http://www.saivas.no/visartikkel.asp?a rt=53>. Last access: 19/09/2017
- Sebastiá, M. T., Estornell, J., Rodilla, M., Martí, J., & Falco, S. 2012. Estimation of chlorophyll «A» on the Mediterranean coast using a QuickBird image. *Revista de Teledetección*, 37, 23-33.
- Segura, R., Cierpka, C., Rossi, M., & Kähler, C. J. (2015). Thermochromic Liquid Crystals for Particle Image Thermometry. In *Encyclopedia of Microfluidics and Nanofluidics* (pp. 3272-3279). Springer New York.
- Sendra, S., Llario, F., Parra, L., & Lloret, J. (2013a). Smart wireless sensor network to detect and protect sheep and goats to wolf attacks. *Recent Advances in Communications and Networking Technology (Formerly Recent Patents on Telecommunication)* 2(2): 91-101.
- Sendra, S., Lloret, A. T., Lloret, J., & Rodrigues, J. J. P. C. (2014). A wireless sensor network deployment to detect the degeneration of cement used in construction. *International Journal of Ad Hoc and Ubiquitous Computing*, 15(1-3), 147-160.
- Sendra, S., Lloret, J., Jimenez, J. M., & Parra, L. (2015a). Underwater Acoustic Modems. *IEEE Sensors Journal*, 16(11), 4063-4071.
- Sendra, S., Parra, L., Lloret, J., & Jiménez, J. M. (2015b). Oceanographic multisensor buoy based on low cost sensors for posidonia meadows monitoring in Mediterranean Sea. *Journal of Sensors*, 2015.
- Sendra, S., Parra, L., Ortuno, V., & Lloret, J. (2013b). A low cost turbidity sensor development. In *Proceedings of the 7th International Conference on Sensor Technologies and Applications (SENSORCOMM'13)*, Barcelona, Spain, 25-31 of August, 266-272.
- Shahzad, M. K., & Cho, T. H. (2017). A Network Density-adaptive Improved CCEF Scheme for Enhanced Network Lifetime, Energy Efficiency, and Filtering in WSNs. *Adhoc & Sensor Wireless Networks*, 35.
- Shan, X., Xiao, Z., Huang, W., & Dou, S. (2008). Effects of photoperiod on growth, mortality and digestive enzymes in miyu croaker larvae and juveniles. *Aquaculture* 281(1): 70-76.
- Shenoy, M. R., Pal, B. P., & Gupta, B. D. (2012). Design, analysis, and realization of a turbidity sensor based on collection of scattered light by a fiber-optic probe. *IEEE Sensors Journal*, 12(1), 44-50.
- Shifeng, Y., Jing, K., & Jimin, Z. (2007, December). Wireless monitoring system for aquaculture environment. In *Proceedings of the IEEE International Workshop on Radio-Frequency Integration Technology*, Singapore, 9-11 December 2007, pp. 274-277.
- Sigholt, T., Staurnes, M., Jakobsen, H. J., & Åsgård, T. (1995). Effects of continuous light and short-day photoperiod on smolting, seawater survival and growth in Atlantic salmon (*Salmo salar*). *Aquaculture*, 130(4): 373-388.
- Simbeye, D. S., & Yang, S. F. (2014). Water Quality Monitoring and Control for Aquaculture Based on Wireless Sensor Networks. *JNW*, 9(4), 840-849.
- Sims, D. W., Queiroz, N., Humphries, N. E., Lima, F. P., & Hays, G. C. (2009). Long-term GPS tracking of ocean sunfish *Mola mola* offers a new direction in fish monitoring. *PLoS One*, 4(10), e7351.
- Sin, A., Chin, K. C., Jamil, M. F., Kostov, Y., Rao, G., & Shuler, M. L. (2004). The design and fabrication of three-chamber microscale cell culture analog devices with integrated dissolved oxygen sensors. *Biotechnology progress*, 20(1), 338t-345.

- smarTROLL RDO, [https://in-situ.com/wp-content/uploads/2015/08/smarTROLL\\_RDO\\_Handheld\\_Specs1.pdf](https://in-situ.com/wp-content/uploads/2015/08/smarTROLL_RDO_Handheld_Specs1.pdf). Last access: 19/09/2017
- smarTROLL, [https://in-situ.com/wp-content/uploads/2014/11/smarTROLL\\_Multiparameter\\_Handheld\\_Specs.pdf](https://in-situ.com/wp-content/uploads/2014/11/smarTROLL_Multiparameter_Handheld_Specs.pdf). Last access: 19/09/2017
- Smith, D., & Davis-Colley, R. (2001). Turbidity suspended sediment and water clarity. *J Am Water Resour Assoc*, 37, 1085-1101.
- Smith, T. I., Denson, M. R., Heyward, L. D., Jenkins, W. E., & Carter, L. M. (1999). Salinity effects on early life stages of southern flounder *Paralichthys lethostigma*. *Journal of the World Aquaculture Society* 30(2): 236-244.
- Sosna, M., Denuault, G., Pascal, R. W., Prien, R. D., & Mowlem, M. (2007). Development of a reliable microelectrode dissolved oxygen sensor. *Sensors and Actuators B: Chemical*, 123(1), 344-351.
- Sosna, M., Denuault, G., Pascal, R. W., Prien, R. D., & Mowlem, M. (2008). Field assessment of a new membrane-free microelectrode dissolved oxygen sensor for water column profiling. *Limnology and Oceanography: Methods*, 6(4), 180-189.
- Sousa-Lima, R. S., Norris, T. F., Oswald, J. N., & Fernandes, D. P. (2013). A review and inventory of fixed autonomous recorders for passive acoustic monitoring of marine mammals. *Aquatic Mammals*, 39(1), 23.
- STATGRAPHICS, 2017. <http://www.statgraphics.net/descargas-centurion-xvii/> (Last access: February 24, 2017)
- Stuart, K. R., & Drawbridge, M. (2012). The effect of photoperiod on larval culture performance of two marine finfish species. *Aquaculture* 360: 54-57.
- Stubblefield, A. P., Reuter, J. E., Dahlgren, R. A., & Goldman, C. R. (2007). Use of turbidometry to characterize suspended sediment and phosphorus fluxes in the Lake Tahoe basin, California, USA. *Hydrological Processes*, 21(3), 281-291.
- Sun, L., Chen, H., & Huang, L. (2006). Effect of temperature on growth and energy budget of juvenile cobia (*Rachycentron canadum*). *Aquaculture* 261(3): 872-878.
- Suquet, M., Normant, Y., Gaignon, J. L., Quemener, L., & Fauvel, C. (2005). Effect of water temperature on individual reproductive activity of pollack (*Pollachius pollachius*). *Aquaculture* 243(1): 113-120.
- Sutherland, A. B., & Meyer, J. L. (2007). Effects of increased suspended sediment on growth rate and gill condition of two southern Appalachian minnows. *Environmental Biology of Fishes* 80(4): 389-403.
- Sweka, J. A., & Hartman, K. J. (2001). Effects of turbidity on prey consumption and growth in brook trout and implications for bioenergetics modeling. *Canadian Journal of Fisheries and Aquatic Sciences*, 58(2): 386-393.
- T1/T1R, <http://inwusa.com/wordpress/wp-content/uploads/t1.pdf>. Last access: 19/09/2017
- Takaaki, A. B. E., Mizugaki, S., Toyabe, T., Maruyama, M., Murakami, Y., & Ishiya, T. (2012). High range turbidity monitoring in the Mu and Saru river basins: All-year monitoring of hydrology and suspended sediment transport in 2010. *International Journal of Erosion Control Engineering*, 5(1), 70-79.
- Tandler, A., Anav, F. A., & Choshniak, I. (1995). The effect of salinity on growth rate, survival and swimbladder inflation in gilthead seabream, *Sparus aurata*, larvae. *Aquaculture* 135(4): 343-353.
- TD301/TD303, [http://www.saivas.no/upload/TD301-303\\_091026.pdf](http://www.saivas.no/upload/TD301-303_091026.pdf). Last access: 19/09/2017
- Thetmeyer, H., Waller, U., Black, K. D., Inselmann, S., & Rosenthal, H. (1999). Growth of European sea bass (*Dicentrarchus labrax* L.) under hypoxic and oscillating oxygen conditions. *Aquaculture* 174(3): 355-367.
- Thiemann, S., & Kaufmann, H. (2002). Lake water quality monitoring using hyperspectral airborne data—a semiempirical multisensor and multitemporal approach for the Mecklenburg Lake District, Germany. *Remote sensing of Environment*, 81(2-3), 228-237.
- Tokhtuev, E., Owen, C., Skirda, A., Slobodyan, V., & Goin, J. (2005). U.S. Patent No. 6,842,243. Washington, DC: U.S. Patent and Trademark Office.
- Tran-Duy, A., Schrama, J. W., van Dam, A. A., & Verreth, J. A. (2008). Effects of oxygen concentration and body weight on maximum feed intake, growth and hematological parameters of Nile tilapia, *Oreochromis niloticus*. *Aquaculture* 275(1): 152-162.
- Trettnak, W., Kolle, C., Reininger, F., Dolezal, C., & O'Leary, P. (1996). Miniaturized luminescence lifetime-based oxygen sensor instrumentation utilizing a phase modulation technique. *Sensors and Actuators B: Chemical*, 36(1), 506-512.



- Trettnak, W., Kolle, C., Reininger, F., Dolezal, C., O'Leary, P., & Binot, R. A. (1998). Optical oxygen sensor instrumentation based on the detection of luminescence lifetime. *Advances in Space Research*, 22(10), 1465-1474.
- Trevethan, M., Chanson, H., & Takeuchi, M. (2007). Continuous high-frequency turbulence and suspended sediment concentration measurements in an upper estuary. *Estuarine, Coastal and Shelf Science*, 73(1), 341-350.
- TROLL 9500, [https://in-situ.com/wp-content/uploads/2014/11/TROLL-9500-Water-Quality-Instrument\\_Specs.pdf](https://in-situ.com/wp-content/uploads/2014/11/TROLL-9500-Water-Quality-Instrument_Specs.pdf). Last access: 19/09/2017
- Trotter, A. J., Pankhurst, P. M., Morehead, D. T., & Battaglene, S. C. (2003). Effects of temperature on initial swim bladder inflation and related development in cultured striped trumpeter (*Latris lineata*) larvae. *Aquaculture* 221(1): 141-156.
- Tsuzuki, M. Y., Sugai, J. K., Maciel, J. C., Francisco, C. J., & Cerqueira, V. R. (2007). Survival, growth and digestive enzyme activity of juveniles of the fat snook (*Centropomus parallelus*) reared at different salinities. *Aquaculture* 271(1): 319-325.
- Tucker, B. J., Booth, M. A., Allan, G. L., Booth, D., & Fielder, D. S. (2006). Effects of photoperiod and feeding frequency on performance of newly weaned Australian snapper *Pagrus auratus*. *Aquaculture* 258(1): 514-520. doi:10.1016/j.aquaculture.2006.03.033
- Tyler, A. N., Svab, E., Preston, T., Présing, M., & Kovács, W. A. 2006. Remote sensing of the water quality of shallow lakes: A mixture modelling approach to quantifying phytoplankton in water characterized by high-suspended sediment. *International Journal of Remote Sensing*, 27(8), 1521-1537.
- UN (2015). World Population Prospects: The 2015 Revision. Department of Economic and Social.
- van der Meeren, T., Mangor-Jensen, A., & Pickova, J. (2007). The effect of green water and light intensity on survival, growth and lipid composition in Atlantic cod (*Gadus morhua*) during intensive larval rearing. *Aquaculture* 265(1): 206-217.
- Van Ham, E. H., Berntssen, M. H., Imsland, A. K., Parpoura, A. C., Bonga, S. E. W., & Stefansson, S. O. (2003). The influence of temperature and ration on growth, feed conversion, body composition and nutrient retention of juvenile turbot (*Scophthalmus maximus*). *Aquaculture* 217(1): 547-558.
- Vespe, M., Sciotti, M., Burro, F., Battistello, G., & Sorge, S. (2008, May). Maritime multi-sensor data association based on geographic and navigational knowledge. In Proceedings of the 2008 IEEE Radar Conference (RADAR '08), Rome (Italy), May 26-30, 2008, 1-6.
- Vieira, J. A. B., & Mota, A. M. (2009, July). Thermoelectric generator using water gas heater energy for battery charging. In Proceedings of the 2009 IEEE Control Applications, (CCA) & Intelligent Control, (ISIC), St.Petersburg, Russia, 8-10 July, 2009.
- Vishay, 2017a. <https://www.vishay.com/docs/81078/tshg6200.pdf> (Last access: November, 2017)
- Vishay, 2017b. <http://www.vishay.com/docs/83029/tllg440.pdf> (Last access: February 24, 2017)
- Vishay, 2017c. <http://www.vishay.com/docs/81530/bpw83.pdf> (Last access: February 24, 2017)
- Voulgaris, G., & Meyers, S. T. (2004). Temporal variability of hydrodynamics, sediment concentration and sediment settling velocity in a tidal creek. *Continental Shelf Research*, 24(15), 1659-1683.
- Vousdoukas, M. I., Aleksiadis, S., Grenz, C., & Verney, R. (2011). Comparisons of acoustic and optical sensors for suspended sediment concentration measurements under non-homogeneous solutions. *Journal of coastal research*, (64), 160.
- Wang, J. Q., Lui, H., Po, H., & Fan, L. (1997). Influence of salinity on food consumption, growth and energy conversion efficiency of common carp (*Cyprinus carpio*) fingerlings. *Aquaculture* 148(2): 115-124.
- Wang, J., Tang, S., Yin, B., & Li, X. Y. (2012, March). Data gathering in wireless sensor networks through intelligent compressive sensing. Proceedings of the 31st Annual IEEE International Conference on Computer Communications (IEEE INFOCOM 2012), Orlando, USA, March 25-30
- Wang, L., Yang, Y., Zhao, W., Xu, L., & Lan, S. (2016). Multi-rate Network Coding for Energy-Efficient Multicast in Heterogeneous Wireless Multi-hop Networks. *Adhoc & Sensor Wireless Networks*, 32.
- Wang, N., Xu, X., & Kestemont, P. (2009). Effect of temperature and feeding frequency on growth performances, feed efficiency and body composition of pikeperch juveniles (*Sander lucioperca*). *Aquaculture* 289(1): 70-73.
- Wang, T., Zhang, Y., Cui, Y., & Zhou, Y. (2014). A novel protocol of energy-constrained sensor network for emergency monitoring. *International Journal of Sensor Networks*, 15(3), 171-182.

- Wang, Z., Wang, Q., & Hao, X. (2009, September). The design of the remote water quality monitoring system based on WSN. In *Wireless Communications, Networking and Mobile Computing, 2009. WiCom'09. 5th International Conference on* (pp. 1-4). IEEE.
- Ward, D. P., Hamilton, S. K., Jardine, T. D., Pettit, N. E., Tews, E. K., Olley, J. M., & Bunn, S. E. 2013. Assessing the seasonal dynamics of inundation, turbidity, and aquatic vegetation in the Australian wet-dry tropics using optical remote sensing. *Ecohydrology*, 6(2), 312-323.
- Watanabe, W. O., Lee, C. S., Ellis, S. C., & Ellis, E. P. (1995). Hatchery study of the effects of temperature on eggs and yolk sac larvae of the Nassau grouper *Epinephelus striatus*. *Aquaculture* 136(1): 141-147.
- Wei, Y., Wang, J., Li, D., & Ding, Q. (2009, October). Design of intelligent conductivity meter based on MSP430F149. In *International Conference on Computer and Computing Technologies in Agriculture* (pp. 240-247). Springer, Berlin, Heidelberg.
- White LED VLHW4100. 2018. Available online: <http://www.farnell.com/datasheets/2049319.pdf> (accessed on 13 January 2018).
- Wilber, D. H., & Clarke, D. G. 2001. Biological effects of suspended sediments: a review of suspended sediment impacts on fish and shellfish with relation to dredging activities in estuaries. *North American Journal of Fisheries Management*, 21(4), 855-875.
- Wilhelm Filho, D., Torres, M. A., Zaniboni-Filho, E., & Pedrosa, R. C. (2005). Effect of different oxygen tensions on weight gain, feed conversion, and antioxidant status in piapara, *Leporinus elongatus* (Valenciennes, 1847). *Aquaculture* 244(1): 349-357.
- Winkler, L. W. 1888. The determination of dissolved oxygen in water. *Berichte der Deutschen Chemischen Gesellschaft*, 21, 2843-2854.
- Wood, R. T., Bannazadeh, A., Nguyen, N. Q., & Bushnell, L. G. (2010). A salinity sensor for long-term data collection in estuary studies. In *Proceedings of the IEEE OCEANS 2010 MTS/IEEE SEATTLE*, Seattle, USA, 20-23 of September, 2010, 1-6.
- Woolfe, K. F., Lani, S., Sabra, K. G., & Kuperman, W. A. (2015). Monitoring deep-ocean temperatures using acoustic ambient noise. *Geophysical Research Letters*, 42(8), 2878-2884.
- Xing, K., Wu, W., Ding, L., Wu, L., & Willson, J. (2014). An efficient routing protocol based on consecutive forwarding prediction in delay tolerant networks. *International Journal of Sensor Networks*, 15(2), 73-82.
- Xu, G., Shen, W., & Wang, X. (2014). Applications of wireless sensor networks in marine environment monitoring: A survey. *Sensors*, 14(9), 16932-16954.
- Xu, J., Liu, Y., Cui, S., & Miao, X. (2006). Behavioral responses of tilapia (*Oreochromis niloticus*) to acute fluctuations in dissolved oxygen levels as monitored by computer vision. *Aquacultural engineering* 35(3): 207-217.
- Xu, X., Liu, C., Jia, J., Liu, B., Yang, X., & Dong, S. (2008). A simple and inexpensive method for fabrication of ultramicroelectrode array and its application for the detection of dissolved oxygen. *Electroanalysis*, 20(7), 797t-802.
- Yan, M., Li, Z., Xiong, B., & Zhu, J. (2004). Effects of salinity on food intake, growth, and survival of pufferfish (*Fugu obscurus*). *Journal of Applied Ichthyology* 20(2): 146-149.
- Ye, Y., Tam, N. F. Y., Lu, C. Y., & Wong, Y. S. (2005). Effects of salinity on germination, seedling growth and physiology of three salt-secreting mangrove species. *Aquatic Botany*, 83(3), 193-205.
- Yeh, T. S., Chu, C. S., & Lo, Y. L. (2006). Highly sensitive optical fiber oxygen sensor using Pt (II) complex embedded in sol-gel matrices. *Sensors and Actuators B: Chemical*, 119(2), 701-707.
- Yick, J., Mukherjee, B., & Ghosal, D. (2008). Wireless sensor network survey. *Computer networks*, 52(12), 2292-2330.
- Yoshikawa, T., Kanemata, K., Nakase, G., & Eguchi, M. (2012). Microbial mineralization of organic matter in sinking particles, bottom sediments and seawater in a coastal fish culturing area. *Aquaculture Research*, 43(12), 1741-1755.
- Yue, R., & Ying, T. (2011, March). A water quality monitoring system based on wireless sensor network & solar power supply. In *Cyber Technology in Automation, Control, and Intelligent Systems (CYBER), 2011 IEEE International Conference on* (pp. 126-129). IEEE.
- Zaions, M. I., & Baldisserotto, B. (2000). Na<sup>+</sup> and K<sup>+</sup> body levels and survival of fingerlings of *Rhamdia quelen* (Siluriformes, Pimelodidae) exposed to acute changes of water pH. *Ciência Rural* 30(6): 1041-1045.
- Zhang, G., Shi, Y., Zhu, Y., Liu, J., & Zang, W. (2010a). Effects of salinity on embryos and larvae of tawny puffer *Takifugu flavidus*. *Aquaculture*, 302(1): 71-75.

- Zhang, H., Wei, Q., & Kang, M. (2014). Measurement of swimming pattern and body length of cultured Chinese sturgeon by use of imaging sonar. *Aquaculture*, 434, 184-187.
- Zhang, M., Li, D., Wang, L., Ma, D., & Ding, Q. (2010b, October). Design and development of water quality monitoring system based on wireless sensor network in aquaculture. In *Proceedings of the International Conference on Computer and Computing Technologies in Agriculture*, Nanchang, China, 22-25 October 2010, pp. 629-641.
- Zhao, Y., & Liao, Y. (2002). Novel optical fiber sensor for simultaneous measurement of temperature and salinity. *Sensors and Actuators B: Chemical*, 86(1), 63-67.
- Zhao, Y., Zhang, B., & Liao, Y. (2003). Experimental research and analysis of salinity measurement based on optical techniques. *Sensors and Actuators B: Chemical*, 92(3), 331-336.
- Zhao, Y., Zhang, X., Zhao, T., Yuan, B., & Zhang, S. (2009). Optical salinity sensor system based on fiberoptic array. *IEEE Sensors Journal*, 9(9), 1148-1153.
- Zheng, Z., Ren, J., Li, Y., Huang, C., Liu, G., Du, C., & Lyu, H. 2016. Remote sensing of diffuse attenuation coefficient patterns from Landsat 8 OLI imagery of turbid inland waters: A case study of Dongting Lake. *Science of The Total Environment*, 573, 39-54.
- Zhiyao, Z. J. Baoliang, W. H., & Haiqing, L. (2005). A New Electrical Conductance Measurement Instrument Based on Bi-directional Pulsed Voltage Technique. *Chinese Journal of Scientific Instrument*, S2.
- Zhou, G., Huang, L., Li, W., & Zhu, Z. (2014). Harvesting ambient environmental energy for wireless sensor networks: a survey. *Journal of Sensors*, 2014.
- Zhu, X., Li, D., He, D., Wang, J., Ma, D., & Li, F. (2010). A remote wireless system for water quality online monitoring in intensive fish culture. *Computers and Electronics in Agriculture*, 71, S3-S9.